THEORETICA CHIMICA ACTA

edenda curat
Hermann Hartmann

adiuvantibus
C. J. Ballhausen, København
R. D. Brown, Clayton
E. Heilbronner, Basel
J. Jortner, Tel-Aviv
M. Kotani, Tokyo
J. Koutecký, Praha
J. W. Linnett, Cambridge
E. E. Nikitin, Moskwa
R. G. Pearson, Evanston
B. Pullman, Paris
K. Ruedenberg, Ames
C. Sandorfy, Montreal
M. Simonetta, Milano
O. Sinanoğlu, New Haven

Vol. 29, 1973

Springer-Verlag · Berlin · Heidelberg · New York

The exclusive copyright for all languages and countries, including the right for photomechanical and any other reproductions, also in microform, is transferred to the publisher.

The use of registered names, trademarks, etc. in this publication does not imply, even in the absence of a specific statement, that such names are exempt from the relevant protective laws and regulations and therefore free for general use.

Alle Rechte, einschließlich das der Übersetzung in fremde Sprachen und das der fotomechanischen Wiedergabe oder einer sonstigen Vervielfältigung, auch in Mikroform, vorbehalten. Jedoch wird gewerblichen Unternehmen für den innerbetrieblichen Gebrauch nach Maßgabe des zwischen dem Börsenverein des Deutschen Buchhandels e. V. und dem Bundesverband der Deutschen Industrie abgeschlossenen Rahmenabkommens die Anfertigung einer fotomechanischen Vervielfältigung gestattet. Wenn für diese Zeitschrift kein Pauschalabkommen mit dem Verlag vereinbart worden ist, ist eine Wertmarke im Betrage von DM 0,40 pro Seite zu verwenden. *Der Verlag läßt diese Beträge den Autorenverbänden zufließen.*

Die Wiedergabe von Gebrauchsnamen, Handelsnamen, Warenbezeichnungen usw. in dieser Zeitschrift berechtigt auch ohne besondere Kennzeichnung nicht zu der Annahme, daß solche Namen im Sinne der Warenzeichen- und Markenschutz-Gesetzgebung als frei betrachtet wären und daher von jedermann benutzt werden dürften.

Springer-Verlag Berlin Heidelberg New York
Printed in Germany by Brühlsche Universitätsdruckerei, Gießen
© by Springer-Verlag Berlin Heidelberg 1973

Index

Commentationes et Relationes

Absar,I., Schaad,L.J., Wazer,J.R. Van: An *ab initio* LCAO-MO-SCF Study of the Electronic Structure of Phosphirane and Thiirane 173

Alagona,G., Cimiraglia,R., Lamanna,U.: Theoretical Investigations on the Solvation Process. III. STO Double-ζ SCF Calculations on the Hydrated Proton $H_5O_2^+$ 93

Amos,A.T., Burrows,B.L.: Dispersion Interactions and Solvent-Shift Effects 139

Becker,J.Y., Meyer,A.Y., Klein,J.: Sesquiacetylenes 313

Bendazzoli,G.L., Bernardi,F., Zauli,C., Palmieri,P.: Atomic Wave Functions by Rotational Projections of Floating Orbitals 85

Bernardi,F., s. Bendazzoli,G.L., *et al.* 85

Berthier,G. s. Meunier,A., *et al.* 49

Burnelle,L.A., s. Macaulay,R., *et al.* 1

Burrows,B.L., s. Amos,A.T. 139

Cimiraglia,R., s. Alagona,G., *et al.* 93

Csizmadia,I.G., s. Strausz,O.P., *et al.* 183

Condirston,D.A., Moule,D.C.: Barriers to Molecular Inversion in ($n\pi^*$) Carbonyls: A CNDO Investigation 133

Denis,A., Langlet,J., Malrieu,J.P.: Orbital and Excitonic Descriptions of Molecular Excited and Ionized States. I. Delocalization of the Excitation 117

Fischer-Hjalmars,I., Kowalewski,J.: Simplified Non-Empirical Excited States Calculations
Part II. Interpretation of the Electronic Transitions in the Vacuum-UV Spectrum of Ethylene 345

Francke,E., Moncuit,C.: Le spectre d'absorption électronique du trichloroamminoplatinate de potassium cristallisé 319

Frost,A.A., s. Nelson,J.L. 75

Gamba,A., Tantardini,G.F., Simonetta,M.: Transition Energies and Oscillator Strengths for Electronic Spectra of Non Planar Conjugated Molecules. I. Polyphenyls 335

Haase,D., Ruch,E.: Quantenmechanische Theorie der optischen Aktivität der Methanderivate im Transparenzgebiet 189

Haase,D., Ruch,E.: Bemerkung zur Rayleigh-Schrödinger-Störungstheorie 235

Haase,D., Ruch,E.: Quantenmechanische Theorie der optischen Aktivität der Allenderivate im Transparenzgebiet 247

Hässelbarth,W., s. Ruch,E. 259

Hopkinson,A.C., s. Strausz,O.P., *et al.* 183

Janoschek,R.: *Ab initio*-Behandlung der IR- und Ramanaktivität der Wasserstoffbrücke $(ClHCl)^-$ unter Berücksichtigung der Umgebung 57

Johansson,A., Kollman,P., Rothenberg,S.: An Application of the Functional Boys-Bernardi Counterpoise Method to Molecular Potential Surfaces 167

Jortner,J., s. Nitzan,A. 97

Jug,K.: Effects of Polarization on Charge Distributions and Integral Approximations . . 9

Kahn,O., Kettle,S.F.A.: Couplage vibronique et anisotropie paramagnétique dans un complexe cubique $^2T_2$ soumis à un champ trigonal 359

Karwowski, J.: Matrix Elements of One- and Two-Electron Operators 151

Kettle, S. F. A., s. Kahn, O. 359

Klein, J., s. Becker, J. Y., *et al.* 313

Kollman, P., s. Johansson, A., *et al.* 167

Kowalewski, J., s. Fischer-Hjalmars, I. 345

Lamanna, U., s. Alagona, G., *et al.* 93

Langlet, J., s. Denis, A., *et al.* 117

Lévy, B., s. Meunier, A., *et al.* 49

Macaulay, R., Burnelle, L. A., Sandorfy, C.: Theoretical Investigation of the Carbon Nitrogen Double Bond 1

Malrieu, J. P., s. Denis, A., *et al.* 117

Mead, A., Ruch, E., Schönhofer, A.: Theory of Chirality Functions, Generalized for Molecules with Chiral Ligands 269

Meunier, A., Lévy, B., Berthier, G.: Corrélation électronique et effets de base dans l'étude de la liaison hydrogène: le dimère mixte ammoniac-eau 49

Meyer, A. Y., s. Becker, J. Y., *et al.* 313

Meyer, H., Schweig, A.: Molecular Dipole Polarizabilities Based on MINDO/1 and MINDO/2 Wavefunctions 375

Moncuit, C., s. Francke, E. 319

Moule, D. C., s. Condirston, D. A. 133

Nelson, J. L., Frost, A. A.: Local Orbitals for Bonding in Ethane 75

Niessen, W. von: Density Localization of Atomic and Molecular Orbitals. III. Heteronuclear Diatomic and Polyatomic Molecules 29

Nitzan, A., Jortner, J.: Electronic Relaxation of Small Molecules in a Dense Medium . . . 97

Norstrom, R. J., s. Strausz, O. P., *et al.* 183

Palmieri, P., s. Bendazzoli, G. L., *et al.* 85

Pancíř, J.: Study of Reaction Mechanisms by Semiempirical Methods. I. Optimization of the Geometry of the Molecule in the Framework of a Single Calculation of the Energy Function 21

Rothenberg, S., s. Johansson, A., *et al.* 167

Ruch, E., Hässelbarth, W.: Classifications of Rearrangement Mechanisms by Means of Double Cosets and Counting Formulas for the Numbers of Classes 259

Ruch, E., s. Haase, D. 189, 235, 247

Ruch, E., s. Mead, A., *et al.* 269

Sandorfy, C., s. Macaulay, R., *et al.* 1

Schaad, L. J., s. Absar, I., *et al.* 173

Schoenborn, M., s. Strausz, O. P., *et al.* 183

Schönhofer, A., s. Mead, A., *et al.* 269

Schweig, A., s. Meyer, H. 375

Simonetta, M., s. Gamba, A., *et al.* 335

Strausz, O. P., Norstrom, R. J., Hopkinson, A. C., Schoenborn, M., Csizmadia, I. G.: An *ab initio* Molecular Orbital Study of the C_2F_2 Species: The Difluorovinylidene → Difluoroacetylene Rearrangement 183

Sustmann, R., Vahrenholt, F.: Application of SCF-Perturbation Theory to Hydrogen Bonding in Water Dimers 305

Tantardini, G. F., s. Gamba, A., *et al.* 335

Vahrenholt, F., s. Sustmann, R. 305

Wazer, J. R. Van, s. Absar, I., *et al.* 173

Zauli, C., s. Bendazzoli, G. L., *et al.* 85

Indexed in Current Contents

Theoret. chim. Acta (Berl.) 29, 1—7 (1973)
© by Springer-Verlag 1973

Commentationes

Theoretical Investigation of the Carbon Nitrogen Double Bond

R. Macaulay, L. A. Burnelle*, and C. Sandorfy

Département de Chimie, Université de Montréal, Montréal, Québec, Canada

Received October 26, 1972

Ab initio Gaussian type calculations are reported for the ground and excited states of the hypothetical molecule formaldimine (H_2CNH). The C═N group is compared with the C═O group.

Die Ergebnisse einer *ab initio* Rechnung mit Gauß-Orbitalen für das hypothetische Formaldimin-Molekül (H_2CNH) werden mitgeteilt. Es werden sowohl Grundzustand als auch einige angeregte Zustände untersucht und die beiden Gruppen C═O und N═O verglichen.

On présente les résultats de calculs *ab initio* utilisant une base Gaussienne pour la molécule hypothétique de formaldimine (H_2CNH). L'étude porte sur l'état fondamental et quelques états excités. Une comparaison est faite entre le groupement C═N et le groupement C═O.

Introduction

The carbonyl (C═O) function has been the object of extensive studies for many decades. Much less is known about the azomethine (C═N) group, however, and we therefore felt that a theoretical investigation of this functional group was in order. It was decided to study the simplest system with a C═N function, namely the hypothetical molecule of formaldimine (H_2CNH).

Calculations

The *ab initio* calculations were done using a 4-31G Gaussian basis set [1]. The computer programs were modified versions of the Polyatom system [2, 3]. The $n - n^*$ singlet state was done using Huz, a program we built which is based on Huzinaga's first scheme [4]. This program will be submitted to the Quantum Chemistry Program Exchange very shortly.

Ground State

Complete optimization of the ground state geometry (Fig. 1) of formaldimine gives a planar structure having a total energy of -93.8824 a.u. (Table 1).

Experimentally, the C═N bond length is of the order of 1.29 – 1.30 Å for non conjugated imines (see Ref. [5]), i.e. imines containing alkyl substituents only. The value we obtain for H_2CNH is 1.257 Å.

---

* Present address: Department of Chemistry, New York University, New York, N.Y. 10003, USA.

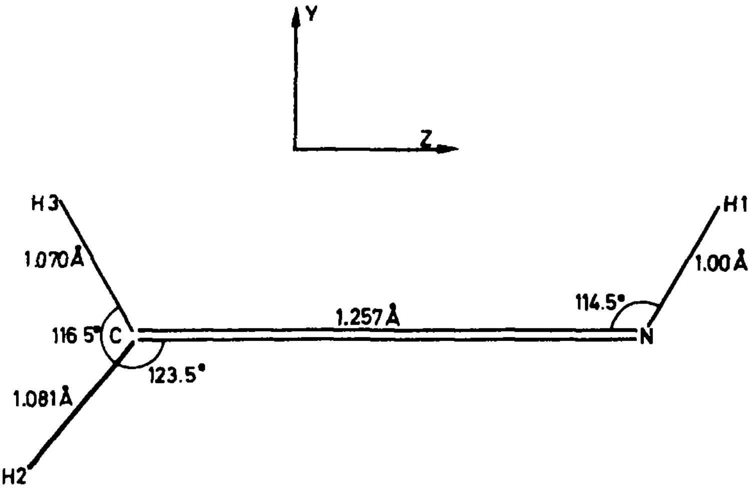

Fig. 1. Geometry of the ground state of formaldimine

Table 1. Results of SCF calculation on the ground state of formaldimine

	Energy breakdown (a.u.)		Orbital eigenvalues (a.u.)
Kinetic	93.9724	$1a'$	−15.5395
One-el. pot.	−286.2296	$2a'$	−11.2622
One-el. energy	−192.2573	$3a'$	−1.2292
Two-el. pot.	65.0770	$4a'$	−0.8521
Total el pot.	−221.1525	$5a'$	−0.6925
Nuclear pot.	33.2978	$6a'$	−0.6142
Total pot.	−187.8547	$1a''(\pi)$	−0.4499
Total electron	−127.1802	$7a'(n)$	−0.4119
		$2a''(\pi^*)$	0.1646
Total energy	−93.8824	$8a'$	0.2414
		$9a'$	0.2806
Virial	−1.9990	$10a'$	0.3411

The following ground state electronic configuration of formaldimine results from the calculations (under C_s symmetry):

$$^1A':(1a')^2(2a')^2(3a')^2(4a')^2(5a')^2(6a')^2(1a'')^2(7a')^2.$$

The first two molecular orbitals are the Nitrogen and Carbon inner-shell orbitals respectively. The $3a'$ orbital is strongly C=N bonding, with most of the charge centered on the Nitrogen. An individual breakdown of the charges in terms of the basis functions (atomic orbitals) shows that 90% of the charge on Nitrogen and 80% of the charge on Carbon are due to the respective $2s$ basis functions. This MO is therefore mainly a $2s-2s$ bonding orbital, with slight contributions from the p_y and p_z orbitals.

Table 2. Results of Mulliken population analysis on formaldimine

MO	Gross populations					Overlap populations			
	H_2	H_3	C	N	H_1	N–H_1	N–C	CH_2	CH_3
1*a*′	0.0000	0.0000	0.0047	1.9942	0.0010	0.0018	0.0075	0.0000	0.0000
2*a*′	0.0017	0.0014	1.9956	0.0016	0.0000	0.0000	0.0027	0.0027	0.0025
3*a*′	0.0141	0.0122	0.5329	1.3613	0.0795	0.1069	0.5183	0.0134	0.0126
4*a*′	0.2580	0.1740	0.8886	0.4870	0.2024	0.2630	−0.1952	0.2905	0.2182
5*a*′	0.0026	0.4033	0.7845	0.5877	0.2219	0.1399	0.2470	0.0031	0.3516
6*a*′	0.4259	0.0504	0.8585	0.5634	0.1017	0.1332	0.0809	0.3903	0.0504
1*a*″	0.0000	0.0000	0.8829	1.1171	0.0000	0.0000	0.4867	0.0000	0.0000
7*a*′	0.1276	0.2098	0.1297	1.4395	0.0934	0.0086	−0.1350	0.0689	0.1360
Total *a*′	0.8197	0.8512	5.1955	6.4347	0.6999	0.6534	0.5261	0.7689	0.7750
Total *a*″	0.0000	0.0000	0.8829	1.1171	0.0000	0.0000	0.4867	0.0000	0.0000
Total	0.8197	0.8512	6.0774	7.5518	0.6999	0.6534	1.0127	0.7689	0.7750

In MO's 4*a*′, 5*a*′, and 6*a*′ most of the charge is on C and N. The 4*a*′ MO is slightly antibonding in CN, and 6*a*′ is practically non bonding in CN. Orbital 7*a*′, which is associated with the free pair orbital has most of the charge localized on the Nitrogen. This orbital is slightly antibonding in CN, and only slightly bonding in $C-H_3$; there is of course a slight delocalization over the entire molecule.

The 1*a*″ MO is the MO which is formed from the $2p_x$ orbitals of Nitrogen and Carbon. The orbital is strongly bonding, and, as expected, is polarized towards the Nitrogen atom.

Taking the sum of populations over all occupied MO's, we see that the Hydrogens bonded to the Carbon lose about 0.16 electrons each while the one bonded to the Nitrogen loses 0.30.

The Carbon atom transfers 0.12 π electrons to the Nitrogen while gaining 0.19 σ electrons. The Nitrogen atom gains 0.43 σ electrons.

Formaldimine is isoelectronic with formaldehyde and we can expect similarities between these molecules. From a qualitative point of view, both molecules are predicted to be planar with formaldimine having a bent $C{=}N-H_1$ part (symmetry group C_s). In both molecules, the ordering of the highest two occupied orbitals, and lowest virtual orbital is predicted to be π, n, π^* [6, 7].

Our calculation and that of Winter, Dunning and Letcher on formaldehyde [8] bear these predictions out. Table 3 contains the orbital eigenvalues, gross atomic and overlap populations of formaldehyde taken from Ref. [8].

Comparing Table 3 with Table 1 and Table 2, we find that the two molecules are not only qualitatively similar, but, except for the sixth molecular orbital, the eigenvalues, gross and overlap populations on Carbon, Nitrogen and Oxygen are quantitatively quite close for each occupied MO. The functional group bonds C=N and C=O have similar overlap populations for corresponding molecular orbitals, and the gross populations on Carbon and Nitrogen in formaldimine correspond very well to the Carbon and Oxygen populations in formaldehyde. The σ, π, and total charge on Carbon is less in formaldehyde

Table 3. Orbital eigenvalues and population analysis of formaldehyde (Results taken from Ref. [8])

MO	ε_i (a.u.)	Gross populations		Overlap populations
		C	O	C–O
$1a_1$	−20.6072	0.0015	1.9985	0.0029
$2a_1$	−11.3576	1.9993	−0.0002	−0.0004
$3a_1$	− 1.4304	0.4042	1.5817	0.4552
$4a_1$	− 0.8609	1.0835	0.3809	−0.1190
$1b_2$	− 0.6893	0.9485	0.6046	0.2609
$5a_1$	− 0.6318	0.4478	1.3731	0.1126
$1b_1(\pi)$	− 0.5238	0.7715	1.2285	0.4270
$2b_2(n)$	− 0.4269	0.1142	1.2528	−0.1169
$2b_1(\pi^*)$	0.1465	—	—	—
σ Sub total		5.0291	7.1914	0.5952
π Sub total		0.7715	1.2285	0.4270
Total		5.8006	8.4199	1.0222

Table 4. Inversion barriers for formaldimine

Configuration	Total energy	Barrier (kcal/mole)	Ref. [9]
Ground state	−93.8824 a.u.		
Rotated transition state	−93.7947 a.u.	55.1	57.5
Planar transition state	−93.8404 a.u.	26.3	27.9

than in formaldimine because of the greater electronegativity of Oxygen relative to Nitrogen. These results exemplify the close relationship these molecules have from a bonding point of view.

Experimental evidence supports a planar inversion mechanism for isomerization of imines [11, 20]. Our results predict that the isomerization process in formaldimine would occur through planar inversion rather than rotation about the molecular axis. From Table 4, we see that our results are quite similar to those of Lehn and Munsch [9], although they used a much better basis than ours. Our calculated value of 26.3 kcal/mole is in good agreement with experimental values for alkyl substituted imines which range from 25 to 27 kcal/mole [10–12].

We obtain a dipole moment of 2.44 D for formaldimine which is quite close to the value obtained for formaldehyde (2.59 D) [8]. The experimental value for formaldehyde's dipole moment is 2.34 D [13].

The positive ion of formaldimine was calculated using the Polyatom open shell SCF program based on Roothaan's [14] one-determinant formalism. We obtain an energy of −93.5499 a.u. This gives us a vertical ionization potential of 0.3325 a.u., which is of course inferior to the Koopmans' theorem value of 0.4119 a.u. since the latter does not take into account the rearrangement of the molecular orbitals in the ion.

Table 5. Transition energies (vertical) for formaldimine

State	CI	SCF
$(n \rightarrow \pi^*)^3$	4.68 eV	3.49 eV
$(n \rightarrow \pi^*)^1$	5.84 eV	4.21 eV
$(\pi \rightarrow \pi^*)^3$	4.57 eV	4.05 eV
$(\pi \rightarrow \pi^*)^1$	10.33 eV	—
$(n \rightarrow \sigma^*)^3$	9.59 eV	—

Excited States

The $n \rightarrow \pi^*$ transition energy should be about the same for most alkyl substituted imines, since the transition goes from a non bonding orbital largely localized on the Nitrogen, to a π^* orbital which is still largely localized on the C=N group. The transition energies for various excited states of formaldimine are given in Table 5. The energies were calculated by two different methods: singly excited configuration interaction using the ground state molecular orbitals, and the open-shell SCF procedure applied to the excited state wavefunctions. Because of the limited size of our basis set, CI did not lower the transition energies very much. The calculations were done with the ground state geometry, and therefore correspond to the vertical transitions.

Experimentally, the far ultra-violet spectrum of alkyl substituted imines [5] consists of broad bands and this feature makes the interpretation difficult. The fact that all types of transitions are permitted does not simplify matters either. There is a strong and diffuse band centered around 1700 Å (7.3 eV), with a molecular extinction coefficient of nearly 8000. This transition occurs at too low a frequency to be caused by the alkyl groups, and the molecular extinction coefficient would seem to indicate that in all likelihood, this is the first $(\pi \rightarrow \pi^*)^1$ transition. The asymmetrical shape of the band, which extends to 2000 Å indicates a composite character, probably due to a $(n \rightarrow \sigma^*)^1$ or $(n \rightarrow 3s)^1$ Rydberg transition. The $(n \rightarrow \pi^*)^1$ transition is usually located between 5.0 and 5.4 eV in this type of molecule [15, 16].

Our CI calculation gives a value of 10.33 eV for the $(\pi \rightarrow \pi^*)^1$ transition, which is about 30% higher than the experimental value. Del Bene, Ditchfield, and Pople's study of excited states (using the same basis as ours) by configuration interaction [20] shows that for $(\pi \rightarrow \pi^*)^1$ transitions, the calculated value is usually between 20% and 30% higher than the experimental values.

Similarly, $(n \rightarrow \pi^*)^1$ transitions are between 5% and 15% higher than the experimental values. If we reduce our calculated value by 10%, we obtain 5.2 eV, which is in good agreement with the experimental data for this type of transition.

The open-shell SCF results for the vertical transitions are lower than the CI results and the experimental values. This is presumably because the correlation energy is smaller in the excited states than in the ground state. Buenker and Peyerimhoff [17] obtained similar results for formaldehyde, their CI calculations being quite close to the experimental value while the SCF value was much lower.

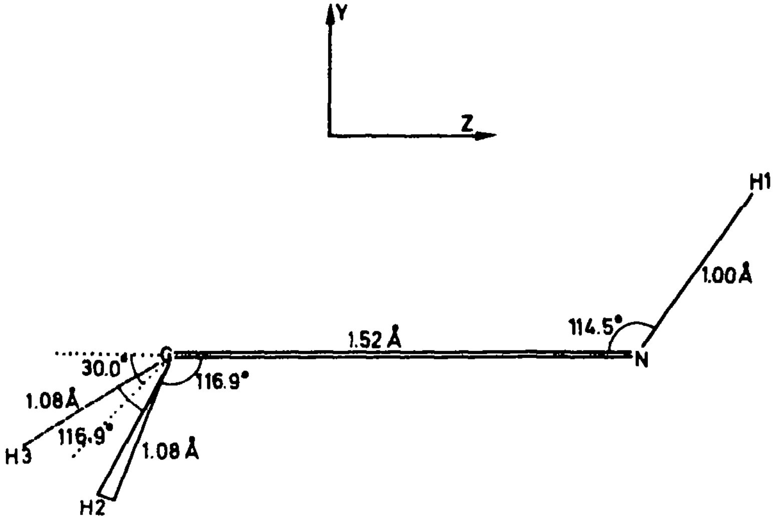

Fig. 2. Geometry of the excited triplet state of formaldimine

Symmetry considerations [6, 7, 18] predict that excitation of a non bonding electron to an anti-bonding orbital ($n \to \pi^*$) should result in bending the CH_2 group out of the molecular plane and a rotation of the N–H bond about the same plane (Fig. 2).

We have partially optimized the $(n \to \pi^*)^3$ state geometry, using the open-shell SCF method. The Hydrogen bond lengths were kept constant (1.08 Å for CH, and 1.00 Å for NH), the CNH angle was not varied, and the HCH angle was kept equal to the HCN angle. The minimum energy configuration (Fig. 2) gives an energy of −93.8108 a.u. We note that the CH_2 group is bent out of plane by 30°, the CN bond length is lengthened to 1.52 Å, and the NH bond is rotated 90° out of plane to give a trans conformation. This structure no longer represents the $(n \to \pi^*)^3$ state however since the geometry variations have destroyed the original symmetry plane. The resulting state is a mixture of the original ($n \to \pi^*$) and ($\pi \to \pi^*$) triplet states. Buenker and Peyerimhoff [18] obtained an out-of-plane bending angle of 32° for the formaldehyde $(n \to \pi^*)^3$ state: this is quite close to the value we obtain for formaldimine. The experimental out-of-plane bending angle is approximately 35° for formaldehyde (see Ref. [17]).

Conclusion

This paper has attempted to elucidate the structural characteristics of the imine functional group. We have drawn attention to similarities between the imine group and the carbonyl group throughout the article. The results are quite satisfying in that the two groups are very similar in the ground state, and the low-lying electronic states also seem to have a great deal in common.

Acknowledgements. We would like to thank the National Research Council of Canada, and the «Centre de calcul de l'Université de Montréal» for their support.

References

1. Ditchfield, R., Hehre, W. J., Pople, J. A.: J. Amer. chem. Soc. **54**, 724 (1971).
2. Neumann, D. B., Basch, H., Kornegay, R. L., Snyder, L. C., Moskowitz, J. W., Hornback, C., Liebmann, S. P.: Q.C.P.E. Program 199, (POLYATOM), Indiana University. Indiana, USA.
3. Duke, A. J.: Chem. Physics Letters **13**, 76 (1972).
4. Huzinaga, S.: Physic. Rev. **122**, 131 (1961).
5. Sandorfy, C.: The chemistry of the carbon-nitrogen double bond, ed. by Saul Patai, Ch. 1, p. 2. New York: Interscience publishers 1970.
6. Walsh, A. D.: J. chem. Soc. **1953**, 2306.
7. Gimarc, B. M.: J. Amer. chem. Soc. **93**, 815 (1971).
8. Winter, N. W., Dunning, T. H., Letcher, J. H.: J. chem. Physics **49**, 1871 (1968).
9. Lehn, J. M., Munsch, B.: Theoret. chim. Acta (Berl.) **12**, 91 (1968).
10. Koeppl, G. W., Sagatys, D. S., Krishnamurthy, G. S., Miller, S. I.: J. Amer. chem. Soc. **89**, 3396 (1968).
11. Curtin, D. Y., Grubbs, E. J., McCarthy, C. G.: J. Amer. chem. Soc. **88**, 2775 (1966).
12. Wurmb-Gerlich, D., Vogtle, F., Mannschreck, A., Staab, H. A.: Liebigs Ann. Chem. **708**, 36 (1967).
13. Schoolery, J. N., Sharbaugh, A. H.: Physic. Rev. **82**, 92 (1951).
14. Roothaan, C. C. J.: Rev. mod. Physics **32**, 179 (1960).
15. Nelson, D. A., Worman, J. J.: Tetrahedron Letters **1966**, 507.
16. Bonnett, R.: J. chem. Soc. **2**, 2313 (1965).
17. Buenker, R. J., Peyerimhoff, S. D.: J. chem. Physics **53**, 1368 (1970).
18. Pearson, R. G.: Chem. Physics Letters **10**, 31 (1971).
19. Kessler, H.: Tetrahedron Letters **1968**, 2041.
20. Del Bene, J. E., Ditchfield, R., Pople, J. A.: J. chem. Physics **55**, 2236 (1971).

Prof. Dr. C. Sandorfy
Département de Chimie
Université de Montréal
Montréal, Québec, Canada

Theoret. chim. Acta (Berl.) 29, 9—20 (1973)
© by Springer-Verlag 1973

Effects of Polarization on Charge Distributions and Integral Approximations

Karl Jug*
Institut für Theoretische Chemie der Universität Stuttgart

Received July 14, 1972

Polarization factors derived in a previous paper [1] are presented for $1s$, $2s$, $2p\sigma$ and $2p\pi$ orbitals on two centers. The formulas for gross atomic populations and integral approximations are tested in diatomics. It is found that our definition of atomic charges proposed earlier is far superior to the Mulliken approximation. With proper partitioning into charge and hybrid parts the total dipole moment of the wavefunction can be obtained with great accuracy. The application of the formulas to two-center hybrid repulsion integrals is less satisfactory in the lowest-order approximation.

Die Polarisationsfaktoren einer früheren Arbeit [1] werden für $1s$-, $2s$-, $2p\sigma$- und $2p\pi$-Orbitale an zwei Zentren angegeben. Die Formeln für Atomladungsverteilungen und Integralapproximationen werden in zweiatomigen Molekülen geprüft. Man findet, daß unsere vorgeschlagene Definition von Atomladungen der Mulliken-Näherung weit überlegen ist. Bei geeigneter Aufteilung in Ladungs- und Hybridanteil kann das Dipolmoment der Wellenfunktion mit großer Genauigkeit erhalten werden. Die Anwendung der Formeln auf Zwei-Zentren-Hybridintegrale der Elektronenwechselwirkung ist weniger zufriedenstellend in der niedrigsten Approximationsstufe.

1. Introduction

Recently, we developed the basis for an approximate molecular orbital method whose chief characteristic is the lack of empirical adjustment [1, 2]. The basic idea was to use commutator equations $u=[t,x]$ between hermitian and antihermitian operators to establish approximate integral relations on the basis of truncated expansions for integrals over atomic orbitals μ, ν on different centers. We have tested the accuracy of approximations for β integrals over a core Hamiltonian in the case of two equal $2s$, $2p\sigma$ and $2p\pi$ orbitals on different centers [2]. In this paper, we test the accuracy of charge distributions and certain selected repulsion integrals in heteropolar diatomics. After a brief formulation of the method, we present the polarization factors for $1s$, $2s$, $2p$ orbitals. We then discuss the dipole moments of various diatomics and show that a satisfactory definition of atomic charge distributions in molecules can be gained on the basis of our considerations. The use of this definition of atomic charge distributions in polyatomics is straightforward. Our results for repulsion integrals show that the lowest order expansions are sometimes insufficient to guarantee the same accuracy as in one-electron integrals.

---

* Permanent address: Department of Chemistry, Saint Louis University, Saint Louis, Missouri 63156, USA.

2. The General Method

A commutator equation

$$u=[t,x] \tag{2.1}$$

with hermitian and antihermitian operators u, t, x is equivalent to a matrix representation in a complete orthogonal or non-orthogonal basis set. For the case of one-electron operators the following expansion over non-orthogonal orbitals χ, χ' seems to be most convenient

$$\begin{aligned} u_{\mu\nu} &= \sum_{\chi,\chi'} t_{\mu\chi}(S^{-1})_{\chi\chi'}x_{\chi'\nu} - x_{\mu\chi}(S^{-1})_{\chi\chi'}t_{\chi'\nu} \\ \text{with} \qquad u_{\mu\nu} &= \langle\mu|u|\nu\rangle \quad \text{etc.} \end{aligned} \tag{2.2}$$

if μ and ν are atomic orbitals on different centers. S^{-1} is the inverse of the overlap matrix. We denote the adjugate matrix by $\tilde{S}$. By definition of S^{-1}

$$\tilde{S}=S^{-1}\det S \tag{2.3}$$

holds. With (2.2) and (2.3) an element $x_{\mu\nu}$ can be expressed exactly in the following way

$$\begin{aligned} x_{\mu\nu} = {} & \left(\sum_{\chi} t_{\mu\chi}\tilde{S}_{\chi\mu} - t_{\chi\nu}\tilde{S}_{\chi\nu}\right)^{-1} \\ & \times\Bigg[\tfrac{1}{2}\sum_{\chi}(t_{\chi\nu}\tilde{S}_{\chi\mu} - t_{\mu\chi}\tilde{S}_{\chi\nu})(x_{\mu\mu}+x_{\nu\nu}) \\ & + \tfrac{1}{2}\sum_{\chi}(t_{\chi\nu}\tilde{S}_{\chi\mu} + t_{\mu\chi}\tilde{S}_{\chi\nu})(x_{\mu\mu}-x_{\nu\nu}) \\ & + \sum_{\substack{\mu'\neq\mu \\ \nu'\neq\nu}}\Bigg\{\tfrac{1}{2}\sum_{\chi}(t_{\chi\nu}\tilde{S}_{\chi\mu'} - t_{\mu\chi}\tilde{S}_{\chi\nu'})(x_{\mu\mu'}+x_{\nu'\nu}) \\ & + \tfrac{1}{2}\sum_{\chi}(t_{\chi\nu}\tilde{S}_{\chi\mu'} + t_{\mu\chi}\tilde{S}_{\chi\nu'})(x_{\mu\mu'}-x_{\nu'\nu}) \\ & + \tfrac{1}{2}\sum_{\chi}(t_{\chi\nu}\tilde{S}_{\chi\nu'} - t_{\mu\chi}\tilde{S}_{\chi\mu'})(x_{\mu\nu'}+x_{\mu'\nu}) \\ & + \tfrac{1}{2}\sum_{\chi}(t_{\chi\nu}\tilde{S}_{\chi\nu'} + t_{\mu\chi}\tilde{S}_{\chi\mu'})(x_{\mu\nu'}-x_{\mu'\nu})\Bigg\} \\ & + u_{\mu\nu}\det S\Bigg]. \end{aligned} \tag{2.4}$$

The right side of (2.4) consists of seven terms: the Mulliken approximation for x and its polarization, the other single-center contributions and their polarization, the rest of the two-center contributions and their polarization and the contribution of u. Our previous work [1, 2] was concerned with the first two terms and the dominant contribution of the third and fourth term in cases where μ and ν are *not equivalent* orbitals on different centers. We have neglected contributions from terms five and six and kept seven where it was different from zero. The following commutator equations seem to be of interest for the property listed on the right

$$[\boldsymbol{r}, 1] = 0 \qquad \text{overlap} \tag{2.5a}$$

$$[\boldsymbol{r}, \boldsymbol{r}] = 0 \qquad \text{dipole moment} \tag{2.5b}$$

$$[\boldsymbol{r}, V] = 0 \qquad \text{potential energy} \tag{2.5c}$$

$$[\boldsymbol{r}, T] = \boldsymbol{p} \qquad \text{kinetic energy} \tag{2.5d}$$

$$[\boldsymbol{r}, h] = \boldsymbol{p} \qquad \text{core energy} \tag{2.5e}$$

$$[\boldsymbol{r}, \boldsymbol{p}] = -1 \qquad \text{slope of overlap} \tag{2.5f}$$

$$\left[\boldsymbol{r}_1 + \boldsymbol{r}_2, \frac{1}{r_{12}}\right] = 0 \qquad \text{electronic interaction energy.} \tag{2.5g}$$

The last equation fits into a two-electron form of (2.4). In all relations $t = \boldsymbol{r}$. For this particular case, the formalism conserves the dipole moment on any level of truncation of (2.4). This is due to the symmetry $x = t$ of (2.5b) as an inspection of (2.2) shows. We derive now an approximate formula for $x_{\mu\nu}$ with four expansion functions, μ, μ' on atom A and ν, ν' on atom B, in the case $t = \boldsymbol{r}$. For the sake of simplicity and practicability we drop all terms containing products of two or more overlap integrals in the polarization factors $\varkappa$. Applications in Section 4 show that this means an insignificant loss of accuracy in the dipole moment.

$$\begin{aligned} x_{\mu\nu} = {} & \tfrac{1}{2} S_{\mu\nu}(1 + \varkappa_{\mu\nu})\, x_{\mu\mu} + \tfrac{1}{2} S_{\mu\nu}(1 - \varkappa_{\mu\nu})\, x_{\nu\nu} \\ & + \tfrac{1}{2} S_{\mu'\nu}(1 + \varkappa_{\mu'\nu})\, x_{\mu\mu'} + \tfrac{1}{2} S_{\mu\nu'}(1 - \varkappa_{\mu\nu'})\, x_{\nu'\nu} \\ & + u_{\mu\nu} \det S \end{aligned}$$

with (2.6)

$$\varkappa_{\mu\nu} = \frac{2 z_{\mu\nu} - S_{\mu\nu}(z_{\mu\mu} + z_{\nu\nu}) - S_{\mu'\nu} z_{\mu\mu'} - S_{\mu\nu'} z_{\nu\nu'}}{S_{\mu\nu}(z_{\mu\mu} - z_{\nu\nu})}$$

$$\det S = \begin{cases} (1 - S_{\mu\nu}^2)(1 - S_{\mu'\nu'}^2) \\ (1 - S_{\mu'\nu}^2)(1 - S_{\mu\nu'}^2) \end{cases} \text{for} \quad \begin{matrix} \left\{\begin{smallmatrix} \mu, \nu \\ \mu', \nu' \end{smallmatrix}\right\} \\ \left\{\begin{smallmatrix} \mu', \nu \\ \mu, \nu' \end{smallmatrix}\right\} \end{matrix} \quad \text{of same type}$$

z is a component of $\boldsymbol{r}$ in a local coordinate system, in particular along the internuclear axis. $\varkappa_{\mu'\nu}$ and $\varkappa_{\mu\nu'}$ are defined similarly to $\varkappa_{\mu\nu}$. Inspection of $\varkappa_{\mu\nu}$ shows that hybrid parts are eliminated from the two-center dipole moment. The rest contributes to the charge redistribution. The corresponding hybrid parts to those of $\varkappa_{\mu\nu}$ are explicitly presented in terms three and four of (2.6). In the following, we calculate polarization factors $\varkappa$ for various ratios of exponents of 1*s*, 2*s*, 2*p* orbitals on two centers.

Then we apply formula (2.6) to overlap, dipole moment and electronic repulsion energy.

3. Polarization Factors

If $\mu\nu$ approaches formally an average of $\mu\mu$ and $\nu\nu$ in the united atom limit, then μ' and ν' are not essential. Otherwise the type of μ' and ν' is fixed by the condition that the united atom limit of $\mu\nu$ is represented by an average of $\mu\mu'$

Table 1. Polarization factors $\varkappa$ for 1s, 2s, 2p orbitals on two centers[a]

$$\varkappa_{11} = 1 - \frac{2\langle 2p\sigma_a(\zeta_a)|1s_b(\zeta_b)\rangle}{\varrho_a\langle 1s_a(\zeta_a)|1s_b(\zeta_b)\rangle}$$

$$\varkappa_{ss} = 1 - \frac{\sqrt{10}\langle 3p\sigma_a(\zeta_a)|2s_b(\zeta_b)\rangle}{\varrho_a\langle 2s_a(\zeta_a)|2s_b(\zeta_b)\rangle}$$

$$\varkappa_{\sigma\sigma} = 1 - \frac{\sqrt{8}\langle 3d\sigma_a(\zeta_a)|2p\sigma_b(\zeta_b)\rangle + \sqrt{10}\langle 3s_a(\zeta_a)|2p\sigma_b(\zeta_b)\rangle}{\varrho_a\langle 2p\sigma_a(\zeta_a)|2p\sigma_b(\zeta_b)\rangle}$$

$$\varkappa_{\pi\pi} = 1 - \frac{\sqrt{6}\langle 3d\pi_a(\zeta_a)|2p\pi_b(\zeta_b)\rangle}{\varrho_a\langle 2p\pi_a(\zeta_a)|2p\pi_b(\zeta_b)\rangle}$$

$$\varkappa_{1s} = 1 - \frac{2\langle 2p\sigma_a(\zeta_a)|2s_b(\zeta_b)\rangle}{\varrho_a\langle 1s_a(\zeta_a)|2s_b(\zeta_b)\rangle}$$

$$\begin{aligned}\varkappa_{1\sigma} = 1 - {} & (2\langle 2p\sigma_a(\zeta_a)|2p\sigma_b(\zeta_b)\rangle - \langle 2p\sigma_a(\zeta_a)|2p\sigma_a(\zeta_a')\rangle\,\langle 2p\sigma_a(\zeta_a')|2p\sigma_b(\zeta_b)\rangle \\ & - \frac{\zeta_a}{\zeta_b'}\langle 1s_a(\zeta_a)|1s_b(\zeta_b')\rangle\,\langle 2p\sigma_b(\zeta_b')|2p\sigma_b(\zeta_b)\rangle)/(\varrho_a\langle 1s_a(\zeta_a)|2p\sigma_b(\zeta_b)\rangle)\end{aligned}$$

$$\begin{aligned}\varkappa_{s\sigma} = 1 - {} & \sqrt{\frac{5}{2}}(2\langle 3p\sigma_a(\zeta_a)|2p\sigma_b(\zeta_b)\rangle - \langle 3p\sigma_a(\zeta_a)|2p\sigma_a(\zeta_a')\rangle\,\langle 2p\sigma_a(\zeta_a')|2p\sigma_b(\zeta_b)\rangle \\ & - \frac{\zeta_a}{\zeta_b'}\langle 2s_a(\zeta_a)|2s_b(\zeta_b')\rangle\,\langle 3p\sigma_b(\zeta_b')|2p\sigma_b(\zeta_b)\rangle)/(\varrho_a\langle 2s_a(\zeta_a)|2p\sigma_b(\zeta_b)\rangle)\end{aligned}$$

[a] Abbreviations: $11 = 1s_a 1s_b$, $ss = 2s_a 2s_b$ etc.

and vv' in a natural way. This suffices to guarantee a proper behaviour of the approximation (2.6) for small and large internuclear distances.

For practical purposes we have listed the polarization factors $\varkappa$ of Eq. (2.6) used for 1s, 2s, $2p\sigma$ and $2p\pi$ orbitals in Table 1. These are simple combinations of overlap integrals over Slater orbitals. Exponents ζ_a and ζ_b refer to the two orbitals on atom A and B for which the polarization factors are calculated; ζ_a' and ζ_b' refer to the complementary orbitals used in the expansion, e.g. $2p\sigma_a$ and $1s_b$ for $\varkappa_{1s_a 2p\sigma_b}$. We have calculated these seven polarization factors for various ratios $\zeta = \zeta_a/\zeta_b$ and internuclear distances $\varrho_a = \zeta_a R$. $\zeta_a' = \zeta_a/3.5$ and $\zeta_b' = 3.5\zeta_b$ was assumed for $\varkappa_{1\sigma}$ and $\zeta_a' = \zeta_a$, $\zeta_b' = \zeta_b$ for $\varkappa_{s\sigma}$. This represents the Slater orbitals for first-row atoms fairly well. In Section 4, we use the actual basis set orbitals for expansion.

The results are in Figs. 1–4. $\varkappa = 0$ means equal weighting factors for contributions to atoms A and B. $\varkappa = 1$ means the whole contribution goes to A, $\varkappa = -1$ the whole contribution goes to B. $\varkappa > 1$ and $\varkappa < -1$ characterizes cases with "overpolarization", *i.e.* where a simple partitioning in two positive parts cannot adequately describe the situation. In Fig. 1 the behaviour of $\varkappa$ for 1s and 2s orbitals can be simply characterized as follows: If the orbital on atom A is more contracted than the orbital on atom B ($\zeta < 1$) the contribution to atom A is increased. For a more diffuse orbital on A ($\zeta > 1$), it is decreased. With increasing internuclear distance the contribution to the atom with the more contracted orbital increases. The polarization factor approaches $+1$ or -1. A similar behaviour is shown in Fig. 2 for $2p\pi$ orbitals. The complicated

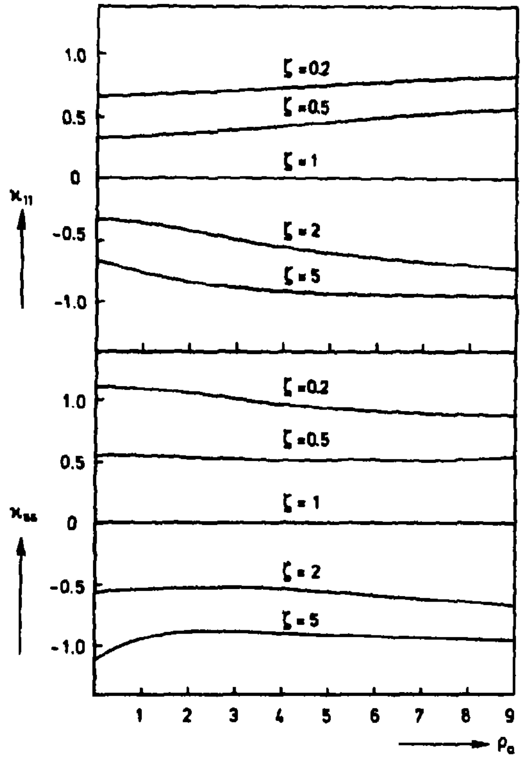

Fig. 1. Polarization factors $\varkappa$ for $1s_a 1s_b$ and $2s_a 2s_b$ charge distributions in dependence of $\varrho_a = \zeta_a R$; ζ_a orbital exponent of atom A, R internuclear distance (in atomic units), $\zeta = \zeta_b/\zeta_a$

dependence of $\varkappa$ for $2p\sigma$ orbitals can be explained in terms of the nodal property of the overlap integral. Here $\varkappa_{a\sigma} S_{\sigma\sigma}$ is the relevant quantity which does not vanish when $S_{a\sigma}$ does. The singularity of $\varkappa$ here means a shift of node of x_{ab} as compared to the Mulliken approximation. Fig. 3 shows the polarization of a $1s_a\, 2s_b$ distribution. Here $\varkappa$ is different from zero for $\zeta = 1$. This means in this case that for equal exponents more charge goes to the atom with the $1s$ orbital than to the atom with the $2s$ orbital. This is not surprising, since the center of charge is not in the middle between atoms A and B, but closer to A.

The curves for $\varkappa_{1\sigma}$ and $\varkappa_{2\sigma}$ show a different asymptotic behaviour for large internuclear distances from the previous ones. However for intermediate distances the interpretation is simpler. For orbitals of equal type more contribution goes to the center with the more contracted orbital, whereas here is an overall shift of weight to atom A similar to $\varkappa_{1s}$. The weights are not equal for $\zeta = 1$. There is a singularity for $R = 0$ in these two cases. This is due to the fact that we are dealing with the first two members of two different complete sets which are overcomplete in this limit. This problem could be avoided by using sets with flexible exponents which approach each other pairwise for $R = 0$. There is, however, no practical importance in the above failure.

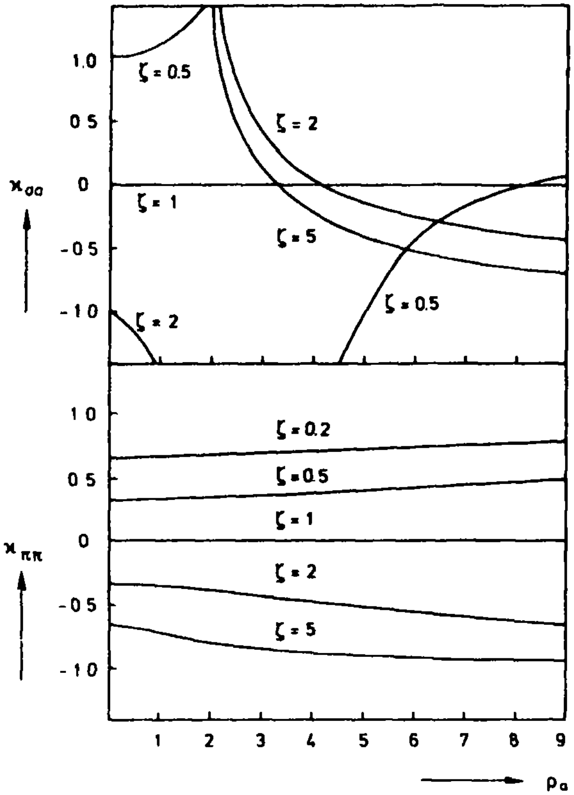

Fig. 2. Polarization factors $\varkappa$ for $2p\sigma_a 2p\sigma_b$ and $2p\pi_a 2p\pi_b$ charge distributions in dependence of $\varrho_a = \zeta_a R$; ζ_a orbital exponent of atom A, R internuclear distance (in atomic units), $\zeta = \zeta_b/\zeta_a$

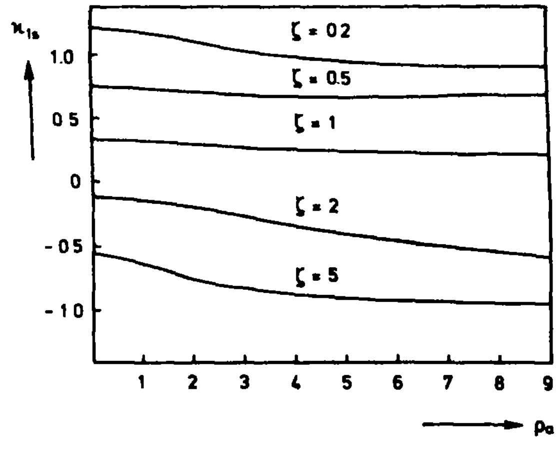

Fig. 3. Polarization factors $\varkappa$ for $1s_a 2s_b$ charge distributions in dependence of $\varrho_a = \zeta_a R$; ζ_a orbital exponent of atom A, R internuclear distance (in atomic units), $\zeta = \zeta_b/\zeta_a$

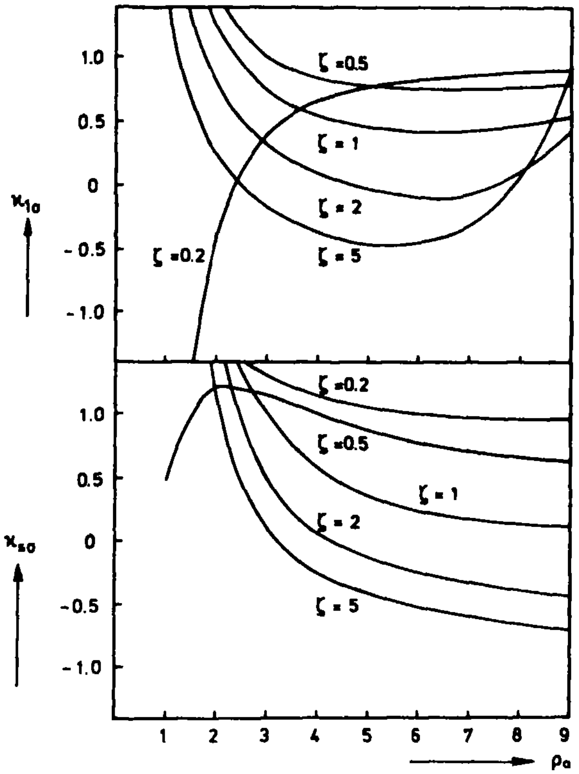

Fig. 4. Polarization factors $\varkappa$ for $1s_a 2p\sigma_b$ and $2s_a 2p\sigma_b$ charge distributions in dependence of $\varrho_a = \zeta_a R$; ζ_a orbital exponent of atom A, R internuclear distance (in atomic units), $\zeta = \zeta_b/\zeta_a$

4. Charge Distributions and Dipole Moments

Among the concepts of molecular orbital theory, which are most popular among chemists is the assignment of a formal charge to an atom in a molecule. Such a definition avoids the complicated analysis of density contour maps and would offer us a simple tool in reactivity considerations. Unfortunately, the assignment of charge contributions to atoms in molecules is not unique, even if we use atomic basis sets centered at the different atoms. There exist overlap contributions $c_a c_b S_{ab}$ between two orbitals a, b on different centers A and B. Most popular is a procedure attributed to Mulliken [3], but also suggested by Daudel [4], to partition this contribution equally among the two atoms. Recently it became apparent, that the Mulliken analysis would lead unsatisfactory conclusions, e.g. about dipole moments. Three different alternatives have been proposed:

a) the use of different weighting factors for the partitioning among two toms [5],

b) the use of Löwdin orthogonalized orbitals [6] each of which is completely ttributed to a particular atom [7],

c) the definition of regions of space which are exclusively attributed to each f the atoms in a molecule [8].

Table 2. Net charges in heteronuclear diatomics

	Ransil wavefunction [12]			STO basis [13]	
	Mulliken	Christoffersen	This work	CNDO	INDO
Li^+H^-	0.35	0.51	0.62	0.27	0.29
B^+H^-	0.02	−0.12	0.30	0.08	0.08
F^-H^+	0.23	0.39	0.06	0.23	0.27
C^+O^-	0.17	0.55	0.19	0.08	0.07
Li^+F^-	0.28	0.48	0.37	0.56	0.58

Approach c) seems to be rather untractable and has been tested only in linear systems [9]. Approach b) is definitely open to critique because orthogonalization can be achieved only by contributions of other atoms to a nonorthogonal orbital. Thus the assignment of the resulting orthogonalized orbital to a particular atom is arbitrary. Cusachs and Politzer [10] have compared the Mulliken analysis and Löwdin analysis in diborane. The charge distributions of the same wavefunction were completely different. To avoid practical and methodogical difficulties approach a) seems to offer the greatest possibilities. Our approach is in fact of this type. It differs from Christoffersen's in a sense that Christoffersen uses the coefficients of an SCF calculation to define weighting factors, whereas we obtain weighting factors from the nature of overlap distribution alone. It would be proper here to state, that our weighting factors come close to Löwdin's idea [11] to distribute the overlap among the atoms in such a way that the dipole moment of the distribution is conserved. In the simplest cases our procedure [1] yields indeed this result. However, in cases where overlap distributions of type $1s_a 2p\sigma_b$ or $2s_a 2p\sigma_b$ are involved our formulas are more general than Löwdin's because they take care of the hybrid dipole parts.

In Table 2 we have compared net charges for several selected diatomics LiH, BH, HF, CO and LiF in Mulliken's, Christoffersen's and our approximation based on Ransil's [12] optimized minimal basis sets as well as CNDO and INDO type calculations [13]. The differences in results could not be more striking. To determine which atomic distribution is most appropriate, we have calculated dipole moments with these charge distributions. These are listed under A in Table 3. The total dipole moment should properly be calculated as consisting of two parts: the charge part and the hybrid part [13]. The charge part is calculated with the weighted overlap integrals according to (2.6) with $x=1$. Only the first two terms contribute in this case. There are four hybrid parts. The first two are the direct single-center contributions for $x=r$ of distributions $2s_a 2p\sigma_a$, $2s_b 2p\sigma_b$ and $1s_a 2p\sigma_a$, $1s_a 2p\sigma_a$. These cannot be accounted for by overlap integrals. In the CNDO and INDO methods, there appears only the $2s\,2p\sigma$ part. The other two result from two-center dipole parts of $2s_a 2p\sigma_b$, $2s_b 2p\sigma_a$ and $1s_a 2p\sigma_b$, $1s_b 2p\sigma_a$. They are in the third and fourth term of (2.6) for $x=r$. The sum of these five dipole parts reproduces the dipole moment of the wavefunction within 1% accuracy. This is not too surprising considering that (2.5b) is defining the weighting factors. But it also shows that the neglect of

Table 3. Dipole moments (in Debye) of heteronuclear diatomics

		Ransil wavefunction [12]					STO basis [13]	
		M	Ch	This work	exact	exp.	CNDO	INDO
Li^+H^-	*A*	−2.71	−3.94	−4.77			−2.04	−2.19
	B			−1.20			−4.12	−4.01
	C			0.06				
	D			0.00				
	E			−0.02				
	F	−2.71	−3.94	−5.93	−5.92	−5.88	−6.16	−6.20
B^-H^+	*A*	−0.14	0.70	−1.81			−0.43	−0.46
	B			3.44			2.56	2.30
	C			−0.04				
	D			0.00				
	E			−0.02				
	F	−0.14	0.70	1.57	1.58		2.13	1.84
F^-H^+	*A*	1.01	1.74	0.25			1.09	1.30
	B			1.21			0.77	0.69
	C			−0.02				
	D			0.00				
	E			−0.01				
	F	1.01	1.74	1.43	1.44	1.74	1.86	1.99
C^-O^+	*A*	−0.94	−2.98	−1.03			−0.46	−0.40
	B			1.69			−0.18	−0.20
	C			−0.02				
	D			−0.04				
	E			0.00				
	F	−0.94	−2.98	0.60	0.59	0.12	−0.64	−0.60
Li^+F^-	*A*	−2.02	−3.16	−2.70			−5.82	−6.03
	B			−0.65			−2.08	−1.83
	C			0.02				
	D			−0.15				
	E			0.01				
	F	−2.02	−3.16	−3.47	−3.43	−6.6	−7.90	−7.86

A charge part,
B single-center $2s2p\sigma$ hybrid part,
C single-center $1s2p\sigma$ hybrid part,
D two-center $2s2p\sigma$ hybrid part,
E two-center $1s2p\sigma$ hybrid part,
F total dipole moment,
M Mulliken,
Ch Christoffersen.

higher-order terms in the weighting factors was not severe. Calculations with other Ransil wavefunctions confirm this result. For this accuracy, the contributions from *D*, i.e. the hybrid parts of the two-center $2s2p\sigma$, are in general not negligeable as can be seen from CO and LiF.

Neither the Mulliken, nor the Christoffersen approximation are in good agreement with the wavefunction's total dipole moment. This is true with or without hybrid parts. With regard to the CNDO and INDO charges, we feel

Table 4. Atomic occupation numbers in heteronuclear diatomics

A^+	B^-	Ransil wavefunction [12]							
		Mulliken				This work			
		1s	2s	2pσ	2pπ	1s	2s	2pσ	2pπ
Li		1.995	0.395	0.256		1.983	0.288	0.107	
	H	1.354				1.622			
B		1.999	1.808	1.169		1.996	1.810	0.888	
	H	1.024				1.305			
	F	1.999	1.946	1.284	2.000	1.999	1.934	1.124	2.000
H		0.771				0.943			
C		1.999	1.663	0.929	1.234	1.990	1.714	0.959	1.148
	O	1.999	1.865	1.545	2.766	1.994	1.858	1.485	2.852
Li		1.996	0.055	0.057	0.613	1.991	0.063	0.072	0.501
	F	1.999	1.943	1.950	3.387	1.998	1.970	1.906	3.499

that they may not be reliable, although the total dipole moments are often well reproduced.

For several reasons, we did not push this investigation farther at this time. Firstly, minimal basis sets are not producing good dipole moments, e.g. in CO and LiF. So the absolute value of these charge calculations is limited. Secondly, very few wavefunctions are published on polyatomics. A test in polyatomics would involve generating good wavefunctions. Thirdly, there is still some freedom in the polarization factors which concerns the functions μ' and ν'. From (2.6) it can be seen that a particular type of function may be necessary, e.g. $2s_b$ and $2p\sigma_a$ for $\chi_{2s_a 2p\sigma_b}$, to ensure a proper united atom limit. For the usual internuclear distances, however, there is no constraint to fix the exponents. We feel that the most consistent scheme is one in which the basis functions of the MO's are used as μ' and ν'. For example, it does not seem consistent to use $\nu' = 2p\sigma$ on hydrogen since this function is not in Ransil's basis set. Further study of this point is necessary.

In Table 4, we have compared the atomic occupation numbers for Mulliken's and our approximation. We observe in the hydrides a shift of charge from $2p\sigma$ of the hetero atoms to $1s$ of hydrogen as the main difference to Mulliken's analysis. CO is characterized by a shift of $2s$ and $2p\sigma$ charge from C to O and an opposite, but smaller shift of $2p\pi$ charge from O to C. This trend is overemphasized in the Mulliken analysis. Yet opposite σ and π transfers cancel each other to a large extent. This effect is somewhat reduced by our polarization factors and leads to an increased overall charge transfer. LiF is bound primarily by a π-bond on top of an ionic σ bond. Transfer of the σ electron of Li is causing the polarity.

5. Electron Repulsion Integrals

Integral approximations for three- and four-center integrals were the starting point of the Mulliken approximation [14]. It was a gratifying idea to

Table 5. Error (%) of Mulliken and this work's integral approximations of two-center hybrid integrals for various ratios of orbital exponents and internuclear distances R (a.u.)

ζ_b/ζ_a	$(1s_A 1s_B \vert 1s_A 1s_A)$		$(2s_A 2s_B \vert 1s_A 1s_A)$		$(2p\sigma_A 2p\sigma_B \vert 1s_A 1s_A)$		$(2p\pi_A 2p\pi_B \vert 1s_A 1s$	
	Mulliken	This work	Mulliken	This work	Mulliken	This work	Mulliken	This work
0.2	− 12	19	− 6	59	− 6	111	− 6	33
	− 9	34	− 16	35	36	*504*	− 1	46
	− 12	43	− 18	32	− 3	− 92	0.7	59
0.5	− 3	4	− 2	13	− 2	26	− 2	7
	− 2	21	− 9	11	− 15	− 46	4	24
	− 2	41	− 10	22	5	14	9	46
1	0	0	0	0	0	0	0	0
	14	14	− 1	− 1	*5701*	*5701*	10	10
	58	58	29	29	*2278*	*2278*	44	44
2	− 3	1	− 4	8	− 4	17	− 4	3
	61	11	25	− 1	2	− 3	29	4
	214	41	123	27	101	39	126	30
5	− 11	0.5	− 16	16	− 16	42	− 16	3
	99	3	52	0.5	22	3	53	1
	256	7	162	6	136	27	162	6

reduce multi-center integrals to two-center Coulomb integrals. Cisek [15] has compared the accuracy of various methods and proposed an expansion to reproduce multipole moments. Harris and Rein [16] also favored empirical adjustment so as to obtain best orbital coefficients for certain standard integrals which then could be used for other integrals.

We have considered the simplest two-center hybrid integrals $(1s_A 1s_B | 1s_A 1s_A)$, $(2s_A 2s_B | 1s_A 1s_A)$, $(2p\sigma_A 2p\sigma_B | 1s_A 1s_A)$, $(2p\pi_A 2p\pi_B | 1s_A 1s_A)$ and compared Mulliken's and our approximations for various ratios ζ_b/ζ_a with the exact values calculated with the formulas of Ruedenberg *et al.* [17]. The results are listed in Table 5. The errors of the Mulliken approximation are usually smaller than those of this work, if the orbital on center B is more diffuse than those on center A. We find our results improved over Mulliken's if the orbital on B is more contracted than those on A. The numbers in italics which indicate very large errors are at those distances where the exact integral is close to zero. Considering the fact that there seems to be not much gain in improved weighting factors, the question arises what the reason for this unsatisfactory behaviour could be. Certainly the influence of the location of distribution of the second electron is important. In this case the redistribution is to generate one-center integrals which are effectively overemphasizing the trend, namely to increase the integral value where the Mulliken approximation yields a too small value. This latter pattern is well pronounced in the table for all cases where the Mulliken approximation is closer to the exact values than ours, i.e. for $\zeta_b/\zeta_a < 1$. Also the neglect of the higher terms in (2.6) might be more crucial than in the single-electron case. We think that exchange integrals would be from symmetry more apt than hybrid integrals to an improved treatment with different weighting factors.

6. Conclusion

The calculations in this paper open the way to a new definition of atomic charges in molecules. Although the formulas were tested only in diatomics with Slater orbitals centered on the nuclei, a generalization is straightforward. A rotation of the results in a local coordinate system to a molecular coordinate system performed in the same way as in Pople's CNDO program would lead directly to atomic distributions in polyatomics. Also, there is no restriction of the formulas to Slater functions. The concepts hold also for Gaussian functions. Pure Gaussian functions would also allow in simple fashion to redistribute off-center orbital contributions. The same considerations hold also for approximations of other integrals. Electronic repulsion integrals are more sophisticated in structure and would need more care to guarantee a desired accuracy.

Acknowledgement. I thank P. Coffey for performing most of the calculations. I appreciate the hospitality and support of Prof. H. Preuß during my stay in his institute. Several discussions with Dr. W Meyer on the topic of this paper are appreciated.

References

1. Jug, K : Theoret. chim Acta (Berl.) **26**, 231 (1972).
2. Jug, K.: Theoret. chim. Acta (Berl.) **23**, 183 (1971).
3. Mulliken, R.S.: J. chem. Physics **23**, 1833 (1955).
4. Daudel, R., Laforgue, A.: Compt. rend. séances Acad. Scie. **233**, 623 (1951).
5. Christoffersen, R. E., Baker, K. A.: Arbeitsbericht No. 16 des Instituts für Theoretische Chemie der Universität Stuttgart (1971).
6. Löwdin, P. O.: J. chem. Physics **18**, 365 (1950).
7. Pople, J. A., Segal, G. A.: J. chem. Physics **43**, S 136 (1965).
8. Stout, Jr., F. W., Politzer, P.: Theoret. chim. Acta (Berl.) **12**, 379 (1968).
9. Politzer, P., Mulliken, R.S.: J. chem. Physics **55**, 5135 (1971).
   Politzer, P., Harris, R. R.: J. Amer. chem. Soc. **92**, 6451 (1970).
10. Cusachs, L. C., Politzer, P.: Chem. Physics Letters **1**, 529 (1968); **2**, 1 (1968).
11. Löwdin, P. O.: J. chem. Physics **21**, 374 (1953).
12. Ransil, B. J.: Rev. mod. Physics **32**, 239 (1960).
13. Pople, J A., Beveridge, D. L.: Approximate molecular orbital theory, p. 87ff. New York: McGraw-Hill 1970.
14. Mulliken, R.S.: J. Chim. physique **46**, 497, 675 (1949).
15. Cisek, J.: Molecular Physics **6**, 19 (1963); **10**, 83 (1965).
16. Harris, F. E., Rein, R.: Theoret. chim. Acta (Berl.) **6**, 73 (1966).
17. Ruedenberg, K., Roothaan, C. C. J., Jaunzemis, W.: J. chem. Physics **24**, 201 (1956).

Prof. Dr. Karl Jug
Department of Chemistry
Saint Louis University
Saint Louis, Missouri 63156, U.S.A.

Theoret. chim. Acta (Berl.) 29, 21—28 (1973)
© by Springer-Verlag 1973

Study of Reaction Mechanisms by Semiempirical Methods. I.

Optimization of the Geometry of the Molecule in the Framework of a Single Calculation of the Energy Function

J. Pancíř

The J. Heyrovský Institute of Physical Chemistry and Electrochemistry, Czechoslovak Academy of Sciences, Prague, Czechoslovakia

Received September 8, 1972

The author suggests a procedure offering the possibility to determine, with the use of a double iteration technique, the equilibrium geometry within the framework of a single calculation of the energy function. The method is used for the ground state and the lowest excited singlet state of formaldehyde and for the formyl radical. The individual contributions of the potential energy are discussed in brief.

Der Autor schlägt ein Verfahren vor, das erlaubt, mittels einer Doppeliterationstechnik die Gleichgewichtsgeometrie im Laufe einer einzigen Berechnung der Energiefunktion zu bestimmen. Das Verfahren wird auf den Grund- und den ersten angeregten Zustand von Formaldehyd und auf das Formylradikal angewendet. Die einzelnen Beiträge zur potentiellen Energie werden kurz diskutiert.

L'auteur propose une méthode par laquelle il est possible de déterminer par une technique iterative double la géometrie d'équilibre dans le cadre d'un seul cálcul de la fonction énergétique. On a appliqué la méthode pour l'état fondamental et l'état excité le plus bas singulet de formaldéhyde et pour HCO. On discute brevement les contributions singulaires de l'énergie potentielle.

Introduction

Semiempirical methods working with all valency electrons [1–5] were successfully employed for determining the equilibrium geometry of molecules [3–7]. The usual procedure in such calculations, i.e., the determination of the shape of the energetic hyper-surface, however, is fairly costly and not feasible for molecules with more than four independent coordinates. The number of the necessary calculations of the energy function was considerably reduced by the procedure of McIver and Komornicki [8], who by means of a quadratically convergent variable metric method minimized the total energy of a molecule obtained with the use of EHT and MINDO/2 programs [1, 5].

In the present paper we have suggested a procedure, which by means of double iteration technique permits the equilibrium geometry in the framework of a single calculation of the energy function to be determined. We have applied this procedure also to the CNDO/2 method [6], of which it is known [9, 10] that it affords a better agreement between the theoretical and the experimental equilibrium geometries than that obtained by the method mentioned earlier. We extended the procedure to the case of excited states (half-electron method [11]) and to radicals (method of Longuet-Higgins and Pople [12]). Although we have tested the procedure on calculations of equilibrium geometries, our main interest is concerned with questions of the reactivity of small molecules and of principal functional groups. To this theme we shall pay our attention in the following papers.

Theoretical Procedure

Among numerical methods used for finding a stationary point of the given function, the most efficient are those which utilize the properties of the gradient [13, 14]. The calculation of the gradient requires a knowledge of the derivative of the overall energy of the molecule with respect to the x-th Cartesian coordinate n_{xA} of the atom A. For the ground singlet state and the CNDO/2 method we can derive the relation

$$\begin{aligned}\frac{\partial E}{\partial n_{xA}} &= \sum_{B \neq A} \left[Z_A Z_B \frac{\partial R_{AB}^{-1}}{\partial n_{xA}} - (P_{AA} Z_B + P_{BB} Z_A - P_{AA} P_{BB}) \frac{\partial \gamma_{AB}}{\partial n_{xA}} \right] \\ &+ \sum_{B \neq A} \sum_{\mu}^{A} \sum_{\nu}^{B} \left[2P_{\mu\nu} \frac{\partial \beta_{\mu\nu}}{\partial n_{xA}} - \frac{1}{2} P_{\mu\nu}^2 \frac{\partial \gamma_{AB}}{\partial n_{xA}} \right]\end{aligned} \tag{1}$$

where R_{AB} and γ_{AB} denote the distance and the bicentric repulsion integral between the atoms A and B; Z_A and P_{AA} stand for the "core" charge and the electron density on the atom A; $P_{\mu\nu}$ and $\beta_{\mu\nu}$ denote the bond order and the resonance integral between the atomic orbitals μ and ν localized on the atoms A and B. For an open shell system we can use the formula

$$\frac{\partial E}{\partial n_{xA}} = D - 0.5 \sum_{B \neq A} \sum_{\mu}^{A} \sum_{\nu}^{B} c_{m\mu}^2 c_{m\nu}^2 \frac{\partial \gamma_{AB}}{\partial n_{xA}} \tag{2}$$

where D is the right hand side of Eq. (1), and $c_{m\mu}$ denotes the expansion coefficient of the μ-th AO in the singly occupied MO (marked with m).

The derivative of the energy change in the excitation of the electron from the level i to j is described by the equation

$$\begin{aligned}\frac{\partial E}{\partial n_{xA}} &= D - 0.5 \sum_{B \neq A} \sum_{\mu}^{A} \sum_{\nu}^{B} (c_{i\mu}^2 c_{i\nu}^2 + c_{j\mu}^2 c_{j\nu}^2 \\ &\quad - 2c_{i\mu} c_{j\mu} c_{i\nu} c_{j\nu} \pm 4c_{i\mu} c_{j\mu} c_{i\nu} c_{j\nu}) \frac{\partial \gamma_{AB}}{\partial n_{xA}}\end{aligned} \tag{3}$$

where the upper sign holds for a singlet state and the lower for a triplet state. For the INDO method, Eqs. (1)–(3) apply without any change. For the MINDO/2 method different formulas are used [5] for electronic and core-core repulsion integrals. These formulas are very easy to differentiate and are not presented here.

From the Eqs. (1)–(3) and from the proportionality of the resonance and the overlap integral [2–4] in the methods employed it is obvious that the main problem lies in the determination of the derivatives of the overlap and the repulsion integral with respect to the Cartesian coordinates. The overlap integrals were differentiated in a similar way as in Ref. [8] with the use of the formulas of Gerratt and Mills [15]. Since the practical determination of these derivatives and in particular the necessary transformation of the coordinates are very laborious, we give the resultant formulas in Appendix A of this paper. The repulsion integrals were differentiated directly with the use of the corresponding explicit formulas; the results are given in Appendix B. It was found that for practical calculations, where we do not demand an accuracy of the determined coordinates higher than about 10^{-2} Å, it is sufficient to differentiate the repulsion integrals numerically.

In order to study the reactivity, it was indispensable to carry out the minimization in spherical coordinates. The calculation of the geometries of nonequilibrium configurations of the molecule, arising in the formation or in the disappearance of the chemical bond, was performed by means of the fixation of one or more spherical coordinates. This procedure will be described in more detail in the following paper.

The minimization itself was carried out by the variable metric minimization method according to Murtagh and Sargent [14], the necessary formulas for it were taken from Ref. [8]. The calculation began with the conventional CNDO/2 method, which was continued until the average difference in the orbital energies in two successive iterations did not exceed 0.1 eV. Thereupon, the variable metric method was employed as long as the coordinates of the molecule did not change by more than $2 \cdot 10^{-4}$ Å. The control was returned to the CNDO/2 program and the criterion of convergence was halved. The procedure was repeated as long as the average error in the calculation of the orbital energies was larger than 10^{-4} eV. The attainment of self-consistency required about double the number of iterations as were necessary in the case of the simple CNDO/2 calculation. This applies also with the MINDO/2 method.

The program was written in FORTRAN IV for IBM 7040 and IBM 370/155 computers.

Results and Discussion

The usefulness of the method was tested on the formaldehyde molecule. Table 1 presents the results for two different assumed initial geometries in comparison with the calculations by the INDO method [7] and with the experiment [16]. The "exact" equilibrium geometries in both calculations are in agreement with an error of about ±0.0005 Å in the bond lengths and of 0.4° in the values of the angles. For the sake of comparison the values obtained by the numerical differentiation of repulsion integrals are also presented. It can be noticed that the error is sufficiently small for the study of reaction paths. It was found that already after the first application of the variable metric method, the change in the geometry amounted to 80–90% of the total change; it is obvious, therefore, that the geometry of the molecule depends rather on the values of the two-centre atomic integrals than on the density matrix. In this way it is possible to explain, e.g., why the CNDO/2 method and the INDO method give so similar estimates of the bond lengths and of the angles.

It is interesting to consider in more detail the CNDO/2 energy contributions of the individual bonds in the equilibrium configuration in the molecule. These

Table 1. Geometry of formaldehyde $H_1H_2C{=}O$ in a ground state

Method	r_{CH_1}	r_{CH_2}	r_{CO}	$\vartheta_{H_1CH_2}$	ϑ_{H_2CO}	ζ[a]	Energy (eV)
1. Initial	0.99	1.00	1.4	90°	135°	10°28′	—
CNDO/2	1.114	1.114	1.247	115°48′	122°6′	0°37′	-730.287
CNDO/2[b]	1.102	1.102	1.234	115°20′	122°20′	0°16′	-730.261
MINDO/2	1.220	1.220	1.204	108°11′	126°	0°20′	-472.112
2. Initial	0.939	1.090	1.238	172°20′	132°40′	0°	—
CNDO/2	1.114	1.114	1.247	115°48′	122°6′	0°	-730.287
INDO[c]	1.12	1.12	1.25	115°	122°30′	0°	—
exp.[d]	1.116	1.116	1.208	116°30′	121°40′	0°	—

[a] $(180 - \zeta)$ is the angle which bond C=O makes with the bisector of H_1–C–H_2.

[b] Numerical differentiation of repulsion integrals was used.

[c] Ref. [7].

[d] Ref. [16].

Table 2. Geometry of formyl radical

Method	r_{CH}	r_{CO}	ϑ_{HCO}	Energy (eV)
Initial	1.2	1.2	120°	—
CNDO/2	1.129	1.223	130°35′	-704.345
CNDO/2[a]	1.106	1.204	130°50′	-704.326
MINDO/2	1.230	1.175	139°30′	-455.353
INDO[b]	1.11	1.22	131°10′	—
Exp.[c]	1.148	1.177	123°20′	—

[a] Numerical differentiation of repulsion integrals was used.

[b] Ref. [7].

[c] Ref. [17].

contributions can be roughly divided into resonance energy, electrostatic attractive (core-electron), and repulsive energy (core-core and electron-electron). The attractive and the repulsive contributions (-522 and $+525$ eV at the C=O bond) are by an order higher than the resonance energy (-48 eV), but they almost compensate each other, so that the overall energy of the bond is, in principle, the resonance energy. The attractive and the repulsive forces, too, compensate each other to a considerable extent (323 and -375 eV/A for the C=O bond), the contribution of the resonance force is somewhat more significant (53 eV/A). The forces of electrostatic character are inversely proportional to the square of the distance of the atoms; the bond angles are given, in principle by the resonance forces. Consequently it becomes understandable that the extended Hückel method, which neglects the electron repulsion, gives so good estimates of the bond angles.

For testing the open shell minimization procedure we selected the radical HCO. The initial and the final geometries as well as the experimental data are listed in Table 2.

It is known that formaldehyde is non-planar in the first excited singlet state [18], whereas the virtual orbital calculation predicts a planar configuration of the atoms [19].

Our calculations (Table 3) favored the non-planar arrangement of the atoms, in this case the theoretical geometry being in somewhat poorer accordance with

Table 3. Geometry of formaldehyde in excited singlet state

Method	r_{CH}	r_{CO}	ϑ_{HCH}	ξ[a]	Energy (eV)
Initial	0.99	1.4	120°	39°30′	—
CNDO/2	1.131	1.287	109°33′	37°35′	−726.498
Exp.[b]	1.093	1.323	119°	31°	—

[a] $(180-\xi)$ is the angle which bond C=O makes with the bisector of H_1–C–H_2.

[b] Ref. [19].

experimental data than for the ground state. The calculated dipole moment is, however, in a good agreement with the experimental one (theor. 1.67 *D*, exp. 1.56 *D*, cf., Ref. [20]). The MINDO/2 applied to the excited state of formaldehyde failed badly for the reaction $H_2CO \rightarrow H_2 + CO$ was predicted to occur without any energy barrier. It is noteworthy that in the unrestricted Hartree-Fock CNDO/2 calculation the energy minimum of the excited state of formaldehyde pertains to the planar molecule (cf., Fig. 2, Ref. [21]).

Acknowledgement. The author should like to express his thanks to Mr. K. Mašek for checking of the formulas given in this paper and to Prof. P. O. Löwdin for making use of the computing facility.

Appendix A

Master formulas of the derivatives of the overlap integrals. (Differentiated is always the first member of the pair of the Slater orbitals in the brackets, the differentiation is carried out with respect to the *z* coordinate. The derivatives with respect to the Cartesian coordinates *x* and *y* can be easily ascertained by cyclic interchange of the axes of the coordinate system.)

$$\left\langle \frac{\partial(1s)}{\partial z} \middle| 1s \right\rangle = -(k/\sqrt{3}) \cos\psi \langle 1p_z | 1s \rangle ,$$

$$\left\langle \frac{\partial(1s)}{\partial z} \middle| 2s \right\rangle = -(k/\sqrt{3}) \cos\psi \langle 1p_z | 2s \rangle .$$

$$\left\langle \frac{\partial(1s)}{\partial z} \middle| 2p_x \right\rangle = -(k/\sqrt{3}) \sin\varphi \sin\psi \cos\psi [\langle 1p_x | 2p_x \rangle + \langle 1p_z | 2p_z \rangle] ,$$

$$\left\langle \frac{\partial(1s)}{\partial z} \middle| 2p_y \right\rangle = -(k/\sqrt{3}) \cos\varphi \sin\psi \cos\psi [\langle 1p_x | 2p_x \rangle + \langle 1p_z | 2p_z \rangle] ,$$

$$\left\langle \frac{\partial(1s)}{\partial z} \middle| 2p_z \right\rangle = -(k/\sqrt{3}) (\cos^2\psi \langle 1p_z | 2p_z \rangle - \sin^2\psi \langle 1p_x | 2p_x \rangle) ,$$

$$\left\langle \frac{\partial(2s)}{\partial z} \middle| 1s \right\rangle = k \cos\psi [(1/3) \langle 1p_z | 1s \rangle - (1/\sqrt{3}) \langle 2p_z | 1s \rangle] ,$$

$$\left\langle \frac{\partial(2p_x)}{\partial z} \middle| 1s \right\rangle = (k/\sqrt{5}) \sqrt{3} \sin\varphi \sin\psi \cos\psi \langle 2d_{z^2} | 1s \rangle ,$$

$$\left\langle \frac{\partial(2p_y)}{\partial z} \middle| 1s \right\rangle = (k/\sqrt{5}) \sqrt{3} \cos\varphi \sin\psi \cos\psi \langle 2d_{z^2} | 1s \rangle ,$$

$$\left\langle \frac{\partial(2p_z)}{\partial z} \middle| 1s \right\rangle = -k \langle 1s | 1s \rangle + (k/\sqrt{3}) \langle 2s | 1s \rangle + (k/\sqrt{15}) (3\cos^2\psi - 1) \langle 2d_{z^2} | 1s \rangle ,$$

$$\left\langle \frac{\partial(2s)}{\partial z} \middle| 2s \right\rangle = k\cos\psi\,[(1/3)\langle 1p_z|2s\rangle - (1/\sqrt{3})\langle 2p_z|2s\rangle]\,,$$

$$\begin{aligned}\left\langle \frac{\partial(2s)}{\partial z} \middle| 2p_x \right\rangle = {} & k\sin\varphi\,\sin\psi\,\cos\psi\,[(1/3)(\langle 1p_x|2p_x\rangle + \langle 1p_z|2p_z\rangle)\\ & -(1/\sqrt{3})(\langle 2p_x|2p_x\rangle + \langle 2p_z|2p_z\rangle)]\,,\end{aligned}$$

$$\begin{aligned}\left\langle \frac{\partial(2s)}{\partial z} \middle| 2p_y \right\rangle = {} & k\cos\varphi\,\sin\psi\,\cos\psi\,[(1/3)(\langle 1p_x|2p_x\rangle + \langle 1p_z|2p_z\rangle)\\ & -(1/\sqrt{3})(2p_x|2p_x\rangle + \langle 2p_z|2p_z\rangle)]\,,\end{aligned}$$

$$\begin{aligned}\left\langle \frac{\partial(2s)}{\partial z} \middle| 2p_z \right\rangle = {} & (k/3)(\cos^2\psi\,\langle 1p_z|2p_z\rangle - \sin^2\psi\,\langle 1p_x|2p_x\rangle)\\ & -(k/\sqrt{3})(\cos^2\psi\,\langle 2p_z|2p_z\rangle - \sin^2\psi\,\langle 2p_x|2p_x\rangle)\,,\end{aligned}$$

$$\left\langle \frac{\partial(2p_x)}{\partial z} \middle| 2s \right\rangle = (k/\sqrt{5})\sqrt{3}\,\sin\varphi\,\sin\psi\,\cos\psi\,\langle 2d_{z^2}|2s\rangle\,,$$

$$\begin{aligned}\left\langle \frac{\partial(2p_x)}{\partial z} \middle| 2p_x \right\rangle = {} & -(k/\sqrt{5})\cos\psi\,[(1-2\sin^2\varphi\,\sin^2\psi)\langle 2d_{xz}|2p_x\rangle\\ & -\sqrt{3}\sin^2\varphi\,\sin^2\psi\,\langle 2d_{z^2}|2p_z\rangle]\,,\end{aligned}$$

$$\left\langle \frac{\partial(2p_x)}{\partial z} \middle| 2p_y \right\rangle = (k/\sqrt{5})\sin\varphi\,\cos\varphi\,\sin^2\psi\,\cos\psi(2\langle 2d_{xz}|2p_x\rangle + \sqrt{3}\langle 2d_{z^2}|2p_z\rangle)\,,$$

$$\begin{aligned}\left\langle \frac{\partial(2p_x)}{\partial z} \middle| 2p_z \right\rangle = {} & (k/\sqrt{5})\sin\varphi\,\sin\psi\,[(\cos^2\psi - \sin^2\psi)\langle 2d_{xz}|2p_x\rangle\\ & +\sqrt{3}\cos^2\psi\,\langle 2d_{z^2}|2p_z\rangle]\,,\end{aligned}$$

$$\left\langle \frac{\partial(2p_y)}{\partial z} \middle| 2s \right\rangle = (k/\sqrt{5})\sqrt{3}\,\cos\varphi\,\sin\psi\,\cos\psi\,\langle 2d_{z^2}|2s\rangle\,,$$

$$\left\langle \frac{\partial(2p_y)}{\partial z} \middle| 2p_x \right\rangle = (k/\sqrt{5})\sin\varphi\,\cos\varphi\,\sin^2\psi\,\cos\psi(2\langle 2d_{xz}|2p_x\rangle + \sqrt{3}\langle 2d_{z^2}|2p_z\rangle)\,,$$

$$\begin{aligned}\left\langle \frac{\partial(2p_y)}{\partial z} \middle| 2p_y \right\rangle = {} & (k/\sqrt{5})\cos\psi\,[(1-2\sin^2\varphi\,\sin^2\psi)\langle 2d_{xz}|2p_x\rangle\\ & +\sqrt{3}\cos^2\varphi\,\sin^2\psi\,\langle 2d_{z^2}|2p_z\rangle]\,,\end{aligned}$$

$$\begin{aligned}\left\langle \frac{\partial(2p_y)}{\partial z} \middle| 2p_z \right\rangle = {} & (k/\sqrt{5})\cos\varphi\,\sin\psi\,[(\cos^2\psi - \sin^2\psi)\langle 2d_{xz}|2p_x\rangle\\ & +\sqrt{3}\cos^2\psi\,\langle 2d_{z^2}|2p_z\rangle]\,,\end{aligned}$$

$$\left\langle \frac{\partial(2p_z)}{\partial z} \middle| 2s \right\rangle = -k\langle 1s|2s\rangle + (k/\sqrt{3})\langle 2s|2s\rangle + (k/\sqrt{15})(3\cos^2\psi - 1)\langle 2d_{z^2}|2s\rangle\,,$$

$$\begin{aligned}\left\langle \frac{\partial(2p_z)}{\partial z} \middle| 2p_x \right\rangle = {} & -k\sin\varphi\,\sin\psi\,[\langle 1s|2p_z\rangle - (1/\sqrt{3})\langle 2s|2p_z\rangle]\\ & +(2k/\sqrt{15})\sin\varphi\,\sin\psi\,[\sqrt{3}\cos^2\psi\,\langle 2d_{xz}|2p_x\rangle\\ & +(1/2)(3\cos^2\psi - 1)\langle 2d_{z^2}|2p_z\rangle]\,,\end{aligned}$$

$$\begin{aligned}\left\langle \frac{\partial(2p_z)}{\partial z} \middle| 2p_y \right\rangle = {} & -k\cos\varphi\,\sin\psi\,[\langle 1s|2p_z\rangle - (1/\sqrt{3})\langle 2s|2p_z\rangle]\\ & +(2k/\sqrt{15})\cos\varphi\,\sin\psi\,[\sqrt{3}\cos^2\psi\,\langle 2d_{xz}|2p_x\rangle\\ & +(1/2)(3\cos^2\psi - 1)\langle 2d_{z^2}|2p_z\rangle]\,,\end{aligned}$$

$$\begin{aligned}\left\langle \frac{\partial(2p_z)}{\partial z} \middle| 2p_z \right\rangle = {} & -k\cos\psi\,[\langle 1s|2p_z\rangle - (1/\sqrt{3})\langle 2s|2p_z\rangle]\\ & -(2k/\sqrt{15})\cos\psi\,[\sqrt{3}\sin^2\psi\,\langle 2d_{xz}|2p_x\rangle - (1/2)\\ & \cdot(3\cos^2\psi - 1)\langle 2d_{z^2}|2p_z\rangle]\end{aligned}$$

where k is the Slater exponent of the differentiated orbital, the Euler angles are defined as follows (the differentiated orbital has the coordinates x_1, y_1, z_1):

$$\sin\varphi = \frac{\Delta x}{r}, \qquad \sin\psi = \frac{r}{R}, \qquad r^2 = \Delta x^2 + \Delta y^2,$$

$$R^2 = r^2 + \Delta z^2$$

$$\cos\varphi = \frac{\Delta y}{r}, \qquad \cos\psi = \frac{\Delta z}{R}, \qquad \Delta x = x_1 - x_2$$

$$\Delta y = y_1 - y_2$$

$$\Delta z = z_1 - z_2 .$$

Appendix B

Differentiation of the bicentric repulsion integrals with respect to the Cartesian coordinates

$$\frac{\partial \gamma_{\mathrm{AB}}}{\partial x_{\mathrm{A}}} = 27.20974\, G \cdot \frac{x_{\mathrm{A}} - x_{\mathrm{B}}}{d} .$$

Case 1: $s = \sigma$

$$G(1s,1s) = \frac{1}{d}\left\{-\frac{1}{d} + e^{-2sd}\left[\left(1 + \frac{11}{8}sd + \frac{3}{4}s^2d^2 + \frac{1}{6}s^3d^3\right)\left(\frac{1}{d} + 2s\right)\right.\right.$$
$$\left.\left. - \frac{11}{8}s - \frac{3}{2}s^2d - \frac{1}{2}s^3d^2\right]\right\},$$

$$G(1s,2s) = \frac{1}{d}\left\{-\frac{1}{d} + e^{-2sd}\left[\left(1 + \frac{25}{16}sd + \frac{9}{8}s^2d^2 + \frac{23}{48}s^3d^3\right.\right.\right.$$
$$\left. + \frac{1}{8}s^4d^4 + \frac{1}{60}s^5d^5\right)\left(\frac{1}{d} + 2s\right) - \frac{25}{16}s - \frac{9}{4}s^2d - \frac{23}{16}s^3d^2$$
$$\left.\left. - \frac{1}{2}s^4d^3 - \frac{1}{12}s^5d^4\right]\right\},$$

$$G(2s,2s) = \frac{1}{d}\left\{-\frac{1}{d} + e^{-2sd}\left[\left(1 + \frac{419}{256}sd + \frac{163}{128}s^2d^2 + \frac{119}{192}s^3d^3\right.\right.\right.$$
$$\left. + \frac{5}{24}s^4d^4 + \frac{1}{20}s^5d^5 + \frac{1}{120}s^6d^6 + \frac{1}{1260}s^7d^7\right)\left(\frac{1}{d} + 2s\right)$$
$$- \frac{419}{256}s - \frac{163}{64}s^2d - \frac{163}{64}s^2d - \frac{119}{64}s^3d^2 - \frac{5}{6}s^4d^3 - \frac{1}{4}s^5d^4$$
$$\left.\left. - \frac{1}{20}s^6d^5 - \frac{1}{180}s^7d^6\right]\right\}.$$

Case 2: $s \neq \sigma$

$$G(1s,1s) = \frac{1}{d}\left\{-\frac{1}{d} + n^2e^{-2sd}\left[\frac{2 + a + sd}{4}\left(\frac{1}{d} + 2s\right) - \frac{s}{4}\right]\right.$$
$$\left. + b^2e^{-2\sigma d}\left[\frac{2 - a + \sigma d}{4}\left(\frac{1}{d} + 2\sigma\right) - \frac{\sigma}{4}\right]\right\},$$

$$G(1s,2s) = \frac{1}{d}\left\{-\frac{1}{d} + n^3e^{-2sd}\left[\left(\frac{1 - 5a - 4a^2}{16} - \frac{asd}{8}\right)\left(\frac{1}{d} + 2s\right) + \frac{as}{8}\right]\right.$$
$$+ b^2e^{-2\sigma d}\left[\left(\frac{15 - 22a + 15a^2 - 4a^3}{16} + 3\,\frac{3 - 3a + a^2}{8}\sigma d + \frac{2 - a}{4}\sigma^2d^2\right.\right.$$
$$\left.\left.\left. + \frac{\sigma^3d^3}{12}\right)\left(\frac{1}{d} + 2\sigma\right) - 3\,\frac{3 - 3a + a^2}{8}\sigma - \frac{2 - a}{2}\sigma^2d - \frac{\sigma^3d^2}{4}\right]\right\}.$$

$$G(2s, 2s) = \frac{1}{d}\left\{-\frac{1}{d} + n^3 e^{-2sd}\left[\left(\frac{8 - a - 27a^2 - 30a^3 - 10a^4}{16} + \frac{11 - 19a - 44a^2 - 20a^3}{32}\right.\right.\right.$$

$$\left.\cdot sd + \frac{1 - 5a - 4a^2}{16} s^2 d^2 - \frac{a}{24} s^3 d^3\right)\left(\frac{1}{d} + 2s\right) - \frac{11 - 19a - 44a^2 - 20a^3}{32} s$$

$$\left. - \frac{1 - 5a - 4a^2}{8} s^2 d + \frac{a}{8} s^3 d^2\right] + b^3 e^{-2\sigma d}\left[\left(\frac{8 + a - 27a^2 + 30a^3 - 10a^4}{16}\right.\right.$$

$$\left. + \frac{11 + 19a - 44a^2 + 20a^3}{32} \sigma d + \frac{1 + 5a - 4a^2}{16} \sigma^2 d^2 + \frac{a}{24} \sigma^3 d^3\right)\left(\frac{1}{d} + 2\sigma\right)$$

$$\left.\left. \frac{11 + 19a - 44a^2 + 20a^3}{32} \sigma - \frac{1 + 5a - 4a^2}{8} \sigma^2 d - \frac{a}{8} \sigma^3 d^2\right]\right\}$$

where x_A and x_B are coordinates of atoms, s, σ are Slater exponents, d is the distance of the atoms in atomic units, $a = 0.5(t + 1/t)$, $b = 1 + a$, $n = 1 - a$, $t = \dfrac{s - \sigma}{s + \sigma}$.

References

1. Hoffmann, R.: J. chem. Physics **39**, 1397 (1963).
2. Pople, J. A., Santry, D. P., Segal, G. A.: J. chem. Physics **43**, S129, S136 (1965).
3. Pople, J. A., Beveridge, D. L., Dobosh, P. A.: J. chem. Physics **47**, 2026 (1967).
4. Pople, J. A., Segal, G. A : J. chem. Physics **44**, 3289 (1966).
5. Dewar, M. J. S., Haselbach, E.: J. Amer. chem. Soc. **92**, 590 (1970).
6. Segal, G. A.: J. chem. Physics **47**, 1876 (1967).
7. Gordon, M. S., Pople, J. A.: J. chem. Physics **49**, 4643 (1968).
8. McIver, J. W., Jr., Komornicki, A.: Chem. Physics Letters **10**, 303 (1971).
9. Klopman, G., O'Leary, B.: Fortschr. chem. Forschung **15**, 445 (1970).
10. Čársky, P.: Chem. Listy **66**, 910 (1972).
11. Ellison, F. O., Matheu, F. M.: Chem. Physics Letters **10**, 322 (1971).
12. Longuet-Higgins, H. C., Pople, J. A.: Proc. physic. Soc. (London) A**68**, 591 (1955).
13. Davidon, W. C.: A.E.C. Res. Develop. Rep., ANL 5990 (1959).
14. Murtagh, B. A., Sargent, R. W. H.: Computer J. **13**, 185 (1970).
15. Gerratt, J., Mills, I. M.: J. chem. Physics **49**, 1730 (1968).
16. Tokagi, K., Oka, T.: J. physic. Soc. Japan **18**, 1174 (1963).
17. Pedersen, L.: J. molecular Structure **5**, 21 (1970).
18. Brand, J. C. D.: J. chem. Soc. **1946**, 858.
19. Kroto, H. W., Santry, D. P.: J. chem. Physics **47**, 792 (1967).
20. Freeman, D. E., Lombardi, J. R., Klemperer, W.: J. chem. Physics **45**, 58 (1966).
21. Kroto, H. W., Santry, D. P.: J. chem. Physics **47**, 2756 (1967).

Dr. J. Pancíř
The J. Heyrovský Institute of
Physical Chemistry and Electrochemistry
Czechoslovak Academy of Sciences
7 Máchova
Prague 2, Vinohrady
Czechoslovakia

Theoret. chim. Acta (Berl.) 29, 29—48 (1973)
© by Springer-Verlag 1973

Density Localization of Atomic and Molecular Orbitals

III. Heteronuclear Diatomic and Polyatomic Molecules

W. von Niessen

Max-Planck-Institut für Physik und Astrophysik, 8 München 40, Germany

Received October 30, 1972

Density localized molecular orbitals are computed for the molecules LiH, LiF, BF, BN, CO, C_2H_2, CH_4, NH_3, H_2O, and HF. The density localization method is based on the minimization of the sum of the interorbital density overlap integrals. The results of this method are compared to the results of the energy localization method of Edmiston and Ruedenberg and the localization procedures of Boys and of Magnasco and Perico. The agreement among the results obtained by these four methods is in general good. With a few exceptions the localized molecular orbitals agree with the classical chemical concepts.

Dichtelokalisierte Molekülorbitale sind berechnet worden für die Moleküle LiH, LiF, BF, BN, CO, C_2H_2, CH_4, NH_3, H_2O und HF. Die Dichtelokalisierungsmethode beruht auf der Minimisierung der Summe der Dichteüberlappungsintegrale zwischen verschiedenen Orbitalen. Die Ergebnisse dieses Verfahrens werden verglichen mit den Resultaten der Energielokalisierungsmethode von Edmiston und Ruedenberg und den Verfahren von Boys und von Magnasco und Perico. Die Übereinstimmung zwischen den verschiedenen Methoden ist im allgemeinen gut. Mit einigen Ausnahmen werden die klassischen chemischen Vorstellungen von Elektronenpaaren reproduziert.

1. Introduction

In a previous paper [1] (we refer to it as I) we have given the general theory of the density localization method. In a subsequent work [2] (we refer to it as II) we have applied this method to the homonuclear diatomic molecules Li_2, Be_2, B_2, C_2, N_2, and F_2 and have compared the results with those of the energy localization method of Edmiston and Ruedenberg [3, 4] and the localization procedures of Boys [5, 6] and of Magnasco and Perico [7]. In the present paper we apply these four methods to the molecules LiH, LiF, BF, BN, CO, C_2H_2, CH_4, NH_3, H_2O, and HF. We find – as in II – that the calculated localized molecular orbitals (LMO's) agree in general with the classical chemical concepts of inner shells, lone pairs of electrons and bonds which are used to describe the electronic structure of molecules. Exceptions are the molecules LiF, BN, and CO. However, just these exceptions offer additional insight into the concept of localized orbitals. The numerical agreement among the results of the four methods is in most cases quite satisfactory. For a few molecules – in particular those involving lone pairs of electrons – the results of the Magnasco-Perico method exhibit greater deviations from the general agreement, but it does not seem possible to establish a general trend. After describing briefly the four localization methods under investigation in Sect. 2 we discuss the calculations in detail in Sect. 3. In Sect. 4 we analyze the atomic hybrids for all molecules examined so far.

2. Short Outline of the Four Localization Methods

We present only a short outline of the general idea of the energy, density, Boys, and Magnasco-Perico localization methods. For all details we refer to the original papers [1–7] and to review articles [8–10]. The considerations will be restricted to closed shell cases, where the wavefunction is approximated by a single Slater determinant. The doubly filled orthonormal real orbitals are determined by a SCF calculation. For the wavefunction of a system with $2n$ electrons we write

$$|\Psi\rangle = (2n!)^{1/2} \mathscr{A}\{|1+\rangle\,|1-\rangle \cdots |n+\rangle\,|n-\rangle\}. \tag{1}$$

where $\mathscr{A}$ is the antisymmetric projection operator with $\mathscr{A}^2 = \mathscr{A}$. Let $|\Phi\rangle$ denote the row vector of molecular orbitals (MO's).

$$|\Phi\rangle := (|1\rangle, \ldots, |i\rangle, \ldots, |n\rangle). \tag{2}$$

Any unitary transformation, applied to $|\Phi\rangle$ leaves the wavefunction $|\Psi\rangle$ invariant. This can be used to transform the canonical molecular orbitals (CMO's) to the LMO's. Such a unitary transformation is common to all the localization methods under investigation, they only differ by the choice of a functional which is to be extremized by the transformation. This functional will be called localization function and is chosen by physical arguments.

They energy localized molecular orbitals (ELMO's) of Edmiston and Ruedenberg [3, 4] are obtained by maximizing the sum of the orbital self-interaction energies

$$D = \sum_i [ii|ii]. \tag{3}$$

Because of the separate invariance of the total Coulomb and total exchange interaction energy this is equivalent to minimizing separately the sum of the interorbital exchange energies and the sum of the interorbital Coulomb energies.

The density localized molecular orbitals (DLMO's) are defined to be those orbitals resulting from the unitary transformation which minimizes the sum of the interorbital density overlap integrals [1]

$$D = \sum_{i<j} [i^2 j^2]. \tag{4}$$

The density overlap between the MO's is given by

$$[i^2 j^2] := \int |\langle \boldsymbol{r}|i\rangle|^2 \, |\langle \boldsymbol{r}|j\rangle|^2 \, d^3\boldsymbol{r}, \tag{5}$$

where $|\langle \boldsymbol{r}|i\rangle|^2$ is the charge density of orbital $|i\rangle$.

The localized molecular orbitals of Boys (BLMO's) are determined by minimizing the sum of the quadratic repulsions of the orbitals with themselves [5, 6]:

$$I = \sum_i \langle ii|r_{12}^2|ii\rangle. \tag{6}$$

This has been shown by Boys to be equivalent to a maximization of the sum of the squares of the distances between the orbital charge centroids:

$$D = \sum_{i,j} [\langle i|\boldsymbol{r}|i\rangle - \langle j|\boldsymbol{r}|j\rangle]^2. \tag{7}$$

The latter formula is more appropriate for numerical implementation.

The localization procedure of Magnasco and Perico [7] is an external method [11], i.e. a concept of the orbital structure is required prior to localization. The starting point is the definition of local electron populations for each MO, which have to be localized around atoms or between pairs of atoms. The localization function in this case is the sum of these local populations:

$$P = \sum_i P_i, \tag{8}$$

where

$$P_i = \sum_{p,q \in \Gamma_i} C_{pi} C_{qi} \langle p | q \rangle \tag{9}$$

and where Γ_i denotes the set of functions making up this population. Maximization of P defines the uniformly localized molecular orbitals of Magnasco and Perico (MPLMO's).

The actual process of localization is done via a sequence of pairwise rotations of the MO's which are chosen to extremize the localization function.

3. The Calculations

Localized molecular orbitals have been computed using the formalism described above for the molecules LiH, LiF, BF, BN, CO, C_2H_2, CH_4, NH_3, H_2O, and HF. The calculations are based on SCF wavefunctions obtained with a program written by the author. The MO's are expanded in a set of Gaussian lobe functions. As basis set we used: at the H atom 4 s-type functions, the two functions with the largest exponents contracted into one group, at the Li atom 9 s-type functions, the five functions with the largest exponents contracted into one group, and 2 p-type functions, and at the atoms B to F 9 s-type functions, the five functions with the largest exponents contracted into one group, and 5 p-type functions, the three functions with the largest exponents contracted into one group. The exponential parameters and contraction coefficients of the s-type functions are taken from Huzinaga's paper [12], of the p-type functions (atoms B to F) from Whitten's paper [13]. For the Li atom the exponents η of the p-type functions and the distance R from the center are: $\eta_1 = 0.5$, $R_1 = \pm 0.075$ a.u., $\eta_2 = 2.0$, $R_2 = \pm 0.065$ a.u. Table 1 contains information about the geometry of the molecules used in the calculations and about the total energies computed.

The LMO's which we have obtained agree for most of the molecules with the results of Edmiston and Ruedenberg [4, 14] and other authors [15, 16], wherever a comparison is possible, except for the molecules LiF, BF, and CO. We are going to discuss these results in detail below.

Before examining in detail the individual molecules we make a few general statements about the numerical results. We find again – as has been found in II – that the numerical agreement among the results of the four localization methods is in general quite satisfactory, the best agreement being found among the results of the three intrinsic methods, where differences of about 1% in the value of the more "important" coefficients ($c \geq 0.1$) are typical. For some of the molecules the MPLMO's show greater differences. Whereas the results of all four localization

Table 1. Geometries and total energies

Molecule	Geometrical parameters^a	E [a.u.]
LiH	R = 3.01483	− 7.978159
LiF	R = 2.8535	− 106.953533
BF	R = 2.3849	− 124.100587
BN	R = 2.4208	− 78.868576
CO	R = 2.132	− 112.693805
C_2H_2	R_{CH} = 2.0101, $R_{CC'}$ = 2.2696	− 76.807095
CH_4	R_{CH} = 2.0617	− 40.183581
NH_3	R_{NH} = 1.9162 HNH = 106.8°	− 56.174877
H_2O	R_{OH} = 1.663 HOH = 104.5°	− 75.993520
HF	R = 1.7328	− 100.019503

^{a} distances are given in atomic units

Table 2. $2p$-type populations of unnormalized hybrids on different atoms in bond and lone pair LMO's

	Bond orbital				Lone pair orbital			
Atom	ELMO	DLMO	BLMO	MPLMO	ELMO	DLMO	BLMO	MPLMO
B in B_2	0.1973	0.2045	0.1904	0.2492	0.2067	0.2006	0.2122	0.1673
N in N_2	0.3046	0.3119	0.2997	0.3362	0.2618	0.2417	0.2735	0.1883
F in F_2	0.3768	0.3909	0.3452	0.3695	0.6888	0.6847	0.6956	0.6904
F in LiF	0.7039	0.7000	0.7008	0.5701	0.7413	0.7407	0.7426	0.7842
B in BF	0.0525	0.0600	0.0477	0.0457	0.1118	0.1039	0.1170	0.1188
F in BF	0.5735	0.5753	0.5828	0.6074	0.6756	0.6768	0.6714	0.6571
N in BN	0.3863	0.3359	0.4087	0.4328	0.2245	0.3533	0.1601	0.0619
C in CO	0.1259	0.1371	0.1223	0.1387	0.1765	0.1615	0.1928	0.1722
O in CO	0.5091	0.3912	0.5130	0.5834	0.4007	0.5142	0.3823	0.1749
N in NH_3	0.3303	0.3316	0.3280	0.2999	0.7026	0.6982	0.7095	0.7912
O in H_2O	0.3929	0.3954	0.3884	0.3497	0.7005	0.6979	0.7051	0.7423
F in HF	0.4799	0.4803	0.4712	0.4973	0.7162	0.7162	0.7197	0.7109

methods agree well in the structure of the inner shell orbitals the agreement for the lone pair and bond orbitals is sometimes less good. The MPLMO's show the greatest differences from the ELMO's in molecules with lone pair orbitals, except for the HF molecule where the agreement is very good. It appears difficult to establish general trends; in addition a dependence of the results on the basis set size seems probable.

For the inner shell orbitals we find the strongest participation of the Gaussian basis functions with the smallest exponents in the MPLMO's, the contribution decreasing for the DLMO's, ELMO's, and BLMO's in the given order. For molecules containing lone pairs of electrons it is stated in the literature that the MPLMO's have a greater local $2p$-type population in the localized lone pair orbitals than do the ELMO's and that the reverse is true for the bond orbitals [7, 17]. In II we have already commented on this feature.

Analyzing the localized orbitals for a fairly large number of molecules we cannot confirm the above statement. Table 2 contains the local $2p$-type populations in the lone pair and bond orbitals for several atoms. For some molecules the quoted behaviour is found, for others not. The MPLMO's show the greatest differences, but no general trend seems to emerge.

We describe qualitatively the LMO's resulting from the four localization methods. The lengthy expansions of the orbitals in terms of the Gaussian basis functions will not be given because of limitation of space[1], but we present the transformation matrices from CMO's to LMO's which appear to be the most useful result because of their approximate independency of the basis set choice [4]. (For the notation used see Ref. [4]). In order to compare the results of the different localization methods the transformation matrices resulting from the Magnasco-Perico localization method have been subjected to an additional unitary transformation, which mixes the orbitals of σ- and π-symmetry [7]. The signs of the orbitals are chosen in the following way: The largest coefficient of an s-type or of a $2p\pi$-type function is chosen to be positive for each orbital. If there are two or more coefficients of equal magnitude, the first one carries the positive sign. In cases of degeneracy or wavefunctions calculated with greatly differing basis sets this might not suffice, but the major uncertainties should be eliminated in this way.[1]

LiH *(Table 3)*

The orbitals of LiH are changed insignificantly by a localization. One obtains an inner shell on the Li atom and a bond orbital which is strongly polarized towards the H atom. From the transformation matrices given in Table 3 we see that the transformation is closest to the identity for the Boys method, and has greater deviations from the identity for the energy, the density and the Magnasco-Perico method. The exchange integrals calculated with the LMO's are reduced by a factor of about four compared to the exchange integrals calculated with the CMO's, for the density overlap integrals the factor is about ten.

Table 3

```
TRANSFORMATION MATRICES FOR   LIH

ENERGY LOCALIZATION                      BOYS LOCALIZATION

         iLi        bσLiH                         iLi        bσLiH

1σ    0.99768    0.06811                 1σ    0.99954    0.03020
2σ   -0.06811    0.99768                 2σ   -0.03020    0.99954


DENSITY LOCALIZATION                     MAGNASCO-PERICO LOCALIZATION

         iLi        bσLiH                         iLi        bσLiH

1σ    0.99477    0.10213                 1σ    0.99010    0.14035
2σ   -0.10213    0.99477                 2σ   -0.14035    0.99010
```

---

[1] The detailed results (basis set, expansion coefficients for the CMO's and LMO's and transformation matrices) can be obtained upon request from the author.

LiF *(Table 4)*

For the LiF molecule one would anticipate a structure with a single bond and three lone pairs of electrons on the F atom. But Edmiston and Ruedenberg obtained besides the two inner shells a σ-type lone pair orbital on the F atom and three trigonally equivalent banana bonds strongly polarized towards the F atom [4]. Our calculations gave the following results: With the energy and the density localization method we obtained a single bond, but the methods of Boys and of Magnasco and Perico tended towards three strongly polarized banana bonds and a single lone pair which has a large $2p\sigma$-contribution. Since the method of Magnasco and Perico requires a concept of the LMO's for the calculation, it might thus be expected to yield any answer. But to the credit of this method it was found that only the three bond picture represents a solution. Obtaining each of the two possibilities twice is puzzling. But it should be recalled that, although the concept of the LMO's is a very convenient and useful one, it is basically arbitrary.

Table 4

TRANSFORMATION MATRICES FOR LIF

ENERGY LOCALIZATION

	iF	iLi	bσLiF	ℓt1F	ℓt2F	ℓt3F
1σ	0.98994	-0.00216	0.06848	0.07144	0.07160	0.07135
2σ	-0.00560	0.99605	0.08756	0.00832	0.00669	0.00888
3σ	-0.14082	-0.06058	0.55089	0.47394	0.47289	0.47411
4σ	-0.01243	0.06493	-0.82685	0.31622	0.34279	0.30734
1π	0.00001	-0.00013	0.02130	-0.00327	0.69702	-0.71673
	-0.00001	0.00006	-0.00632	0.81866	-0.40971	-0.40237

DENSITY LOCALIZATION

	iF	iLi	bσLiF	ℓt1F	ℓt2F	ℓt3F
1σ	0.98040	-0.00521	0.09524	0.09989	0.09944	0.09924
2σ	-0.00648	0.99152	0.12961	-0.00658	-0.00189	0.00019
3σ	-0.19618	-0.06827	0.54243	0.46902	0.47019	0.47071
4σ	-0.01685	0.11045	-0.82370	0.35427	0.31210	0.29345
1π	0.00000	-0.00007	0.03215	0.78070	-0.57643	-0.23916
	-0.00000	0.00004	-0.01948	-0.18708	-0.58254	0.79074

BOYS LOCALIZATION

	iF	iLi	bt1LiF	bt2LiF	bt3LiF	ℓσF
1σ	0.99642	-0.00078	0.04160	0.04162	0.04162	0.04410
2σ	-0.00407	0.99667	0.04591	0.04556	0.04544	-0.01957
3σ	-0.08421	-0.06110	0.50869	0.50833	0.50820	0.46233
4σ	-0.00575	0.05397	-0.27138	-0.26523	-0.26299	0.88538
1π	-0.00001	-0.00001	-0.66038	0.74638	-0.08253	-0.00334
	-0.00001	-0.00001	-0.47713	-0.33221	0.81361	-0.00409

MAGNASCO-PERICO LOCALIZATION

	iF	iLi	bt1LiF	bt2LiF	bt3LiF	ℓσF
1σ	0.97437	-0.00528	0.08605	0.08605	0.08605	0.16844
2σ	-0.00649	0.99310	0.06516	0.06516	0.06516	-0.03118
3σ	-0.21922	-0.07371	0.45726	0.45726	0.45726	0.56501
4σ	-0.05013	0.09106	-0.33555	-0.33555	-0.33555	0.80710
1π	0.0	0.0	0.81650	-0.40825	-0.40825	0.0
	0.0	0.0	0.0	0.70711	-0.70711	0.0

For the particular case of LiF we can suggest a model to rationalize the results. Instead of regarding the LiF molecule as being covalently bonded we can regard it as an ionic structure with a partial covalent character. Essentially we would have $Li^+ F^-$. For the F^- ion we would obtain four tetrahedrally equivalent lone pair orbitals (see the results for the Ne atom in I). Because of the presence of the Li^+ ion this tetrahedron will be distorted. Recalling the van't Hoff model for carbon compounds one could form a single bond by letting a corner of the tetrahedron point towards the Li^+ ion, and a double or a triple bond by letting two or three lobes point in this direction. One could thus expect all three possibilities as the results of a localization. We have obtained two of them. Since we are dealing with different localization methods this is quite reasonable. With a different wavefunction it is feasible that the double bond picture could emerge, because a strong dependence of the results on the wavefunction is very probable. It could be

Table 5

TRANSFORMATION MATRICES FOR BF

ENERGY LOCALIZATION

	1F	1B	$b\sigma BF$	$\ell t1F$	$\ell t2F$	$\ell t3F$	$\ell\sigma B$
1σ	0.98970	-0.00081	0.06388	0.07395	0.07389	0.07380	-0.00692
2σ	-0.00111	0.99293	0.05162	-0.00303	-0.00297	-0.00286	0.10680
3σ	-0.13744	-0.03800	0.65201	0.42794	0.42787	0.42792	0.07226
4σ	0.03868	-0.05896	0.73306	-0.38094	-0.37976	-0.37657	0.16282
1π	-0.00001	0.00001	-0.00110	0.26498	-0.80069	0.53728	0.00003
	0.00001	-0.00001	0.00218	0.77135	-0.15834	-0.61639	-0.00002
5σ	0.01084	-0.09579	-0.17537	0.03265	0.03247	0.03188	0.97817

DENSITY LOCALIZATION

	1F	1B	$b\sigma BF$	$\ell t1F$	$\ell t2F$	$\ell t3F$	$\ell\sigma B$
1σ	0.97995	-0.00198	0.09173	0.10238	0.10203	0.10176	-0.00480
2σ	-0.00091	0.98505	0.06654	-0.00865	-0.00813	-0.00773	0.15825
3σ	-0.19120	-0.05242	0.64663	0.41934	0.41980	0.42011	0.11825
4σ	0.05287	-0.08798	0.71860	-0.39026	-0.38147	-0.37476	0.18657
1π	-0.00000	0.00000	-0.00414	-0.03374	-0.68666	0.72618	0.00007
	-0.00000	0.00001	-0.00779	-0.81208	0.44236	0.38051	0.00013
5σ	0.01828	-0.13849	-0.22925	0.02617	0.02420	0.02271	0.96236

BOYS LOCALIZATION

	1F	1B	$b\sigma BF$	$\ell t1F$	$\ell t2F$	$\ell t3F$	$\ell\sigma B$
1σ	0.99604	-0.00045	0.03256	0.04772	0.04772	0.04772	-0.00268
2σ	-0.00084	0.99804	0.03564	0.00183	0.00183	0.00184	0.05139
3σ	-0.08416	-0.02677	0.63980	0.44049	0.44049	0.44049	0.02760
4σ	0.02854	-0.03274	0.75485	-0.36755	-0.36759	-0.36733	0.15218
1π	-0.00000	0.0	-0.00005	-0.81646	0.41099	0.40556	-0.00000
	0.00000	0.00000	0.00014	0.00307	0.70547	-0.70874	0.00000
5σ	0.00071	-0.04618	-0.13610	0.04440	0.04441	0.04437	0.98663

MAGNASCO-PERICO LOCALIZATION

	1F	1B	$b\sigma BF$	$\ell t1F$	$\ell t2F$	$\ell t3F$	$\ell\sigma B$
1σ	0.96748	-0.00303	0.07739	0.13901	0.13901	0.13901	-0.00110
2σ	-0.00171	0.97468	0.08490	-0.00418	-0.00418	-0.00418	0.20670
3σ	-0.23774	-0.05960	0.59356	0.44112	0.44112	0.44112	0.06204
4σ	0.08573	-0.08903	0.78787	-0.34555	-0.34555	-0.34555	0.07596
1π	0.0	0.0	0.0	0.81650	-0.40825	-0.40825	0.0
	0.0	0.0	0.0	0.0	-0.70711	0.70711	0.0
5σ	0.00991	-0.19622	-0.11724	-0.00011	-0.00011	-0.00011	0.97348

argued that we have the case of multiple extrema, some localization methods find one minimum, others a second one. But although this cannot be ruled out, it was made improbable by taking different starting points and examining another wavefunction with a smaller basis set. Our model is supported when we consider the charge centroids of the LMO's. For the ELMO's (DLMO's) the charge centroids of the lone pair orbitals are at a distance of about 0.52 a.u. (0.52 a.u.) from the F atom and of the bond orbital at a distance of about 0.57 a.u. (0.58 a.u.). For the BLMO's (MPLMO's) the charge centroid of the lone pair orbital is at a distance of about 0.52 a.u. (0.57 a.u.) from the F atom and for the three bond orbitals at a distance of about 0.54 a.u. (0.51 a.u.). This is consistent in all cases with the model of a distorted tetrahedron of LMO's surrounding the F atom. The transformation matrices are given in Table 4.

BF *(Table 5)*

Edmiston and Ruedenberg obtained for the BF molecule (as for the LiF molecule) three polarized bond orbitals and a σ-type lone pair orbital on the B and on the F atom (besides the inner shells). They stated that in addition the F lone pair orbital seemed to have gained some bonding character. In the case of the wavefunction we are examining all four localization methods gave the same answer which was a single bond orbital connecting the B and F atoms and polarized towards the latter, a single lone pair orbital on the B atom and three lone pair orbitals on the F atom (Table 5). In this case the ionic model does not seem to be so appropriate.

BN *(Table 6)*

To the knowledge of the author no LMO's have so far been obtained for the BN molecule. (We consider the $1\sigma^2\, 2\sigma^2\, 3\sigma^2\, 4\sigma^2\, 1\pi^4$, ${}^1\Sigma^+$ state.) In this case again the different localization methods yield different results. An anticipated structure would involve, besides the obligatory inner shells on the B and N atoms, a triple bond polarized towards the N atom and a lone pair of electrons on the N atom. This picture is found with the energy, the Boys and the Magnasco-Perico method, but the N-lone pair is found to have a fairly strong bonding character (Table 6). This is seen from the relatively large coefficients of the B atom s-type functions contributing to this lone pair orbital. The charge centroid of this orbital is only at a distance of about 0.14 a.u. from the N atom. A similar result was found by Edmiston and Ruedenberg for the F-lone pair orbital in BF [4]. The three trigonally equivalent BN bond orbitals are slightly polarized towards the N atom. The agreement between the results of the method of Boys and of Magnasco and Perico is quite good, between the ELMO's and the BLMO's only fair, although these generally agree well. The density localization method gives on a first superficial examination the picture of a double bond and two lone pairs of electrons on the N atom. But a closer investigation reveals that the lone pair orbitals are strange in so far as they are turned inside the bond region towards the B atom. They seem to be hybrids between bond and lone pair orbitals and one could call them lone pair orbitals which have become bonding in character. Peters [18] obtained with his localization method hybrids which pointed in the

Table 6

TRANSFORMATION MATRICES FOR BN

ENERGY LOCALIZATION

	1N	1B	tσN	bt1BN	bt2BN	bt3BN
1σ	0.99145	-0.00192	0.09844	0.04945	0.04943	0.04943
2σ	-0.00167	0.99440	-0.04632	0.05488	0.05486	0.05477
3σ	-0.11637	-0.07058	0.37190	0.53041	0.53018	0.52984
4σ	0.05900	-0.07864	-0.92187	0.21681	0.21652	0.21586
1π	0.00001	-0.00001	-0.00025	-0.79182	0.56802	0.22447
	-0.00000	-0.00000	0.00041	0.19806	0.58646	-0.78539

DENSITY LOCALIZATION

	1N	1B	bd1BN	bd2BN	ℓd1N	ℓd2N
1σ	0.98207	-0.00390	0.07990	0.07991	0.10666	0.10665
2σ	-0.00201	0.98703	0.10226	0.10223	-0.04931	-0.04934
3σ	-0.16817	-0.09866	0.62227	0.62224	0.30631	0.30622
4σ	0.08515	-0.12661	0.30988	0.30968	-0.62633	-0.62650
1π	0.0	0.0	0.45405	-0.45425	0.54208	-0.54189
	0.0	-0.00000	0.54199	-0.54198	-0.45412	0.45418

BOYS LOCALIZATION

	1N	1B	ℓσN	bt1BN	bt2BN	bt3BN
1σ	0.99690	-0.00094	0.06660	0.02413	0.02413	0.02413
2σ	-0.00125	0.99860	-0.00035	0.03052	0.03052	0.03052
3σ	-0.07109	-0.04435	0.53663	0.48477	0.48477	0.48477
4σ	0.03358	-0.02878	-0.84119	0.31115	0.31115	0.31115
1π	0.0	0.0	-0.00000	0.57849	-0.78825	0.20976
	0.0	0.0	-0.00000	0.57620	0.21289	-0.78909

MAGNASCO-PERICO LOCALIZATION

	1N	1B	ℓσN	bt1BN	bt2BN	bt3BN
1σ	0.96506	-0.01481	0.25260	0.03928	0.03928	0.03928
2σ	-0.00629	0.95594	0.00105	0.16944	0.16944	0.16944
3σ	-0.23728	-0.19001	0.73076	0.35288	0.35288	0.35288
4σ	0.11096	-0.22327	-0.63418	0.42256	0.42256	0.42256
1π	0.0	0.0	0.0	0.81650	-0.40825	-0.40825
	0.0	0.0	0.0	0.0	0.70711	-0.70711

wrong direction from what they should. He called them negative hybrids. We have examined whether such negative hybrids can arise as well with the intrinsic density localization method. But this was not found. The hybrids on the N atom (which are used to construct the lone pair orbitals) do not point into the bonding region but away from it. It is the contributions from the B atom which cause the orbitals to have their charge centroids within the bonding region. They have consequently gained substantial bonding character. We thus obtain for the BN molecule either three bond orbitals and a partially bonding N-lone pair orbital or two bond orbitals and two partially bonding lone pair orbitals on the N atom. Since the DLMO's can also be regarded as giving the picture of a quadruple bond one could argue that this result does not make too much sense, because such a bond is unknown in chemistry. Also the other result of a σ-type lone pair orbital which has gained some bonding character does not make too much sense either in view of the classical chemical concepts. But it should be noted that both concepts, the classical chemical ones as well as the concept of the LMO's are basically arbitrary and derive their justification from their usefulness.

CO *(Table 7)*

The energy and the Boys localization method give an inner shell and a lone pair orbital on each atom and a set of trigonal bond orbitals polarized towards the O atom. Both lone pair orbitals have gained a partial bonding character, but a much smaller one than in the case of the BN molecule. With the density localization method we obtain a lone pair orbital on the C atom, a σ-type bond orbital slightly polarized towards the O atom and three lone pair orbitals on the O atom which are partially bonding in character so that their charge centroids fall

Table 7

TRANSFORMATION MATRICES FOR CO

ENERGY LOCALIZATION

	1O	1C	ℓσO	bt1CO	bt2CO	bt3CO	ℓσC
1σ	0.99057	-0.00110	0.09317	-0.05765	-0.05763	-0.05750	-0.01154
2σ	-0.00158	0.99203	-0.02532	-0.03652	-0.03642	-0.03552	0.10639
3σ	-0.11875	-0.06614	0.26123	-0.55041	-0.54937	-0.54258	0.11890
4σ	-0.06816	0.07132	0.91692	0.12910	0.12769	0.11718	-0.32065
1π	-0.00001	0.00002	-0.00531	0.80989	-0.34661	-0.47320	-0.00005
	-0.00001	-0.00005	0.00607	0.07683	-0.73712	0.67135	0.00008
5σ	0.00414	-0.08015	0.28569	0.11793	0.11730	0.11260	0.93359

BOYS LOCALIZATION

	1O	1C	ℓσO	bt1CO	bt2CO	bt3CO	ℓσC
1σ	0.99688	-0.00057	0.05256	0.03387	0.03387	0.03387	-0.00510
2σ	-0.00124	0.99732	-0.01141	0.02643	0.02643	0.02643	0.05599
3σ	-0.07110	-0.04406	0.29455	0.54826	0.54826	0.54826	0.06695
4σ	-0.03427	0.03945	0.91478	-0.15195	-0.15195	-0.15195	-0.30195
1π	0.00000	0.0	0.00000	0.81593	-0.43423	-0.38170	0.00000
	-0.00000	0.0	0.0	0.03033	0.69146	-0.72178	-0.00000
5σ	-0.00045	-0.04317	0.27115	-0.08838	-0.08837	-0.08838	0.94931

MAGNASCO-PERICO LOCALIZATION A

	1O	1C	ℓσO	bt1CO	bt2CO	bt3CO	ℓσC
1σ	0.98035	-0.00361	0.17653	0.05075	0.05075	0.05075	-0.00395
2σ	-0.00318	0.98219	-0.01055	0.06005	0.06005	0.06005	0.15609
3σ	-0.17352	-0.10166	0.58042	0.44604	0.44604	0.44604	0.16063
4σ	-0.09363	0.11019	0.78196	-0.30859	-0.30859	-0.30859	-0.28628
1π	0.0	0.0	0.0	0.40825	0.40825	-0.81650	0.0
	0.0	0.0	0.0	0.70711	-0.70711	0.0	0.0
5σ	0.00584	-0.11320	0.14273	-0.18158	-0.18158	-0.18158	0.93159

DENSITY LOCALIZATION

	1O	1C	bσCO	ℓt1O	ℓt2O	ℓt3O	ℓσC
1σ	0.98104	-0.00267	0.09119	0.09897	0.09849	0.09822	-0.00992
2σ	-0.00171	0.98303	0.09337	-0.00934	-0.00892	-0.00866	0.15710
3σ	-0.16765	-0.09559	0.79382	0.31619	0.31658	0.31692	0.17881
4σ	-0.09671	0.10956	-0.48817	0.46680	0.46096	0.45748	-0.31729
1π	-0.00000	0.00000	-0.00447	-0.79681	0.26185	0.54453	0.00014
	-0.00000	0.00000	-0.00085	0.16377	-0.77389	0.61178	0.00002
5σ	0.01013	-0.11178	-0.33837	0.10254	0.10023	0.09884	0.91792

MAGNASCO-PERICO LOCALIZATION B

	1O	1C	bσCO	ℓt1O	ℓt2O	ℓt3O	ℓσC
1σ	0.98035	-0.00361	0.08791	0.10192	0.10192	0.10192	-0.00395
2σ	-0.00318	0.98219	0.10400	-0.00609	-0.00609	-0.00609	0.15609
3σ	-0.17352	-0.10166	0.77257	0.33511	0.33511	0.33511	0.16063
4σ	-0.09363	0.11019	-0.53449	0.45146	0.45146	0.45146	-0.28628
1π	0.0	0.0	0.0	0.81650	-0.40825	-0.40825	0.0
	0.0	0.0	0.0	0.0	-0.70711	0.70711	0.0
5σ	0.00584	-0.11320	-0.31451	0.08241	0.08241	0.08241	0.93159

into the bonding region (by about 0.15 a.u.) instead of outside. Starting with the ELMO's instead of the CMO's as input to the density localization calculation, results identical with the DLMO's as described above were obtained eliminating the possibility of a second minimum. Using the IBMOL Version 4 program (which uses the Cartesian Gaussian functions as basis functions) a calculation was performed for the CO molecule to check the results for the DLMO's. Complete agreement was found between the results of the two wavefunctions. The Magnasco-Perico method can give both results, three bond orbitals (A in Table 7) or three partially bonding lone pair and one bond orbital (B in Table 7) depending on which σ-orbital is mixed with the π-orbitals.

C_2H_2 *(Table 8)*

The structure of acetylene is similar to the structure of nitrogen which was discussed in II. We obtain two inner shells, two equivalent CH bond orbitals and three equivalent CC′ bond orbitals (Table 8). These bond orbitals have a

Table 8

TRANSFORMATION MATRICES FOR C2H2

ENERGY LOCALIZATION

	1C	1C'	bσCH	bσC'H'	bt1CC'	bt2CC'	bt3CC'
$1\sigma_g$	0.70059	0.70059	0.04189	0.04189	0.07034	0.07034	0.07024
$1\sigma_u$	0.70465	-0.70465	0.05893	-0.05894	-0.00000	-0.00000	0.00000
$2\sigma_g$	-0.09556	-0.09557	0.26556	0.26557	0.52961	0.52959	0.52890
$2\sigma_u$	-0.05893	0.05894	0.70464	-0.70465	-0.00001	0.00002	0.00000
$3\sigma_g$	-0.00607	-0.00607	0.65401	0.65400	-0.21961	-0.21959	-0.21916
$1\pi_u$	-0.00000	0.00000	0.00006	0.00004	0.81572	-0.38213	-0.43425
	-0.00000	0.00001	-0.00005	-0.00007	0.03042	-0.72135	0.69190

DENSITY LOCALIZATION

	1C	1C'	bσCH	bσC'H'	bt1CC'	bt2CC'	bt3CC'
$1\sigma_g$	0.69332	0.69332	0.06057	0.06057	0.10248	0.10202	0.10186
$1\sigma_u$	0.70135	-0.70135	0.09005	-0.09005	0.0	0.0	0.00000
$2\sigma_g$	-0.13876	-0.13876	0.26722	0.26722	0.52425	0.52186	0.52106
$2\sigma_u$	-0.09005	0.09005	0.70125	-0.70135	-0.00000	-0.00000	0.00000
$3\sigma_g$	-0.00754	-0.00754	0.65186	0.65186	-0.22486	-0.22328	-0.22276
$1\pi_u$	0.00000	0.00000	0.00035	0.00035	0.79008	-0.22455	-0.57039
	0.0	0.0	-0.00000	-0.00000	-0.19967	0.78548	-0.58580

BOYS LOCALIZATION

	1C	1C'	bσCH	bσC'H'	bt1CC'	bt2CC'	bt3CC'
$1\sigma_g$	0.70500	0.70501	0.01994	0.01994	0.04139	0.04139	0.04139
$1\sigma_u$	0.70663	-0.70663	0.02601	-0.02601	0.0	-0.00000	0.00000
$2\sigma_g$	-0.05448	-0.05448	0.25290	0.25290	0.53732	0.53732	0.53732
$2\sigma_u$	-0.02601	0.02601	0.70663	-0.70663	0.0	0.0	0.0
$3\sigma_g$	-0.00043	-0.00043	0.66003	0.66003	-0.20713	-0.20713	-0.20713
$1\pi_u$	0.00000	-0.00000	0.0	0.0	-0.37846	0.81579	-0.43733
	0.0	0.00000	0.0	0.0	-0.72349	0.03399	0.68950

MAGNASCO-PERICO LOCALIZATION

	1C	1C'	bσCH	bσC'H'	bt1CC'	bt2CC'	bt3CC'
$1\sigma_g$	0.69185	0.69185	0.06723	0.06723	0.10592	0.10592	0.10592
$1\sigma_u$	0.70070	-0.70070	0.09500	-0.09500	0.0	0.0	0.0
$2\sigma_g$	-0.14551	-0.14551	0.26015	0.26015	0.52355	0.52355	0.52355
$2\sigma_u$	-0.09500	0.09500	0.70070	-0.70070	0.0	0.0	0.0
$3\sigma_g$	-0.01324	-0.01324	0.65407	0.65407	-0.21912	-0.21912	-0.21912
$1\pi_u$	0.0	0.0	0.0	0.0	-0.77125	0.15350	0.61775
	0.0	0.0	0.0	0.0	-0.26803	0.80194	-0.53391

Table 9

TRANSFORMATION MATRICES FOR CH4

ENERGY LOCALIZATION

	1C	bσCH	bσCH'	bσCH''	bσCH'''
$1a_1$	0.99420	0.05380	0.05380	0.05379	0.05380
$2a_1$	-0.10759	0.49711	0.49710	0.49708	0.49710
$1t_2$	-0.00000	0.10111	-0.40304	-0.47425	0.77516
	-0.00000	-0.13504	0.75607	-0.64012	0.01907
	-0.00000	0.84943	-0.12615	-0.33963	-0.38368

DENSITY LOCALIZATION

	1C	bσCH	bσCH'	bσCH''	bσCH'''
$1a_1$	0.98727	0.07953	0.07953	0.07953	0.07953
$2a_1$	-0.15907	0.49363	0.49363	0.49363	0.49363
$1t_2$	0.0	0.10112	-0.40302	-0.47426	0.77616
	0.0	-0.13503	0.75608	-0.64011	0.01906
	0.0	0.84944	-0.12614	-0.33961	-0.38368

BOYS LOCALIZATION

	1C	bσCH	bσCH'	bσCH''	bσCH'''
$1a_1$	0.99836	0.02862	0.02862	0.02862	0.02862
$2a_1$	-0.05724	0.49918	0.49918	0.49918	0.49918
$1t_2$	-0.00000	0.10112	-0.40302	-0.47426	0.77616
	-0.00000	-0.13503	0.75608	-0.64011	0.01906
	-0.00000	0.84944	-0.12614	-0.33961	-0.38368

MAGNASCO-PERICO LOCALIZATION

	1C	bσCH	bσCH'	bσCH''	bσCH'''
$1a_1$	0.97589	0.10913	0.10913	0.10913	0.10913
$2a_1$	-0.21826	0.48795	0.48795	0.48795	0.48795
$1t_2$	0.0	0.10112	-0.40302	-0.47426	0.77616
	0.0	-0.13503	0.75608	-0.64011	0.01906
	0.0	0.84944	-0.12614	-0.33961	-0.38368

Table 10

TRANSFORMATION MATRICES FOR NH3

ENERGY LOCALIZATION

	1N	bσNH	bσNH'	bσNH''	ℓσN
$1a_1$	0.99262	0.05477	0.05477	0.05477	0.07556
$2a_1$	-0.11410	0.54359	0.54368	0.54367	0.31675
1e	-0.00000	0.81655	-0.40819	-0.40820	-0.00007
	-0.00000	-0.00002	0.70710	-0.70711	0.00002
$3a_1$	-0.04110	-0.18642	-0.18656	-0.18653	0.94550

DENSITY LOCALIZATION

	1N	bσNH	bσNH'	bσNH''	ℓσN
$1a_1$	0.98452	0.08016	0.08022	0.08022	0.10686
$2a_1$	-0.16611	0.53897	0.53940	0.53940	0.31623
1e	0.00001	0.81676	-0.40799	-0.40799	-0.00022
	-0.00000	0.0	0.70711	-0.70711	0.00000
$3a_1$	-0.05588	-0.18970	-0.19014	-0.19014	0.94265

BOYS LOCALIZATION

	1N	bσNH	bσNH'	bσNH''	ℓσN
$1a_1$	0.99755	0.02812	0.02812	0.02812	0.05032
$2a_1$	-0.06199	0.54756	0.54751	0.54751	0.31113
1e	-0.00000	0.81647	-0.40827	-0.40827	0.00000
	0.0	0.0	0.70711	-0.70711	0.00000
$3a_1$	-0.03256	-0.18101	-0.18099	-0.18099	0.94903

MAGNASCO-PERICO LOCALIZATION

	1N	bσNH	bσNH'	bσNH''	ℓσN
$1a_1$	0.98151	0.08932	0.08932	0.08932	0.11271
$2a_1$	-0.17251	0.56015	0.56006	0.56006	0.17071
1e	0.00002	0.81646	-0.40829	-0.40829	-0.00005
	0.0	0.0	0.70711	-0.70711	0.00000
$3a_1$	-0.08293	-0.10793	-0.10797	-0.10797	0.97885

TRANSFORMATION MATRICES FOR H2O

ENERGY LOCALIZATION

	1O	bσOH	bσOH'	ℓd1O	ℓd2O
$1a_1$	0.99106	0.05675	0.05674	0.07539	0.07538
$2a_1$	-0.12370	0.60253	0.60252	0.35962	0.35957
$1b_2$	-0.00001	0.70710	-0.70711	-0.00000	0.0
$3a_1$	-0.05003	-0.36571	-0.36570	0.60410	0.60422
$1b_1$	0.00001	0.00005	0.00005	-0.70715	0.70707

DENSITY LOCALIZATION

	1O	bσOH	bσOH'	ℓd1O	ℓd2O
$1a_1$	0.98209	0.08155	0.08155	0.10534	0.10535
$2a_1$	-0.17596	0.59683	0.59683	0.35821	0.35821
$1b_2$	0.0	0.70711	-0.70711	-0.00000	0.00000
$3a_1$	-0.06732	-0.37034	-0.37033	0.60048	0.60050
$1b_1$	0.0	0.00000	0.00001	-0.70711	0.70710

BOYS LOCALIZATION

	1O	bσOH	bσOH'	ℓd1O	ℓd2O
$1a_1$	0.99671	0.03034	0.03034	0.04860	0.04860
$2a_1$	-0.07175	0.60915	0.60915	0.35548	0.35548
$1b_2$	0.00000	0.70711	-0.70711	-0.00000	0.00000
$3a_1$	-0.03764	-0.35780	-0.35780	0.60932	0.60932
$1b_1$	0.00000	0.00000	0.00000	-0.70711	0.70711

MAGNASCO-PERICO LOCALIZATION

	1O	bσOH	bσOH'	ℓd1O	ℓd2O
$1a_1$	0.97584	0.09367	0.09367	0.12285	0.12285
$2a_1$	-0.19152	0.63734	0.63734	0.27469	0.27469
$1b_2$	0.00000	0.70711	-0.70711	-0.00000	-0.00000
$3a_1$	-0.10513	-0.29158	-0.29158	0.63989	0.63989
$1b_1$	0.0	0.0	0.0	-0.70711	0.70711

TRANSFORMATION MATRICES FOR HF

ENERGY LOCALIZATION

	1F	bσHF	ℓt1F	ℓt2F	ℓt3F
1σ	0.98973	0.05279	0.07676	0.07667	0.07665
2σ	-0.13733	0.60909	0.45129	0.45086	0.45079
3σ	0.03967	0.79135	-0.35294	-0.35196	-0.35178
1π	-0.00001	-0.00046	-0.79743	0.24945	0.54944
	0.00001	0.00003	0.17316	-0.77765	0.60438

DENSITY LOCALIZATION

	1F	bσHF	ℓt1F	ℓt2F	ℓt3F
1σ	0.98010	0.07618	0.10603	0.10589	0.10553
2σ	-0.19152	0.60546	0.44649	0.44617	0.44533
3σ	0.05212	0.79222	-0.35330	-0.35181	-0.34797
1π	0.00000	0.00098	-0.30243	0.80723	-0.50686
	-0.00000	-0.00235	-0.75705	0.11968	0.64230

BOYS LOCALIZATION

	1F	bσHF	ℓt1F	ℓt2F	ℓt3F
1σ	0.99600	0.02898	0.04881	0.04881	0.04881
2σ	-0.08411	0.62365	0.44870	0.44870	0.44870
3σ	0.03020	0.78116	-0.36003	-0.36003	-0.36003
1π	-0.00000	0.00000	0.75396	-0.10557	-0.64839
	0.00000	0.0	0.31340	-0.80964	0.49625

MAGNASCO-PERICO LOCALIZATION

	1F	bσHF	ℓt1F	ℓt2F	ℓt3F
1σ	0.96579	0.09579	0.13913	0.13913	0.13913
2σ	-0.25126	0.57554	0.44930	0.44930	0.44930
3σ	0.06415	0.81214	-0.33482	-0.33482	-0.33482
1π	0.0	0.0	0.15075	0.61957	-0.77033
	0.0	0.0	0.80246	-0.53178	-0.27068

numbers
38967
24.4.86

Table 13 Angles between bond and lone pair orbitals and hybrids resulting from different localization methods in H_2O and NH_3 [a]

Angle formed by	ELMO	DLMO	BLMO	MPLMO
OH bond orbitals	103°	102°	103.5°	107°
O-hybrids for bond orbitals	96	93°	96.5°	104°
O-lone pair orbitals	114	116	113.5°	110°
O-hybrids for lone pair orbitals	115.5	117.5°	116°	110.5°
NH bond orbitals	106	105.5°	106°	109°
N-hybrids for bond orbitals	101.5°	100°	102°	109°

[a] The experimental values are $\measuredangle$ HOH = 104.45°, $\measuredangle$ HNH = 107°.

smaller $2p$-character than the corresponding orbitals in N_2, a fact anticipated by Hall and Lennard-Jones [19]. The CH bond orbital is slightly polarized towards the H atom as measured by the charge centroids.

CH_4, NH_3, H_2O, HF *(Tables 9, 10, 11, 12, 13)*

Finally we consider the molecules CH_4, NH_3, H_2O and HF. We obtain upon localization for each molecule an inner shell orbital, 4, 3, 2, and 1 equivalent XH bond orbitals and 0, 1, 2, and 3 equivalent lone pair orbitals respectively. The CH bond orbital is polarized towards the H atom as is the NH and the OH bond orbital as measured by the charge centroids, only the FH bond orbital is slightly polarized towards the heavy atom. In LiF the bond orbital (for ELMO's and DLMO's) was much more polarized towards the F atom in agreement with the very polar structure of LiF. The results for the different localization methods are numerically in good agreement with each other for the CH_4 and FH molecules, but for NH_3 and H_2O the MPLMO's differ appreciably from the other results. (For the transformation matrices see Tables 9 (CH_4), 10 (NH_3), 11 (H_2O), and 12 (HF).)

In Table 13 we give for the molecules H_2O and NH_3 the angles between the bond orbitals, between the lone pair orbitals, and the angles between the hybrids leading to these orbitals. The experimental angle between the two OH bonds in H_2O is 104.45°, between two NH bonds in NH_3 approximately 107°. We conclude from the table that the angles between the bond orbitals all agree reasonably well with the experimental values. The angles formed by the hybrids resulting from the Magnasco-Perico method agree best with the angles formed by the internuclear directions. In addition the Magnasco-Perico bond orbitals show the smallest degree of bending whereas the DLMO's show the greatest one.

4. Analysis of the Hybrids

A number of theories have been developed to calculate approximate wavefunctions by starting with the construction of optimal hybrids and combining them to one and two center LMO's [20]. These theories require a concept of the orbital structure and of the structure of these hybrids. The problem of constructing these hybrids becomes certainly much more difficult when extended basis sets are used for the calculations. This is one reason for examining the hybrids which result without a preconception from the application of the localization methods to SCF wavefunctions. We obtain information on the differences in the structure of the hybrids resulting from the different methods and thus obtain information on the behaviour of the methods in applications. Also we are looking for trends in the structure of hybrids and the similarity of hybrids contributed to the same type of LMO for a fixed atom in different molecules. (Because we consider only

Table 14. s, $2p\sigma$, and $2p\pi$-type populations of normalized hybrids on different atoms in localized lone pair orbitals

Atom	Type	ELMO	DLMO	BLMO	MPLMO
Be in Be_2	s	0.9996	0.9996	0.9996	0.9997
	$2p\sigma$	0.0004	0.0004	0.0004	0.0003
B in B_2	s	0.8269	0.8322	0.8219	0.8609
	$2p\sigma$	0.1731	0.1678	0.1781	0.1391
B in BF	s	0.8990	0.9055	0.8944	0.8927
	$2p\sigma$	0.1010	0.0945	0.1056	0.1073
C in CO	s	0.8465	0.8592	0.8312	0.8498^{a,b}
	$2p\sigma$	0.1535	0.1408	0.1688	0.1502^{a,b}
N in N_2	s	0.7666	0.7863	0.7543	0.8353
	$2p\sigma$	0.2334	0.2137	0.2457	0.1647
N in BN	s	0.7577	0.5177	0.8380	0.9377
	$2p\sigma$	0.2423	0.1339	0.1620	0.0623
	$2p\pi$	0	0.3484	0	0
N in NH_3	s	0.3084	0.3128	0.3016	0.2154
	$2p$	0.6916	0.6872	0.6984	0.7846
O in CO	s	0.5835	0.3504	0.6076	0.8317^{a} 0.3633^{b}
	$2p\sigma$	0.4164	0.0846	0.3924	0.1683^{a} 0.0735^{b}
	$2p\pi$	0.0001	0.5650	0	0 ^{a} 0.5632^{b}
O in H_2O	s	0.3186	0.3213	0.3139	0.2739
	$2p\sigma$	0.1951	0.1925	0.1995	0.2370
	$2p\pi$	0.4863	0.4862	0.4866	0.4891
F in F_2	s	0.3282	0.3303	0.3210	0.3264
	$2p\sigma$	0.0133	0.0103	0.0197	0.0145
	$2p\pi$	0.6585	0.6594	0.6593	0.6591
F in LiF	s	0.2531	0.2537	0.2908	0.4263
	$2p\sigma$	0.0797	0.0776	0.7092	0.5737
	$2p\pi$	0.6672	0.6687	0.0000	0
F in BF	s	0.2862	0.2855	0.2895	0.3085
	$2p\sigma$	0.0724	0.0726	0.0676	0.0522
	$2p\pi$	0.6414	0.6419	0.6429	0.6393
F in HF	s	0.2945	0.2953	0.2917	0.3004
	$2p\sigma$	0.0493	0.0494	0.0522	0.0436
	$2p\pi$	0.6563	0.6553	0.6561	0.6560

[a] MPLMO's corresponding to ELMO's.

[b] MPLMO's corresponding to DLMO's.

small molecules this is possible only in a few cases.) Because of limitation of space we do not give the expansion form of the hybrids. We present only the results for a particular aspect of the problem, we are going to analyze the *s*, $2p\sigma$, and $2p\pi$ character of the hybrids which are contributed by the atoms to the localized lone pair and bond orbitals. In Table 14 we give the *s*, $2p\sigma$, and $2p\pi$-type populations in localized lone pair orbitals for normalized hybrids on different atoms. Table 15 contains the equivalent information for the bond orbitals. We have compiled the data of II and the present work. One should not attach too much importance to the numbers or to a disagreement among the methods because we refer to *normalized hybrids* which do not reflect the weight of these hybrids in the LMO.

Let us consider first the lone pair orbitals. There is one saliant overall trend, which is very reasonable. If we regard the atoms from Be to F the $2p$ contribution to the hybrids steadily increases with one marked exception - the hybrid leading to the lone pair orbital in NH_3. This has an extremely large $2p$ character leading to the large extension of the lone pair orbital into the direction away from the rest of the molecule in congruence with its chemical behaviour. The Be hybrid in Be_2 is practically a $2s$ atomic orbital, so are the hybrids on the B atom. The *s*-character steadily decreases with increasing atomic number, but for atoms having only one lone pair orbital the *s*-character remains dominant with the noted exception of NH_3. The same trend can be observed for the hybrids on atoms with three lone pair orbitals. (See e.g. XF, X = H, Li, B, F.) An increase of the $2p$ character is necessary in going from one to several lone pair orbitals on the same atom, because these lone pair orbitals have to have a stronger directional

Table 15 *s*, $2p\sigma$, and $2p\pi$-type populations of normalized hybrids on different atoms in localized bond orbitals

Atom	Type	FLMO	DLMO	BLMO	MPLMO
Li in Li_2	*s*	0.9973	0.9974	0.9973	0.9975
	$2p\sigma$	0.0027	0.0026	0.0027	0.0025
Li in LiH	*s*	0.9126	0.9116	0.9171	0.9144
	$2p\sigma$	0.0874	0.0884	0.0829	0.0856
Li in LiF	*s*	0.4837	0.2193	0.3693	0.1927
	$2p\sigma$	0.5162	0.7804	0.3134	0.4394
	$2p\pi$	0.0001	0.0003	0.3173	0.3679
B in B_2	*s*	0.3340	0.3121	0.3573	0.1958
	$2p\sigma$	0.6660	0.6879	0.6427	0.8042
B in BF	*s*	0.1403	0.1294	0.2155	0.2455
	$2p\sigma$	0.8597	0.8706	0.7845	0.7545
B in BN	*s*	0.2905	0.4704	0.3528	0.4367
	$2p\sigma$	0.0391	0.0537	0.0344	0.0221
	$2p\pi$	0.6704	0.4759	0.6128	0.5412
C in C_2	*s*	0.6982	0.6988^{a} 0.4037^{b} 0.6543^{c}	0.9925^{d} 0.0060^{e} 0.1409^{f} 0.9120^{g}	-
	$2p\sigma$	0.0014	0.0014^{a} 0.0431^{b} 0.0283^{c}	0.0075^{d} 0.0830^{e} 0.0155^{f} 0.0041^{g}	

Table 15 (Continued)

Atom	Type	ELMO	DLMO	BLMO	MPLMO
C in C_2	$2p\pi$	0.3004	0.2998[a] 0.5532[b] 0.3174[c]	0.0 [d] 0.9110[e] 0.8436[f] 0.0839[g]	
C in CO	s	0.0782	0.1708	0.1286	0.0848[h] 0.2297[i]
	$2p\sigma$	0.2250	0.8292	0.1903	0.2843[h] 0.7703[i]
	$2p\pi$	0.6968	0.0000	0.6811	0.6309[h] 0.0 [i]
C in C_2H_2	s	0.4348	0.4421	0.4212	0.4380
(CH bond)	$2p\sigma$	0.5652	0.5579	0.5788	0.5620
C in C_2H_2	s	0.1783	0.1763	0.1847	0.1789
(CC bond)	$2p\sigma$	0.1118	0.1123	0.1066	0.1104
	$2p\pi$	0.7099	0.7115	0.7087	0.7107
C in CH_4	s	0.3221	0.3235	0.3218	0.3266
	$2p$	0.6779	0.6765	0.6782	0.6734
N in N_2	s	0.1322	0.1115	0.1464	0.0580
	$2p\sigma$	0.1497	0.1805	0.1349	0.2350
	$2p\pi$	0.7181	0.7080	0.7187	0.7070
N in BN	s	0.1668	0.2082	0.0789	0.0042
	$2p\sigma$	0.0995	0.1902	0.1541	0.2128
	$2p\pi$	0.7337	0.6016	0.7670	0.7830
N in NH_3	s	0.2915	0.2898	0.2960	0.3610
	$2p$	0.7085	0.7102	0.7040	0.6390
O in CO	s	0.1941	0.2257	0.1746	0.0463[h] 0.1717[i]
	$2p\sigma$	0.1021	0.7743	0.1066	0.2234[h] 0.8283[i]
	$2p\pi$	0.7038	0.0000	0.7187	0.7303[h] 0 [i]
O in H_2O	s	0.2250	0.2210	0.2343	0.3187
	$2p\sigma$	0.7750	0.7790	0.7657	0.6813
F in F_2	s	0.0380	0.0189	0.0937	0.0498
	$2p\sigma$	0.9620	0.9811	0.9063	0.9502
F in LiF	s	0.2450	0.2441	0.2378	0.1923
	$2p\sigma$	0.7545	0.7544	0.0889	0.1292
	$2p\pi$	0.0005	0.0015	0.6734	0.6786
F in BF	s	0.2337	0.2451	0.2067	0.1589
	$2p\sigma$	0.7663	0.7549	0.7933	0.8411
F in HF	s	0.1570	0.1570	0.1732	0.1281
	$2p\sigma$	0.8430	0.8430	0.8268	0.8719

[a] DLMO A (see Ref. [2]).
[b] DLMO B (symmetric bonding orbital b3CC′, b4CC′, see Ref. [2]).
[c] DLMO B (unsymmetric bonding orbital b1CC′, b2CC′, see Ref. [2]).
[d] BLMO A (orbital b1CC′, see Ref. [2]).
[e] BLMO A (orbital b2CC′, b3CC′, b4CC′, see Ref. [2]).
[f] BLMO B (symmetric bonding orbital b3CC′, b4CC′, see Ref. [2]).
[g] BLMO B (unsymmetric bonding orbital b1CC′, b2CC′, see Ref. [2]).
[h] MPLMO's corresponding to ELMO's.
[i] MPLMO's corresponding to DLMO's.

character. This can be seen quite clearly for the CO molecule where the energy localization leads to single lone pair orbitals on the O atom and the density localization to trigonal ones. (See also the O-hybrids in CO and H_2O.)

Quite remarkable is the similarity of the hybrids for the F-lone pair orbitals among the different localization methods and among the investigated molecules (In this case we can fortunately examine four molecules which is, if not sufficient, at least indicative.) This is not unexpected since they lie outside the bonding region and are consequently affected least by the atoms to which the F atom is bound. These data speak favourably for the transferability of LMO's.

The examination of the hybrids leading to the bond orbitals reveals some reasonable trends too (Table 15). As observed for the hybrids leading to lone pair orbitals we see here too that with increasing atomic number the $2p$ character of the hybrids for the bond orbitals increases. This has been anticipated and qualitatively discussed for the C_2H_2 and N_2 molecules by Hall and Lennard-Jones [19].

The more polar the bond becomes in a molecule involving one fixed atom the greater is the reduction in s-character of the hybrids for the less electronegative atom and the greater is the increase in s-character for the more electronegative atom. The more electronegative atom tends to attract the charge around its own nucleus, the s-character of its hybrids contributed to the bond orbital must therefore increase. We see this clearly from the series: $Li_2 \rightarrow LiH \rightarrow LiF$, $B_2 \rightarrow BF$, $F_2 \rightarrow HF$, $BF \rightarrow LiF$, and $C_2H_2 \rightarrow CO$.

The agreement among the results of the four localization methods in Tables 14 and 15 is satisfactory in general, but in a few cases (where one could expect a better agreement because the qualitative structure of the LMO's is the same) it is only fair. In the larger fraction of the molecules it is the Magnasco-Perico method which gives the greatest differences, but there are also some molecules where the agreement among all methods is only fair.

5. Discussion and Conclusions

We summarize the results and attempt an explanation. The density localization method which we have introduced in these three publications has been established as a useful new intrinsic localization method. This method adds information to our knowledge about localized orbitals in atoms and molecules and helps us to understand the concept of localization itself. The concept of localized orbitals has been proved in many publications to be of great usefulness and it allows to bridge the gap between the qualitative chemical concepts on the one hand and the quantitative Hartree-Fock theory on the other hand. The classical chemical concepts can be reproduced in the quantum mechanical description of molecules by wavefunctions.

Because there are many different localization methods it could well be that they yield somewhat different types of LMO's. Greater differences are improbable and would in fact be quite embarrassing, but smaller differences are possible because we are dealing with external methods and intrinsic methods based on different separation functions for orbital separation [11]. It is thus gratifying that for the greater part of the molecules, which we have examined so far, the four localization methods under investigation give the same qualitative answer and even a satisfactory or good quantitative agreement. There are, however, a few exceptions and they offer additional insight into the concept of localized orbitals. (It seems, though, that such problems as unconventional orbital structures arise mainly in diatomic molecules [4, 15, 17] and it is quite probable that for polyatomic molecules there will be no or only few qualitative differences among the localization methods, except that the arbitrariness of the external methods will play a greater role.) There is the C_2 molecule which presents some difficulties. We have discussed this problem in II. One might expect a lone pair on each C atom and a double bond. This would result from the Magnasco-Perico method by not mixing the orbitals of σ- and π-symmetry. But then the CC′ double bond would be a pure π-bond – a rather peculiar answer. Besides that the energy, the density, and the Boys localization methods do not support it. There is furthermore the LiF molecule, for which both the triple and the single bond seems to be a possible solution. On the assumption of an ionic model for this molecule this result can be explained. But the results for the BN and CO molecules are more difficult to rationalize. One can argue about the meaning of such results. They may arise from a certain arbitrariness of the localized orbitals (which does not preclude the usefulness of the results). But one can argue as well that they reflect details of the molecular electronic structure. One could also extract chemical information from some such results. (This might work in some cases and fail in others.) Let us take only one example which we considered already in II. (See also Ref. [19] NH_3 will accept a proton to form NH_4^+. The N-lone pair orbital will become a bond orbital. The N atoms in N_2 have lone pairs of electrons too, but N_2 will not accept a proton. If we consider the detailed structure of these lone pair orbitals, this fact is understandable. The lone pair orbital in N_2 is close to a 2*s* atomic orbital, whereas the lone pair orbital in NH_3 has a large extension in the direction away from the H atoms by making heavy use of the 2*p* functions. LMO's and bonds are a breakdown of the total electronic density into components, which might be very useful. (E.g. for the transfer of LMO's between molecules, the calculation of correlation effects, or to extract some chemical information which might be more difficult to get otherwise.) We have stressed this point before. LMO's are not observables of any one state of any one system, but, as Ruedenberg *et al.* [10] have pointed out, "properties of individual orbitals can nonetheless be related to differences in expectation values of different states or different systems."

Acknowledgement. The author wishes to thank Dr. J. Schäfer and Dr. W. Meyer for several discussions and Dr. G. Diercksen for reading the manuscript. Financial aid of the Deutsche Forschungsgemeinschaft is gratefully acknowledged.

References

1. Niessen, W. von: J. chem. Physics **56**, 4290 (1972).
2. Niessen, W. von: Density localization of atomic and molecular orbitals. II. Homonuclear diatomic molecules. Theoret. chim. Acta (Berl.) **27**, 9 (1972).
3. Edmiston, C., Ruedenberg, K.: Rev. mod. Physics **35**, 457 (1963).
4. Edmiston, C., Ruedenberg, K.: J. chem. Physics **43**, S 97 (1965).
5. Foster, J. M., Boys, S. F.: Rev. mod. Physics **32**, 300 (1960).

6. Boys, S. F.: Quantum theory of atoms, molecules, and the solid state, P. O. Löwdin, Ed., p. 253. New York: Academic Press 1966.
7. Magnasco, V., Perico, A.: J. chem. Physics **47**, 971 (1967); **48**, 800 (1968).
8. Gilbert, T. L.: Molecular orbitals in chemistry, physics, and biology, P. O. Löwdin and B. Pullman, Eds. p. 405 New York: Academic Press 1964.
9. Weinstein, H., Pauncz, R., Cohen, M.: Advances At Mol. Phys., Vol. 7, p. 97. New York: Academic Press 1971.
10. England, W., Salmon, L.S., Ruedenberg, K.: Topics in current chemistry, Vol. 23, p. 31. Berlin: Springer 1971
11. Ruedenberg, K: Modern quantum chemistry, Vol. 1, p. 85. O. Sinanoğlu, Ed., New York: Academic Press 1965
12. Huzinaga, S.: J. chem. Physics **42**, 1293 (1965).
13. Whitten, J. L.: J. chem. Physics **44**, 359 (1966).
14. Edmiston, C., Ruedenberg, K: Quantum theory of atoms, molecules, and the solid state, P. O. Löwdin, Ed., p. 263 New York: Academic Press 1966.
15. Rothenberg, S.: J. chem. Physics **51**, 3389 (1969).
16. Newton, M. D., Switkes, E., Lipscomb, W. N.: J. chem. Physics **53**, 2645 (1970).
17. Trindle, C., Sinanoglu, O.: J. chem. Physics **49**, 65 (1968)
18. Peters, D.: J. chem. Soc. **372**, 2003 (1963).
19. Hall, G. G., Lennard-Jones, J.: Proc. Royal Soc. (London) A **205**, 357 (1951).
20. Mc Weeny, R., Del Re, G.: Theoret. chim. Acta (Berl.) **10**, 13 (1968). Letcher, J. H., Dunning, T. H.: J. chem. Physics **48**, 4538 (1968). Urland, M. L., Dunning, T. H., Van Wazer, J. R.: J. chem. Phys. **50**, 3208 (1969). Sovers, O. J., Kern, C. W., Pitzer, R. M., Karplus, M.: J. chem. Phys. **49**, 2592 (1968). Petke, J. D., Whitten, J. L.: J. chem. Phys. **51**, 3166 (1969). Hoyland, J. R.: J. Amer. chem. Soc. **90**, 2227 (1968). J. chem. Physics **50**, 473 (1969). Letcher, J. H.: J. chem. Physics **54**, 3215 (1971).

Dr. W. von Niessen
Institut für Theoretische Chemie
der Technischen Universität München
8 München 2, Arcisstr. 21
Federal Republic of Germany

Theoret. chim. Acta (Berl.) 29, 49—55 (1973)
© by Springer-Verlag 1973

Corrélation électronique et effets de base dans l'étude de la liaison hydrogène: le dimère mixte ammoniac-eau

Annie Meunier, Bernard Lévy et Gaston Berthier

Laboratoire de Chimie ENSJF, 1 rue Maurice Arnoux, 92120 Montrouge et Laboratoire de Biochimie associé au CNRS, 13 rue Pierre et Marie Curie, 75005 Paris, France

Reçu le 24 juillet 1972

Electron Correlation and Basis Effects in the Theory of Hydrogen Bonds: The Mixed Dimer Ammonia-Water

The energy of the hydrogen bond N···H—O in the dimer (NH_3, H_2O) has been computed by the LCAO MO method, using a minimal set of Slater-type orbitals optimized for the isolated monomers. The doubly occupied and virtual orbitals have been determined by the standard SCF technique, and electron correlation has been introduced by a complete second-order perturbation calculation, using different sets of equivalent MO's. The bonding energy is found to be equal to 7.66 kcal/mol at the SCF step and to 9.65 kcal/mol after second order corrections. The latter value is given by a set of equivalent MO's obtained by projecting the canonical MO's of the monomers into the space of the dimer MO's. The preceding values are reduced to 3.96 kcal/mol at the SCF step and to 4.63 kcal/mol at the second-order, if the basis extension arising from the vicinity of the two monomers inside the dimer is taken into account.

L'énergie de la liaison hydrogène N···H—O dans le dimère ammoniac – eau a été calculée par la méthode LCAO–MO, à l'aide d'une base minimale d'orbitales de Slater dont les exposants sont déterminés variationnellement dans les monomères isolés. Les orbitales moléculaires occupées et virtuelles ont été déterminées par un calcul SCF classique; la corrélation électronique a été introduite par un calcul de perturbation du second ordre utilisant différentes bases d'orbitales moléculaires équivalentes. L'énergie de liaison du dimère est de 7,66 kcal/mole à l'étape SCF et de 9,65 kcal/mole après correction du second ordre. Ce dernier résultat est donné par un jeu d'orbitales moléculaires équivalentes obtenues par projection des orbitales canoniques des monomères dans l'espace des orbitales du dimère. Les valeurs précédentes sont réduites à 3,96 kcal/mole à l'étape SCF et à 4,63 kcal/mole au second ordre, si l'on tient compte de l'élargissement de base provenant de la proximité des monomères dans le dimère.

Mit Hilfe der LCAO MO-Methode wurde die Energie der N···H—O-Wasserstoffbrücke im Dimeren (NH_3, H_2O) berechnet. Es wurde dazu ein minimaler, für die isolierten Monomeren optimierter Basissatz von Slater-Orbitalen benutzt. Die doppelt besetzten und die virtuellen Orbitale sind mit Standard-SCF-Techniken bestimmt worden, die Elektronenkorrelation wurde durch eine Störungsrechnung zweiter Ordnung unter Benutzung von anderen Sätzen äquivalenter Orbitale eingeführt. Mit der SCF-Rechnung erhielt man eine Bindungsenergie von 7,66 kcal/mol und nach Berücksichtigung der Störung zweiter Ordnung von 9,65 kcal/mol. Der letztgenannte Wert wird aus einem Satz äquivalenter Orbitale erhalten, die durch Projektion der kanonischen Orbitale der Monomeren in den Raum der MO's der Dimeren entstehen. Diese beiden Werte werden zu 3,96 kcal/mol im SCF-Schritt und zu 4,63 kcal/mol in der zweiten Ordnung reduziert, wenn die Basiserweiterung, die durch die Annäherung der beiden Monomeren im Dimeren zustande kommt, in Betracht gezogen wird.

Les calculs non-empiriques qui ont été effectués ces dernières années à propos de la liaison hydrogène utilisent presque tous la méthode des orbitales moléculaires LCAO–SCF. Le but de ces travaux était en général d'étudier la force des liaisons hydrogène qui peuvent s'établir entre un composé donneur d'électrons et un composé accepteur et de déterminer la conformation géométrique d'énergie la plus basse pour le dimère qui en résulte (Voir Ref. [1, 2 et 3]). Le succès de tels calculs paraît plutôt surprenant si l'on remarque que ce type de liaison chimique met en jeu des atomes situés assez loin les uns des autres et des énergies très faibles par rapport aux liaisons chimiques habituelles [4]. Or, la méthode des orbitales moléculaires sous sa forme la plus simple met en oeuvre des fonctions d'onde dont le comportement devient de plus en plus incorrect à mesure que les distances internucléaires grandissent; en outre, l'énergie de la liaison hydrogène (quelques kcal/mole) est un nombre extrêmement petit par rapport aux énergies totales des molécules elles-mêmes ($5 \cdot 10^4$ kcal/mole pour l'eau), de telle sorte qu'une évaluation de cette quantité par différence des énergies trouvées pour le dimère et les monomères exige en principe une précision considérable sur les énergies totales. On a bien observé empiriquement que les différences d'énergies obtenues par la théorie du champ self-consistant sont quand même utilisables pour l'interprétation de certains phénomènes chimiques, pourvu que la transformation envisagée mette en jeu des molécules à couches électroniques complètes et n'entraîne pas un changement du nombre total d'électrons appariés, ce qui signifie probablement que l'énergie de corrélation reste approximativement constante au cours de la réaction [5]; une condition un peu plus stricte serait que ni le nombre de paires d'électrons, ni celui des termes d'interaction entre liaisons adjacentes ne changent [6]. Mais il semble difficile de décider *ex nihilo* si et comment les critères précédents s'appliquent aux associations par liaison hydrogène, et cela justifie à notre avis la réalisation de calculs dépassant le stade SCF, même si par ailleurs les orbitales moléculaires utilisées à cet effet proviennent d'un calcul SCF encore loin de la limite Hartree-Fock.

Dans ce travail, nous nous sommes intéressés au dimère mixte ammoniac-eau qui contient une liaison hydrogène $N \cdots H—O$. Les raisons de ce choix sont les suivantes: une énergie d'association assez forte, probablement voisine de celle des dimères $(NH_3)_2$ et $(H_2O)_2$ ($\Delta H_{exp} = 4{,}4$ kcal/mole et 5,0 kcal/mole [8]), et une structure géométrique partiellement connue (la distance d_{N-O} séparant les atomes d'azote et d'oxygène dans la liaison $N \cdots H—O$ vaut 2,775 Å [7], les trois atomes étant vraisemblablement sur la même droite).

Pour réaliser la présente étude, nous avons fait l'hypothèse que dans le dimère mixte (NH_3, H_2O) chacun des monomères conserve le plus possible sa conformation géométrique d'équilibre. Les seuls degrés de liberté qui ont été considérés sont la distance d'approche d_{N-O} et la longueur $d_{O-H'_1}$ de la liaison impliquée dans la liaison hydrogène. Les deux monomères ont été placés en position décalée, les liaisons extérieures N—H et O—H et les angles au voisinage de l'azote et de l'oxygène ont été pris égaux aux données expérimentales relatives aux monomères ($d_{N-H} = 1.014$ Å, $\widehat{HNH} = 107°$, $d_{O-H'_2} = 0{,}958$ Å, $\widehat{HOH} = 105°$); les mêmes valeurs ont été utilisées pour l'étude des monomères isolés.

Pour évaluer l'énergie du dimère et de ses composantes, nous avons choisi comme base de développement des orbitales moléculaires les fonctions déterminées par Switkes *et coll.* [10]; il s'agit d'une base d'orbitales atomiques de Slater usuelle, mais dont les exposants orbitaux ont été obtenus par minimisation de l'énergie SCF totale des monomères. Du point de vue énergétique, une telle base donne au stade SCF des résultats relativement proches de ceux d'une base double-zêta (pour NH_3 $E_{SCF} = -56{,}007$ u.a. contre $-56{,}099$ u.a. avec une base double-zêta [11]). D'après les renseignements qu'on peut tirer des calculs multiconfigurationnels effectués sur des molécules polyatomiques simples [20], l'énergie de corrélation susceptible d'être retirée d'une base minimale n'est que de 20 % environ de l'énergie de corrélation totale (pour NH_3 $E_{cor} = -0{,}38$ u.a.), mais il a été montré dans l'étude des barrières de rotation, phénomène mettant en jeu des variations d'énergie du même ordre de grandeur que dans les associations par liaison hydrogène, qu'une base assez restreinte donne déjà des informations significatives sur l'importance des effets de corrélation [13].

Le principe de la méthode suivie ici consiste à utiliser la théorie des perturbations pour évaluer la correction du second ordre qu'il convient d'apporter aux énergies SCF de chaque molécule (dimère et monomères isolés) par suite de l'interaction de configuration; la partition d'Epstein-Nesbet est utilisée pour construire l'hamiltonien d'ordre zéro de la perturbation et toutes les configurations diexcitées sont prises en compte (voir par exemple [14]). Le calcul de perturbation a été fait pour plusieurs bases d'orbitales moléculaires équivalentes à l'ordre zéro, mais différant entre elles à l'ordre deux à la suite de transformations unitaires ayant pour but de relocaliser les orbitales moléculaires du traitement SCF.

1. Résultats

Le Tableau 1 contient les valeurs qu'on trouve pour l'énergie de la liaison $N\cdots H—O$ en faisant la différence entre la somme des énergies des monomères isolés et l'énergie du dimère au même stade de calcul. A l'issue du traitement SCF on obtient une énergie de liaison ΔE_{SCF} de 6,74 kcal/mole en prenant pour les paramètres géométriques du système les valeurs standard $d_{N-O} = 2{,}775$ Å, $d_{O-H'_1} = 0{,}958$ Å. Si l'on fait varier la distance $d_{O-H'_1}$ en maintenant d_{N-O} fixe, l'énergie de liaison passe à 7,66 kcal/mole pour le minimum d'énergie, qui est obtenu pour une distance $O—H'_1$ un peu plus grande: 0,980 Å.

Quand on calcule par perturbation la fraction de l'énergie de corrélation contenue dans la base d'orbitales atomiques des monomères et du dimère, et qu'on évalue par différence la correction de corrélation ΔE_{cor} sur l'énergie de liaison ΔE_{SCF} déterminée précédemment, on constate que l'effet de corrélation ainsi introduit agit différemment selon les orbitales moléculaires utilisées:

1) en partant des orbitales moléculaires canoniques qui proviennent des calculs LCAO–SCF effectués sur les trois molécules (ammoniac, eau et dimère), c'est-à-dire d'un jeu d'orbitales occupées et virtuelles diagonalisant les opérateurs de Fock correspondants, on trouve au minimum d'énergie du dimère une faible diminution de l'énergie de liaison $(\Delta E_{SCF} + \Delta E_{cor})$: 7,50 kcal/mole pour $d_{O-H'_1} = 1{,}007$ Å, d_{N-O} restant fixé à 2,775 Å.

2) en partant d'orbitales équivalentes, localisées sur les différentes liaisons chimiques par application de la transformation de Boys [15] d'une part aux

Tableau 1. Energie de liaison du système ammoniac-eau
Les corrections d'ordre 1 dues aux défauts de self-consistance des orbitales des monomères après extension de base (cas (e)) ont été incluses dans ΔE_{SCF}

d_{N-O} (Å)	d_{O-H_1} (Å)		Energie de liaison N···H—O (en kcal/mole)			
			ΔE_{SCF}	ΔE_{cor}		
				(a)	(b)	(c)
2,700	0,958	(d)	+6,7388	−1,3881	+0,9093	+0,4462
2,775	0,958	(d)	+7,1938	−1,4646	+0,7762	+0,3909
		(e)	+3,6565			−0,6269
2,837	0,958	(d)	+7,2848	−1,5274	+0,6633	+0,3326
2,775	0,980	(d)	+7,6487	−0,6639	+1,5732	+1,2908
		(e)	+3,9853			+0,2228
	1,000	(d)	+7,4435	+0,0634	+2,3080	+2,1009
		(e)	+3,6527			+0,9764
	1,015	(d)	+6,9453	+0,5986	+2,8658	+2,6964
		(e)	+3,0666			+1,5437
	1,030	(d)	+6,1810	+1,1176	+3,4306	+3,2806
		(e)	+2,2070			+2,0890

(a) perturbation en O.M. canoniques
(b) perturbation en O.M. localisées.
(c) perturbation en O.M. projetées.
(d) H_2O et NH_3 calculés dans leur base propre.
(e) H_2O et NH_3 calculés dans la base du dimère.

orbitales canoniques occupées et d'autre part aux orbitales canoniques virtuelles de chaque molécule, on constate au contraire une augmentation de l'énergie de liaison: 9,82 kcal/mole pour $d_{O-H'_1} = 1{,}011$ Å (d_{N-O} restant à 2,775 Å).

3) en partant d'orbitales canoniques pour les monomères et d'orbitales équivalentes construites par projection *ad hoc* dans le dimère, on trouve un résultat peu différent du précédent: 9,65 kcal/mole pour $d_{O-H'_1} = 1{,}013$ Å. La transformation effectuée sur le dimère consiste à projeter les orbitales canoniques occupées φ_{1i} des monomères dans l'espace engendré par les orbitales canoniques occupées φ_{2j} du dimère, ce qui fournit pour le dimère un nouveau jeu d'orbitales:

$$\varphi'_{2i} = \sum_j \langle \varphi_{1i} | \varphi_{2j} \rangle \varphi_{2j}$$

où les $\langle \varphi_{1i} | \varphi_{2j} \rangle$ sont des intégrales de recouvrement entre orbitales moléculaires; ces fonctions sont ensuite réorthogonalisées par la méthode d'orthogonalisation symétrique de Löwdin [16]. On construit de la même façon un jeu d'orbitales virtuelles φ''_{2i} en projetant les virtuelles canoniques φ_{1i} des monomères dans l'espace orthogonal aux orbitales occupées φ'_{2j} construites précédemment:

$$\varphi''_{2i} = \varphi_{1i} - \sum_j \langle \varphi_{1i} | \varphi'_{2j} \rangle \varphi'_{2j}$$

et en les réorthogonalisant par la méthode de Löwdin. Un tel procédé au lieu de transformer les orbitales moléculaires du dimère en orbitales de liaison ou de paire libre équivalentes, comme les méthodes de localisation usuelles, fait réapparaître du mieux possible les orbitales canoniques des deux monomères à l'intérieur de la fonction d'onde du dimère, en accord avec la description classique d'un complexe moléculaire.

Il ressort du Tableau 1 que, quel que soit le jeu d'orbitales moléculaires utilisées, l'énergie de la liaison hydrogène N···H—O est grandement modifiée (de l'ordre de 20%) sous l'effet de la corrélation électronique introduite par un calcul de perturbation du second ordre, alors que l'énergie totale de chaque molécule (−75,703, −56,007 et −131,721 u.a. pour H_2O, NH_3 et $HO—H\cdots NH_3$) est seulement modifiée de moins de 0,1%; d'autre part la valeur numérique finale $\Delta E_{SCF}+\Delta E_{cor}$ est sans doute trop forte par rapport à l'énergie à laquelle on s'attend pour une liaison hydrogène de ce type.

Les conclusions précédentes subsistent si on fait varier la distance d_{N-O} des deux monomères dans le dimère en maintenant la longueur de la liaison O—H impliquée dans le pont hydrogène à la valeur standard $d_{O-H'_1}=0{,}958$ Å. L'énergie totale du dimère est minimum pour la distance $d_{N-O}=2{,}837$ Å au stade SCF; cette longueur d'équilibre est légèrement diminuée au second ordre: d_{N-O} vaut *2,815 Å, 2,810 Å et 2,815 Å après perturbation en orbitales canoniques (jeu n° 1),* localisées (jeu n° 2) ou projetées (jeu n° 3), se rapprochant ainsi de la valeur expérimentale de 2,775 Å. Des calculs antérieurs limités au stade SCF attribuaient au dimère ammoniac-eau une énergie de liaison un peu plus faible: $\Delta E_{SCF}=5{,}8$ kcal/mole mais pour une distance d'équilibre beaucoup plus grande: $d_{N-O}=3{,}12$ Å [1].

La stabilisation exagérée du dimère dans les calculs précédents s'explique facilement si l'on remarque que la description réalisée par une approximation du type LCAO s'améliore quand on passe de deux monomères isolés à un dimère: en effet, chacun d'eux peut alors utiliser les orbitales de l'autre pour enrichir sa propre base, ce qui déséquilibre le bilan énergétique de l'association au profit du dimère. Pour compenser cet effet de base propre au dimère, on peut prendre comme énergie d'association des deux monomères la différence entre l'énergie totale du dimère et celles des monomères, chacune d'elles étant calculée à l'aide d'une base élargie comprenant les orbitales atomiques de l'autre monomère telles qu'elles sont placées dans le dimère. En outre, au lieu de déterminer les orbitales canoniques dans la base élargie par un calcul SCF direct, on a préféré modifier les orbitales occupées primitives en y incorporant les termes représentant le mélange des configurations fondamentale et monoexcitées (voir par exemple [17]).

Les résultats du Tableau 1 confirment l'hypothèse que les effets de base sont à l'origine des valeurs trop élevées qu'on trouve tant à l'ordre zéro qu'à l'ordre deux pour l'énergie de liaison du dimère. Au stade SCF, celle-ci est réduite de moitié: $\Delta E_{SCF}=3{,}96$ kcal/mole pour $d_{N-O}=2{,}775$ Å et $d_{O-H'_1}=0{,}983$ Å. Les calculs de perturbation ont été faits pour les monomères avec les orbitales canoniques et pour le dimère avec les orbitales projetées. Si l'on ajoute aux orbitales moléculaires virtuelles de chaque monomère l'ensemble des orbitales occupées et virtuelles de l'autre, on constate que la correction du second ordre ΔE_{cor} à l'énergie de liaison du dimère est très diminuée: 0,67 kcal/mole au lieu de 2,0 d'où une énergie de liaison $(\Delta E_{SCF}+\Delta E_{cor})$ égale à 4,63 kcal/mole pour $d_{N-O}=2{,}775$ Å et $d_{O-H'_1}=1{,}013$ Å. Ce dernier résultat est par son ordre de grandeur en accord avec ce qu'on doit attendre d'une liaison hydrogène du type N···H—O.

Il a été proposé par ailleurs d'évaluer l'effet d'enrichissement de base sur chaque monomère en incluant dans le calcul de perturbation uniquement les orbitales moléculaires virtuelles de l'autre monomère [18]. Dans le cas présent la correction du second ordre ΔE_{cor} passe de 0,7 à 1,3 kcal/mole, d'où une énergie de liaison du même ordre de grandeur que précédemment.

2. Analyse structurale de l'énergie de la liaison H

Selon un procédé d'analyse développé récemment (voir par exemple [19–21]), il est possible de décomposer l'énergie de liaison du dimère, telle qu'elle est donnée par la méthode des orbitales moléculaires, en plusieurs composantes reliées directement au mécanisme de formation de la liaison hydrogène.

Les résultats du Tableau 2 montrent que les composantes de l'énergie de liaison, tant attractives (énergies coulombienne ΔE_C et de réarrangement ΔE_R) que répulsive (énergie d'échange ΔE_E), sont toutes supérieures en valeur absolue à l'énergie de liaison ΔE_{SCF} elle-même. Si l'élargissement de base décrit plus haut modifie la valeur numérique de ces composantes, il laisse à peu près inchangée la résultante (répulsive) des termes coulombien et d'échange; il a pour effet principal de diminuer l'énergie de réarrangement ΔE_R et par suite l'énergie de la liaison N···H—O.

Grâce à l'emploi d'orbitales localisées par projection, il est également possible de présenter une analyse structurale de la contribution de la corrélation ΔE_{cor} à l'énergie de liaison du dimère. Les composantes du second ordre de l'énergie de liaison s'obtiennent par différence entre les termes relatifs aux monomères et ceux relatifs au dimère et comprennent donc deux composantes intragroupement (l'une pour H_2O, l'autre pour NH_3), une composante de dispersion et une de transfert de charge.

Alors que les composantes intra-H_2O et intra-NH_3 donnent la plus grande partie de l'énergie de corrélation obtenue au second ordre pour le dimère (respectivement 40 et 50%), leur contribution à l'énergie de la liaison H est en général

Tableau 2. Décomposition de l'énergie de liaison N···H—O (en u.a.)

		ΔE_{SCF}			ΔE_{cor}			
		Coulomb	Echange	Réarrangement	Intra-H_2O	Intra-NH_3	Transfert de charge	Dispersion
d_{O-H_1} Å		ΔE_C	ΔE_E	ΔE_R				
0,958	(1)	+0,0284	−0,0321	+0,0152	−0,00354	−0,00077	+0,00432	+0,00061
	(2)	+0,0351	−0,0388	+0,0095	−0,00354	−0,00070	+0,00262	+0,00061
0,980	(1)	+0,0303	−0,0351	+0,0165	−0,00245	−0,00082	+0,00467	+0,00065
	(2)	+0,0375	−0,0422	+0,0106	−0,00245	−0,00074	+0,00289	+0,00065
1,015	(1)	+0,0332	−0,0402	+0,0188	−0,00081	−0,00090	+0,00529	+0,00072
	(2)	+0,0412	−0,0480	+0,0124	−0,00081	−0,00081	+0,00337	+0,00072

(1) H_2O et NH_3 étant calculés dans leur base propre.

(2) H_2O et NH_3 étant calculés dans la base du dimère.

inférieure à celle de la composante de transfert de charge (Tableau 2). L'influence du terme de dispersion est minime, tant en ce qui concerne les diexcitations du type $OH'_1\ NH \rightarrow OH'^{*}_1\ NH^*$ que les diexcitations mettant en jeu le doublet de l'azote et les électrons de la liaison $O—H'_1$.

L'emploi d'une base élargie pour le calcul de l'énergie des monomères laisse inchangée la composante de dispersion et ne modifie pas sensiblement les composantes intra-groupements de l'énergie de liaison du dimère. L'effet principal produit par cet élargissement est une diminution de la composante de transfert de charge, du fait qu'il apparaît alors une composante de ce type dans l'énergie d'ordre 2 de chaque monomère: c'est essentiellement là l'origine de l'abaissement de l'énergie de liaison.

Remerciements. L'ensemble des calculs rapportés ici a été effectué sur les ordinateurs du CIRCE (Orsay) que nous remercions pour son assistance.

Bibliographie

1. Kollman, P. A., Allen, L. C.: J. Amer. chem. Soc. **93**, 4991 (1971).
2. Dreyfus, M., Maigret, B., Pullman, A.: Theoret. chim. Acta (Berl.) **17**, 109 (1970).
3. Clementi, E., Mehl, W., Von Niessen, W.: J. Chem. Physics **54**, 508 (1971).
4. Coulson, C. A.: Research (London) **10**, 149 (1957).
5. Snyder, L. C., Basch, H.: J. Amer. chem. Soc. **91**, 2189 (1969).
6. Gélus, M., Ahlrichs, R., Staemmler, V., Kutzelnigg, W.: Chem. Physics Letters **7**, 503 (1970).
7. Olovsson, I., Templeton, D. H.: Acta crystallogr. **12**, 827 (1959).
8. Pimentel, G. C., McClellan, A. L.: The hydrogen bond, Appendix 3. San Francisco Freeman and Co. 1960.
9. Kollman, P. A.: J. Amer. chem. Soc. **94**, 1837 (1972).
10. Switkes, E., Stevens, R. M., Lipscomb, W. N.: J. chem. Physics **51**, 5229 (1969).
11. Kaldor, U., Shavitt, I.: J. chem. Physics **45**, 888 (1966).
12. Lévy, B.: Int. J. quant. Chemistry **4**, 297 (1970); Thèse, N° CNRS AO 5271, Paris (1971).
13. Lévy, B., Moireau, M. C.: J. chem. Physics **54**, 3316 (1971).
14. Masson, A., Lévy, B., Malrieu, J. P.: Theoret. chim. Acta (Berl.) **18**, 193 (1970).
15. Foster, J. M., Boys, S. F.: Rev. mod. Physics **32**, 300 (1960).
16. Löwdin, P. O.: J. chem. Physics **18**, 365 (1950).
17. Lefebvre, R.: In: Modern quantum chemistry, Part I, p. 125. New York: Academic Press 1965.
18. Daudey, J. P., Claverie, P., Malrieu, J. P.: J. chem. Physics, à paraître.
19. Löwdin, P. O.: Philos. Mag. Suppl. 5, 1 (1956).
20. Dreyfus, M., Pullman, A.: Theoret. chim. Acta (Berl.) **19**, 20 (1970).
21. Kollman, P. A., Allen, L. C.: Theoret. chim. Acta (Berl.) **18**, 399 (1970).

Dr. G. Berthier
Institut de Biologie Physico-chimique
13, rue P. et M. Curie
F-75005 Paris, France

Theoret. chim. Acta (Berl.) 29, 57—74 (1973)
© by Springer-Verlag 1973

Ab initio-Behandlung der IR- und Ramanaktivität der Wasserstoffbrücke $(\mathrm{ClHCl})^-$ unter Berücksichtigung der Umgebung

R. Janoschek
Institut für Theoretische Chemie der Universität Stuttgart

Eingegangen am 16. Oktober 1972

Ab initio Investigation of the IR- *and Raman Activity of the Hydrogen Bond* $(\mathrm{ClHCl})^-$ *with Different Environments*

In order to get an explanation for the IR continous absorption of solutions in which symmetric hydrogen bonds occur the systems HCl, $(\mathrm{ClHCl})^-$ as well as the model structures $(\mathrm{HClHClH})^+$ and $(\mathrm{HClHClH})^-$ have been investigated by means of an *ab initio* treatment (SCF-MO-LCGO-method). The Cl...Cl-distances as well as the position of the proton of the hydrogen bonds have been variied. For all these hydrogen bonds the energy levels, the frequencies, the corresponding transition intensities and the polarizability for the nuclear motion were calculated. The temperature dependency of the IR-activity is discussed. The influence of an electrical field due to the ions in respect to the hydrogen bonds is taken into account by means of an external electrical field in the Hamiltonian of the nuclear motion. The high polarizability caused by the proton of the hydrogen bond - in the system $(\mathrm{HClHClH})^-$ effects a continous IR-absorption in the range 1600–2700 cm^{-1} in a good agreement with measurements. For the Cl...Cl vibration an extremely intensive Raman activity is predicted.

Zur Deutung des IR-Kontinuums für Lösungen, in denen symmetrische Wasserstoffbrücken auftreten, werden mit Hilfe von *ab initio*-Rechnungen (SCF-MO-LCGO-Methode) die Systeme HCl, $(\mathrm{ClHCl})^-$, sowie die Modellstrukturen $(\mathrm{HClHClH})^+$ und (HClHClH) berechnet, wobei stets sowohl die Cl ..Cl-Abstände als auch die Lagen des Brückenprotons variiert werden. Für diese H-Brückensysteme werden jeweils die Energietermschemata, die Übergangsfrequenzen und die zugehörigen Übergangsintensitäten, sowie die Polarisierbarkeiten für die Kernbewegung berechnet, wobei auch die Temperaturabhängigkeit diskutiert wird. Der Einfluß der Ionenfelder auf die Brückensysteme wird durch elektrische Felder im Hamiltonoperator für die Kernbewegung berücksichtigt und diskutiert. Auf Grund der hohen Polarisierbarkeit, die durch das Brückenproton entsteht, tritt für das System $(\mathrm{HClHClH})^-$ ein IR-Kontinuum im Bereich 1600–2700 cm^{-1} auf, in guter Übereinstimmung mit Messungen. Für die Cl...Cl-Schwingung wird eine extrem intensive Ramanaktivität berechnet.

1. Einführung

Das IR-Spektrum von wäßriger Imidazollösung in Abhängigkeit von der Protonierung zeigt eine kontinuierliche Absorption, deren Intensität mit steigender Protonierung zunächst steigt [1, 2]. Diese Absorption erstreckt sich von etwa 3000 cm^{-1} bis zu den kleinsten noch beobachtbaren Frequenzen. Wenn die Protonierung stärker als 50% wird, so sinkt die Intensität der kontinuierlichen Absorption zunächst wieder (Figs. 1, 2)[1]. Bringt man die Ursache der kontinuierlichen Absorption mit dem Entstehen von symmetrischen $\mathrm{N}...\mathrm{H}^+...\mathrm{N}$-

---

[1] Fig. 1 ist in [2] auf S. 547 zu finden.

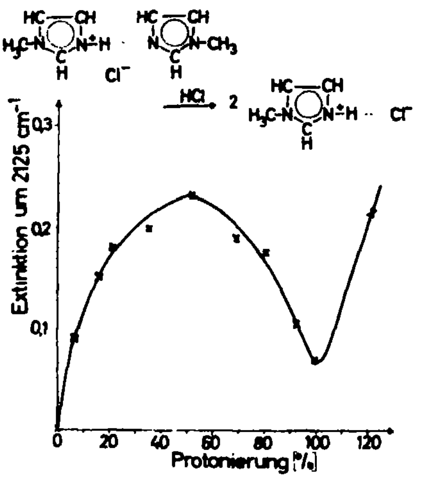

Fig. 2 Extinktion des kontinuierlichen Spektrums von wäßriger N-Methylimidazollösung in einem Frequenzbereich, der keine Wasser- oder NH-Banden enthält

Brücken in Verbindung, so ist das Intensitätsmaximum bei 50% Protonierung verständlich. Bei weiterer Protonierung sinkt die Intensität des IR-Kontinuums wieder und erreicht schließlich bei 100% Protonierung ein Minimum. Bei Protonierungen von über 100% steigt die Intensität wieder steil an und übertrifft dabei den Wert für 50%. Die kontinuierliche Absorption beginnt aber jetzt bei etwa 2600 cm^{-1} und erstreckt sich bis zu den kleinsten beobachtbaren Frequenzen. Die minimale Intensität bei 100% Protonierung kann so erklärt werden, daß die zunächst gebildeten symmetrischen $\mathrm{N}\ldots\mathrm{H}^+\ldots\mathrm{N}$-Brücken wieder verschwinden und dabei durch unsymmetrische Brücken der Form $\mathrm{N{-}H}^+\ldots\mathrm{Cl}^-$ ersetzt werden. Die hohe Intensität des IR-Kontinuums für mehr als 100% Protonierung läßt auf die Entstehung einer neuen symmetrischen Brücke $\mathrm{Cl}^-\ldots\mathrm{H}^+\ldots\mathrm{Cl}^-$ schließen. Wasserstoffbrücken dieser Form sind in Kristallen bekannt. Allerdings zeigen die in Kristallen auftretenden Brücken keine kontinuierliche IR-Absorption, sondern lediglich breite Banden. Die Ursache dieses Unterschieds ein und derselben Brücke für Flüssigkeiten und Kristalle muß also in der Umgebung der Brücke liegen.

In dieser Arbeit wird versucht, die unterschiedlichen spektroskopischen Eigenschaften einer Wasserstoffbrücke einerseits im Kristall, andererseits im flüssigen Zustand mit Hilfe von *ab initio*-Berechnungen von Modellsubstanzen zu erklären.

Im Kristall wird die Umgebung der H-Brücke vor allem durch Kationenfelder gebildet. Als einfache Modellsubstanz eignet sich deshalb das System

$$\mathrm{H}^+\ldots\mathrm{Cl}^-\ldots\mathrm{H}^+\ldots\mathrm{Cl}^-\ldots\mathrm{H}^+ .$$

Bezüglich des Brückenmittelpunktes unsymmetrische Kationenfelder können dabei durch ein zusätzliches äußeres elektrisches Feld erzeugt werden.

Befindet sich die $\mathrm{Cl}^-\ldots\mathrm{H}^+\ldots\mathrm{Cl}^-$-Brücke in einer Flüssigkeit, so werden sich in der unmittelbaren Umgebung der Cl^--Anionen keine Atom-Kationen befinden, wie das Beispiel des protonierten Imidazols in Fig. 1 zeigt. Die positive Ladung wird sich in diesem Falle über den Imidazolring so verteilen, daß hier das System

$$H...Cl^-...H^+...Cl^-...H$$

als Modellsubstanz geeignet sein dürfte. Für die Abstände der äußeren Protonen von den entsprechenden Cl-Atomen wird der feste Wert 2 Å verwendet.

Für die beiden bereits genannten Systeme, sowie für die freie Brücke $Cl^-...H^+...Cl^-$ werden durch Variation der $Cl^-...Cl^-$-Abstände, sowie der $Cl^-...H^+$-Abstände Energieflächen und Dipolmomentflächen *ab initio* berechnet. In einem zweiten Schritt wird dann die erhaltene Energiefläche zur Lösung der Schrödingergleichung für die Kernbewegung verwendet. Es resultieren dabei Schwingungszustände, die in einem dritten Schritt unter Verwendung der Dipolmomentfläche als Operator die IR-Übergangsintensitäten liefern. Mit Hilfe dieser Dipolmomentfläche wird auch der Einfluß äußerer elektrischer Felder auf das Termschema und die IR-Übergangsintensitäten untersucht. Schwingungs-Raman-Übergangsintensitäten werden mit Hilfe des Polarisierbarkeits-Operators berechnet.

2. Methode

Zur Berechnung der Gesamtenergien sowie der Dipolmomente und der Elektronendichten der angegebenen Systeme wurde ein selbst geschriebenes Programm der SCF-MO-LC (LCGO)-Methode verwendet. Als Basisfunktionen dienten Linearkombinationen von reinen Gaußfunktionen (LCGO). Bei der Auswahl der Basisfunktionen wurde von dem Gesichtspunkt ausgegangen, daß die Erzielung einer besonders tiefen Gesamtenergie alleine nicht der Sinn der Rechnungen ist, sondern daß die Form der Potentialkurven, insbesondere Gleichgewichtsabstände und Kraftkonstanten, sowie Dipolmomente in gleichem Maße in guter Übereinstimmung mit eventuellen Meßwerten resultieren. Die Größe des hier verwendeten Basissatzes war Cl (7*s*, 3*p*), H (1*s*). Am Cl-Atom wurden somit 7 *s*-Funktionen und 3 *p*-Funktionen verwendet, die am Cl^--Ion bestimmt wurden. Am H-Atom wurde eine *s*-Funktion angeboten. Die scheinbare Unausgewogenheit dieser Basis am H-Atom beruht auf der Erfahrung, daß an den Brückenprotonen nicht nur wenig Elektronenladung lokalisiert ist, sondern daß darüber hinaus die Elektronendichte am Brückenproton bezüglich der Protonbewegung relativ unveränderlich ist. Bei der Behandlung der Protonenbewegung wäre es verfehlt, die Elektronendichte am Proton besonders gut beschreiben zu wollen, denn der Einfluß der Protonlage auf die Elektronen macht sich im wesentlichen in den einsamen Elektronenpaaren der Protonenakzeptoren bemerkbar.

Die exponentiellen Parameter der verwendeten Basis, wobei auch die Abstände der *p*-Funktionen-bildenden Gaußorbitale vom entsprechenden Atomzentrum in atomaren Längeneinheiten angegeben sind, lauten wie folgt:

Cl (3000,0, 691,0, 159,0, 45,0, 4,0, 0,55, 0,21; 19,0/±0,01, 3,9/±0,05, 0,4/±0,2),

H (0,283).

Für H-Brücken der Art $(\mathrm{Cl}\ldots\mathrm{H}\ldots\mathrm{Cl})^-$ liegen bis jetzt keine Vergleichsrechnungen vor. Die Güte der verwendeten Basisfunktionen bezüglich der erwähnten spektroskopischen Eigenschaften wurde deshalb am HCl geprüft. Die Ergebnisse sollen später diskutiert werden.

Bei der theoretischen Behandlung von Wasserstoffbrücken hat man sich bisher meistens mit der Angabe der Gleichgewichtsgeometrie und der Bindungsenergie begnügt. Die Berechnung der Grundschwingungsfrequenzen in harmonischer Näherung wurde bis jetzt nur in wenigen Fällen durchgeführt [3, 4]. Für die Behandlung der Kernbewegung von H-Brücken ist jedoch die harmonische Approximation zur Darstellung der potentiellen Energie nicht ausreichend. Dies wurde, allerdings nur an Hand von Modellüberlegungen, bereits von Ibers erkannt [5]. Führt man in der H-Brücke $(\mathrm{Cl}\ldots\mathrm{H}\ldots\mathrm{Cl})^-$ die Bewegungskoordinaten x und y ein, wobei x die Auslenkung des Protons aus der Mitte längs der Brückenachse und y die Änderung des Cl...Cl-Abstandes bezüglich eines festen Wertes ist, so läßt sich die Energiefläche $V(x, y)$ als

$$V(x, y) = \sum_{k,l} a_{kl} x^k y^l \tag{1}$$

schreiben. Diese Gestalt der potentiellen Energie wird in der Schrödingergleichung für die Kernbewegung verwendet, wobei die Indizes k und l jeweils bis 4 laufen. Dadurch wird gewährleistet, daß für große y (Cl...Cl-Abstand) bezüglich x ein Doppelminimumpotential vorliegen kann. Weiter wird insbesondere bei schwachen H-Brücken der stark ausgeprägten Anharmonizität bezüglich der Cl...Cl-Auslenkung Rechnung getragen. Schließlich liefern gemischte Glieder wie beispielsweise $a_{21} x^2 y$ die durch die Kopplung der beiden Schwingungen verursachten Effekte, die besonders durch das Auftreten von Übergängen charakterisiert sind, die im entkoppelten Fall verboten sind.

Die Schrödingergleichung wird durch eine Linearkombination von Produkten von Oszillatoreigenfunktionen gelöst. Die Einzelheiten zur Bestimmung dieser Basisfunktionen sind in [6] beschrieben. Die Verwendung von 32 Basisfunktionen der Gestalt

$$u^{n}_{ij}(x - x_i, \lambda_j)\cdot v^{n'}_{i'j'}(y - y_{i'}, \lambda_{j'})\,, \tag{2}$$

wobei die Funktionen im Punkt $(x_i, y_{i'})$ lokalisiert sind und $\lambda_j, \lambda_{j'}$ exponentielle Parameter sind und n, n' die Anzahl der Knotenlinien bezüglich x und y ist, erhält man im Energietermschema Konsistenz für etwa die tiefsten 10 Zustände.

Die SCF-Rechnungen liefern neben der Energie auch das Dipolmoment in Abhängigkeit von den beiden Bewegungskoordinaten. In Analogie zur Energiefläche wird die Dipolmomentfläche durch

$$\mu(x, y) = \sum_{k,l} b_{kl} x^k y^l \tag{3}$$

dargestellt. Auch hier treten in Analogie zur mechanischen Kopplung und zur mechanischen Anharmonizität elektrische Kopplung und elektrische Anharmonizität auf, was sich bei der Verwendung von (3) als Dipoloperator zur Berechnung von Übergangsmomenten durch das Auftreten neuer Übergänge bemerkbar macht [7–9].

Die Dipolmomentfläche hat im Zusammenhang mit Wasserstoffbrücken allerdings noch eine weitere wichtige Bedeutung. Wie bereits in der Einführung erwähnt, sind H-Brücken der Form (Cl...H...Cl)$^-$ stets irgendwelchen Kationenfeldern ausgesetzt. Diese elektrischen Felder F können in der Rechnung dadurch berücksichtigt werden, daß die potentielle Energie den Zusatz $-\mu(x, y)\cdot F$ erhält. Dieser feldverursachte Zusatz zur potentiellen Energie ist deshalb richtig, weil noch bei Feldern bis $5\cdot 10^7$ V/cm die Einwirkung des äußeren Feldes auf die Elektronen vernachlässigbar ist gegenüber der Wirkung des Brückenprotons auf die Elektronen [6]. Ein äußeres elektrisches Feld bewirkt die Aufhebung der Symmetrie der potentiellen Energie bezüglich der x-Koordinate. Dadurch treten eine Reihe neuer Übergänge auf, die vorher aus Symmetriegründen verboten waren.

Ein äußeres elektrisches Feld induziert in einer Wasserstoffbrücke ein Dipolmoment, aus dem die Polarisierbarkeit errechnet werden kann. Die Polarisierbarkeit von Wasserstoffbrücken in Brückenrichtung kann wesentlich höher als die bekannten Elektronenpolarisierbarkeiten sein [6]. Während für IR-Übergänge der Operator des Dipolmoments als Funktion der Kernkoordinaten verantwortlich ist, ist für Raman-Übergänge der Operator des induzierten Dipolmoments als Funktion der Kernkoordinaten heranzuziehen. Die Entstehungsursache des induzierten Dipolmoments ist bei Wasserstoffbrückenbindungen eine ganz andere als bei Molekülen mit Valenzbindungen. Ein elektrisches Feld vom Betrage F in x-Richtung bewirkt im Hamiltonoperator den Zusatz

$$F\cdot\left(\sum_i x_i^{\mathrm{el}} - \sum_k Q_k X_k\right). \tag{4}$$

wobei x_i^{el} die x-Koordinate des i-ten Elektrons ist und X_k die x-Koordinate des k-ten Kerns ist. Aus der Lösung der Schrödingergleichung für die Elektronenbewegung erhält man das induzierte Dipolmoment der Elektronenverteilung als Funktion der Kernkoordinaten $\ldots X_k, Y_k, Z_k\ldots$ und der Feldstärke F als

$$\mu_{\mathrm{ind}}^{\mathrm{el}}(\ldots, X_k, Y_k, Z_k, \ldots, F) \tag{5}$$

Für Moleküle mit Valenzbindungen ist der Einfluß von Feldern bis $5\cdot 10^7$ V/cm auf die Kernlagen noch vernachlässigbar, so daß (5) alleine das induzierte Dipolmoment und somit den Operator für Raman-Übergänge darstellt. Bei Wasserstoffbrückenbindungen kann jedoch die Situation genau umgekehrt sein. In den meisten Fällen von Wasserstoffbrücken kann nämlich ein elektrisches Feld die Lage der Kerne so stark verändern, daß das induzierte Dipolmoment im wesentlichen durch die Verschiebung der Kerne entsteht, so daß dann $\mu_{\mathrm{ind}}^{\mathrm{el}}$ aus (5) vernachlässigbar ist [6]. Faßt man in (5) für den zweidimensionalen linearen Fall die Koordinaten X_1, X_2 als Normalkoordinaten auf und separiert die Schrödingergleichung für die Kernbewegung bezüglich X_1 und X_2, so lautet der Operator für die Raman-Übergänge der Schwingung längs X_2

$$\mu_{\mathrm{ind}}^{1}(X_2, F), \tag{6}$$

wobei über X_1 bereits integriert wurde. Für die Frequenzen muß dabei natürlich $\omega_1 \gg \omega_2$ erfüllt sein. Die Kopplung zwischen der symmetrischen und antisymmetrischen Schwingung ist in symmetrischen Wasserstoffbrücken so gering, daß eine Separation das induzierte Dipolmoment nicht wesentlich ändert in bezug auf eine kopplungsbehaftete Behandlung dieser beiden Schwingungsarten [7].

Zur Lösung der Schrödingergleichung für ein zweidimensionales Potential in Polynomgestalt wurde das Programm DOM 2 (Doppelminimumpotential, 2-dimensional) entwickelt. Als Ergebnisse werden Termschema, Wellenfunktionen, IR- und Raman-Übergangsintensitäten (thermisch gemittelt), induzierte Dipolmomente (thermisch gemittelt) ausgedruckt. Die Rechnungen wurden auf der Maschine CDC 6600 des Regionalen Rechenzentrums, Stuttgart durchgeführt. Wenn nicht anders vermerkt, beziehen sich thermisch gemittelte Größen auf 300 °K.

3. Ergebnisse und Diskussion

A. Das HCl-*Molekül*

Das HCl-Molekül soll in dieser Arbeit nur insoweit behandelt werden, als es als Prüfung der hier angewendeten Methoden dienen soll. Einerseits eignet sich dieses Molekül infolge der umfangreichen vorliegenden Meßwerte zu einem solchen Vergleich mit errechneten Eigenschaften recht gut, andererseits muß aber berücksichtigt werden, daß mit den hier verwendeten Methoden nur "closed shell"-Zustände behandelt werden können. Die Potentialkurve und auch die Dipolmomentkurve des HCl-Moleküls werden für größere Atomabstände insofern verfälscht, als die Dissoziationsprodukte Cl^- und H^+ entstehen. Für die errechnete Potentialkurve ergab sich in atomaren Einheiten

$$\Delta V = 0{,}20386(\Delta R_{HCl})^2 - 0{,}15850(\Delta R_{HCl})^3 \tag{7}$$

mit einer Gesamtenergie von $-454{,}94654$ at.E. beim Gleichgewichtsabstand 1,345 Å (Experimenteller Wert 1,275 Å [10]). Die Dipolmomentkurve resultierte zu

$$\mu = 0{,}44222 - 0{,}04398(\Delta R_{HCl}) + 0{,}05087(\Delta R_{HCl})^2 \tag{8}$$

in at.E. Das Dipolmoment im Gleichgewichtszustand von 1,12 D stimmt mit dem gemessenen Wert von 1,07 D [11] sehr gut überein. Die mit Hilfe von (7) errechnete Grundschwingungsfrequenz, die 1. und 2. Oberschwingung, sowie die berechneten zugehörigen relativen Übergangsintensitäten werden in folgender Tab. 1 mit gemessenen Werten verglichen.

Sowohl die berechneten Frequenzen, als auch die relativen Übergangsintensitäten zeigen im Gang das Verhalten der gemessenen Werte. Die Intensitäten der Oberschwingungen gehen in I mit wachsender Frequenz zu langsam zurück, was durch den zu groß berechneten Term mit $(\Delta R_{HCl})^2$ im Dipolmoment verursacht wird. Dieser zu groß berechnete Term entsteht durch das fehlerhafte Dipolmoment für große Kernabstände, das durch die Dissoziationsprodukte Cl^- und H^+ verursacht wird. In II wurde die elektrische Anharmonizität vernachlässigt, das heißt, daß die Oberschwingungen alleine durch die mechanische Anharmonizität auftreten. Literaturzitate für Berechnungen am HCl-Molekül sind in [12] aufgeführt.

Tabelle 1. Berechnete und gemessene [10] Frequenzen und Übergangsintensitäten des HCl-Moleküls. I: Mit Dipolmomentoperator (8). II: Ohne elektrische Anharmonizität

		Grundschwingung	1. Oberschwingung	2. Oberschwingung
Frequenz [cm^{-1}]	berechnet	3158	6121	8931
	gemessen	2886	5668	8347
Relative Intensität	I	1	0,216	0,0124
Relative Intensität	II	1	0,0158	0,000222
Relative Intensität	gemessen	1	0,0201	0,0016

B. Die Energieflächen

Beim Vergleich der Energieflächen für die Systeme H$^+$...Cl$^-$...H$^+$...Cl$^-$...H$^+$ und H...Cl$^-$...H$^+$...Cl$^-$...H in Fig. 3 stellt man zunächst fest, daß in beiden Fällen das Brückenproton ein einfaches Energieminimum vorfindet. Jedoch ist beim zuerst genannten System dieses Minimum besonders ausgeprägt, so daß der Cl...Cl-Abstand um mindestens 1 Å aufgeweitet werden muß, um für das Brückenproton ein Doppelminimumpotential zu erzwingen. Beim zweiten System ist diese Energiemulde bezüglich des Cl...Cl-Abstandes extrem flach. Bereits eine Aufweitung des Cl...Cl-Abstandes um 0,4 Å erzeugt für das Brückenproton ein Doppelminimumpotential. Die bezüglich des Cl...Cl-Abstandes flache Energiemulde des zweiten Systems läßt auf eine schwache Wasserstoffbrücke schließen, was sich auch beim Vergleich der beiden Cl...Cl-Abstände zeigt, der beim ersten System 3,109 Å und beim zweiten System 3,532 Å beträgt. Die Koeffizienten der analytischen Darstellung der potentiellen Energie sind für beide Systeme in Tab. 2 aufgeführt.

Tabelle 2. Koeffizienten a_{kl} der potentiellen Energie (in at. E.) und Koeffizienten b_{kl} der Dipolmomentfläche (in at. E.). Der Ursprung der Variablen y entspricht einem Cl... Cl-Abstand von 6,2 bzw. 7,0 at. E.

Koeffizienten a_{kl} zu $x^k y^l$	H$^+$...Cl$^-$...H$^+$...Cl$^-$...H$^+$	H...Cl$^-$...H$^+$...Cl$^-$...H
a_{00}	0,00790	0,00208
a_{20}	0,04967	0,03067
a_{40}	0,06458	0,07708
a_{01}	0,03940	0,01166
a_{02}	0,04022	0,01228
a_{03}	−0,02019	−0,00661
a_{04}	0,00796	0
a_{21}	−0,07096	−0,15335
Koeffizienten b_{kl} zu $x^k y^l$		
b_{10}	1,60	−3,45
b_{30}	−0,29	0,15
b_{11}	0,42	−0,52

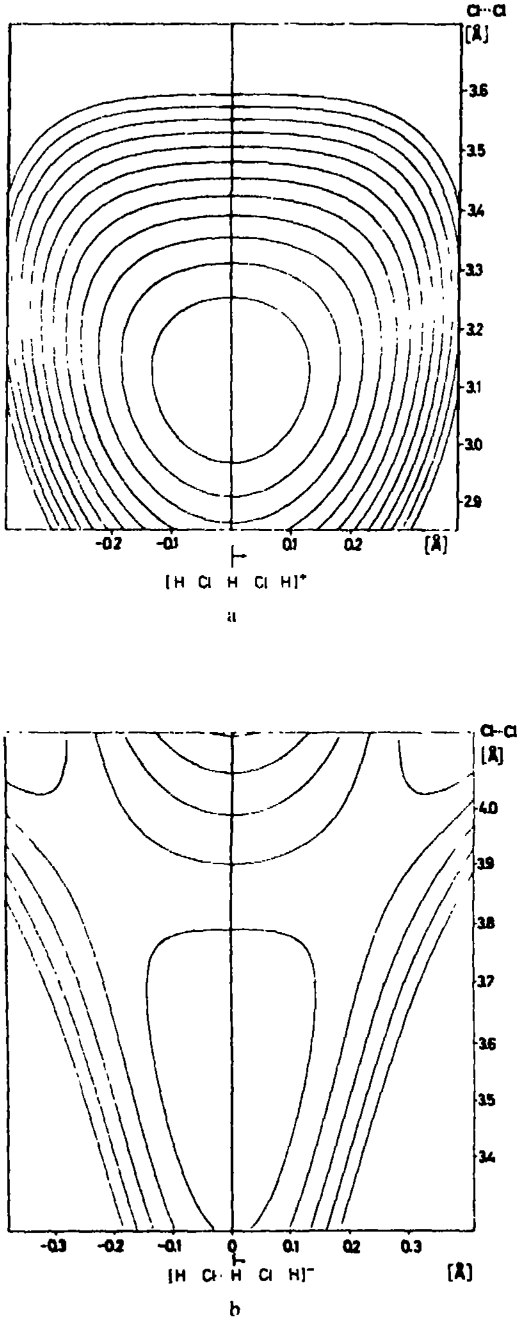

Fig. 3.a Energiefläche für das System $H^{\cdot}\ldots Cl\ldots H^{+}\ldots Cl\ldots H^{\cdot}$. b Energiefläche für das Syst $H\ldots Cl^{-}\ldots H^{+}\ldots Cl^{-}\ldots H$

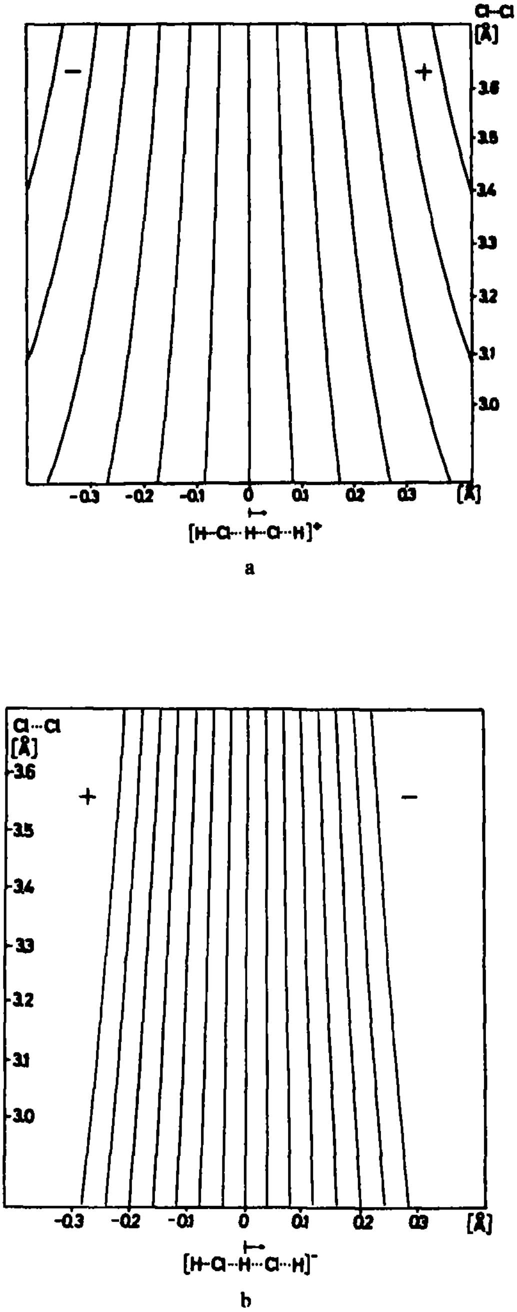

Fig. 4. a Dipolmomentfläche für das System $H^+ \ldots Cl^- \ldots H^+ \ldots Cl^- \ldots H^+$. b Dipolmomentfläche für das System $H \ldots Cl^- \ldots H^+ \ldots Cl^- \ldots H$

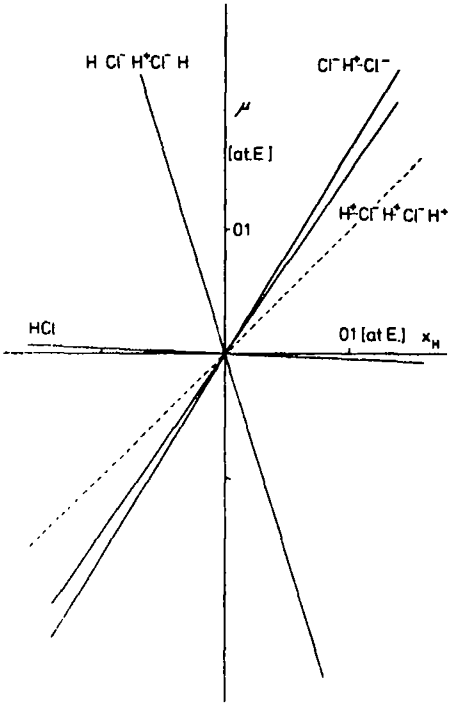

Fig. 5. Dipolmomentkurven in Abhängigkeit von der Protonbewegung. (Für HCl entspricht $x_H = 0$ dem berechneten Gleichgewichtsabstand; die Dipolmomentkurve für HCl ist um 0.441 at.E. nach unten verschoben). (- - -) Dipolmomentgerade für das nackte Proton

C. *Die Dipolmomentflächen*

Die Dipolmomentflächen der beiden Wasserstoffbrücken haben die gemeinsame Eigenschaft, daß das Dipolmoment nicht nur von der Lage des Brückenprotons, sondern auch vom Cl...Cl-Abstand abhängt (Fig. 4). Für kleine Auslenkungen des Brückenprotons aus der Gleichgewichtslage ändert sich das Dipolmoment in beiden Fällen nahezu linear. Ein Vergleich in Fig. 4 und in Tab. 2 zeigt aber, daß einerseits die Vorzeichen der Dipolmomente für gleiche Protonauslenkung in den beiden H-Brücken verschieden sind und daß andererseits die Anstiege der Dipolmomentgeraden dem Betrage nach wesentlich größer als 1 sind. Dies besagt, daß das Dipolmoment hier nicht alleine durch die Protonladung verursacht wird (dieser Fall entspricht der gestrichelt gezeichneten Geraden in Fig. 5), sondern daß in der einen Brücke bei der Auslenkung des Protons die Elektronen in die entgegengesetzte Richtung verschoben werden, während bei der anderen H-Brücke die Elektronen mit dem Proton mitgeführt werden.

D. *Die Elektronendichten*

Diese Elektronenverschiebungen, durch das Brückenproton verursacht, werden in Fig. 6 deutlich, wo die Elektronendichte entlang der Achse der Wasserstoff-

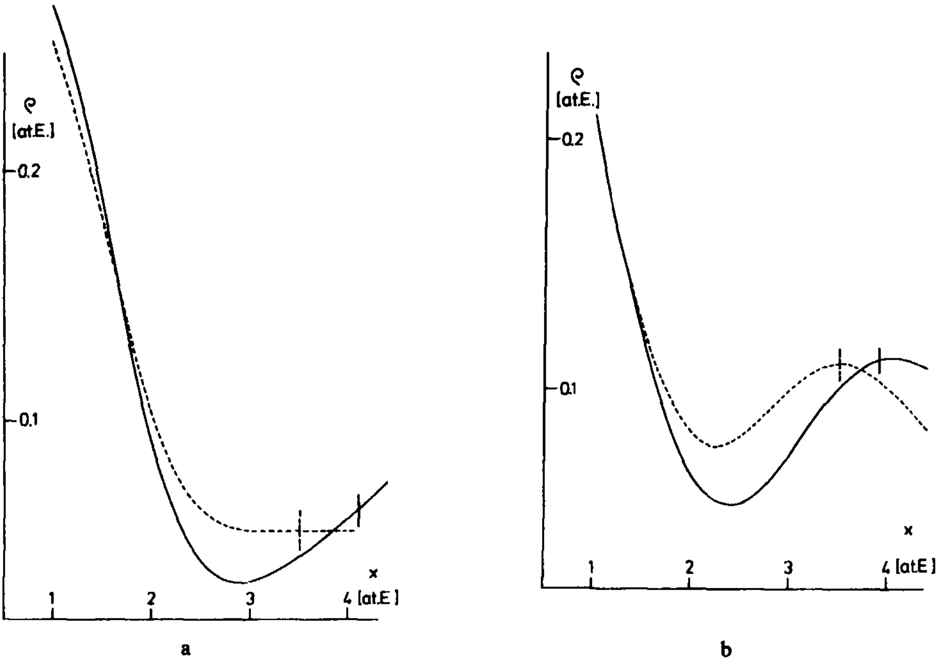

Fig. 6. a Elektronendichten längs der H-Brückenbindung im System $H^+ \ldots Cl^- \ldots H^+ \ldots Cl^- \ldots H^+$. Die Cl-Atome liegen bei $x = 0$ und $x = 7$ at.E. (- - -) Brückenproton bei $x = 3.5$ at.E. (——) Brückenproton bei $x = 4.1$ at.E. b Elektronendichten längs der H-Brückenbindung im System $H \ldots Cl^- \ldots H^+ \ldots Cl^- \ldots H$. Die Atome liegen bei $x = 0$ und $x = 7$ at.E. (- - -) Brückenproton bei $x = 3.5$ at.E. (——) Brückenproton bei $x = 3.9$ at.E.

brücke aufgetragen ist. In beiden Fällen liegen die Cl-Atome bei $x = 0$ und $x = 7$ at.E. Die gestrichelten Kurven stellen die Elektronendichten längs der Brückenachse dar, wobei sich das Brückenproton jeweils in der Mitte zwischen den beiden Cl-Atomen befindet (3,5 at.E.). Die durchgehenden Kurven geben den Verlauf der Elektronendichte wieder, wenn das Proton um 0,6 beziehungsweise um 0,4 at.E. nach rechts ausgelenkt wird. Im Falle des Systems $H^+ \ldots Cl^- \ldots H^+ \ldots Cl^- \ldots H^+$ werden die gegen das Proton sich bewegenden Elektronen in Fig. 6 besonders deutlich dargestellt. Wird das Proton aus der Wasserstoffbrückenmitte heraus nach rechts ausgelenkt, so zieht das bei $x = 0$ befindliche Cl-Atom Elektronen zurück, so daß im Bereich von 2 bis 4 at.E. die Elektronendichte abnimmt, während sie im Bereich von weniger als 2 at.E. zunimmt. Das bei $x = 7$ at.E. befindliche zweite Cl-Atom schiebt dem sich nähernden Proton Elektronen entgegen, was durch den Dichteanstieg im Bereich von mehr als 4 at.E. ersichtlich ist.

Im System $H \ldots Cl^- \ldots H^+ \ldots Cl^- \ldots H$ bewegen sich die Elektronen in gleicher Richtung wie das Proton.

E. Der Einfluß eines elektrischen Feldes auf Wasserstoffbrücken

Der Einfluß eines elektrischen Feldes auf ein Elektronensystem (Atom, Molekül) ist seit der Entdeckung des Stark-Effekts (1913) bekannt. Als Ergebnis einer Störungsrechnung 2. Ordnung erhält man für die Verschiebung zweier nicht entarteter Terme mit den Energien E_i und E_j mit $E_i > E_j$ und für hinreichend kleine Felder F

$$\Delta E_{ij} = \pm \frac{\mu_{ij}^2 F^2}{|E_i - E_j|} . \tag{9}$$

Dabei gilt für ΔE_i das Plus-Zeichen und für ΔE_j das Minus-Zeichen; μ_{ij} ist das Dipolübergangsmoment der Zustände i und j und F ist die elektrische Feldstärke. Die Bedeutung des Stark-Effekts ist für die meisten Systeme wegen der Kleinheit des Effekts gering. Aus Gl. (9) folgt jedoch, daß für Protonenzustände in Wasserstoffbrücken der Stark-Effekt eine dominierende Rolle spielen kann, weil für die beiden tiefsten Protonenzustände 0 und 1 $|E_1 - E_0|$ klein ist im Vergleich zu den Schwingungszuständen von Molekülen und weil das Übergangsmoment μ_{01} für Protonenzustände wesentlich größer sein kann als für Schwingungszustände von Molekülen, wie dies beispielsweise im $H_5O_2^+$ der Fall ist [6]. Der Einfluß eines elektrischen Feldes auf eine Wasserstoffbrücke ist aus zweierlei Gründen von Bedeutung: Durch ein äußeres elektrisches Feld lassen sich einerseits die Polarisierbarkeitstensoren der Brücken bestimmen, die ausschlaggebend für die Raman-Aktivität sind. Andererseits läßt sich die Feldabhängigkeit der IR- und Raman-Spektren diskutieren.

1. Die Termschemata

In der Fig. 7 sind die Termschemata als Funktion der elektrischen Feldstärke dargestellt. In beiden Fällen ist die Frequenz der asymmetrischen Schwingung groß gegen die Frequenz der symmetrischen Schwingung. Berücksichtigt man für die symmetrische Schwingung jeweils die vier tiefsten Terme, so treten selbst bei Feldern von $5 \cdot 10^7$ V/cm noch keine Termüberschneidungen auf. Im gesamten Feldbereich können deshalb den Termen Quantenzahlentupel zugeordnet werden. Die erste Quantenzahl bezieht sich dabei auf die asymmetrische Schwingung, während die zweite Quantenzahl den symmetrischen Schwingungszustand kennzeichnet. Das System $H\ldots Cl^-\ldots H^+\ldots Cl^-\ldots H$ hat im Verhältnis zu dem anderen System bezüglich der Brückenprotonbewegung die stärkere Dipolmomentänderung und somit das größere Dipolübergangsmoment, was nach (9) eine stärkere Feldeinwirkung auf die Terme verursacht. Demnach sind im System $H^+\ldots Cl^-\ldots$ $\ldots H^+\ldots Cl^-\ldots H^+$ keine merklichen feldverursachten Frequenzverschiebungen zu erwarten. Im System $H\ldots Cl^-\ldots H^+\ldots Cl^-\ldots H$ dagegen bewirkt das elektrische Feld Frequenzänderungen, deren Auswirkungen auf das IR-Spektrum aber erst durch die Berechnung der Übergangsintensitäten ersichtlich werden.

Bei der Betrachtung der symmetrischen Schwingungszustände des Systems $H\ldots Cl^-\ldots H^+\ldots Cl^-\ldots H$ fällt auf, daß die Termdifferenzen $n\,k+1 - n\,k$ für steigende k zunehmen, obwohl die hier berücksichtigte mechanische Anharmonizität einen umgekehrten Verlauf liefern müßte. Auf Grund des Gliedes $a_{21}x^2y$ in der potentiellen Energie kann jedoch die Kopplung über die Anharmonizität $a_{03}y^3 + a_{04}y^4$ dominieren. In der Energiematrix treten Beiträge der Gestalt

$$\langle n\,k|x^2y|\,n\,k+1\rangle \sim \sqrt{k+1}$$

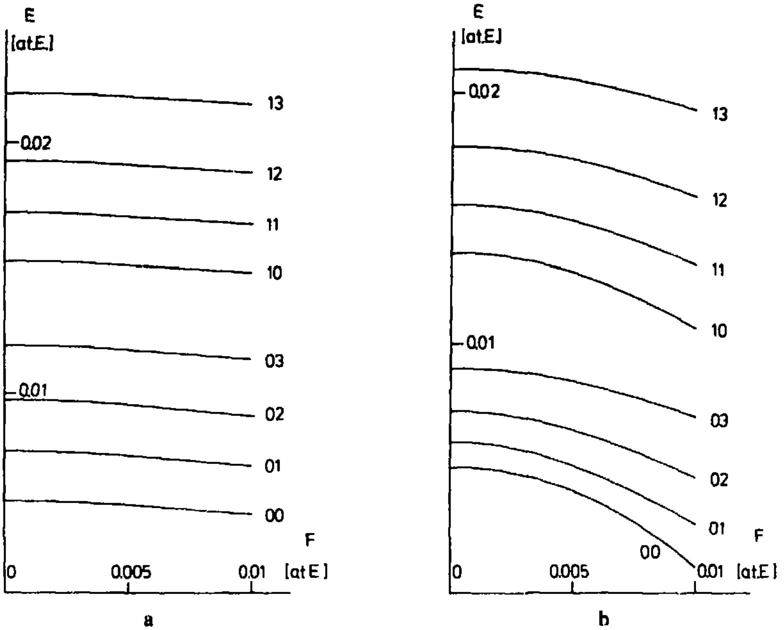

Fig. 7. a Termschema für das System $H^+ \ldots Cl^- \ldots H^+ \ldots Cl^- \ldots H^+$. Die erste Quantenzahl bezieht sich auf die asymmetrische Schwingung, die zweite Quantenzahl bezieht sich auf die symmetrische Schwingung. b Termschema für das System $H \ldots Cl^- \ldots H^+ \ldots Cl^- \ldots H$

auf, die für steigendes k wachsen. Simuliert man eine Energiematrix, in der die Diagonalglieder proportional k sind und die Nichtdiagonalglieder benachbarter Indizes proportional $\sqrt{k+1}$ gehen, so kann der Termverlauf in Fig. 7b wiedergegeben werden.

Die Entwicklungskoeffizienten der Schwingungszustände zeigen, daß die Begriffe „symmetrische“ und „asymmetrische“ Schwingung, die nur in der harmonischen Näherung streng gültig sind, nicht mehr ganz zutreffend sind. Trotzdem lassen sich auf Grund dominierender Entwicklungskoeffizienten diese Begriffe noch sinnvoll anwenden.

2. IR-*Übergänge*

Wie schon auf Grund des Termschemas zu erwarten ist, gibt es im System $H^+ \ldots Cl^- \ldots H^+ \ldots Cl^- \ldots H^+$ nur einen intensiven Dipolübergang, nämlich den fundamentalen Übergang 00–10, der bei 2098 cm^{-1} liegt (Fig. 8a). Wächst das elektrische Feld auf $5 \cdot 10^7$ V/cm an, so verschiebt sich die Frequenz des Übergangs nur geringfügig nach 2133 cm^{-1}, wobei sich die Intensität kaum ändert. Die Intensität des fundamentalen Dipolüberganges ist temperaturabhängig, was jedoch im Experiment nicht beobachtet werden kann, weil im selben Maße, wie die Intensität des Überganges 00–10 mit wachsender Temperatur sinkt, die Intensität des Überganges 01–11 steigt.

Im System $H\ldots Cl^-\ldots H^+\ldots Cl^-\ldots H$ treten eine ganze Reihe intensiver Dipolübergänge auf (Fig. 8b). Dominierend ist wieder der fundamentale Übergang 00–10, der aber im Vergleich zum vorhergehenden Fall eine viermal stärkere Intensität hat und sich bei einem Feld von $5\cdot 10^7$ V/cm von 1879 cm^{-1} nach 2100 cm^{-1} verschiebt, wobei dieser Übergang noch intensiver wird. Gleichzeitig gibt es intensive kopplungsbedingte Übergänge, die mit steigender Feldstärke an Intensität verlieren. Alle Übergangsintensitäten sind stark temperaturabhängig. Der verschiedene Gang der Intensitäten mit der Temperatur wirkt auch hier ausgleichend, so daß insgesamt keine merkliche Temperaturabhängigkeit vorliegt. Bei einer Variation der elektrischen Feldstärke von 0 bis $5\cdot 10^7$ V/cm überstreichen die Übergänge einen Frequenzbereich von 1600–2700 cm^{-1}. Die Frequenzen und Übergangsintensitäten in Abhängigkeit von der elektrischen Feldstärke und von der Temperatur sind in Tab. 3 aufgeführt.

Tab. 3a Frequenzen ν_{ij} und relative Absorptionsintensitäten I_{ij} für das System $H^+\ldots Cl^-\ldots H^+\ldots Cl^-\ldots H^+$ (I: Fundamentale Übergänge der asymmetrischen Schwingung; II: Kopplungsbedingte Übergänge)

Übergang		$F = 0$					$F = 5{,}14\cdot 10^7$ V/cm				
		ν_{ij}	I_{ij}				ν_{ij}	I_{ij}			
		[cm^{-1}]	100 K	200 K	300 °K	400 K	[cm^{-1}]	100 °K	200 °K	300 °K	400 K
I	00 10	2098	545	523	481	435	2133	544	522	478	433
	01 11	2089	1	21	55	85	2124	1	22	57	87
	02 12	2095	0	1	7	17	2134	0	1	7	18
	03 13	2193	0	0	1	3	2228	0	0	1	3
II	00 11	2531	11	10	9	8	2562	9	8	8	7

Tabelle 3b Frequenzen ν_{ij} und relative Absorptionsintensitäten I_{ij} für das System $H\ldots Cl^-\ldots H^+\ldots Cl^-\ldots H$. (I. Fundamentale Übergänge der asymmetrischen Schwingung; II: Kopplungsbedingte Übergänge; III: Übergänge der symmetrischen Schwingung)

Übergang		$F = 0$					$F = 5{,}14\cdot 10^7$ V/cm				
		ν_{ij}	I_{ij}				ν_{ij}	I_{ij}			
		[cm^{-1}]	100 K	200 K	300 K	400 °K	[cm^{-1}]	100 °K	200 K	300 K	400 °K
I	00 10	1879	1881	1585	1342	1172	2100	2938	2755	2478	2222
	01 11	2083	54	222	319	362	2285	13	175	385	541
	02 12	2325	2	49	132	206	2474	0	9	51	117
	03 13	2620	0	4	27	66	2704	0	0	4	17
II	00-11	2303	948	799	676	591	2659	45	42	38	34
	00-12	2809	37	31	26	23	3263	0	0	0	0
	01 10	1658	41	169	243	276	1725	0	4	8	11
	01 12	2589	25	101	145	165	2888	0	5	12	17
	02 10	1394	0	3	8	13	1310	0	0	0	0
	02 11	1818	1	15	40	63	1870	0	0	2	5
	02 13	3001	0	5	12	19	3236	0	0	1	2
III	00-01	221	0	0	0	0	375	17	16	14	13
	00-02	485	0	0	0	0	789	4	4	3	3
	00 03	866	0	0	0	0	1322	2	2	2	1

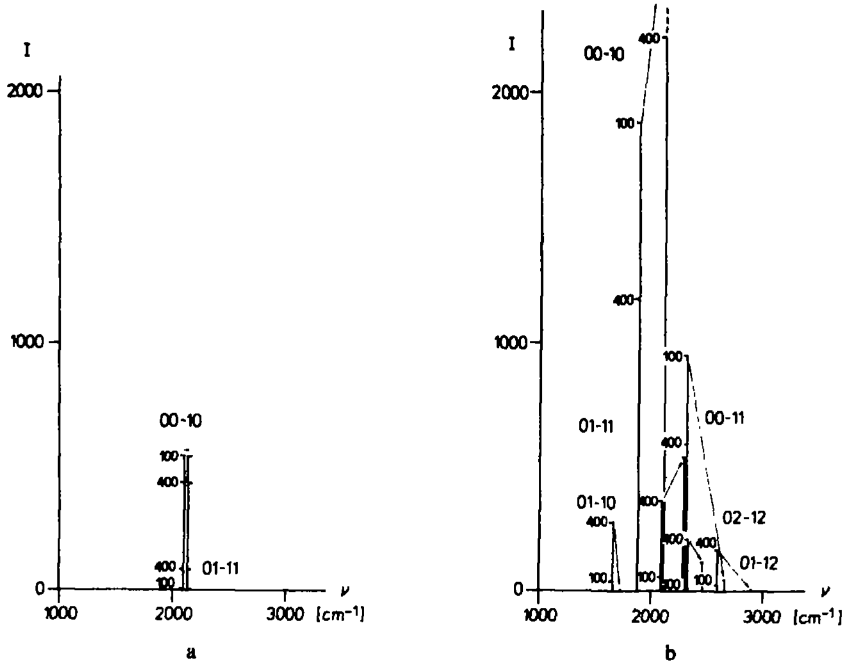

Fig. 8. a Relative Absorptionsintensitäten I_{ij} der IR-Übergänge im System $H^+ \ldots Cl^- \ldots H^+ \ldots Cl^- \ldots H^+$ für die Feldstärken 0 und $5{,}14 \cdot 10^7$ V/cm (0.01 at.E.) – durch Pfeile gekennzeichnet – für die Temperaturen 100 und 400 K. b Relative Absorptionsintensitäten I_{ij} der IR-Übergänge im System $H \ldots Cl^- \ldots H^+ \ldots Cl^- \ldots H$ für die Feldstärken 0 und $5{,}14 \cdot 10^7$ V/cm (0.01 at.E.) durch Pfeile gekennzeichnet für die Temperaturen 100 und 400 K

3. Raman-Übergänge

Der Raman-Effekt war bis jetzt für quantenchemische Berechnungen unzugänglich. Der Grund dafür ist darin zu sehen, daß neben einer Energiefläche für die Kernbewegung die Polarisierbarkeitstensorfläche zur Berechnung der Schwingungs-Raman-Übergänge nötig ist, was eine große Anzahl von Einzelrechnungen zur Folge hätte.

Für symmetrische Wasserstoffbrücken der Form A...H...A sind die Schwingungs-Raman-Übergänge zur direkten Bestimmung der Frequenzen der symmetrischen Schwingung von Bedeutung, da diese Schwingungen keine IR-Aktivität aufweisen. Unter gewissen Bedingungen ist es möglich, für Wasserstoffbrückensysteme Schwingungs-Raman-Übergänge mit minimalem rechnerischen Aufwand zu bestimmen. Diese Bedingungen lauten:

1. Der Polarisierbarkeitstensor hat extreme Excentrizität, das heißt, die Polarisierbarkeit in Brückenrichtung ist dominierend.

2. Die Separation der Schrödingergleichung bezüglich der symmetrischen und der asymmetrischen linearen Schwingung ist wegen $\omega_a \gg \omega_s$ möglich und wirkt sich nicht wesentlich auf das induzierte Dipolmoment aus.

Beide Bedingungen sind bei den hier behandelten Fällen erfüllt. Die Bedingung 1 besagt, daß während der Schwingung die Form des Polarisierbarkeitstensors erhalten bleibt, so daß die eindimensionale Behandlung der Raman-Übergänge möglich ist. Die Bedingung 2 gestattet es, die symmetrische Schwingung ungekoppelt mit der Protonbewegung zu behandeln und für verschiedene A...A-Abstände die Polarisierbarkeit zu berechnen. Die Polarisierbarkeit kann bei Wasserstoffbrücken bezüglich des A...A-Abstandes stark variieren, was eine extrem starke Schwingungs-Raman-Aktivität zur Folge hat [6]. Die Frequenzen der $Cl^-...Cl^-$ Schwingungen, sowie die zugehörigen relativen Ramanintensitäten sind in Tab. 4 aufgeführt. Die Frequenzen I, die mit Hilfe eines eindimensionalen Potentials bestimmt wurden, zeigen den erwarteten Gang, der durch die Anharmonizität $a_{03}y^3$ bedingt ist. Die Frequenzen II wurden unter Berücksichtigung der Ankopplung der asymmetrischen Schwingung berechnet, wobei der Term $a_{21}x^2y$ in der potentiellen Energie Frequenzänderungen bezüglich der eindimensionalen Behandlung hervorruft, was in 1. bereits diskutiert wurde. Für das System $H^+...Cl^-...H^+...Cl^-...H^+$, beziehungsweise für $H...Cl^-...H^+...Cl^-...H$, wurden die Polarisierbarkeitsoperatoren (6) zur Berechnung der Raman-Intensitäten verwendet, die nach Division durch F im einzelnen folgende Gestalt haben:

$$\alpha(y) = 11{,}840 + 16{,}475\,y + 11{,}625\,y^2$$

beziehungsweise

$$-\alpha(y) = 54{,}970 + 108{,}450\,y + 153{,}750\,y^2\,.$$

Die Variable y bedeutet die Änderung des $Cl^-...Cl^-$-Abstandes bezüglich der Gleichgewichtslage, wobei atomare Einheiten zu verwenden sind.

Die Intensitäten sind auf die Grundschwingung des ersten Systems bezogen. Beim Vergleich der relativen Intensitäten für die beiden Wasserstoffbrückensysteme fällt auf, daß die hohe Polarisierbarkeit in Brückenrichtung eine hohe Raman-Aktivität bewirkt. Die Polarisierbarkeit des ersten Systems ist von der Größenordnung der üblichen Elektronenpolarisierbarkeiten, so daß der Tab. 4 entnommen werden kann, daß bei symmetrischen Wasserstoffbrückensystemen die Raman-Aktivität der symmetrischen Schwingung um zwei Zehnerpotenzen stärker sein kann als bei Molekülen mit ausgeprägten Valenzbindungen.

Tabelle 4 Frequenzen und relative Raman-Intensitäten der $Cl^-...Cl^-$-Schwingungen (I: eindimensionale Behandlung; II: zweidimensionale Behandlung)

	$H^+...Cl^-...H^+...Cl^-...H^+$	
	Frequenz [cm^{-1}]	Relat. Raman-Intens.
Grundschwingung	447	1,0
1. Oberschwingung	892	0,07889
2 Oberschwingung	1336	0,00178

	$H...Cl^-...H^+...Cl^-...H$		
	Frequenz [cm^{-1}]		Relat. Raman-Intens.
	I	II	
Grundschwingung	237	221	5,14968
1. Oberschwingung	473	485	4,79458
2. Oberschwingung	707	866	0,22878

4. Vergleich mit dem Experiment

Wie bereits in der Einführung erwähnt, beobachtet man bei wäßriger Imidazollösung für einen Protonierungsgrad von über 100% ein IR-Kontinuum von 2600 cm^{-1} bis zu den kleinsten beobachtbaren Frequenzen (Fig. 1)[2]. Das System $H...Cl^-...H^+...Cl^-...H$ besitzt nach den hier diskutierten Rechenergebnissen ein IR-Kontinuum zwischen 2700 und 1600 cm^{-1}. Beim Vergleich von Fig. 8b und Fig. 1 stellt man fest, daß mit dem in dieser Arbeit verwendeten Mechanismus das IR-Kontinuum offensichtlich erklärt und auch quantitativ beschrieben werden kann. Die wesentlichen Gesichtspunkte sollen noch einmal genannt werden:

1. Die Modellsubstanz $H...Cl^-...H^+...Cl^-...H$ eignet sich gut zur Beschreibung der Vorgänge in wäßriger Imidazollösung bei über 100% Protonierung, wenn man sich auf den IR-Kontinuumsbereich 2700–1600 cm^{-1} beschränkt, der nach Fig. 1 als besonders glatt verlaufende Intensitätskurve auffällt.
2. Zur Beschreibung des IR-Kontinuums für den in 1. genannten Bereich reicht eine zweidimensionale Behandlung aus, wobei die Kopplung der symmetrischen und der asymmetrischen Brückenschwingung Ursache für das Auftreten zahlreicher IR-Übergänge ist.
3. Mitentscheidend für das Zustandekommen eines IR-Kontinuums ist ein gewisser Feldstärkebereich, der durch die Ionenfelder der Umgebung verursacht wird.

Der Verlauf der Intensitätskurven in Fig. 1[2] ist im Bereich kleinerer Frequenzen als 1600 cm^{-1} auffallend strukturiert. Diese Banden rühren von Schwingungen benachbarter Systeme her, die mit denen der H-Brücke mehr oder weniger stark gekoppelt sind. Beispielsweise liegt bei 1588 cm^{-1} eine Ringschwingung des Imidazolringes, während bei 1180 cm^{-1} die NH-Winkelschwingung in Ringebene liegt [2]. Der Intensitätsverlauf in diesem Frequenzbereich ist allerdings

belle 5. Berechnete Eigenschaften von HCl und von $Cl^-...H^+...Cl^-$-Brücken (gemessene Werte in Klamme

Cl		$H^+...Cl^-...H^+...$ $...Cl^-...H^+$	$Cl^-...H^+...Cl^-$	$H...Cl^-...H^+...$ $...Cl^-...H$	$Cl^-...H^+...Cl^-$ in Kristallen [1
Cl: 1,345 (1,275)	Cl ...Cl [Å]	3,109	3,155	3,532	(3,16)
3158	ω_s	447	483	221	(210– 240)
(2886)	ω_a	2098	2133	1879	(730–1660)
	ω_b [cm^{-1}]		1061		(1050–1185)
2635,536	ϱ_{Cl}	2634,368	2634,574	2636,420	
0,141	ϱ_H [at.E.]	0,073	0,080	0,110	
	α_0 $\left[\begin{matrix}10^{-24}\\ cm^3\end{matrix}\right]$	1,89	2,21	11,30	
μ: 1,12 D (1,07)					

---

[2] Siehe Fußnote 1.

schon vor der Ausbildung symmetrischer $Cl^-...H^+...Cl^-$-Brücken deutlich erkennbar und ist deshalb für den Nachweis dieser H-Brücken unbedeutend.

Zum Vergleich der berechneten Eigenschaften der $Cl^-...H^+...Cl^-$-Brücken mit Messungen am Kristall sind die wichtigsten Ergebnisse in Tab. 5 zusammengefaßt. Neben dem bereits erwähnten System $H^+...Cl^-...H^+...Cl^-...H^+$ wurde auch noch die freie $Cl^-...H^+...Cl^-$-Brücke berechnet. Auffallend ist die Ähnlichkeit der berechneten Eigenschaften dieser beiden Systeme. Vergleicht man die berechneten Eigenschaften mit an Kristallen gemessenen Werten, so stellt man nur für den $Cl^-...Cl^-$-Abstand und für die Winkelschwingung ω_b gute Übereinstimmung fest [13]. Für die anderen beiden Eigenschwingungen ist ein Vergleich nicht gerechtfertigt, denn einerseits hängt insbesondere die Frequenz der asymmetrischen Schwingung stark von der Art der Kationen des Kristalls ab, während für die symmetrische Schwingung nur in Einzelfällen eine IR-Aktivität beobachtet werden kann, was dann auf eine unsymmetrische Lage des Brückenprotons schließen läßt.

Literatur

1. Seßler, W., Zundel, G.: Z. physik. Chem. **79**, 180 (1972).
2 Zundel, G., Muehlinghaus, J.: Z. Naturforsch. **26**b, 546 (1971).
3. Swanstrøm, P., Janoschek, R., Preuß, H.: Int. J. quant. Chemistry **III**, 115 (1969).
4. Janoschek, R., Diercksen, G., Preuß, H.: Int. J. quant. Chemistry **II**, 159 (1968).
5. Ibers, J. A.: J. chem. Physics **41**, 25 (1964)
6. Janoschek, R., Weidemann, E. G., Pfeiffer, H., Zundel, G.: J. Amer. Chem. Soc. **94**, 2387 (1972).
7. Janoschek, R., Weidemann, E. G., Zundel, G.: Trans. Faraday Soc. (im Druck).
8. Bertie, J. E., Millen, D. J.: J. chem. Soc. 514 (1965).
9 Singh, T. R., Wood, J. L.: J. chem. Physics **48**, 4567 (1968).
10 Herzberg, G.: Spectra of diatomic molecules. New York: D. van Nostrand Comp. 1961
11. McClellan, A. L.: *Tables of experimental dipole moments. San Francisco: Freeman and Co. 1963.*
12 Richards, W. G., Walker, T. E. H., Hinkley, R. K.: A bibliography of *ab initio* molecular wave functions. Oxford Science Research Papers 1971
13. Nibler, J. W., Pimentel, G. C.: J. chem. Physics **47**, 710 (1967).

Dr. R. Janoschek
Institut für Theoretische Chemie
der Universität Stuttgart
D-7000 Stuttgart 1
Relenbergstr. 32
Bundesrepublik Deutschland

Theoret. chim. Acta (Berl.) 29, 75—83 (1973)
© by Springer-Verlag 1973

Local Orbitals for Bonding in Ethane

John L. Nelson and Arthur A. Frost
Department of Chemistry, Northwestern University, Evanston, Illinois 60201

Received August 8, 1972/November 13, 1972

An extension of the FSGO model is used to construct local bonding orbitals for ethane. These improved functions provide for a more accurate description of the internal rotational barrier in ethane, while retaining the computational simplicity and intuitive nature of the simple FSGO model.

Eine Erweiterung des FSGO-Modells wird für die Konstruktion lokalisierter Bindungsorbitale bei Äthan angewendet. Die verbesserten Funktionen vermitteln eine genauere Beschreibung der inneren Rotationsbarriere in Äthan; die einfache Berechnungsweise und die intuitive Natur des ursprünglichen einfachen FSGO-Modells bleiben jedoch erhalten.

Une extension du mode FSGO est utilisée pour construire les orbitales liantes localisées de l'éthane Ces nouvelles functions donnent une description plus exacte de la barriere de rotation interne de l'éthane, tout en retenant la simplicité de calcul et la nature intuitive du model FSGO original.

Introduction

Floating orbitals (orbitals not constrained to be centered on nuclei) have been used for many years as basis functions for quantum mechanical calculations on molecules. Early work [1, 2] and some more recent investigations [3] have utilized Slater type orbitals which were allowed to float. However, the use of floating exponential functions have the disadvantage of putting cusps in regions between nuclei. Floating gaussian functions were proposed and developed by other investigators in the form of lobe functions (as opposed to the cartesian gaussian type functions) [4, 5]. More in the spirit of the earlier calculations, an attempt was made to use floating gaussians in a valence bond calculation on H_2 [6]. Also attempts have been made to augment atomic orbital basis sets with floating gaussian functions [7–9]. These investigations found that floating functions can be very efficient for obtaining polarization effects and for building-up charge in the bonding region.

Several investigators [10–14] have developed methods where the concept of atomic orbitals is abandoned entirely in favor of floating orbitals. In particular a technique was developed [10] (the Floating Spherical Gaussian Orbitals Model – FSGO) using an absolute minimum basis set, where each orbital is doubly-occupied. As currently applied, the model has been used to predict the electronic and geometric structure of singlet ground states of molecules with local orbitals without the use of any arbitrary or semiempirical parameters. The local orbitals were constructed by using single normalized spherical Gaussian functions

$$\Phi(\vec{r}-\vec{R}_i)=\left(\frac{2}{\pi\varrho_i^2}\right)^{3/4}\exp[(\vec{r}-\vec{R}_i)^2/\varrho_i^2]$$

with orbital radius, ϱ_i, and position, R_i. A single Slater determinant represents the total electronic wave function. If S is the overlap matrix of the set of non-orthogonal localized orbitals Φ_i and $T=S^{-1}$, then the energy expression for a molecule is

$$E=2\sum_{j,k}(j|k)\,T_{jk}+\sum_{k,l,p,q}(kl|pq)\,[2T_{kl}\,T_{pq}-T_{kp}\,T_{lq}]$$

where

$$(j|k)=\int\Phi_j\,h\,\Phi_k\,dv\ (h=\text{on-electron operator})$$

and

$$(kl|pq)=\int\Phi_k(1)\,\Phi_l(1)\,(1/r_{12})\,\Phi_p(2)\,\Phi_q(2)\,dv_1\,dv_2\,.$$

The energy is minimized by a direct search procedure with respect to all parameters: orbital radii, ϱ_1, orbital positions, $\vec{R}_i$, are nuclear positions. (Numerical difficulties have forced the inter-orbital distances for π-bonds and lone pair orbitals to be held fixed.)

In all previous work each double-occupied orbital has been constructed from a single gaussian function (SG), or at most a linear combination of two concentric gaussians (concentric double gaussian - CDG) [15]. In light of the recent renewed interest in floating orbitals, it was decided to make an extensive investigation of an extended FSGO model. The orbitals for these calculations are made up of linear combinations of up to four gaussians. (One should note here the difference between the FSGO orbitals, which are "local" orbitals, and the more commonly used "localized" orbitals, e.g., localized orbitals obtained from an Edmiston-Ruedenberg localization scheme. The localized orbital schemes start with diffuse canonical molecular orbitals, and transform them, via a unitary transformation, to localized orbitals. The FSGO orbitals are centered in a restricted region of space in their makeup, and are therefore orbitals local to that area.)

The first system to be investigated was the ethane molecule. This was done with the idea of improving upon the description given by the simple FSGO model. In particular the simple FSGO predicts a rotational barrier of 5.7 kcal/mole (concentric double gaussians give 5.0 kcal/mole), compared with an experimental value of 3.0 kcal/mole [16]. The idea was to obtain basis functions from simple systems and then transfer them to ethane. In particular methane and a "simplified" ethane molecule were used to develop the basis functions.

Other models have been developed for transferring bonding functions to "large" molecules. In particular, Christoffersen and coworkers [11] have developed a modification of the simple FSGO model to obtain a basis set for such calculations. The problem of optimizing the wave function for changes in molecular environment is handled via an SCF-MO procedure in Christoffersen's FSGO model, abandoning the concept of local orbitals. The calculations described in this paper retain the concept of non-orthogonal local orbitals, but optimize only the linear combination coefficients (a procedure borrowed from the SCF-MO method). (The effect of assuming local orbitals vs. the more general SCF-MO procedure was investigated, vide infra.)

Procedure

The orbitals necessary for ethane are: inner shells, C–H bonding orbitals, and C–C bonding orbitals.

Tests were made on methane with single (SG), double (DG), and triple (TG) gaussian inner shells. The nuclear geometry, and all orbital radii and orbital positions were optimized.

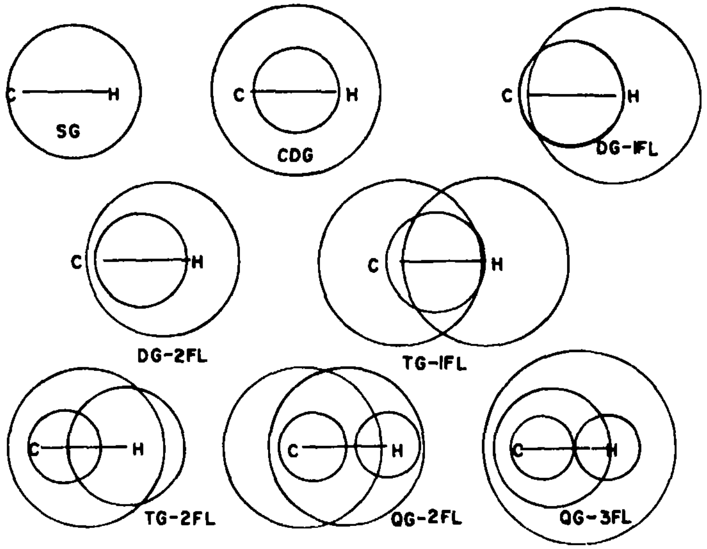

Fig. 1. C–H Bonding functions (Circle size proportional to orbital radius)

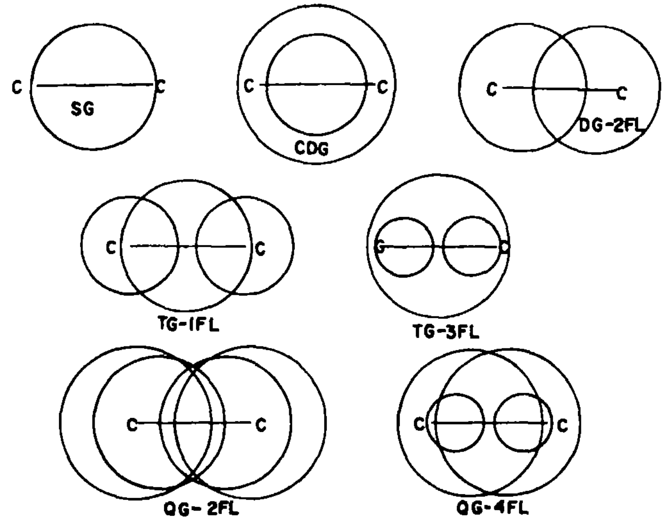

Fig. 2. C–C Bonding functions (Circle size proportional to orbital radius)

The C-H bonding orbitals were likewise constructed from calculations on methane. The various basis sets that were used are described in Fig. 1. A DG was used for the inner shell in all cases, and the orbital radii, orbital positions, and nuclear geometry were all optimized. The idea of using some floating and some fixed gaussians, either centered on the proton or on the carbon nucleus, was also investigated. [It was thought that the use of a gaussian on the proton (to help build a cusp) or on the carbon (to simulate the effect of a 2*s* atomic orbital) was reasonable from a chemical point of view.] If fixing the gaussian did not significantly affect the results of the calculation (compared to the same calculation where the constraint was removed) then using these fixed gaussians would provide increased efficiency due to the decrease in the number of parameters.

The C-C bonding orbitals (Fig. 2) were obtained from the ethane molecule, with SG everywhere except for the inner shells (DG) and for the C–C bond orbital itself. Again an attempt was made to fix some of the gaussians on the carbon nuclei.

The inner shell orbitals and the C-H and C–C bonding functions were then transferred to ethane with only linear combination coefficient optimization. Nuclear geometry was held fixed to that of Clementi and Davis [17], and orbital radii and positions fixed from the calculations on the simpler systems. (For some of the simpler orbital schemes full optimization on ethane were performed.) Both the staggered and eclipsed conformations were investigated, assuming rigid rotation [18].

Results

While the inner shell orbitals have little effect on the geometry, the energy is strongly dependent upon their form. (Table 1 shows results for methane with various inner shells.) A large decrease in energy is obtained from SG to DG inner shells. Compared to this decrease, adding a third gaussian improved the energy relatively slightly. It was also found that orbital and nuclear parameters were unchanged as the inner shell was improved. It was decided to use the DG inner shell representation in all further calculations - as it appeared that little was to be gained by using the TG representation. The lack of importance of the inner shell has been pointed out in several recent papers [19, 20]. In particular Hehre *et al.* [19] found that going to a better form for the inner shells did not affect any of the chemically important properties (geometry, relative energies).

The results for the C-H bonding orbitals appear in Table 2. The following comments are applicable to this data. (1) Fixing an orbital of the DG set on the proton (DG-1 FL, double gaussian with one floating gaussian) is too restrictive, as the elimination of this constraint (DG-2 FL) gives a much different result. (2) Fixing one gaussian on the proton with a TG set (TG-2 FL) appears to be a reasonable restriction - as it differs very little from the result when the constraint is removed. With this in mind, it was assumed that the quadruple gaussian with no gaussians fixed (QG-4 FL) would be very nearly the same as that with one orbital fixed (QG-3 FL), and this simpler set was used in place of the more complex one. (3) In all cases where an attempt was made to fix one gaussian on the carbon (TG-1 FL, QG-2 FL), results were very different from the cases without the

Table 1. Inner shell orbitals from CH_4

Orbital type				
Inner shell	SG	DG	DG	TG
C–H bond	SG	SG	CDG	CDG
Inner shell				
ϱ_1(a.u.)	0.328	0.148	0.148	0.074
C_1	1.0	0.267	0.267	0.056
ϱ_2		0.389	0.389	0.193
C_2		0.830	0.719	0.365
ϱ_3				0.441
C_3				0.707
C–H orbital				
ϱ_1	1.694	1.698	1.174	1.161
C_1	1.0	1.0	0.338	0.329
X_1[a]	0.598	0.593	0.405	
ϱ_2			2.188	2.178
C_2			0.719	0.727
X_2[a]			0.537	0.528
C–H bond length (Å)	1.110	1.115	1.040	1.036
$-E$ (a.u.)	33.992	38.246	38.484	39.250

[a] X is the ratio of (carbon to orbital distance)/(C–H bond length).

constraint, so these basis sets were regarded as unsatisfactory. (4) It would appear that at least a TG is necessary to give a resonable description of the electron density around the proton. Only with TG-2 FL, TG-3 FL, and QG-3 FL was a cusp-like condition developed at the proton.

The results for the C–C bonding function are given in Table 3. One can make the following observations about this data. (1) The DG-2 FL set is judged to be unsatisfactory on the grounds that it gives a very poor approximation to the C–C bond length. One should be careful about using basis sets which lead to poor geometrical predictions. To try to circumvent this problem by attempting to calculate a rotational barrier with idealized geometry, for example, is a very unrealistic procedure. (2) As with the C–H bonding functions, fixing gaussians on the carbon nuclei (TG-1 FL, and QG-2 FL) gives results very different from the cases where the constraints are removed. (3) Three to four gaussians are necessary for a reasonable description of the C–C bond. Only then does one begin to obtain a cylindrical charge distribution along the C–C bond.

Referring to Fig. 3 of the electron density along the C–H bond, only the TG-2 FL and QG-3 FL bond functions give the correct qualitative picture of a relative minimum near the midpoint of the bond and a "cusp" on the proton. (Densities for the CDG, DG-2 FL, and TG-1 FL resemble those of the SG and DG-1 FL.) Likewise in Fig. 4 (the total electron density along the C–C bond in ethane), only the TG-3 FL and QG-4 FL bond functions approach the correct picture of a relative minimum at the midpoint of the C–C bond. (CDG, TG-1 FL, and QG-2 FL resemble SG and DG-2 FL plots.)

Table 2. C–H Bonding orbitals from CH_4 [a]

	SG	CDG	DG-1 FL	DG-2 FL	TG-1 FL	TG-2 FL	TG-3 FL	QG-2 FL	QG-3 FL
ϱ_1(a.u.)	1.694	1.174	1.339	0.811	1.924	0.941	0.938	2.104	0.709
C_1	1.000	0.332	0.617	0.167	0.010	0.234	0.234	0.900	0.109
X_1 [b]	0.598	0.525	0.494	0.244	0.000	0.262	0.260	0.000	0.216
ϱ_2		2.192	2.264	1.870	1.335	2.097	2.096	0.899	1.551
C_2		0.724	0.465	0.901	0.605	0.793	0.794	0.051	0.489
X_2		0.525	1.000	0.612	0.492	0.524	0.526	0.111	0.355
ϱ_3					2.247	0.730	0.731	2.068	2.521
C_3					0.469	0.109	0.110	0.075	0.454
X_3					1.000	1.000	0.994	0.525	0.665
ϱ_4								0.756	0.752
C_4								0.011	0.104
X_4								1.000	1.000
R(C–H) (Å)	1.115	1.040	1.077	1.083	1.078	1.129	1.130	1.114	1.132
$-E$(a.u.)	38.24689	38.48489	38.48004	38.52158	38.47995 [c]	38.84232	38.84250	38.87572	38.88746

[a] All calculations with DG inner shell.

[b] Ratio of (carbon to orbital distance)/(C–H distance).

[c] Apparently a local minimum.

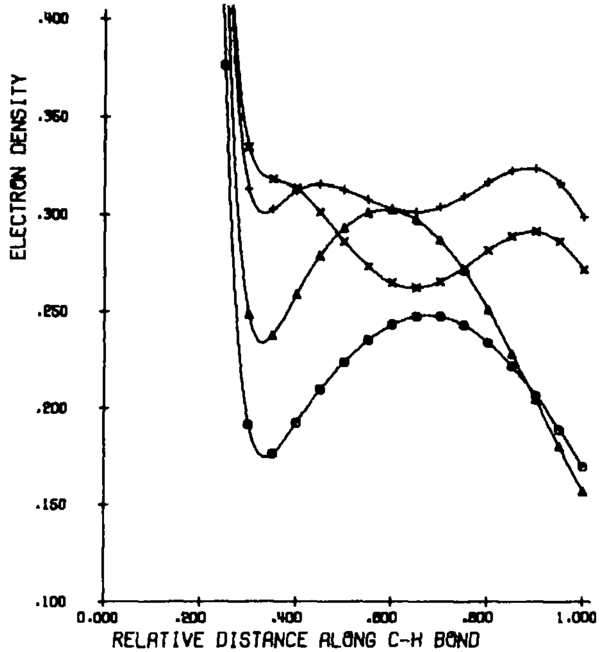

Fig. 3. Total electron density along C–H bond in methane for SG (○), DG-1 FL (△), TG-2 FL (+), and QG-3 FL (×)

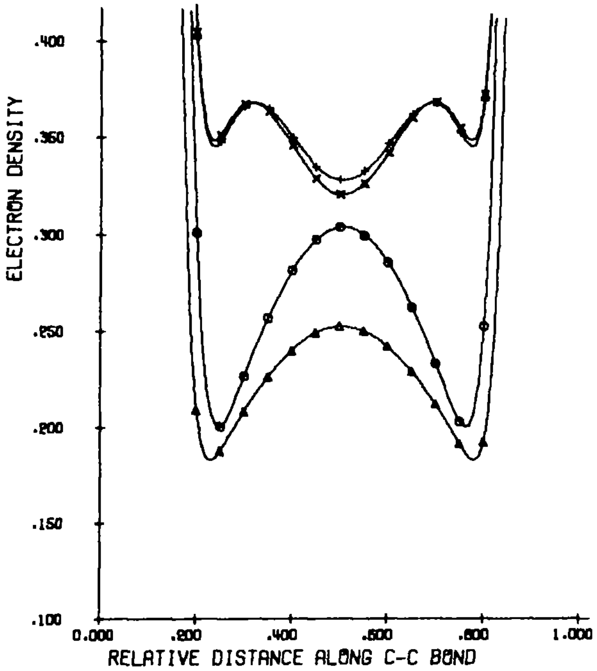

Fig. 4. Total electron density along C–C bond in ethane for SG (○), DG-2 FL (△), TG-3 FL (+), and QG-4 FL (×)

Table 3. C–C Bonding orbitals from C_2H_6 [a]

	SG	CGD	DG-2 FL	TG-1 FL	TG-3 FL	QG-2 FL	QG-4 FL
ϱ_1 (a.u.)	1.646	1.300	1.639	1.745	1.844	1.725	1.846
C_1	1.000	0.316	0.587	0.779	0.886	0.568	0.452
X_1 [b]	0.000	0.000	0.655	0.000	0.000	0.600	0.304
ϱ_2		2.020		1.382	0.741	1.959	0.740
C_2		0.740		0.169	0.110	$<10^{-8}$	0.116
X_2		0.000		1.000	0.562	1.000	0.561
R(C–C) (Å)	1.504	1.487	1.669	1.553	1.581	1.660	1.552

[a] SG C–H orbitals, and DG inner shells, except for CDG calculations where CDG everywhere. All calculations had only C–C geometry optimization, except for SG and CDG, where a full optimization was performed.

[b] X is relative distance from center of C–C bond. X = 0 at midpoint, X = 1 at carbon nucleus.

Table 4. Barrier to internal rotation in C_2H_6 from FSGO basis sets

Bonding type I.S.	C–C	Orbital C–H	-Energy (staggered) (a.u.)	Rotational barrier (kcal/mole)
DG [a]	SG	SG	75.5134	6.3
DG [a]	CDG	CDG	75.8620	5.0
DG	TG-3 FL	TG-2 FL	76.5070	3.7
DG	QG-4 FL	QG-3 FL	76.5633	4.0
DG	TG-3 FL	TG-2 FL (SCF)	76.8762	3.8
STO-3 G [b]			78.8623	3.3
Experimental [c]				

[a] Optimized geometry.

[b] Pople, J. A., Radom, L.: J. Amer. chem. Soc. 92, 4786 (1970).

[c] Lide, D. R.: J. chem. Physics 29, 1426 (1958).

The results for the rotational barrier calculations appear in Table 4. These results show that acceptable values for the rotational barrier in ethane are obtained with the extended FSGO functions. Values of 3.7–4.0 kcal/mole are given by the three and four gaussian extended FSGO basis sets.

To test the effect of the restriction of local orbitals, SCF–MO calculations (using POLYATOM II) [21] were performed on the staggered and eclipsed forms of ethane, using the DG (inner shell), TG-2 FL (C–H), and TG-3 FL (C–C) basis set. (All gaussians were treated as uncontracted orbitals, except for the DG inner shell gaussians which were contracted to a single orbital, with relative coefficients as found in the local orbital FSGO calculation.) The results (Table 4) show that while there is a considerable decrease in the total energy (0.37 a.u.), the rotational barrier is only very slightly affected (0.1 Kcal/mole).

Discussion

The results of these calculations indicate that an extended FSGO model can be used to obtain local bonding functions. The main advantages in using this type of function are that they are transferable, and that polarization effects can be accounted for with them. Other bond function approaches [22, 23] have been built upon an LCAO framework. The LCAO framework has the advantage of being less arbitrary in choosing basis functions (for example where the extended FSGO method assumed fixed orbital positions). However the extended FSGO basis set is much more adaptable for including polarization effects. It is also encouraging to note that the restriction to local orbitals does not seem to invalidate the results.

Work is continuing on developing computational procedures for handling the extended FSGO model and in the development of "bonding functions" for pi bonds and lone-pair orbitals.

Acknowledgements. Many helpful discussions were held with Klaus Mueller. We would also like to thank the referee for several helpful suggestions. This research was supported by a grant from the National Science Foundation. O. H. Crawford suggested the expression "local orbital" in order to differentiate from "localized orbital".

References

1. Gurnee, E. F., Magee, J. L.: J. chem. Physics **18**, 142 (1950).
2. Schull, H., Ebbing, D. D.: J. chem. Physics **28**, 866 (1958).
3. Adamov, M. N., Evarestov, R. A.: Chem. Physics Letters **3**, 726 (1969); **9**, 465 (1971).
4. Preuss, H.: Z. Naturforsch. **11** a, 823 (1956); **19** a, 1335 (1964); **20** a, 18, 21, 1290 (1965).
5. Whitten, J. L.: J. chem. Physics **44**, 359 (1966).
6. Reeves, C. M.: J. chem. Physics **39**, 1 (1963).
7. Rothenberg, S., Schaefer, H. F.: J. chem. Physics **54**, 2764 (1971).
8. Chu, S. Y.: Theoret. chim. Acta (Berl.) **25**, 200 (1972).
9. Russegger, P., Lischka, H., Schuster, P.: Chem. Physics Letters **12**, 392 (1971).
10. Nelson, J. L., Frost, A. A.: J. Amer. chem. Soc. **92**, 3727 (1972); Chem. Physics Letter **13**, 610 (1972); and references therein.
11. Christoffersen, R. E.: Advances in quant. Chemistry **6**, 333 (1972); and references therein.
12. Ford, B., Hall, G. G., Packer, J. C.: Int. J. quant. Chemistry IV, 533 (1970).
13. Van Duijnen, P. T., Cook, D. B.: Molecular Physics **21**, 475 (1971).
14. Barthelot, J. C., Durand, Ph.: Chem. Physics Letters **16**, 63 (1972).
15. Rouse, R. A., Frost, A. A.: J. chem. Physics **50**, 1705 (1969).
16. Lide, D. R.: J. chem. Physics **29**, 1426 (1958).
17. Clementi, E., Davis, D. R.: J. chem. Physics **45**, 2593 (1966).
18. Computational details. Calculations were performed on the CDC 6400 computer at Vogelback Computing Center, Northwestern University. The total time required for optimization of linear parameters for both staggered and eclipsed ethane with a DG/TG basis set was less than two minutes.
19. Hehre, W. J., Ditchfield, R., Pople, J. A.: J. chem. Physics **56**, 2257 (1972).
20. Johansen, H.: Theoret. chim. Acta (Berl.) **21**, 9 (1971).
21. Quantum chemistry program exchange, program number 199.
22. Hoyland, J. R.: J. Amer. chem. Soc. **90**, 2227 (1968); J. chem. Physics **50**, 473 (1969).
23. Letcher, J. H., Dunning, T. H.: J. chem. Physics **48**, 4538 (1968).

Prof. Dr. A. A. Frost
Northwestern University
Department of Chemistry
Evanston, Illinois 60201, USA

Theoret. chim. Acta (Berl.) 29, 85—91 (1973)
© by Springer-Verlag 1973

Atomic Wave Functions by Rotational Projections of Floating Orbitals

G. L. Bendazzoli, F. Bernardi, and C. Zauli

Istituto di Chimica Fisica e Spettroscopia, Università di Bologna,
Viale Risorgimento 4, I-40136 Bologna

P. Palmieri

Istituto Chimico "G. Ciamician", Via Selmi 2, I-40126 Bologna

Received August 23, 1972

Floating orbitals and the rotational projector operators defined by Percus and Rotenberg, are used to obtain approximate wavefunctions for the ground states of He-like ions and for the first excited ${}^1P$ state of helium.

Mit Hilfe von "Floating Orbitals" und Rotationsprojektionsoperatoren, wie sie von Percus und Rotenberg definiert worden sind, werden näherungsweise Wellenfunktionen für die Grundzustände von He-ähnlichen Ionen und für den ersten angeregten He-Zustand ${}^1P$ erhalten.

The present paper reports the results obtained with a simple procedure based on the idea of different orbitals for different spins [1] together with the "floating gaussian" technique [2], which is able to take into account part of the correlation energy. Some preliminary results obtained with this procedure were already reported for He [3]. Here the procedure is described in a more detailed way and results for He-like systems in their ground states and an application to an excited state of He, $(1s\,2p)\ {}^1P$ are given.

In the ground state of He-like atoms an easy way of introducing electron correlation, especially the angular correlation, is to displace the two space functions on opposite sides of the nucleus [3]. However this procedure involves two main difficulties: 1) a substantial loss in potential energy occurs as a result of taking away charge from the nucleus, and 2) the resulting wavefunction has no longer the required symmetry. As far as the first difficulty is concerned, a possible solution is to assume that the one-electron functions can be written as linear combination of the form

$$\varphi_i = \sum_k \lambda_k^i \varphi_k(\boldsymbol{r} - \boldsymbol{\delta}_k^i) \tag{1}$$

or more generally

$$\varphi_i = \int_0^\infty \lambda_i(\delta)\, \phi(\boldsymbol{r} - \boldsymbol{\delta})\, d\delta \tag{1a}$$

where $\phi_k(\mathbf{r}-\boldsymbol{\delta}_k^i)$ are orbitals centred at points, defined by the vectors $\boldsymbol{\delta}_k^i$, along an oriented line containing the nucleus and where λ_k^i and $|\delta_k^i|$ are taken as variational parameters. In the following we shall deal only with a discrete two-terms expansion, where one term is on the nucleus and the other at a distance δ_i:

$$\varphi_i(\mathbf{r}) = \phi_{i0}(\mathbf{r}) + \lambda_i \phi_{i1}(\mathbf{r}-\boldsymbol{\delta}_i) \tag{2}$$

As far as the lack the correct symmetry is concerned one can solve the difficulty by averaging the rotations of the impure state, with a suitable weight factor. This can be accomplished by the use of the formalism of rotational projectors introduced by Percus and Rotenberg [4] O_{JM}, defined by the following equation:

$$\begin{aligned} O_{JM}\Psi = \frac{2J+1}{8\pi^2} \iiint e^{iM(\phi+\chi)} \cos^{2M}(\Theta/2) \\ \cdot F[M-J, 1+M+J, 1; \sin^2(\Theta/2)]\, R_{\phi\theta\chi} S_{\phi\theta\chi}\, \Psi \sin\theta \, d\phi \, d\theta \, d\chi \end{aligned} \tag{3}$$

where Ψ is the impure state function and $O_{JM}\Psi$ is the corresponding projected wavefunction of definite angular momentum J and its z component M. In Eq. (3) the integration variables ϕ, θ, χ are Eulerian angles and R, S are rotation operators in the ordinary and spin space respectively. The calculation of the expectation value of the hamiltonian with the projected wavefunction can be greatly simplified since: 1) the hamiltonian operator commutes with the projector O_{JM} [5]. The expectation value of the energy thus becomes

$$\langle H \rangle = \frac{\langle O_{JM}\Psi | H | O_{JM}\Psi \rangle}{\langle O_{JM}\Psi | O_{JM}\Psi |} = \frac{\langle \Psi | H | O_{JM}\Psi \rangle}{\langle \Psi | O_{JM}\Psi \rangle} \tag{4}$$

2) the spin factor for singlet states is left unchanged by the projection; 3) the order of the integrations in Eq. (4) may be interchanged and one can integrate first over the space coordinates and then over the Eulerian angles ϕ, θ and χ; 4) when states with $M=0$ are considered, a significant simplification in the expression of the projector O_{JM} is obtained. In this case, as it has been pointed out in the previous paper [3], a suitable choice of the reference system for the Eulerian angles makes the integrations over the variables φ and χ easily performed, resulting in a constant factor.

Ground State

In this section we describe the results obtained for some He-like systems in their ground state ^1S. According to Eq. (2) the orbitals φ_i are taken to be linear combinations of two STO – 1s, the first at the nucleus and the second at distance δ_i from it. Therefore we will write the total (unnormalized) wavefunction in the form:

$$\begin{aligned} \Psi(\mathbf{r}_1, \mathbf{r}_2) = O_{00} A [(e^{-\zeta_1 r_1} + \lambda_1 e^{-\zeta_1' |\mathbf{r}_1 - \boldsymbol{\delta}_1|})(e^{-\zeta_2 r_2} + \lambda_2 e^{-\zeta_2' |\mathbf{r}_2 - \boldsymbol{\delta}_2|})] \\ \cdot [\alpha(1)\beta(2) - \beta(1)\alpha(2)] \end{aligned} \tag{5}$$

where O_{00} and A stand for rotational projector and antisymmetrizer respectively. If the ζ_i's, λ_i's and δ_i's are considered as adjustable parameters, function (5) contains as particular cases: 1) the uncorrelated single determinant for $\lambda_1 = \lambda_2 = 0$ and $\zeta_1 = \zeta_2$; 2) the conventional DODS approach of Hylleraas and Eckart [1] for $\lambda_1 = \lambda_2 = 0$ and $\zeta_1 \neq \zeta_2$. In our case the optimisation of variational parameters is performed after the projection, and when function (5) is optimized it corresponds to a restricted form of the Extended Hartree-Fock for He-like ions. Therefore one cannot expect to obtain from (5) the exact value of the energy, which requires, in that scheme, the use of hypercomplex spin orbitals [6]. It is easy to see that many centre integrals are needed for the computation of the energy in the present scheme. Therefore it was found convenient to expand each STO appearing in Eq. (5) as a linear combination of gaussian-type orbitals (GTO). A three term expansion according to McWeeny and Huzinaga [7] was considered adequate to approximate each STO for the present purposes. The optimisation of non-linear variational parameters was carried out by a simple modification of the procedure used by Roos *et al.* [8].

Table 1. Optimum values of variational parameters, computed total energy and correlation energy (a.u.) for H^-, He, Li^+

	H^-	He	Li^+
ζ_1	2.636	5.712	12.884
ζ'_1	0.372	2.086	3.290
δ_1	1.991	0.167	0.127
λ_1	21.831	11.348	20.187
ζ_2	3.768	3.547	6.831
ζ'_2	1.051	1.265	2.050
δ_2	− 0.550	− 0.601	− 0.201
λ_2	16.159	9.712	15.513
Total energy	− 0.51693	− 2.88780	− 7.26258
Correlat. energy	0.02910 (73%)	0.02613 (62%)	0.02618 (60%)
Exact energy [11]	− 0.52775	− 2.90372	− 7.27993
Radial limit [12]	− 0.51449	− 2.87903	− 7.25249
Best single ζ	− 0.4727	− 2.84765	− 7.22266
Conventional DODS [9]	− 0.5133	− 2.8757	− 7 2490

In Table 1 the computed total energies and correlation energies are reported together with optimum values of variational parameters. The comparison of total energies with the uncorrelated best-ζ single determinant and the DODS values of Shull and Löwdin [9], reported in the same Table 1, is satisfactory. The fraction of correlation energy here computed are beyond the limit of radial correlation. This means that, as expected, the procedure here proposed allows the introduction of a significant amount of angular correlation. In the case of

H^- the present results (-0.5169 a.u.) are better than the value (-0.5150 a.u.) computed by Banyard [10] by his configuration interaction-floating-orbital (CIFO) method. The wavefunction considered by this author is closely related to (5), buth with important differences. The CIFO function is a complete configuration interaction built from three 1s-STO, one of them centred on the nucleus, the other two being symmetrically placed at the two opposite sides of the nucleus itself. Thus the main differences between Banyard's and the present function can be summarized as follows: 1) function (5) has the correct spherical symmetry; 2) function (5) is equivalent to a restricted rather than to a complete CI; 3) the STO displaced from the nucleus are free to have different exponential factors and distances from the nucleus.

As far as the wavefunctions are concerned, qualitative information can be obtained by examining the shape of the two optimized orbitals for each system. In Fig. 1 are reported the sections of orbitals φ_1 and φ_2 for He in a plane containing the three centers of the STO's, together with the corresponding sections of the orbitals optimized by Shull and Löwdin in the conventional DODS scheme [9].

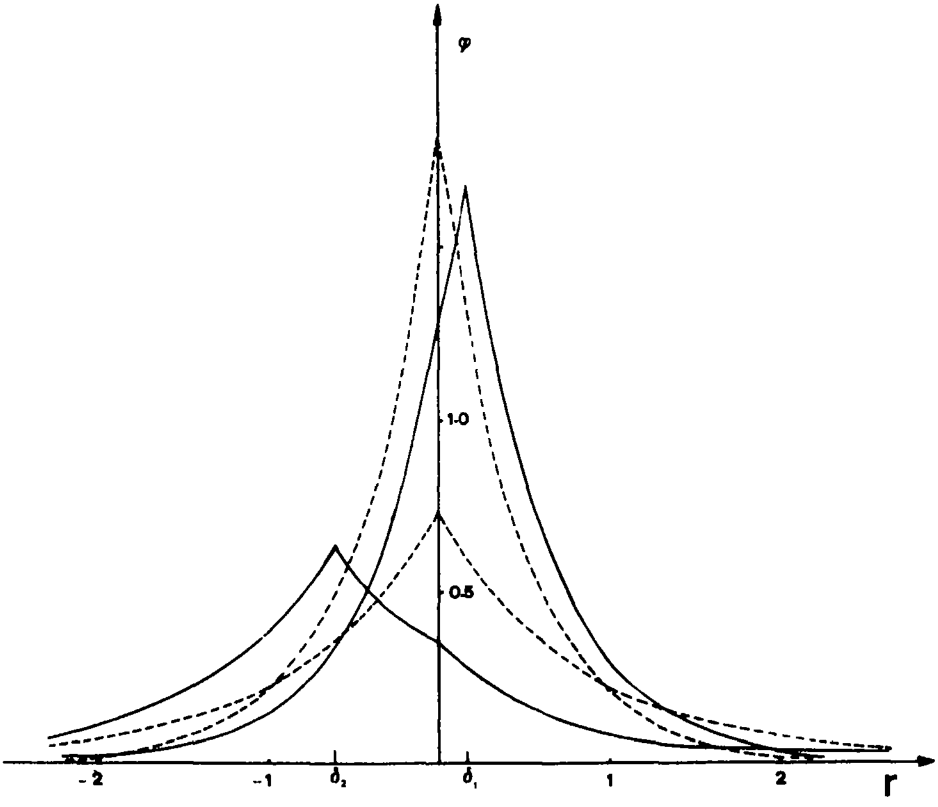

Fig. 1. Sections of the optimum orbitals in a plane containing the centers of the STO's, in case of He. Full lines refer to the orbitals described in this paper and dashed lines to the orbitals of Shull and Löwdin

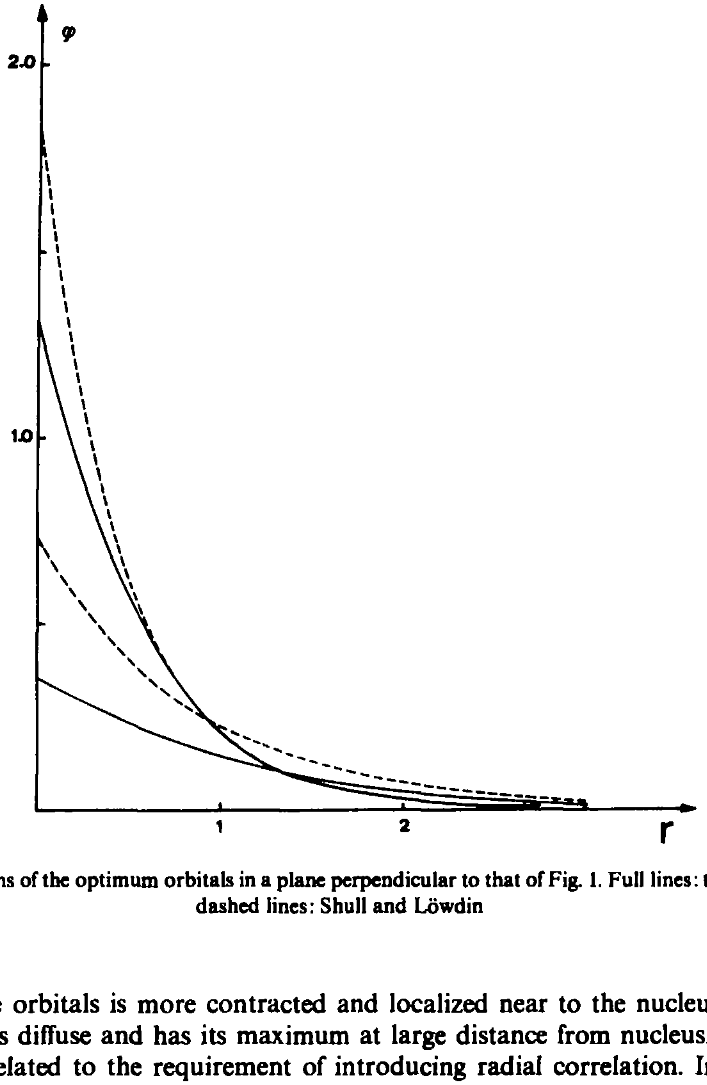

Fig. 2. Sections of the optimum orbitals in a plane perpendicular to that of Fig. 1. Full lines: this paper; dashed lines: Shull and Löwdin

One of the orbitals is more contracted and localized near to the nucleus, while the other is diffuse and has its maximum at large distance from nucleus. This is certainly related to the requirement of introducing radial correlation. In Fig. 2 are reported the sections of the same orbitals in the plane perpendicular to that of the previous figure and containing the nucleus. In this case the differences among the orbitals are less pronounced.

It should be pointed out that, relaxing the restriction that ϕ_0 and ϕ_1 in Eq. (2) are STO's, one can obtain better energies than those reported above. A simple example of such functions was obtained by arbitrarily putting in Eq. (2)

$$\begin{aligned} \varphi_1 &= \sum_{j=1}^{3} c_j \exp(-\alpha_j \eta_1 r^2) + \lambda_1 \sum_{j=4}^{5} c_j \exp[-\alpha_j \eta_1' (r-\delta_1)^2] \\ \varphi_2 &= \sum_{j=1}^{2} c_j \exp(-\alpha_j \eta_2 r^2) + \lambda_2 \sum_{j=3}^{5} c_j \exp[-\alpha_j \eta_2' (r-\delta_2)^2] \end{aligned} \qquad (6)$$

where the coefficients c_j and α_j are chosen in such a way as to give, for $\eta_i = \eta_i' = \lambda_i = 1$ and $\delta_i = 0$, a five terms gaussian expansion of the two "different orbitals for different spins" of Shull and Löwdin [9]. The λ, η and δ parameters were optimized for He and the corresponding minimum energy was found to be -2.89170 a.u. corresponding to the 71% of the correlation energy, to be compared with 62% reported in Table 1. The function defined by orbitals (6) could certainly be improved or extended. Unfortunately this problem appears to be complicate and brute force optimisation of many non linear parameters seems to be unavoidable. For these reasons it was decided not to pursue this approach further.

Application to Excited States

It follows from the previous discussion that the present method, in principle, can be applied to states of symmetry different from that of the ground state as well. To test the applicability of the method, we have computed the total energy of the ^1P state of He atom. The trial function used is again of the type (5), with the projector replaced by the appropriate one for this state, O_{10}. The 1s function centered on the nucleus has been approximated again by a three term gaussian expansion according to McWeeny [4] and Huzinaga [5], while the orbitals at the distance δ_i have been approximated by the following two-term expansion

$$\varphi_i = 0.82018 \exp[-0.131373(r-\delta_i)^2 \eta_i^2] + 0.274057 \exp[-0.852787(r-\delta_i)^2 \eta_i^2] \quad (7)$$

where η_i is a scaling parameter. This two-term expansion roughly simulates the radial part of a 2*p* Slater orbital. With this simple wave-function a total energy of -2.10768 a.u. has been obtained[1], which compares favourably with the experimental value of -2.12384 a.u. It must be underlined that the value computed here was obtained from an impure state function Ψ built on only with 1*s* Slater functions. Nevertheless the projected wavefunction $O_{10}\Psi$ can be considered, on the basis of the energy value obtained, a reasonably accurate wavefunction for ^1P state of He. The energy value could certainly be improved, using in the wavefunction orbitals of *p* type together with orbitals of *s* type. Here we wanted only to show that the method can be satisfactorily applied to states of symmetry different from that of the ground state and we believe that the computation just described fulfills this purpose.

Acknowledgments. The authors thank the CNR of Italy for financial support. The numerical computations were carried out on the CDC 6600 Computer of Bologna University.

References

1. Hylleraas, E. A.: Z. Physik **54**, 347 (1929); Eckart, C.: Physic. Rev. **36**, 878 (1930).
2. Gurnee, F. G., Magee, J. L.: J. chem. Physics **18**, 142 (1950); Hurley, A. C.: Proc. Roy. Soc. (London) A**226**, 170, 179, 193 (1954); Barker, R. S., Giddings, J. C., Eyring, H.: J. chem. Physics **23**, 344 (1955); Shull, H., Ebbing, D. D.: J. chem. Physics **28**, 866 (1958).

---

[1] The optimum parameters are:

$$\zeta_1 = 1.260; \quad \zeta_1' = 1.879; \quad \delta_1 = 0.010; \quad \lambda_1 = 0.968$$
$$\zeta_2 = 0.820; \quad \zeta_2' = 0.484; \quad \delta_2 = 2.692; \quad \lambda_2 = -1.134$$

3. Bendazzoli, G. L., Palmieri, P., Zauli, C.: Chem. Physics Letters **8**, 556 (1971).
4. Percus, J. K., Rotenberg, A.: J. math. Physics **3**, 928 (1962).
5. Lefebvre, R., Prat, R.: Chem. Physics Letters **1**, 388 (1967).
6. Prat, R. F., Lefebvre, R.: Int. J. quant. Chemistry 3, 503 (1969).
7. Huzinaga, S.: J. chem. Physics **42**, 1293 (1965).
8. Roos, B., Salez, C., Veillard, A., Clementi, E.: IBM Research note RJ518 (1968).
9. Shull, H., Löwdin, P. O.: J. chem. Physics **25**, 1035 (1956).
10. Banyard, K. E.: J. chem. Physics **44**, 4645 (1966); ibid. **48**, 2121 (1968).
11. Midtal, J.: Phys. Mat. Univ. Oslo **32** (1966).
12. Davis, H. L.: J. Chem. Physics **39**, 1827 (1963).

Dr. D. L. Bendazzoli
Istituto di Chimica Fisica e Spettroscopia
Università di Bologna
Viale Risorgimento 4
I-40136 Bologna, Italy

Theoret. chim. Acta (Berl.) 29, 93—96 (1973)
© by Springer-Verlag 1973

Relatio

Theoretical Investigations on the Solvation Process

III. STO Double-ζ SCF Calculations on the Hydrated Proton $H_5O_2^+$

Giuliano Alagona, Renzo Cimiraglia
Laboratorio di Chimica Quantistica ed Energetica Molecolare del CNR, Via Risorgimento 35,
56100 Pisa, Italy

Ugo Lamanna
Istituto di Chimica Analitica dell'Università, Bari, Italy

Received July 31, 1972/November 7, 1972

STO double-zeta SCF wavefunctions for various configurations of the $H_5O_2^+$ associate have been computed. Results are discussed and compared with other authors' similar calculations on gaussian bases.

An electrostatic picture of the monosolvation of H_3O^+ is proposed as a fairly satisfactory one.

In a previous paper of this series [1], hereafter referred to as I, a simple electrostatic procedure for obtaining a first order picture of the conformational energy of hydration adducts was tested on the water dimer, where the association energy is about 5 kcal/mole. In the present note we make a similar test on $H_3O^+ \cdot H_2O$ where the association energy is considerably larger, about 40 kcal/mole.

As in Paper I, the test is performed by comparing the results of the electrostatic procedure with a picture of the conformational energy obtained by "*ab initio*" SCF LCAO MO calculations on the whole associate.

In contrast with *I* the internal geometries of the partners are not kept fixed at the experimental ones because the association energy range does not allow one to neglect the hypothesis of sensible deformations.

All SCF calculations have been performed on a double-ζ STO basis set (ζ values for O in Ref. [2], for H in Ref. [3]). Such results may be used as a control of the compatibility of SCF geometry optimization via limited basis sets. There are, in fact, analogous investigations on the same associate relying on GTO basis sets of different complexity [4–6]. The essential information of the search for the best geometries is collected in Table 1.

The results on H_2O and H_3O^+ show that double-ζ STO basis sets give sufficiently correct geometries which compare well with the best calculations [7–8].

The optimized structure of $H_5O_2^+$ belongs to the D_{2d} symmetry group, i.e. it is linear with staggered terminal hydrogens, the other hydrogen lying at the molecular centre (see the model at the top of Fig. 1). The same disposition was found to be the optimum one also in Refs. [4–6]. Optimization of geometry was made in Ref. [6]: the best values quoted are $r_{OH} = 0.95$ Å, $r_{O-O} = 2.36$ Å, $\alpha = 115°$.

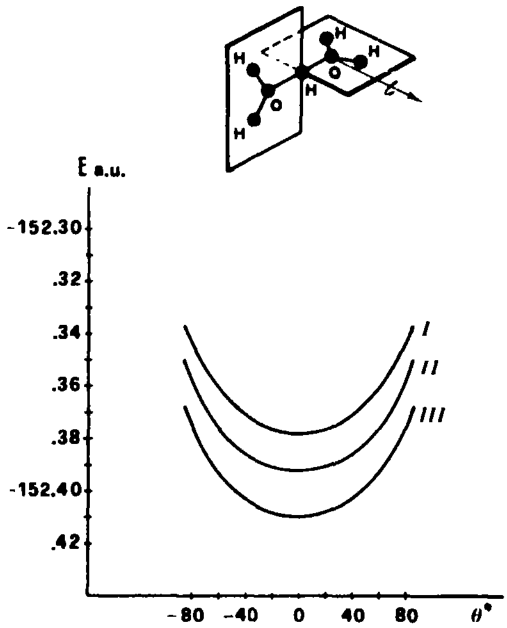

Fig. 1 Trend of the interaction energy for rotations of the HOH molecule, as shown at the top of the figure. The curves may be fitted by the following quartics (θ in radians, energy in atomic units): Eq. I $E^{SCF}(\theta) - E^{SCF}(0) = 0.012736\,\theta^2 + 0.002487\,\theta^4$. Eq. II $E^{El}(\theta) - E^{El}(0) = 0.006561\,\theta^2 + 0.005519\,\theta^4$. Eq. III $E^{H}(\theta) - E^{H}(0) = 0.011706\,\theta^2 + 0.003010\,\theta^4$

Table 1

	H_2O	H_3O^+	$H_5O_2^+$
E(a.u.)	− 76.00574	− 76.30141	− 152.37793
r_{O-H}(Å)	0.962 (0.958)	0.970	0.966
α_{HOH}	108.8° (104.52°)	120°	114.4°
r_{O-O}(Å)			2.36
hydration energy[d]	—	185.5	44.4
(kcal/mole)		(172[a] 188.4[b])	(44.5[c] 38.5[b])

Experimental values in parenthesis.

[a]: Ref. [9], [b]: [10], [c]: [11], all corrected for zero-point energy.

[d] $\Delta E(H_{2n+1}O_n^+) = E(H_{2n+1}O_n^+) - E(H_{2n-1}O_{n-1}^+) - E(H_2O)$.

The total energy of $H_5O_2^+$ and binding energy ΔE relative to H_2O and H_3O^+ reported in Table 1 are to be compared with those found by Kollman and Allen [4]: $E = -152.36230$ a.u., $\Delta E = 36.9$ kcal/mole, by Kraemer and Diercksen [5]: -152.42848 and 32.3, by Newton and Ehrenson: -152.1791 and 44.0.

The influence of the optimization of the internal geometry of the partners may be illustrated by examining the investigation made by Kraemer and Diercksen [5] on two possible reaction paths: a) H_2O and H_3O^+ approach each other retaining their internal geometries, b) two water molecules (at fixed internal geometries) approach each other keeping a proton fixed midway between the two O atoms. The minima they found are at $r_{O-O} = 2.47$ Å for case a) and $r_{O-O} = 2.39$ Å for case b), their difference in energy favouring b) by 0.6 kcal/mole. Furthermore a displacement of the proton along the O–O axis in the b) structure shows a very slight double well character.

Our results are very similar to those of Ref. [5] for large O–O distances. Near the equilibrium, if one releases the internal geometries of the partners, the difference between a) and b) structures increases notably. According to our calculations the difference between b) ($r_{O-O} = 2.45$ Å) and a) ($r_{O-O} = 2.36$ Å) is about 4 kcal/mole and further, the double well character of the proton displacement curve in b) structure disappears, leaving a very flat minimum. Such differences in stability between the two structures a) and b) show how in the present case geometry deformations are essential: it is, therefore, questionable whether the electrostatic assumption of Paper I may be still supported. Since the associate considered here may be regarded as a limiting case in the set of monohydration associates $M^+ H_2O$, where M^+ is a molecular ion, it is convenient to elucidate to what extent the electrostatic approximation is still valid. Simple estimates based on the interaction of a point dipole (H_2O) with a point charge (H_3O^+) have already shown [6] how it is possible in such a way to allow for about 70% of the interaction energy. A less naive approximation considers the two entities H_3O^+ and H_2O at the geometries of the associate (see Table 1) and calculates fully the electrostatic energy between them. Rotations of one of the partners around the corresponding O nucleus give an electrostatic picture of the potential energy hypersurface around the minimum. Such a picture is in fairly satisfactory accordance with the SCF one.

As an example Fig. 1 shows the energy hypersurface section corresponding to the rotation of H_2O around the axis visible in the figure. Curve I provides the SCF section, curve II the electrostatic one.

The application of point charge models performed in Paper I would not be appropriate in this case. A larger interpenetration of the charge clouds leads to the possibility of there being different models of the H_2O molecule, all reaching the same degree of reliability, as defined in I, which gives erratic results. Introduction of polarization effects is more influential in the present case. Curve III of Fig. 1 corresponds to a picture allowing for also the polarization (Hartree SCF function). The larger difference of $E_{III} - E_I$ with respect to $E_{II} - E_I$ is offset by a better approximation to I as far as curvature in the minimum region is concerned (compare the fitting with quartic curves reported at the bottom of Fig. 1).

In conclusion, it seems that the validity range of the electrostatic assumption may be extended to associates involving also "strong" hydrogen bonds, whereas the ultrasimple charge point model of Paper I seems to be too poor an approximation in such cases.

Acknowledgments. It is a pleasure for the authors to thank Professor E. Scrocco and Professor J. Tomasi for continuous and stimulating discussions throughout this work.

References

1. Bonaccorsi, R., Petrongolo, C., Scrocco, E., Tomasi, J.: Theoret. chim. Acta (Berl.) **20**, 331 (1971).
2. Clementi, E.: J. chem. Physics **40**, 1944 (1964).
3. Guidotti, C., Salvetti, O.: Theoret. chim. Acta (Berl.) **10**, 454 (1968).
4. Kollman, P. A., Allen, L. C.: J. Amer. chem. Soc. **92**, 6101 (1970).
5. Kraemer, W. P., Diercksen, G. H. F.: Chem. Physics Letters **5**, 463 (1970).
6. Newton, M. D., Ehrenson, S.: J. Amer. chem. Soc. **93**, 4971 (1971).
7. Neumann, D., Moskowitz, J. W.: J. chem. Physics **49**, 2056 (1968).
8. Moskowitz, J. W., Harrison, M. C.: J. chem. Physics **43**, 3550 (1965).
9. Long, J., Munson, B.: J. chem. Physics **53**, 1356 (1970).
10. De Paz, M., Leventhal, J. J., Friedman, L.: J. chem. Physics **51**, 3748 (1969).
11. Kebarle, P., Searles, S. K., Zolla, A., Scarborough, J., Arshadi, M.: J. Amer. chem. Soc. **89**, 6393 (1967).

Dr G. Alagona
Laboratorio di Chimica
Quantistica ed Energetica Molecolare del CNR
Via Risorgimento 35
56100 Pisa, Italy

Theoret. chim. Acta (Berl.) 29, 97 – 116 (1973)
© by Springer-Verlag 1973

Electronic Relaxation of Small Molecules in a Dense Medium

Abraham Nitzan and Joshua Jortner

Department of Chemistry, Tel-Aviv University, Tel-Aviv, Israel

Received October 2, 1972

In this paper we present a theoretical study of radiationless transitions in a small molecule embedded in a dense inert medium. Two extreme situations of the molecule-medium coupling were considered, involving the case of zero displacements of the medium modes between the two electronic states (i.e. the Shpolskii matrix) and the limit of strong molecule-medium coupling. The Fourier transform of the non radiative decay probability of a small molecule in a Shpolskii matrix involves exponential damping, while for the strong coupling situation Gaussian damping is involved. In the case of the Shpolskii matrix the decay rate of a small molecule can be expressed in terms of an infinite series where each term corresponds to a product of an (intramolecular) Poisson distribution and a (medium induced) Lorentzian distribution. The Lorentzian widths were explicitly expressed in terms of the vibrational relaxation widths. The Robinson-Frosch formula can be obtained for the extreme case of near degeneracy in a Shpolskii matrix. In the limit of strong molecule-medium coupling the decay rate of a small molecule can be recast in terms of an infinite sum where each term involves a superposition of a Poisson distribution and a Gaussian distribution. The medium induced Gaussian distribution is determined by intramolecular phonon broadening. We have elucidated some new features of the electronic relaxation of a small molecule in a dense medium pertaining to the problem of off-resonance intramolecular coupling which modifies the energy gap law and the deuterium isotope effect.

Strahlungslose Übergänge in einem kleinen Molekül, das von einem dichten inerten Medium umgeben ist, werden untersucht, wobei zwei Grenzfälle bei der Kopplung Molekül/Medium zugrunde gelegt werden: keine Verschiebungen der Medium-Bewegungen beim Übergang (d.h. der Shpolskii-Matrix) einerseits und starke Kopplung Molekül/Medium andererseits. Die Fouriertransformierte für die Wahrscheinlichkeit des strahlungslosen Zerfalls eines kleinen Moleküls in Form einer Shpolskii-Matrix schließt exponentielle Dämpfung ein, wohingegen bei starker Kopplung die Dämpfung einer Gauss-Funktion entspricht. Im ersteren Fall läßt sich der Zerfall als unendliche Reihe von Produkten einer intramolekularen Poisson-Verteilung mit einer vom Medium induzierten Lorentz-Verteilung formulieren, wobei die Lorentz-Breite explizit mittels der Schwingungsrelaxationsbreiten angegeben wird. Die Robin-Frosch-Formel ergibt sich für den Grenzfall der Fastentartung der Shpolskii-Matrix. Bei starker Molekül-Medium-Kopplung laßt sich der Zerfallsverlauf als unendliche Summe von Überlagerungen von Poisson- und Gaussverteilungen angeben. Dabei wird die Medium-induzierte Gauss-Verteilung durch die intramolekulare Phononen-Verbreiterung bestimmt. In diesem Zusammenhang zeigten sich einige neue Gesichtspunkte für die elektronische Relaxation kleiner Moleküle in dichten Medien, wie z. B. das Problem von Nicht-Resonanz bei intramolekularer Kopplung, wo der Satz vom Energie-Sprung und der Deuterium-Isotopie-Effekt modifiziert werden müssen.

1. Introduction

In considering the implications of intramolecular interstate coupling on the radiative decay of electronically excited states of polyatomic molecules, it is important to realize that the existence of interstate coupling provides a necessary but by no means a sufficient condition for the occurrence of an intramolecular electronic relaxation process. Intramolecular non-radiative decay is exhibited in the statistical limit for excited state of "isolated" large molecular which are characterized by a large energy gap (~ 1 eV) [1]. In the case of small molecules in the low pressure gas phase no intramolecular relaxation occurs, while the effects of intramolecular coupling are exhibited as follows: a) A complex molecular absorption spectrum of some triatomic molecules [2] (i.e. NO_2) is observed, which may be sensitive to external fields ($^2\Sigma - {}^2\Pi$ mixing in the CN molecule [3]). b) Anomalously long radiative decay times of the first spin allowed excited states of some triatomic molecules (i.e. NO_2, SO_2 and CS_2) [4] are observed, while the emission quantum yields are unity.

One can extend the concept of the decay of electronically excited states of a "small molecule" to include the following two categories:

1. Electronically excited states of diatomic and triatomic molecules (i.e. NO_2, SO_2 and CS_2), which are characterized by a small number of vibrational degrees of freedom.
2. Electronically excited states of some large molecules which are characterized by a small electronic energy gap. Such excited states will exhibit the small molecule case encountered within a large molecule [5]. Experimental verification of this theoretical prediction was recently obtained for the radiative decay of the second excited singlet state of 3,4 Benzopyrene [6] and of naphthalene [7] (where the $S_2 - S_1$ energy gap is ~3000 cm^{-1}) and of the lowest excited singlet state of Benzophenone [8, 9] (where the $S_1 - T_1$ energy gap is 2800 cm^{-1}) in the low pressure gas phase, which exhibit anomalously long radiative decay times (relative to the expectations on the basis of the integrated oscillator strength).

Most of previous theoretical work on electronic relaxation in large molecules focused attention on the "isolated" molecule in the statistical limit [1]. Little theoretical attention has been devoted to medium effects on electronic relaxation of a guest molecule. Consider the simplest model for an "inert" medium which is characterized by the following features:

1. It does not modify the relevant energy levels.
2. It does not affect the interstate coupling matrix elements.
3. It does not provide promoting modes for electronic relaxation.

Thus the electronic wave functions of the guest molecule are practically invariant with respect to charges in the medium nuclear coordinates.

Such an "inert" medium may affect the electronic relaxation of a guest molecule as follows: a) It may provide accepting modes for the intramolecular decay process. The equilibrium configurations of the medium phonon modes (and their frequencies) usually vary between different electronic states of the impurity molecule. Indirect information concerning this effect may be obtained from the phonon broadening of optical lines of impurity molecules in inert matrices [10]. It is well known that the low lying excited electronic states (where the contribution of intramolecular decay to the linewidth is small) in mixed crystals and in hydrocarbon matrices exhibit appreciable phonon broadening, and only in special cases [11] (which are referred to as Shpolskii matrices) the equilibrium configurations of the medium phonons do not vary between the ground and the electronically excited states. We may conclude that in many cases of physical interest low frequency medium vibrations may act as accepting modes in the electronic relaxation process. b) The medium provides a heat bath for vibrational relaxation of the intramolecular vibrations. This vibrational relaxation (and vibrational excitation) processes may occur both in the initial and in the final electronic manifold.

In the statistical limit the non-radiative decay probability (in the weak electronic vibrational coupling limit) is dominated by the high frequency vibrational modes [12], whereupon the contribution of the low frequency medium accepting modes is negligible. Furthermore, it is asserted that in the statistical limit the vibrational relaxation in the final dense electronic manifold does not affect the non-radiative transition [13]. Thus the non-radiative decay of an individual vibronic level in the statistical limit is unaffected by an inert medium. From the experimental point of view provided that the vibrational relaxation process (in the initial electronic manifold) is fast on the time scale of the electronic transition, the non-radiative decay probability in an inert medium is obtained in terms of a thermal average over the decay of the individual vibronic levels of the isolated molecule.

The situation is drastically different in the small molecule case. As is well established both experimentally and theoretically an isolated small molecule does not exhibit intramolecular electronic relaxation [4], while external perturbations (in the gas phase or by a dense host matrix) may induce a non-radiative decay process [14–22]. The relevant experimental evidence may be summarized as follows: a) From the study of the emission spectra of NO in rare gas solid matrices experimental evidence was obtained for the $a^4\Pi - x^2\Pi$ intersystem crossing [14]. The lifetime of the quartet state in Ne, Ar and Kr was found to be 156, 93 and 35 msec respectively, and this shortenting of the lifetime can be assigned to externally induced spin orbit coupling which enhances the non-radiative decay. It should be noted however that this interpretation is not conclusive as the enhanced spin orbit coupling can also reduce the pure radiative decay time of the $a^4\Pi$ state, and quantum yield experiments are required to resolve this point. b) A strong temperature dependence of the phosphorescence ($T_1 \rightarrow S_0$) intensity of SO_2 in inert rare gas and molecular matrices intitially excited to the S_1 state was reported [15], while the $T_1 \rightarrow S_0$ radiative decay times were temperature independent. These results were interpreted in terms of the temperature and medium effects on the rate of the $T_1 \rightarrow S_0$ intersystem crossing. c) The S_1 state of the benzophenone molecule, which is separated by a small ($\sim 2800\,\mathrm{cm}^{-1}$) gap from the T_1 state, exhibits ultrafast $S_1 - T_1$ intersystem crossing in solution [16] (fluorescence quantum yield $\sim 10^{-6}$, non-radiative decay rate from the vibrationless S_1 level ~ 5 psec). On the other hand efficient fluorescence from the S_1 state is observed from the isolated benzophenone molecule [8], which exhibits predominantly the features of strong interstate $S_1 - T_1$ coupling as is the case for small molecules.

The theoretical treatment of the non-radiative decay of a small molecule embedded in a medium pertains to the following theoretical problems: a) The conventional golden rule rate formula, or related expressions, which are adequate for the treatment of the statistical limit, are not of general applicability for the electronic relaxation of a small molecule embedded in a medium. This point was not always realized and some authors [17, 18] have used second order perturbation theory to handle non-radiative processes in small molecules with-

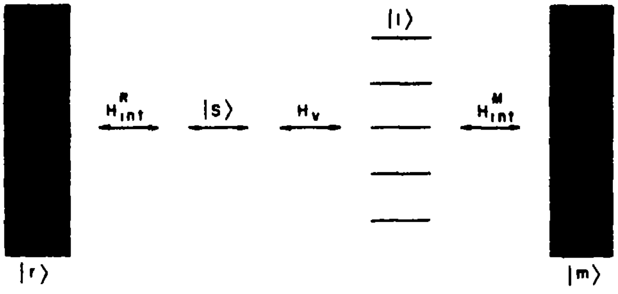

Fig. 1. Scheme for consecutive decay. $|s\rangle$ – initial molecular state; $|r\rangle$ – radiative continuum; $|l\rangle$ – sparse intramolecular manifold; $|m\rangle$ – medium states

out proper modifications. It should be pointed out that the pioneering work of Robinson and Frosch handled the vibrational relaxation in the final manifold. The Robinson-Frisch formula [19] for the non-radiative decay probability $W = (2\pi/\hbar\alpha)\sum_n \beta_n^2$ (where β_n are the intramolecular coupling matrix elements, while α is the vibrational relaxation width in the final manifold) is valid only for special cases and is inadequate for the small molecule case. Recently Takahashi and Yokota [20] attempted to consider the decay of small molecules by an ad-hoc inclusion of a vibrational relaxation rate into the Kubo-Toyozawa generating functions formalism, and provided a distinction between the small molecule and the large molecule case in terms of the corresponding vibrational relaxation width. b) When the medium does not supply accepting modes, the non-radiative decay rate of a small molecule may be considered in terms of a consecutive decay process. Here the initial molecular state is intramolecularly coupled to final molecular states which in turn decay by vibrational relaxation which originates from intermolecular coupling to the medium states. c) The consecutive decay process for a small molecule can be described phenomenologically (see Fig. 1) by assigning a vibrational relaxation width to the final molecular states. A more elaborate model should involve the details of the vibrational relaxation process [21].

In this paper we explore the problem of electronic relaxation of small molecules in a dense medium. In the first stage of this treatment we consider the idealized situation of a Shpolskii medium [10] whereupon the medium vibrations do not provide accepting modes. In this context we shall attempt to resolve the following problems: a) To establish the criteria for the validity of an exponential decay law (described in terms of the golden rule rate constant) for a small molecule subjected to a consecutive decay process. b) To elucidate the effects of vibrational relaxation on electronic relaxation of small molecules. We shall demonstrate that in general the decay rate of a small molecule will exhibit a linear dependence on the (medium induced) vibrational relaxation width. c) To clarify the connection between the consecutive decay scheme and the Robinson and Frosch expression [19]. Only in the rare and special case of accidental degeneracy between the initial and the final molecular vibronic states, a reciprocal relation is expected to exist between the decay rate and the vibrational relaxation width. d) To study the contribution of the vibrational relaxation width to the non-radiative decay rate of a small molecule in terms of a harmonic model which considers vibrational relaxation as a ladder process.

In the second stage of the present treatment we shall relax the restinction of a Spolskii medium and consider the role of medium modes as accepting modes for the electronic relaxation of a small molecule. This physical situation will bring back the features of the statistical limit whereupon the electronic relaxation rate will be independent of the vibrational relaxation rate for intramolecular and intermolecular vibrations.

2. Model System

We consider non-radiative relaxation of a molecule embedded in an inert dense host matrix. We do not need to concern ourselves with the relatively complex description of relaxation by collisions but rather consider coupling of the guest molecule to the medium phonons. The Hamiltonian of the system may be conveniently factorized into the molecular Hamiltonian (which in itself consists of the Born Oppenheimer Hamiltonian, H_{BO}, and a term H_V responsible for the non-adiabatic coupling), the medium Hamiltonian H_{Med}, an interaction term, H_{int}^{M}, between the medium and the molecule

$$H = H_{BO} + H_V + H_{Med} + H_{int}^{M} \tag{2.1}$$

Our molecular model will be similar to that presented in previous work. We shall also apply the same notations (see Ref. [21], Section 2).

Utilizing some approximate symmetry arguments it may be demonstrated that within our model: a) Interference effect resulting from the coupling of different levels to the same medium levels, are negligible. b) Intramolecular interference effects will be neglected. c) We consider the fast vibrational relaxation limit, whereupon electronic relaxation is slow on the time scale of vibrational relaxation.

These basic assumptions will be utilized to handle the phenomenology of the non-radiative decay of a (large or small) molecule in an inert medium which does not provide accepting modes (Section 3). These results are then applied in Section 4 for the non-radiative decay of a small molecule in a Shpolskii matrix. In Section 5 we consider the details of the vibrational relaxation (induced by the H_{int}^{M} term) and its effect on the electronic relaxation of a small molecule in a Shpolskii medium. Finally we consider (Section 6) a medium which provides accepting modes, whereupon the electronic relaxation of a small molecule is now reminescent of the statistical limit.

3. Theory of Consecutive Decay

In this section we shall briefly consider the problem of the time evolution of an "initially prepared" state $|si\rangle$ subjected to a coupling scheme represented by Fig. 1, which has been previously handled by Freed and Jortner [22] who utilized the Green's function technique, and more recently by Nitzan *et al.* [5], using the Wigner-Weisskopf method. The Green's function method is based on the observation that the time evolution of an initially prepared state $|si\rangle$ is given by the Fourier transform of the diagonal element $\langle si|G|si\rangle$ of the Green's operator for the system, $G = (E - H + i\eta)^{-1}$, $\eta \rightarrow 0^{+}$, and that the decay characteristics of this state are determined by the complex poles of this diagonal matrix element, whose explicit form in our model is (see Appendix A)

$$\langle si|G|si\rangle = \left(E - \tilde{E}_{si} + \frac{i}{2}\Gamma_{si}(E) + \frac{i}{2}\Delta_{si}(E)\right)^{-1} \tag{3.1}$$

where $\Gamma_{si}(E)$ is a smooth function of the energy E which is nearly a constant in the vicinity of $E \approx E_{si}$ and whose magnitude for $E = E_{si}$ corresponds to the radiative width of the state $|si\rangle$; and where $\Delta_{si}(E)$ is given by

$$\Delta_{si}(E) = 2\sum_j \frac{\frac{1}{2}\Gamma_{lj}|(H_v)_{si,lj}|^2}{(E - \tilde{E}_{lj})^2 + \frac{1}{4}\Gamma_{lj}^2} \tag{3.2}$$

Γ_{lj} is the width of the state $|l_j\rangle$ due to its coupling with the medium states (strictly speaking this is a smooth and nearly constant function of E, near $E = E_{lj}$). E_{si} and E_{lj} are the modified (by the appropriate level shifts) energies of the states $|si\rangle$ and $|lj\rangle$ respectively.

The crucial point is now the form of $\Delta_{si}(E)$ as a function of E. Freed and Jortner [22] have demonstrated that the statistical limit corresponds to the case in which this function is a smooth and nearly constant function of E. In this case it may be shown that the function $G_{si,si}$, Eq. (3.1) has only a single pole $E = E_s - \frac{1}{2}i(\Gamma_{si} + \Delta_{si})$. In this case the decay will be smoothly exponential in time, and Δ_{si} is the non-radiative contribution to the decay rate.

A more interesting behaviour results in the situation where $\Delta_{si}(E)$ is not a smooth function of E, which corresponds to the case where the density of states in the manifold $\{|lj\rangle\}$ is low. This case is much more difficult to mathematical treatment (a general exact solution has been obtained [5] only for the case where the manifold $\{|lj\rangle\}$ consists of one state only). However it will be sufficient to consider the time evolution of the system in two important limits. a) The strong intramolecular coupling limit characterized by

$$|(H_v)_{si,lj}| \gg |E_{lj} - E_{lj'}| \tag{3.3a}$$

where $|lj\rangle$ and $|lj'\rangle$ are two adjacent levels in the $\{|li\rangle\}$ manifold. b) The weak intramolecular coupling limit which is defined by the inequality for all j,

$$|(H_v)_{si,lj}| \ll \left|E_{si} - E_{lj} + \frac{i}{2}(\Gamma_{si} - \Gamma_{lj})\right|. \tag{3.3b}$$

A small molecule embedded in a dense medium where fast vibrational relaxation occurs can be often described by the weak coupling limit. If the density of states in the $\{|lj\rangle\}$ manifold is low (for example in a diatomic or in a triatomic molecule), the term $|E_{si} - E_{lj}|$ is sufficiently large to satisfy condition (3.3b) (excluding cases of accidental degeneracy). Even if this is not the case, the other term $|\Gamma_{si} - \Gamma_{lj}|$ in which $\Gamma_{lj} \sim 1 - 10\,\mathrm{cm}^{-1} \gg \Gamma_{si}$ will in most cases be much greater than $|(H_v)_{si,ll}|$. We may thus conclude that the relaxation of a molecule in a medium will correspond in most cases to the weak coupling situation.[1]

---

[1] In the case of a strong coupling situation a prediagonalization of the strongly coupled levels should be performed. A discussion of this situation is provided in Refs. [5, 9].

The time evolution of a prepared $|si\rangle$ state in our model has been evaluated by Nitzan *et al.* [5], and is given by

$$|\langle\psi(t)|si\rangle|^2 = \exp(-\gamma^{s}t) + \sum_j \frac{|(H_v)_{si,lj}|^2 \exp(-\gamma^{lj}t)}{(E_{si}-E_{lj})^2 + \frac{1}{4}(\Gamma_{si}-\Gamma_{lj})^2} + \text{interference terms} \qquad (3.4)$$

where $\psi(t)$ is the state vector of the system at time t given that $\psi(0) = |si\rangle \cdot \gamma^{si}$ is given by

$$\gamma^{si} = \Gamma_{si} + \sum_j \frac{|(H_v)_{si,lj}|^2 (\Gamma_{lj}-\Gamma_{si})}{(E_{si}-E_{lj})^2 + \frac{1}{4}(\Gamma_{lj}-\Gamma_{si})^2} \qquad (3.5a)$$

(see also Eq. (A.11)), while γ^{lj} takes the form

$$\gamma^{lj} = \Gamma_{lj} - \frac{|(H_v)_{si,lj}|^2 (\Gamma_{lj}-\Gamma_{si})}{(E_s-E_l)^2 + \frac{1}{4}(\Gamma_{lj}-\Gamma_{si})^2}\,. \qquad (3.5b)$$

The interference terms in Eq. (3.4) decay as $\exp(-\frac{1}{2}\gamma^{lj}t)$. Now in the weak coupling limit, we have

$$\gamma^{lj} \cong \Gamma_{lj} \gg \gamma^{si} \qquad (3.6)$$

which is also consistent with the restriction that vibrational relaxation is faster than the electronic transitions. In this case the time evolution of our system will be essentially characterized by the exponentially decaying term $\exp(-\gamma^{si}t)$, as the other terms in Eq. (3.3) are characterized by much smaller amplitudes and also decay much more rapidly.

We conclude that our model molecule subjected to weak coupling conditions and to the restriction that relaxation due to the coupling with the medium is much faster than the radiative decay, i.e. $\Gamma_{lj} \gg \Gamma_{si}$ for all j, if prepared initially in the state $|si\rangle$ will decay exponentially with a decay rate given by Eq. (3.5a). The non-radiative decay rate is thus

$$W_{si} = \frac{1}{\hbar} \sum_j \frac{|(H_v)_{si,lj}|^2 \Gamma_{lj}}{(E_{si}-E_{lj})^2 + (\Gamma_{lj}/2)^2} \qquad (3.7)$$

where Γ_{si} has been neglected relative to Γ_{lj}. The result (3.7) is a slight generalization of Fermi's golden rule. The latter is obtained in the limit $\Gamma_{lj} - 0$ and when $\{|lj\rangle\}$ is a continuous manifold of states. An alternative derivation of (3.7) using sum rules for non-radiative decay is given in Appendix B.

Returning to Eq. (3.7), it is easy to show that with the simplifying assumption that Γ_{li} is a constant over the manifold $\{|lj\rangle\}$

$$\Gamma_{lj} = \Gamma_l \quad \text{for all } j\,. \qquad (3.8)$$

Eq. (3.7) may be expressed as a Fourier transform of a generating function. To achieve this goal we note that a Lorentzian may be expressed as a Fourier transform in the following way

$$\frac{\Gamma}{(E_{si}-E_{lj})^2 + (\Gamma/2)^2} = \frac{1}{\hbar} \int_{-\infty}^{\infty} dt \exp\left[\frac{it}{\hbar}(E_{lj}-E_{si}) - \frac{\Gamma}{2\hbar}|t|\right]$$

where the variable t has dimensions of time. Thus Eq. (3.7) may be recast in the form

$$\begin{aligned} W_{si} &= \frac{1}{\hbar^2}\int_{-\infty}^{\infty} dt \exp\left(-\frac{\Gamma}{2\hbar}|t|\right)\sum_j |(H_v)_{si,lj}|^2 \exp\left[\frac{it}{\hbar}(E_{lj}-E_{si})\right] \\ &= \frac{1}{\hbar^2}\int_{-\infty}^{\infty} dt \exp\left(-\frac{i\Delta E}{\hbar}t-\frac{\Gamma}{2\hbar}|t|\right)\sum_j |(H_v)_{si,lj}|^2 \exp\left[\frac{it}{\hbar}(E_j^l-E_i^s)\right] \end{aligned} \tag{3.9}$$

where

$$\Delta E = E_{s0} - E_{l0} \tag{3.10}$$

corresponds to the energy gap between the pure electronic origins of the two electronic manifolds, and where E_j^l and E_i^s are vibrational energies above the corresponding electronic origins.

Averaging now over the initial distribution, we obtain

$$\begin{aligned} \langle W_s\rangle_T &= \frac{1}{\hbar^2}\int_{-\infty}^{\infty} dt \exp\left(-\frac{i\Delta E t}{\hbar}-\frac{\Gamma}{2\hbar}|t|\right) \\ &\otimes \sum_i P_i \sum_j |(H_v)_{si,lj}|^2 \exp\left[\frac{it}{\hbar}(E_j^l-E_i^s)\right] \end{aligned} \tag{3.11}$$

where

$$\begin{aligned} &P_i = Z^{-1}\exp(-\beta E_i^s) \\ &Z = \sum_i \exp(-\beta E_i^s); \qquad \beta = (k_B T)^{-1}. \end{aligned} \tag{3.12}$$

We note that Eqs. (3.9) and (3.11) yield rigorous expressions for the non-radiative decay rate also for the statistical limit case. It also applies for the isolated molecule case, where now Γ will correspond to the infrared and or radiative width of the levels $|lj\rangle$. The results previously obtained [12, 23–24] which have not included the factor $\exp\left(-\frac{\Gamma}{2\hbar}|t|\right)$ in the generating function where conceptually deficient as, bearing in mind that we actually handle a quasicontinuum and not a real continuum, the result with $\Gamma=0$ will diverge at any point where exact conservation of energy occurs, as is easy to see from Eq. (3.7). However, as we shall demonstrate elsewhere, the non-radiative transition probability in the statistical limit does not depend on Γ and reduces to the previously obtained results of Lin and Bersohn [24], Engleman, Freed and Jortner [12] and Fisher [23].

The sum over i in Eq. (3.9), and over i and j in Eq. (3.11) may now be evaluated using the Green's function (or density matrix) expression for the harmonic oscillator, or alternatively the Feynman's operator calculus together with a simple closure relation.

The result may be written generally in the form

$$W_{si} = \frac{1}{\hbar^2}\int_{-\infty}^{\infty} dt \exp\left(-i\frac{\Delta E}{\hbar}t-\frac{\Gamma}{2\hbar}|t|\right)F(t), \tag{3.13a}$$

$$\langle W_s\rangle_T = \frac{1}{\hbar^2}\int_{-\infty}^{\infty} dt \exp\left(-i\frac{\Delta E}{\hbar}t-\frac{\Gamma}{2\hbar}|t|\right)\langle F(t)\rangle_T \tag{3.13b}$$

where expressions for $F(t)$ and $F(t)$ have been previously obtained [12b, 25] for a molecule characterized by identical displaced potential surfaces:

$$
\begin{aligned}
F(t) = {} & \tfrac{1}{2} \sum_{\varkappa} |C^{\varkappa}_{sl}|^2 \exp\left(- \sum_{\mu} (\Delta_{\mu}^2/2)\right) \int_{-\infty}^{\infty} dt \\
& \cdot \{[(v_{s\varkappa} + 1) \exp(i\omega_{\varkappa} t) + v_{s\varkappa} \exp(-i\omega_{\varkappa} t)]\} \exp\left[\sum_{\mu} (\Delta_{\mu}^2/2) \exp(i\omega_{\mu} t)\right] \qquad (3.14\text{a}) \\
& \otimes \prod_{\mu \neq \varkappa} (v_{s\mu})! \sum_{r=0}^{v_{s\mu}} (-\Delta\mu)^{2r} \frac{[1 - \cos(\omega_{\mu} t)]^r}{(v_{s\mu} - r)!\,(r!)^2}
\end{aligned}
$$

$$
\begin{aligned}
\langle F(t) \rangle_T = {} & \tfrac{1}{4} \sum_{\varkappa} |C^{\varkappa}_{sl}|^2 \exp\left\{- \tfrac{1}{2} \sum_{\mu} \Delta_{\mu}^2 (2\langle v_{\mu} \rangle_T + 1)\right\} \qquad (3.14\text{b}) \\
& \otimes \int_{-\infty}^{\infty} dt \left\{\{[\coth(\beta\hbar\omega_{\varkappa/2}) + 1] \exp(i\omega_{\varkappa} t) + [\coth(\beta\hbar\omega_{\varkappa}) - 1] \exp(-i\omega_{\varkappa} t)\}\right. \\
& \otimes \left.\exp\left[\tfrac{1}{2} \sum_{\mu} \Delta_{\mu}^2 (\langle v_{\mu} \rangle + 1) \exp(i\omega_{\mu} t) + \tfrac{1}{2} \sum_{\mu} \Delta\mu^2 \langle v_{\mu} \rangle \exp(-i\omega_{\mu} t)\right]\right\}
\end{aligned}
$$

and for a molecule characterized by displaced potential surfaces which differ also in the frequencies of the normal modes [12b, 26]. The result for this case in the zero temperature limit is

$$
\begin{aligned}
\langle F(t) \rangle_0 = {} & \tfrac{1}{2} \sum_{\kappa} |C^{\varkappa}_{sl}|^2 \prod_{\mu} (\beta_{\mu})^{-1/2} \exp[i\omega_{l\varkappa} t - i\delta_{\mu} t] \\
& \otimes \left\{1 + \frac{(1 - \beta_{\varkappa})^2}{4\beta_{\varkappa}} [1 - \exp(i\omega_{l\varkappa} t)]\right\}^{-1} \\
& \otimes \prod_{\mu} \left\{1 + \frac{(1 - \beta_{\mu})^2}{4\beta_{\mu}} [1 - \exp(2i\omega_{l\mu} t)]\right\}^{-1/2} \qquad (3.15) \\
& \otimes \exp\left\{- \sum_{\mu \neq \varkappa} \frac{\beta_{\mu} \Delta_{\mu}^2 [1 - \exp(i\omega_{l\mu} t)]}{1 + \beta_{\mu} + (\beta_{\mu} - 1) \exp(i\omega_{l\mu} t)}\right\}.
\end{aligned}
$$

An approximate result for W_{sl} for any i is given in Ref. [26]. In these expressions $v_{s\mu}$ is the initial population in the mode μ while $\langle v_{\mu} \rangle_T = [\exp(\beta\hbar\omega_{\mu}) - 1]$, $C^{\varkappa}_{sl}$ is the electronic matrix element [12], $\omega_{l\mu}$ and $\omega_{s\mu}$ are the frequencies of the mode μ in the l-th and s-th electronic states respectively. Finally, δ_{μ} and β_{μ} are defined by

$$\delta_{\mu} = \tfrac{1}{2}(\omega_{s\mu} - \omega_{l\mu})$$

$$\beta_{\mu} = (\omega_{s\mu}/\omega_{l\mu}).$$

It is important to note that expressions (3.14) and (3.15) are valid for both large and small molecules interacting with an inert medium and subjected to the conditions (3.8) and (3.3b) (the last condition is not important for the large molecule case). We now turn to study the particular characteristics of the small molecule case.

4. The Small Molecule Case

It has been asserted in Section 3 that within the restrictions imposed by the weak coupling limit, a small molecule embedded in a medium, if initially prepared in some excited electronic-vibrational state will exhibit an exponential non-radiative decay (basides its radiative decay). The non-radiative decay rate is given by Eq. (3.13b).

In order to handle Eq. (3.13b) analytically we shall consider the simple molecular model system characterized by identical frequencies in the two electronic states which just differ in their origins. The non-radiative decay probability in the zero temperature limit is (taking for the sake of simplicity the contribution of only one promoting mode)

$$\langle W\rangle_T = \frac{1}{2\hbar^2}|C^{x}_{sl}|^2 \exp\left(-\sum_\mu a_\mu\right) J \tag{4.1}$$

where the vibrational integral has the form

$$\begin{aligned} J &= \int_{-\infty}^{\infty} dt \exp\left\{-\frac{i}{\hbar}(\Delta E - \hbar\omega_x)t + \sum_\mu a_\mu \exp(i\omega_\mu t) - \frac{\Gamma}{2\hbar}|t|\right\} \\ &= \frac{1}{\omega_N}\int_{-\infty}^{\infty} dx \exp\left\{-i\varepsilon x + \sum_\mu a_\mu \exp(i\bar{\omega}_\mu x) - \frac{1}{2}\gamma|x|\right\} \end{aligned} \tag{4.2}$$

here we have set $a_\mu = \frac{1}{2}\sum_\mu \Delta_\mu^2$. The intramolecular frequencies have been normalized by a common divider ω_N so that $\bar{\omega}_\mu = \frac{\omega_\mu}{\omega_N}$ are integers and where $\gamma = \Gamma/\omega_N$ while $\varepsilon = E - \hbar\omega_x/\omega_N$.

In the small molecule case the exponential damping factor in the integral (4.2) cannot be neglected and thus the saddle point method which was popular in the statistical limit is now inapplicable. To proceed we now expand the exponent in (4.2) in the form

$$\begin{aligned} \exp\left\{\sum_\mu a_\mu \exp(i\bar{\omega}_\mu x)\right\} &= \prod_{\mu=1}^{N} \exp[a_\mu \exp(i\bar{\omega}_\mu x)] \\ &= \sum_{n_1=0}^{\infty}\sum_{n_2=0}^{\infty}\cdots\sum_{n_N=0}^{\infty}\prod_{\mu=1}^{N}\frac{(a_\mu)^{n_\mu}}{(n_\mu)!}\exp(i\bar{\omega}_\mu n_\mu x) \\ &= \sum_{\{n\}}\exp\left[i\left(\sum_{\mu=1}^{N} n_\mu\bar{\omega}_\mu\right)x\right]\prod_{\mu=1}^{N}\frac{(a_\mu)^{n_\mu}}{(n_\mu)!} \end{aligned} \tag{4.3}$$

where N is the number of vibrational degrees of freedom and $\sum_{\{n\}}$ is a sum over all the sets of any N integers (including zero). We thus obtain

$$J = \frac{1}{\omega_N}\sum_{\{n\}}\left[\left(\prod_{\mu=1}^{N}\frac{(a_\mu)^{n_\mu}}{n_\mu!}\right)\int_{-\infty}^{\infty} dx \exp\left\{i\epsilon x + i\sum_{\mu=1}^{N} n_\mu\bar{\omega}_\mu x - \frac{\gamma}{2}|x|\right\}\right]. \tag{4.4}$$

The integral in Eq. (4.4) is easily performed to give a Lorentzian of width γ, so that J takes the form of a superposition of Lorentzians

$$J = \frac{1}{\omega_N} \sum_{\{n\}} \frac{\gamma}{\left(\varepsilon - \sum_{\mu=1}^{N} n_\mu \bar{\omega}_\mu\right)^2 + \left(\frac{\gamma}{2}\right)^2} \prod_{\mu=1}^{N} \frac{(a_\mu)^{n_\mu}}{(n_\mu)!} . \tag{4.5a}$$

This expression can be easily transformed to an alternative form which contains the conventional energy parameters. Multiplying the numerator and the denominator by $\hbar^2 \omega_N^2$ Eq. (4.5a) then takes the form

$$J = \hbar \sum_{\{n\}} \frac{\Gamma}{\left(\Delta E - \hbar\omega_x - \hbar \sum_{\mu=1}^{N} n_\mu \omega_\mu\right)^2 + (\Gamma/2)^2} \prod_{\mu} \frac{(a_\mu)^{n_\mu}}{n_\mu!} . \tag{4.5b}$$

Eqs. (4.1) and (4.5b) provide an explicit expression for the non-radiative transition probability (Eq. (3.7)), where the widths Γ_{li} are assumed to be independent of the particular vibronic levels $|lj\rangle$, and where the coupling matrix elements have been evaluated for the simple model at hand. These expressions are still general being applicable for both the small molecule case and for the statistical limit. The statistical limit is characterized by the relation $\Gamma \ll \varrho^{-1}$ (where ϱ is the density of states in the $|li\rangle$ manifold). In this case the overlapping Lorentzian peaks in (4.5b) yield a smooth function of the energy so that J (and $\langle W \rangle$) is a smooth function of the energy, being independent of Γ [13].

Turning now the small molecule case we specialize in the simple situation where only a single intramolecular vibrational mode acts as an accepting mode. This physical situation prevails for spin orbit coupling in a diatomic molecule (i.e. $^4\Pi - {^2\Pi}$ coupling in NO). Eq. (4.5b) takes the form

$$J = \hbar \sum_{n} \frac{\Gamma}{(\Delta E - n\hbar\omega)^2 + (\Gamma/2)^2} \left(\frac{a^n}{n!}\right) . \tag{4.6}$$

Provided that the widths of the final states originate from vibrational relaxation then for the low temperature limit the vibrationless level $n = 0$ does not contribute to the final result and the sum in (4.6) has to be taken over $n = 1 \cdots \infty$.

The following comments are now in order: a) The decay rate of a small molecule in a dense medium is expressed in terms of an infinite series where each term corresponds to a product of a Lorentzian distribution and of a Poisson (Pekerian) distribution. b) In the simple case considered herein the density of vibronic states in the final electronic manifold is constant, whereupon only the magnitudes of the Lorentzian and of the Pekerian will determine the relative contributions of the various terms in Eq. (4.6). For $a \lesssim 1$ *it may happen that the largest contribution* to the decay rate of the $|s0\rangle$ level will not originate from the close lying $|lj\rangle$ levels, but rather from low lying $|lj\rangle$ states which contribute via the tails of their Lorentzian (uncertainty) distributions. c) In the case of accidental degeneracy when $(\Delta E - \hbar\omega) \ll \Gamma$, and provided that a is not too small[2], the dominating contribution to J originates from a single level, whereupon one gets

---

[2] Reasonable order of magnitude estimates are $\Delta E = 10^4 \mathrm{cm}^{-1}$, $\hbar\omega = 10^3 \mathrm{cm}^{-1}$, $a \sim 1$ and $\Gamma \sim 1 \mathrm{cm}^{-1}$. This value of Γ corresponds to fast vibrational relaxation.

$$J = \frac{4\hbar}{\Gamma}\left[a^{(\Delta E/\hbar\omega)}/(\Delta E/\hbar\omega)!\right] \tag{4.7a}$$

and

$$w_{s0} = \frac{2}{\hbar\Gamma}|c_{sl}|^2 e^{-a}\left[a^{\Delta E/\hbar\omega}/(\Delta E/\hbar\omega)!\right]. \tag{4.7b}$$

Eq. (4.7) corresponds to the Robinson-Frosch formula, obtained for our simplified model system. The main feature of this result is the dependence of w_{s0} on the reciprocal of the width Γ. It is also easy to verify that the result (4.7) is model independent, for the case of accidental degeneracy one gets

$$J = 4\hbar\,|(H_v)_{si,lj}|^2/\Gamma_{lj}. \tag{4.8}$$

Thus the Robinson-Frosch formula is applicable only for the case of near degeneracy in a small molecule embedded in a Shpolskii matrix. This theoretical result is of little use in real life. d) When accidental degeneracy is not encountered i.e. $\Delta E - n\hbar\omega \gg \Gamma$, we have

$$J = \hbar\Gamma \sum_n \frac{1}{(\Delta E - n\hbar\omega)^2}\,\frac{a^n}{n!} \tag{4.9}$$

so that the non-radiative probability is linear with the coupling to the medium, expressed in terms of the width Γ. This physical situation may be encountered in real life for small molecules in a Shpolskii matrix. e) The energy gap law for the non-radiative decay of a small molecule in a dense medium is not expected to be of general validity, as in the case for large molecules. If the major contribution to J (and to W) originates from off resonance low lying levels, W will vary as $(\Delta E)^{-2}$. On the other hand only when the major contribution will originate from near resonance coupling the usual energy law $W \sim a^{(\Delta E/\hbar\omega)}/(\Delta E/\hbar\omega)!$ will apply.

5. Details of Vibrational Relaxation

Up to this point we have been concerned with a phenomenological description of the vibrational relaxation widths of the final molecular states involved in the electronic relaxation process. The details of the vibrational relaxation process and its effect on the electronic relaxation of a small molecule can be handled by considering a simplified model of a harmonic molecule interacting with a harmonic medium via interaction terms which are linear in the molecular nuclear coordinates and of arbitrary order (within the rotating wave approximation) in the medium phonons [21, 27]. The limit of fast vibrational relaxation which is of interest for us can be defined in terms of the relation [21]

$$\gamma_\mu t \gg 1$$

for all $\mu = 1 \cdots N$.

Where t is the time scale and the indices μ refer to the vibrational mode. The thermally averaged non-radiative transition probability for spin allowed internal conversion in the fast vibrational relaxation limit is [21]

$$
\begin{aligned}
\langle W_s\rangle_T = \frac{2}{\hbar^2}\sum_{\varkappa}|C_{sl}^{\varkappa}|^2 \; \exp\left[-\frac{1}{2}\sum_{\mu}\Delta_{\mu}^2(2\langle v_{\mu}\rangle_T+1)\right] \\
\otimes\left\{\left[\coth\left(\frac{\beta\hbar\omega_{\varkappa}}{2}\right)+1\right]\int_{-\infty}^{\infty}dt\exp\left[-i\left(\frac{\Delta E}{\hbar}-\omega_{\varkappa}\right)t+\sum_{\mu}\left(\frac{\Delta_{\mu}^2}{2}\right)\right.\right. \\
\left.\cdot(\langle v_{\mu}\rangle_T+1)\exp\left(i\omega_{\mu}t-\frac{\gamma_{\mu}}{2\hbar}|t|\right)+\frac{1}{2}\sum_{\mu}\Delta_{\mu}^2\langle v_{\mu}\rangle_T\exp\left(-i\omega_{\mu}t-\frac{\gamma_{\mu}}{2\hbar}|t|\right)\right] \\
+\left[\coth\left(\frac{\beta\hbar\omega_{\varkappa}}{2}\right)-1\right]\otimes\int_{-\infty}^{\infty}dt\exp\left[-i\left(\frac{\Delta E}{\hbar}+\omega_{\varkappa}\right)t+\sum_{\mu}\left(\frac{\Delta_{\mu}^2}{2}\right)\right. \\
\left.\cdot(\langle v_{\mu}\rangle_T+1)\exp\left(i\omega_{\mu}t-\frac{\gamma_{\mu}}{2\hbar}|t|\right)+\frac{1}{2}\sum_{\mu}\Delta_{\mu}^2\langle v_{\mu}\rangle_T\exp\left(-i\omega_{\mu}t-\frac{\gamma}{2\hbar}|t|\right)\right].
\end{aligned}
\tag{5.1}
$$

Where $C_{sl}^{\varkappa}$ is the intramolecular electronic coupling matrix element induced by the $\varkappa$ promoting mode. ω_{μ} is the frequency of the μ-th vibrational mode characterized by the displacement Δ_{μ} and by the thermal occupation number $\langle v_{\mu}\rangle_T$. The effective electronic energy gap $\Delta E_{\varkappa}=\Delta E-\hbar\omega_{\varkappa}$ is reduced by the promoting mode frequency. Eq. (5.1) bears a close resemblance to the thermally averaged non-radiative transition probability in the statistical limit except that each frequency is now replaced by the complex frequency $\omega_{\mu}+i\gamma_{\mu}$.

To simplify matters we consider the electronic relaxation probability of the vibrationless level (corresponding to the zero temperature limit of Eq. (5.1)) which is given by

$$
\begin{aligned}
W_{s0} = \frac{1}{2h^2}\sum_{\varkappa}|C_{sl}^{\varkappa}|^2\exp\left(-\frac{1}{2}\sum_{\mu}\Delta_{\mu}^2\right)\int_{-\infty}^{\infty}dx\left\{\exp\left[-\frac{i\Delta E_{\varkappa}x}{\hbar}-\gamma_{\varkappa}|x|\right]\right. \\
\left.\otimes\exp\left[\frac{1}{2}\sum_{\mu}\Delta_{\mu}^2\exp(i\omega_{\mu}x-\gamma_{\mu}|x|)\right]\right\}.
\end{aligned}
\tag{5.2}
$$

Utilizing the expansion of the exponential function

$$
\begin{aligned}
\exp\left[\frac{1}{2}\sum_{\mu}\Delta_{\mu}^2\exp(i\omega_{\mu}x-\gamma_{\mu}|x|)\right] \\
=\sum_{\{n\}}\exp\left[i\left(\sum_{\mu}n_{\mu}\omega_{\mu}x\right)-\sum_{\mu}n_{\mu}\gamma_{\mu}|x|\right]\prod_{\mu}\frac{(\frac{1}{2}\Delta_{\mu}^2)^{n_{\mu}}}{n_{\mu}!}
\end{aligned}
\tag{5.3}
$$

Eq. (5.2) takes the form

$$
\begin{aligned}
W_{s0} = \frac{1}{2\hbar^2}\sum_{\varkappa}|C_{sl}^{\varkappa}|^2\exp\left|-\frac{1}{2}\sum_{\mu}\Delta_{\mu}^2\right| \\
\otimes\sum_{\{n\}}\frac{\gamma_{\varkappa}+\sum\limits_{\mu\neq\varkappa}n_{\mu}\gamma_{\mu}}{\left(\Delta E-\hbar\omega_{\varkappa}-\hbar\sum\limits_{\mu\neq\varkappa}n_{\mu}\omega_{\mu}\right)^2+\frac{1}{4}\left(\gamma_{\varkappa}+\sum\limits_{\mu\neq\varkappa}n_{\mu}\omega_{\mu}\right)^2}.
\end{aligned}
\tag{5.4}
$$

We have thus obtained a generalized microscopic expression for the non-radiative decay probability in the fast vibrational relaxation limit. The width of the lj level characterized by the vibrational occupation numbers $j \equiv \{M\}$ (for the harmonic model) is given by

$$\Gamma_{lj} = \gamma_\kappa + \sum_{\mu \neq \kappa} n_\mu \gamma_\mu \tag{5.5}$$

The linear dependence of the thermal relaxation widths of the multimode harmonic oscillator on the population number is well known [28]. It should be noted that Eq. (5.4) is equivalent to the phenomelogical equation (3.2) except that now an explicit expression has been obtained (Eq. (5.5)) for the level widths. Thus in the small molecule case when a small number of vibrational modes contributes to (5.4) the conclusions derived in section 4 are of general applicability.

6. The Contribution of Medium Modes

Up to this point we have disregarded the displacement of the origins of the medium modes, assuming that the inert medium does not contribute accepting modes for electronic relaxation. In order to extend the relaxation theory of a small molecule in a medium we shall consider the small number of intramolecular vibrations and the intermolecular vibrations on the same footing. Our model system consists of a supermolecule with a single intramolecular vibrational mode (specified by the frequency ω and the reduced displacement Δ) and N intermolecular modes (characterized by frequencies ω_α and reduced displacements Δ_α; $\alpha = 1 \cdots N$). The physical situation now corresponds to the statistical limit, whereupon the non-radiative decay probability is independent of the vibrational relaxation widths γ_μ. Separating the intramolecular and the intermolecular contributions the transition probability (Eq. (3.13)) takes the form

$$\begin{aligned} W_{s0} = {} & \frac{1}{2\hbar^2} \sum_\kappa |C^\kappa_{sl}|^2 \exp\left[-\frac{1}{2} \Delta^2 - \frac{1}{2} \sum_\alpha \Delta_\alpha^2 \right] \\ & \otimes \int_{-\infty}^{\infty} dx \exp\left(-\frac{iE_\kappa}{\hbar} x \right) \otimes \exp\left[\frac{1}{2} \Delta^2 \exp(i\omega x) \right] \\ & \otimes \exp\left[\frac{1}{2} \sum_\alpha \Delta_\alpha \exp(i\omega_\alpha x) \right]. \end{aligned} \tag{6.1}$$

The non-radiative decay probability can be expressed in terms of separate contributions of the intramolecular high frequency mode and intermolecule low frequency modes. Utilizing the expansion (4.3) we now have

$$W_{s0} = \frac{1}{2\hbar^2} \sum_\kappa |C^\kappa_{sl}|^2 \sum_n \exp\left(-\frac{1}{2} \Delta^2 \right) \frac{(\Delta^2/2)^n}{n!} F(\Delta E_\kappa - n\omega) \tag{6.2}$$

where

$$\begin{aligned} F(\Delta E_\kappa - n\omega) = {} & \exp\left[-\frac{1}{2} \sum_\alpha \Delta_\alpha^2 \right] \int_{-\infty}^{\infty} dx \exp\left[\frac{i}{\hbar} (\Delta E_\kappa - n\omega) x \right] \\ & \otimes \exp\left[\frac{1}{2} \sum_\alpha \Delta_\alpha^2 \exp(i\omega_\alpha x) \right]. \end{aligned} \tag{6.3}$$

Thus the non-radiative transition probability can be recast as a sum of products of the intramolecular Franck Condon factors and the medium contributions (5.3). The F functions (5.3) just correspond to the line shape functions at the energies $(\Delta E_x - n\omega)$, which were previously treated in detail [29]. Thus the effect of the accepting medium modes, amounts to the replacement of the Lorentzian distributions Eq. (5.4) by the equivalent medium line shape functions.

As is well known from the theory of radiative and non-radiative processes in molecules and solids Eq. (6.3) can be considerably simplified in the limit of strong coupling to the medium phonons whereupon

$$\sum_{\alpha} (\Delta_\alpha^2/2) \gg 1 \,. \tag{6.4}$$

In this case the exponential function in the integral can be expanded in a power series of X retaining terms up to X^3 [12]. This procedure leads to the well known Gaussian line shape

$$F(\varepsilon) = \int_{-\infty}^{\infty} dx \exp(i\varepsilon x/\hbar) \exp(-D^2 X^2) = \left(\frac{2\pi}{D^2}\right)^{1/2} \exp[-(\varepsilon - E_M)^2/D^2] \tag{6.5}$$

where

$$D^2 = \tfrac{1}{2} \sum_{\alpha} \hbar\omega_\alpha^2 \Delta_\alpha^2 \tag{6.6a}$$

is the second moment of the distribution, while the Stokes shift is

$$E_M = \tfrac{1}{2} \sum_{\alpha} \hbar\omega_\alpha \Delta_\alpha^2 \,. \tag{6.6b}$$

Utilizing Eqs. (6.2), (6.3) and (6.5) the transition probability in the strong molecule-medium coupling limit takes the form

$$\begin{aligned} W_{s0} = {} & \left(\frac{\pi}{2}\right)^{1/2} \left(\frac{1}{\hbar^2 D}\right) \sum_{x} |C_{sl}^{x}|^2 \sum_{n} \exp(-\Delta^2/2) \frac{(\Delta^2/2)^n}{n!} \\ & \otimes \exp[-(\Delta E - n\hbar\omega - E_M)^2/D^2] \,. \end{aligned} \tag{6.7}$$

Thus the non-radiative decay of a small molecule strongly coupled to the medium can be recast in terms of a superposition of a Poisson and a Gaussian distribution. It is important to notice that as in the case of the Shpolskii matrix the non-radiative decay probability (6.7) may be dominated by off resonance coupling to the tails of the distributions of low lying states in the final manifold.

To conclude this discussion we would like to point out that a phenomenological model can be provided which accounts simultaneously for the medium broadening D (Eq. (6.6a)) and for vibrational relaxation broadening γ_μ (Eq. (4.1)). Provided that medium accepting modes are not active in intramolecular and intermolecular vibrational relaxation the non-radiative decay probability is given by Eq. (6.2) which includes both the intramolecular mode and the intermolecular mode. It is easy to demonstrate that when the γ_μ terms are retained Eq. (6.3) will include additional contribution of the form $\exp\left(-\sum_{\alpha} \gamma_\alpha |x|\right)$ in the integral. In the case of strong molecule medium coupling the Gaussian distribution (6.5) is replaced by a Voigt line shape function [30]. Now in this limit the phonon broadening will appreciably exceed the vibrational relaxation broadening, i.e. $D \gg \gamma_\mu$ for all μ, the Gaussian distribution (6.5) will be regained.

7. Discussion

In this paper we have considered the features of the electronic relaxation of a small molecule in a dense medium. We have focused attention on two limiting cases and considered the limit of zero displacements of the medium modes between the two electronic states (i.e. a Shpolskii matrix) and the case of strong molecule-medium coupling. In both cases we were able to recost the non-radiative decay probability in terms of a sum, where each term is a product of an intramolecular Franck Condon factor and a medium assisted distribution function. In the case of the Shpolskii matrix the latter term involves a Lorentzian distribution while in the limit of strong molecule medium coupling this term involves a Gaussian distribution. From the mathematical point of view we can assert *that the Fourier transform of the non-radiative decay probability of a small* molecule in a Shpolskii matrix involves exponential damping while in the strong molecule medium coupling Gaussian damping is involved.

The main new features of the decay of a small molecule can be summarized as follows:

a) Interaction of the small molecule with a medium via vibrational relaxation or phonon broadening is a prerequisite for the occurrence of non-radiative relaxation.

b) The non-radiative relaxation probability of the small molecule in a medium is dominated by the coupling to the medium, being determined by the vibrational relaxation width γ_μ in the Shpolskii matrix or by the distribution width, D, in the strong coupling case.

c) The electronic relaxation of a small molecule may involve non-resonant coupling originating from overlapping widths of low lying final state.

d) The popular energy gap law will not hold when off resonance coupling dominates.

e) In the case of dominating of resonance coupling the deuterium isotope effect in the electronic relaxation will be negligibly small.

These features drastically differ from the decay characteristics in the statistical limit occurs via near resonance coupling, which are independent of the medium induced widths (γ_μ or D), which exhibit the energy gap law and the large deuterium isotope effect.

Appendix A.
Sequential Decay by the Green's Function Method

To verify Eqs. (3.1) and (3.2) we start from a model (see Fig. 1) where a single molecular vibronic level $|s\rangle$ is coupled to a radioactive continuum $|r\rangle$ and to a discrete molecular manifold $|l\rangle$. The $|l\rangle$ manifold is in turn coupled to a continuum of level states $|m\rangle$, assuming that the levels $\{|l\rangle\}$ do not interfere through their interaction with the medium, so that each $|l\rangle$ level is coupled to a different set of $\{|m\rangle\}$ states. Making use of the Dyson equation

$$G + G_0 + G_0 VG \tag{A. 1}$$

we obtain the following forms for the matrix elements of the Green's function

$$G_{ss} = \frac{1}{E - E_s} + \frac{1}{E - E_s} \sum_r (H^{\mathrm{R}}_{\mathrm{int}})_{sr} G_{rs} + \frac{1}{E - E_s} \sum_l (H_v)_{ls} G_{ls}, \tag{A. 2}$$

$$G_{rs} = \frac{1}{E - E_r} (H^{\mathrm{R}}_{\mathrm{int}})_{rs} G_{ss}, \tag{A. 3}$$

$$G_{ls} = \frac{1}{E - E_l} (H_v)_{ls} G_{ss} + \frac{1}{E - E_l} \sum_m (H^M_{\mathrm{int}})_{lm} G_{ms}, \tag{A.4}$$

$$G_{ms} = \frac{1}{E - E_m} \sum_l (H^{\mathrm{M}}_{\mathrm{int}})_{ml} G_{ls}. \tag{A.5}$$

Inserting Eq. (A.5) into Eq. (A.4) we get

$$G_{ls} = \frac{1}{E - E_l} \left[(H_v)_{ls} G_{ss} + \sum_{l'} G_{l's} \sum_m (H^{\mathrm{M}}_{\mathrm{int}})_{lm} (H^{\mathrm{M}}_{\mathrm{int}})_{ml'} \otimes \frac{1}{E - E_m} \right]. \tag{A.6}$$

If interference between different 1 and 1′ states is neglected we obtain

$$G_{ls} = \frac{1}{E - E_m} \left[(H_v)_{ls} G_{ss} + G_{ls} \sum_m \frac{|(H^{\mathrm{M}}_{\mathrm{int}})_{lm}|^2}{E - E_l} \right] \tag{A.7}$$

which after some algebraic manipulations results in

$$G_{ls} = \frac{(H_v)_{ls}}{E - \tilde{E}_l + \frac{i}{2} \Gamma_l} G_{ss} \tag{A.8}$$

where the modified energy

$$\tilde{E}_l = E_l + pp \sum_m \frac{|(H^{\mathrm{M}}_{\mathrm{int}})_{lm}|^2}{E - E_m} \tag{A.9}$$

and the width

$$\Gamma_l = 2\pi \sum_m |(H^{\mathrm{M}}_{\mathrm{int}})|^2 \, \delta(E - E_m) \tag{A.10}$$

are assumed to be weakly dependent on the energy variable E. Inserting now Eqs. (A.8) and (A.3) into Eq. (A.2) we obtain after some further algebraic manipulation

$$G_{ss} = \frac{1}{E - \tilde{E}_s + \frac{i}{2} \, \Gamma_s(E) + \Delta_s(E))} \tag{A.11}$$

where

$$\Delta_s = \sum_l \frac{\Gamma_l |(H_v)_{sl}|^2}{(E - \tilde{E}_l)^2 + (\Gamma_{l/2})^2}, \tag{A.11a}$$

$$\Gamma_s = 2\pi \sum_r |(H^{\mathrm{R}}_{\mathrm{int}})_{sr}|^2 \, \delta(E - E_r) \tag{A.11b}$$

and where

$$E_s = \tilde{E}_s + pp\sum_r \frac{|(H^R_{int})_{sr}|^2}{E-E_r} + \sum_l \frac{2(E-\tilde{E}_l)|(H_v)_{sl}|^2}{(E-\tilde{E}_l)^2+(\Gamma_{l/2})^2}. \tag{A.12}$$

The radiative contributions to the width and level shift of the state s are usually nearly constant functions of the energy variable E. Eqs. (3.1) and (3.2) are now obtained by replacing the notations $|s\rangle$ and $|l\rangle$ by $|si\rangle$ and $|lj\rangle$ respectively.

Appendix B. Sum Rules for Non Radiative Decay

The effect of the broadening of the "final" molecular levels $|lj\rangle$ on the non radiative decay rate may be obtained in the following less concise but simpler procedure. As a starting point we take the well known expression [31] for the probability distribution in the dissipative manifold. The probability to be at time $t = \infty$ in a particular state $|f\rangle$ of this manifold is given by

$$P_f = \frac{|V_{kf}|^2}{(E_f-\tilde{E}_k)^2+(\Gamma_{k/2})^2} \tag{B.1}$$

where $|k\rangle$ is the initial metastable state, with the corresponding decay width Γ_k and the (shifted) energy $\tilde{E}_k$ · V_{kf} denotes the coupling between the states k and f. Summing over all the final states f we obtain (assuming that f is the only decay channel)[3]

$$\sum_f P_f = \sum_f \frac{|V_{kf}|^2}{(E_f-\tilde{E}_k)^2+(\Gamma_{k/2})^2} = 1\,. \tag{B.2}$$

This trivial sum rule may be applied to derive an expression for Γ_k provided that is may be assumed that Γ_k is weakly dependent on E_f. This restriction should be recognized as the condition for an exponential decay of the state $|k\rangle$. Assuming that this condition is satisfied we may apply Eq. (B.2) to our model taking $|k\rangle$ to be our initial state $|si\rangle$ and taking the states $\{|f\rangle\}$ to be the states which result from a partial diagonalization of the "final" molecular levels $\{|lj\rangle\}$ and the continuous manifold of medium levels. Denoting the (continuous) medium levels by $\{|m\rangle\}$ we have

$$|f\rangle = a^f_{lj}|lj\rangle + \sum_m b^f_m|m\rangle \tag{B.3}$$

where the absolute square of the amplitudes a^f_{lj} is given by Fano [32] to be

$$|a^f_{lj}|^2 = \frac{|V_{lj,m}|^2_{E_m=E_f}}{(E_f-E_{lj})^2+(\Gamma_{lj/2})^2} \tag{B.4}$$

where $\Gamma_{lj} = 2\pi\varrho_m|V_{lj,m}|^2$ is the width of the level $|lj\rangle$ and where level shifts have been neglected. To derive these results one should invoke the assumption that each molecular level $|lj\rangle$ decays into its own set of levels $\{|m\rangle\}$, namely, that the levels $|lj\rangle$ do not interfere through their interaction with the medium levels. The same assumption has been invoked in deriving Eq. (3.7).

---

[3] Other independent decay channels will contribute in an additive manner.

Assuming further that there is no direct interaction between the initial molecular state $|si\rangle$ and the medium levels $\{|m\rangle\}$ (so that the only interaction occurs through the molecular levels $|lj\rangle$) and utilizing Eq. (B.3) we obtain[4]

$$V_{si,f} = a^f_{lj}(H_v)_{si,lj}\,. \tag{B.5}$$

Inserting this result into Eq. (B.2) we now have

$$\sum_{lj}\sum_{f}\frac{|(H_v)_{si,lj}|^2\,|a^f_{lj}|^2}{(E_f-\bar{E}_{si})^2+(\gamma^{si/2})^2}=1 \tag{B.6}$$

where γ^{si} now replaces Γ_k in order to match the notation in Section 3.

Utilizing Eq. (B.4) and replacing the summation over f by an integration over E_f with the corresponding density of states, Eq. (B.6) takes the form

$$\frac{1}{2\pi}\sum_{lj}\int dE_f\,\frac{|(H_v)_{si,lj}|^2\,\Gamma_{lj}}{[(E_f-\bar{E}_{si})^2+(\gamma^{si}/_2)^2]\,[(E_f-E_{lj})^2+(\Gamma_{lj/2})^2]}=1\,. \tag{B.7}$$

The integral over E_f is easily evaluated assuming that Γ_{lj} does not depend on this variable leading to

$$W_{si}=\frac{\Gamma_{si}}{\hbar}=\frac{1}{\hbar}\sum_{lj}\frac{|(H_v)_{si,lj}|^2\,(\gamma^{si}+\Gamma_{lj})}{(E_{si}-E_{lj})^2+[\frac{1}{2}(\gamma^{si}+\Gamma_{lj})^2]}\,. \tag{B.8}$$

This result corresponds to the physical situation only in the limit $\Gamma_{lj} \ll \gamma^{si}$. Neglecting γ^{si} relative to Γ_{lj} in the r.h.s. of Eq. (B.8) we regain Eq. (3.7). It should be noted that if γ^{si} and Γ_{lj} were comparable in magnitude, the present procedure which is based on the condition (3.6) leads to an incorrect result as is seen by comparing Eqs. (B.8) and (3.5a).

References

1a. Henry, B. R., Kasha, M.: Ann. Rev. physic. Chem. **19**, 161 (1968).
1b. Jortner, J., Bixon, M.: Israel J. Chem. **48**, 715 (1968).
1c. Jortner, J.: Pure Appl. Chem. **24**, 165 (1970).
1d. Schlag, E. W., Schneider, S., Fischer, S. F.: Annu. Rev. physic. Chem. in press **22**, 465 (1971).
1e. Henry, B. R., Siebrand, W.: (to be published).
2. Douglas, A. E., Huben, K. P.: Canad. J. Physics **43**, 74 (1965).
3. Radford, H. E., Broida, H. P.: J. chem. Physics **38**, 644 (1963); physic. Rev. **128**, 231 (1963).
4. Bixon, M., Jortner, J.: J. chem. Physics **50**, 3284 (1969).
5. Nitzan, A., Jortner, J., Rentzepis, P. M.: Proc. Royal Soc. A **327**, 367 (1972).
6. Wannier, P., Rentzepis, P. M., Jortner, J.: Chem. Physics Letters **10**, 102 (1971).
7. Wannier, P., Rentzepis, P. M., Jortner, J.: Chem. Physics Letters **10**, 193 (1971).
8. Busch, G. E., Rentzepis, P. M., Jortner, J.: Chem. Physics. Letters **12**, 129 (1971).
9. Busch, G. E., Rentzepis, P. M., Jortner, J.: J. chem. Physics **56**, 531 (1972).
10. Rebane, K.: Impurity spectra of solids. New York: Plenum Press 1971.
11. Shpolskii, E. V.: Sov. Phys. Usp. **5**, 522 (1972); **6**, 411 (1963).
12a. Englman, R., Jortner, J.: Molecular Physics **18**, 145 (1970).
12b. Freed, K. F., Jortner, J.: J. chem. Physics **52**, 6272 (1970).
13. Nitzan, A., Jortner, J.: to be published.
14. Frosch, R. P., Robinson, G. W.: J. chem. Physics **41**, 367 (1964).
15. Meyer, B., Phillips, L. F., Smith, J. J.: Proc. nat. Acad. Sci. **61**, 7 (1968).

---

[4] In Eq. (B.5) only one level $|lj\rangle$ contributes as we have assumed that only one such level participates in a particular $|f\rangle$ state.

16. Nitzan, A., Jortner, J., Rentzepis, P. M.: Chem. Physics Letters **8**, 445 (1971).
17. Lin, S. H.: J. chem. Physics **46**, 279 (1967).
18. Jug, K., von Weyssenhoff, H.: J. chem. Physics **56**, 517 (1972).
19. Robinson, G. W., Frosch, R. P.: J. chem. Physics **37**, 1962 (1962); **38**, 1187 (1963).
20. Takahashi, K., Yokota, M.: Molecular Physics **20**, 663 (1971).
21. Nitzan, A., Jortner, J.: Effects of vibrational relaxation on electronic transitions, in chem. Physics (in press).
22. Freed, K. F., Jortner, J.: J. chem. Physics **50**, 2916 (1968).
23. Fischer, S.: J. chem. Physics **53**, 3195 (1970).
24a. Lin, S. H.: J. chem. Physics **44**, 3759 (1966).
24b. Lin, S. H., Bersohn, R.: J. chem. Physics **48**, 2732 (1968).
25. Nitzan, A., Jortner, J.: J. chem. Physics **55**, 1355 (1971).
26. Nitzan, A., Jortner, J.: J. chem. Physics **56**, 2079 (1972).
27. Nitzan, A., Jortner, J.: Vibrational relaxation of a molecule in a dense medium; in Molecular Physics *(in press)*.
28. Trifonov, E. D.: Sov. Phys. Solid State **9**, 2680 (1968).
29a. Kubo, R., Toyozawa, Y.: Progr. theoret. Physics (Osaka) **13**, 161 (1955).
29b. Lax, M.: J. chem. Physics **20**, 1752 (1952).
30. Posener, D. W.: Austral. J. Physics **12**, 184 (1959).
31. Heitler, W.: The quantum theory of radiation. Oxford: University Press 1954.
32. Fano, U.: Physic. Rev. **124**, 1866 (1961).

Prof. Dr. J. Jortner
Department of Chemistry
Tel-Aviv University
Tel-Aviv, Israel

Theoret. chim. Acta (Berl.) 29, 117–131 (1973)
© by Springer-Verlag 1973

Orbital and Excitonic Descriptions of Molecular Excited and Ionized States

I. Delocalization of the Excitation

Armelle Denis, Jacqueline Langlet, and J. P. Malrieu

Institut de Biologie Physico-Chimique, Laboratoire de Biochimie Théorique associé au C.N.R.S.
13, rue P et M. Curie, Paris 5è

Received October 9, 1972

The single determinantal Virtual Orbital description of the excited state is compared with the excitonic description for an homogeneous chain of n subunits. The single determinant built from canonical delocalized MO's represents the excited state as a "democratic" mixture of Charge Transfer excitations; the long distances electron jumps are highly probable while the local excitations within the bonds have a vanishing weight when the dimension increases. On the contrary the excitonic treatment (and therefore the Configuration Interaction between singly excited configurations) describes the excited state as mainly built from local excitations and Charge Transfer excitations between adjacent bonds; the long distance electron transfer probability decreases exponentially with the amplitude of the electron jump. Therefore one may say that the Orbital description of the excited state overestimates the electronic delocalization in the excited state. It is shown that the fluctuation of the dipole moment in the excited state varies as n^2 in the Orbital description while in the excitonic model this fluctuation is bounded.

On compare les descriptions excitonique et monodeterminantale (dite Approximation d'Orbitale Virtuelle) des etats excités d'une chaîne homogène de n sous-unités. La représentation à un seul déterminant à l'aide d'orbitales SCF canoniques décrit l'état excité comme un mélange «démocratique» d'«excitations» de transfert de charge: les transferts d'électrons à longue distance y sont très probables, tandis que le poids des excitations locales à l'intérieur des liaisons tend vers zéro quand n augmente. Au contraire le traitement excitonique (et donc l'interaction de configuration des configurations monoexcitées) décrit l'état excité à l'aide d'excitations locales et d'excitations de transfert de charge à courte distance; la probabilité de transferts à longue distance décroît exponentiellement avec l'ampleur du saut. On peut donc dire que la description à un seul déterminant surestime qualitativement la délocalisation électronique dans l'état excité. On montre que la fluctuation quantique du moment dipolaire dans l'état excité croît comme n^2 dans la description orbitale, tandis qu'elle reste bornée dans le modèle excitonique.

Die Beschreibung eines angeregten Zustandes einer homogenen Kette von n Untereinheiten durch eine Determinante mit virtuellen Orbitalen wird mit der excitonischen Beschreibung verglichen. Die einzelne Determinante, die aus kanonischen delokalisierten MO's aufgebaut wird, stellt den angeregten Zustand als eine Mischung von Anregungen mit Ladungsübertragung dar; die Übertragungen von Elektronen über große Entfernungen sind sehr wahrscheinlich, während lokale Anregungen innerhalb der Bindungen ein verschwindendes Gewicht haben, falls die Zahl n ansteigt. Im Gegensatz dazu beschreibt die excitonische Darstellung (und somit die Konfigurationenwechselwirkung mit einfach angeregten Konfigurationen) die angeregten Zustände hauptsächlich durch lokale Anregungen mit Ladungsübertragung zwischen benachbarten Bindungen; die Wahrscheinlichkeit der Übertragung über größere Entfernungen nimmt exponentiell mit der Weite des „Elektronensprungs" ab. Man kann deshalb sagen, daß die Orbitalbeschreibung eines angeregten Zustands die Elektronendelokalisierung überbewertet. Es wird gezeigt, daß die Fluktuation des Dipolmoments im angeregten Zustand wie n^2 in der Orbitalbeschreibung variiert, während sie im excitonischen Modell beschränkt bleibt.

Localized Molecular Orbitals are beginning to be widely used for the study of ground state properties (total ground state energy[1], conformational properties[2], Electron Spin Resonance[3] and Nuclear Magnetic Resonance[4] coupling constants). They have even been used for the study of the stereoselectivity of concerted reactions [7, 8], i.e. outside of the ground state equilibrium region, for nuclear configurations where the bond definition begins to be ambiguous.

The main objection against the localized MO's concerns the representation of excited and ionized states [9]. The idea that the ESCA or ESR experiments show the orbital energy or the orbital repartition as physical features, can only be regarded as naive. But it is clear that the use of symmetry delocalized MO's allows a rather satisfactory single determinantal representation of the excited or ionized states, and the adequacy of the delocalized symmetry MO's for a simple single determinantal representation of the delocalized spectroscopic phenomena certainly explains the complete domination of the delocalized MO's methods over the research and pedagogic works of quantum chemistry [10].

The excited or ionized states may be represented as well from the equivalent sets of localized MO's, using then multideterminantal wave-functions; the excited state appears then as a linear combination of local single excitations, the coefficients of this combination resulting from a partial Configuration Interaction between the local excitations. This is simply the "excitonic" representation of excited states, which has received some applications in molecular physics [11 – 14]. In some sense the situation may be summarized as follows.

The use of symmetry delocalized MO's, generally implies the variational diagonalization of a one-electron effective hamiltonian (a Hückel type one, or an Hartree-Fock hamiltonian, with possible modifications of the internal field representation in order to get better representations of the excited state). This rather blind procedure allows a single determinantal zeroth order representation of the excited state.

– The excitonic model may use chemically meaningfull localized MO's, atomic core orbitals, bonding and antibonding bond MO's and lone pairs but the description of the excited state requires the diagonalization of a partial CI matrix; the blind procedure is simply displaced from the MO construction to the total WF construction.

In the present paper the two descriptions will be compared on a simple model case, the case of linear homogeneous polymer. It will be shown that the charge-fluctuations (i.e. the probability electron transfers between distant bonds) are overestimated in the single determinantal orbital description of the excited state.

---

[1] For single determinantal approximation, see Ref. [1a]; for multiconfigurational perturbative method from SCF localized MO's, *ab initio* calculations, see Ref. [2a], semiempirical calculations, see Ref. [2b]; for multiconfigurational perturbative method from non-SCF bond MO's, one must quote the semi-empirical PCILO method, see Ref. [3], and a few *ab initio* calculations, see first Ref. of [2a] and last Ref. of [3].

[2] *Ab initio* calculations, see Ref. [4]; for semiempirical calculations, the applications of the PCILO method (Ref. [3]) are too numerous to be quoted here.

[3] The fundamental McConnell relationship was already based on the use of localized MO's, [5a]; for some recent *ab initio* calculations see Ref. [5b]; for semiempirical calculations see the PCILO method for localized free radicals [5c].

[4] For *ab initio* calculations, see Ref. [6a]; for semiempirical calculations, see Ref. [6b].

1. Translation of the Single-Determinantal Delocalized Description of the Excitation in Terms of Local Excitations

Let us consider a regular chain of n equivalent bonds. This might be a chain of H_2 molecules, or the π bonds of a linear polyene. Let us consider the (SCF) localized MO's on these bonds, p_i, and the corresponding antibonding (SCF) localized MO's in the valence shell p_{i^*}[5]. One may establish easily the expression of the occupied delocalized (SCF) MO's, by diagonalizing the Fock operator between the bonding localized MO's. Neglecting end effects, and assuming that the Fock operator between non adjacent bonds are negligible in comparison of the Fock operator between adjacent bonds,

$$\begin{aligned} &\langle p_s|F|\,p_s\rangle = E\,\forall s \\ &\langle p_s|F|\,p_{s+1}\rangle = \langle p_s|F|\,p_{s-1}\rangle = F\,\forall s \\ &\langle p_s|F|\,p_{s+r}\rangle \ll F \qquad\qquad \forall s \quad \text{and } |r|>1 \end{aligned} \tag{1}$$

one gets a Fock operator which keeps the form of a Hückel type topological matrix, and the delocalized MO's P_j are given by

$$P_j = \sum_s c_{js} p_s \qquad c_{js} = \sqrt{\frac{2}{n+1}} \sin \frac{j\pi s}{n+1}. \tag{2}$$

The corresponding energies increase when j varies from 1 to n. The form of the Fock operator between the virtual orbitals would be the same

$$\begin{aligned} &\langle p_s^*|F|\,p_s^*\rangle = E^*\,\forall s \\ &\langle p_s^*|F|\,p_{s+1}^*\rangle = F^*\,\forall s \\ &\langle p_s^*|F|\,p_{s+r}^*\rangle = 0 \quad \forall s, \quad r>1 \end{aligned} \tag{3}$$

and the delocalized HF MO's are given by

$$P_j^* = \sum_s c_{js}^* p_s^* \qquad c_{js}^* = \sqrt{\frac{2}{n+1}} \sin \frac{j\pi s}{n+1}. \tag{4}$$

The corresponding energies now decrease when n varies from 1 to n, because $FF^* < 0$, as may be easily understood by considering the respective phase behaviour of the occupied and virtual localized MO's.

$$\underset{p_i}{\underline{+\quad +}}\qquad \underset{p_{i+1}}{\underline{+\quad +}},$$

$$\underset{p_i^*}{\underline{+\quad -}}\qquad \underset{p_{i+1}^*}{\underline{+\quad -}}.$$

Therefore the ordering of the delocalized SCF MO's is given by Fig. 1, which shows the "pairing" of occupied and virtual MO's.

---

[5] These SCF localized MO's may be obtained from the usual canonical MO's through any localization process, see Ref. [15].

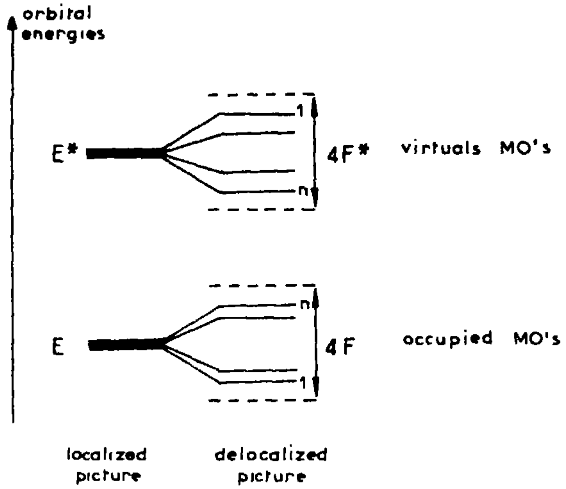

Fig 1 Ordering of the delocalized MO's obtained from the diagonalization of the Fock operators for the occupied and virtual (HF) localized MO's. The dashed lines represent the limit of the orbital energies when n tends to infinity

The canonical and localized descriptions of the SCF ground state determinant are given by

$$\Phi_0 = \mathscr{A} \prod_{i=1}^{n} P_i = \pm \mathscr{A} \prod_{r=1}^{n} p_r . \tag{5}$$

These two descriptions are equivalent since the two sets $\{p_r\}$ and $\{P_i\}$ are obtained from each other through a unitary transformation [16].

N.B. If the p_r MO's are SCF localized MO's, the Fock operator is zero between occupied and virtual MO's (due to the Brillouin's theorem). This is the reason why we diagonalized separately the two blocks of the Fock operator. If the p_r MO's where fully localized MO's (as in the PCILO method and the usual excitonic treatments), the Fock operator would not split in two blocks, but the diagonalization of the two blocks for occupied and virtual MO's would still give delocalized MO's very close to the SCF ones, since the SCF localized and fully localized MO's are very close [2].

Then the unoptimized single determinantal representation of the excited state (which is frequently called the Virtual Orbital approximation) is obtained by the substitution of a virtual MO P_{j^*} to an occupied one P_i. In the 2nd quantization formalism, this may be written as:

$$\Phi\begin{pmatrix} j^* \\ i \end{pmatrix} = a_{j^*}^{+} a_0 \Phi_0 . \tag{6}$$

Expressing the canonical creation and annihilation operators in terms of local creation and annihilation operators (through Eqs. (2) and (4)) one gets an equivalent *expression of the excitation procedure*

$$\Phi\begin{pmatrix} j^* \\ i \end{pmatrix} = \frac{2}{n+1} \sum_{r} \sum_{s} \sin \frac{i\pi r}{n+1} \sin \frac{j\pi s}{n+1} a_{p_{s^*}}^{+} a_{p_r} \Phi_0 \tag{7}$$

where Φ_0 may expressed now as the antisymmetrized product of local MO's

$$\Phi\binom{j^*}{i} = \frac{2}{n+1}\sum_r\sum_s \sin\frac{i\pi r}{n+1}\sin\frac{j\pi s}{n+1}\,\Phi\binom{s^*}{r}. \tag{8}$$

The single excitation from P_i to P_{j^*} appears as the linear combination of local excitations from the bonds r toward the antibonding MO of the bonds s. These excitations may be described in general as electron transfer from one region to another. Some of the local excitations, for which $s = r$, do not imply such an electron transfer since they simply represent a $(\pi\pi^*)$ excitation in the ethylenic system of a (double) bond. These excitations $(r = s)$ will be called local excitations (LEs) while the former ones $(r \neq s)$ will be called Charge Transfer excitations (CTEs). The CTEs will be characterized by the amplitude of the electron jump through the quantity $p = |r - s|$ and identified as ^{p}CTE.

Let us analyze now the relative weight of local and charge transfer excitations in the (lowest) excitations. The weight of LE is given by

$$d_{\mathrm{LE}}\binom{j^*}{i} = \left(\frac{2}{n+1}\right)^2 \sum_r \left(\sin\frac{j\pi r}{n+1}\sin\frac{i\pi r}{n+1}\right)^2. \tag{9}$$

Since $\sin^2\alpha \leqq 1$

$$d_{\mathrm{LE}}\binom{j^*}{i} \leqq \frac{4}{n+1}. \tag{10}$$

A more accurate calculation gives $d_{\mathrm{LE}}\binom{j^*}{i} = \frac{1}{n+1}\left[1 + \frac{f(i,j,n)}{n+1}\right]$ where f is bounded by a constant whatever i, j, n.

Therefore the relative weight of LE in the Virtual Orbital description of excited states decreases as $1/n$ when the dimension n of the conjugated system increases[6].

On the contrary the weight of the CTE increases towards 1. The excitations are treated almost democratically, whatever the distance between the departure and arrival bonds, i.e. the amplitude of the electron jump. It will be seen in Appendix 1 that a jump over p intermediate bonds becomes as probable as the local excitations when n is much larger than p.

2. The Excitonic Wave-Function

Let us turn back now towards the excitonic model, in order to analyze the structure of the lowest excited states. The excitonic matrix appears as built from several blocks. One block deals with the LE excitations $\binom{p^*}{p}$ and their matrix

---

[6] These results are not modified by considering the proper S^2 eigenfunctions for the excited state

$$\Psi\binom{j^*}{i}^{1,3} = 1/\sqrt{2}\left(\Phi\binom{j^*}{i} \pm \Phi\binom{j^*}{i}\right)$$

instead of the single determinant $\Phi\binom{j^*}{i}$ of Eq (6) elements. For singlet states these matrix elements are essentially transition dipole-transition dipole interactions

$$\left\langle \Phi\begin{pmatrix} r^* \\ r \end{pmatrix} \middle| H \middle| \Phi\begin{pmatrix} s^* \\ s \end{pmatrix} \right\rangle = 2(p_r p_r^*, p_s p_s^*) - (p_r p_s^*, p_s p_r^*). \tag{11}$$

The second term decreases exponentially with the distance R_{rs} between the bonds r and s, and the first one decreases as $1/R_{rs}^3$. For the triplet state the dipolar interaction disappears. In both cases one may consider that the only important off diagonal elements occur between excitations on adjacent bonds

$$(p_r p_r^*, p_{r+1} p_{r+1}^*) = (p_r p_r^*, p_{r-1} p_{r-1}^*) = b. \tag{12}$$

The LE are less energetic than the CTE, as may be seen from the zeroth-order

$$\Delta E\begin{pmatrix} s^* \\ r \end{pmatrix} = \langle p_s^* | F | p_s^* \rangle - \langle p_r | F | p_r \rangle - J p_r p_s^* + K p_r p_s^* \pm K p_r p_s^*. \tag{13}$$

In this expression the difference between the diagonal elements of the Fock operator are independant on the distance between r and s, while the charge-charge interaction $J p_r p_s^*$ decreases as R_{rs}^{-1}. $K p_r p_s^*$ decreases exponentially with R_{rs} but remains always much smaller than $J p_r p_s^*$ and the localized transition energies may be ordered in the following way:

$$\begin{aligned} &\left(\Delta E_0 = \Delta E\begin{pmatrix} r^* \\ r \end{pmatrix}\right) < \left(\Delta E_1 = \Delta E\begin{pmatrix} (r\pm 1)^* \\ r \end{pmatrix}\right) < \left(\Delta E_2 = \Delta E\begin{pmatrix} (r\pm 2)^* \\ r \end{pmatrix}\right) \\ &< \cdots < \left(\Delta E_p = \Delta E\begin{pmatrix} (r\pm p)^* \\ r \end{pmatrix}\right) < \cdots < (\langle p_s^* | F | p_s^* \rangle - \langle p_r | F | p_r \rangle). \end{aligned} \tag{14}$$

One may build therefore the excitonic matrix in a basis of localized excited determinants in which the LE occur first, followed by CTExcitations between adjacent bonds, and so on ... The LE determinants are coupled with the CTE ones, through

$$\left\langle \Phi\begin{pmatrix} r^* \\ r \end{pmatrix} \middle| H \middle| \Phi\begin{pmatrix} s^* \\ t \end{pmatrix} \right\rangle = \langle p_r p_{t^*} | p_r^* p_s \rangle.$$

If r, s and t are all different this matrix element may be approximated through the Mulliken's approximation

$$\left\langle \Phi\begin{pmatrix} r^* \\ r \end{pmatrix} \middle| H \middle| \Phi\begin{pmatrix} s^* \\ t \end{pmatrix} \right\rangle = 1/2 \langle p_s | p_t^* \rangle \left[\langle rs | r^* s \rangle + \langle rt^* | r^* t^* \rangle \right] \tag{15}$$

$\langle ps | pt^* \rangle$ decreases exponentially as $\exp(-R_{st})$, and the two integrals decrease as R_{rs}^{-2} and R_{rt}^{-2} respectively. The matrix element will be negligible except when $t = r$ or $s^* = r^*$. In such a case

$$\begin{aligned} \left\langle \Phi\begin{pmatrix} r^* \\ r \end{pmatrix} \middle| H \middle| \Phi\begin{pmatrix} s^* \\ r \end{pmatrix} \right\rangle &= \langle p_r^* | F - J_r | p_s^* \rangle \\ \left\langle \Phi\begin{pmatrix} r^* \\ r \end{pmatrix} \middle| H \middle| \Phi\begin{pmatrix} r^* \\ s \end{pmatrix} \right\rangle &= \langle p_r | F + J_{r^*} | p_s \rangle. \end{aligned} \tag{16}$$

If s and r are adjacent bonds ($s = r \pm 1$), these matrix elements are rather important

$$\begin{aligned}
\left\langle \Phi\begin{pmatrix} r^* \\ r \end{pmatrix} \middle| H \middle| \Phi\begin{pmatrix} (r \pm 1)^* \\ r \end{pmatrix} \right\rangle &= \langle p_r^* | F - J_r | p_{r\pm 1}^* \rangle = A_1 \\
\left\langle \Phi\begin{pmatrix} r^* \\ r \end{pmatrix} \middle| H \middle| \Phi\begin{pmatrix} r^* \\ (r \pm 1) \end{pmatrix} \right\rangle &= -\langle p_r | F + J_{r^*} | p_{r\pm 1} \rangle = B_1
\end{aligned} \tag{17}$$

and we shall keep only these interactions, as we did when diagonalizing the ground state Fock operator. In the same way the CTE between adjacent bonds are coupled with some CTE at two bonds distances.

$$\begin{aligned}
\left\langle \Phi\begin{pmatrix} (r+1)^* \\ r \end{pmatrix} \middle| H \middle| \Phi\begin{pmatrix} (r+2)^* \\ r \end{pmatrix} \right\rangle &= \langle p_{r+1}^* | F - J_r | p_{r+2}^* \rangle = A_2 \\
\left\langle \Phi\begin{pmatrix} (r+1)^* \\ r \end{pmatrix} \middle| H \middle| \Phi\begin{pmatrix} (r+1)^* \\ r+2 \end{pmatrix} \right\rangle &= -\langle p_r | F + J_{(r+1)}^* | p_{r+2} \rangle = B_2 .
\end{aligned} \tag{18}$$

The structure of the excitonic CI matrix is shown in Fig. 2. Then, taking benefit of the fact that $\Delta E_0 < \Delta E_1 < \Delta E_2$ etc... one may try to search the eigenfunctions of the CI matrix by a two steps procedure.

a) diagonalization of the CI matrix of the LE only. This is the original excitonic treatment proposed by Simpson [11]. This step gives some zeroth order wave-functions Ψ_m^0.

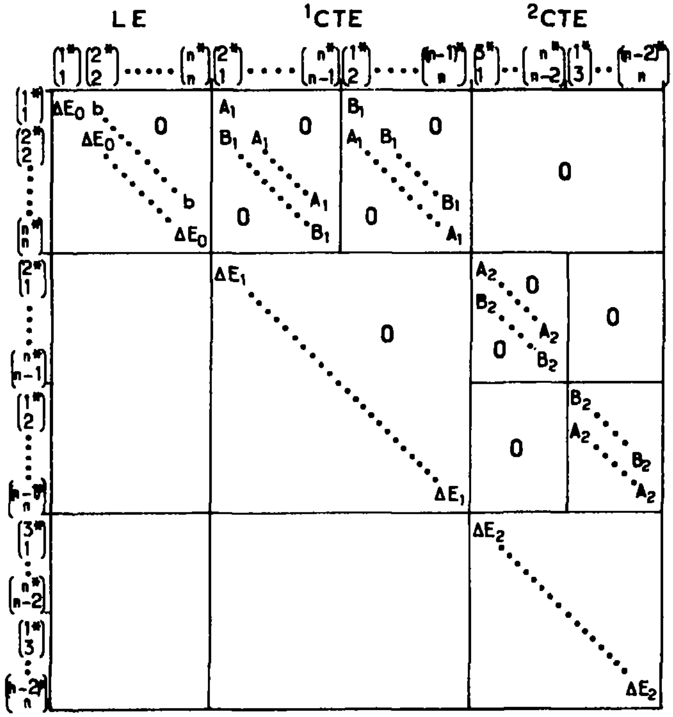

Fig. 2. Structure of the excitonic matrix

b) perturbation of these zeroth order wave functions under the influence of the CTE, through a classical RS procedure.

Since the CI matrix restricted to the LE has a Hückel-type structure, one knows its eigenfunctions and eigenvalues

$$\Psi_m^0 = \sum_{r=1}^{n} C_{mr}\Phi\begin{pmatrix} r^* \\ r \end{pmatrix} \quad \text{with} \quad C_{mr} = \sqrt{\frac{2}{n+1}}\sin\frac{m\pi r}{n+1}, \tag{19}$$

$$\Delta E_m^0 = \Delta E_0 + 2b\cos\frac{m\pi}{n+1}. \tag{20}$$

Then one may perturb Ψ_m^0 under the influence of the CTE. The theoretical details of such a procedure may be found elsewhere [17]. Due to the structure of the CI matrix when one neglects the long distances overlap distributions, the first order wave-function Ψ_m^1 will only involve the ^{1}CTE, i.e. the CTE between adjacent bonds.

$$\Psi_m^1 = \sum_r \left[\left\langle \Psi_m^0 \middle| H \middle| \Phi\begin{pmatrix} (r+1)^* \\ r \end{pmatrix}\right\rangle \Phi\begin{pmatrix} (r+1)^* \\ r \end{pmatrix} + \left\langle \Psi_m^0 \middle| H \middle| \Phi\begin{pmatrix} (r-1)^* \\ r \end{pmatrix}\right\rangle \Phi\begin{pmatrix} (r-1)^* \\ r \end{pmatrix}\right] \times (\Delta E_m^0 - \Delta E_1)^{-1}. \tag{21}$$

In order to analyse the relative weight of the LE and CTE in that model, we must calculate the norm of the first order perturbed wave-function.

$$\begin{aligned} \langle \Psi_m^1 | \Psi_m^1 \rangle &= (\Delta E_m^0 - \Delta E_1)^{-2} \sum_r \left\langle \Psi_m^0 \middle| H \middle| \Phi\begin{pmatrix} (r+1)^* \\ r \end{pmatrix}\right\rangle^2 \\ &\quad + \left\langle \Psi_m^0 \middle| H \middle| \Phi\begin{pmatrix} (r-1)^* \\ r \end{pmatrix}\right\rangle^2 \left\langle \Psi_m^0 \middle| H \middle| \Phi\begin{pmatrix} (r+1)^* \\ r \end{pmatrix}\right\rangle \\ &= C_{mr}\left\langle \Phi\begin{pmatrix} r^* \\ r \end{pmatrix} \middle| H \middle| \Phi\begin{pmatrix} (r+1)^* \\ r \end{pmatrix}\right\rangle + C_{m(r+1)}\left\langle \Phi\begin{pmatrix} (r+1)^* \\ (r+1) \end{pmatrix} \middle| H \middle| \Phi\begin{pmatrix} (r+1)^* \\ r \end{pmatrix}\right\rangle \\ &= C_{mr}A_1 + c_{m(r+1)}B_1\,. \end{aligned} \tag{23}$$

Thus

$$\langle \Psi_m^1 | \Psi_m^1 \rangle = \frac{2}{n+1}(\Delta E_m^0 - \Delta E_1)^{-2} \sum_{r=1}^{n-1}\left(\sin\frac{mr\pi}{n+1}A_1 + \sin\frac{m(r+1)\pi}{n+1}B_1\right)^2. \tag{24}$$

This summation is easy to perform through elementary trigonometrical transformations and gives

$$\langle \Psi_m^1 | \Psi_m^1 \rangle = 4\left(\frac{A_1 + B_1}{\Delta E_m^0 - \Delta E_1}\right)^2 + \frac{1}{n+1}f(n,m) = N_1 + \frac{1}{n+1}f(n,m) \tag{25}$$

where $f(n,m)$ is a trigonometric function of n and m bounded by a constant. Therefore the weight of the CTE in the first order perturbed wave functions tends towards a constant when n increases. Since $\langle \Psi_m^0 | \Psi_m^0 \rangle = 1$, the ratio of the LE in the first order perturbed wave function tends towards a constant

$$\frac{\langle \Psi_m^0 | \Psi_m^0 \rangle}{\langle \Psi_m^0 | \Psi_m^0 \rangle + \langle \Psi_m^1 | \Psi_m^1 \rangle} \simeq \frac{1}{1+N_1} \quad \text{when} \quad n \to \infty\,. \tag{26}$$

The further ^{p}CTE excitations would appear with exponentially decreasing weights: in the first order wave-function the coefficients would imply exponentially decreasing overlap distributions $\varphi_r\varphi_{(r+p)}$, and if one only keeps the interactions between adjacent bonds, they would only appear at the p^{th} order of perturbation with a weight proportional to x^p (See Appendix 2).

3. Discussion of the Electronic Delocalization in the Excited State

This analysis rests upon the convergence of the perturbation expansion. This convergence is questionable for the higher eigenfunctions of the LE CI matrix, but is certainly valid for the lowest excitations. The numerical diagonalizations of the full excitonic matrix actually show that the relative weight of LE tends towards 45% in the series of linear polyenes [18].

The result of the CI procedure gives therefore a description of the excited states which differs qualitatively from the Virtual Orbital single determinant description. The single determinant built from canonical delocalized MO's represents the excited state as a "democratic" mixture of Charge Transfer Excitations. The long distance electron jumps are highly probable while the local excitations in the bonds have a vanishing weight when the dimension increases. On the contrary the excitonic treatment describes the excited state as mainly built from local excitations in the bond (the corresponding probability decreases but tends towards a constant when the number of equivalent bonds increases) and from ^{1}CTE between adjacent bonds. The electron jumps probabilities decrease exponentially with the amplitude of the jump.

It had been noticed already that in the Hückel theory the Orbital description of the excited state only involves exchange or delocalization effects which are therefore overestimated to reproduce implicitely the bielectronic effects[7] One sees here that going from the Hückel to the SCF model does not change quatitatively the validity of the single determinantal description of the excited state as regard the electronic delocalization.

This result concerns not only the excitonic treatment but the usual Configuration Interaction between the singly excited configurations; since the canonical MO's are obtained from the localized ones by two unitary transformations in the spaces of occupied and virtual MO's, the space of the singly excited determinants is invariant in these changes of the MO's, and the eigenvectors of the CI matrix of singly excited determinants are the same, regardless of the localized or delocalized character of the MO's. The excitonic treatment gives therefore some insight upon the physical effect of the CI of singly excited states, which, in the delocalized scheme, seems rather intricate and difficult to analyse, since all the matrix elements loose their local character. Once again the localized picture demonstrates its higher handiness and its interpretative power.

But the most surprising result is that the canonical orbital model of the excitation in a certain sense overestimates the electronic delocalization in the excited state. Of course quantum mechanics describes the excitation as delocalized. In the statistical interpretation of quantum mechanics [20] the Hamiltonian and the wave-function only deal with a set of similarly prepared systems, not with a unique system, and we cannot know what happens in the excitations of a given molecule. The delocalization is linked to the symmetry properties of the Hamiltonian and does not prove anything about the local or global character of the excitation in each molecular system. Even in the excitonic model which only implies the local excitations, the excitation is delocalized, and, this "delocalization" due to the basic principles, cannot be removed in homogenous symmetrical systems.

---

[7] See Refs. [12] and [19].

But the delocalization of the electrons is completely different from the delocalization of the excitation. In this loge theory [21], Daudel has proposed some intrinsic criteria to analyse the extent of electronic delocalization; the probability of finding two and only two electrons in each loge of a partition of space may be maximized with respect to the definition of the loge and this maximum gives an estimate of the physical electronic localization. The higher this probability, the less probable are the situations with 1 electron in loge *i* and 3 electrons in loge *j*.

Along the same direction, and according to the statistical interpretation of the wave-function we proposed to study the fluctuation of the number of electrons in each loge [22]. When the fluctuations are important, the system is not well localizable. One may also consider as a measure of the electronic delocalization the fluctuations of the dipole moment; in a symmetric or non polar system, the "permanent" or mean dipole moment will be zero but the ionic structures in which one electron has jumped from its box *i* to the box *j* introduce some transient dipoles. This concept may be applied to the excited states, and from that point of view it is clear that the orbital description of the excited state overestimates the electronic delocalization. This description (Eq. (8)) is very close the "fully democratic" delocalized description of the excited state where each configuration $\Phi\begin{pmatrix} s^* \\ r \end{pmatrix}$ would appear with a probability $1/n^2$.

$$\Psi = 1/n \sum_r \sum_s \Phi\begin{pmatrix} s^* \\ r \end{pmatrix} \tag{27}$$

for a linear system, the configuration $\Phi\begin{pmatrix} s^* \\ r \end{pmatrix}$ introduces a dipole moment equal to

$$\vec{\mathcal{M}}_{rs} = e\overrightarrow{Rrs} = e\vec{l}(r-s) \tag{28}$$

where l is the standard distance between two bonds $(\vec{r}, \vec{r}+1)$. We shall neglect here the transition dipole moment between different CTE excitations, even when they differ by two adjacent MO's

$$\left\langle \Phi\begin{pmatrix} s^* \\ r \end{pmatrix} \middle| \overrightarrow{\Sigma \boldsymbol{R}} \middle| \Phi\begin{pmatrix} (s+1)^* \\ r \end{pmatrix} \right\rangle = \langle s^* | \boldsymbol{R} | (s+1)^* \rangle \simeq 0 ,$$

as would be done in the CNDO hypotheses for fully localized MO's. All the configurations where $r-s=q$ contribute to the same value $\vec{\mathcal{M}}_q = e\vec{l}q$, which appears with the probability $p_q = \frac{n-|q|}{n^2}$. One knows therefore the full histogram of the dipole moment of the excited state, i.e. the spectral decomposition of the dipole moment in the excited state, which is reported in Fig. 3.

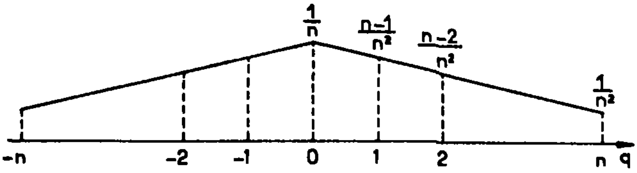

Fig. 3. Distribution of the dipole moment of the excited state for the delocalized single determinantal description

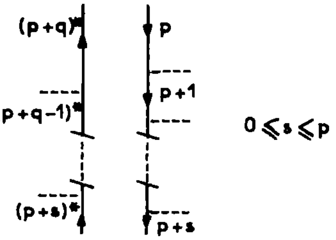

Fig. 4. Appearance of the $\binom{(p+q)^*}{p}^q$ CTE's configurations from the $\binom{(p+s)^*}{(p+s)}$ LE's configurations

The fluctuation of the dipole moment in the excited state may be calculated immediately

$$\mathcal{F} = 2\sum_{q=1}^{n-1} \mathcal{M}_q^2\, p_q = 2\Sigma(el)^2\, q^2\, \frac{n-q}{n^2} = 2(el)^2 \sum_{q=1} (nq^2 - q^3)\,.$$

Since

$$\sum_{q=1}^{n-1} q^2 \simeq \frac{n^3}{3} \quad \text{and} \quad \sum_{q=1}^{n-1} q^3 \simeq \frac{n^4}{4}$$

$$\mathcal{F} = 2(el)^2\, n^2/6\,.$$

The fluctuation of the dipole moment increases as n^2 when the dimension of the system increases. One may see easily that this feature is kept when one uses Eq. (8) for the wave-function, instead of the "fully democratic" single determinantal representation of Eq. (27).

On the contrary the excitonic model (i.e. the full CI of singly excited determinants, whatever the basis set of MO's) will give a completely different histogram. Since the wave-function appears as mainly built from the LE and ^{1}CTE between adjacent bonds, in a ratio which tends towards a constant, the histogram tends towards a constant shape and the fluctuation of the dipole moment also increases towards a constant when n increases.

This result remains valid when one takes into account the long distances ^{p}CTE with their exponentially decreasing weight e^{ap} (cf. Appendix 2). Their contribution to the fluctuation of the dipole moment is indeed proportional to $2\sum_{p=1}^{n-1} p^2 e^{ap}$. This sum may be bracketed through the integration

$$\int_1^n p^2 e^{ap}\, dp < \sum_{p=1}^{n-1} p^2 e^{ap} < \int_0^{n-1} p^2 e^{ap}\, dp\,.$$

$\int_0^n p^2 e^{ap} dp = e^{an}\left(\frac{n^2}{a} - \frac{2n}{a^2} + \frac{2}{a^3}\right)$ is bonded whatever n and therefore the fluctuation of the dipole moment is bonded, a being negative as may be seen from Appendix 2.

The configuration Interaction between the singly excited configurations qualitatively changes the picture of the excited state. In the Orbital description, the mean number of electrons per bond is correct, but the fluctuations of electronic positions are much too large. The CI tends to bring back the electrons two by two in each loge. One may say that the orbital description of the excited state is too disordered, and that the CI brings some order in the excited state, diminishes the entropy of the description. The excitonic model looses the single determinantal character and its related advantages, but it gives inmediately a more correct representation of the excited state. Table 1 summarizes the main conclusions of this work.

In the following paper, we shall demonstrate that the qualitative differences between the Orbital and Excitonic descriptions of the excited state imply some qualitative differences in the descriptions of the $\sigma-\pi$ coupling effect on the $\pi\pi^*$ transition, and in the orbital reorganisation of the excited states.

Table 1 Summary of the comparison between delocalized and localized pictures of the excitation

	Delocalized picture		Localized picture
s	Delocalized P_i, P_{j^*}		Localized p_r, p_{s^*} $\{p\} = \mathbf{U}\{\mathbf{P}\}$ $\mathbf{U}$ unitary
ınd State determinant	Φ_0	identical	Φ_0
:ed determinants	$\Phi\begin{pmatrix} j^* \\ i \end{pmatrix}$		Local excitations $\Phi\begin{pmatrix} r^* \\ r \end{pmatrix}$ charge transfer excitations $\Phi\begin{pmatrix} (r+p)^* \\ r \end{pmatrix}$
esentation of the excited			
e determinantal approx	*Virtual orbital approximation* $\Phi\begin{pmatrix} j^* \\ i \end{pmatrix}$ may be expressed in terms of $\Phi\begin{pmatrix} s^* \\ r \end{pmatrix}$ The weight of LE's $\rightarrow 0$, of PCTE's $\rightarrow 1$ $\Big\}$ when $n \rightarrow \infty$ The fluctuation of the dipole moment in the excited state behaves like n^2		no single determinantal approximation
:tween the single excited minants	*Usual CIS approximation* This treatment is identical to the excitonic one. The conclusions obtained for the excitonic treatment hold for the CIS approximation, which therefore relocalizes the excitation with respect to the VO approximation	$\equiv$	*Excitonic method* The weight of LE's → constant C (~ 50%) ^{1}CTE's → 1-C (~ 50%) when $n \rightarrow \infty$ The fluctuation of the dipole moment in the excited state → constant.

Appendix 1

Weight of the ^{p}CTEs in the Orbital Model

According to Eq. (8) the weight of the ^{p}CTEs in the orbital model is given by

$$Q(n, p) = \frac{8}{(n+1)^2} \sum_{r=1}^{n-p} \sin^2 \frac{i\pi r}{n+1} \sin^2 \frac{j\pi(r+p)}{n+1}$$

for the transition $i \to j^*$. For sake of simplicity, the analysis will be limited to the lowest transition, the $N-V$ transition, corresponding to $i=j=n$. Then

$$Q(n, p) = \frac{8}{n+1^2} \sum_{r=1}^{n-p} \sin^2 \frac{n\pi r}{n+1} \sin^2 \frac{2n\pi(r+p)}{n+1}$$

$$= \frac{8}{(n+1)^2} \sum_{r=1}^{n-p} \left(\sin \frac{\pi r}{n+1} \sin \pi \frac{r+p}{n+1} \right)^2$$

$$= \frac{2}{(n+1)^2} \sum_{r=1}^{n-p} \left(\cos \frac{\pi p}{n+1} - \cos \frac{2\pi}{n+1} (r+p/2) \right)^2$$

$$= \frac{2}{(n+1)^2} \sum_{r=1}^{n-p} \left(\cos^2 \frac{\pi p}{n+1} + \cos^2 \frac{2\pi(r+p/2)}{n+1} - 2 \cos \frac{\pi p}{n+1} \frac{\cos 2\pi(r+p/2)}{n+1} \right)$$

$$\Sigma \cos^2 \frac{\pi p}{n+1} = (n-p-1) \cos^2 \frac{\pi p.}{n+1}$$

$$\Sigma \cos^2 \frac{\pi(2r+p)}{n+1} = \frac{n-p-1}{2} + \sin \frac{2p\pi}{n+1} - \cos \frac{2p\pi}{n+1} \left(1 + tg \frac{2\pi}{n+1} \right)$$

$$-\Sigma 2 \cos \frac{p\pi}{n+1} \cos \frac{(2r+p)\pi}{n+1} = \sin \frac{2p\pi}{n+1} - 1 + \cos \frac{2p\pi}{n+1} \left(1 + \mathrm{tg} \frac{\pi}{n+1} \right).$$

Therefore

$$Q(n, p) = \frac{2}{(n+1)^2} \left[(n-p-1) \left(1/2 + \cos \frac{2\pi p}{n+1} \right) + f(n, p) \right]$$

where $f(n, p)$ is a trigonometric function bonded by a constant. $Q(n, p)$ behaves as $\frac{n-p}{(n+1)^2} \left(1 + 2 \cos^2 \frac{\pi p}{n+1} \right)$, and when n increases for a fixed value of p, this quantity tends towards $3/n$.

Appendix 2

Weight of the Long Distances Charge Transfer Excitations in the Excitonic Model

The configuration $\binom{(r+p)^*}{r}$ may be reached from the LE $\binom{(r+s)^*}{(r+s)}$ in Ψ^0_m (where $0 \leq s \leq p$) by changing progressively the hole from r to $r+s$ through s hole-hole interactions, and by changing progressively the particle from $(r+s)^*$ to $(r+p)^*$ through $(p-s)$ particle particle interactions. The corresponding diagram is drawn in Fig. 4. For a given value of s, the s hole-hole interaction lines and the

$p - s$ particle-particle interaction lines may have any relative position. The number of relative positions of s balls in $p - s + 1$ boxes is $\binom{s}{p}$ and the total number of different diagrams is $N = \sum_{s=0}^{p} \binom{s}{p} = 2^p$. One may have an estimate of the corresponding propagator by assuming all the denominators to be equal to ΔE_1 (which is a minorant). If one takes

$$\left.\begin{aligned} \left\langle \binom{u^*}{t} \middle| H \middle| \binom{u^*}{t+1} \right\rangle &= B \\ \left\langle \binom{u^*}{t} \middle| H \middle| \binom{(u+1)^*}{t} \right\rangle &= A \end{aligned}\right\} \forall u, t$$

as occurs in the CNDO hypotheses, the $\binom{s}{p}$ diagrams with s hole-hole interaction lines give a contribution

$$\binom{s}{p} B^s A^{p-s} / \Delta E^p .$$

The coefficient of the configuration $\binom{(r+p)^*}{r}$ in the p^{th} order correction Ψ_m^p is equal to

$$\begin{aligned} \left\langle \Psi_m^p \middle| \Phi \binom{(r+p)^*}{r} \right\rangle &= \sum_{s=0}^{p} \binom{s}{p} B^s A^{p-s} \Delta E^{-p} \\ &= [(A+B)/\Delta E]^p . \end{aligned}$$

Therefore the ^{p}CTE's appear with coefficients exponentially decreasing with the amplitude of the electron jump. Their weight in the perturbed wave function follows the same variation.

References

1a McWeeny, R., Ohno, K.: Proc. Royal Soc. (London) A **255**, 367 (1960). Tsuchida, A., Ohno, K.: J. chem. Physics **39**, 600 (1963). McWeeny, R., Del Re, G.: Theoret. chim. Acta (Berl.) **10**, 13 (1968)

1b. Petke, J. D., Whitten, J. L.: J. chem. Physics **51**, 3166 (1969)

1c Hoyland, J. R.: J. Amer. chem. Soc. **90**, 2227 (1968), J. chem. Physics **50**, 473 (1969).

2a Masson, A., Levy, B., Malrieu, J. P.: Theoret. chim. Acta (Berl.) **18**, 193 (1970). Berthier, G., Meyer, A. Y., Praud, L.: In: Jerusalem Symposia on Quantum Chemistry and Biochemistry **3**, 174 (1971). Serre, J., Praud, L., Berthier, G.: Jerusalem Symposia on Quantum Chemistry and Biochemistry, p. 198; Bonaccorsi, R., Petrongolo, C., Scrocco, E., Tomasi, J.: Theoret. chim. Acta (Berl.) **15**, 332 (1969).

2b Diner, S., Malrieu, J. P., Jordan, F., Claverie, P.: Theoret. chim. Acta (Berl.) **15**, 86 (1970).

3. Diner, S., Malrieu, J. P., Claverie, P.: Theoret. chim. Acta (Berl.) **13**, 1, 18 (1969). Diner, S., Jordan, F., Gilbert, M.: Theoret. chim. Acta (Berl.) **15**, 100 (1969). Jordan, F., Gilbert, M., Malrieu, J. P., Pincelli, U.: Theoret. chim. Acta (Berl.) **15**, 211 (1969). – Diner, S., Malrieu, J. P., Claverie, P., Jordan, F.: Chem. Physics Letters **2**, 319 (1969). Daudey, J. P., Diner, S.: Int. J. quant. Chemistry **6**, 575 (1972)

4 Sovers, O. J., Kern, C. W., Pitzer, R. M., Karplus, M.: J. chem. Physics **49**, 2592 (1968); Cadioli, R., Pincelli, U., Levy, B.: Chem. Physics Letters (in press) - Lehn, J. M., Munsch, B., Levy, B., Millié, Ph.: Theoret. chim. Acta (Berl.) **18**, 143 (1970).

5a. McConnell, H.: J. chem. Physics **24**, 764 (1956).

5b. Maeder, F., Berthier, G., Millié, Ph.: Int. J. quant. Chemistry **4** s, 175 (1970). – Levy, B., Berthier, G., Millié, Ph.: Int. J. quant. Chemistry **6**, 155 (1972). – Ellinger, Y., Rassat, A., Subra, R., Berthier, G., Millié, Ph.: Chem. Physics Letters **11**, 362 (1971).

5c. Langlet, J., Malrieu, J. P.: Theoret. chim Acta (Berl.) **22**, 80 (1971).

6a. Hiroike, E.: J. physic. Soc. Japan **22**, 379 (1967). - Armour, E. A. G., Stone, A. J.: Proc. Royal Soc. (London) A **302**, 25 (1967). Barbier, C., Gagnaire, D., Berthier, G., Levy, B.: J. Magn. Res. **5**, 11 (1971). Barbier, C., Lévy, B., Millié, Ph.: Chem. physic. Letters **17**, 122 (1972).

6b. Pople, J. A., Santry, D. P.: Molecular Physics **8**, 1 (1964). - Denis, A., Malrieu, J P.: Molecular Physics **23**, 581 (1972).

7. Trindle, C.: J Amer. chem. Soc. **91**, 4054 (1969); 3251, 3255 (1970); Theoret. chim. Acta (Berl.) **18**, 261 (1970).

8. Langlet, J., Malrieu, J. P.: J. Amer. chem. Soc **94**, 7254 (1972).

9. See the discussion of the report by G. Berthier about localized pictures, Colloque international du CNRS Menton (1970), related in "Aspects de la Chimie Quantique Contemporaine, CNRS, (Paris) p 49 (1971).

10. Malrieu, J. P.: J. Photochem. Photobiol **7**, 531 (1968).

11 Simpson, W. T.: J. Amer. chem. Soc **73**, 5363 (1951); **77**, 6164 (1955)

12. Pople, J. A., Walmsley, S M.: Trans. Faraday Soc **58**, 441 (1962).

13. Murrell, J. N.: J. chem. Physics **37**, 1162 (1962).

14 Langlet, J.: Theoret. chim. Acta (Berl.), **27**, 223 (1972).

15. Edmiston, C., Ruedenberg, K.: J. chem. Physics **43**, 597 (1963); Rev. mod. Physics **35**, 457 (1963). Gilbert, T. L.: In: Molecular orbitals in chemistry, Physics and Biology, Löwdin, P. O., Pullman, B. (Eds.) p. 405 New York: Acad. Press 1964. Foster, J. M., Boys, S F.: Rev. mod. Physics **32**, 300 (1960) Magnasco, V., Perico, A.: J chem. Physics **47**, 971 (1967).

16. Lennard-Jones, J. E.: Proc. Royal Soc. (London) A **198**, 114 (1949) Hall, G. G., Lennard-Jones, J. E.: Proc. Royal Soc (London) A **202**, 155 (1950); A **205**, 367 (1951); Hall, G. G.: Proc Royal Soc. (London) A **202**, 166 (1950); A **203**, 102 (1952).

17. Huron, B., Malrieu, J. P., Rancurel, P: J chem. Physics (in press)

18. Langlet, J., Malrieu, J. P: Theoret. chim. Acta, (Berl.) (in press).

19. Salem, L.: The molecular orbital theory of conjugated systems. p. 448-452. New York: W. A. Benjamin (1966).

20. See e g. Ballantine: Rev. mod. Physics **42**, 358 (1970).

21. Daudel, R.: Les *fondements de la chimie théorique* Paris: Gauthier Villars 1956

22 Diner, S., Claverie, P., Malrieu, J. P., to be published.

Dr. J. P. Malrieu
Institut de Biologie Physico-Chimique
Laboratoire de Biochimie Théorique
associé au C.N.R.S.
13, rue P et M. Curie
Paris, 5 è, France

Theoret. chim. Acta (Berl.) 29, 133 – 137 (1973)
© by Springer-Verlag 1973

Barriers to Molecular Inversion in ($n\pi^*$) Carbonyls: A CNDO Investigation

D. A. Condirston and D. C. Moule

Department of Chemistry, Brock University, St. Catharines, Ontario, Canada

Received June 15, 1972

CNDO/2 calculations performed on a series of carbonyl-containing compounds have shown that inductive effects by electronegative substituents with respect to hydrogen play the major role in determining the height of the inversion barrier relative to formaldehyde. The change in density flow at the central carbon atom for different carbonyl substituents parallels the calculated inversion barriers in accordance with Walsh's rules.

Mit Hilfe von CNDO/2-Rechnungen wurde für eine Reihe von Verbindungen mit Carbonylgruppen gezeigt, daß die Höhe der Inversionsbarriere relativ zu Formaldehyd vorwiegend durch induktive Effekte der elektronegativen Substituenten in bezug auf Wasserstoff bestimmt wird. Die Ladungsflußänderungen am zentralen Kohlenstoffatom entsprechen in Übereinstimmung mit den Walshschen Regeln den berechneten Inversionsbarrieren.

Des calculs CNDO/2 effectués sur une série de composés carbonylés ont montré que les effets inductifs dûs à des substituants électronégatifs par rapport à l'hydrogène jouent un rôle essentiel dans la détermination de la hauteur de la barrière d'inversion par rapport au formaldéhyde. Les variations de transfert de charge sur l'atome de carbone central selon les différents substituants carbonylés sont parallèles aux barrières d'inversion calculées en accord avec les règles de Walsh.

Introduction

During the past several years optical spectroscopists have studied the electronic transitions from the ground electronic state to the first $^1n\pi^*$ states of simple aldehydes and ketones such as formaldehyde [1], formyl fluoride [2], propynal [3], phosgene [4], and cyclobutanone [5]. While infrared and microwave studies have established that these molecules are planar in the ground electronic state, evidence has been provided to show that the excited state structures of these molecules are pyramidal. One interesting observation that can be made when looking at the excited state structures is that there is a great variation in the barrier heights to molecular inversion. For example, the inversion barrier for propynal is close to 0 cm^{-1}, whereas for H_2CO it is 356 cm^{-1} and for Cl_2CO it is 3170 cm^{-1}. It appears, then, that the barrier to inversion is very sensitive to the type of substituent on the carbonyl group.

In view of the success of the CNDO method developed by Pople, Santry, and Segal [6] in the calculation of a number of properties of simple polyatomic molecules, we thought that we could use it to obtain an understanding of the role that the substituents play in determining the height of the inversion barrier.

Calculations

For the ground state and for the first triplet state, CNDO/2 calculations were performed for the molecules F_2CO, HFCO, H_2CO, C_4H_6O (cyclobutanone), CH_3CHO, and HCCCHO. The CNDO/2 program as introduced by Pople and Segal [7] was not modified for our purposes. The out-of-plane angle, which is defined as the angle between the C=O bond and the projection of the C=O bond onto the molecular plane, was varied in each calculation, while the XCY angle (where C is the carbonyl carbon atom and X and Y are the substituents) and the C=O bond length were clamped at their ground state values throughout the inversion process. While Kroto and Santry [8] have demonstrated, through calculations on the formaldehyde molecule, that the barrier is sensitive to the choice of inversion coordinate, we felt that this procedure was acceptable, since we were concerned only with the relative barriers to inversion. The geometries used in the calculations for the molecular series $F_2CO/HFCO/H_2CO/C_4H_6O/CH_3CHO/$ HCCCHO are found in references [9] to [14] respectively.

Results and Discussion

Table 1 presents the calculated barrier heights and out-of-plane angles for the molecules studied, along with the experimental values for comparison purposes. It is evident that the CNDO method is successful in predicting the relative order of the barrier heights to molecular inversion, with the exception of cyclobutanone. A direct comparison of the calculated and experimental data should not be made, though, since the calculated data refer to the triplet excited state, while the experimental data refer to the corresponding singlet state. For planar $n\pi^*$ states, however, the exchange integral vanishes in the CNDO approximation, and the two states become degenerate [15].

To obtain an insight into the factors responsible for the variation in barrier with change in carbonyl substituent, we attempted to extend Walsh's rules to the series of substituted carbonyl compounds. In 1953 Walsh [16] qualitatively

Table 1 Calculated and experimental barriers to inversion and out-of-plane angles for the $(n\pi^*)$ states of some carbonyl compounds

Molecule	Barrier (cm^{-1})		Angle (degrees)		Ref.
	expt.[a]	calc.[b]	expt.[a]	calc.[b]	
F_2CO	>4000	4600	-	40	[19]
HFCO	2800 4200	1900	30–35	38	[2]
H_2CO[c]	356	760	33.6	35	[20]
C_4H_6O	1550	180		23	[5]
CH_3CHO		50	—	18	
HCCCHO	~0	0	0 4	0	[21]

[a] For the $^1(n\pi^*)$ state.

[b] For the $^3(n\pi^*)$ state.

[c] A value of 776 cm^{-1} has been calculated [20] from the observed inversion levels of $^1A_2$ H_2CO.

Table 2. Electron densities at the C=O group

Molecule	Atom	Ground state				Planar excited state				Non-planar excited state			
		$2s$	$2p_x$	$2p_y$	$2p_z$	$2s$	$2p_x$	$2p_y$	$2p_z$	$2s$	$2p_x$	$2p_y$	$2p_z$
F_2CO	C	0.9950	0.7791	0.7344	0.8299	0.9208	1.2548	0.7357	0.7471	1.1101	0.9984	0.7370	0.7714
	O	1.7144	1.3631	1.8841	1.3118	1.7251	1.8410	1.0105	1.4607	1.7298	1.6604	1.0172	1.6417
HFCO	C	1.0394	0.8211	0.8273	0.8828	0.9897	1.2457	0.8322	0.7923	1.1227	1.0497	0.8322	0.8123
	O	1.7202	1.2419	1.9065	1.3584	1.7308	1.7990	1.0525	1.4646	1.7323	1.6517	1.0620	1.6021
H_2CO	C	1.0888	0.8358	0.9321	0.9245	1.0505	1.2356	0.9298	0.8467	1.1389	1.0858	0.9271	0.8794
	O	1.7281	1.1642	1.9188	1.3738	1.7364	1.7644	1.0833	1.4610	1.7371	1.6443	1.0945	1.5703
C_4H_6O	C	1.0175	0.8183	1.0363	0.8728	0.9719	1.1919	1.0203	0.7914	1.0222	1.1177	1.0176	0.8106
	O	1.7357	1.2415	1.9425	1.3391	1.7438	1.8019	1.1082	1.4453	1.7444	1.7295	1.1110	1.5172
CH_3CHO	C	1.0429	0.8258	0.9569	0.9244	1.0049	1.2063	0.9509	0.8399	1.0249	1.1603	0.9675	0.8435
	O	1.7318	1.2118	1.9367	1.3506	1.7406	1.7947	1.0806	1.4540	1.7408	1.7686	1.1053	1.4558
HCCCHO	C	1.0219	0.8385	0.9623	0.9165	0.9897	1.1737	0.9640	0.8416				
	O	1.7312	1.1936	1.9368	1.3497	1.7393	1.7899	1.0786	1.4479				

correlated molecular geometry and orbital energy for a variety of molecules. For H_2CO, the Walsh diagram correctly predicts a non-planar excited state equilibrium structure. The main principle on which he based his correlation is the following: whether or not an orbital becomes more tightly bound with change of angle is determined primarily by whether or not it changes from being built from a *p* orbital on an atom to being built from an *s* orbital on that atom. The *s* and *p* orbital character at each atomic center is given by the elements of the CNDO density matrix. An interpretation of the CNDO density matrices for the ground and excited electronic states of the series $F_2CO/HFCO/H_2CO/C_4H_6O/CH_3CHO/HCCCHO$ from the viewpoint of the Walsh postulate should provide information about the non-planarity of the upper state. Table 2 compares the electron densities at the carbonyl group for each of the molecules studied in their ground, planar excited, and non-planar excited states. For the planar configurations the coordinate axes were set up such that the C=O bond is parallel to the *z* axis, and the *x* axis is perpendicular to the molecular plane. In the calculations on the non-planar configurations, the *XCY* framework was taken to be in the *yz* plane.

In a $\pi^* \leftarrow n$ electronic transition, an electron is promoted from a filled *n* orbital to a previously unoccupied π^* orbital. The electron densities listed in Table 2 for the carbonyl group illustrates this clearly, in that for H_2CO, the *n* orbital on oxygen $[2p_y(O)]$ has a density of 1.9188 for the $^1A_1$ state, while for the $^1A_2$ state it takes a value of 1.0833. The ground state density in the π orbital for the carbon and oxygen atoms is given respectively as 0.8358 and 1.1642. The corresponding densities for the excited electronic state are 1.2356 and 1.7644. The loss in density for the *n* orbital is therefore -0.8355, while the gain in density in the *x* direction for carbon and oxygen is, respectively, 0.3998 and 0.6002. These density differences for the series of molecules studied are given in Δ_1 of Table 3. The Δ_2 values in this table are the differences in electron densities which result from a transition from the ground state to a non-planar excited state, and were obtained from the first and third sets of data listed in Table 2. $\Delta_2 - \Delta_1$, then, gives the difference in electron density between the non-planar and planar excited states.

Table 3. Density differences

Molecule	Atom	Δ_1				Δ_2				$\Delta_2 - \Delta_1$			
		$2s$	$2p_x$	$2p_y$	$2p_z$	$2s$	$2p_x$	$2p_y$	$2p_z$	$2s$	$2p_x$	$2p_y$	$2p_z$
F_2CO	C	-0.0742	0.4757	0.0013	-0.0828	0.1151	0.2193	0.0026	-0.0585	0.1893	-0.2564	0.0013	0.0243
	O	0.0107	0.4779	-0.8736	0.1489	0.0154	0.2973	-0.8679	0.3299	0.0047	-0.1806	0.0057	0.1810
HFCO	C	-0.0497	0.4246	0.0049	-0.0905	0.0833	0.2286	0.0049	-0.0705	0.1330	-0.1960	0.0000	0.0200
	O	0.0106	0.5571	-0.8540	0.1062	0.0121	0.4098	-0.8445	0.2437	0.0015	-0.1473	0.0095	0.1375
H_2CO	C	-0.0383	0.3998	-0.0023	-0.0778	0.0501	0.2500	-0.0050	-0.0451	0.0884	-0.1498	-0.0027	0.0327
	O	0.0083	0.6002	-0.8355	0.0880	0.0090	0.4801	-0.8243	0.1973	0.0007	-0.1201	0.0112	0.1039
C_4H_6O	C	0.0456	0.3736	-0.0160	-0.0814	-0.0047	0.3014	-0.0187	-0.0622	0.0409	-0.0722	-0.0027	0.0192
	O	0.0081	0.5604	0.8343	0.1026	0.0087	0.4880	-0.8315	0.1781	0.0006	-0.0724	0.0028	0.0755
CH_3CHO	C	0.0380	0.3805	0.0060	-0.0845	-0.0180	0.3345	0.0131	-0.0809	0.0200	-0.0460	0.0191	0.0036
	O	0.0088	0.5829	-0.8561	0.1034	0.0090	0.5568	-0.8314	0.1052	0.0002	-0.0261	0.0247	0.0018
HCCCHO	C	0.0322	0.3352	0.0017	-0.0749								
	O	0.0081	0.5963	0.8582	0.0982								

For H_2CO, the $\Delta_2 - \Delta_1$ values for the $2p_x$(C) orbital and the $2s$(C) orbital are, respectively, -0.1498 and 0.0884. That is, when planar formaldehyde in the $n\pi^*$ configuration is distorted from the plane by 35°, there is a shift in electron density away from the $2p_x$ orbital on the carbon atom into the $2s$ orbital. This is in agreement with the Walsh postulate, in that a gain in s density leads to a more stable configuration, which in the case of H_2CO corresponds to a non-planar structure. Since Walsh's rule states that the degree of non-planarity in the $n\pi^*$ states depends upon the amount of s character acquired by the π^* orbital, the height of the inversion barrier should then parallel the $2p_x$ and $2s$ density changes at the carbonyl carbon atom. Hence, it should be possible to establish a correlation between the $\Delta_2 - \Delta_1$ values and the inversion barriers for the series of molecules studied. From Table 3, $\Delta_2 - \Delta_1$ values for the $2p_x$ orbital for the molecular series F_2CO/HFCO/H_2CO/C_4H_6O/CH_3CHO/HCCCHOare, respectively, -0.2564, -0.1960, -0.1498, -0.0722, -0.0460, and 0. The corresponding gain in carbon $2s$ electron density for the same series is 0.1893, 0.1330, 0.0884, 0.0409, 0.0200, and 0.

The orbitals on the oxygen atom also show significant density changes. The $\Delta_2 - \Delta_1$ values for the $2p_x$(O) orbital for the series are -0.1806, -0.1473, -0.1201, -0.0724, -0.0261, and 0. The corresponding gain in the oxygen $(2s + 2p_z)$ density is 0.1857, 0.1390, 0.1100, 0.0749, 0.0020, and 0, with nearly all of this density going into the $2p_z$ orbital. This indicates that density flow on the oxygen atom, as on the carbon atom, is in the direction from the π to the σ framework.

Brundle *et al.* [17] have recently demonstrated in a photoelectron study of H_2CO and F_2CO that the effect of substitution of fluorine for hydrogen has a much larger stabilization effect on the σ MO's than on the π MO's. Therefore, the $2p_x$(C) AO which goes to form the π MO is relatively unaffected by substitution on the carbonyl group. The σ MO's in these compounds belong to the representations A_1 and B_2, while the π MO belongs to the B_1 representation. When the molecule is distorted from the planar (C_{2v}) to the non-planar (C_s) form, the A_1 and B_1 representations correlate with A', and the A_2 and B_2 representations correlate with A''. Therefore, in a non-planar system, the $\sigma - \pi$ distinction is no longer valid, and it follows that the $2p_x$(C) orbital can be perturbed by an electronegative substituent. In the case of F_2CO, the carbon $2p_x$ AO responds to fluorine induction, with the result that there is a net charge flow from the $2p_x$(C) into the $2s$(C) AO. From the viewpoint of the Walsh postulate, a change in electron density in this direction would result in a non-planar distortion at the carbon center. The height of the inversion barrier and the out-of-plane angle can be considered, then, to result from an inductive effect of the attached group.

In the case of propynal, the π and π^* orbitals are delocalized over four atomic centers, and consequently the necessity for a density flow from the $2p_x$(C) to the $2s$(C) AO is reduced. Both the calculated and observed barrier heights for propynal reflect this. The lack of agreement in the data for cyclobutanone may be attributed to molecular strain arising from the four-membered ring. For the case of inverting nitrogen heterocycles [18], however, this deficiency has been overcome by a reparametrization of the CNDO electronegativities.

References

1. Brand, J. C. D.: J. chem. Soc. (London) **1956**, 858.
2. Fischer, Gad: J. molecular Spectroscopy **29**, 37 (1969).
3. Lin, C. T., Moule, D. C.: J. molecular Spectroscopy **37**, 280 (1971).
4. Moule, D. C., Foo, P. D.: J. chem. Physics **55**, 1262 (1971).
5. Moule, D. C.: Canad. J. Physics **47**, 1235 (1969).
6. Pople, J. A., Santry, D. P., Segal, G. A.: J. chem. Physics **43**, S129 (1965).
7. Pople, J. A., Segal, G. A.: J. chem. Physics **44**, 3289 (1965).
8. Kroto, H. W., Santry, D. P.: J. chem. Physics **47**, 2736 (1967).
9. Laurie, V. W., Pence, D. T., Jackson, R. H.: J. chem. Physics **37**, 2995 (1962).
10. Favero, P., Mirri, A. M., Baker, J. G.: J. chem. Physics **31**, 566 (1959).
11. Townes, C. H., Schawlow, A. L.: Microwave spectroscopy. New York: McGraw-Hill Co. 1955.
12. Scharpen, L. H., Laurie, V. W.: J. chem. Physics **49**, 221 (1968).
13. Kilb, R. W., Lin, C. C., Wilson, E. B.: J. chem. Physics **26**, 1695 (1957).
14. Costain, C. C., Morton, J. R.: J. chem. Physics **41**, 3453 (1964).
15. Del Bene, J., Jaffé, H. H.: J. chem. Physics **48**, 1807 (1968).
16. Walsh, A. D.: J. chem. Soc. (London) **1953**, 2306.
17. Brundle, C. R., Robin, M. B., Kuebler, N. A., Basch, H.: J. Amer. chem. Soc. **94**, 1451 (1972).
18. Rauk, A., Andose, J. D., Frick, W. G., Tang, R., Mislow, K.: J. Amer. chem. Soc. **93**, 6507 (1971).
19. Condirston, D. A., Moule, D. C.: Unpublished results.
20. Jones, V. T., Coon, J. B.: J. molecular Spectroscopy **31**, 137 (1969).
21. Brand, J. C. D., Callomon, J. H., Watson, J. K. G.: Discuss. Faraday Soc. **35**, 175 (1963).

Dr. D. C. Moule
Department of Chemistry
Brock University
St. Catharines, Ontario
Canada

Theoret. chim. Acta (Berl.) 29, 139–150 (1973)
© by Springer-Verlag 1973

Dispersion Interactions and Solvent-Shift Effects

A. T. Amos
Department of Mathematics, University of Nottingham

B. L. Burrows
Department of Mathematics, The Polytechnic, Stafford

Received October 13, 1972

The problem of relating solvent-shift effects to excited-state polarizabilities is discussed. It is found that the chief difficulty is that of estimating the dispersion term in the interaction energy between a solvent molecule and a solute molecule, and it is shown that the differences in the values of excited-state polarizabilities which have been deduced from solvent-shift data are due to widely differing estimates of this dispersion term. In order to obtain meaningful results it is found necessary to assume that the change in the dispersion term is related to the change in the polarizability of a solute molecule on excitation. On the basis of this assumption, the use of a semi-empirical formula which connects solvent-shifts with these changes in the polarizability is discussed and it is found that the accuracy is such that very little useful information can be obtained.

Das Problem, Lösungsmittelverschiebungen mit der Polarisierbarkeit angeregter Zustände in Verbindung zu bringen, wird diskutiert. Dabei zeigt sich, daß die Hauptschwierigkeit im Abschätzen des Dispersionsterms der Wechselwirkung Solvent-Solut-Molekül liegt und daß die Unterschiede in den Polarisierbarkeiten, die sich aus Daten für Lösungsmittelverschiebungen ergeben, auf die sehr unterschiedliche Abschätzung dieses Dispersionsterms zurückgehen. Um sinnvolle Resultate zu erhalten, muß angenommen werden, daß die Änderung des Dispersionsterms mit der Änderung der Polarisierbarkeit eines angeregten Solutmoleküls zusammenhängt. Auf dieser Grundlage wird eine entsprechende semiempirische Formel diskutiert; jedoch deren mangelnde Genauigkeit läßt keine eindeutigen Aussagen mehr zu.

1. Introduction

When a conjugated molecule -- the solute molecule - is placed in a solvent there will be interaction effects between the solute and the surrounding solvent molecules. These effects will change the solute energy levels and, since they are not all changed by equal amounts, there will be a change in the excitation energies between the ground and excited states, which can be observed in the spectrum. These changes, called solvent shifts, can clearly be related to the basic interaction terms between the solute and the solvent molecules, and these, to a certain degree of approximation, can be expressed as electrostatic type terms depending on the dipole moments and polarizabilities of the solute molecule in both ground and excited states and the solvent molecules in their ground state. In this way the solvent shifts can, so it is believed, give information on the difference in the dipole moment and polarizability of the solute molecule in its ground and excited states.

Unfortunately, while this seems to work none too badly for dipole moments, the results have been interpreted in very different ways in the case of polarizabilities so that, for example, one authority believes that the polarizability change between the ground and the lowest excited state of naphthalene is small [1] while another believes it is very large indeed [2]. The purpose of this note is to try to examine how far the solvent-shift effects can be related to polarizability changes and, in passing, to resolve these apparent contradictions. Although in a fairly *ad hoc* way it is possible to find a rough correlation between theoretical values of excited-state polarizabilities and solvent-shift effects the approximations involved are so dubious that we tend to doubt whether any really convincing evidence on the magnitude of polarizability changes can be obtained in this way.

2. Electrostatic Interpretation of Solvent-Shift Effects

There have been many reviews and original papers (Refs. [3-8] are a small selection) giving detailed quantum-mechanical derivations of the equations relating solvent shifts to the electric properties of the solute and solvent molecules, so we shall only quote the main results here. However, in passing, we ought to point out that these results are based on quite a severe approximation, namely that solvent and solute molecules are sufficiently far apart for exchange of electrons to be neglected and for the interaction potential to be expressed as a truncated dipolar expansion. In many cases this will hardly be the case and one can only hope that any errors due to this fortuitously cancel.

If $\boldsymbol{\mu}_u^s$, $\boldsymbol{\mu}_v$, $\boldsymbol{\alpha}_u^s$, $\boldsymbol{\alpha}_v$ refer to the dipole moments and the polarizability tensors of the solute molecule in the state s and the pth solvent molecule $v(p)$ in its ground state, the change in the energy of the s state of the solute due to the interaction with the solvent is

$$\begin{aligned}\Delta E_s = {} & \sum_{p=1}^{N} R_p^{-3}\,\boldsymbol{\mu}_u^s\cdot\boldsymbol{\theta}^{uv(p)}\cdot\boldsymbol{\mu}_{v(p)} \\ & -\tfrac{1}{2}\sum_{p=1}^{N} R_p^{-6}\,\boldsymbol{\mu}_u^s\cdot\boldsymbol{\theta}^{uv(p)}\cdot\boldsymbol{\alpha}_{v(p)}\cdot\boldsymbol{\theta}^{uv(p)}\cdot\boldsymbol{\mu}_u^s \\ & -\tfrac{1}{2}\sum_{p,q=1}^{N} R_p^{-3}R_q^{-3}\,\boldsymbol{\mu}_{v(p)}\cdot\boldsymbol{\theta}^{uv(p)}\cdot\boldsymbol{\alpha}_u^s\cdot\boldsymbol{\theta}^{uv(q)}\cdot\boldsymbol{\mu}_{v(q)} + D_s\end{aligned} \tag{1}$$

where the solute is assumed to be placed with its mean centre of charge at the origin and R_p is the distance from the origin to the mean centre of charge of the pth solvent molecule, $\boldsymbol{\theta}^{uv(p)}$ is an angular term taking into account the relative orientations of the solute and solvent molecule and the sums are over all N solvent molecules in the system. In (1) terms which depend on solvent molecules only have been omitted since they cancel when the solvent shift is calculated and terms depending on higher powers of R^{-1} than the sixth are ignored.

In Eq. (1) D_s is the dispersion-interaction term and is given by

$$D_s = -\sum_{p=1}^{N}\sum_{e\neq 0}\sum_{t\neq s} R_p^{-6}\,\frac{\langle 0|\boldsymbol{\mu}_{v(p)}|e\rangle\cdot\boldsymbol{\theta}^{uv(p)}\cdot\langle t|\boldsymbol{\mu}_u|s\rangle\cdot\langle s|\boldsymbol{\mu}_u|t\rangle\cdot\boldsymbol{\theta}^{uv(p)}\cdot\langle e|\boldsymbol{\mu}_{v(p)}|0\rangle}{\varepsilon_v^e-\varepsilon_v^0+\varepsilon_u^t-\varepsilon_u^s} \tag{2}$$

where, for example, $\langle 0|\boldsymbol{\mu}_{v(p)}|e\rangle$ is the transition dipole moment between the pth solvent molecule ground state $|0\rangle$ of energy ε_v^0 amd the excited state $|e\rangle$ of energy ε_v^e and similarly for $\langle s|\boldsymbol{\mu}_u|t\rangle$.

As it happens many conjugated hydrocarbons have zero dipole moments in their ground and lowest excited states. Therefore Eq. (1) will simplify considerably because the first two terms will vanish. Even with this simplification, however, Eq. (1) is not yet ready for use. This is because it it obtained on the basis that all the molecules are rigidly fixed in position and orientation, as is indicated by the presence of the R_p and the $\theta^{uv(p)}$ in the formulae. The true energy change of the liquid system ought, therefore, to be computed by a statistical averaging over the various possible configurations, each weighted by the appropriate Boltzmann factor. In practice, of course, this is too difficult so one can either use an approach in which the solvent is replaced by a continuous dielectric or else use a semi-classical result and compute $\langle V \exp(-V/kT)\rangle$ where V is the angular-dependent interaction term [9]. The latter, which will not be valid for low temperatures but should be reasonably accurate for normal laboratory temperatures, gives:

$$\Delta E_s = -\sum_{p=1}^{N} R_p^{-6}\{(\mu_{v(p)})^2\,\alpha_u^s + d_{uv}^s\} \tag{3}$$

where $\alpha_u = \frac{1}{3}$ trace $\boldsymbol{\alpha}_u$ and d_{uv}^s is the van der Waals coefficient between the solute molecule and a solvent molecule:

$$d_{uv}^s = \frac{2}{3}\sum_{t\neq s}\sum_{e\neq 0}\frac{|\langle e|\boldsymbol{\mu}_v|0\rangle|^2\,|\langle t|\boldsymbol{\mu}_u|s\rangle|^2}{\varepsilon_e^v - \varepsilon_0^v + \varepsilon_t^u - \varepsilon_s^u}\,. \tag{4}$$

In (3) we have assumed the molecules are isotropic so that both α_u and d_{uv}^s represent average values. This actually, is neither necessary nor true, but the approximations made in the theory are, in our view, too drastic to allow anisotropic effects to be estimated with any sort of accuracy so that we prefer not to include them.

There remains the evaluation of the sum $\Sigma\, R_p^{-6}$. It is probably simplest to assume that the solvent molecules are distributed uniformly outside a spherical cavity of radius a (the cavity radius) which contains the solute molecule. This gives the result

$$\Sigma\, R_p^{-6} = 4\pi A d/3\, M a^3 \tag{5}$$

where M and d are the mass and density of the solvent molecules and A is Avogadro number. Alternatively one can use the method of Abe [10] who places each solvent molecule inside a sphere of radius $r_v = (4\pi A d/3\,M)^{\frac{1}{3}}$ which are closely packed around the sphere of radius $r_u = (4\pi A d_u/3\,M_u)^{\frac{1}{3}}$ containing the solute molecule, where M_u and d_u denote the mass and density of the solute. As we have pointed out elsewhere [4] the two approaches give much the same results if one assumes not that $r_u = a$, as might be expected, but rather that $a \approx r_u + \frac{1}{2}\, r_v$. The basic reason for this is that the sum $\Sigma\, R_p^{-6}$ dies off so quickly with distance that only the solvent molecules close to the solute contribute strongly. In fact more than 90% of the whole solvent-shift effect arises from interactions between the solute molecule and the solvent molecules forming the first "layer" around it.

This gives, therefore,

$$\Delta E_s = -\frac{4\pi A d}{3\,M}\, a^{-3}\{d_{uv}^s + \alpha_u^s(\mu_v)^2\}\,. \tag{6}$$

Table 1. Experimental values for the solvent-shifts of the two lowest excited states of naphthalene in a number of solvents

Solvent	Solvent shift in cm^{-1} [13]	
	$^1B_{1u}$	$^1B_{2u}$
n-pentane	−258	−870
n-hexane	−288	−912
n-heptane	−287	−917
n-nonane	−322	−951
Cyclohexane	−296	−954
Cyclopentane	−296	−950
Ethyl ether	−236	−919
Ethanol	−256	−979
Acetronitrile	−266	−1189

The solvent shift between the ground state G and the excited state E will be

$$\begin{aligned} \Delta_{EG} &= \Delta E_E - \Delta E_G \\ &= -\frac{4\pi A d}{3 M a^3} \left[\Delta d + (\mu_v)^2 \Delta\alpha \right] \end{aligned} \tag{7}$$

where Δd represents the change in the dispersion term between ground and excited state, and $\Delta\alpha$ the similar quantity for the polarizability. Clearly if (7) is to be used to estimate $\Delta\alpha$ from the experimental values of Δ_{EG}, some method of estimating the change in the dispersion term Δd must be found. We now turn to this problem.

3. The Dispersion Term

The contribution of dispersion forces to the solvent-shift effect is most difficult to estimate since we require the dispersion interaction between a solvent molecule and the solute molecule. Even for very small atomic systems the calculation of the d^n_{uv} term is by no means easy and any hope of computing it accurately for the type of complex molecules we are interested in must be abandoned. This is particularly so since we require it not only for the ground state of the solute but also for its excited state, and, as far as we know, there has been no attempt to compute d^n_{uv} for excited states even for small systems except, that is, for degenerate excited states where the problem is altogether different [11]. Thus if we are not to give up the problem as altogether intractable, there are only three reasonable ways to proceed.

Firstly we could try to eliminate the dispersion term from the problem. This is basically what is done by Suppan in order to estimate excited state dipole moments [1, 12] and he does this by the simple expedient of subtracting the solvent shift for two separate solvents. On the assumption that the dispersion term is the same for both it is eliminated from the problem. To examine how this would work for naphthalene consider the data given in Table 1. For the three solvents, ethyl-ether, ethanol and acetronitrile with non-zero dipole moments, there will be, according to Eq. (7), two terms in the solvent shift, the dispersion term and the term involving $(\mu_v)^2\,\Delta\alpha$. If we assume that the dispersion term is more or less the same in all three polar solvents then taking the difference of any two X and Y say will give

$$\Delta^X_{EG} - \Delta^Y_{EG} = \frac{4\pi A}{3}\left\{\frac{d_Y}{M_Y a_Y^3}\mu_Y^2 - \frac{d_X}{M_X a_X^3}\mu_X^2\right\}\Delta\alpha \tag{8}$$

Now these differences $\Delta^X_{EG} - \Delta^Y_{EG}$ are of the order of 20 cm^{-1} for the ${}^1B_{1u}$ excited state of naphthalene and 60–200 cm^{-1} for the ${}^1B_{2u}$ excited state. (Results given by Weigang [13] show the same trend of results for phenanthrene and azulene.) However, if we now examine the non-polar solvents where the solvent shift is caused entirely by the dispersion term, we see that here, too, there are differences of the order of 20 cm^{-1} for the lowest state and 40–80 cm^{-1} for the ${}^1B_{2u}$ excited state. Thus the errors involved in assuming the dispersion terms cancel, so that Eq. (8) is obtained, are the same order of magnitude as the differences $(\Delta^X_{EG} - \Delta^Y_{EG})$ themselves. For this reason we do not believe that the dispersion term can be eliminated from the problem in such a way as to enable estimates of $\Delta\alpha$ to be made. [The case of dipole-moment changes is, of course, entirely different since the differences between solvent shifts of a polar solute in different polar solvents is much greater than those for non-polar solutes so that the error in cancelling the dispersion term is relatively unimportant.]

The second possible way to proceed is to use semi-empirical methods to estimate the value of $d^s_{uv'}$. By this we mean that the wave functions for the solute and solvent molecules could be divided up into bond-orbitals and pi-type orbitals. The dispersion forces could then be written as the sum of bond interaction terms, pi-sigma and pi-pi terms [14]. Such a procedure would be difficult but by no means impossible. However, one thing is quite clear: such semi-empirical estimates could only give order of magnitude results and the errors would be quite large. Since the estimated dispersion term would have to be substituted into (7) and the difference between this and the experimental shift used to determine $\Delta\alpha$, the value of $\Delta\alpha$ thus determined would be subject to such possible error as to be practically useless.

In fact both the two methods just discussed fail for very similar reasons. In Eq. (7) the two terms which together contribute to the solvent shift are of very different orders of magnitude, the term proportional to $\Delta\alpha$ being, in our view, only about 10% of the dispersion term. Thus, if Eq. (7) is to be used to determine $\Delta\alpha$, then either the dispersion term must be estimated accurately to within a few percent, which we have shown to be impractical or else, and this is the third possible method of procedure, the dispersion term must be related to polarizability changes.

Almost from the first introduction of the idea of dispersion interaction, it has been believed that they can be approximately related to the polarizabilities of the molecules involved. In their recent book on Intermolecular Forces [11], Margenau and Kestner list various of these approximations and show how they can be derived. The more important and most useful of these when applied to the interaction between a solvent molecule and the solute molecule in the state s take the forms:

$$\text{(i)}\ d^s_{uv} = \frac{3}{2}\,\frac{\bar{\varepsilon}^s_u\bar{\varepsilon}_v}{\bar{\varepsilon}^s_u+\bar{\varepsilon}_v}\,\alpha^s_u\alpha_v \tag{9}$$

where $\bar{\varepsilon}^s_u$ and $\bar{\varepsilon}_v$ are "average" (or Unsöld) energy denominators which are often identified with ionization potentials.

$$\text{(ii)}\ d^s_{uv} = \frac{3}{2}\,\frac{\alpha^s_u\alpha_v}{\left(\frac{\alpha^s_u}{N_u}\right)^{\frac{1}{2}}+\left(\frac{\alpha_v}{N_v}\right)^{\frac{1}{2}}} \tag{10}$$

where N_u and N_v are the "average" number of electrons in closed shells. This is the Slater-Kirkwood formula. A modification of this is

$$\text{(iii)}\ d^s_{uv} = \frac{6}{B}\,\frac{\alpha_v\alpha^s_u}{\alpha^s_u/\chi^s_u+\alpha_u/\chi_v} \tag{11}$$

where χ^s_u and χ_v are the diamagnetic susceptibilities.

Equations (10) and (11) can be considered as modifications of (9) in which the average energies $\bar{\varepsilon}^s_u$ and $\bar{\varepsilon}_v$ are related to the polarizabilities and susceptibilities. In particular it should follow that

$$\bar{\varepsilon}^s_u : \left(\frac{N_u}{\alpha^s_u}\right)^{\frac{1}{2}} : \left(\frac{\chi^s_u}{\alpha^s_u}\right). \tag{12}$$

This equation shows quite clearly that to a large extent the results for the change in α_u between the ground and excited state depends on the assumption made concerning the variation in the value of $\bar{\varepsilon}_u$ between these two states. Since N_u will remain constant, the first proportionality sign indicates that a decrease in $\bar{\varepsilon}_u$ in going from the ground to excited state implies an increase in α_u. The second proportionality sign indicates that the change in α_u is proportional to the change in the square of the diamagnetic susceptibility. The latter should be proportional to the mean value of r^2 for the molecule, i.e. should vary with molecular size. Generally the bond lengths of a conjugated molecule increase on excitation but not by very much [15]. This suggests a small increase in $(\chi^s_u)^2$ on excitation and hence a small increase in α^s_u. On the other hand if the $\bar{\varepsilon}^s_u$ is approximated by ionization potentials there will be a large change in $\bar{\varepsilon}_u$ in going from the ground to the lowest excited states.

To summarize, therefore, the results obtained from solvent shift data using these approximate forms for the dispersion energy will depend on how the 'average' energy denominators are varied from the ground to the excited state. A small change will lead to a small change in the polarizability whereas a large change will lead to a large change in the polarizability.

In the theory developed by Abe [10] it is assumed that large changes in the $\bar{\varepsilon}^s_u$ do occur and that is why calculations based on Abe's method do indeed give rise to such large values of excited-state polarizabilities [2, 16]. On the other hand those calculations which obtain relatively small excited-state polarizabilities [1, 12, 18] in one way or another are assuming the dispersion terms are not very different in the ground and excited states which is equivalent to the assumption that the $\bar{\varepsilon}_u^s$ are roughly the same in the two states. If simple dispersion formulae like (9) are to be used in this field, therefore, it is essential to decide whether the average energies are changed by large or small amounts in going from the ground to the excited state.

To resolve this crucial point let us set out the arguments for the two possible choices. Firstly the reasons for making a small change in $\bar{\varepsilon}_u^s$:

(a) Equation (12) suggests that $\Delta\bar{\varepsilon}_u$ should depend on $\Delta\chi_u$ and since the molecular size varies only slightly on excitation so should χ_u and, hence, α_u.

(b) Equation (12) also suggests $\Delta\bar{\varepsilon}_u$ should change with $(\alpha_u)^{-\frac{1}{2}}$ and theoretical calculations imply relatively minor changes in α_u.

(c) A large change in α_u would imply that the assumption that polarizability terms could be ignored, which is made in deriving dipole-moment changes from solvent-shift data, would have to be revised. Yet the dipole-moment results seem consistent and acceptable (c.f. Ref. [12]).

(d) Attempts made to find excited-state polarizabilities from the electrostatic terms by considering non-polar solvents and also non-polar solutes in non-polar solvents suggest that d^s_{ur} is roughly proportional to the polarizability change and that this is relatively small [1].

The main arguments for making a large change in $\bar{\varepsilon}_u$ are:

(a) For atoms in their ground states, $\bar{\varepsilon}_u^s$ is often replaced by the ionization potential and the ionization potential of a conjugated molecule in its excited state is much less than in its ground state.

(b) An examination of (4) shows that the energy denominators are decreased in going from the ground to the excited state.

We believe these last two points are not really valid. Point (a) assumes that the results for atoms will apply equally to molecules which may well not be the case. Even if the result does hold for most molecules, conjugated hydrocarbons provide a special case where there are relatively low-lying excited states with large transition moments connecting them to the ground state. Point (b) is valid only if the energy denominators are the determining quantity, i.e. only if the numerators remain the same for the ground and excited state which is not the case since the transition dipoles $|\langle t|\mu_u|s\rangle|^2$ will vary depending on whether s is the ground or excited state. The effect of this is almost impossible to determine which is why the whole problem is so difficult.

Our opinion at the moment is that what evidence there is suggests that the energy denominators $\bar{\varepsilon}_u^s$ should be given approximately the same values for both the ground and excited states. Further evidence that this is so can be obtained by comparing values of excited-state polarizabilities obtained from solvent-shift data with theoretical values. There have been two sets of theoretical calculations of the polarizabilities of the p-excited states of a number of conjugated hydrocarbons. Those of Trsic et [16] were made for quite a large number of molecules and were based on the Hückel method. We ourselves [17] have made calculations on a restricted number of molecules but have used relatively sophisticated methods. The results obtained in the two sets of calculations are given in Table 2 and are in quite good agreement. (Note that the values of Trsic *et al.* are given in units of $e^2 d^2 \beta^{-1}$ and a conversion factor of 100 was used to bring them into units

Table 2. Polarizabilities of the ground and excited states of a number of conjugated molecules (units of 10^{-25} cm^3)

Molecule	Excited state polarizabilities obtained from solvent-shift data		Theoretical excited state polarizabilities		Ground state polarizabilities	
	$\bar{\varepsilon}' = \bar{\varepsilon}$ (ground)[a]	$\bar{\varepsilon} =$ I.P.	[16]	[17]	Experiment[e]	Theory [20]
Naphthalene $^1B_{1u}$	223	346[c]	—	206	175	194
Naphthalene $^1B_{2u}$	337	556[c]	257	256	175	194
Anthracene	391	685[b]	429	461	259	289
Phenanthrene	332	[d]	488	322	247	278
Azulene	[d]	201[b]	224	229	180	212

[a] Computed from experimental data in [13] and [19].

[b] Quoted in [16].

[c] Quoted in [2].

[d] Not available.

[e] For experimental references see [20].

of 10^{-25} cm^3, the reasons for this choice being discussed in Ref. [17]). In Table 2 we also give the values of the excited-state polarizabilities for the same molecules (in the case of naphthalene results are given for the two lowest excited states) computed from solvent-shift data using formula (9) for the dispersion interaction. In column 1 the energy denominators are assumed to be the same for the excited state as for the ground state (i.e. to be the ground-state ionization potentials) while in column 2 the values of $\bar{\varepsilon}_u'$ for the excited states are the ionization potentials of those states and are, therefore, much smaller. Thus the second column results are based on Abe's formula [10] without any qualification. The table makes explicit the point we have made earlier that the use of the same $\bar{\varepsilon}_u'$ in the ground and excited states leads to excited-state polarizabilities which are relatively close to the groundstate values (these are quoted in columns 5 and 6 of Table 2) while the very different values for $\bar{\varepsilon}_u'$ used in Abe's formula leads to large changes. Clearly the former case gives "experimental" values in better agreement with the calculated ones (columns 3 and 4).

However, although, at least on empirical grounds, it seems that the average energies in the formula (9) for the London coefficient should be the same or approximately the same in the ground and excited states, we are not entirely happy with the choice of the ground-state ionization potentials for these average energies. This may not be too bad an approximation for the solvent molecules where the ground state is well separated from the excited state but the solute conjugated hydrocarbons have many low-lying excited states so that it is not so clear what would be a reasonable value of $\bar{\varepsilon}_u'$ in this case. Another difficulty is the proper choice for the cavity radius. Although the choice $a \approx r_u + \frac{1}{2} r_v$ is the proper one for spherical molecules which are well separated; in practice we have large planar molecules with certain regions of the solute and surrounding solvent molecules very much closer together than the distance, a, between the molecular centres. On the whole, therefore, it would seem better to try and replace both by some

Table 3. Comparison of *n*-pentane solvent shifts of a number of conjugated molecules and the Hückel polarizability changes between the ground and the excited *p*-states

Molecule	N	Experimental Δ_{EG} (cm^{-1}) [19]	Theoretical $\Delta\alpha(10^{-25}$cm^3)[16]	$C\Phi(n^2)=\frac{N\Delta_{EG}}{\Delta\alpha}$	$C\Phi(n^2)=\frac{N^2\Delta_{EG}}{\Delta\alpha}$
Naphthalene	2	902	68.5	26.3	52.6
Anthracene	3	866	138.2	18.8	56.4
Naphthacene	4	854	266.9	12.8	51.2
Phenanthrene	3	1012	215.5	14.1	42.3
Pyrene	4	1061	73.3	57.9	289.5
Chyrene	4	1030	383.4	10.8	42.4
1-2 Benzanthracene	4	884	284.3	12.4	49.6
1, 2, 5, 6 Dibenzanthracene	5	3706	509.9	36.3	181.7

type of semi-empirical parameter. Certainly it is the case [13] that the dispersion part of the solvent shift of any particular solute molecule in a number of solvents can be represented quite well by the relation

$$\Delta_{EG} = C_u \Phi(n^2)\,\Delta\alpha \tag{13}$$

where

$$\Phi(n^2) = \frac{n^2-1}{n^2+2} = \frac{4\pi A d}{3M}\alpha_v \tag{14}$$

represents the solvent property and C_u depends only on the solute and is equal to

$$\frac{3}{2}\,\frac{\bar{\varepsilon}_u \bar{\varepsilon}_v}{\bar{\varepsilon}_u + \bar{\varepsilon}_v}\,a^{-3}\,. \tag{15}$$

We say that C_u depends on only the solute even though (15) contains $\bar{\varepsilon}_v$ and a which actually do depend on the solvent because this dependence, at least for commonly used solvents, is so slight that it can be ignored. An examination of the solvent-shift data for a number of molecules shows that Eq. (13) gives a good representation of the dispersion effect. However to use this equation to obtain $\Delta\alpha$ from the experimental Δ_{EG} values an estimate of C_u must be found.

It would clearly be most satisfactory if the same value of C_u could be used for all solute molecules but this cannot be correct, for, even if the $\bar{\varepsilon}_u$ were independent of the solute molecule, the cavity radius would not be. If we use the ground-state ionization potentials for $\bar{\varepsilon}_u$ the quality $\bar{\varepsilon}_u\bar{\varepsilon}_v/\bar{\varepsilon}_u + \bar{\varepsilon}_v$ shows some relatively slight dependence on the particular solute. For polyenes and polyacenes there is a slight decrease as the size of the molecule increases. Similarly, since a^3 depends on the size of the molecule, the term a^{-3} decreases as the molecular size increases. Therefore, the value of C_u varies inversely with molecular size. If N is the number of rings in a solute molecule and we take no account of the variation of the average energies, we would expect C_u to be proportional to $1/N$. This suggests that a reasonable procedure is to try and fit the experimental Δ_{EG} and the theoretical $\Delta\alpha$ by a relationship of the form:

$$\Delta_{EG} = \frac{C}{N}\Phi(n^2)\,\Delta\alpha \tag{16}$$

Table 4. Predictions of $\Delta\alpha$ from Eqs. (16) and (17)

Molecule	$\Delta\alpha$ $[C\Phi(n^2) = 16$ (from (16))]	$\Delta\alpha$ $[C\Phi(n^2) = 50$ (from (17))]	$\Delta\alpha$ (theoretical [16])
Naphthalene	112.0	72.1	68.5
Anthracene	162.4	155.9	138.2
Naphthacene	213.5	273.3	266.9
Phenanthrene	189.8	182.2	215.5
Chyrene	257.5	329.6	383.4
1, 2 Benzanthracene	221.0	282.9	284.3

where C is some constant more or less independent of solute and solvent. C should be fixed empirically and, for this to be done in a satisfactory way, it is clearly best to use a large number of molecules. Unfortunately, self-consistent calculations of $\Delta\alpha$ have been done only for a very few conjugated molecules so for the theoretical values we have used the Hückel calculations of Trsic *et al.* [16]. We have assumed that these theoretical values correspond to the p-bands. For the Δ_{EG} values we have considered only the solvent-shift effects in n-pentane. We do not anticipate that the choice of one solvent only is very significant since variations in Δ_{EG} for different solvents will be adequately taken care of by the $\Phi(n^2)$ term.

In Table 3 we compare values of the experimental Δ_{EG} with theoretical $\Delta\alpha$ and the measure N of molecular size. The ratio $N\Delta_{EG}/\Delta\alpha$, which should be a constant $C\Phi(n^2)$ if the expression (16) is correct, is also computed and the values given in Table 3. Even if we exclude the two highly anomalous results of pyrene (where $\Delta\alpha$ seems anomalous) and 1, 2, 5, 6 dibenzanthracene (where Δ_{EG} seems anomalous), the values of $C\Phi(n^2)$ for the different solute molecules are not by any means constant.

The problem is clearly that while the values of Δ_{EG} do not vary in any significant way with the size of the solute molecule and indeed are fairly constant for all of them, the values of $\Delta\alpha$ display a size dependence greater than $\Delta\alpha$ proportional to N which is implied by Eq. (16). Indeed, if we replace (16) by

$$\Delta_{EG} = \frac{C}{N^2}\,\Phi(n^2)\,\Delta\alpha\,, \tag{17}$$

then as Table 3 shows the resulting values of $C\Phi(n^2)$ are very much more constant.

Using these two different formulae, Eqs. (16) and (17), with the value of $C\Phi(n^2) = 16$ in the first and $C\Phi(n^2) = 50$ in the second we have used the experimental values of Δ_{EG} to find values of $\Delta\alpha$ to compare with the theoretical ones. These values are given in Table 4. It is fairly clear from that table that the second formula (17) gives decidedly better results. Taking the average energy $\bar{\varepsilon}_u$ for naphthalene to be its ground state ionization potential these values of C correspond to a cavity radius of 5.35 Å and 4.607 Å respectively. These are not out of line with previously used values.

The results in Tables 3 and 4 are not very encouraging. Provided we use Eq. (17) there is a correlation between Δ_{EG} and $\Delta\alpha$ but not a good one. Essentially, since the Δ_{EG} do not vary very much, the formula is really giving a correlation between $\Delta\alpha$ and N^2 rather than $\Delta\alpha$ and the solvent shift. A better test of this type of relationship could be made if values of $\Delta\alpha$ were available for the α and β bands of the solute molecules since Δ_{EG} for the α band is smaller (approximately 300 cm^{-1}) than for the other two bands. Actually we do have a calculated value for the α band of naphthalene of $\Delta\alpha = 12.10^{-25}$ cm^3 which does fit the expression (17) (c.f. 20.64×10^{-25} cm^3) reasonably well but it would be unwise to draw any conclusion from this one value. On the whole therefore one would have to conclude that Table 4 shows that very little useful information on excited state polarizabilities can be gleaned from solvent shift data.

4. Summary and Conclusions

We have examined the possibility of using solvent-shift data to obtain "semi-experimental" values for the polarizabilities of excited states of conjugated molecules. We decided that for this to be done in a satisfactory way the dispersion-interaction term had to be related to the polarizability changes of the solute molecule between its ground and excited state. This can only be done by assuming that the dispersion interaction can be approximated by a London-type formula involving average excitation energies. The use of this formula involves the crucial decision of whether the average solute excitation energy should have approximately the same value for the solute in its ground state as in its excited state or whether the values in the two states should be very different. This is crucial since the former choice will inevitably mean that the polarizability changes deduced from the solvent-shift data will be small while the latter choice will lead to large changes. This explains the very different values which can be found in the literature. For a number of reasons, the most important of which was comparison with theoretical values, we decided that the average energies ought to be taken the same for both ground and excited state. When this is done the final relation between the experimental solvent shift Δ_{EG} and the polarizability change $\Delta\alpha$ takes the form

$$\Delta_{EG} = -\frac{C}{f(N)}\,\Phi(n^2)\,\Delta\alpha \tag{18}$$

where $f(N)$ is a function of the solute molecular size (measured by the number of benzene rings N) which takes account of the cavity volume occupied by the solute and the variation of the average energy between the different molecules. One might expect that the dominant term in $f(N)$ depends on the cavity volume which, in turn, should vary as N. However, we have found that this choice of $f(N)$ proportional to N does not lead to very good agreement between Δ_{EG} and the Hückel values of $\Delta\alpha$. It turned out to be much better to take $f(N)$ proportional to N^2. It is difficult to see, using the usual cavity-field type arguments, why the volume should depend on a higher power of N than the first. The extra power of N could come from the average energy, which, since it is something of an unknown quantity might perhaps vary in this way, although it is rather unlikely. It may well be, however, that with increasing size of the solute molecules the whole basis of the usual theory of solute-solvent interaction breaks down. It is not, after all, very realistic to replace the interaction between two large molecules by a dipolar expansion in terms of the distance between their centres when, in fact, the periferies of the two molecules are in closer contact than either perifery to their respective centres. The rather odd variation with molecular size which we appear to have found may well be an indication that these considerations are becoming important. Using Eq. (18) with theoretical values of excited-state polarizabilities and experimental solvent-shift values it has proved possible to obtain at least some indication of the empirical status of the relationship between solvent shift effects and polarizability changes. It seems quite clear that for the *p*-bands of conjugated hydrocarbons the relationship is not very good. The solvent shifts do not vary very much for the different solute molecules, whereas the polarizabilities vary considerably more or less as the square of the molecular size. This is why, in order to get any sort of correlation, we are forced to include a term proportional to N^2 in the formula relating Δ_{EG} and $\Delta\alpha$ and this is not easy to justify theoretically.

Our general conclusion is that, while it is possible to find a rough correlation between theory and experiment, the exact basis of this relationship is hard to understand. Moreover, the crudity of the correlation is such that the values of $\Delta\alpha$ obtained from the solvent-shift data are very approximate indeed. Thus such values are not very useful for confirming and comparing theoretical calculation. As a final point, however, we recognise that these disappointing conclusions are based only on results for the *p* excited states. It would be useful to have more theoretical values of excited state polarizabilities, particularly of the α and β excited states, available to make a more extensive comparison in order to try to confirm our findings. However, there are beginning to become available direct measurements of excited state polarizabilities [18] which can be used to confirm the theoretical calculations directly and so make it unnecessary to use the solvent-shift data in this way. There will, of course, still remain the problem of estimating the dispersion contribution to the solvent shift theoretically. The results in this paper certainly suggest that the use of the London approximation is not a suitable way to do this.

References

1. Suppan, P.: Spectrochim. Acta **24**, 1161 (1964).
2. Abe, T., Amako, Y., Nishioka, T., Azumi, H.: Bull. chem. Soc. Japan **39**, 845 (1966).
3. Liptay, W.: In: Modern quantum chemistry, Part II p. 173. New York: Academic Press 1965.
4. Amos, A. T., Burrows, B. L.: Advances in quant. Chemistry, in press (1973).
5. Suppan, P.: J. chem. Soc. (A), 3126 (1968).
6. Ooshika, Y.: J. physic. Soc. Japan **9**, 594 (1954).
7. MacRae, E. G.: J. physic. Chem. **61**, 562 (1957).
8. Liptay, W., Walz, G : Z. Natur **26a**, 2007 (1971).
9. Margenau, H.: Rev. mod. Physics **11**, 1 (1939).
10. Abe, T.: Bull. chem. Soc. Japan **38**, 1314 (1965).
11. Margenau, H., Kestner, N.: Theory of intermolecular forces. Oxford: Pergamon Press 1969.
12. Ledger, M. B., Suppan, P.: Spectrochim. Acta **23**, 641 (1967).
13. Weigang Jr., O. E.: J. chem. Physics **33**, 892 (1960).
14. Haugh, E. F., Hirschfelder, J. O.: J. chem. Physics **23**, 1778 (1955).
15. Dixon, R. N.: Spectroscopy and structure. London: Methuen 1965.
16. Trsic, M., Uzhinov, B. M., Matzke, P.: Molecular Physics **18**, 851 (1970).
17. Amos, A. T., Burrows, B. L.: Theoret. chim. Acta (Berl.) **23**, 327 (1972).
18. Eisenthal, K. B., Rieckhoff, K. E.: J. chem. Physics **55**, 3317 (1971) Liptay, W., Walz, G., Baumann, W., Schlosser, H. J., Deckers, H., Detzer, N.: Z. Natur **26a**, 2020 (1971).
19. Weigang Jr., O. E., Robertson, W. W., Matsen, F. A.: J. molecular Spectroscopy **1**, 1 (1959).
20. Amos, A. T., Hall, G. G.: Theoret. chim. Acta (Berl.) **6**, 159 (1966).

Dr. A. T. Amos, Department of Mathematics,
University of Nottingham, Nottingham NG 7 2RD, England

Theoret. chim. Acta (Berl.) 29, 151 – 166 (1973)
© by Springer-Verlag 1973

Matrix Elements of One- and Two-Electron Operators*

Jacek Karwowski**

Institute of Physics, Nicholas Copernicus University, Toruń, Poland

Received February 1, 1972

A graphical representation of matrix elements of spin-free one- and two-electron operators is used for deriving a simple algorithm for the evaluation of their values. The method covers all the cases which may occur when wave functions are taken as mutually orthogonal antisymmetrized products of spinorbitals (which are assumed to form an orthonormal set) and are eigenfunctions of $\mathscr{S}^2$ and $\mathscr{S}_z$ operators. The resulting formulas are suitable as well for computer programming as for hand calculations.

Mit Hilfe einer graphischen Darstellung wird ein einfacher Algorithmus zur Bestimmung der Werte der Matrix-Elemente von spinfreien Ein- und Zweielektronenoperatoren abgeleitet. Durch diese Methode werden alle Fälle erfaßt, die auftreten, wenn die Wellenfunktionen wechselweise orthogonale, antisymmetrisierte Produkte von Spinorbitalen (von denen angenommen wird, daß sie einen orthogonalen Satz bilden) darstellen und Eigenfunktion der $\mathscr{S}^2$ und $\mathscr{S}_z$ Operatoren sind. Die erhaltenen Formeln eignen sich für Rechnungen mit und ohne Verwendung eines Computers.

1. Introduction

Although the multiexcited configurations were shown to be fundamentally important in the energy levels calculations, they are included rather exceptionally. One of the most important barriers for extension of configuration interaction expansions by inclusion of multiexcited configurations presents the problem of evaluation of matrix elements for open shell configurations. A simple method, originally formulated by Pauling [10], was further extended by numerous authors in spin-dependent [11] as well as in spin-free [8] formulation of quantum chemistry. However an applicability of the algorithms obtained is limited to the valence-bond wave functions. In the case of spin-projected wave functions the problem has been solved in its general form by Harris [2]. Evaluation of the matrix elements is considerably more troublesome when the wave functions (being antisymmetric eigenfunctions of $\mathscr{S}^2$ and $\mathscr{S}_z$ operators) are mutually orthogonal. Tables of formulas for different types of the matrix elements, published occasionally by various authors [9] are really convenient in some special cases, but are completely insufficient for an authomatic construction of configuration interaction matrices. The main source of difficulty lies in an enormous number of different types of formulas, which rapidly grows up with the number of singly occupied orbitals. The tables of Yamazaki [16], probably the most complete in this type, cover the configurations with at most six singly occupied orbitals and contain a few thousands of formulas. Another, signifficantly more condensed type of formulas, however limited to the singlet configurations being no more than doubly excited relatively to a closed shell ground-state, was derived by Čížek [1]. A very interesting algebraic approach making use of the permutational symmetry of the space part of the wave function was recently given by Kaplan [4]. The method enables to evaluate all the types of diagonal and some types of the off diagonal matrix elements. Recently, the second quantization formalism has been used for evaluation of the matrix elements by Kuprievich *et al.* [7][1].

---

* Sponsored by the Mathematical Institute, Polish Academy of Sciences.

** Temporary address (till October 1973): Division of Theoretical Chemistry, Department of Chemistry, University of Alberta, Edmonton, Canada.

A different and probably the most general is the Serber-Yamanouchi-Kotani approach [6] which may be easily applied in the case of an orthogonal set of antisymmetric configurations being eigenfunctions of $\mathscr{S}^2$ and $\mathscr{S}_z$ operators. The most important obstacle in its direct application is that the matrix elements, in the case of N-electron system, are expressed as sums over $N!$ terms. However when the wave functions are taken as linear combinations of antisymmetrized products of orthogonal one-electron spinorbitals, these sums contain only a few non-zero terms [2, 5, 12]. An efficient method enabling to select the nonvanishing terms and to determine the coefficients with which the appropriate integrals there appear was recently presented in two different versions by Ruedenberg, Salmon and Poshusta [12–14]. An alternative handling of the subject was independently proposed by the author [5]. In the present paper the Ruedenberg's formulas are rederived using a diagram technique[2] which is shown to be a very useful tool as well for general considerations as for practical calculations. An example of such calculation is given as an illustration of the method. Moreover a further simplification of these formulas, being particulary important from the point of view of an applicability of the method to computer-programming, is here performed.

2. Formulation of the Problem

We are concerned with one-electron operators

$$\mathscr{H}_1 = \sum_{i=1}^{N} h_1(\mathbf{r}_i) \tag{1}$$

and two-electron operators

$$\mathscr{H}_2 = \sum_{j=i+1}^{N} \sum_{i=1}^{N-1} h_2(\mathbf{r}_i, \mathbf{r}_j) \tag{2}$$

where $\mathbf{r}_i$ denote the spatial coordinates of electron i, N means number of the electrons and $h_2(\mathbf{r}_i, \mathbf{r}_j) = h_2(\mathbf{r}_j, \mathbf{r}_i)$. In particular, Hamiltonian of a system of N electrons can always be written in the form

$$\mathscr{H} = \mathscr{H}_1 + \mathscr{H}_2 \,. \tag{3}$$

---

[1] A very complete review of literature concerning the subject is presented in an article of Ruedenberg and Poshusta [13] where the reader is referred to.

[2] This paper was completed before the Ruedenberg *et al.* results [12–14] have got to the author's knowledge. Therefore an approach of Kotani *et al.* [6] was taken as a starting point in this discussion and the notation used here is as close as it is possible to that of Kotani and rather different from the Ruedenberg's one

Let us define a primitive function Ψ^0_λ as a product of N one-electron orbitals chosen from an orthonormal set

$$\psi_1, \psi_2, \ldots, \psi_K (K \geqq N/2)$$

$$\psi^0_\lambda(\boldsymbol{r}_1, \boldsymbol{r}_2, \ldots, \boldsymbol{r}_N) = \prod_{i=1}^{N} \psi_{\lambda_i}(\boldsymbol{r}_i). \tag{4}$$

Every primitive function corresponds to an electronic configuration λ, described by the set of indices $[\lambda_1, \lambda_2, \ldots, \lambda_N]$. Some orbitals can be doubly occupied. Then they appear twice in the product (4) and are there written after the singly occupied orbitals. Moreover, both kinds of orbitals are put in (4) in the growing order of their indices. It means that

$$\begin{gathered} \lambda_1 < \lambda_2 < \cdots < \lambda_p \\ \lambda_{p+1} = \lambda_{p+2} < \lambda_{p+3} = \lambda_{p+4} < \cdots < \lambda_{N-1} = \lambda_N \end{gathered} \tag{5}$$

where p denotes the number of singly occupied orbitals in configuration λ.

In order to construct a wave function with the proper spin and space symmetry properties, based on the orbital product (4), it is convenient to follow the work of Kotani *et al.* [6][3]. For this purpose we introduce an orthonormal set $\Theta_{SM,k}$ of all the linearly independent N-electron eigenfunctions of $\mathscr{S}^2$ and $\mathscr{S}_z$ operators corresponding to the eigenvalues $S(S+1)\hbar^2$ and $M\hbar$, which span a subspace of the whole 2^N dimensional N-spin space. This subspace is called the SM subspace. Its dimension f^N_S can be evaluated from the formula [6]:

$$f^N_S = \frac{(2S+1)\,N!}{(N/2+S+1)!\,(N/2-S)!}. \tag{6}$$

Index k numbers the basis functions of SM subspace and varies from 1 to f^N_S.

The SM subspace is invariant in respect to permutation operators $\mathscr{P}_\sigma$ acting on the spin coordinates of electrons

$$\mathscr{P}_\sigma \Theta_{SM,k} = \sum_{j=1}^{f^N_S} V^N_S(\mathscr{P})_{jk}\,\Theta_{SM,j}. \tag{7}$$

The $V^N_S(\mathscr{P})$ matrices form an irreducible representation of the N!th order permutation group $\mathfrak{S}_N$ [6]. The basis $\Theta_{SM,k}$ of SM subspace has been chosen as orthonormal. Then V^N_S matrices are unitary. As the basis $\Theta_{SM,k}$ is complete in the spin space, every normalized eigenfunction $\Phi_{SM}(\boldsymbol{r}, \boldsymbol{\sigma})$ of $\mathscr{S}^2$ and $\mathscr{S}_z$, depending on space ($\boldsymbol{r}$) and spin ($\boldsymbol{\sigma}$) coordinates of N electrons, can be expanded as

$$\Phi_{SM}(\boldsymbol{r}, \boldsymbol{\sigma}) = \frac{1}{\sqrt{f^N_S}} \sum_{k=1}^{f^N_S} \chi_{S,k}(\boldsymbol{r})\,\Theta_{SM,k}(\boldsymbol{\sigma}) \tag{8}$$

where $\chi_{S,k}(\boldsymbol{r})$ are normalized to unity and M-independent functions of the spatial coordinates of electrons. In the case when $\Phi_{SM}(\boldsymbol{r}, \boldsymbol{\sigma})$ satisfies the Pauli principle, and $\mathscr{P}$ is an operator of permutation of the space coordinates of electrons, then

$$\mathscr{P}\chi_{S,k} = \varepsilon_{\mathscr{P}} \sum_{j=1}^{f^N_S} V^N_S(\mathscr{P}^{-1})_{kj}\,\chi_{S,j} \equiv \sum_{j=1}^{f^N_S} U^N_S(\mathscr{P})_{jk}\,\chi_{S,j} \tag{9}$$

---

[3] The most complete treatment of the problem is given in a recent paper of Salmon [15].

where $\varepsilon_{\mathscr{P}}$ is parity of the permutation $\mathscr{P}$ and $U_S^N(\mathscr{P})_{jk} = \varepsilon_{\mathscr{P}} V_S^N(\mathscr{P}^{-1})_{kj}$. As the V_S^N are unitary,

$$U_S^N(\mathscr{P}) = \varepsilon_{\mathscr{P}} V_S^N(\mathscr{P}). \tag{10}$$

Hence the matrices $U_S^N(\mathscr{P})$ form a dual representation of $\mathfrak{S}_N$. It is easy to observe, that $\chi_{S,k}(k = 1, 2, \ldots, f_S^N)$ are mutually orthogonal. Every normalizable function of space coordinates of electrons, when transforming according to (9), may be used as basis for construction of the wave function (8) which is an eigenfunction of $\mathscr{S}^2$ and $\mathscr{S}_z$ operators and satisfies the Pauli principle.

When some orbitals are doubly occupied in configuration λ, then there exists a subgroup $\mathfrak{H}_\lambda$ of $\mathfrak{S}_N$ for which Ψ_λ^0 is invariant. Every permutation $\mathscr{Q} \in \mathfrak{H}_\lambda$ only inverts ordering within doubly occupied pairs. Since $\mathfrak{H}_\lambda$ is Abelian and $\mathscr{Q}^2 = \mathscr{I}$ ($\mathscr{I}$ means the identity operator) all $U_S^N(\mathscr{Q})$ can be as follows:

$U_S^N(\mathscr{Q})_{ik} = \pm\delta_{ik}, (i, k = 1, 2, \ldots, f_S^N)$; and
$U_S^N(\mathscr{Q})_{kk} = +1$ when $k \leqq f$, while
$U_S^N(\mathscr{Q})_{kk} = -1$ for at least one $\mathscr{Q}$ when $k > f$.
It can be shown [6], that

$$f = f_S^p$$

and that the functions

$$\chi_{S,k}^{(m)} = \sqrt{f_S^N/(N!\,2^{(N-p)/2})} \sum_{\mathscr{P}} U_S^N(\mathscr{P})_{km} \mathscr{P} \Psi_\lambda^0 \tag{11}$$

form an orthonormal set and fulfill relation (9) for $m \leqq f$, while for $m > f$ vanish identically. The sum is here extended over all $N!$ elements of $\mathfrak{S}_N$.

From (11) results, that for every configuration λ there exist f linearly independent functions

$$\Phi_{SM,m}^{(\lambda)}(r, \sigma) = 2^{(p-N)/4}/\sqrt{N!} \sum_{k=1}^{f_S^N} \sum_{\mathscr{P}} U_S^N(\mathscr{P})_{km}\, \Theta_{SM,k}(\sigma)\, \mathscr{P} \Psi_\lambda^0(r) \tag{12}$$

$$m = 1, 2, \ldots, f;\ \mathscr{P} \in \mathfrak{S}_N,$$

which fulfil the following conditions:

$$\mathscr{P}_\sigma \mathscr{P} \Phi_{SM,m}^{(\lambda)} = \varepsilon_{\mathscr{P}} \Phi_{SM,m}^{(\lambda)}, \tag{13}$$

$$\mathscr{S}^2 \Phi_{SM,m}^{(\lambda)} = \hbar^2 S(S+1)\, \Phi_{SM,m}^{(\lambda)}, \tag{14}$$

$$\mathscr{S}_z \Phi_{SM,m}^{(\lambda)} = \hbar M \Phi_{SM,m}^{(\lambda)}, \tag{15}$$

$$\langle \Phi_{SM,m}^{(\lambda)} | \Phi_{S'M',n}^{(\mu)} \rangle = \delta_{\lambda\mu} \delta_{SS'} \delta_{MM}\, \delta_{mn}. \tag{16}$$

The matrix elements of an arbitrary Hermitean and spin-free operator $\mathscr{H}$ between the wave functions (12) can now be expressed as

$$\langle \Phi_{SM,m}^{(\lambda)} | \mathscr{H} | \Phi_{S'M',n}^{(\mu)} \rangle = \delta_{SS'} \delta_{MM'} H_{mn}^{(\lambda\mu)} \tag{17}$$

where [6]

$$H_{mn}^{(\lambda\mu)} = {\sum_{\mathscr{P}}}' \alpha_{\lambda\mu}(\mathscr{P})\, [U_S^N(\mathscr{P})]_{nm}^{fg} \langle \mathscr{P} \Psi_\lambda^0 | \mathscr{H} | \Psi_\mu^0 \rangle \tag{18}$$

$$m = 1, 2, \ldots, f; \quad n = 1, 2, \ldots, g;$$

$$f = f_S^p; \quad g = f_S^q; \quad f \geqq g;$$

p and q are the numbers of singly occupied orbitals in configurations λ and μ respectively ; $[U_S^N(\mathscr{P})]^{fg}$ is the rectangular part of $U_S^N(\mathscr{P})$ containing first f

rows and g columns;

$$\alpha_{\lambda\mu}(\mathcal{P}) = 2^{(p+q)/4 - N/2} \operatorname{ord}\{\mathfrak{P}_{\lambda\mu}(\mathcal{P})\} \tag{19}$$

where $\operatorname{ord}\{\mathfrak{P}_{\lambda\mu}(\mathcal{P})\}$ is the order of a subset $\mathfrak{P}_{\lambda\mu}(\mathcal{P})$ of $\mathfrak{S}_N$ defined as follows: $\mathcal{R} \in \mathfrak{P}_{\lambda\mu}(\mathcal{P})$ if there exist $\mathcal{Q}_\lambda \in \mathfrak{H}_\lambda$ and $\mathcal{Q}_\mu \in \mathfrak{H}_\mu$, such that $\mathcal{R} = \mathcal{Q}_\lambda \mathcal{P} \mathcal{Q}_\mu$[4]; Σ' means that from each set $\mathfrak{P}_{\lambda\mu}(\mathcal{P})$ only one element should be included.

In the primitive function (4) there appear N orbitals ψ_{λ_i}, which are numbered from 1 to N by the index i. It is convenient to define, in paralell to the operators $\mathcal{P}$ which act on the space coordinates of electrons, also operators $\bar{\mathcal{P}}$ acting on the indices i numbering the orbitals. The operators $\mathcal{P}$ and $\bar{\mathcal{P}}$ are connected by a simple relation

$$\bar{\mathcal{P}} = \mathcal{P}^{-1} \tag{20}$$

when they act on Ψ_λ^0. For the representation matrices $U_S^N(\mathcal{P})$ it gives

$$U_S^N(\bar{\mathcal{P}}) = U_S^N(\mathcal{P})^+ \tag{21}$$

The formula (18) can be written involving $\bar{\mathcal{P}}$ operators:

$$H_{mn}^{(\lambda\mu)} = \sum_{\bar{\mathcal{P}}}{}' \alpha_{\lambda\mu}(\bar{\mathcal{P}}) \, [U_S^N(\mathcal{P})]_{mn}^{fg} \langle \bar{\mathcal{P}} \Psi_\lambda^0 | \mathcal{H} | \Psi_\mu^0 \rangle \tag{22}$$

The formulas (18) and (22) are not satisfactory for application to many-electron systems, because the sums are extended over almost all $N!$ permutations of $\mathfrak{S}_N$. However only a few terms give nonvanishing contributions to the matrix elements. The problem to be solved is to choose these nonvanishing terms and to determine the coefficients with which they do appear. The corresponding formulas were recently derived by Ruedenberg, Salmon and Poshusta [12–14]. An alternative, and completely independently obtained, derivation (partly based on previous results of the author [5]) is outlined in the following.

3. Graphical Representation

In order to simplify the Eq. (22) we have found to be convenient to introduce a graphical representation of a pair of configurations. The orbitals appearing in the primitive functions corresponding to a pair of configurations are represented by asterisks (if singly occupied) and by circles (if doubly occupied). The symbol corresponding to ψ_{λ_i} (ψ_{μ_i}) orbital is labelled with the number $\lambda_i(\mu_i)$. The asterisks and circles are distributed in two rows and N columns. The symbols describing the configuration μ are placed in the first row and in the second one – the configuration λ. According to (18), always $f \geqq g$ (i.e. $p \geqq q$). The sequence of the symbols in both rows is the same as in the corresponding orbital products (4). The symbols corresponding to identical orbitals are joined by lines. If it is possible to join them in a few distinct ways, then the joining lines are drawn as short as possible. Such system circles, asterisks and joining lines is called *configuration-pair diagram* and denoted $D_{\lambda\mu}$. For example the pair of configurations:

$$\begin{aligned} \Psi_\mu^0 &= \psi_1(\boldsymbol{r}_1)\,\psi_3(\boldsymbol{r}_2)\,\psi_4(\boldsymbol{r}_3)\,\psi_4(\boldsymbol{r}_4)\,\psi_6(\boldsymbol{r}_5)\,\psi_6(\boldsymbol{r}_6) \\ \Psi_\lambda^0 &= \psi_3(\boldsymbol{r}_1)\,\psi_4(\boldsymbol{r}_2)\,\psi_6(\boldsymbol{r}_3)\,\psi_8(\boldsymbol{r}_4)\,\psi_1(\boldsymbol{r}_5)\,\psi_1(\boldsymbol{r}_6) \end{aligned} \tag{23}$$

---

[4] Some useful properties of the double coset $\mathfrak{P}_{\lambda\mu}(\mathcal{P})$ are derived by Junker and Klein [3].

is represented by the diagram:

$D_{\lambda\mu} =$ 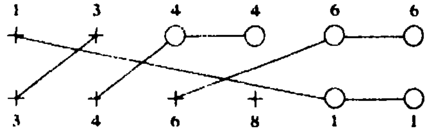 . (24)

In such a way to every rectangular $H^{(\lambda\mu)}$ matrix corresponds one $D_{\lambda\mu}$ diagram.

Every $D_{\lambda\mu}$ diagram generates a set of $N!$ diagrams $\mathscr{D}_{\lambda\mu}(\bar{\mathscr{P}})$ called *numbered diagrams of a configuration pair*. The graphical representation of $\mathscr{D}_{\lambda\mu}(\mathscr{I})$ is the same as that of $D_{\lambda\mu}$, however the symbols representing the orbitals are now additionally provided with their consecutive numbers in the orbital product (4) (number i for φ_{λ_i} orbital). In $\mathscr{D}_{\lambda\mu}(\bar{\mathscr{P}})$ diagram the order of orbitals in the first row is the same as in $\mathscr{D}_{\lambda\mu}(\mathscr{I})$ while in the second one it is changed in respect to $\mathscr{D}_{\lambda\mu}(\mathscr{I})$ and is the same as in $\bar{\mathscr{P}}\Psi^0_\lambda$. The joining lines are also properly changed. If we accept the convention that the operators $\bar{\mathscr{P}}$ may properly permute the orbitals in the second row of the numbered diagrams and do not affect the first row, then all $N!$ diagrams $\mathscr{D}_{\lambda\mu}(\bar{\mathscr{P}})$ can be expressed as

$$\mathscr{D}_{\lambda\mu}(\bar{\mathscr{P}}) = \bar{\mathscr{P}}\mathscr{D}_{\lambda\mu}(\mathscr{I}). \tag{25}$$

For example, for the diagram (24)

$\mathscr{D}_{\lambda\mu}(\mathscr{I}) =$ 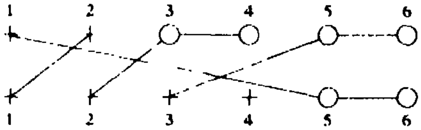

and

$(\overline{1432})\,\mathscr{D}_{\lambda\mu}(\mathscr{I}) =$ 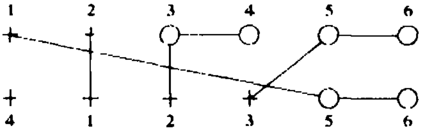 $= \mathscr{D}_{\lambda\mu}((\overline{1432}))$

In these diagrams the indices λ_i and μ_i are for simplicity sake omitted.

In the case when identical orbitals are on the same positions in Ψ^0_μ and $\bar{\mathscr{P}}\Psi^0_\lambda$, the corresponding joining lines in the numbered diagram $\mathscr{D}_{\lambda\mu}(\bar{\mathscr{P}})$ are "vertical". The difference between number of electrons (N) and number of the vertical lines is called *rank* of the numbered diagram. The diagram $\mathscr{D}_{\lambda\mu}(\bar{\mathscr{P}})$ in which all the lines joining its rows are vertical is called the *ordered diagram*. Of course, there may be a few ordered diagrams for a given configuration-pair diagram. From among the permutations which transform $\mathscr{D}_{\lambda\mu}(\mathscr{I})$ into the ordered diagram we choose one and denote it $\bar{\mathscr{P}}_0$[5]. Then, this permutation is kept fixed for a given pair of configurations. In our example $\bar{\mathscr{P}}_0$ can be any permutation from the sets $\mathfrak{P}_{\lambda\mu}((\overline{1532}))$ or $\mathfrak{P}_{\lambda\mu}((\overline{46})(\overline{1532}))$. The rank of an ordered diagram is called rank of the configuration-pair diagram and equals the number of orbitals by which the two involved configurations differ. Where it is essential we write it as a superscript in the correspondent symbol: $D^r_{\lambda\mu}$.

---

[5] The permutation $\bar{\mathscr{P}}_0$ is identical with the *line-up permutation* introduced by Ruedenberg [12].

The relation (22) states that the configuration-pair diagram $D_{\lambda\mu}$ is a superposition of the numbered diagrams $\mathscr{D}_{\lambda\mu}(\mathscr{P})$

$$D_{\lambda\mu} = \sum_{\mathscr{P}}{}' \alpha_{\lambda\mu}(\mathscr{P})\, \mathscr{D}_{\lambda\mu}(\mathscr{P}). \tag{26}$$

The prime in the sum means, that only one element from every set $\mathfrak{P}_{\lambda\mu}(\mathscr{P})$ should be included. The orthogonality of the orbitals causes, that in the case of n-electron operators (we are interested in $n = 1$ and $n = 2$) only these diagrams will contribute to the sum (26) whose ranks do not exceed n. In our example $r = 2$. Therefore non-zero contributions appear for two-electron operators and come from ordered diagrams only: one from the set $\mathfrak{P}_{\lambda\mu}((\overline{1532}))$ and one from $\mathfrak{P}_{\lambda\mu}((\overline{46})(\overline{1532}))$, say

$\mathscr{D}_{\lambda\mu}((\overline{1532})) =$

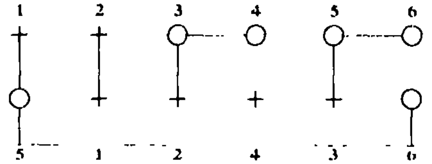

$\mathscr{D}_{\lambda\mu}((\overline{46})(\overline{1532})) =$

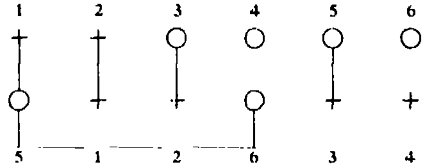

4. Classification of Configuration-Pair Diagrams

Every permutation $\mathscr{P}$ may be expressed in the form

$$\mathscr{P} = \mathscr{P}^{sd}\mathscr{P}^{s}\mathscr{P}^{d} \tag{27}$$

where $\mathscr{P}^{s}$ causes a mixing of singly occupied orbitals, $\mathscr{P}^{d}$ of doubly occupied ones, and $\mathscr{P}^{sd}$ is a product of transpositions interchanging singly and doubly occupied orbitals. Decomposition (27) is always performed in such way, that $\mathscr{P}^{sd}$ consists of the least possible number of transpositions.

The decomposition (27) of $\mathscr{P}_0$ permutation

$$\mathscr{P}_0 = \mathscr{P}_0^{sd}\mathscr{P}_0^{s}\mathscr{P}_0^{d} \tag{28}$$

can be used as a basis for an useful classification of configuration-pair diagrams. Namely, as will be seen, the type of formula for the matrix element (22), (26) is determined by this part of $\mathscr{D}_{\lambda\mu}(\mathscr{P}_0^{s}\mathscr{P}_0^{d})$ diagram, where non-identical orbitals are located on the same positions in the rows. Therefore it is convenient to classify the $D_{\lambda\mu}$ diagrams in such way, that to one class belong these diagrams for which $\mathscr{D}_{\lambda\mu}(\mathscr{P}_0^{s}\mathscr{P}_0^{d})$ has the same form.

All the distinct types of $\mathscr{D}_{\lambda\mu}(\mathscr{P}_0^{s}\mathscr{P}_0^{d})$ diagrams corresponding to $D^{r}_{\lambda\mu}$ diagrams with $r \leq 2$ are collected in Table 1. These parts of the diagrams, where identical orbitals (when singly occupied) or identical pairs of orbitals (when doubly occupied) are located on the same positions in both rows, are there omitted. As

Table 1. Types of $\mathcal{D}_{\lambda\mu}(\mathcal{F}_0^\lambda\mathcal{F}_0^\mu)$ diagrams

No	$\mathcal{D}_{\lambda\mu}(\mathcal{F}_0^\lambda\mathcal{F}_0^\mu)$	Rank of $D_{\lambda\mu}$	$\alpha_{\lambda\mu}(\mathcal{F}_0)$	$p-q$
1	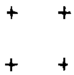	2	1	0
2	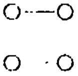	2	1	0
3	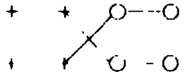	2	2	0
4	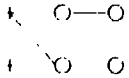	2	2	0
5	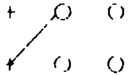	2	2	0
6	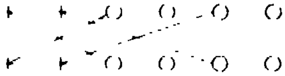	2	4	0
7	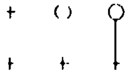	2	$\sqrt{2}$	2
8	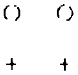	2	$\sqrt{2}$	2
9	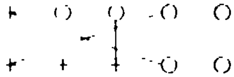	2	$2\sqrt{2}$	2
10	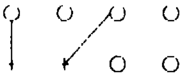	2	$2\sqrt{2}$	2
11	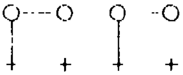	2	2	4
12	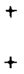	1	1	0
13	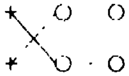	1	2	0
14	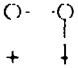	1	$\sqrt{2}$	2
15		0	1	0

seen, all the $D^r_{\lambda\mu}$ diagrams ($r \leqq 2$) have been distributed into 15 classes. According to the rank r, there are 11 classes for $r = 2$, 3 classes for $r = 1$ and one class for $r = 0$.

Let the number of orbitals being singly occupied in configuration $\lambda(\mu)$ and doubly occupied in configuration $\mu(\lambda)$ be denoted by $t_\lambda(t_\mu)$ and $\max(t_\lambda, t_\mu)$ be the bigger of these numbers. If $p = q$ then $\bar{\mathcal{P}}_0^{sd}$ consists of $t = \max(t_\lambda, t_\mu)$ transpositions. If $p \neq q$ then $(p - q)/2$ singly occupied orbitals of configuration λ may be brought into coincidence with the corresponding doubly occupied orbitals of configuration μ by means of $\bar{\mathcal{P}}_0^s$ (a pair of doubly occupied orbitals in μ may always be placed in a proper position as the representation matrix corresponding to a *transposition of two doubly occupied pairs is unit). Hence, if* $\max(t_\lambda, t_\mu) > (p - q)/2$ then $\bar{\mathcal{P}}_0^{sd}$ consists of

$$t = \max(t_\lambda, t_\mu) - (p - q)/2 \tag{29}$$

transpositions, and $\bar{\mathcal{P}}_0^{sd} = \mathcal{I}$ (i.e. $t = 0$) in the opposite case.

5. Evaluation of $\alpha_{\lambda\mu}(\bar{\mathcal{P}}_0)$

If $\mathfrak{P}_{\lambda\mu}(\bar{\mathcal{P}}_0)$ is decomposed after (28), then

$$\mathfrak{P}_{\lambda\mu}(\bar{\mathcal{P}}_0) = \{\mathfrak{H}_\mu \bar{\mathcal{P}}_0^{sd} \bar{\mathcal{P}}_0^{d} \mathfrak{H}_\lambda \bar{\mathcal{P}}_0^{s}\} . \tag{30}$$

$\bar{\mathcal{P}}_0^d$ may always be expressed as a product of operators transposing pairs of doubly occupied orbitals. Then $\{\bar{\mathcal{P}}_0^d \mathfrak{H}_\lambda\} = \{\mathfrak{H}_\lambda \bar{\mathcal{P}}_0^d\}$[6] and

$$\operatorname{ord}\{\mathfrak{P}_{\lambda\mu}(\bar{\mathcal{P}}_0)\} = \operatorname{ord}\{\mathfrak{H}_\mu \bar{\mathcal{P}}_0^{sd} \mathfrak{H}_\lambda\} \tag{31}$$

Now, if $\bar{\mathcal{P}}_0^{sd} = \mathcal{I}$, then $\operatorname{ord}\{\mathfrak{P}_{\lambda\mu}(\bar{\mathcal{P}}_0)\} = \operatorname{ord}\{\mathfrak{H}_\mu \mathfrak{H}_\lambda\} = 2^{(N-q)/2}$ (because $\mathfrak{H}_\lambda$ is a subgroup of $\mathfrak{H}_\mu$ and $\mathfrak{H}_\mu \mathfrak{H}_\lambda = \mathfrak{H}_\mu$). Therefore, according to (19), in this case

$$\alpha_{\lambda\mu}(\bar{\mathcal{P}}_0) = 2^{(p-q)/4} . \tag{32}$$

If $\bar{\mathcal{P}}_0^{sd}$ consists of one transposition $(d's)$, where ψ_{λ_s} is a singly occupied orbital and $\psi_{\lambda_{d'}} = \psi_{\lambda_{d''}}$ is a doubly occupied one, then

$$\alpha_{\lambda\mu}(\bar{\mathcal{P}}_0) = 2^{(p-q)/4+1} \tag{33}$$

Indeed, if $\mathcal{Q}_\lambda \in \mathfrak{H}_\lambda$ then either $(d's)\,\mathcal{Q}_\lambda = \mathcal{Q}_\lambda(d's)$ (if $\mathcal{Q}_\lambda$ does not invert the $(d'd'')$ pair) or $(d's)\,\mathcal{Q}_\lambda = \mathcal{Q}_\lambda(d''s)$ (if $\mathcal{Q}_\lambda$ inverts $(d'd'')$). Hence the set $\{\mathfrak{H}_\mu \bar{\mathcal{P}}_0^{sd} \mathfrak{H}_\lambda\}$ consists of permutations $\mathfrak{H}_\mu(d's)$ and $\mathfrak{H}_\mu(d''s)$. Generally, if $\bar{\mathcal{P}}_0^{sd}$ involves t distinct doubly occupied orbitals then

$$\alpha_{\lambda\mu}(\bar{\mathcal{P}}_0) = 2^{(p-q)/4+t} \tag{34}$$

where t is determined by Eq. (29).

6. Representation Matrices

The appropriate rectangular parts of $U_S^N(\mathcal{P})$, necessary to evaluate the $H^{(\lambda\mu)}$ matrix (22) may be relatively easily obtained after the genealogical scheme [6] or using the SAAP formalism [14] (for the most important cases tables of $U_S^N(\mathcal{P})$

---

[6] It means that the sets $\{\bar{\mathcal{P}}_0^d \mathfrak{H}_\lambda\}$ and $\{\mathfrak{H}_\lambda \bar{\mathcal{P}}_0^d\}$ are identical. However the elements of $\mathfrak{H}_\lambda$ in general do not commute with $\bar{\mathcal{P}}_0^d$.

are available [6, 16]). As compromise between a time-consuming construction of every actually desired representation matrix and a storage-consuming keeping of the all $N!$ matrices in the machine core, it seems to be reasonable to store only the matrices of a few transpositions expressing the others, actually desired matrices, as their products. However in such case, to obtain the $f \times g$ part of $U_S^N(\mathscr{P})$, full representation matrices for the component transpositions are needed, dimension (6) of whom violently grow up with the number of electrons. A considerable reduction of the necessary dimension is possible, basing on the following properties of U_S^N matrices [6]:

1. If in the primitive function (4) $\lambda_{d'} = \lambda_{d''}$ and $\lambda_r \neq \lambda_{d'}, \lambda_s \neq \lambda_{d'}$ then

$$[U_S^N((d'd'')\,\mathscr{T})]^{ff} = [U_S^N(\mathscr{T})]^{ff}\,, \tag{35}$$

$$[U_S^N((d'r)\,\mathscr{T})]^{ff} = [U_S^N((d''r)\,\mathscr{T})]^{ff} = -\tfrac{1}{2}[U_S^N(\mathscr{T})]^{ff}\,, \tag{36}$$

$$[U_S^N((d'r)(d''s)\,\mathscr{T})]^{ff} = \tfrac{1}{2}[U_S^N(\mathscr{T})]^{ff} + \tfrac{1}{2}[U_S^N((rs)\,\mathscr{T})]^{ff} \tag{37}$$

where $\mathscr{T}$ is an arbitrary permutation not containing d' nor d''.

2. Let $\mathfrak{S}_p$ be permutation group of the orbitals singly occupied in configuration λ. If $\mathscr{P} \in \mathfrak{S}_p$ then

$$[U_S^N(\mathscr{P})]^{ff} = U_S^p(\mathscr{P})\,. \tag{38}$$

Hence, only the representation matrices U_S^p, corresponding to permutations $\mathscr{P} \in \mathfrak{S}_p$, are necessary for evaluating of all the matrix elements. This fact is of fundamental importance for application, as in general $p \ll N$.

7. The Matrix Elements

According to rank r of $D_{\lambda\mu}^r$ diagrams, four kinds of formulas are possible.

a) $r > 2$

As the orbitals are orthogonal, all the matrix elements of one- and two-electron operators are equal to zero in this case.

b) $r = 2$

In (26) there are at most two non-zero components, namely

$$D_{\lambda\mu}^2 = \alpha_{\lambda\mu}(\bar{\mathscr{P}}_0)\,\mathscr{D}_{\lambda\mu}(\bar{\mathscr{P}}_0) + \alpha_{\lambda\mu}((ik)\,\bar{\mathscr{P}}_0)\,\mathscr{D}'_{\lambda\mu}((ik)\,\bar{\mathscr{P}}_0) \tag{39}$$

where i and k are the numbers of the orbitals of configuration λ which do not link to any orbital of μ. Prime in the second term means, that it appears only in the case when $(ik)\,\bar{\mathscr{P}}_0 \notin \mathfrak{P}_{\lambda\mu}(\bar{\mathscr{P}}_0)$. As can be easily verified, for all the diagrams with $r = 2$

$$\alpha_{\lambda\mu}((ik)\,\bar{\mathscr{P}}_0) = \alpha_{\lambda\mu}(\bar{\mathscr{P}}_0)\,. \tag{40}$$

Hence the relation (39) may be written as

$$\begin{aligned} H^{(\lambda\mu)} = \alpha_{\lambda\mu}(\bar{\mathscr{P}}_0)\,\{&[U_S^N(\bar{\mathscr{P}}_0)]^{fg}\,\langle\bar{\mathscr{P}}_0\Psi_\lambda^0|\mathscr{H}|\Psi_\mu^0\rangle \\ &+ [U_S^N((ik)\,\bar{\mathscr{P}}_0)]^{fg}\,\langle(ik)\,\bar{\mathscr{P}}_0\Psi_\lambda^0|\mathscr{H}|\Psi_\mu^0\rangle'\}\,. \end{aligned} \tag{41}$$

Let φ_{μ_j} and φ_{μ_l} be the orbitals of configuration μ located in the diagram $\mathscr{D}_{\lambda\mu}(\bar{\mathscr{P}}_0)$ on the positions corresponding to φ_{λ_i} and φ_{λ_k} respectively. Then, after

Table 2. $a_{\lambda\mu}$ coefficients and $A_{\lambda\mu}$ matrices

No.	$\mathscr{D}_{\lambda\mu}(\mathscr{F}_0^{\lambda}\mathscr{F}_0^{\mu})^a$	$a_{\lambda\mu}$	$A_{\lambda\mu}$
1	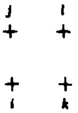	1	$U_\xi((ik))$
2	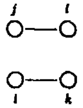	1	0
3	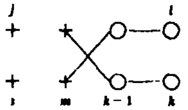	-1	$1+U_\xi((im))$
4	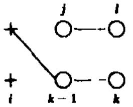	-1	0
5	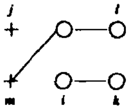	-1	0
6	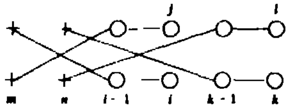	1	$U_\xi((mn))$
7	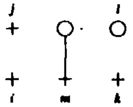	$\sqrt{2}$	$\sqrt{2}\,U_\xi((ik))$
8	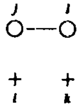	$\sqrt{2}$	0
9	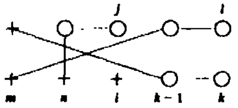	$-\sqrt{2}$	$\sqrt{2}[1+U_\xi((im))]$
10	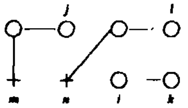	$-\sqrt{2}$	0
11	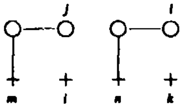	2	$2\,U_\xi((ik))$

---

[a] Where essential, the orbitals are provided with their consecutive numbers in the orbital product (4) (i for ψ_{λ_i} (φ_{μ_i}) orbital). The indices λ_i and μ_i are for simplicity sake omitted.

performing in (41) integration over all the variables but j-th and l-th, and making use of the orthogonality of orbitals, we get[7]

$$H^{(\lambda\mu)} = \alpha_{\lambda\mu}(\bar{\mathscr{P}}_0)\,[\{[\lambda_i\mu_j|\lambda_k\mu_l] + [\lambda_k\mu_j|\lambda_i\mu_l]\,U_S^N((ik))\}\,U_S^N(\bar{\mathscr{P}}_0)]^{f\theta} \tag{42}$$

where

$$[\lambda_i\mu_j|\lambda_k\mu_l] = \int \psi^*_{\lambda_i}(\boldsymbol{r}_1)\,\psi^*_{\lambda_k}(\boldsymbol{r}_2)\,h_2(\boldsymbol{r}_1,\boldsymbol{r}_2)\,\psi_{\mu_j}(\boldsymbol{r}_1)\,\psi_{\mu_l}(\boldsymbol{r}_2)\,\mathrm{d}\tau_{12}\,. \tag{43}$$

Of course, the contributions from one-electron operators in this case vanish.

Formula (42) presents the most compact expression for the matrix elements in the case of $r = 2$. However the representation matrices appearing in it are formed for the whole operators $\bar{\mathscr{P}}_0$ and $(ik)\bar{\mathscr{P}}_0$, including contributions from $\bar{\mathscr{P}}_0^d$ and from $\bar{\mathscr{P}}_0^{sd}$. As was previously explained, it is rather inconvenient in applications. Therefore we will perform a further simplification of (42). Making use of (28) we get

$$U_S^N(\bar{\mathscr{P}}_0) = U_S^N(\bar{\mathscr{P}}_0^{sd})\,U_S^N(\bar{\mathscr{P}}_0^{s})\,U_S^N(\bar{\mathscr{P}}_0^{d})\,. \tag{44}$$

From (35) and (37) it directly results that $[U_S^N(\bar{\mathscr{P}}_0^d)]^{ff} = \mathbf{1}$ ($\mathbf{1}$ is $f \times f$ unit matrix). Using formulas (35)–(38) the matrices $[U_S^N(\bar{\mathscr{P}}_0)]^{ff}$ and $[U_S^N((ik)\bar{\mathscr{P}}_0)]^{ff}$ can be transformed as follows:

$$\alpha_{\lambda\mu}(\bar{\mathscr{P}}_0)\,[U_S^N(\bar{\mathscr{P}}_0)]^{ff} = a_{\lambda\mu}\,U_S^p(\bar{\mathscr{P}}_0^s)\,, \tag{45}$$

$$\alpha_{\lambda\mu}(\bar{\mathscr{P}}_0)\,[U_S^N((ik)\bar{\mathscr{P}}_0)]^{ff} = A_{\lambda\mu}\,U_S^p(\bar{\mathscr{P}}_0^s) \tag{46}$$

where $a_{\lambda\mu}$ is a number and $A_{\lambda\mu}$ – an $f \times f$ matrix. The values of $a_{\lambda\mu}$ and $A_{\lambda\mu}$ depend on the specific form of the appropriate configuration-pair diagram. Coefficients $\alpha_{\lambda\mu}(\bar{\mathscr{P}}_0)$ have been included into $a_{\lambda\mu}$ and $A_{\lambda\mu}$ in order to simplify the notation. The $A_{\lambda\mu}$ matrices can be constructed involving only $f \times f$ parts of the representation matrices corresponding to transpositions of singly occupied orbitals and are listed in Table 2. Also the values of $a_{\lambda\mu}$ are there given[8]. The formula (42) takes now the form:

$$H^{(\lambda\mu)} = \{a_{\lambda\mu}[\lambda_i\mu_j|\lambda_k\mu_l] + A_{\lambda\mu}[\lambda_k\mu_j|\lambda_i\mu_l]\}\,[U_S^p(\bar{\mathscr{P}}_0^s)]^{f\theta}\,. \tag{47}$$

As an illustration of the method of treatment let us derive the $A_{\lambda\mu}$ matrix and calculate the value of $a_{\lambda\mu}$ for diagram No. 6. Applying (36), (37) and (38) we get:

$$\begin{aligned}
[U_S^N(\bar{\mathscr{P}}_0)]^{ff} &= [U_S^N((i-1,m)(k-1,n)\bar{\mathscr{P}}_0^s)]^{ff} = \tfrac{1}{4}[U_S^N(\bar{\mathscr{P}}_0^s)]^{ff} = \tfrac{1}{4}\,U_S^p(\bar{\mathscr{P}}_0^s)\,,\\
[U_S^N((ik)\bar{\mathscr{P}}_0)]^{ff} &= [U_S^N((ik)(i-1,m)(k-1,n)\bar{\mathscr{P}}_0^s)]^{ff}\\
&= \tfrac{1}{2}[U_S^N((k-1,n)\bar{\mathscr{P}}_0^s)]^{ff} + \tfrac{1}{2}[U_S^N((km)(k-1,n)\bar{\mathscr{P}}_0^s)]^{ff}\\
&= \tfrac{1}{4}[U_S^N((mn)\bar{\mathscr{P}}_0^s)]^{ff} = \tfrac{1}{4}\,U_S^p((mn))\,U_S^p(\bar{\mathscr{P}}_0^s)\,.
\end{aligned}$$

Hence $a_{\lambda\mu} = \alpha_{\lambda\mu}(\bar{\mathscr{P}}_0)/4 = 1$, and $A_{\lambda\mu} = U_S^p((mn))$. Numbering of the orbitals after Table 2.

---

[7] Note a difference between this formula and the corresponding one derived by Ruedenberg *et al.* [12–14]. In the Ruedenberg's formula the both terms do appear also when they are identical, while in (42) only in the case when they are essentially different. For this reason $\alpha_{\lambda\mu}(\bar{\mathscr{P}}_0)$ differs in some cases from the Ruedenberg's $(N_{\lambda\beta}(U)\,N_{\mu\delta}(V))^{1/2}$ coefficient by factor 2.

[8] Let us note that $a_{\lambda\mu} = \varepsilon 2^{(p-q)/4}$, where ε is parity of $\bar{\mathscr{P}}_0^{sd}$ permutation, and $A_{\lambda\mu} \neq 0$ only if neither $\lambda_k = \lambda_i$ nor $\mu_j = \mu_l$.

c) $r = 1$.

Retaining in (26) only nonvanishing terms,

$$D^1_{\lambda\mu} = \alpha_{\lambda\mu}(\bar{\mathscr{F}}_0)\,\mathscr{D}_{\lambda\mu}(\bar{\mathscr{F}}_0) + \sum_{m=1}^{N}{}' \alpha_{\lambda\mu}((mi)\,\bar{\mathscr{F}}_0)\,\mathscr{D}_{\lambda\mu}((mi)\,\bar{\mathscr{F}}_0) \tag{48}$$

where φ_{λ_i} does not link to any orbital of configuration μ. The prime over the sum means that from every set $\mathfrak{P}_{\lambda\mu}((mi)\,\bar{\mathscr{F}}_0)$ only one term is included.

As seen in Table 1, three distinct types of configuration-pair diagrams are possible (No. 12, 13 and 14). The correspondent formulas are as follows:

Diagram 12:

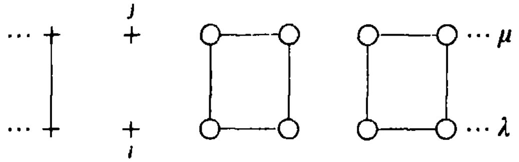

After simple manipulation we obtain

$$\alpha_{\lambda\mu}(\bar{\mathscr{F}}_0) = 1; \quad [U_S^N(\bar{\mathscr{F}}_0)]^{ff} = U_S^p(\bar{\mathscr{F}}_0^s); \quad \text{and} \quad (\text{if } m \neq i),$$

$$\alpha_{\lambda\mu}((im)\,\bar{\mathscr{F}}_0) = \begin{cases} 1 & (\text{if } m \leqq p) \\ 2 & (\text{if } m > p), \end{cases}$$

$$[U_S^N((im)\,\bar{\mathscr{F}}_0)]^{ff} = \begin{cases} U_S^p((im))\,U_S^p(\bar{\mathscr{F}}_0^s) & (\text{if } m \leqq p) \\ -U_S^p(\bar{\mathscr{F}}_0^s)/2 & (\text{if } m > p). \end{cases}$$

Thus, Eq. (48) can be rewritten

$$H^{(\lambda\mu)} = \left\{ \langle \bar{\mathscr{F}}_0 \Psi_\lambda^0 | \mathscr{H} | \Psi_\mu^0 \rangle + \sum_{\substack{m=1 \\ (m \neq i)}}^{p} [\lambda_i \lambda_m | \lambda_m \mu_j]\, U_S^p((im)) \right.$$
$$\left. - \sum_{m=1}^{(N-p)/2} [\lambda_i \lambda_{p+2m} | \lambda_{p+2m} \mu_j] \right\} U_S^p(\bar{\mathscr{F}}_0^s). \tag{49}$$

Diagramm 13:

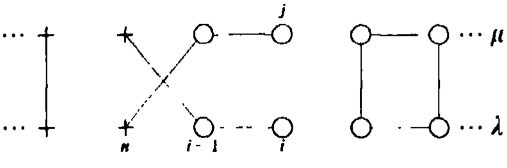

Analogically,

$$\alpha_{\lambda\mu}(\bar{\mathscr{F}}_0) = 2; \quad [U_S^N(\bar{\mathscr{F}}_0)]^{ff} = -U_S^p(\bar{\mathscr{F}}_0^s)/2; \quad \text{and } (\text{if } m \neq i, m \neq i-1)$$

$$\alpha_{\lambda\mu}((im)\,\bar{\mathscr{F}}_0) = \begin{cases} 2 & (\text{if } m \leqq p) \\ 4 & (\text{if } m > p), \end{cases}$$

$$[U_S^N((im)\,\bar{\mathscr{F}}_0)]^{ff} = [U_S^N((im)\,(i-1, n)\,\bar{\mathscr{F}}_0^s)]^{ff}$$
$$= \begin{cases} [1 + U_S^p((mn))]\,U_S^p(\bar{\mathscr{F}}_0^s)/2 & (\text{if } m \leqq p) \\ U_S^p(\bar{\mathscr{F}}_0^s)/4 & (\text{if } m > p). \end{cases}$$

Thus, in this case

$$H^{(\lambda\mu)} = \Bigg\{ -\langle \bar{\mathscr{P}}_0 \Psi_\lambda^0 | \mathscr{H} | \Psi_\mu^0 \rangle + \sum_{\substack{m=1 \\ (m \neq n)}}^{p} [\lambda_i \lambda_m | \lambda_m \mu_j] \left(1 + U_S^g((mn))\right) + \sum_{\substack{m=1 \\ (m \neq (i-p)/2)}}^{(N-p)/2} [\lambda_i \lambda_{p+2m} | \lambda_{p+2m} \mu_j] \Bigg\} U_S^g(\bar{\mathscr{P}}_0^{sd}) . \tag{50}$$

Diagram 14:

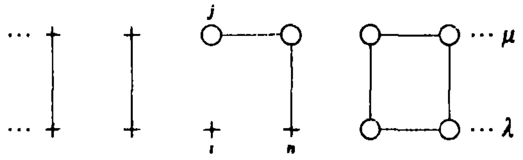

In the same way

$$H^{(\lambda\mu)} = \sqrt{2} \Bigg\{ \langle \bar{\mathscr{P}}_0 \Psi_\lambda^0 | \mathscr{H} | \Psi_\mu^0 \rangle + \sum_{\substack{m=1 \\ (m \neq i, m \neq n)}}^{p} [\lambda_i \lambda_m | \lambda_m \mu_j] \, U_S^g((im)) - \sum_{m=1}^{(N-p)/2} [\lambda_i \lambda_{p+2m} | \lambda_{p+2m} \mu_j] \Bigg\} [U_S^g(\bar{\mathscr{P}}_0^{sd})]^{fg} . \tag{51}$$

Equations (49) (51) present the final expressions for the matrix elements in the case of $r = 1$. Contributions from one-electron operators appear there only in integrals

$$\langle \bar{\mathscr{P}}_0 \Psi_\lambda^0 | \mathscr{H} | \Psi_\mu^0 \rangle = [\lambda_i \mu_j] + \sum_{\substack{m=1 \\ (m \neq i)}}^{N} [\lambda_i \mu_j | \lambda_m \lambda_m] \tag{52}$$

where

$$[\lambda_i \mu_j] = \int \psi_{\lambda_i}^*(\mathbf{r}_1) \, h_1(\mathbf{r}_1) \, \psi_{\mu_j}(\mathbf{r}_1) \, d\tau_1 . \tag{53}$$

Then, the $H_1^{(\lambda\mu)}$ matrix of one-electron operator (1) in the case of $r = 1$ can be written in a condensed form

$$H_1^{(\lambda\mu)} = \varepsilon 2^{(p-q)/4} [\lambda_i \mu_j] \, [U_S^g(\bar{\mathscr{P}}_0^{sd})]^{fg} \tag{54}$$

where ε is parity of $\bar{\mathscr{P}}_0^{sd}$ permutation

d) $r = 0$.

In this case $U_S^N(\bar{\mathscr{P}}_0) = 1$, as $\bar{\mathscr{P}}_0$ is the identity operator. Thus

$$D_{\lambda\mu}^0 = \mathscr{D}_{\lambda\mu}(\mathscr{I}) + \sum_{(ij)}{}' \alpha_{\lambda\mu}((ij)) \, \mathscr{D}_{\lambda\mu}((ij)) \tag{55}$$

where the sum is extended over the all distinct $\mathfrak{P}_{\lambda\mu}((ij))$ sets. The explicit expression for $H^{(\lambda\mu)}$ is

$$H^{(\lambda\mu)} = \langle \Psi_\lambda^0 | \mathscr{H} | \Psi_\mu^0 \rangle + \sum_{i=j+1}^{p} \sum_{j=1}^{p-1} [\lambda_i \lambda_j | \lambda_j \lambda_i] \, U_S^g((ij)) - \sum_{i=1}^{p} \sum_{j=1}^{(N-p)/2} [\lambda_i \lambda_{p+2j} | \lambda_{p+2j} \lambda_i] - 2 \sum_{i=j+1}^{(N-p)/2} \sum_{j=1}^{(N-p)/2-1} [\lambda_{p+2i} \lambda_{p+2j} | \lambda_{p+2j} \lambda_{p+2i}] \tag{56}$$

where

$$\langle \Psi_\lambda^0 | \mathscr{H} | \Psi_\mu^0 \rangle = \sum_{i=1}^{N} [\lambda_i \lambda_i] + \sum_{i=j+1}^{N} \sum_{j=1}^{N-1} [\lambda_i \lambda_i | \lambda_j \lambda_j] \tag{57}$$

8. Example of Application

Let us evaluate the matrix elements of $\mathscr{H}$ operator (3) for the pair of configurations (23). In this case

$$\mathscr{F}_0^s = (23)(12); \quad \mathscr{F}_0^d = 1$$

and

$$\mathscr{D}_{\lambda\mu}(\mathscr{F}_0^s \mathscr{F}_0^d) =$$

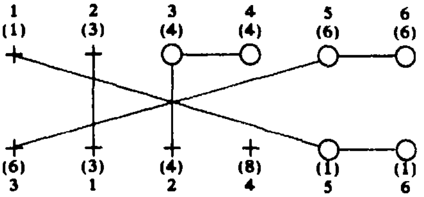

Names of the orbitals (the numbers $\lambda_i(\mu_i)$ for $\psi_{\lambda_i}(\psi_{\mu_i})$ orbitals) are given in parenthesis. As seen, the diagram corresponds to the case No. 9 (Tables 1 and 2). Making use of Table 2 and Eq. (47)

$$H^{(\lambda\mu)} = \{-\sqrt{2}[84|16] + \sqrt{2}[14|86][1 + U_S^4((34))]\}[U_S^4((23)(12))]^{fg}$$

For the singlet configurations[9] ($S = 0$):

$$f = f_0^4 = 2; \quad g = f_0^2 = 1$$

$$U_0^4((12)) = \begin{bmatrix} 1 & 0 \\ 0 & -1 \end{bmatrix}; \quad U_0^4((23)) = \begin{bmatrix} -1/2 & \sqrt{3}/2 \\ -\sqrt{3}/2 & 1/2 \end{bmatrix}; \quad U_0^4((34)) = \begin{bmatrix} 1 & 0 \\ 0 & -1 \end{bmatrix}$$

Thus

$$H^{(\lambda\mu)} = \begin{bmatrix} 1/\sqrt{2} \\ \sqrt{3}/2 \end{bmatrix}[84|16] - \begin{bmatrix} \sqrt{2} \\ 0 \end{bmatrix}[14|86].$$

For the triplet configurations ($S = 1$):

$$f = f_1^4 = 3; \quad g = f_1^2 = 1$$

$$U_1^4((12)) = \begin{bmatrix} -1 & 0 & 0 \\ 0 & -1/3 & -2\sqrt{2}/3 \\ 0 & -2\sqrt{2}/3 & 1/3 \end{bmatrix}$$

$$U_1^4((23)) = \begin{bmatrix} -1/2 & -\sqrt{3}/2 & 0 \\ -\sqrt{3}/2 & 1/2 & 0 \\ 0 & 0 & -1 \end{bmatrix}; \quad U_1^4((34)) = \begin{bmatrix} 1 & 0 & 0 \\ 0 & -1 & 0 \\ 0 & 0 & -1 \end{bmatrix}$$

Thus

$$H^{(\lambda\mu)} = \begin{bmatrix} -1/\sqrt{2} \\ -\sqrt{3/2} \\ 0 \end{bmatrix}[84|16] + \begin{bmatrix} \sqrt{2} \\ 0 \\ 0 \end{bmatrix}[14|86]$$

9. Numerical Procedure

Basing on the above presented method, an ALGOL procedure was written and run in a few programmes at GIER computer at the Department of Numerical

---

[9] The representation matrices U_0^4 and U_1^4 are taken from [16].

Calculations, Warsaw University. The procedure evaluates the matrix elements for an arbitrary pair of configurations corresponding to a given spin multiplicity.

Acknowledgements The author would like to thank Professor K. Ruedenberg for his valuable remarks and constructive criticism which enabled to improve this paper in many points, as well as for supplying typescripts of his papers prior to publication. Criticism of Dr. W. Salmon is also appreciated.

References

1. Čizek,J.: Theoret. chim. Acta (Berl.) **6**, 292 (1966).
2. Harris,F.E.: J. chem. Physics **46**, 2769; **47**, 1047 (1967).
3. Junker,B.R., Klein,D.J.: J. chem. Physics **55**, 5532 (1971).
4. Kaplan,I.G.: Theor. and exptl. chem. **1**, 608, 619 (1965); **2**, 441 (1966); **3**, 150 (1967).
5. Karwowski,J.: Preprint No. 33 of Theoretical Physics Department. Toruń: Nicholas Copernicus University, May 1968 (Thesis).
6. Kotani,M., Amemiya,A., Ishiguro,E., Kimura,T.: Table of molecular integrals. Tokyo: Maruzen Co. Ltd. 1955.
7. Kuprievich,V.A., Kruglyak,Yu.A., Mozdor,E.V.: Croat. chem. acta **43**, 15 (1971).
8. Matsen,F.A.: Adv. in quant. Chemistry **1**, 59 (1964). Matsen,F.A., Cantu,A.A., Poshusta,R.D.: J. Physic. Chem. **70**, 1558 (1966). Klein,D.J., Junker,B.R.: J. chem. Physics **54**, 4290 (1971).
9. Murrell,J.N., McEwen,K.L.: J. chem. Physics **25**, 1143 (1956). Ito,H., I'Haya,Y.: Theoret. chim. Acta (Berl.) **2**, 247 (1964). Nakayama,M., I'Haya,Y.: Intern. J. quantum chemistry **4**, 43 (1970).
10. Pauling,L.: J. chem. physics **1**, 280 (1933).
11. Reeves,C.M.: Commun. ACM **9**, 276 (1966). Cooper,I.L., McWeeny,R.: J. chem. physics **45**, 226 (1966). Sutcliffe,B.T.: J. chem. physics **45**, 235 (1966). Shull,H.: Intern. J. quantum chemistry **3**, 523 (1969).
12. Ruedenberg,K.: Physic. rev. letters **27**, 1105 (1971).
13. Ruedenberg,K., Poshusta,R.D.: Advances quant. Chemistry **6**, 267 (1972).
14. Salmon,W.I., Ruedenberg,K.: J. chem. Physics **57**, 2776 (1972). Salmon,W.J., Ruedenberg,K., Cheung,L.M.: J. chem. physics **57**, 2787 (1972).
15. Salmon,W.I.: Genealogical electronic spin eigenfunctions and antisymmetric many-electron wavefunctions generated directly from Young diagrams. To be published.
16. Yamazaki,M.: Sci. rep. of Kanazawa University **8**, 397 (1963).

Dr. Jacek Karwowski
Division of Theoretical Chemistry
Department of Chemistry
University of Alberta
Edmonton 7, Alberta, Canada

Theoret. chim. Acta (Berl.) 29, 167 – 172 (1973)
© by Springer-Verlag 1973

An Application of the Functional Boys-Bernardi Counterpoise Method to Molecular Potential Surfaces

Allan Johansson
Department of Inorganic Chemistry, Helsinki University of Technology, Otaniemi, Helsinki, Finnland

Peter Kollman
Department of Pharmaceutical Chemistry, School of Pharmacy, University of California, San Francisco, California 94122

Steve Rothenberg
Information Systems Design, 7817 Oakport Avenue, Oakland, California

Received July 28, 1972/November 23, 1972

The "functional" counterpoise method, proposed by Boys and Bernardi [1], is applied to the theoretical prediction of hydrogen bonding potential surfaces, using a minimal basis to represent the atomic orbitals (STO-3G). Using this method, with a systematically chosen "correction factor", one can compute potential surfaces with an STO-3G basis as accurately as with a much more flexible atomic basis.

Die „funktionale" Ausgleichsmethode, von Boys and Bernardi [1] vorgeschlagen, wird zur theoretischen Vorhersage der Potentialflächen von Wasserstoff-Bindungen benutzt. Dabei werden die Atomorbitale durch einen minimalen Basissatz (STO-3G) dargestellt. Indem man diese Methode mit einem systematisch ausgewählten „Korrekturfaktor" benutzt, kann man Potentialflächen mit einer STO-3G Basis ebenso gut wie sonst nur mit einem sehr viel flexibleren Atombasissatz berechnen.

Introduction

One of the important problems in molecular orbital potential surface calculations is the basis set choice; for most systems of chemical interest, one must use a relatively, small contracted gaussian basis. For small H-bonded complexes, the energies of dimerization found using an exhaustive basis set (with polarization functions) are in good agreement with available experimental data. The next level of basis set choice, a "double-zeta" representation of the atomic valence shells, exaggerates H-bond energies because it substantially overestimates the monomer dipole moments. Finally, small contracted *ab initio* bases (such as the STO-3G used here) predict a dimerization energy in better agreement with the "most accurate" calculations than the "double-zeta"; the STO-3G also predicts a greater dimerization energy than the "most accurate" (for $(H_2O)_2$, ΔE (most accurate) = 4.7 kcal/mole, ΔE (double zeta) = 7.9 kcal/mole ΔE (STO or STO-4G) = 6.4 kcal/mole) [2], despite the fact that the STO-3G predicted water dipole moment (1.8 D) is in excellent agreement with experiment, in contrast to the "most accurate" ($\mu = 2.1$ D).

In the present work we rationalize why the STO-3G dimerization energy is larger than that found with the "most accurate" basis set and attempt to improve the STO-3G [3] computed potential curve by applying the so-called "functional counterpoise method" originally suggested by Boys and Bernardi [1].

Description of Calculations

The potential surface of the following hydrogen bonded systems was studied:

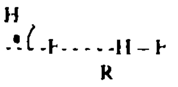

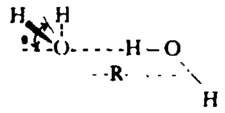

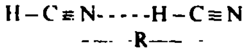

The energies for each geometry were computed by the well documented Roothaan SCF procedure for closed shell systems [4]. In the counterpoise method, the dimer energies E_{12} are computed in the usual way, but the monomer energies E_1 and E_2 are evaluated for each geometry point by using the full set of expansion

Table 1. All energies are in a.u.

$(HF)_2$ $E_0 = -98.57060$

R(a.u.)	θ	E dimer (a.u.)	E_1 + basis func. (2)	ΔE[a]	$\Delta\varepsilon$[b]	$\Delta\varepsilon + 1/6\,\Delta\varepsilon$
4.5	0	−197.14232	−98.58307	−0.0011	0.0125	0.0010
5.0	0	−197.14656	−98.57754	−0.0054	0.0069	−0.0044
5.5	0	−197.14548	−98.57374	−0.0042	0.0031	−0.0038
6.0	0	−197.14413	−98.57183	−0.0029	0.0012	−0.0027
6.5	0	−197.14332	−98.57107	−0.0021	0.0004	−0.0021
5.0	60	−197.14968	−98.58095	−0.0085	0.0104	−0.0068

$(H_2O)_2$ $E_0 = -74.96177$ a.u.

R(a.u.)	θ	E dimer, (a.u.)	E_1 + basis func. (2)	ΔE[a]	$\Delta\varepsilon$[b]	$\Delta\varepsilon + 2/7\,\Delta\varepsilon$
4.75	54	−149.93217	−74.97735	−0.0087	0.0156	−0.0042
5.25	54	−149.93396	−74.97094	−0.0105	0.0092	−0.0079
5.75	54	−149.93120	−74.96631	−0.0077	0.0045	−0.0064
6.25	54	−149.92858	−74.96371	−0.0050	0.0019	−0.0050
5.25	39	−149.933897	−74.97047	−0.0104	0.0087	−0.0079
5.25	0	−149.932995	−74.96966	−0.0095	0.0079	−0.0072

$(HCN)_2$ $E_0 = -91.67527$ a.u.

R(a.u.)	E dimer	E_1 + basis func. (2)	ΔE[a]	$\Delta\varepsilon$[b]	$\Delta\varepsilon + 4/11\,\Delta\varepsilon$
5.1	−183.34595	−91.68015	0.0047	0.0049	0.0064
5.67	−183.35564	−91.67847	−0.0050	0.0032	−0.0039
6.24	−183.35634	−91.67701	−0.0057	0.0017	−0.0051
6.68	−183.35522	−91.67606	−0.0046	0.0008	−0.0043

[a] E dimer $- 2\,E_0$.

[b] $E_0 - (E_1$ + basis func. (2)).

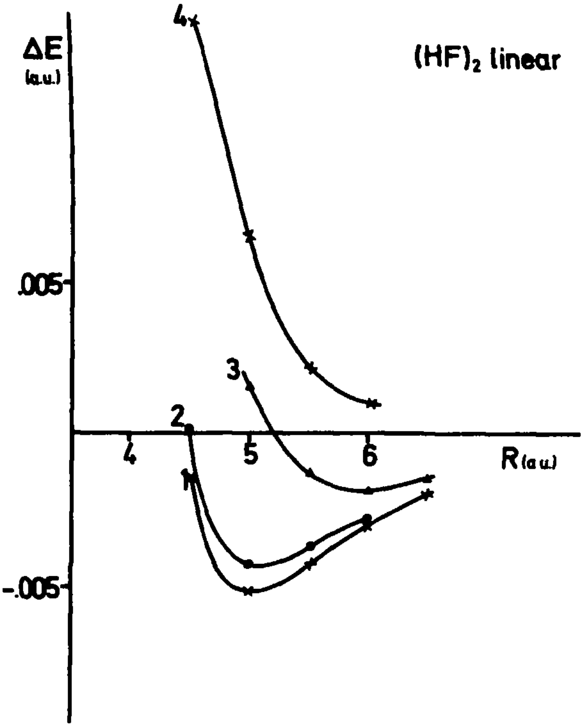

Fig. 1. Curve 1: $\Delta E = E$ dim $- 2\,E_0$. Curve 2: $\Delta E - f\Delta\varepsilon$; $f = 1/6$ for HF, 2/7 for H_2O, 4/11 for HCN. Curve 3: $\Delta E - \Delta\varepsilon \equiv \Delta E$ − basis function correction. Curve 4: $\Delta\varepsilon \equiv$ basis function correction

functions for the dimer; that is, the dimer calculation for a given geometry is repeated first with all the nuclear charges set equal to zero on center 1 and then with all the nuclear charges set equal to zero on center 2. In this way the monomer energies, E_1 and E_2 will contain the "extra" stabilization induced by the increased basis set upon dimerization and the "true" stabilization will be $E_{12} - E_1 - E_2$ rather than $E_{12} - 2E$ (isolated monomer). The difference between $2E$ (isolated monomer) and $E_1 + E_2$ we designate the basis function connection $\equiv \Delta\varepsilon$.

Results and Discussions

In the three cases studied here, a significant lowering of the monomer energy (at reasonable H-bond distances) was obtained in the calculations on the electron donor fragment (1) with the basis functions from the electron acceptor (2). E_2, the monomer energy for the electron acceptor with basis functions from the electron donor, did not differ significantly from the isolated monomer energy.

It is clear from Table 1 that a large portion of the dimerization energy comes from "extra" stabilization. One of the main reasons for this "extra" stabilization is the poor representation of core orbital in a single Slater basis. Thus, the "extra

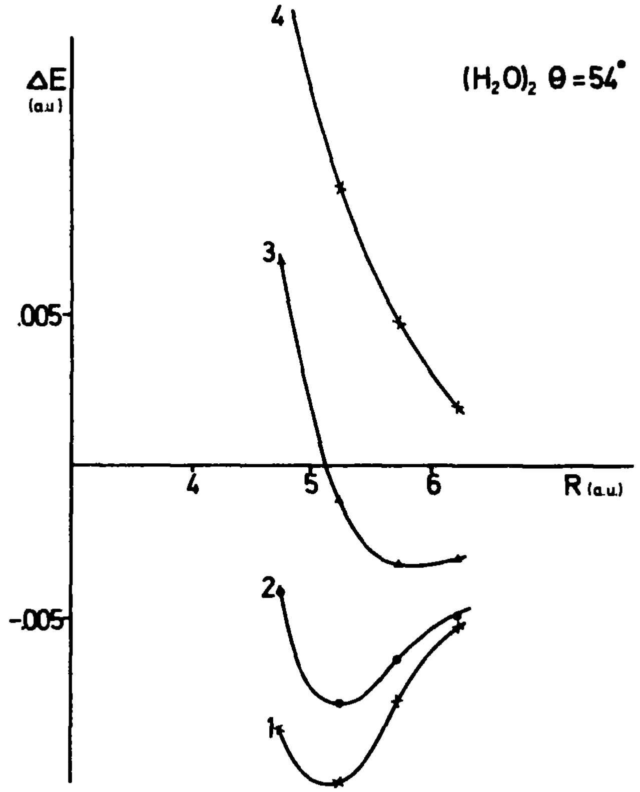

Fig. 2. Curve 1: $\Delta E = E\,\mathrm{dim} - 2E_0$. Curve 2: $\Delta E - f\Delta\varepsilon$; $f = 1/6$ for HF, 2/7 for H_2O, 4/11 for HCN. Curve 3: $\Delta E - \Delta\varepsilon = \Delta E$ – basis function correction. Curve 4: $\Delta\varepsilon$ = basis function correction

stabilization" comes mainly from an improvement in the representation of the 1s core by the additional basis functions. Support from this comes from the fact that the calculations on the electron acceptor with basis functions of the electron donor show no large stabilization because the orbitals are too far away from the electronegative atom.

However, the fact that for $R = 5.0$ au., the $\Delta\varepsilon$ computed for $(HF)_2$, $\theta = 0$ is so much less than that for $\theta = 60$ indicates that the improvement of the 1s representation is closely linked to the "charge transfer" of electrons out of the valence shell. Newton and Ehrenson have shown in their study of hydronium ions that an energy optimized representation of the water 1s core results in an "extra" stabilization at $R(O–O) = 2.4$ Å of less than 1 kcal/mole, in contrast to the 9.4 kcal/mole "stabilization" found here for water dimer at $R(O–O) = 2.51$ Å, $\theta = 54°$. Thus, it is unlikely that this counterpoise procedure will greatly change the dimerization energy computed with "double zeta" bases and the exaggerated ΔE found in those cases is really due to the overestimated monomer dipole moment.

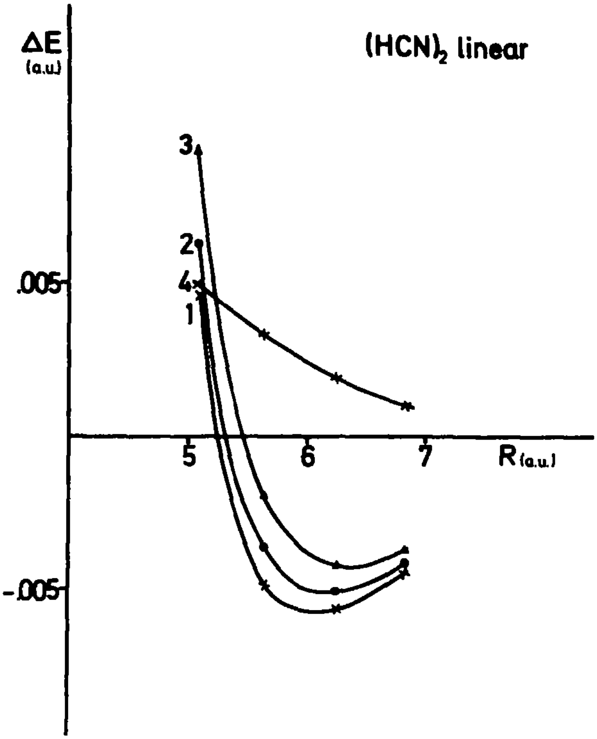

Fig. 3. Curve 1: $\Delta E = E\text{dim} - 2E_0$. Curve 2: $\Delta E - f\Delta\varepsilon$; $f = 1/6$ for HF, 2/7 for H_2O, 4/11 for HCN Curve 3: $\Delta E - \Delta\varepsilon \equiv \Delta E$ − basis function correction. Curve 4: $\Delta\varepsilon \equiv$ basis function correction

The results of the calculations are presented in Table 1 and graphically summarized in the three figures. It is obvious from Fig. 2 that if the total correction $\Delta\varepsilon$ (defined as the difference between the monomer energies with and without additional basis functions) is added to the uncorrected stabilization energy, the resulting potential curve shows a too small an energy of dimerization and a too large an intermolecular separation as compared with the most accurate calculations; thus, we have somewhat "overcorrected" our original potential curve.

In order to give results in better agreement with the best *ab initio* calculations and experiment an empirical "correction factor" was sought. Since the electron pair acceptor in the actual dimer (in the case of HF) has only one unoccupied orbital and we have included six extra orbitals in the calculation of E_1, each $\Delta\varepsilon$ was multiplied by 1/6 and added to the uncorrected ΔE to give a dimerization energy of 4.4 kcal/mole at $R = 2.6$ Å, $\theta = 60°$. A similar analysis of the water dimer surface (multiplying the $\Delta\varepsilon$ by 2/7) and the HCN surface (multiplication by 4/11) led to the results summarized in Table 2. As one can see, the results, albeit suspect because of our correction factor, are in excellent agreement with the experimental (where available) values and "most accurate" calculations. The "agreement" with experiment is somewhat fortuitous, since no dispersion attraction can be found within the SCF framework.

Table 2. Comparison of counterpoise results with more accurate calculations
Distances in Å and ΔE in kcal/mole

	R(STO-3G)[a]	ΔE(STO-3G)	R(CP)[b]	ΔE(CP)	R(DZ + P)[c]	ΔE(DZ + P)
$(HF)_2$ $\theta = 60°$	2.6	5.4	2.6	4.4	2.85[d,e]	4.2[d]
(H_2O) $\theta = 54$	2.7	6.6	2.8	5.0	3.0[f]	4.7[f]
$(HCN)_2$ linear	3.3	3.6	3.3	3.3	3.4	3.3

[a] STO-3G-direct calculation of ΔE. R refers to the minimum energy separation between monomers.

[b] CP – counterpoise $\Delta E - f\Delta\varepsilon$; $f = 1/6$ for HF, 2/7 for H_2O, 4/11 for HCN.

[c] DZ + P – very accurate calculation of molecular potential surface "double zeta + polarization" atomic basis for $(HCN)_2$ no such accurate calculation exists, so the ΔE is taken from the experimental one in Ref. [6] and the R is assumed to be that of the infinite crystal (Ref. [7]).

[d] See Ref [8]; the minimum energy geometry occurs at $\theta = 40°$.

[e] See Ref. [9].

[f] See Ref. [10].

Conclusions

The above results indicate that the functional counterpoise method, with a systematically chosen empirical factor, can be useful in improving potential surface calculations carried out with limited *ab initio* bases. No new integrals need be calculated, and with starting vectors from the isolated monomer, the additional SCF calculations converge very rapidly; thus the extra computational effort required to implement the counterpoise method is minimal.

References

1. Boys, S. F., Bernardi, F.: Molecular Physics **19**, 558 (1970).
2. Kollman, P. A., Allen, L. C.: Chem. Reviews **72**, 283 (1972).
3. Hehre, W. J., Stewart, R. F., Pople, J. A.: J. chem. Physics **51**, 2657 (1968).
4. Roothaar, C. J.: Rev. mod. Physics **23**, 65 (1951).
5. Newton, M., Ehrenson, S.: J. Amer. chem. Soc. **93**, 4971 (1971).
6. Giaque, W. F., Ruhrwein, R. A.: J. Amer. chem. Soc. **61**, 2626 (1939).
7. Dulmage, W. J., Lipscomb, W. N.: Acta crystallogr. **4**, 330 (1951).
8. Dierchsen, G. H. F., Kraemers, W. P.: Chem. Physics Letters **6**, 419 (1970).
9. Dyke, T. R., Howard, B. T., Klemperer, W.: J. chem. Physics **56**, 2442 (1972).
10. Hankins, D., Moscowitz, J., Stillinger, F.: J. chem. Physics **53**, 4544 (1970).

Dr. P. Kollman
Department of Pharmaceutical Chemistry
School of Pharmacy
University of California
San Francisco, California 94122
USA

Theoret. chim. Acta (Berl.) 29, 173 – 181 (1973)
© by Springer-Verlag 1973

An *ab initio* LCAO-MO-SCF Study of the Electronic Structure of Phosphirane and Thiirane

Ilyas Absar, Lawrence J. Schaad, and John R. Van Wazer

Department of Chemistry, Vanderbilt University, Nashville, Tennessee 37235

Received August 18, 1972/November 27, 1972

Wave functions have been determined for the C_2H_4PH and C_2H_4S cyclic molecules, using (951/52/3) and (95/52/3) uncontracted Gaussian basis sets for each molecule. From Mulliken population analyses and electron-density plots, it is shown that the valence orbitals of C_2H_4PH and C_2H_4S are closely related and that these are similar to the respective orbitals of cyclopropane.

Für die zyklischen Moleküle C_2H_4PH und C_2H_4S wurden mit den nichtkontrahierten Basissätzen ((951/52/3) und (95/52/3)) von Gaußfunktionen Wellenfunktionen bestimmt. Die Mullikenschen Populationsanalysen sowie Diagramme der Elektronendichte zeigen, daß die Valenzorbitale von C_2H_4PH und C_2H_4S in enger Beziehung stehen und daß diese den entsprechenden Orbitalen des Cyclopropans ähnlich sind.

1. Introduction

As part of the study of the electronic structure of phosphorus compounds e.g. [1–4] which has been underway in our laboratory, it seemed desirable to investigate the strained-ring compound called phosphirane, C_2H_4PH, for which no prior quantum-mechanical study has been reported. For comparison purposes, we then calculated in the same basis sets wave functions for the related molecule (thiirane) in which a sulfur atom is substituted for the PH fragment, and for which several prior *ab initio* studies [5–8] have been reported. Our thiirane energy is lower than all except those from the contracted Gaussian basis calculations of Strausz, Gosavi, Denes, and Csizmadia [8] which appeared after our work was completed.

2. Calculational Details

The calculations on phosphirane, C_2H_4PH, were carried out using the following reported microwave C_s geometry [9]: $C–C = 1.502$ Å, $C–P = 1.867$ Å, $C–H_{cis} = 1.092$ Å, $C–H_{trans} = 1.093$ Å, and $P–H = 1.428$ Å; with $\angle CPC = 47.44°$, $\angle HPC = 95.22°$, $\angle CCH_{cis} = 118.00°$, and $\angle CCH_{trans} = 117.00°$. For thiirane, C_2H_4S, the calculations were carried out for a single atomic arrangement corresponding to the C_{2v} microwave structure [10]: $C–C = 1.492$ Å, $C–S = 1.819$ Å, and $C–H = 1.078$ Å, with $\angle CSC = 48.43°$, $\angle HCH = 116.00°$, and $\angle CCH = 117.82°$.

The LCAO-MO-SCF calculations were carried out with uncontracted (95/52/3) Gaussian basis sets containing a total of 58 *sp* functions for thiirane and 61 for phosphirane and uncontracted (951/52/3) sets containing 64 spd functions for thiirane and 67 for phosphirane, using the program MOSES. Atom-optimized exponents were employed for the *s* and *p* orbitals [4, 11], along with values of 0.435 for the sulfur and 0.360 for the phosphorus *d* orbitals. These *d*-orbital exponents were obtained from optimization on phosphine [12] and phosphine oxide [13] for the phosphorus and on hydrogen sulfide [11] and sulfoxylic acid tautomer [11] for sulfur. Further details of the calculational methods have been described elsewhere [4].

3. Results and Discussion

3.1. Molecular Results

The total energy and dipole moment obtained for thiirane in the various prior calculations are compared with our results in Table 1. Obviously the (52) description of sulfur by Clark [5] is inadequate and not in balance with that of the other atoms, since it led to both a poor total energy and dipole moment. It is interest to compare our single-determinant SCF results for thiirane with the group-function calculations on this molecule by Franchini and Zandomeneghi [7]. They used the group-function method with and without configuration interaction, but even their best CI energy of −474.6465 a.u. is inferior to our single-determinant result of −474.8717 a.u. The SCF group-function method introduces correlation within each electron group [14]. The first-order correlation corrections to the SCF group function then involve only doubly excited states [15], and it is these states that Franchini and Zandomeneghi mixed into their CI function. One might have expected that this much configuration interaction would push the energy below the Hartree-Fock limit; this being the rationale of the group function approach. But the fact is, it does not. Expanding the basis set in a single-determinant SCF calculation is more worthwhile than configuration interaction with a limited basis. This might be surprising except that Allen and Karo [16] observed the same thing long ago in comparing minimal-Slater SCF calculations on hydrogen fluoride, with and without CI, to the Hartree-Fock limit. Strausz, Gosavi, Denes, and Csizmadia [8] have used a [641/41/1] Gaussian set contracted from (1291/116/3) in their very recently published work on thiirane. Their energy is 0.39 a.u. = 245 kcal/mole lower than our best, and is a strong demonstration of

Table 1. Values of total energy and of dipole moment calculated for the C_2H_4S molecule

Calculation	E_{tot}(a.u.)	$\mu(D)$
(52/52/2) GTO [5]	−456.0016	5.17
Min. basis STO, no *d* [6]	−474.4759	1.56
Min. basis STO, with *d* [6]	−474.5159	0.84
Group-function (GF), geminals, min STO with *d* [7]	−474.6197	0.56
CI GF, geminals, min. STO with *d* [7]	−474.6465	—
(95/52/3) GTO (our work)	−474.8387	1.24
(951/52/3) GTO (our work)	−474.8717	0.97
[641/42/1] GTO [8]	−475.2622	—
Experimental value	−477.74	1.84 [10]

Table 2. Atomic charges from a Mulliken population analysis of C_2H_4S

	S	C	H
(52/52/2) GTO [5]	+1.072	−0.908	+0.186
Min. STO, no *d* [6]	+0.066	−0.435	+0.201
Min. STO, with *d* [6]	+0.070	−0.425	+0.195
(95/52/3) GTO	+0.123	−0.470	+0.204
(951/52/3) GTO	−0.036	−0.362	+0.190

the power of such contracted bases. These authors present a thorough study of the orbital and total energy relations between thiirane and its isomers; but, although they compute the oscillator strength of several thiirane transitions, they do not give a computed dipole moment for the ground state.

The so-called "atomic charges" obtained by subtracting the Mulliken gross population [17] from the atomic number are shown in Table 2 for various calculations on thiirane. These data are unfortunately not available for the low-energy wave function of Strausz, Gosavi, Denes, and Csizmadia. If one assumes that a minimum-basis set of Slater orbitals epitomizes a balanced basis set in the Mulliken sense [18], the charges given in Table 2 indicate that the (95/52/3) Gaussian set is a reasonably well balanced one; whereas the (52/52/3) set of Gaussian orbitals [5] is horribly unbalanced, with the sulfur being starved for atomic orbitals. Note that adding a set of *d* orbitals to the minimum Slater basis set has very little effect on the atomic charges, whereas the effect is quite pronounced when going from our (95/52/3) to (951/52/3) Gaussian basis set. We attribute this difference to the choice of too large a radius for the *d* orbital in the Slater calculations [6]. Instead of using a Slater exponent of 1.7 for the *d* orbital, a value around 2.7 would have been more appropriate [19]. The *d* orbital corresponding to the 1.7 exponent obviously exhibited too large a radius to give the proper bonding contributions to the thiirane molecule, although it undoubtedly contributed to the desired polarization of the *s* and *p* orbitals [20]. As shown in Table 1, the fact that the change in total energy when allowing *d* orbitals to the Slater minimum-basis set and to the (95/52/3) Gaussian set was about the same is attributable to the fact that the absolute change in inner-orbital energies upon allowing *d* character is considerably greater than that for the outer orbitals for either basis set.

The "experimental" value for the thiirane energy was obtained by subtracting the sum of the atomic ionization potentials [21] (+476.74401 a.u.) and the standard heat of formation of the atoms [22] at 0 K (+0.9762 a.u.) from the heat of formation of thiirane [22] at 0 K (+0.0360 a.u.) and the zero-point vibration corrections (−0.0530 a.u.) obtained from an analysis of the IR spectrum [23]. The resulting energy of −477.737 a.u. is 68 kcal/mole above that given by Bonaccorsi, Scrocco, and Tomasi [6] for the same quantity. It seems most likely that the difference is due to our use of revised atomic ionization potentials! Both values are sufficiently far below all calculated thiirane energies so that the difference is not yet significant. But as calculations become more exact, the problem of obtaining accurate experimental energies promises to become a serious one.

The fundamental vibrational frequencies for phosphirane are available [24, 25], but thermochemical data are not. Nevertheless, the heat of formation of phosphirane from atoms at 298 °K can be estimated from the corresponding quantity for thiirane and Cottrell's [26] empirical bond energies.

$$\begin{aligned}\Delta H^{\circ}_{298}(\text{phosphirane}) &\approx \Delta H^{\circ}_{298}(\text{thiirane}) + 2\,E_{PC} - 2\,E_{SC} + E_{PH}\\ &= -597.988 - 126 + 130 - 77 = -671\ \text{kcal}\end{aligned}$$

where E_{PC} is Cottrell's energy of a phosphorus-carbon bond, and E_{SC} and E_{PH} are defined similarly. Using the heat of formation of cyclopropane instead of that of thiirane gives instead an estimate of -654 kcal for phosphirane. The two estimates differ by only 0.027 a.u. so either is probably accurate enough to give a useful estimate of the total energy of phosphirane relative to separated particles. Since P and S are more nearly alike than are P and C, we choose the -671 value. Then

$$\begin{aligned}\Delta E_{298} &= \Delta H^{\circ}_{298} + 7\,RT = -666.7\ \text{kcal}\\ &= \Delta E_{\text{variational}} + \Delta(\text{trans}) + \Delta(\text{rot}) + \Delta(\text{zero-point})\\ &= \Delta E_{\text{variational}} - \tfrac{21}{2}\,RT + \tfrac{3}{2}RT + 0.0613\ \text{a.u.}\end{aligned}$$

This gives a $\Delta E_{\text{variational}}$, the phosphirane energy relative to separated atoms, of -1.1152 a.u. Including the atomic ionization potentials [21] gives $(-1.1152 - 420.1555) = -421.27$ a.u. as the experimental energy of the phosphirane potential minimum relative to separated electrons and nuclei.

In all of these calculations, the most recent values of the fundamental constants [27] were used, corresponding to

$$1\ \text{a.u.} = 27.2117\ \text{eV} = 627.52\ \text{kcal/mole} = 219475\ \text{cm}^{-1}\,.$$

The total energy, dipole moment, and atomic charges from a Mulliken population analysis are shown in Table 3 for the phosphirane molecule, which has not been studied previously. Note that the percentage difference between the SCF value of the total energy and the experimental value is about the same for thiirane as for phosphirane in the same basis set. Likewise, the increase in total energy upon allowing *d* orbitals is also similar (0.033 a.u. for C_2H_4S and 0.050 a.u. for C_2H_4PH). However, the atomic charge on the phosphorus is appreciably

Table 3. Calculated values for the C_2H_4PH molecule

Basis set	(95/52/3)	(951/52/3)
Total energy (a.u.)[a]	−418.6923	−418.7422
Dipole mom. (*D*)[b]	0.921	0.647
Atomic charges (*e*)		
P	+ 0.53	+ 0.30
C	− 0.49	− 0.35
H_r	+ 0.21	+ 0.20
H_p	+ 0.01	+ 0.09

[a] Experimental value: −421.27 a.u.

[b] Experimental value [9]: $\mu = 1.12\,D$.

higher than that on the sulfur whether or not *d* orbitals are allowed, and this is also true for the change in charge upon allowing *d* orbitals to the molecule.

3.2. Orbital Results

The Mulliken population analyses for the valence orbitals of phosphirane and thiirane are compared in Table 4 from which it can be seen that there is great similarity between the valence orbitals of these two molecules. This similarity extends to the valence-orbital energies which are reported in Table 5. The close correspondence between the P–C overlap of an orbital of phosphirane and the S–C overlap of the related orbital of thiirane should be particularly noted in Table 4, along with the similarities in the other overlap populations as well as in the gross populations of the carbon atoms and their attached hydrogens. Interestingly enough, the phosphorus gross population varies from orbital to orbital in about the same way as does the sulfur gross population between the related orbitals.

It also seemed desirable to find out whether or not the valence orbitals of cyclopropane in a comparable basis set would also be closely related to those of phosphirane and thiirane. Accordingly a calculation was carried out on cyclopropane using a (52/2) uncontracted Gaussian basis [28]. In order to carry out a proper comparison, it seemed appropriate to select sets of orbitals of *e* symmetry corresponding to the linear combination which would be directly comparable to molecules of C_{2v} symmetry. This was achieved by a 2′ diminution in the HCH angle at only one of the carbon atoms of cyclopropane, which resulted in a transformation of the D_{3h} symmetry of cyclopropane into C_{2v} without appreciable distortion of the wave function. As can be seen in Table 4, the resulting gross and overlap populations for cyclopropane agree quite well orbital-by-orbital with those of phosphirane and thiirane. Note, however, that the difference in the number of the valence-shell electrons of carbon (4), phosphorus (5), and sulfur (6) shows up predominantly in the molecular orbitals $3e'$ and $1e''$ for C_3H_6 and $11a'$ for C_2H_4PH.

Since a population analysis results from integrations over space thus producing numbers which do not reflect electronic spatial distributions, appropriate electron-density plots should be much more suitable for showing the details of interrelations between wave functions of different molecules. For intercomparing the orbitals of phosphirane with those of thiirane and cyclopropane, three-dimensional plots are shown in Fig. 1 for those orbitals exhibiting electron densities in the ring plane. In these plots the magnitude of the electron-density in the plane of the ring is plotted perpendicular to this plane. Figure 1 shows that the intermolecular-orbital correlations made between these three molecules on the basis of the population analysis of Table 4 are clearly recognizable in the electron-density plots. Of particular interest is the good comparison between the two $2e'$ orbitals of cyclopropane and the respective orbitals of phosphirane ($3a''$ and $7a'$) and thiirane ($3b_2$ and $6a_1$), all of which are dominated by *s*-type atomic orbitals. The suitable choice of the pair of $3e'$ orbitals is also demonstrated by their correspondence to the related orbitals of phosphirane ($10a'$ and $5a''$) and thiirane ($8a_1$ and $4b_2$), all of which are based on *p*-type atomic orbitals.

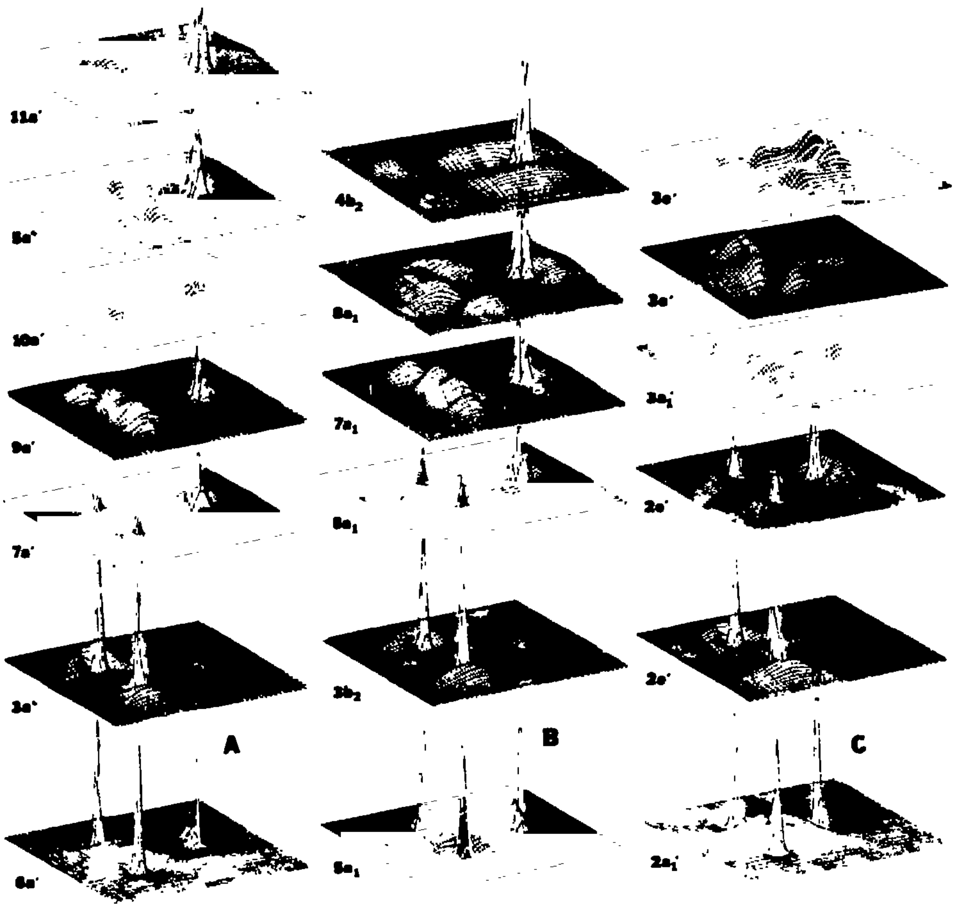

Fig. 1. Three-dimensional plots of the electron-densities in the ring plane (electron density shown on the vertical axis) for the valence molecular orbitals of (*A*) phosphirane, (*B*) thiirane, and (*C*) cyclopropane

The electron-density plots show that the main difference between orbital $6a'$ of phosphirane, $5a_1$ of thiirane, and $2a'$ of cyclopropane lies in the fact that the third carbon of cyclopropane bonds through its second (and hence outermost) *s*-orbital antinode; whereas for phosphorus and sulfur, the bonding is through overlap of the third *s*-orbital antinode. This acts to push the concentration of electrons in the bonding region away from the region of the phosphorus or sulfur nuclei. Similarly, the *p*-type orbitals of phosphirane and thiirane ($9a'$, $10a'$, $5a''$, $11a'$ of C_2H_4PH; $7a_1$, $8a_1$, and $4b_2$ of C_2H_4S) exhibit bonding through the outermost of the two *p*-orbital antinodes of the phosphorus and sulfur thereby leading to the observed differences in electron-density distribution between these orbitals

Table 4. Electronic population analysis[a] for the valence orbitals of C_2H_4X molecules

X	Orbs.	Gross population					Overlap population				
		M[b]	C	H_M	H_C[c]	H'_C	M–C	C–C	M–H	C–H_C	C–H'_C
P(H)	$6a'$	0.435	0.789	0.014	0.048	0.048	0.271	0.372	0.001	0.049	0.049
S	$5a_1$	0.524	0.670	—	0.034		0.217	0.326	—	0.038	
$C(H_2)$	$2a'_1$	0.614	0.614	0.027	0.027		0.276	0.277	0.029	0.029	
P(H)	$3a''$	0.108	0.665	0.000	0.163	0.162	0.069	−0.150	0.000	0.193	0.193
S	$3b_2$	0.068	0.655	—	0.155		0.036	−0.151	—	0.192	
$C(H_2)$	$2e'$	0.101	0.646	0.000	0.152		0.054	−0.147	0.000	0.181	
P(H)	$7a'$	0.954	0.217	0.197	0.027	0.044	−0.086	0.072	0.221	0.048	0.063
S	$6a_1$	1.157	0.315	—	0.053		−0.063	0.119	—	0.065	
$C(H_2)$	$2e'$	0.827	0.283	0.202	0.051		−0.079	0.121	0.240	0.060	
P(H)	$8a'$	0.182	0.593	0.045	0.221	0.123	0.091	0.139	0.017	0.193	0.095
S	$2b_1$	0.095	0.603	—	0.175		0.040	0.153	—	0.154	
$C(H_2)$	$1a''_2$	0.448	0.449	0.109	0.109		0.101	0.102	0.095	0.095	
P(H)	$9a'$	0.338	0.529	0.131	0.043	0.157	0.009	0.232	0.147	0.032	0.132
S	$7a_1$	0.451	0.587	—	0.094		0.170	0.271	—	0.077	
$C(H_2)$	$3a'_1$	0.475	0.470	0.099	0.097		0.093	0.093	0.104	0.103	
P(H)	$4a''$	0.007	0.514	0.000	0.245	0.241	0.005	−0.198	0.000	0.236	0.232
S	$1a_2$	0.002	0.520	—	0.240		0.001	−0.203	—	0.236	
$C(H_2)$	$1e''$	0.000	0.523	0.000	0.239		0.000	−0.199	0.000	0.227	
P(H)	$10a'$	0.507	0.371	0.434	0.039	−0.003	−0.148	0.239	0.210	0.031	0.003
S	$8a_1$	0.773	0.604		0.005		0.016	0.269		0.005	
$C(H_2)$	$3e'$	0.298	0.773	0.052	0.013		−0.092	0.461	0.033	0.008	
P(H)	$5a''$	1.070	0.485	0.000	0.016	0.021	0.374	−0.212	0.000	0.015	0.019
S	$4b_2$	1.094	0.397	—	0.028		0.255	−0.193	—	0.017	
$C(H_2)$	$3e'$	0.927	0.458	0.000	0.039		0.278	−0.275	0.000	0.025	
P(H)	$11a'$	1.109	0.184	0.090	0.002	0.007	−0.193	0.111	−0.177	0.003	0.014
S	$3b_1$	1.874	0.009		0.027		−0.036	0.004	—	0.014	
$C(H_2)$	$1e''$	0.697	0.174	0.318	0.080		−0.132	0.066	0.302	0.075	
P(H)	total	14.702	6.346	0.911	0.803	0.799	0.380	0.598	0.426	0.798	0.799
S	total	16.036	6.362	—	0.810		0.480	0.587	—	0.794	
$C(H_2)$	total	6.389	6.389	0.805	0.806	0.494	0.492	0.800	0.800		

[a] These values are calculated from a (951/52/3) basis set for the phosphirane and thiirane molecules and a (52/2) basis set for cyclopropane.

[b] The M stands for P of X = P(H), or C of X = $C(H_2)$.

[c] For the C_2H_4PH molecule, the H_C corresponds to the hydrogen which is *cis* to the H_M hydrogen and H'_C to that which is *trans*.

and the respective cyclopropane molecular orbitals ($3a'$, $3e'$, and $3e'$) which are also dominated by *p*-type atomic orbitals. The most pronounced case of this pushing of bonding electrons away from the region of the phosphorus or sulfur nuclei is found for orbitals $9a'$ of C_2H_4PH and $7a_1$ of C_2H_4S, as can be seen in Fig. 1.

The figure clearly shows that the most stable valence-shell molecular orbital of each molecule (bottom plots) is strongly bonding and involves the *s* atomic orbitals of all three of the ring atoms. The next two valence-shell molecular orbitals are also based on the *s* atomic orbitals of the three ring atoms but exhibit

Table 5. Orbital energies calculated for C_2H_4PH and C_2H_4S, with *d* orbitals allowed

C_2H_4PH		C_2H_4S	
Orbital	Energy (eV)	Orbital	Energy (eV)
$1a'$ P "1*s*"	2176.2	$1a_1$ S "1*s*"	−2502.2
$2a'$ C "1*s*"	− 308.4	$2a_2$ C "1*s*"	− 308.9
$1a''$ C "1*s*"	− 308.4	$1b_2$ C "1*s*"	− 308.9
$3a'$ P "2*s*"	204.6	$3a_1$ S "2*s*"	− 243.9
$4a'$ P "2*p*"	147.0	$4a_1$ S "2*p*"	− 180.5
$5a'$ P "2*p*"	− 146.9	$2b_2$ S "2*p*"	− 180.5
$2a''$ P "2*p*"	− 146.9	$1b_1$ S "2*p*"	− 180.4
$6a'$	29.7	$5a_1$	− 30.8
$3a''$	22.4	$3b_2$	− 22.8
$7a'$	20.7	$6a_1$	− 22.4
$8a'$	17.3	$2b_1$	− 17.6
$9a'$	15.4	$7a_1$	− 15.7
$4a''$	13.7	$1a_2$	− 14.1
$10a'$	− 12.0	$8a_1$	− 11.3
$5a''$	9.7[a]	$4b_2$	− 10.5
$11a'$	9.7	$3b_1$	− 8.0

[a] When given with more accuracy, the $5a''$ molecular orbital of phosphirane is found to be higher in energy than orbital $11a'$.

either no-bonding or antibonding characteristics within the ring. The remaining orbitals which contribute to bonding of the ring atoms all involve the *p* atomic orbitals of these atoms, with the two more stable of these molecular orbitals being $(\overline{p_\sigma - p_\sigma - p}_\sigma)$. With respect to the interactions of the ring atoms, the phosphorus or sulfur (or alternatively the third carbon of cyclopropane) is strongly π-bonded to the C_2H_4 group by atomic *p* orbitals with nodal planes perpendicular to the ring plane ($5a''$, $4b_2$, $3e'$); whereas similar π antibonding is achieved for the case where the nodal plane of the *p* atomic orbitals lies in the ring plane. By looking at plots similar to those given in Fig. 1 corresponding to the planes passing through each of the ring atoms and the center of the ring, the same kind of information concerning the bonds to the hydrogen atoms is obtained as is given by Fig. 1 for the bonding within the ring plane.

Acknowledgment. We wish to thank the Air Force Office of Scientific Research for partial support of this work under contract number AFOSR-72-2265.

References

1. Absar, I., Robert, J. B., Van Wazer, J. R.: J. chem. Soc. Faraday transactions II **68**, 1055 (1972).
2. Absar, I., Van Wazer, J. R.: J. Amer. chem. Soc. **94**, 2382 (1972).
3. Absar, I., Van Wazer, J. R.: J. chem. Physics **56**, 1284 (1972).
4. Robert, J. B., Marsmann, H., Absar, I., Van Wazer, J. R.: J. Amer. chem. Soc. **93**, 3320 (1971).
5. Clark, D. T.: Theoret. chim. Acta (Berl.) **15**, 225 (1969).
6. Bonaccorsi, R., Scrocco, E., Tomasi, J.: J. chem. Physics **52**, 5270 (1970).
7. Franchini, P. F., Zandomeneghi, M.: Theoret. chim. Acta (Berl.) **21**, 90 (1971).
8. Strausz, O. P., Gosavi, R. K., Denes, A. S., Csizmadia, I. G.: Theoret. chim. Acta (Berl.) **26**, 367 (1972).
9. Bowers, M. T., Beaudet, R. A., Goldwhite, H., Tang, R.: J. Amer. chem. Soc. **91**, 17 (1969).

10. Cunningham, G. L., Jr., Boyd, A. W., Myers, R. J., Gwinn, W. D. J. chem. Physics **19**, 676 (1951); Shoemaker, R. L., Flygare, W. H.: J. Amer. chem. Soc. **90**, 6263 (1968).
11. Van Wazer, J. R., Absar, I.: In: Sulfar research trends. Advances in chemistry series, Vol. 110, p. 20. American Chemical Society 1972.
12. Robert, J. B., Marsmann, H., Schaad, L. J., Van Wazer, J. R.: Phosphorus **2**, 11 (1972).
13. Marsmann, H., Groenweghe, L. C. D., Schaad, L. J., Van Wazer, J. R.: J. Amer. chem. Soc. **92**, 6107 (1970).
14. Franchini, P. F., Vergani, C.: Theoret. chim. Acta (Berl.) **13**, 46 (1969).
15. McWeeny, R.: Rev. mod. Physics **32**, 335 (1960).
16. Allen, L. C., Karo, A. M.: Rev. mod. Physics **32**, 275 Fig. 1 (1960).
17. Mulliken, R. S.: J. chem. Physics **23**, 1833, 1841, 2338, 2343 (1955).
18. Mulliken, R.S.: J. chem. Physics **36**, 3428 (1962).
19. Absar, I., Van Wazer, J. R.: Chem. Physics Letters **11**, 310 (1971).
20. Coulson, C. A.: Nature **221**, 1106 (1969).
21. Moore, C. E.: Ionization potentials and ionization limits derived from the analysis of optical spectra, NSRDS-NBS 34. Washington: U.S. Government printing office 1970.
22. Wagman, D. D., Evans, W. H., Parker, V. B., Halow, I., Bailey, S. M., Schumm, R. H.: Selected values of chemical thermodynamic properties, NBS technical note 270-3. Washington: U.S. Government printing office 1968.
23. Guthrie, G. B., Jr., Scott, D. W., Waddington, G.: J. Amer. chem. Soc. **74**, 2795 (1952).
24. Mitchell, R. W., Kuzma, L. J., Pirkle, R. J., Merritt, J. A.: Spectrochim. Acta A**25**, 819 (1969).
25. Chan, S., Goldwhite, H., Keyzer, H., Tang, R.: Spectrochim. Acta A**26**, 249 (1970).
26. Cottrell, T. L.: The strengths of chemical bonds, 2nd edition. London: Butterworth's 1958.
27. Taylor, B. N., Parker, W. H., Langenberg, R. N.: Rev. mod. Physics **41**, 375 (1969).
28. Marsmann, H., Robert, J.-B., Van Wazer, J. R.: Tetrahedron **27**, 4377 (1971).

Dr. John R. Van Wazer
Department of Chemistry
Vanderbilt University
Nashville, Tennessee 37235, USA

Theoret. chim. Acta (Berl.) 29, 183 – 187 (1973)
© by Springer-Verlag 1973

Relatio

An *ab initio* Molecular Orbital Study of the C_2F_2 Species: The Difluorovinylidene → Difluoroacetylene Rearrangement

Otto P. Strausz and Ross J. Norstrom
Department of Chemistry, University of Alberta, Edmonton, Alberta, Canada

Alan C. Hopkinson
Department of Chemistry, York University, Downsview, Ontario, Canada

Michael Schoenborn and Imre G. Csizmadia
Department of Chemistry, University of Toronto, Toronto 5, Ontario, Canada

Received November 8, 1972

An *ab initio* MO study, using medium size Gaussian basis sets has been made of vinylidene carbene, acetylene and the isomeric cyclic intermediate presumed to represent the transition state of their interconversion reaction, along with their perfluorinated analogs. The total energies of the acetylenes are lower than the vinylidenes and the estimated activation energy of their interconversion is considerably higher for the fluorinated molecules. The results are in line with experimental observations.

The difluorovinylidene carbene, $F_2C=C:$, has been shown to be the principal primary product of the triplet mercury photosensitization of trifluoroethylene [1]. Thermodynamically, it is likely to be less stable than its structural isomer difluoroacetylene, nonetheless its unimolecular isomerization to acetylene is slow at room temperature and consequently the carbene can be readily scavenged. It reacts with the C–H bonds of paraffins to give a 1,1-difluoro-1-alkene and with the π-bonds of olefins to give a difluoromethylene cyclopropane or its secondary fragmentation or rearrangement product.

In order to gain an understanding of the cause of the stability of difluorovinylidene and to elucidate details of the hypothetical reaction path leading to acetylene formation, non-empirical MO calculations were performed on three C_2F_2 species including the vinylidene (I) and acetylene (II) structures and the cyclic intermediate (III) assumed to be the transition state of the expected isomerization reaction:

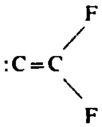
$:C=C\genfrac{}{}{0pt}{}{\diagup F}{\diagdown F}$

(I)

$F-C\equiv C-F$

(II)

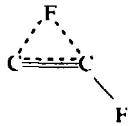

(III)

Theoret. chim. Acta (Berl.) 29, 183 – 187 (1973)
© by Springer-Verlag 1973

Relatio

An *ab initio* Molecular Orbital Study of the C_2F_2 Species: The Difluorovinylidene → Difluoroacetylene Rearrangement

Otto P. Strausz and Ross J. Norstrom
Department of Chemistry, University of Alberta, Edmonton, Alberta, Canada

Alan C. Hopkinson
Department of Chemistry, York University, Downsview, Ontario, Canada

Michael Schoenborn and Imre G. Csizmadia
Department of Chemistry, University of Toronto, Toronto 5, Ontario, Canada

Received November 8, 1972

An *ab initio* MO study, using medium size Gaussian basis sets has been made of vinylidene carbene, acetylene and the isomeric cyclic intermediate presumed to represent the transition state of their interconversion reaction, along with their perfluorinated analogs. The total energies of the acetylenes are lower than the vinylidenes and the estimated activation energy of their interconversion is considerably higher for the fluorinated molecules. The results are in line with experimental observations.

The difluorovinylidene carbene, $F_2C = C$:, has been shown to be the principal primary product of the triplet mercury photosensitization of trifluoroethylene [1]. Thermodynamically, it is likely to be less stable than its structural isomer difluoroacetylene, nonetheless its unimolecular isomerization to acetylene is slow at room temperature and consequently the carbene can be readily scavenged. It reacts with the C–H bonds of paraffins to give a 1,1-difluoro-1-alkene and with the π-bonds of olefins to give a difluoromethylene cyclopropane or its secondary fragmentation or rearrangement product.

In order to gain an understanding of the cause of the stability of difluorovinylidene and to elucidate details of the hypothetical reaction path leading to acetylene formation, non-empirical MO calculations were performed on three C_2F_2 species including the vinylidene (I) and acetylene (II) structures and the cyclic intermediate (III) assumed to be the transition state of the expected isomerization reaction:

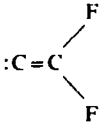

(I)

$F-C\equiv C-F$

(II)

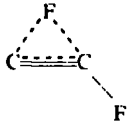

(III)

Table 1. Computed energy values for the three C_2F_2 species

Energy (hartree)	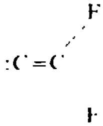	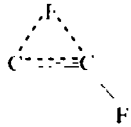	F–C≡C–F
Electronic attraction	– 374.269680	279.957668	– 365.535053
Nuclear repulsion	+ 102.667484	+ 108.572154	+ 93.874888
Total molecular	– 271.602196	– 271.385514	– 271.660165
Relative energy (kcal mole)	0.00	E_a = + 135.96	ΔE = – 36.37

Table 2. Computed molecular orbital[a] energy values (in Hartree a.u.) for the C_2F_2 species

Species	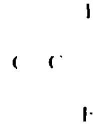				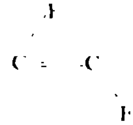		F–C≡C–F	
MO	$a_1(\sigma)$	$b_1(\sigma)$	$b_2(\pi)$	$a_2(\pi)$	σ	π	σ	π_x and π_y
1	26.4752	26.4751	0.7426	– 0.6341	26.6128	– 0.8579	26.5007	– 0.7064
2	11.4790	1.7037	– 0.3781	+ 3.7010	– 26.5074	– 0.6919	– 26.5001	– 0.6784
3	– 11.3391	0.7588	+ 0.2083		– 11.4684	– 0.3236	– 11.4153	– 0.3930
4	1.7674	0.6145	+ 1.5526		11.3359	+ 0.1866	– 11.4136	+ 0.2746
5	1.1030	+ 0.0467			1.9665	+ 1.5592	1.7245	+ 1.5680
6	0.8990	+ 0.5879			1.7352		– 1.7224	
7	0.6535				– 1.0956		– 1.1081	
8	– 0.4411				– 0.9453		– 0.8100	
9	+ 0.4470				– 0.8071		– 0.7507	
10	+ 0.6689				0.6999		+ 0.2591	
11					– 0.6120		+ 0.5263	
12					– 0.3962		+ 1.0204	
13					+ 0.2252			
14					+ 0.3989			

[a] The broken line indicates the occupancy limit.

Because of the relatively large size of the molecule only a "medium" Gaussian basis set could be used to expand the molecular orbitals. It consisted of five *s* and two *p* Gaussian type functions [2] (GTF), for both carbon and fluorine, resulting in a total of 44 GTF. This basis set has been used successfully by Clark [3] for studying fluoro hydrocarbons and related molecules and it should be suitable for the present case as well. The calculations were carried out on an IBM 7094-II computer using the POLYATOM system [4].

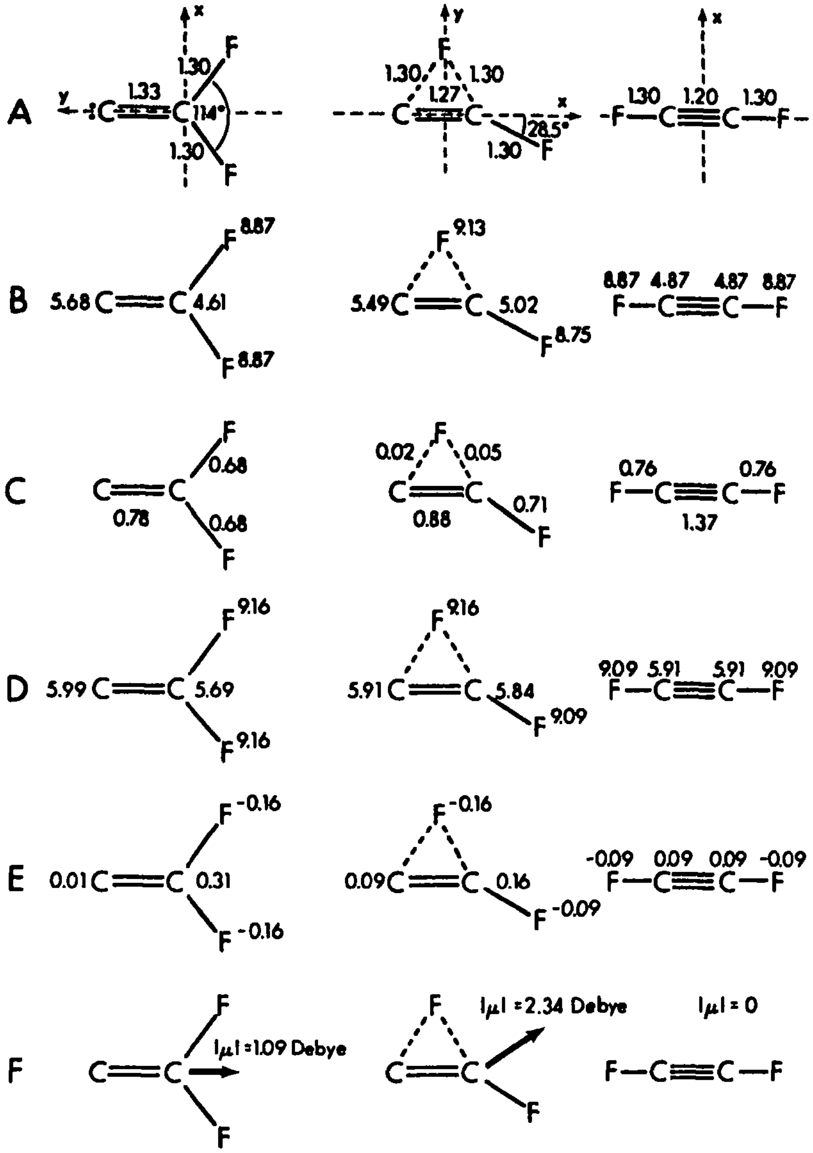

Fig. 1. Geometries and electron distributions for C_2F_2 species. A Bond length (Å) and bond angles. B Net atomic electron populations. C Overlap electron populations. D Gross atomic electron populations. E Net atomic charges. F Dipole moments

The electronic attraction, nuclear repulsion as well as the total energy values computed for the species I to III are summarized in Table 1. The results show that the carbene is indeed less stable than the acetylene as anticipated on the grounds that the former contains one less π bond and the same number of σ bonds as the latter. The energy value computed for the transition state III of the hypothetical unimolecular isomerization is prohibitively large.

Table 3. Computed energy values for the three C_2H_2 species

Energy (hartree)	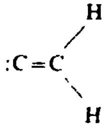	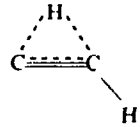	H−C≡C−H
Electronic attraction	−100.19584	−102.58358	−101.49828
Nuclear repulsion	23.59257	26.10265	24.83465
Total molecular	−76.60327	−76.48093	−76.66363
Relative energy (kcal/mole)	0.00	$E_a = +76.79$	$\Delta E = -37.89$

In addition to total energies the orbital energies, given in Table 2, the dipole moments and electron populations, presented in Fig. 1, were also calculated. The latter data clearly indicate that the properties of III lie intermediate between I and II. However, the binding of the bridged fluorine to the two carbon atoms, as measured by the overlap populations, is diminishingly small.

For comparison the corresponding calculations were also carried out on the unfluorinated species, vinylidene, acetylene, and the cyclic intermediate representing the transition state for their interconversion. In order to ensure that the two sets of calculations are directly comparable their quality must be commensurate and this requires the use of basis sets of approximately identical sizes.

The basis set used for the C_2F_2 species consisted of 5^s, 2^p GTF on both C and F, which resulted in a total of 44 basis functions. On going from C_2F_2 to C_2H_2 the number of carbon atom orbitals was increased because for the description of hydrogen atoms one normally needs fewer orbitals than for the description of fluorine atoms. In this set of calculations the carbon atoms were represented by 7^s, 3^p GTF while the hydrogen atoms were described [2] by a set of 3^s GTF. This yielded a total of 38 GTF in the basis set, which is comparable to the previous basis set size of 44.

The results, computed for the C_2H_2 species, are given in Table 3. It is seen that the enthalpy changes of the two reactions are very similar but the activation energy associated with the rearrangement of the fluoro compound is nearly twice the value of the unfluorinated molecule. This is in line with expectation since H-atom migration is known to be more facile than F-atom migration while the enthalpy change would be expected to be affected only slightly [1].

Since no literature report exists on the detection or trapping of vinylidene it is quite probable that the isomerization to acetylene is very rapid and features a very low activation energy. Even if we take the activation energy as being zero the estimated value of the activation energy for the fluoro analog is still about 59 kcal/mole, which would adequately explain the reluctance of difluorovinylidene to isomerize.

Acknowledgements. The authors thank the donors of the Petroleum Research Fund, administered by the American Chemical Society and the National Research Council of Canada, for support of the research.

References

1. Strausz, O. P., Norstrom, R. J., Salahub, D., Gosavi, R. K., Gunning, H. E., Csizmadia, I. G.: J. Amer. chem. Soc. **92**, 6395 (1970).
2. Csizmadia, I. G., Harrison, M. C., Moskowitz, J. W., Sutcliffe, B. T.: Theoret. chim. Acta (Berl.) **6**, 217 (1966).
3. Clark, D. T.: J. Chem. Soc. *D* (Chem. Comm.) **1970**, 1042.
4. Csizmadia, I. G., Harrison, M. C., Moskowitz, J. W., Seung, S. S., Sutcliffe, B. T., Barnett, M. P.: The POLYATOM System QCPE No. 47 A.

Prof. Dr. O. P. Strausz
Department of Chemistry
University of Alberta
Edmonton, Alberta, Canada

Announcement

A NATO-Advanced Study Institute on
"Chemical Spectroscopy and Photochemistry in the Vacuum Ultraviolet"
will be held from August 5 to 17, 1973
at the Far Hills Inn, Val Morin, Québec, Canada
under the joint sponsorship of the Royal Society of Canada and The Scientific Affairs Division of the North Atlantic Treaty Organization.

Members of Organizing Committee	Dr. P. Ausloos, Radiation Chemistry Section, U.S. National Bureau of Standards, Washington, D.C. 20234, U.S.A.
	Dr. M. B Robin, Bell Laboratories 600 Mountain Ave, Murray-Hill, New Jersey 07974, U.S.A.
	Dr. C. Sandorfy, Département de Chimie Université de Montréal, C.P. 6128, Montréal, Québec, Canada.
Director of the Institute.	C. Sandorfy.

The number of participants is limited to 80.
Those who wish to attend should contact one of the members of Organizing Committee.

Theoret. chim. Acta (Berl.) 29, 189—234 (1973)
© by Springer-Verlag 1973

Commentationes

Quantenmechanische Theorie der optischen Aktivität der Methanderivate im Transparenzgebiet

Dietrich Haase und Ernst Ruch
Institut für Quantenchemie der Freien Universität Berlin

Eingegangen am 22. Juni 1972

Quantum Mechanical Theory of Optical Rotatory Power of Methane Derivatives in the Transparent Region

The optical rotatory power of methane derivatives depending on substituent properties is discussed by means of quantum mechanics following an algebraic theory for this molecular class [17]. With proper definitions of "formally bonded ligands" and a "model Hamiltonian" and by means of a perturbation treatment using the interaction between ligands as perturbation, the Ansatz according to the so called second method is exactly confirmed if the perturbation treatment is performed up to and including the second order. Perturbation corrections of zeroth and first order yield only contributions related to geometrical deviations from the so called T_d-situation. Therefore the only contribution which is present in all methane derivatives with four different ligands and which represents the main contribution to optical rotatory power if such deviations from the T_d-situation are small is described by the second order. The corrections of zeroth and first order are also discussed. With simplifying assumptions about the perturbation operator we arrive at an interpretation of the result by dipole moments and electromagnetic polarisibilities of the ligands and geometrical parameters. Finally further assumptions are discussed in order to obtain simplified formulas.

Die optische Aktivität von Methanderivaten in Abhängigkeit von den Eigenschaften der Substituenten wird entsprechend einer algebraischen Theorie für diese Molekülklasse [17] quantenmechanisch diskutiert. Mit geeigneten Festsetzungen über die Begriffe „formal gebundener Ligand" und „Modelloperator für die Energie" und mit den Mitteln einer Störungsrechnung, bei der die Wechselwirkung zwischen den Liganden als Störung betrachtet wird, läßt sich der Ansatz nach der sogenannten zweiten Methode exakt bestätigen, wenn man die Störungsrechnung mit der zweiten Ordnung abbricht. Da störungstheoretische Korrekturen nullter und erster Ordnung nur Zusatzbeiträge liefern, die auf geometrische Abweichungen von der sogenannten T_d-Situation zurückzuführen sind, wird der einzige Beitrag, der bei allen Methanderivaten mit vier verschiedenen Liganden auftritt und bei kleinen Abweichungen von der T_d-Situation den Hauptbeitrag zum optischen Drehwinkel darstellt, erst in zweiter Ordnung beschrieben. Die Korrekturen nullter und erster Ordnung werden ebenfalls besprochen. Mit vereinfachenden Annahmen über die Form der Störung gelingt die Interpretation des Resultats durch Dipolmomente und elektromagnetische Polarisierbarkeiten der Liganden und geometrische Parameter. Schließlich werden weitere Näherungsannahmen mit dem Ziel einer Vereinfachung der gefundenen Formel diskutiert.

Inhaltsverzeichnis

I. Vorbemerkung 190
  1. Die Rosenfeld-Gleichung 191
  2. Struktur der Chiralitätsfunktionen für die Klasse der T_d-Derivate 192
II. Die quantenmechanische Behandlung 194
  1. Das Modell 194

2. Struktur der Rosenfeldgleichung im Modell des Energieoperators $\bar{\mathscr{H}}$ 197
3. Polarisierbarkeitstensoren und ihre Zerlegung nach Teilsystemen des Modells 199
4. Lösung für $[\omega]$ im Modell des ungestörten Operators $\mathscr{H}_0$ 201
5. Gegenüberstellung der störungstheoretischen Approximationsaspekte, Gültigkeitsbereich des Modells $\bar{\mathscr{H}}$ und der vereinfachte Modelloperator $\tilde{\mathscr{H}}$ 202
6. Störungsrechnung erster Ordnung. 205
7. Störungsrechnung zweiter Ordnung 208
III. Diskussion des Resultats 215
1 Allgemeiner Gültigkeitsanspruch und spezielle Form für Methanderivate 215
2 T_d-Derivate 217
a) Der formale Strukturaspekt des Resultats im Model $\bar{\mathscr{H}}$ und seine praktische Bedeutung 217
b) Der optische Drehwinkel von T_d-Derivaten im Modell $\tilde{\mathscr{H}}$ 219
c) Vereinfachende Annahmen für die T_d-Komponente im Modell $\tilde{\mathscr{H}}$ 222
IV. Schlußbemerkungen 226
V. Anhang 227
A. Störungsrechnung 227
B Elektromagnetische Tensoren 228
C Koordinatensysteme 232
D Die 2-Liganden-Funktionen 233
Literatur 234

I. Vorbemerkung

Unter „natürlicher optischer Aktivität" versteht man die Eigenschaft eines Mediums, die Polarisationsebene eines durchtretenden linear polarisierten Lichtstrahles ohne zusätzliche Einflüsse von außen, insbesondere ohne ein äußeres statisches Magnetfeld, zu drehen. Das Phänomen der Drehung folgt aus unterschiedlichen Fortpflanzungsgeschwindigkeiten der links- und rechtszirkular polarisierten Komponente einer linear polarisierten Lichtwelle. In Medien mit natürlicher optischer Aktivität sind diese Geschwindigkeiten verschieden. In gasförmigen und flüssigen Stoffen, allgemein in Stoffen ohne bevorzugte Anordnung und Orientierung der Moleküle, kann für die optische Drehung nur die Tatsache verantwortlich gemacht werden, daß die Moleküle von ihren Spiegelbildern verschieden sind.

Der Einfluß auf die rechts- und linkszirkular polarisierte Komponente des Lichtes wird vertauscht, wenn man statt eines Ensembles chiraler Moleküle das Ensemble der Antipoden durchstrahlt. Der Drehwinkel ändert dabei also das Vorzeichen. Die Drehung von linear polarisiertem Licht bei Durchstrahlung einer gegebenen Menge eines statistischen Ensembles chiraler Moleküle einer Sorte ist somit eine pseudoskalare Eigenschaft des Moleküls. Das gilt auch für Lösungen von chiralen Molekülen in einem achiralen Lösungsmittel. Für eine chirale Molekülklasse mit achiralem Gerüst und achiralen Liganden von der Symmetrie der Lagegruppe wird das optische Drehvermögen des entsprechenden statistischen Ensembles also durch eine Funktion der Ligandensorten und ihrer Verteilung auf die Gerüstplätze beschrieben, die wir in [17] Chiralitätsfunktion genannt haben.

Wir werden im folgenden eine approximative Chiralitätsfunktion für den optischen Drehwinkel der Methanderivate aus der Quantenmechanik ableiten und können uns dabei auf zwei Resultate stützen, die Rosenfeldgleichung und die Theorie der Chiralitätsfunktionen.

1. Die Rosenfeld-Gleichung [13]

Der molare Drehwinkel $[\omega]$ für chirale Moleküle in statistischer Verteilung, z. B. für die Lösung einer optisch aktiven chemisch reinen Substanz in einem achiralen Lösungsmittel, wird im Transparenzgebiet durch die Rosenfeldgleichung beschrieben[1]:

$$[\omega] = K\,\mathrm{Sp}\,{}^{(J)}\gamma \tag{1}$$

mit

$$K = \frac{48\,\pi N}{c}\,\frac{n^2+2}{3}\,\nu^2 \quad \text{und} \quad {}^{(J)}\gamma = \frac{2}{h}\,\mathrm{Im}\sum_{s}\frac{\langle o|\vec{m}|s\rangle \circ \langle s|\vec{\mu}|o\rangle}{\nu_{so}^2-\nu^2}.$$

Dabei ist vorausgesetzt, daß sich alle Moleküle im nichtentarteten Grundzustand $|o\rangle$ befinden und die Frequenz ν des Lichts nicht in der Nähe der Resonanzstellen, den Eigenfrequenzen ν_{so}, liegt. Falls der Grundzustand g-fach entartet ist, haben wir in der Definitionsgleichung für ${}^{(J)}\gamma$ die Summe durch das arithmetische Mittel von g entsprechenden Summen mit linear unabhängigen Grundzuständen zu ersetzen.[2] $\vec{m} = \sum_t e_t \vec{r}_t$ ist der Operator des elektrischen, $\vec{\mu} = \sum_t e_t/2M_t c \cdot (\vec{r}_t \times \vec{p}_t + 2\vec{s}_t)$ der des magnetischen Dipolmomentes bei Abwesenheit äußerer Felder. e_t, M_t, $\vec{p}_t$, $\vec{s}_t$ bezeichnen Ladung, Masse, Impuls und Spin des Teilchens t am Ort $\vec{r}_t$; c ist die Lichtgeschwindigkeit, h das Plancksche Wirkungsquantum und N die Loschmidtsche Zahl. Durch $\circ$ ist das unbestimmte Produkt von Operatoren bezeichnet, die Spurbildung „Sp“ liefert das skalare Produkt. Das Matrixelement $\langle s|\mathcal{O}|t\rangle$ eines Operators $\mathcal{O}$ wird mit den Eigenfunktionen ψ_s und ψ_t des Hamiltonoperators für das von äußeren Feldern unbeeinflußte Molekül gebildet. Im bezeichnet den Imaginärteil der Summe, die sich über die Molekülzustände $|s\rangle$ mit der Bedingung $\nu_{so} \neq 0$ erstreckt. Der Faktor $(n^2+2)/3$ beschreibt die Lorentz-Korrektur für das elektromagnetische Feld im Inneren eines Mediums mit dem Brechungsindex n; Einflüsse, die nicht von dieser Korrektur erfaßt und hauptsächlich in stark polaren Medien maßgebend werden, sind vernachlässigt.[3]

Ein weiterer Schritt der allgemeinen Theorie der natürlichen optischen Aktivität besteht in der Spezialisierung auf Molekülklassen mit einem bestimmten Molekülgerüst und in der entsprechenden Behandlung des Rosenfeldschen Ausdrucks bis zur Form einer Funktion, die die Abhängigkeit von den Eigenschaften der Liganden des Moleküls ausdrückt.

In den uns aus der Literatur bekannten quantenmechanischen Arbeiten mit diesem Ziel, z. B. [6, 9], werden verschiedene Modellvorstellungen im Rahmen einer Störungsrechnung erster Ordnung diskutiert. Die Ordnung der quantenmechanischen Störungsrechnung ist aber gerade im Falle der optischen Aktivität ein äußerst fragwürdiges Kriterium für die physikalische Kompetenz eines Ansatzes (vgl. z. B. [8]). Die Methanderivate sind dafür insofern typisch, als gerade die einfachste chirale Situation und damit der idealisierte Grenzfall nicht, wie sich zeigen wird, in erster störungstheoretischer Ordnung zu beschreiben ist. Wir wollen diesen Idealfall zunächst präzisieren und nennen entsprechende Moleküle T_d-Derivate des Methans.

---

[1] Der Drehwinkel φ wird in Grad pro dcm durchsetzter Schicht angegeben (oder in Radian pro cm; 1 Grad/dcm $= \pi/1800$ Radian/cm). Die Größe $[\varphi] = \varphi/\varrho_c$ heißt „spezifischer Drehwinkel“, $[\omega] = [\varphi]\,M_c/100 = \varphi/100 \cdot N/N_c$ heißt „molarer Drehwinkel“. Dabei ist: N_c = Anzahl der chiralen Moleküle pro cm^3 Lösung, M_c = Molgewicht der optisch aktiven Substanz, $\varrho_c = N_c M_c/N$ = Dichte der optisch aktiven Substanz in g pro cm^3 Lösung.

[2] Die Symmetriegruppe optisch aktiver T_d-Derivate ist C_1, also gilt bei gerader Elektronenzahl $g = 1$, bei ungerader $g = 2$.

[3] Eine Diskussion dieser Einflüsse findet sich bei Maaskant und Oosterhoff [11].

Der Kohlenstoff mit vier T_d-symmetrisch orientierten σ-Bindungen sei als Molekülgerüst betrachtet, als das gemeinsame Merkmal einer Klasse von Verbindungen, die sich durch Art und Verteilung von Liganden unterscheiden; wenn dabei die Art und die Fixierung der Liganden der Bedingung genügen, daß die Symmetrieelemente der C_{3v}-Achsen auch Symmetrieelemente der jeweiligen Liganden sind, nennen wir die Verbindungen T_d-Derivate.

Es ist klar, daß T_d-Derivate mit verschiedenartigen Liganden chiral sind. Da sich, wie schon erwähnt, in erster störungstheoretischer Ordnung kein Beitrag zum optischen Drehwinkel ergibt, beschreibt eine Störungsrechnung für Methanderivate, die mit der ersten Ordnung abbricht, wie z. B. die Kirkwoodsche Theorie, Beiträge zum optischen Drehwinkel, die ausschließlich auf der Abweichung von der Situation in T_d-Derivaten beruhen. Die Störungstheorie erster Ordnung behandelt einen Effekt erster Ordnung in den Abweichungen von der T_d-Situation; die zweite störungstheoretische Ordnung dagegen wird den Effekt nullter Ordnung, nämlich die optische Aktivität von T_d-Derivaten ohne Korrekturen ihrer Geometrie, beschreiben. Die Kirkwoodsche oder entsprechende Rechnungen liefern bei kleiner Deformation also Beiträge zum optischen Drehwinkel, die als Korrektur des Resultats einer Störungsrechnung zweiter Ordnung anzusehen sind.

Die hier vorweggenommenen Aussagen über Eigenschaften der Störungsrechnung basieren auf Informationen über die algebraische Struktur von Chiralitätsfunktionen.

2. *Struktur der Chiralitätsfunktionen für die Klasse der* T_d*-Derivate* [16, 17]

Die Theorie der Chiralitätsfunktionen betrifft pseudoskalare Eigenschaften von den Molekülen einer chiralen Molekülklasse mit einem jeweils festgelegten achiralen Gerüst. Die Chiralitätsfunktionen für die Klasse der T_d-Derivate zeichnen sich durch folgende Besonderheiten aus:

α) Das Transformationsverhalten gegenüber allen möglichen Ligandenpermutationen ist durch das Transformationsverhalten gegenüber den Symmetrieoperationen des Gerüstes völlig festgelegt.

β) Es gibt keine chiralen Moleküle mit zwei gleichartigen Liganden (Chiralitätsordnung $o = 1$). Aus diesem Grund können nur Funktionen von mindestens drei Liganden ($n - o = 3$, n = Zahl der Gerüststellen) von Null verschiedene additive Beiträge zur Chiralitätsbeobachtung liefern (vgl. [17]). Dementsprechend lautet die Chiralitätsfunktion nach dem zweiten Näherungsverfahren (vgl. [16])

$$\tilde{\chi}(l_1, l_2, l_3, l_4) = \varphi(l_2, l_3, l_4) - \varphi(l_3, l_4, l_1) + \varphi(l_4, l_1, l_2) - \varphi(l_1, l_2, l_3) \qquad (2)$$

mit Funktionen φ der Eigenschaft

$$\mathscr{P}(ijk)\, \varphi(l_i, l_j, l_k) = \varphi(l_i, l_j, l_k)\,,$$

wobei $\mathscr{P}(ijk)$ ein Projektionsoperator ist, der sich gemäß der Definition

$$\mathscr{P}(ijk) = \tfrac{1}{6}\{\mathscr{O}((1)) + \mathscr{O}((ijk)) + \mathscr{O}((ikj)) - \mathscr{O}((ij)) - \mathscr{O}((jk)) - \mathscr{O}((ki))\}$$

aus Permutationsoperatoren $\mathcal{O}(s)$ zusammensetzt, in denen die spezielle Permutation s jeweils in der Zyklenschreibweise bezeichnet ist. Man überzeugt sich damit ohne Mühe, daß keine additiven Beiträge von der Form

$$f(l_i),\ f(l_i l_j) \quad \text{oder} \quad f(l_i, l_j)\, f(l_k, l_l)$$

auftreten können.

γ) Eine qualitativ vollständige Chiralitätsfunktion für unsere Klasse besteht aus einer einzigen Komponente. Damit ist jede Chiralitätsfunktion, also auch Ansatz (2) und alle daraus durch Spezialisierung entstehenden Ansätze, qualitativ vollständig. Mit dieser Eigenschaft ist bei der vorliegenden Klasse eine Reihe von kritischen Schwächen in der Beschreibung des optischen Drehwinkels, die in fast allen übrigen Klassen auftreten können (vgl. [17]), *a priori* ausgeschlossen.

Die Darstellung der Chiralitätsfunktion (2) als Funktion einer einparametrigen Eigenschaft $\lambda(l)$ der Liganden führt zum Chiralitätsprodukt

$$\chi(\lambda(l_1), \lambda(l_2), \lambda(l_3), \lambda(l_4)) = \varepsilon \prod_{i<j}^{1,4} (\lambda(l_i) - \lambda(l_j)), \tag{2a}$$

wenn wir uns entsprechend den Grundsätzen des ersten Näherungsverfahrens auf das Polynom niedrigsten Grades in $\lambda(l)$ beschränken und mit ε einen molekülunabhängigen Proportionalitätsfaktor bezeichnen. Im Sinne der Darstellung (2) ist damit folgende Spezialisierung vorgenommen:

$$\varphi(l_i, l_j, l_k) = 6\varepsilon\, \mathscr{P}(ijk)\, \lambda(l_i)\, \lambda^2(l_j)\, \lambda^3(l_k) = \varepsilon \begin{vmatrix} \lambda(l_i) & \lambda(l_j) & \lambda(l_k) \\ \lambda^2(l_i) & \lambda^2(l_j) & \lambda^2(l_k) \\ \lambda^3(l_i) & \lambda^3(l_j) & \lambda^3(l_k) \end{vmatrix}.$$

Weniger speziell ist folgende Struktur

$$\varphi(l_i, l_j, l_k) = 6\, \mathscr{P}(ijk) \sum_r \lambda_r(l_i)\, \mu_r(l_j)\, \nu_r(l_k) = \sum_r \begin{vmatrix} \lambda_r(l_i) & \lambda_r(l_j) & \lambda_r(l_k) \\ \mu_r(l_i) & \mu_r(l_j) & \mu_r(l_k) \\ \nu_r(l_i) & \nu_r(l_j) & \nu_r(l_k) \end{vmatrix}$$

mit mehreren ligandenspezifischen Parametern λ_r, μ_r, ν_r; damit erhalten wir Ansatz (2) in der Form

$$\tilde{\chi}(l_1, l_2, l_3, l_4) = \sum_r \begin{vmatrix} 1 & 1 & 1 & 1 \\ \lambda_r(l_1) & \lambda_r(l_2) & \lambda_r(l_3) & \lambda_r(l_4) \\ \mu_r(l_1) & \mu_r(l_2) & \mu_r(l_3) & \mu_r(l_4) \\ \nu_r(l_1) & \nu_r(l_2) & \nu_r(l_3) & \nu_r(l_4) \end{vmatrix}. \tag{2b}$$

δ) Die Klasse gehört zur Kategorie „a", d. h., es gibt Chiralitätsfunktionen ohne „chirale Nullstellen", z. B. das Chiralitätsprodukt (2a), und jede stetige Chiralitätsfunktion in $\lambda(l)$ kann als Produkt von (2a) mit einem stetigen und in den Permutationen der l_i totalsymmetrischen Faktor geschrieben werden (vgl. [14]). Hat der totalsymmetrische Faktor für einen bestimmten Variablenbereich keine Nullstellen, dann können wir aus der Sequenz der λ-Parameter das Vorzeichen des Drehwinkels entnehmen. In Formel (2a) steckt die Annahme, daß bei geeigneter Wahl von $\lambda(l)$ und entsprechender Beschränkung des Variabilitätsbereiches der Liganden der totalsymmetrische Faktor durch eine Konstante approximiert werden kann.

Zusammenfassend können wir feststellen:

Für Methanderivate mit T_d-Bedingung gibt es Struktureigenheiten in der Beschreibung des optischen Drehwinkels, für Methanderivate ohne T_d-Bedingung darf angenommen werden, daß diese Strukturen zumindest noch für einen Teil des Phänomens maßgebend sind. Aus β) entnehmen wir, daß in einer quantenmechanischen Rechnung Wechselwirkungen zwischen je drei Liganden berücksichtigt werden müssen, um von Null verschiedene Ausdrücke für den Drehwinkel von T_d-Derivaten zu erhalten. Wir erwarten daher wertvolle Gesichtspunkte für die praktische Durchführung der Störungsrechnung mit der Aussicht auf eine interessante physikalische Interpretation von Teilausdrücken. Die Formen (2a) und (2b) aus γ) geben uns eine Vorstellung von der möglichen Struktur einer quantenmechanischen Theorie für T_d-Derivate und einen Hinweis auf sinnvolle Vereinfachungen. Wegen δ) kann nach einer Beziehung zwischen der Sequenz einer geeigneten ligandenspezifischen Größe für die verschiedenen Liganden in einem Derivat und dem Vorzeichen des optischen Drehwinkels gesucht werden. Außerdem dürfen wir auf eine physikalische Bewertung der Güte von den verschiedenen Ansätzen für Chiralitätsfunktionen im speziellen Fall „optischer Aktivität von Methanderivaten" hoffen.

II. Die quantenmechanische Behandlung

1. Das Modell

Um den optischen Drehwinkel im Falle der T_d-Derivate auf Eigenschaften der Liganden und die Geometrie ihrer Anordnung zurückzuführen, ist es nötig, Besonderheiten der Eigenfunktionen eines entsprechend spezialisierten Hamiltonoperators in der Born-Oppenheimer-Näherung formal für die Diskussion der Matrixelemente in (1) auszunutzen. Wir betrachten die Atomkerne als klassische Teilchen mit einer fixierten relativen Lage.

Wir können annehmen, daß für alle Methanderivate die kinetische Energie der beiden 1s-Elektronen des zentralen Kohlenstoffatoms in guter Näherung dieselbe ist, und dürfen daher den entsprechenden Term im Hamiltonoperator für unsere Zwecke streichen. Den Beitrag der beiden 1s-Elektronen zusammen mit dem Beitrag des nackten Kohlenstoffkerns zur potentiellen Energie der übrigen Teilchen wollen wir durch das Feld einer vierfach positiven um den Kern konzentrierten und geeignet gewählten Ladungsverteilung beschreiben. Unser Hamiltonoperator enthält also zwei Elektronen weniger als tatsächlich vorhanden und einen zweifach abgeschirmten Kohlenstoffkern. In der Zerlegung

$$\mathscr{H} = \sum_{i}^{1,4} \mathscr{H}_i + \sum_{i<j}^{1,4} \mathscr{H}_{ij}$$

sei $\mathscr{H}_i$ der Energieoperator für ein Teilsystem mit klassischen positiven Ladungen, das aus dem zweifach abgeschirmten Kohlenstoffrumpf und all den Teilchen besteht, die wir im Rahmen einer physikalisch evidenten Modellvorstellung einem Liganden in der Tetraederachsenrichtung i zuordnen. Dazu gehören Atomkerne mit der Ladung $eZ_{i,k}$ und zusammen mit den beiden Bindungselektronen zum zentralen Kohlenstoff n_i Elektronen. Die negative Gesamtladung ist also $-en_i$, die positive ergibt sich zu $e(4+Z_i)$, wenn $Z_i = \sum_k Z_{i,k}$ die Ladung aller Atomkerne des Liganden ausschließlich der des Kohlenstoffrumpfes bezeichnet. In $\mathscr{H}_i$ sind alle Beiträge vom Elektronenspin enthalten, während in $\mathscr{H}_{ij}$ Spin und relativistische Effekte nicht berücksichtigt sind, d. h., hier finden sich nur Coulombterme zwischen den Teilchen der Systeme in den Valenzrichtungen i und j ausschließlich des Kohlenstoffrumpfes.

Die damit gegebene Zerlegung in Teilsysteme entspricht zwar dem physikalischen Bild von der Zuordnung der Teilchen zu Liganden, sie eignet sich aber nicht für eine Störungsrechnung, da die Teilsysteme auch im Falle neutraler Derivate geladen sind und der zweite Term in $\mathscr{H}$ als Störterm zu große Energiebeträge repräsentiert.

Wir verändern daher die Zerlegung, ohne an der Zuordnung der Teilchen etwas zu ändern, durch Verwendung eines T_d-symmetrischen Potentials $\Phi = \sum_i^{1,4} \Phi_i$, das sich aus Komponenten Φ_i zusammensetzt, die die Symmetrie der dreizähligen Tetraederachsen haben und sich wie diese nur in ihrer Orientierung unterscheiden.

Die dem Potential Φ_i entsprechende Ladungsdichte $-\frac{1}{4\pi}\operatorname{div}\operatorname{grad}\Phi_i$ repräsentiere die C_{3v}-symmetrische Verteilung einer dreifach negativen Ladung, mit der wir eine im wesentlichen von den σ-Bindungselektronen der Nachbarliganden herrührende Abschirmung des zentralen Kohlenstoffs gegenüber den übrigen Teilchen des Liganden in der Valenzrichtung i beschreiben wollen. In dieser Abschirmung drückt sich die individuelle Natur der Nachbarliganden nicht aus. Die ligandenspezifische Wechselwirkung kommt dagegen im Störterm des folgendermaßen zerlegten Hamiltonoperators zum Ausdruck:

$$\mathscr{H} = \sum_i^{1,4} (\mathscr{H}_i + \mathscr{V}_i') + \sum_{i<j}^{1,4} (\mathscr{H}_{ij} - \tfrac{1}{3}\{\mathscr{V}_i' + \mathscr{V}_j'\}) .$$

Die Komponenten $\mathscr{H}_i + \mathscr{V}_i'$ des ungestörten Operators

$$\mathscr{H}_0 = \sum_i^{1,4} (\mathscr{H}_i + \mathscr{V}_i')$$

enthalten jetzt zusätzlich die potentielle Energie $\mathscr{V}_i'$ der Teilchen eines Liganden im Feld der Abschirmladung $-\frac{1}{4\pi}\int \operatorname{div}\operatorname{grad}\Phi_i\,d\tau$. Sie sind damit Operatoren für ein im Normalfall $(Z_i = n_i - 1)$ ungeladenes System, das wir den „formal gebundenen Liganden" l_i nennen wollen. Die Komponenten $\mathscr{H}_{ij} - \frac{1}{3}(\mathscr{V}_i' + \mathscr{V}_j')$ beschreiben die verbleibende Wechselwirkung jeweils zwischen den Systemen l_i und l_j.

Die nochmalige Abspaltung eines Terms $\bar{\mathscr{H}}_{ij}$ von $\mathscr{H}_{ij}$, der im Falle neutraler Liganden l_i and l_j ebenfalls als Wechselwirkungsoperator zwischen ungeladenen Systemen gelten kann und für die weitere Diskussion Vorteile bietet, ist durch die folgenden Definitionsgleichungen erklärt:

$$\mathscr{H}_{ij} = \bar{\mathscr{H}}_{ij} + \bar{\bar{\mathscr{H}}}_{ij},$$

$$\bar{\mathscr{H}}_{ij} = \frac{(n_i - 1)(n_j - 1)}{n_i n_j}\,\mathscr{H}_{\mathfrak{E}_i,\mathfrak{E}_j} + \frac{n_i - 1}{n_i}\,\mathscr{H}_{\mathfrak{E}_i,\mathfrak{K}_j} + \frac{n_j - 1}{n_j}\,\mathscr{H}_{\mathfrak{K}_i,\mathfrak{E}_j} + \mathscr{H}_{\mathfrak{K}_i,\mathfrak{K}_j},$$

$$\bar{\bar{\mathscr{H}}}_{ij} = \frac{(n_i - 1) + (n_j - 1) + 1}{n_i n_j}\,\mathscr{H}_{\mathfrak{E}_i,\mathfrak{E}_j} + \frac{1}{n_i}\,\mathscr{H}_{\mathfrak{E}_i,\mathfrak{K}_j} + \frac{1}{n_j}\,\mathscr{H}_{\mathfrak{K}_i,\mathfrak{E}_j}.$$

Dabei bezeichnet $\mathfrak{E}_i$ das System der n_i Elektronen im Liganden l_i, $\mathfrak{K}_i$ das System der Kerne mit Ausnahme des zentralen Kohlenstoffatoms und die Operatoren $\mathscr{H}_{\mathfrak{E}_i,\mathfrak{E}_j}$, $\mathscr{H}_{\mathfrak{E}_i,\mathfrak{K}_j}$, $\mathscr{H}_{\mathfrak{K}_i,\mathfrak{E}_j}$, $\mathscr{H}_{\mathfrak{K}_i,\mathfrak{K}_j}$ die Wechselwirkungsenergien zwischen den entsprechenden Systemen vom Liganden l_i und l_j. Der zentrale Kohlenstoff tritt in $\mathscr{H}_{ij}$, $\bar{\mathscr{H}}_{ij}$ und $\bar{\bar{\mathscr{H}}}_{ij}$ nicht auf. Wir erhalten $\bar{\mathscr{H}}_{ij}$ aus $\mathscr{H}_{ij}$, wenn wir die Elementarladung der Elektronen von den Liganden l_i und l_j um den Faktor $\kappa_i = \frac{n_i - 1}{n_i}$ bzw. $\kappa_j = \frac{n_j - 1}{n_j}$ reduzieren.

In der entsprechenden Zerlegung des Hamiltonoperators

$$\mathscr{H} = \sum_{i}^{1,4} (\mathscr{H}_i + \mathscr{V}_i) + \sum_{i<j}^{1,4} \bar{\mathscr{H}}_{ij} + \sum_{i<j}^{1,4} \left(\bar{\bar{\mathscr{H}}}_{ij} - \tfrac{1}{3}\{\mathscr{V}_i + \mathscr{V}_j\}\right)$$

beurteilen wir die Größenordnung des letzten Terms anhand seiner Erwartungswerte für Eigenfunktionen von T$_d$-Derivaten. Gemäß der Definition von $\bar{\bar{\mathscr{H}}}_{ij}$ erhalten wir für die Erwartungswerte $\langle s|\bar{\bar{\mathscr{H}}}_{ij}|s\rangle$ einen Ausdruck, der auf die Form

$$\langle s|\bar{\bar{\mathscr{H}}}_{ij}|s\rangle = (n_i - 1)\,\frac{e^2}{\bar{r}(s, \mathfrak{E}_i, \mathfrak{E}_j)} + (n_j - 1)\,\frac{e^2}{\bar{r}(s, \mathfrak{E}_i, \mathfrak{E}_j)} + \frac{e^2}{\bar{r}(s, \mathfrak{E}_i, \mathfrak{E}_j)}$$
$$- Z_j\,\frac{e^2}{\bar{r}(s, \mathfrak{E}_i, \mathfrak{K}_j)} - Z_i\,\frac{e^2}{\bar{r}(s, \mathfrak{E}_j, \mathfrak{K}_i)}$$

gebracht werden kann, wobei die $\bar{r}$ Abstände zwischen zwei Orten im Liganden l_i und l_j bezeichnen, an denen wir für den Zweck der Berechnung der potentiellen Energie die Gesamtladung der negativen bzw. positiven Teilchen der beiden Liganden lokalisieren können. Eine entsprechende Zerlegung der Erwartungswerte $\frac{1}{3}\langle s|\mathscr{V}_i + \mathscr{V}_j|s\rangle$ führt auf

$$\frac{1}{3}\langle s|\mathscr{V}_i + \mathscr{V}_j|s\rangle = (n_i - 1)\,\frac{e^2}{\bar{\bar{R}}(s, \mathfrak{E}_i, \Phi_i)} + (n_j - 1)\,\frac{e^2}{\bar{\bar{R}}(s, \mathfrak{E}_j, \Phi_j)} + \frac{e^2}{\bar{\bar{R}}(s, \mathfrak{E}_i, \Phi_i)}$$
$$+ \frac{e^2}{\bar{\bar{R}}(s, \mathfrak{E}_j, \Phi_j)} - Z_j\,\frac{e^2}{\bar{\bar{R}}(s, \Phi_j, \mathfrak{K}_j)} - Z_i\,\frac{e^2}{\bar{\bar{R}}(s, \Phi_i, \mathfrak{K}_i)}.$$

Dabei bezeichnen die $\bar{R}$ entsprechende Abstände von einem repräsentativen Punkt für die dreifach negative Ladung des Abschirmfeldes.

Die Ähnlichkeit in der Struktur der beiden Zerlegungen zusammen mit der speziellen Geometrie der Ligandenanordnung läßt erwarten, daß mit einer geeigneten Wahl der Φ_i die Erwartungswerte $\langle s|\bar{\bar{\mathscr{H}}}_{ij} - \frac{1}{3}(\mathscr{V}_i + \mathscr{V}_j)|s\rangle$ weitgehend unabhängig von der Natur der Liganden den Charakter einer bedeutungslosen Korrektur bekommen.

Das damit formulierte Prinzip zur Festlegung ligandenunabhängiger Φ_i deckt sich mit der Vorstellung, daß jeweils eine Elementarladung aus jeder der benachbarten σ-Bindungen eine positive Kohlenstoffrumpfladung abschirmt. Die beiden Erwartungswerte $\langle s|\bar{\mathcal{H}}_{ij}|s\rangle$ und $\langle s|\bar{\bar{\mathcal{H}}}_{ij}|s\rangle$ haben grundlegend verschiedene Struktur. Der erste hat die Eigenschaft einer Wechselwirkungsenergie zwischen den Teilchen der beiden Teilsysteme mit einer geringfügig veränderten Abschirmung, während der zweite sich aus Anteilen potentieller Energie zusammensetzt, bei denen jeweils eines der beiden Teilsysteme aus einer Elementarladung besteht. Es kann also nur dieser Term für verschiedene Moleküle einer Molekülklasse dem Zahlenwert von $-\frac{1}{3}\langle s|\mathcal{V}_i+\mathcal{V}_j|s\rangle$ ähnlich gemacht werden. Damit wird der Sinn unserer Zerlegung in $\bar{\mathcal{H}}_{ij}$ und $\bar{\bar{\mathcal{H}}}_{ij}$ offenbar.

Das Modell unserer Theorie geht dementsprechend von der Annahme aus, daß für eine umfangreiche Auswahl von T_d-Derivaten der dritte Term im Hamiltonoperator mit einem fest gewählten Abschirmfeld vernachlässigt werden kann, und unser Modelloperator lautet demgemäß:

$$\bar{\mathcal{H}}=\sum_{i}^{1,4}(\mathcal{H}_i+\mathcal{V}_i)+\sum_{i<j}^{1,4}\bar{\mathcal{H}}_{ij}. \tag{3}$$

$\bar{\mathcal{H}}_{ij}$ ist ein Operator, in dem die vom Operator $\mathcal{H}_{ij}-\frac{1}{3}(\mathcal{V}_i+\mathcal{V}_j)$ beschriebene Wechselwirkung zwischen den Systemen l_i und l_j näherungsweise durch die Wechselwirkung zwischen den veränderten Teilsystemen $\bar{l}_i$ und $\bar{l}_j$ ersetzt ist. Man erhält $\bar{l}_i$ und $\bar{l}_j$ aus l_i und l_j, indem man den gemeinsamen Kohlenstoffrumpf einschließlich des Abschirmfeldes unberücksichtigt läßt und die Elementarladung der Elektronen um den Faktor κ_i bzw. κ_j reduziert. Da die Wechselwirkung zwischen l_i und l_j als eine Störung betrachtet werden soll, halten wir den Ersatz von $\mathcal{H}_{ij}-\frac{1}{3}(\mathcal{V}_i+\mathcal{V}_j)$ durch $\bar{\mathcal{H}}_{ij}$ für vertretbar.

Wir orientieren uns noch einmal am Extremfall des isolierten Kohlenstoffatoms über den physikalischen Gehalt des Modelloperators. Im neutralen Kohlenstoffatom enthalten die formal gebundenen Liganden nach unserer Definition jeweils ein Elektron, es gilt also $n_i=1$, alle $\bar{\mathcal{H}}_{ij}$ verschwinden, und unser Modelloperator reduziert sich auf $\mathcal{H}_0$. Die dazugehörigen Eigenfunktionen lassen sich als Zustandsfunktionen des „tetravalenten Kohlenstoffatoms“ interpretieren. Unser Modell bleibt also auch in diesem Grenzfall vernünftig.

2. Struktur der Rosenfeldgleichung im Modell des Energieoperators $\bar{\mathcal{H}}$

Operatoren für elektrische und magnetische Multipolmomente in T_d-Derivaten können nach dem Muster der Zerlegung von $\bar{\mathcal{H}}$ in eine Summe von Operatoren entsprechender Momente der formal gebundenen Liganden l_i zerlegt werden. Insbesondere gilt also für die elektrischen und magnetischen Dipolmomente $\vec{m}$ und $\vec{\mu}$

$$\vec{m}=\sum_{i}^{1,4}\vec{m}_i,\qquad \vec{\mu}=\sum_{i}^{1,4}\vec{\mu}_i.$$

wobei $\vec{m}_i$ und $\vec{\mu}_i$ für alle i auf einen gemeinsamen Aufpunkt im Molelül bezogen sind. Sie sind folgendermaßen definiert:

$$\begin{aligned} \vec{m}_i &= e\left\{Z_i\vec{r}_i - \sum_{k\in\mathfrak{E}_i} \vec{r}_{i,k} + 4\vec{r}_0 - \frac{1}{4\pi e}\int \vec{r}\operatorname{div}\operatorname{grad}\Phi_i(\vec{r})\,d\tau\right\}, \\ \vec{\mu}_i &= -\frac{e}{2M_e c}\sum_{k\in\mathfrak{E}_i}(\vec{r}_{i,k}\times\vec{p}_{i,k} + 2\vec{s}_{i,k}). \end{aligned} \tag{4}$$

Dabei bezeichnen $\vec{r}_0$, $\vec{r}_i$, $\vec{r}_{i,k}$ und $\vec{r}$ Ortsvektoren von dem gemeinsamen, beliebig gewählten Bezugspunkt, und zwar

$\vec{r}_0$ zum Ort des zentralen Kohlenstoffatoms,
$\vec{r}_i$ zum positiven Ladungsschwerpunkt des Teilsystems $\mathfrak{K}_i$,
$\vec{r}_{i,k}$ zum Ort des Elektrons k aus dem System $\mathfrak{E}_i$ und
$\vec{r}$ zum Integrationspunkt mit der infinitesimalen Ladung

$$-\frac{1}{4\pi}\operatorname{div}\operatorname{grad}\Phi_i\,d\tau.$$

M_e bezeichnet die Elektronenmasse.

Wegen

$$\frac{1}{4\pi}\int \vec{r}_0\operatorname{div}\operatorname{grad}\Phi_i(\vec{r})\,d\tau = 3e\vec{r}_0$$

erhalten wir (4) in der Form (4a):

$$\begin{aligned} \vec{m}_i &= e\left\{(Z_i + 1 - n_i)\vec{r}_0 + Z_i(\vec{r}_i - \vec{r}_0) - \sum_{k\in\mathfrak{E}_i}(\vec{r}_{i,k} - \vec{r}_0) - \frac{1}{4\pi e}\int(\vec{r} - \vec{r}_0)\operatorname{div}\operatorname{grad}\Phi_i(\vec{r})\,d\tau\right\}, \\ \vec{\mu}_i &= -\frac{e}{2M_e c}\left\{\sum_{k\in\mathfrak{E}_i}((\vec{r}_{i,k} - \vec{r}_0)\times\vec{p}_{i,k} + 2\vec{s}_{i,k}) + \vec{r}_0\times\sum_{k\in\mathfrak{E}_i}\vec{p}_{i,k}\right\}. \end{aligned} \tag{4a}$$

Die Bedingung $Z_i = n_i - 1$ für neutrale Liganden, die von jetzt ab vorausgesetzt wird und wesentlich in die weitere Diskussion eingeht, führt dazu, daß die elektrischen Dipolmomente $\vec{m}_i$ der Liganden nicht vom Aufpunkt abhängen. Da andere Operatoren wie z. B. die magnetischen Ligandenmomente davon nicht unabhängig sind und da es sich als notwendig herausstellt, gelegentlich für die einzelnen Liganden individuelle Bezugspunkte zu verwenden, wollen wir dafür eine geeignete Nomenklatur benutzen. Wir verändern die Bezeichnung von Operatoren $\mathcal{O}_i$ für einzelne Liganden l_i mit einem gemeinsamen Bezugspunkt im Molekül in $\mathcal{O}(l_i)$, wenn sie auf individuelle Ligandenorte bezogen werden.

Mit dem Ortsvektor $\vec{x}(l_i)$ vom gemeinsamen Bezugspunkt zu dem individuellen Ligandenort von l_i ergibt sich damit für unsere Dipolmomente

$$\begin{aligned} &\vec{m}_i = \vec{m}(l_i) \\ \text{und}\quad &\vec{\mu}_i = \vec{\mu}(l_i) - \frac{e}{2M_e c}\,\vec{x}(l_i)\times\sum_{k\in\mathfrak{E}_i}\vec{p}_{i,k} \end{aligned} \tag{5}$$

und für ihre Matrixelemente

$$\begin{aligned} &\langle s|\vec{m}_i|t\rangle = \langle s|\vec{m}(l_i)|t\rangle \\ \text{und}\quad &\langle s|\vec{\mu}_i|t\rangle = \langle s|\vec{\mu}(l_i)|t\rangle + \frac{i\pi}{c}\,\nu_{st}\,\vec{x}(l_i)\times\langle s|\vec{m}(l_i)|t\rangle. \end{aligned} \tag{5a}$$

da mit fixierten Kernen die Beziehung gilt

$$\frac{1}{2M_e c}\left\langle s\left|-e\sum_{k\in\mathfrak{E}_l}\vec{p}_{l,k}\right|t\right\rangle=\frac{i\pi}{c}\nu_{st}\left\langle s\left|-e\sum_{k\in\mathfrak{E}_l}\vec{r}_{l,k}\right|t\right\rangle=\frac{i\pi}{c}\nu_{st}\langle s|\vec{m}(l_l)|t\rangle .$$

Für die Wechselwirkung zwischen Liganden benötigen wir elektrische Multipolmomente, die an der Wechselwirkung teilnehmen, also den abgeschirmten Systemen $\bar{l}_l$ zugeschrieben werden können. Magnetische Multipolmomente tragen in unserem Modell zur Wechselwirkung definitionsgemäß nichts bei. Für das elektrische Dipolmoment $\vec{m}(\bar{l}_l)$ ergibt sich

$$\vec{m}(\bar{l}_l)=e\kappa_l\left(n_l\vec{r}_l-\sum_{k\in\mathfrak{E}_l}\vec{r}_{l,k}\right)$$

und durch Vergleich mit (4a)

$$\vec{m}(\bar{l}_l)=\kappa_l(\vec{m}(l_l)+\vec{c}_l)$$

mit

$$\vec{c}_l=e(\vec{r}_l-\vec{r}_0)+\frac{1}{4\pi}\int(\vec{r}-\vec{r}_0)\operatorname{div}\operatorname{grad}\Phi_l(\vec{r})\,d\tau . \tag{6}$$

3. *Polarisierbarkeitstensoren und ihre Zerlegung nach Teilsystemen des Modells*

Der Tensor ${}^{(J)}\gamma$ hat klassisch die Bedeutung einer elektromagnetischen Polarisierbarkeit, die als Proportionalitätsfaktor des magnetischen Feldes $\vec{H}$ auftritt, wenn man das durch äußere Felder induzierte elektrische Dipolmoment $\vec{m}^{\text{ind.}}$ eines elektrischen Systems nach den induzierenden Feldern $\vec{E}$ und $\vec{H}$ entwickelt.

$$m_\varrho^{\text{ind.}}=\sum_\sigma^{1,3}\{\alpha_{\varrho\sigma}E_\sigma+\gamma_{\varrho\sigma}H_\sigma+\cdots\} . \tag{7}$$

Dabei ist α der Tensor der elektrischen Polarisierbarkeit. Im Falle zeitlich periodischer Felder gilt dieselbe Entwicklung mit komplexen Tensoren $\alpha={}^{(R)}\alpha-i\nu{}^{(J)}\alpha$ und $\gamma={}^{(R)}\gamma-i\nu{}^{(J)}\gamma$.

Für eine klassische Interpretation der späteren Störungsrechnung ist es zweckmäßig, entsprechende Entwicklungen von α und γ nach einem induzierenden elektrostatischen Feld $\vec{E}'$ zu verwenden. Sie lauten:

$$\begin{aligned}\alpha_{\varrho\sigma}(\vec{E}')&=\alpha_{\varrho\sigma}+\sum_\tau^{1,3}A_{\varrho\sigma\tau}E'_\tau+\cdots,\\ \gamma_{\varrho\sigma}(\vec{E}')&=\gamma_{\varrho\sigma}+\sum_{\tau,\upsilon}^{1,3}\{\Gamma_{\varrho\sigma\tau}E'_\tau+\tfrac{1}{2}\Delta_{\varrho\sigma\tau\upsilon}E'_\tau E'_\upsilon+\cdots\} .\end{aligned} \tag{7a}$$

Dabei sind A und Γ die elektrische und elektromagnetische Hyperpolarisierbarkeit und Δ eine Hyperpolarisierbarkeit höherer Stufe. Sie sind ebenso wie α und γ komplex. Mit Ausnahme von Δ findet sich die quantenmechanische Definition der hier auftretenden Tensoren in Anhang *B*.

Wir benötigen für unsere Aufgabe die oben erklärten Tensoren für das Molekül und für Teilsysteme des Moleküls. Die entsprechenden Zerlegungen erfolgen allgemein nach Prinzipien, die wir jetzt am speziellen Tensor ${}^{(J)}\gamma$ besprechen wollen.

Da es darauf ankommt, Eigenschaften des Moleküls auf Eigenschaften von Teilsystemen und diese weiter auf Eigenschaften von Liganden zurückzuführen, ist eine Nomenklatur erforderlich, die uns eindeutig zeigt, wann individuelle Eigenschaften von Teilsystemen vorliegen. Es ist daher zu beachten, daß in der quantenmechanischen Form von Tensoren des Typs ${}^{(J)}\gamma$ individuelle Teilsysteme nur dann charakterisiert sind, wenn einerseits nur Operatoren für dieses Teilsystem enthalten sind, wenn außerdem die Eigenfunktionen sich auf dieses Teilsystem beziehen und wenn der Ort, an dem diese Eigenschaft beschrieben wird, individueller Ort des Teilsystems ist, also nicht notwendig mehreren Teilsystemen gemeinsam ist.

Die interessierenden Teilsysteme sind durch folgende Energieoperatoren definiert:

$$\langle l_i\rangle \doteqdot \mathscr{H}_i + \mathscr{V}_i,$$
$$\langle l_i, l_j\rangle \doteqdot \mathscr{H}_i + \mathscr{V}_i + \mathscr{H}_j + \mathscr{V}_j + \bar{\mathscr{H}}_{ij},$$
$$\langle l_i, l_j, l_k\rangle \doteqdot \mathscr{H}_i + \mathscr{V}_i + \mathscr{H}_j + \mathscr{V}_j + \mathscr{H}_k + \mathscr{V}_k + \bar{\mathscr{H}}_{ij} + \bar{\mathscr{H}}_{jk} + \bar{\mathscr{H}}_{ki}.$$

Falls in ${}^{(J)}\gamma$ nur die Operatoren eines solchen Teilsystems auftreten, verwenden wir die Bezeichnung

$${}^{(J)}\gamma^{\langle i\rangle},\ {}^{(J)}\gamma^{\langle i,j\rangle} \quad \text{bzw.} \quad {}^{(J)}\gamma^{\langle i,j,k\rangle}.$$

Diese Tensoren beschreiben verschiedene Teilsysteme betreffende Eigenschaften im Molekül. Falls die Tensoren mit den Eigenfunktionen der jeweiligen Teilsysteme gebildet sind und mit individuellen Aufpunkten verstanden werden dürfen, bezeichnen wir sie mit

$${}^{(J)}\gamma(l_i),\ {}^{(J)}\gamma(l_i, l_j) \quad \text{bzw.} \quad {}^{(J)}\gamma(l_i, l_j, l_k).$$

Erst wenn diese Schreibweise vorliegt, können wir schließen, daß es sich um individuelle Eigenschaften der Teilsysteme handelt.

Die Zerlegung von ${}^{(J)}\gamma$ gelingt mit der Umformung[4]

$$\begin{aligned}{}^{(J)}\gamma &= \frac{2}{h}\,\mathrm{Im}\sum_s \sum_i^{1,4} \frac{\langle o|\vec{m}_i|s\rangle \cdot \langle s|\vec{\mu}_i|o\rangle}{\nu_{so}^2 - \nu^2} + \frac{2}{h}\,\mathrm{Im}\sum_s \sum_{i\neq j}^{1,4} \frac{\langle o|\vec{m}_i|s\rangle \cdot \langle s|\vec{\mu}_j|o\rangle}{\nu_{so}^2 - \nu^2}\\ &= -\frac{4}{h}\,\mathrm{Im}\sum_s \sum_i^{1,4} \frac{\langle o|\vec{m}_i|s\rangle\,\langle s|\vec{\mu}_i|o\rangle}{\nu_{so}^2 - \nu^2} + \frac{2}{h}\,\mathrm{Im}\sum_s \sum_{i<j}^{1,4} \frac{\langle o|\vec{m}_i + \vec{m}_j|s\rangle\,\langle s|\vec{\mu}_i + \vec{\mu}_j|o\rangle}{\nu_{so}^2 - \nu^2},\end{aligned}$$

so daß mit den Definitionsgleichungen

$${}^{(J)}\gamma^{\langle i\rangle} = \frac{2}{h}\,\mathrm{Im}\sum_s \frac{\langle o|\vec{m}_i|s\rangle\,\langle s|\vec{\mu}_i|o\rangle}{\nu_{so}^2 - \nu^2}$$

$${}^{(J)}\gamma^{\langle i,j\rangle} = \frac{2}{h}\,\mathrm{Im}\sum_s \frac{\langle o|\vec{m}_i + \vec{m}_j|s\rangle\,\langle s|\vec{\mu}_i + \vec{\mu}_j|o\rangle}{\nu_{so}^2 - \nu^2}$$

---

[4] Es sei daran erinnert, daß der Fall entarteter Grundzustände nur der Übersichtlichkeit halber in den Formeln nicht aufgenommen ist. Die entsprechende Ergänzung kann an allen Stellen dieser Arbeit ohne Mühe vorgenommen werden.

die Zerlegung in der folgenden Form erscheint:

$$^{(J)}\gamma = -2\sum_{i}^{1,4} {}^{(J)}\gamma^{\langle i\rangle} + \sum_{i<j}^{1,4} {}^{(J)}\gamma^{\langle i,j\rangle}\,. \tag{8}$$

4. *Lösung für* $[\omega]$ *im Modell des ungestörten Operators* $\mathscr{H}_0$

Mit den Vorbereitungen des letzten Kapitels ist unser Problem im Modell des verkürzten Hamiltonoperators $\mathscr{H}_0 = \sum_{i}^{1,4} (\mathscr{H}_i + \mathscr{V}_i)$ einfach zu lösen.

Die Eigenfunktionen von $\mathscr{H}_0$ sind Produkte von Eigenfunktionen zu $\mathscr{H}_i + \mathscr{V}_i$, wir haben also

$$|s\rangle^{(0)} = |s_1\rangle\,|s_2\rangle\,|s_3\rangle\,|s_4\rangle = |s_1\,s_2\,s_3\,s_4\rangle$$

mit dem Grundzustand

$$|o\rangle^{(0)} = |o_1\,o_2\,o_3\,o_4\rangle\,.$$

Da die Quantenzahlen s die Eigenfunktionen des Moleküls, die Quantenzahlen s_i die Eigenfunktionen des Liganden l_i numerieren, ist zu bemerken, daß aus $t \neq s$ nur für einen der Indizes $i = 1, 2, 3, 4$ notwendig eine Ungleichung $t_i \neq s_i$ folgt. Für die Matrixelemente der Dipolmomente in nullter störungstheoretischer Ordnung notieren wir demgemäß

$$[\langle o|\vec{m}_i|s\rangle]^{(0)} = \langle o_i|\vec{m}_i|s_i\rangle \prod_{k(\neq i)}^{1,4} \delta_{s_k o_k}\,,$$

$$[\langle s|\vec{\mu}_i|o\rangle]^{(0)} = \langle s_i|\vec{\mu}_i|o_i\rangle \prod_{k(\neq i)}^{1,4} \delta_{s_k o_k}$$

und wegen $[\nu_{so}]^{(0)} = \sum_{i}^{1,4} \nu_{s_i o_i}$

$$\left[\frac{1}{\nu_{so}^2 - \nu^2}\right]^{(0)} \prod_{k(\neq i)}^{1,4} \delta_{s_k o_k} = \frac{1}{\nu_{s_i o_i}^2 - \nu^2}\,.$$

Daraus folgt

$$[{}^{(J)}\gamma^{\langle i\rangle}]^{(0)} = \frac{2}{h}\,\mathrm{Im}\sum_{s_i} \frac{\langle o_i|\vec{m}_i|s_i\rangle\;\langle s_i|\vec{\mu}_i|o_i\rangle}{\nu_{s_i o_i}^2 - \nu^2}\,,$$

$$[{}^{(J)}\gamma^{\langle i,j\rangle}]^{(0)} = [{}^{(J)}\gamma^{\langle i\rangle}]^{(0)} + [{}^{(J)}\gamma^{\langle j\rangle}]^{(0)}\,.$$

$^{(J)}\gamma$ ist eine ortsabhängige Größe, $\mathrm{Sp}\,^{(J)}\gamma$ dagegen nicht. Demnach erhalten wir die Gleichungen

$$[\mathrm{Sp}\,^{(J)}\gamma^{\langle i\rangle}]^{(0)} = \mathrm{Sp}\,^{(J)}\gamma(l_i), \qquad [\mathrm{Sp}\,^{(J)}\gamma^{\langle i,j\rangle}]^{(0)} = \mathrm{Sp}\,^{(J)}\gamma(l_i) + \mathrm{Sp}\,^{(J)}\gamma(l_j)$$

und wegen (8)

$$[\mathrm{Sp}\,^{(J)}\gamma]^{(0)} = \sum_{i}^{1,4} \mathrm{Sp}\,^{(J)}\gamma(l_i)\,. \tag{9a}$$

Da die Eigenfunktionen in $^{(J)}\gamma(l_i)$ exakte Eigenfunktionen für l_i sind und $\mathrm{Sp}\,^{(J)}\gamma(l_i)$ eine pseudoskalare Funktion ist, muß $\mathrm{Sp}\,^{(J)}\gamma(l_i)$ für achirale Liganden verschwinden. Die entsprechende Argumentation auf phänomenologischer Basis lautet:

$K\,\mathrm{Sp}\,^{(J)}\gamma(l_i)$ ist der Rosenfeldausdruck für den formal gebundenen Liganden l_i, beschreibt also den optischen Drehwinkel für den Liganden l_i im Rahmen des Rosenfeldschen Ansatzes. Wir erhalten daher das Resultat:

$$[\omega]^{(0)} = \sum_i^{1,4} [\omega(l_i)] \quad \text{mit} \quad [\omega(l_i)] = K\,\mathrm{Sp}\,^{(J)}\gamma(l_i)\,. \tag{9b}$$

Der optische Drehwinkel des Moleküls ist in nullter störungstheoretischer Ordnung die Summe der Drehwinkel der einzelnen Liganden l_i. Er verschwindet, wenn die einzelnen Liganden inaktiv, also achiral sind. Chirale Liganden sind aber mit den Voraussetzungen über T_d-Derivate ausgeschlossen.

Wir haben demnach zur Berechnung der optischen Aktivität bei T_d-Derivaten die Wechselwirkung zwischen den Liganden zu berücksichtigen und wollen diesen Effekt nach den Prinzipien einer Störungsrechnung mit $\sum_{i<j}^{1,4} \mathcal{H}_{ij}$ als Störoperator behandeln.

Es sei bemerkt, daß $[\omega]^{(0)}$ eine Komponente zum optischen Drehwinkel für Methanderivate mit chiralen Liganden darstellt, die bei großer Aktivität der Liganden möglicherweise den relevanten Anteil des Phänomens beschreibt. Unter diesem erweiterten Aspekt gibt uns die folgende Störungsrechnung die noch nicht erfaßten Komponenten einer qualitativ vollständigen Chiralitätsfunktion für Methanderivate mit T_d-symmetrischen Bindungsrichtungen und Liganden beliebiger Symmetrie.

5. *Gegenüberstellung der störungstheoretischen Approximationsaspekte, Gültigkeitsbereich des Modells $\bar{\mathcal{H}}$ und der vereinfachte Modelloperator $\tilde{\mathcal{H}}$*

Ausgangspunkt für unsere Theorie ist der Rosenfeldterm, ein Ausdruck für den Drehwinkel, der selbst das Resultat einer Störungsrechnung ist und als erstes Glied in einer Reihenentwicklung des Drehwinkels nach Multipolen erscheint. Der vollständige quantenmechanische Ausdruck für den Drehwinkel im Transparenzgebiet gestattet nach Chiu [4] eine Entwicklung der Form

$$[\omega] = \mathrm{Sp} \sum_L K_L \left(\mathrm{Im} \sum_s \frac{\langle o|\mathcal{O}_L|s\rangle\ \langle s|\bar{\mathcal{O}}_L|o\rangle}{\nu_{so}^2 - \nu^2} \right) \tag{10}$$

mit Operatoren $\mathcal{O}_L$ und $\bar{\mathcal{O}}_L$ für elektrische und magnetische Multipolmomente vom Rang L, also mit der speziellen Bedeutung $\mathcal{O}_1 = \vec{m}$, $\bar{\mathcal{O}}_1 = \vec{\mu}$ und $K_1 = \frac{2}{3}K$.

Die Argumentation des letzten Kapitels für den ungestörten Modelloperator $\mathcal{H}_0$ läßt sich in allen Punkten entsprechend auf die Glieder mit $L > 1$ übertragen und führt wieder zur Gl. (9b) mit dem Unterschied, daß $[\omega(l_i)]$ durch den Rosenfeldausdruck und alle seine Korrekturterme beschrieben wird. Es wird sich zeigen, daß entsprechende Beziehungen zwischen dem Drehwinkel des Moleküls und den Drehwinkeln von Teilsystemen in jeder störungstheoretischen Ordnung davon unabhängig sind, ob der Rosenfeldausdruck allein oder zusammen mit Korrekturtermen aus (10) zur Diskussion gestellt wird. Da Beziehungen der genannten Art der Zerlegung des Drehwinkels nach Komponenten einer qualitativ vollständigen Chiralitätsfunktion entsprechen, insoweit sie mit der vorgegebenen störungstheoretischen Ordnung beschreibbar sind, kann geschlossen werden, daß in der quantenmechanischen Beschreibung des optischen Drehwinkels in jeder vorgegebenen störungstheoretischen Ordnung keine qualitativen Züge verlorengehen, wenn man sich im Ausdruck (10) auf die Diskussion des Rosenfeldgliedes beschränkt.

Wir werden die Störungsrechnung einerseits mit $\sum\limits_{i<j}^{1,4} \bar{\mathscr{H}}_{ij}$ als Störterm bis zur zweiten Ordnung durchführen und dabei eine physikalische Interpretation des zweiten Näherungsverfahrens erhalten. Für eine detaillierte Form des Drehwinkels in Abhängigkeit von Eigenschaften einzelner Liganden machen wir andererseits von einer weiteren Näherung Gebrauch, die sich aus einer Reihenentwicklung des Störterms in $\bar{\mathscr{H}}$ ergibt.

Eine Entwicklung von $\bar{\mathscr{H}}_{ij}$ nach Potenzen der reziproken Abstände zwischen ligandenspezifischen Punkten der Systeme l_i und l_j führt zur Form

$$\bar{\mathscr{H}}_{ij} = \sum_p \bar{\mathscr{H}}_{ij}^{[p]},$$

wobei der Index $p = L_i + L_j$ die Summe der Ränge von elektrischen Multipolmomenten der Liganden l_i und l_j bezeichnet. Wir können die Entwicklungsstellen mit den positiven Ladungsschwerpunkten $\vec{r}_i$ und $\vec{r}_j$ der Kernsysteme $\mathfrak{K}_i$ und $\mathfrak{K}_j$ identifizieren. Wegen der Voraussetzung $Z_i = n_i - 1$ für neutrale Liganden ist das erste von Null verschiedene Glied $\bar{\mathscr{H}}_{ij}^{[2]}$ der Operator für die Dipol-Dipol-Wechselwirkungsenergie:

$$\bar{\mathscr{H}}_{ij}^{[2]} = \vec{m}(\bar{l}_i) \cdot T_{ij} \cdot \vec{m}(\bar{l}_j)\,.$$

In dem Tensor

$$T_{ij} = \frac{1}{a_{ij}^3}\left(1 - 3\,\frac{\vec{a}_{ij} \circ \vec{a}_{ij}}{a_{ij}^2}\right)$$

sind die Bezeichnungen $\vec{r}_j - \vec{r}_i = \vec{a}_{ij}$ und $|\vec{a}_{ij}| = a_{ij}$ verwendet; später werden auch entsprechende Bezeichnungen für Vektoren vom zentralen Kohlenstoff zur Entwicklungsstelle, $\vec{r}_i - \vec{r}_0 = \vec{a}_i$, und ihre Beträge $|\vec{a}_i| = a_i$ benutzt.

$\bar{\mathscr{H}}_{ij}^{[3]}$ gibt die Dipol-Quadrupol-Wechselwirkungsenergie

$$\bar{\mathscr{H}}_{ij}^{[3]} = \vec{m}(\bar{l}_i) \cdot S_{ij} \cdot \Theta(\bar{l}_j) \cdot \vec{a}_{ji} + \vec{m}(\bar{l}_j) \cdot S_{ji} \cdot \Theta(\bar{l}_i) \cdot \vec{a}_{ij}$$

mit

$$S_{ij} = \frac{2}{a_{ij}^5}\left(1 - \frac{5}{2}\,\frac{\vec{a}_{ij}\,\vec{a}_{ij}}{a_{ij}^2}\right)$$

und dem auf den Ort $\vec{r}_i$ bezogenen Quadrupolmoment $\Theta(\bar{l}_i)$ (s. Anhang *B*). $\bar{\mathscr{H}}_{ij}^{[4]}$ gibt die Dipol-Oktopol- und Quadrupol-Quadrupol-Wechselwirkungsenergie usw.

Der früher besprochene Einfluß der Abschirmung auf die Wechselwirkung äußert sich darin, daß in den obigen Formeln die Multipolmomente der Systeme $\bar{l}_i$ und $\bar{l}_j$ statt l_i und l_j erscheinen.

Entsprechend der Zerlegung

$$\bar{\mathscr{H}} = \mathscr{H}_0 + \sum_{p \geqq 2}\sum_{i} \bar{\mathscr{H}}_{i}^{[p]} = \mathscr{H}' + \sum_{p \geqq 3}\sum_{i<j} \bar{\mathscr{H}}_{ij}^{[p]}$$

diskutieren wir im folgenden zwei Modelle: das schon besprochene zum Operator $\bar{\mathscr{H}}$ und ein vereinfachtes, durch $\tilde{\mathscr{H}}$ definiertes Modell,

$$\bar{\mathscr{H}} = \mathscr{H}_0 + \sum_{i<j} \bar{\mathscr{H}}_{ij} \quad \text{und} \quad \tilde{\mathscr{H}} = \mathscr{H}_0 + \sum_{i<j} \bar{\mathscr{H}}_{ij}^{[2]} .$$

Wir bezeichnen mit $[\ ]^{(m)}$ störungstheoretische Korrekturen der Ordnung m mit dem Störoperator $\sum_{i<j} \bar{\mathscr{H}}_{ij}$ und mit $[\ ]^{(\tilde{m})}$ die entsprechenden Korrekturen mit $\sum_{i<j} \bar{\mathscr{H}}_{ij}^{[2]}$ als Störoperator. Im Modell $\tilde{\mathscr{H}}$ tragen nur elektrische Dipolmomente zur Wechselwirkung bei; für die auf Eigenfunktionen der Liganden bezogenen Matrixelemente gelten wegen (6) die Beziehungen

$$\begin{aligned} \langle s_i|\vec{m}(\bar{l}_i)|t_i\rangle &= \kappa_i \langle s_i|\vec{m}(l_i)|t_i\rangle \quad \text{für} \quad s_i \neq t_i , \\ \langle s_i|\vec{m}(\bar{l}_i)|s_i\rangle &= \kappa_i(\langle s_i|\vec{m}(l_i)|s_i\rangle + \vec{c}_i) . \end{aligned} \tag{11}$$

Der Approximationsgrad des Modells $\tilde{\mathscr{H}}$ hängt im Gegensatz zu $\bar{\mathscr{H}}$ von einer glücklichen Wahl der Entwicklungsstellen ab. Wir können annehmen, daß die positiven Ladungsschwerpunkte der Teilsysteme $\mathfrak{K}_i$ mit den Stellen einer optimalen Konvergenz in der Multipolentwicklung in guter Näherung zusammenfallen, die formalen Konsequenzen hängen von dieser Frage nicht ab. Die Bedeutung der Vektoren $\vec{d}_i$ und $\vec{d}_{jt}$ ist also nicht auf Ladungsschwerpunkte festgelegt.

Sowohl der Rosenfeldausdruck wie der Modelloperator $\tilde{\mathscr{H}}$ beziehen sich auf das jeweils erste Glied verschiedener Multipolentwicklungen. In beiden Fällen nimmt der Beitrag zum optischen Drehwinkel mit wachsendem Grad in den Multipolen rasch ab. Trotzdem sind wir mit zwei nichtkommensurablen Approximationsprinzipien konfrontiert. Erst die Feststellung, daß in einer bestimmten störungstheoretischen Ordnung auftretende Beiträge zum optischen Drehwinkel, die für besondere geometrische Zusatzbedingungen wie z. B. die T_d-Bedingung im Modell $\tilde{\mathscr{H}}$ verschwinden, auch im Modell $\bar{\mathscr{H}}$ und damit auch für alle Glieder in (10) verschwinden, rechtfertigt eine Approximation des Drehwinkels auf der Basis des Rosenfeldterms durch störungstheoretische Korrekturen zunehmender Ordnung im Modell $\tilde{\mathscr{H}}$.

Obwohl die vorliegende Arbeit zum Ziel hat, den optischen Drehwinkel für T_d-Derivate in Einzelheiten zu diskutieren, und dabei vom Modell $\tilde{\mathscr{H}}$ Gebrauch macht, wird die Störungsrechnung so ausführlich vorgeführt, daß gewünschtenfalls auch allgemeine Methanderivate mit den bereitgestellten Mitteln behandelt werden können. Die dazu erforderliche Übersicht kann bereits im Modell $\bar{\mathscr{H}}$ gefunden werden. Wir wollen daher die vorbereitenden Bemerkungen zur Störungsrechnung mit einer Diskussion über den Gültigkeitsbereich des Modells $\bar{\mathscr{H}}$ abschließen.

Im Modelloperator $\bar{\mathscr{H}}$ manifestiert sich ein bewußter Verzicht auf gewisse Details, ein Verzicht, der unvermeidbar mit der Absicht verbunden ist, Eigenschaften von verschiedenen Molekülen einer Molekülklasse allgemein zu formulieren. Im Rahmen des damit festgelegten Modells gibt die störungstheoretische Ordnung, bis zu der das Problem behandelt wird, einen Approximationsaspekt. Das Modell $\bar{\mathscr{H}}$ und ebenso $\tilde{\mathscr{H}}$ enthält von der Voraussetzung über T_d-Derivate nur die T_d-Symmetrie der Bindungsrichtungen in Form eines Abschirmfeldes entsprechender Symmetrie. Eine Abweichung von dieser Voraussetzung wird also in unserem Modell nur insoweit nicht erfaßt, als eine Veränderung des Abschirmpotentials unberücksichtigt bleibt. Es darf daher angenommen werden, daß geringfügige Deformationen der Bindungswinkel beliebiger Art in den Gültigkeitsbereich des Modelloperators $\bar{\mathscr{H}}$ fallen, also zwar nicht im verkürzten Operator $\mathscr{H}_0$, aber über entsprechende Abstände in den Wechselwirkungstermen hinreichend Berücksichtigung finden.

In der nullten störungstheoretischen Ordnung für $\bar{\mathscr{H}}$ sind Effekte dieser Art ohne Einfluß auf den Drehwinkel. Ausschließlich chirale Liganden führen zu einem Beitrag nullter Ordnung.

Eine Preisgabe von Symmetrievoraussetzungen in der T_d-Bedingung wie z. B. Verdrehungen C_{3v}-symmetrischer Liganden um ihre Bindungsachsen, die Miteinbeziehung von Liganden beliebiger achiraler Symmetrie oder merkliche Abweichungen von der T_d-Symmetrie des Gerüstes im Sinne einer Reduktion auf eine achirale Untersymmetrie D_{2d}, C_{3v}, C_{2v} oder C_s liefern also keine Beiträge nullter Ordnung, werden aber mit der Störungsrechnung im Modell $\bar{\mathscr{H}}$ und $\tilde{\mathscr{H}}$ erfaßt. Die formale Behandlung beider Modelle bleibt dieselbe, wenn Abschirmfelder mit den genannten Untersymmetrien verwendet werden.

Abweichungen der genannten Art können dazu führen, daß der optische Drehwinkel eine Chiralitätsfunktion mit mehreren Komponenten wird und demzufolge in der Störungsrechnung der T_d-Derivate zutreffende Schlüsse über das Verschwinden gewisser Teilausdrücke nicht mehr gültig bleiben. Aus der allgemeinen Übersicht, die uns die Theorie der Chiralitätsfunktionen zur Verfügung stellt, wissen wir, daß es sich bei diesen Teilausdrücken um Chiralitätsfunktionen handelt, die neu auftretende Beiträge zum optischen Drehwinkel für Moleküle veränderter Molekülklassen beschreiben. Die bei T_d-Derivaten ausschließlich auftretende Chiralitätsfunktion repräsentiert für Methanderivate mit den genannten Symmetrieabweichungen eine nichtverschwindende T_d-Komponente. Ihr Beitrag zum optischen Drehwinkel kann auch nicht näherungsweise durch andere Komponenten, z. B. durch Glieder niedrigerer Ordnung, beschrieben werden. Die Relevanz dieses Beitrags hängt vom Ausmaß der oben genannten Abweichungen ab, die T_d-Komponente beschreibt bei kleinen Abweichungen den relevanten Teil des Gesamtphänomens und bekommt für zunehmende Abweichungen schließlich den Charakter einer bedeutungslosen Korrektur. Die Signifikanz der Beiträge von verschiedenen Komponenten entspricht erst bei hinreichend großen Abweichungen von der T_d-Situation der störungstheoretischen Ordnung, in der sie erstmals beschrieben werden.

6. *Störungsrechnung erster Ordnung*

Im Anhang *A* findet sich ein kurzer Abriß der allgemeinen Störungstheorie bis zur zweiten Ordnung mit spezieller Ausrichtung auf das hier vorliegende Problem. Es wird dort auch gezeigt, daß alle Schlüsse, die wir aus den nachfolgenden Formeln für die Matrixelemente mit nichtentarteten Eigenfunktionen ziehen, unverändert bleiben, wenn Entartung vorliegt.

Die Korrektur erster Ordnung für den Tensor ${}^{(J)}\gamma$ lautet:

$$[{}^{(J)}\gamma]^{(1)} = \sum_{\varrho,\sigma,\tau}^{\varrho+\sigma+\tau=1} \left\{ \frac{2}{h} \operatorname{Im} \sum_{s} \sum_{i,j} \left[\frac{1}{\nu_{so}^2 - \nu^2} \right]^{(\varrho)} [\langle o|\vec{m}_i|s\rangle]^{(\sigma)} \circ [\langle s|\vec{\mu}_j|o\rangle]^{(\tau)} \right\}.$$

Die Störungsrechnung liefert

$$[\langle o|\vec{m}_i|s\rangle]^{(1)}=\frac{1}{h}\sum_{k}^{k\neq i}\left\{\begin{aligned}&\sum_{t}{}'\frac{\langle o_i o_k|\bar{\mathcal{H}}_{ik}|t_i t_k\rangle}{\sum\limits_{\kappa}\nu_{o_\kappa t_\kappa}}\langle t_i|\vec{m}_i|s_i\rangle\prod_{\kappa}^{\kappa\neq i,k}\delta_{t_\kappa o_\kappa}\prod_{\kappa}^{\kappa\neq i}\delta_{t_\kappa s_\kappa}\\&+\sum_{t}{}'\langle o_i|\vec{m}_i|t_i\rangle\frac{\langle t_i t_k|\bar{\mathcal{H}}_{ik}|s_i s_k\rangle}{\sum\limits_{\kappa}\nu_{s_\kappa t_\kappa}}\prod_{\kappa}^{\kappa\neq i,k}\delta_{t_\kappa s_\kappa}\prod_{\kappa}^{\kappa\neq i}\delta_{t_\kappa o_\kappa}\end{aligned}\right\},$$

$$[\langle s|\vec{\mu}_j|o\rangle]^{(1)}=\frac{1}{h}\sum_{k}^{k\neq j}\left\{\begin{aligned}&\sum_{t}{}'\frac{\langle s_j s_k|\bar{\mathcal{H}}_{jk}|t_j t_k\rangle}{\sum\limits_{\kappa}\nu_{s_\kappa t_\kappa}}\langle t_j|\vec{\mu}_j|o_j\rangle\prod_{\kappa}^{\kappa\neq j,k}\delta_{t_\kappa s_\kappa}\prod_{\kappa}^{\kappa\neq j}\delta_{t_j o_j}\\&+\sum_{t}{}'\langle s_j|\vec{\mu}_j|t_j\rangle\frac{\langle t_j t_k|\bar{\mathcal{H}}_{jk}|o_j o_k\rangle}{\sum\limits_{\kappa}\nu_{o_\kappa t_\kappa}}\prod_{\kappa}^{\kappa\neq j,k}\delta_{t_\kappa o_\kappa}\prod_{\kappa}^{\kappa\neq j}\delta_{t_\kappa s_\kappa}\end{aligned}\right\}$$

und damit

$$\left|\frac{1}{\nu_{so}^2-\nu^2}\right|^{(0)}[\langle o|\vec{m}_i|s\rangle]^{(1)}\cdot[\langle s|\vec{\mu}_j|o\rangle]^{(0)}=-\frac{1}{h}\,\frac{1}{\nu_{s_j o_j}^2-\nu^2}\prod_{\kappa}^{\kappa\neq j}\delta_{s_\kappa o_\kappa}$$

$$\cdot\sum_{k}^{k\neq i}\left\{\begin{aligned}&\sum_{t}{}'\frac{\langle o_i o_k|\bar{\mathcal{H}}_{ik}|t_i t_k\rangle}{\nu_{o_i t_i}+\nu_{o_k t_k}}\langle t_i|\vec{m}_i|s_i\rangle\circ\langle s_j|\vec{\mu}_j|o_j\rangle\prod_{\kappa}^{\kappa\neq i,k}\delta_{t_\kappa o_\kappa}\prod_{\kappa}^{\kappa\neq i}\delta_{t_\kappa s_\kappa}\\&+\sum_{t}{}'\frac{\langle t_i t_k|\bar{\mathcal{H}}_{ik}|s_i s_k\rangle}{\nu_{s_i t_i}+\nu_{s_k t_k}}\langle o_i|\vec{m}_i|t_i\rangle\circ\langle s_j|\vec{\mu}_j|o_j\rangle\prod_{\kappa}^{\kappa\neq i,k}\delta_{t_\kappa s_\kappa}\prod_{\kappa}^{\kappa\neq i}\delta_{t_\kappa o_\kappa}\end{aligned}\right\},$$

$$\left|\frac{1}{\nu_{so}^2-\nu^2}\right|^{(0)}[\langle o|\vec{m}_i|s\rangle]^{(0)}\,[\langle s|\vec{\mu}_j|o\rangle]^{(1)}=-\frac{1}{h}\,\frac{1}{\nu_{s_i o_i}^2-\nu^2}\prod_{\kappa}^{\kappa\neq i}\delta_{s_\kappa o_\kappa}$$

$$\cdot\sum_{k}^{k\neq j}\left\{\begin{aligned}&\sum_{t}{}'\frac{\langle s_j s_k|\bar{\mathcal{H}}_{jk}|t_j t_k\rangle}{\nu_{s_j t_j}+\nu_{s_k t_k}}\langle o_i|\vec{m}_i|s_i\rangle\cdot\langle t_j|\vec{\mu}_j|o_j\rangle\prod_{\kappa}^{\kappa\neq j,k}\delta_{t_\kappa s_\kappa}\prod_{\kappa}^{\kappa\neq j}\delta_{t_\kappa o_\kappa}\\&+\sum_{t}{}'\frac{\langle t_j t_k|\bar{\mathcal{H}}_{jk}|o_j o_k\rangle}{\nu_{o_j t_j}+\nu_{o_k t_k}}\langle o_i|\vec{m}_i|s_i\rangle\circ\langle s_j|\vec{\mu}_j|t_j\rangle\prod_{\kappa}^{\kappa\neq j,k}\delta_{t_\kappa o_\kappa}\prod_{\kappa}^{\kappa\neq j}\delta_{t_\kappa s_\kappa}\end{aligned}\right\}.$$

Für $i\neq j$, $j\neq k$, $k\neq i$ liefern die Kroneckerfaktoren die speziellen Bedingungen $s_i=o_i$, $s_j=o_j$ und $t_k=s_k=o_k$. Die Glieder mit drei verschiedenen Indizes werden also paarweise konjugiert komplex und geben daher keinen Beitrag zum Imaginärteil.

Für den dritten Term ergibt sich

$$\left[\frac{1}{\nu_{so}^2-\nu^2}\right]^{(1)}[\langle o|\vec{m}_i|s\rangle]^{(0)}\,[\langle s|\vec{\mu}_j|0\rangle]^{(0)}$$

$$=-\frac{1}{h}\sum_{k,l}^{k<l}\frac{2\sum\limits_{\kappa}\nu_{s_\kappa o_\kappa}(\langle s_k s_l|\bar{\mathcal{H}}_{kl}|s_k s_l\rangle-\langle o_k o_l|\bar{\mathcal{H}}_{kl}|o_k o_l\rangle)}{\left(\left(\sum\limits_{\kappa}\nu_{s_\kappa o_\kappa}\right)^2-\nu^2\right)^2}$$

$$\cdot\langle o_i|\vec{m}_i|s_i\rangle\circ\langle s_j|\vec{\mu}_j|o_j\rangle\prod_{\kappa}^{\kappa\neq i}\delta_{s_\kappa o_\kappa}\prod_{\kappa}^{\kappa\neq j}\delta_{s_\kappa o_\kappa}.$$

Er verschwindet für $i \neq j$ und zerfällt für $i = j$ in drei Terme, die jeweils von den Indexpaaren (ik) mit $k \neq i$ abhängen.

Damit ist der Tensor $[{}^{(J)}\gamma]^{(1)}$ eine Summe von Komponenten, die nur Eigenwerte und Eigenfunktionen zu jeweils einem Ligandenpaar l_i, l_j und den dazugehörigen Störoperator $\bar{\mathscr{H}}_{ij}$ enthalten.

Mit der Bezeichung $[\ ]^{(1,ij)}$ für Korrekturterme erster Ordnung zum Störoperator $\bar{\mathscr{H}}_{ij}$ gelten daher die Gleichungen

$$[{}^{(J)}\gamma^{\langle i\rangle}]^{(1)} = \sum_{k}^{k \neq i} [{}^{(J)}\gamma^{\langle i\rangle}]^{(1,ik)}$$

und

$$[{}^{(J)}\gamma^{\langle ij\rangle}]^{(1)} = \sum_{k}^{k \neq i,j} [{}^{(J)}\gamma^{\langle i\rangle}]^{(1,ik)} + \sum_{k}^{k \neq i,j} [{}^{(J)}\gamma^{\langle j\rangle}]^{(1,jk)} + [{}^{(J)}\gamma^{\langle ij\rangle}]^{(1,ij)}\,.$$

$[{}^{(J)}\gamma^{\langle ij\rangle}]^{(1,ij)}$ ist die Korrektur erster störungstheoretischer Ordnung für den Tensor ${}^{(J)}\gamma$ des isolierten Teilsystems $\langle l_i, l_j\rangle$ mit $\bar{\mathscr{H}}_{ij}$ als Störterm, also die vollständige Korrektur erster Ordnung innerhalb des Systems $\langle l_i, l_j\rangle$. Wir können daher schreiben

$$[\mathrm{Sp}\,{}^{(J)}\gamma^{\langle ij\rangle}]^{(1,ij)} = [\mathrm{Sp}\,{}^{(J)}\gamma(l_i, l_j)]^{(1)}$$

und haben damit bis auf den Faktor K die Korrektur erster Ordnung für den optischen Drehwinkel des Teilsystems $\langle l_i, l_j\rangle$.

Unter Benutzung von (8) finden wir die Beziehung

$$[\mathrm{Sp}\,{}^{(J)}\gamma]^{(1)} = \sum_{i<j}^{1,4} [\mathrm{Sp}\,{}^{(J)}\gamma(l_i, l_j)]^{(1)} \tag{12a}$$

und entsprechend zur Gleichung (9)

$$[\omega]^{(1)} = \sum_{i<j}^{1,4} [\omega(l_i, l_j)]^{(1)} \quad \text{mit} \quad [\omega(l_i, l_j)]^{(1)} = K[\mathrm{Sp}\,{}^{(J)}\gamma(l_i, l_j)]^{(1)}\,. \tag{12b}$$

Da Beziehungen von der Art (8) für alle Glieder in (10) gelten, können wir schließen, daß Gleichung (12b) formal dieselbe bleibt, wenn der Ausdruck (10) zugrunde gelegt wird. Die $[\omega(l_i, l_j)]^{(1)}$ werden in diesem Falle durch eine Summe entsprechender Glieder beschrieben.

In jedem Falle sehen wir, daß die erste Ordnung des Drehwinkels verschwindet, wenn alle Teilsysteme $\langle l_i, l_j\rangle$ achiral sind. Diese Voraussetzung ist aber mit einem T_d-symmetrischen Abschirmfeld genau dann erfüllt, wenn die T_d-Bedingung gilt.

Über die explizite Form für $[\mathrm{Sp}\,{}^{(J)}\gamma(l_i, l_j)]^{(1)}$ im Modell $\bar{\mathscr{H}}$, die wir hier nicht angeben, finden wir die entsprechende Form im Modell $\tilde{\mathscr{H}}$. Dabei machen wir von der quantenmechanischen Definition (Anhang *B*) für die komplexen Tensoren der elektrischen und elektromagnetischen Polarisierbarkeit $\alpha = {}^{(R)}\alpha - i\nu\,{}^{(J)}\alpha$ und $\gamma = {}^{(R)}\gamma - i\nu\,{}^{(J)}\gamma$ und der elektromagnetischen Hyperpolarisierbarkeit $\Gamma = {}^{(R)}\Gamma - i\nu\,{}^{(J)}\Gamma$ Gebrauch und erhalten damit unser Resultat in Gestalt einer

Funktion von klassischen Größen. Sie hat die Form[5]

$$
\begin{aligned}
[\mathrm{Sp}\,{}^{(J)}\gamma(l_i, l_j)]^{(\bar{1})} = \frac{2\kappa_i\kappa_j}{\nu}\,\mathscr{P}_+(ij)\,\mathrm{Im}\sum_{\varrho,\sigma,\varrho',\sigma'}\Big\{&\Gamma_{\varrho\varrho\sigma}(l_i)\,(\vec{e}^{(i)}_\sigma\cdot T_{ij}\cdot\{\langle\vec{m}(l_j)\rangle+\vec{c}_j\}) \\
&+\alpha_{\varrho\sigma}(l_i)\,\vec{e}^{(i)}_\varrho\cdot\Big(\gamma_{\varrho'\sigma'}(l_j)\,\vec{e}^{(j)}_{\sigma'} - i\,\frac{\pi}{c}\,\nu\alpha_{\varrho'\sigma'}(l_j)\,\vec{r}_j\times\vec{e}^{(j)}_{\sigma'}\Big)(\vec{e}^{(i)}_\sigma\cdot T_{ij}\cdot\vec{e}^{(j)}_{\varrho'})\Big\}
\end{aligned}
\tag{13}
$$

mit der Abkürzung $\langle o_j|\vec{m}(l_j)|o_j\rangle = \langle\vec{m}(l_j)\rangle$.

Als individuelle Bezugspunkte für ortsabhängige Größen wie $\gamma(l_i)$ und $\Gamma(l_i)$ sind dabei die Ladungsschwerpunkte $\vec{r}_i$ der Kernsysteme $\mathfrak{K}_i$ gewählt. Die $\vec{e}^{(i)}_\varrho$ mit $\varrho = 1, 2, 3$ bezeichnen Einheitsvektoren eines rechtwinkligen Koordinatensystems für den jeweiligen Liganden l_i. $\mathscr{P}_+(ij)$ ist der Projektionsoperator

$$\mathscr{P}_+(ij) = \tfrac{1}{2}\{\mathscr{O}((1)) + \mathscr{O}((ij))\}\,.$$

Wenn von Spineffekten abgesehen wird, können die Eigenfunktionen von $\mathscr{H}_0$ reell gewählt werden, damit gilt ${}^{(J)}\alpha = 0$, ${}^{(R)}\gamma = 0$ und ${}^{(R)}\Gamma = 0$.

Die Kirkwoodsche Theorie entspricht der Auswertung eines Terms, der aus einem Teil des zweiten Gliedes in der geschweiften Klammer von (13) ohne Berücksichtigung des Spins nach Anwendung von $\mathscr{P}_+(ij)$ entsteht, und zwar

$$\frac{\pi}{c}\sum_{\varrho,\sigma,\varrho',\sigma'}{}^{(R)}\alpha_{\varrho\sigma}(l_i)\,{}^{(R)}\alpha_{\varrho'\sigma'}(l_j)\,[\vec{a}_{ij}\cdot(\vec{e}^{(i)}_\varrho\times\vec{e}^{(j)}_{\sigma'})]\,(\vec{e}^{(i)}_\sigma\cdot T_{ij}\cdot\vec{e}^{(j)}_{\varrho'})\,.$$

Dieser Term beschreibt also mit zusätzlichen Vernachlässigungen einen Teil des Beitrages zur optischen Aktivität, der ausschließlich bei Methanderivaten mit Abweichungen von der T_d-Bedingung auftritt und bei kleinen Abweichungen den Charakter einer Korrektur hat.

7. *Störungsrechnung zweiter Ordnung*

$[{}^{(J)}\gamma]^{(2)}$ ist folgendermaßen definiert:

$$[{}^{(J)}\gamma]^{(2)} = \sum_{\varrho,\sigma,\tau}^{\varrho+\sigma+\tau=2}\left\{\frac{2}{h}\,\mathrm{Im}\sum_s\sum_{i,j}\left|\frac{1}{\nu_{so}^2-\nu^2}\right|^{(\varrho)}[\langle o|\vec{m}_i|s\rangle]^{(\sigma)}\,[\langle s|\vec{\mu}_j|o\rangle]^{(\tau)}\right\}.$$

Für die Glieder mit festen Werten von ϱ, σ und τ ergibt sich:

$$
\begin{aligned}
&\left|\frac{1}{\nu_{so}^2-\nu^2}\right|^{(1)}[\langle o|\vec{m}_i|s\rangle]^{(1)}\cdot[\langle s|\vec{\mu}_j|o\rangle]^{(0)} \\
&= -\frac{2}{h^2}\sum_{l,r}^{l<r}\frac{\nu_{s_jo_j}(\langle s_ls_r|\bar{\mathscr{H}}_{lr}|s_ls_r\rangle - \langle o_lo_r|\bar{\mathscr{H}}_{lr}|o_lo_r\rangle)}{(\nu_{s_jo_j}^2-\nu^2)^2} \\
&\quad\times\prod_\kappa^{\kappa\neq j}\delta_{s_\kappa o_\kappa}\sum_k^{k\neq i}\sum_t{}'\left\{\begin{aligned}&\frac{\langle o_io_k|\bar{\mathscr{H}}_{ik}|t_it_k\rangle}{\nu_{o_it_i}+\nu_{o_kt_k}}\langle t_i|\vec{m}_i|s_i\rangle\cdot\langle s_j|\vec{\mu}_j|o_j\rangle\prod_\kappa^{\kappa\neq i,k}\delta_{t_\kappa o_\kappa}\prod_\kappa^{\kappa\neq i}\delta_{t_\kappa s_\kappa} \\
&+\frac{\langle t_it_k|\mathscr{H}_{ik}|s_is_k\rangle}{\nu_{s_it_i}+\nu_{s_kt_k}}\langle o_i|\vec{m}_i|t_i\rangle\cdot\langle s_j|\vec{\mu}_j|o_j\rangle\prod_\kappa^{\kappa\neq i,k}\delta_{t_\kappa s_\kappa}\prod_\kappa^{\kappa\neq i}\delta_{t_\kappa o_\kappa}\end{aligned}\right\}.
\end{aligned}
$$

---

[5] Der Faktor i im letzten Ausdruck unter dem Summenzeichen bezeichnet die imaginäre Einheit und muß daher vom Index i unterschieden werden.

Entsprechendes gilt für $\left[\frac{1}{\nu_{so}^2-\nu^2}\right]^{(1)} [\langle 0|\vec{m}_i|s\rangle]^{(0)} \circ [\langle s|\vec{\mu}_j|o\rangle]^{(1)}$.

$$\left[\frac{1}{\nu_{so}^2-\nu^2}\right]^{(0)} [\langle o|\vec{m}_i|s\rangle]^{(2)} \circ [\langle s|\vec{\mu}_j|o\rangle]^{(0)} = \frac{1}{h^2}\,\frac{1}{\nu_{s_jo_j}^2-\nu^2}\prod_{\kappa}^{\kappa\neq j}\delta_{s_\kappa o_\kappa}\sum_{k,l}^{k<l}\sum_{m,n}^{m<n}\sum_{t}{}'\Bigg\{$$

$$\begin{aligned}
\Bigg\{ &\sum_{t'}{}' \frac{\langle o_k o_l|\bar{\mathscr{H}}_{kl}|t_k t_l\rangle}{\nu_{o_k t_k}+\nu_{o_l t_l}}\;\frac{\langle t'_m t'_n|\bar{\mathscr{H}}_{mn}|s_m s_n\rangle}{\nu_{s_m t'_m}+\nu_{s_n t'_n}} \\
&\qquad\cdot\langle t_i|\vec{m}_i|t'_i\rangle\circ\langle s_j|\vec{\mu}_j|o_j\rangle \prod_{\kappa}^{\kappa\neq k,l}\delta_{t_\kappa o_\kappa}\prod_{\kappa}^{\kappa\neq m,n}\delta_{t'_\kappa s_\kappa}\prod_{\kappa}^{\kappa\neq i}\delta_{t'_\kappa t_\kappa} \\
&+\sum_{t'}{}' \frac{\langle t_k t_l|\bar{\mathscr{H}}_{kl}|t'_k t'_l\rangle}{\sum_\kappa \nu_{s_\kappa t_\kappa}}\;\frac{\langle t'_m t'_n|\bar{\mathscr{H}}_{mn}|s_m s_n\rangle}{\nu_{s_m t'_m}+\nu_{s_n t'_n}} \\
&\qquad\cdot\langle o_i|\vec{m}_i|t_i\rangle\circ\langle s_j|\vec{\mu}_j|o_j\rangle \prod_{\kappa}^{\kappa\neq k,l}\delta_{t_\kappa t'_\kappa}\prod_{\kappa}^{\kappa\neq m,n}\delta_{t'_\kappa s_\kappa}\prod_{\kappa}^{\kappa\neq i}\delta_{t_\kappa o_\kappa} \\
&+\sum_{t'}{}' \frac{\langle o_k o_l|\bar{\mathscr{H}}_{kl}|t'_k t'_l\rangle}{\nu_{o_k t_k}+\nu_{o_l t_l}}\;\frac{\langle t'_m t'_n|\bar{\mathscr{H}}_{mn}|t_m t_n\rangle}{\sum_\kappa \nu_{o_\kappa t_\kappa}} \\
&\qquad\cdot\langle t_i|\vec{m}_i|s_i\rangle\circ\langle s_j|\vec{\mu}_j|o_j\rangle \prod_{\kappa}^{\kappa\neq k,l}\delta_{t'_\kappa o_\kappa}\prod_{\kappa}^{\kappa\neq m,n}\delta_{t'_\kappa t_\kappa}\prod_{\kappa}^{\kappa\neq i}\delta_{t_\kappa s_\kappa} \\
&-\frac{\langle t_k t_l|\bar{\mathscr{H}}_{kl}|s_k s_l\rangle\,\langle s_m s_n|\bar{\mathscr{H}}_{mn}|s_m s_n\rangle}{(\nu_{s_k t_k}+\nu_{s_l t_l})^2}\langle o_i|\vec{m}_i|t_i\rangle\circ\langle s_j|\vec{\mu}_j|o_j\rangle \prod_{\kappa}^{\kappa\neq k,l}\delta_{t_\kappa s_\kappa}\prod_{\kappa}^{\kappa\neq i}\delta_{t_\kappa o_\kappa} \\
&-\frac{\langle o_k o_l|\bar{\mathscr{H}}_{kl}|o_k o_l\rangle\,\langle o_m o_n|\bar{\mathscr{H}}_{mn}|t_m t_n\rangle}{(\nu_{o_m t_m}+\nu_{o_n t_n})^2}\langle t_i|\vec{m}_i|s_i\rangle\circ\langle s_j|\vec{\mu}_j|o_j\rangle \prod_{\kappa}^{\kappa\neq m,n}\delta_{t_\kappa o_\kappa}\prod_{\kappa}^{\kappa\neq i}\delta_{t_\kappa s_\kappa} \\
&-\frac{1}{2}\,\frac{\langle s_k s_l|\bar{\mathscr{H}}_{kl}|t_k t_l\rangle\,\langle t_m t_n|\bar{\mathscr{H}}_{mn}|s_m s_n\rangle}{\left(\sum_\kappa \nu_{s_\kappa t_\kappa}\right)^2} \\
&\qquad\cdot\langle o_i|\vec{m}_i|s_i\rangle\circ\langle s_j|\vec{\mu}_j|o_j\rangle \prod_{\kappa}^{\kappa\neq k,l}\delta_{t_\kappa s_\kappa}\prod_{\kappa}^{\kappa\neq m,n}\delta_{t_\kappa s_\kappa}\prod_{\kappa}^{\kappa\neq i}\delta_{s_\kappa o_\kappa} \\
&-\frac{1}{2}\,\frac{\langle o_k o_l|\bar{\mathscr{H}}_{kl}|t_k t_l\rangle\,\langle t_m t_n|\bar{\mathscr{H}}_{mn}|0_m o_n\rangle}{\left(\sum_\kappa \nu_{o_\kappa t_\kappa}\right)^2} \\
&\qquad\cdot\langle o_i|\vec{m}_i|s_i\rangle\circ\langle s_j|\vec{\mu}_j|o_j\rangle \prod_{\kappa}^{\kappa\neq k,l}\delta_{t_\kappa o_\kappa}\prod_{\kappa}^{\kappa\neq m,n}\delta_{t_\kappa o_\kappa}\prod_{\kappa}^{\kappa\neq i}\delta_{s_\kappa o_\kappa}\Bigg\}
\end{aligned}$$

Entsprechendes gilt für $\left[\frac{1}{\nu_{so}^2-\nu^2}\right]^{(0)} [\langle o|\vec{m}_i|s\rangle]^{(0)} \circ [\langle s|\vec{\mu}_j|o\rangle]^{(2)}$.

$$\left[\frac{1}{\nu_{so}^2-\nu}\right]^{(0)} [\langle o|\vec{m}_i|s\rangle]^{(1)} \circ [\langle s|\vec{\mu}_j|o\rangle]^{(1)} = \frac{1}{h^2}\,\frac{1}{\left(\sum_\kappa \nu_{s_\kappa o_\kappa}\right)^2-\nu^2}\sum_{k}^{k\neq l}\sum_{l}^{l\neq j}\sum_{t}{}'\sum_{t'}{}'\Bigg\{$$

$$
\begin{aligned}
&\left\{\frac{\langle o_i o_k|\bar{\mathscr{H}}_{ik}|t_i t_k\rangle}{\nu_{o_i t_i}+\nu_{o_k t_k}}\,\frac{\langle s_j s_l|\bar{\mathscr{H}}_{jl}|t'_j t'_l\rangle}{\nu_{s_j t'_j}+\nu_{s_l t'_l}}\right.\\
&\qquad\cdot\langle t_i|\vec{m}_i|s_i\rangle\,\langle t'_j|\vec{\mu}_j|o_j\rangle\prod_{\kappa}^{\kappa\neq i,k}\delta_{t_\kappa o_\kappa}\prod_{\kappa}^{\kappa\neq j,l}\delta_{t'_\kappa s_\kappa}\prod_{\kappa}^{\kappa\neq i}\delta_{t_\kappa s_\kappa}\prod_{\kappa}^{\kappa\neq j}\delta_{t'_\kappa o_\kappa}\\
&+\frac{\langle o_i o_k|\bar{\mathscr{H}}_{ik}|t_i t_k\rangle}{\nu_{o_i t_i}+\nu_{o_k t_k}}\,\frac{\langle t_j t'_l|\bar{\mathscr{H}}_{jl}|o_j o_l\rangle}{\nu_{o_j t'_j}+\nu_{o_l t'_l}}\\
&\qquad\cdot\langle t_i|\vec{m}_i|s_i\rangle\,\langle s_j|\vec{\mu}_j|t'_j\rangle\prod_{\kappa}^{\kappa\neq i,k}\delta_{t_\kappa o_\kappa}\prod_{\kappa}^{\kappa\neq j,l}\delta_{t'_\kappa o_\kappa}\prod_{\kappa}^{\kappa\neq i}\delta_{t_\kappa s_\kappa}\prod_{\kappa}^{\kappa\neq j}\delta_{t'_\kappa s_\kappa}\\
&+\frac{\langle t_i t_k|\bar{\mathscr{H}}_{ik}|s_i s_k\rangle}{\nu_{s_i t_i}+\nu_{s_k t_k}}\,\frac{\langle s_j s_l|\bar{\mathscr{H}}_{jl}|t'_j t'_l\rangle}{\nu_{s_j t_j}+\nu_{s_l t_l}}\\
&\qquad\cdot\langle o_i|\vec{m}_i|t_i\rangle\,\langle t_j|\vec{\mu}_j|o_j\rangle\prod_{\kappa}^{\kappa\neq i,k}\delta_{t_\kappa s_\kappa}\prod_{\kappa}^{\kappa\neq j,l}\delta_{t_\kappa s_\kappa}\prod_{\kappa}^{\kappa\neq i}\delta_{t_\kappa o_\kappa}\prod_{\kappa}^{\kappa\neq j}\delta_{t'_\kappa o_\kappa}\\
&+\frac{\langle t_i t_k|\bar{\mathscr{H}}_{ik}|s_i s_k\rangle}{\nu_{s_i t_i}+\nu_{s_k t_k}}\,\frac{\langle t_j t'_l|\bar{\mathscr{H}}_{jl}|o_j o_l\rangle}{\nu_{o_j t_j}+\nu_{o_l t_l}}\\
&\qquad\left.\cdot\langle o_i|\vec{m}_i|t_i\rangle\,\langle s_j|\vec{\mu}_j|t'_j\rangle\prod_{\kappa}^{\kappa\neq i,k}\delta_{t_\kappa s_\kappa}\prod_{\kappa}^{\kappa\neq j,l}\delta_{t'_\kappa o_\kappa}\prod_{\kappa}^{\kappa\neq i}\delta_{t_\kappa o_\kappa}\prod_{\kappa}^{\kappa\neq j}\delta_{t'_\kappa s_\kappa}\right\}
\end{aligned}
$$

$$
\begin{aligned}
&\left|\frac{1}{\nu_{so}^2-\nu^2}\right|^{(2)}[\langle o|\vec{m}_i|s\rangle]^{(0)}\,[\langle s|\vec{\mu}_j|0\rangle]^{(0)}\\
&\quad=\frac{1}{h^2}\langle o_i|\vec{m}_i|s_i\rangle\,\langle s_j|\vec{\mu}_j|o_j\rangle\prod_{\kappa}^{\kappa\neq i}\delta_{s_\kappa o_\kappa}\prod_{\kappa}^{\kappa\neq j}\delta_{s_\kappa o_\kappa}\sum_{k,l}^{k<l}\sum_{m,n}^{m<n}\Bigg\{\\
&\left\{\frac{-2\sum\limits_{\kappa}\nu_{s_\kappa o_\kappa}}{\left(\left(\sum\limits_{\kappa}\nu_{s_\kappa o_\kappa}\right)^2-\nu^2\right)^2}\sum_{t}{}'\left(\begin{aligned}&\frac{\langle s_k s_l|\bar{\mathscr{H}}_{kl}|t_k t_l\rangle\langle t_m t_n|\bar{\mathscr{H}}_{mn}|s_m s_n\rangle}{\sum\limits_{\kappa}\nu_{s_\kappa t_\kappa}}\prod_{\kappa}^{\kappa\neq k,l}\delta_{t_\kappa s_\kappa}\prod_{\kappa}^{\kappa\neq m,n}\delta_{t_\kappa s_\kappa}\\
&-\frac{\langle o_k o_l|\bar{\mathscr{H}}_{kl}|t_k t_l\rangle\langle t_m t_n|\bar{\mathscr{H}}_{mn}|o_m o_n\rangle}{\sum\limits_{\kappa}\nu_{o_\kappa t_\kappa}}\prod_{\kappa}^{\kappa\neq k,l}\delta_{t_\kappa o_\kappa}\prod_{\kappa}^{\kappa\neq m,n}\delta_{t_\kappa o_\kappa}\end{aligned}\right)\right.\\
&+\frac{3\left(\sum\limits_{\kappa}\nu_{s_\kappa o_\kappa}\right)^2+\nu^2}{\left(\left(\sum\limits_{\kappa}\nu_{s_\kappa o_\kappa}\right)^2-\nu^2\right)^3}\times\left(\begin{aligned}&(\langle s_k s_l|\bar{\mathscr{H}}_{kl}|s_k s_l\rangle-\langle o_k o_l|\bar{\mathscr{H}}_{kl}|o_k o_l\rangle)\\
\times\,&(\langle s_m s_n|\bar{\mathscr{H}}_{mn}|s_m s_n\rangle-\langle o_m o_n|\bar{\mathscr{H}}_{mn}|o_m o_n\rangle)\end{aligned}\right)\Bigg\}.
\end{aligned}
$$

Entsprechend dem Resultat (12b) des letzten Kapitels kann auch für die zweite Ordnung eine einfache Beziehung ähnlicher Art (14b) abgeleitet werden, die im weiteren Verlauf der Diskussion von entscheidendem Nutzen ist. Da die diesbezügliche Ableitung sehr aufwendig ist, stützen wir uns auf einen allgemeinen Satz der Störungsrechnung, der zu diesem Zweck formuliert und bewiesen wurde [7]. Er betrifft die Störungsrechnung für ein System, dessen Hamiltonoperator in eine Summe von Energieoperatoren für Teilsysteme und Störoperatoren zerlegt ist, die die Wechselwirkungsenergien zwischen allen Paaren von Teilsystemen beschreiben. Er lautet:

Die p-te störungstheoretische Korrektur für das Matrixelement $\langle s|\mathcal{O}_i|t\rangle$ eines Operators zum Teilsystem i ist eine Summe von Ausdrücken, die jeweils zusammen mit i nicht mehr als $p+1$ verschiedene Indizes enthalten, d. h., die auftretenden Eigenfunktionen, Eigenwerte und Störoperatoren betreffen höchstens $p+1$ verschiedene Teilsysteme.

Ist $\mathfrak{M}_1$ eine Indexmenge von $\sigma+1$ ausgewählten Indizes, zu denen auch i gehört, und $\{[\langle s|\mathcal{O}_i|t\rangle]^{(\sigma)}\}^{\mathfrak{M}_1}$ die Teilsumme aus $[\langle s|\mathcal{O}_i|t\rangle]^{(\sigma)}$, die nur von diesen $\sigma+1$ Indizes abhängt, dann gilt

$$\{[\langle s|\mathcal{O}_i|t\rangle]^{(\sigma)}\}^{\mathfrak{M}_1}=\{[\langle s|\mathcal{O}_i|t\rangle]^{(\sigma)}\}^{\mathfrak{M}_1}\prod_{\kappa}^{\bar{\mathfrak{M}}_1}\delta_{s_\kappa t_\kappa},$$

wobei $\bar{\mathfrak{M}}_1$ die Komplementärmenge zu $\mathfrak{M}_1$ in der Menge $\mathfrak{M}$ aller Indizes für Teilsysteme bezeichnet.

Mit zwei Indexmengen $\mathfrak{M}_1$ und $\mathfrak{M}_2$ von $\sigma+1$ und $\tau+1$ ausgewählten Indizes aus $\mathfrak{M}$, zu denen i bzw. j gehören, erhalten wir für das Produkt der Teilsummen von $\{[\langle o|\mathcal{O}_i|s\rangle]^{(\sigma)}\}^{\mathfrak{M}_1}$ und $\{[\langle s|\bar{\mathcal{O}}_j|o\rangle]^{(\tau)}\}^{\mathfrak{M}_2}$

$$\begin{aligned}&\{[\langle o|\mathcal{O}_i|s\rangle]^{(\sigma)}\}^{\mathfrak{M}_1}\cdot\{[\langle s|\bar{\mathcal{O}}_j|o\rangle]^{(\tau)}\}^{\mathfrak{M}_2}\\&\qquad=\{[\langle o|\mathcal{O}_i|s\rangle]^{(\sigma)}\}^{\mathfrak{M}_1}\cdot\{[\langle s|\bar{\mathcal{O}}_j|o\rangle]^{(\tau)}\}^{\mathfrak{M}_2}\prod_{\kappa}^{\bar{\mathfrak{M}}_1\cup\bar{\mathfrak{M}}_2}\delta_{s_\kappa o_\kappa}.\end{aligned}$$

Dieser Ausdruck ist reell, wenn $\bar{\mathfrak{M}}_1\cup\bar{\mathfrak{M}}_2=\mathfrak{M}$ die Menge aller Indizes und damit der Durchschnitt $\mathfrak{M}_1\cap\mathfrak{M}_2=\Phi$ die leere Menge ist; denn wegen $\bar{\mathfrak{M}}_1\cup\bar{\mathfrak{M}}_2=\mathfrak{M}$ gilt für alle κ aus $\mathfrak{M}$ $s_\kappa=o_\kappa$, d. h. aber, der Ausdruck bleibt unverändert, wenn $|s\rangle=|o\rangle$ gesetzt wird, und in diesem Falle handelt es sich um die störungstheoretische Korrektur eines Produktes von Erwartungswerten.

Man entnimmt ebenfalls aus [7], daß das Produkt der Korrektur ϱ-ter Ordnung des Frequenzfaktors beim Rosenfeldausdruck mit einem Produkt von Kroneckerfaktoren zur Indexmenge $\bar{\mathfrak{M}}_3=\bar{\mathfrak{M}}_1\cup\bar{\mathfrak{M}}_2$,

$$\left[\frac{1}{\nu_{so}^2-\nu^2}\right]^{(\varrho)}\prod_{\kappa}^{\bar{\mathfrak{M}}_3}\delta_{s_\kappa o_\kappa},$$

in Teilsummen zerlegbar ist, deren jede von den Indizes aus $\mathfrak{M}_3$ und höchstens ϱ weiteren aus $\mathfrak{M}$ abhängt. Diese Glieder sind natürlich ebenfalls reell.

Demnach ist in

$$\sum_{\varrho,\sigma,\tau}^{\varrho+\sigma+\tau=2}\left[\frac{1}{\nu_{so}^2-\nu^2}\right]^{(\varrho)}[\langle o|\mathcal{O}_i|s\rangle]^{(\sigma)}\cdot[\langle s|\bar{\mathcal{O}}_j|o\rangle]^{(\tau)}$$

wegen der Bedingung $\varrho+\sigma+\tau=2$ für die zweite Ordnung die Maximalzahl von Ligandenindizes, die in den einzelnen Gliedern der Summenzerlegung vorkommen, $\varrho+\sigma+1+\tau+1=4$, und diese Zahl wird nur erreicht für Produkte zweier Teilsummen, deren Indexmengen $\mathfrak{M}_1$ und $\mathfrak{M}_2$ die leere Menge als Durchschnitt haben. Die Maximalzahl von Indizes in Gliedern, die zum Imaginärteil der Summe beitragen, ist demgemäß $\varrho+\sigma+1+\tau+1-1=3$. In der obigen Form haben wir also für alle Glieder in (10), mit $\mathcal{O}_i=\vec{m}_i$ und $\bar{\mathcal{O}}_j=\vec{\mu}_j$ speziell für den Rosenfeldausdruck, das Resultat:

> Die zweite störungstheoretische Korrektur des optischen Drehwinkels setzt sich additiv aus Beiträgen zusammen, die jeweils von nicht mehr als drei Liganden abhängen.

Mit dieser Information ausgestattet, sammeln wir in den Formeln der Störungsrechnung zweiter Ordnung alle Glieder mit Indizes eines ausgewählten Tripels i, j, k und denken daran, daß wir dieselben Glieder bekommen hätten, wenn wir die Störungsrechnung nur für das System $\langle l_i, l_j, l_k\rangle$ mit dem Störoperator $\bar{\mathcal{H}}_{ij}+\bar{\mathcal{H}}_{jk}+\bar{\mathcal{H}}_{ki}$ durchgeführt hätten.

Wir können die Teilsumme für das Indextripel i, j, k mit

$$^{(J)}\gamma_i^{\langle ijk\rangle} = \frac{2}{h}\,\mathrm{Im}\sum_s \frac{\langle o|\vec{m}_i+\vec{m}_j+\vec{m}_k|s\rangle\circ\langle s|\vec{\mu}_i+\vec{\mu}_j+\vec{\mu}_k|o\rangle}{\nu_{so}^2-\nu^2}$$

bezeichnen und analog zum letzten Kapitel schreiben

$$[\mathrm{Sp}\,^{(J)}\gamma^{\langle ijk\rangle}]^{(2,ij,jk,ki)} = [\mathrm{Sp}\,^{(J)}\gamma(l_i, l_j, l_k)]^{(2)}\,.$$

In diesen Ausdrücken kommen auch Glieder vor, die nur von zwei Indizes abhängen und entsprechend mit

$$[^{(J)}\gamma^{\langle ij\rangle}]^{(2,ij)},\quad [^{(J)}\gamma^{\langle jk\rangle}]^{(2,jk)},\quad [^{(J)}\gamma^{\langle ki\rangle}]^{(2,ki)}$$

bzw.

$$[\mathrm{Sp}\,^{(J)}\gamma^{\langle ij\rangle}]^{(2,ij)} = [\mathrm{Sp}\,^{(J)}\gamma(l_i, l_j)]^{(2)}\quad \text{usw.}$$

bezeichnet werden dürfen. Glieder, die nur von einem Index abhängen, treten wie in der störungstheoretischen Korrektur erster Ordnung nicht auf.

Wenn wir nun die gesamte zweite störungstheoretische Korrektur von $^{(J)}\gamma$ nach Indextripeln $i<j<k$ ordnen wollen, müssen Glieder zu Indexpaaren zweimal statt einmal benutzt werden. Daraus ergibt sich das Resultat

$$[\mathrm{Sp}\,^{(J)}\gamma]^{(2)} = -\sum_{i<j}^{1,4}[\mathrm{Sp}\,^{(J)}\gamma(l_i, l_j)]^{(2)} + \sum_{i<j<k}^{1,4}[\mathrm{Sp}\,^{(J)}\gamma(l_i, l_j, l_k)]^{(2)} \tag{14a}$$

und nach Multiplikation mit K

$$[\omega]^{(2)} = -\sum_{i<j}^{1,4}[\omega(l_i, l_j)]^{(2)} + \sum_{i<j<k}^{1,4}[\omega(l_i, l_j, l_k)]^{(2)} \tag{14b}$$

mit

$$[\omega(l_i, l_j)]^{(2)} = K[\mathrm{Sp}\,^{(J)}\gamma(l_i, l_j)]^{(2)} \text{ und } [\omega(l_i, l_j, l_k)]^{(2)} = K[\mathrm{Sp}\,^{(J)}\gamma(l_i, l_j, l_k)]^{(2)}.$$

Auch (14b) bleibt ebenso wie (9b) und (12b) formal unverändert, wenn statt des Rosenfeldterms der Ausdruck (10) zugrunde gelegt wird und die störungstheoretischen Korrekturen zweiter Ordnung für den optischen Drehwinkel auch unter Bezugnahme auf (10) erklärt werden.

Mit demselben Argument wie bei der Korrektur erster Ordnung stellen wir fest, daß alle $[\omega(l_i, l_j)]^{(2)}$ verschwinden, falls die T_d-Bedingung gilt.

Da $[\mathrm{Sp}\,^{(J)}\gamma(l_i, l_j)]^{(2)}$ auch in $[\mathrm{Sp}\,^{(J)}\gamma(l_i, l_j, l_k)]^{(2)}$ auftritt, ist folgende Zerlegung möglich:

$$\begin{aligned}[\mathrm{Sp}\,^{(J)}\gamma(l_i, l_j, l_k)]^{(2)} = {} & [\mathrm{Sp}\,^{(J)}\gamma_0(l_i, l_j, l_k)]^{(2)} + [\mathrm{Sp}\,^{(J)}\gamma(l_i, l_j)]^{(2)} + [\mathrm{Sp}\,^{(J)}\gamma(l_j, l_k)]^{(2)}\\ & + [\mathrm{Sp}\,^{(J)}\gamma(l_k, l_i)]^{(2)},\end{aligned}$$

wobei $[^{(J)}\gamma_0(l_i, l_j, l_k)]^{(2)}$ ein Tensor ist, in dem Anteile, die ausschließlich von Ligandenpaaren herrühren, weggelassen sind. Damit kann (14a) auch in der

Form (14a') geschrieben werden:

$$[\mathrm{Sp}\,^{(J)}\gamma]^{(2)} = \sum_{i<j}^{1,4} [\mathrm{Sp}\,^{(J)}\gamma(l_i, l_j)]^{(2)} + \sum_{i<j<k}^{1,4} [\mathrm{Sp}\,^{(J)}\gamma_0(l_i, l_j, l_k)]^{(2)} \tag{14a'}$$

mit den speziellen Eigenschaften $[\mathrm{Sp}\,^{(J)}\gamma(l_i, l_j)]^{(2)} = 0$ und $[\mathrm{Sp}\,^{(J)}\gamma(l_i, l_j, l_k)]^{(2)} = [\mathrm{Sp}\,^{(J)}\gamma_0(l_i, l_j, l_k)]^{(2)}$ für T_d-Derivate.

Die Aufteilung von $[\mathrm{Sp}\,^{(J)}\gamma]^{(2)}$ gemäß (14a') empfiehlt sich einmal deswegen, weil wir, wie unten dargelegt, mit guten Gründen auch bei Methanderivaten, die die T_d-Bedingung nicht erfüllen, auf die Beiträge von $[\mathrm{Sp}\,^{(J)}\gamma(l_i, l_j)]^{(2)}$ in vielen Fällen verzichten können, zweitens, weil die explizite Auswertung hier auf neue Schwierigkeiten stößt. Während $[\mathrm{Sp}\,^{(J)}\gamma_0(l_i, l_j, l_k)]^{(2)}$ mit den bereitgestellten Mitteln ausgerechnet und im Modell $\mathscr{K}$ in Form einer Funktion von permanenten Momenten, Polarisierbarkeiten und Hyperpolarisierbarkeiten, also als Funktion klassischer Größen, geschrieben werden kann, ist das für $[\mathrm{Sp}\,^{(J)}\gamma(l_i, l_j)]^{(2)}$, ohne von zusätzlichen Approximationen nach Unsöld [18] und London [10] Gebrauch zu machen, nicht möglich. Auch für $[\mathrm{Sp}\,^{(J)}\gamma_0(l_i, l_j, l_k)]^{(2)}$ erfordert die Auswertung eine erhebliche Rechenarbeit, dasselbe gilt für die Übertragung des Resultats in das Modell $\mathscr{K}$. Wir verzichten daher auf die Angabe von Zwischenresultaten und geben unter Benutzung der elektrischen Hyperpolarisierbarkeit $A = {}^{(R)}A - i\nu\,^{(J)}A$ und der elektromagnetischen Hyperpolarisierbarkeit zweiter Stufe $\Delta = {}^{(R)}\Delta - i\nu\,^{(J)}\Delta$ das Ergebnis der Rechnung an.

$$\begin{aligned}
[\mathrm{Sp}\,^{(J)}\gamma_0(l_i, l_j, l_k)]^{(2)} = -\frac{6\kappa_i\kappa_j\kappa_k}{\nu}\,\mathscr{P}_+(ijk)\,\mathrm{Im} \sum_{\substack{\varrho,\sigma,\tau\\ \varrho',\sigma',\tau'\\ \varrho'',\sigma''}} \Bigg\{ & \\
\Bigg\{ \frac{\kappa_i}{2}\,\Delta_{\varrho\varrho\sigma\tau}(l_i)\,(\vec{e}^{(i)}_\sigma \cdot T_{ij} \cdot \{\langle\vec{m}(l_j)\rangle + \vec{c}_j\})\,(\vec{e}^{(i)}_\tau \cdot T_{ik} \cdot \{\langle\vec{m}(l_k)\rangle + \vec{c}_k\}) & \\
+ \kappa_j\,\Gamma_{\varrho\varrho\sigma}(l_i)\,(\vec{e}^{(i)}_\sigma \cdot T_{ij} \cdot \vec{e}^{(j)}_{\varrho'})\,{}^{(R)}\alpha^0{}_{\varrho'\sigma'}(l_j)\,(\vec{e}^{(j)}_{\sigma'} \cdot T_{jk} \cdot \{\langle\vec{m}(l_k)\rangle + \vec{c}_k\}) & \\
+ \kappa_j\,\alpha_{\varrho\sigma}(l_i)\,\vec{e}^{(i)}_\varrho \cdot \left(\Gamma_{\varrho'\sigma'\tau'}(l_j)\,\vec{e}^{(j)}_{\sigma'} - i\frac{\pi}{c}\nu\,A_{\varrho'\sigma'\tau'}(l_j)\,\vec{r}_j \times \vec{e}^{(j)}_{\sigma'}\right) & \\
\cdot (\vec{e}^{(i)}_\sigma \cdot T_{ij} \cdot \vec{e}^{(j)}_{\varrho'})\,(\vec{e}^{(j)}_{\tau'} \cdot T_{jk} \cdot \{\langle\vec{m}(l_k)\rangle + \vec{c}_k\}) & \\
+ \kappa_i\,A_{\varrho\sigma\tau}(l_i)\,\vec{e}^{(i)}_\varrho \cdot \left(\gamma_{\varrho'\sigma'}(l_j)\,\vec{e}^{(j)}_{\sigma'} - i\frac{\pi}{c}\nu\,\alpha_{\varrho'\sigma'}(l_j)\,\vec{r}_j \times \vec{e}^{(j)}_{\sigma'}\right) & \\
\cdot (\vec{e}^{(i)}_\sigma \cdot T_{ij} \cdot \vec{e}^{(j)}_{\varrho'})\,(\vec{e}^{(i)}_\tau \cdot T_{ik} \cdot \{\langle\vec{m}(l_k)\rangle + \vec{c}_k\}) & \\
+ \kappa_k\,\alpha_{\varrho\sigma}(l_i)\,\vec{e}^{(i)}_\varrho \cdot \left(\gamma_{\varrho'\sigma'}(l_j)\,\vec{e}^{(j)}_{\sigma'} - i\frac{\pi}{c}\nu\,\alpha_{\varrho'\sigma'}(l_j)\,\vec{r}_j \times \vec{e}^{(j)}_{\sigma'}\right) & \\
\cdot (\vec{e}^{(i)}_\sigma \cdot T_{ik} \cdot \vec{e}^{(k)}_{\varrho''})\,\alpha_{\varrho''\sigma''}(l_k)\,(\vec{e}^{(k)}_{\sigma''} \cdot T_{kj} \cdot \vec{e}^{(j)}_{\varrho'}) \Bigg\} &
\end{aligned} \tag{15}$$

Dabei ist $\mathscr{P}_+(ijk)$ der Projektionsoperator

$$\mathscr{P}_+(ijk) = \tfrac{1}{6}\{\mathscr{O}((1)) + \mathscr{O}((ijk)) + \mathscr{O}((ikj)) + \mathscr{O}((ij)) + \mathscr{O}((jk)) + \mathscr{O}((ki))\}\,.$$

${}^{(R)}\alpha^0$ ist der Realteil der statischen elektrischen Polarisierbarkeit gemäß ${}^{(R)}\alpha^0 = {}^{(R)}\alpha|_{\nu=0}$.

Wenn von Spineffekten abgesehen wird, gilt wie früher ${}^{(J)}\alpha = 0$, ${}^{(R)}\gamma = 0$, ${}^{(R)}\Gamma = 0$ und außerdem ${}^{(J)}A = 0$.

Die Form (15) für $[\mathrm{Sp}\,{}^{(J)}\gamma_0(l_i, l_j, l_k)]^{(\tilde{2})}$ kann mit Ausnahme des letzten Gliedes als klassische Korrektur zur störungstheoretischen Korrektur erster Ordnung im Modell $\tilde{\mathcal{H}}$ für $\mathrm{Sp}\,{}^{(J)}\gamma(l_i, l_j, l_k)$,

$$[\mathrm{Sp}\,{}^{(J)}\gamma(l_i, l_j, l_k)]^{(\tilde{1})} = [\mathrm{Sp}\,{}^{(J)}\gamma(l_i, l_j)]^{(\tilde{1})} + [\mathrm{Sp}\,{}^{(J)}\gamma(l_j, l_k)]^{(\tilde{1})} + [\mathrm{Sp}\,{}^{(J)}\gamma(l_k, l_i)]^{(\tilde{1})},$$

verstanden und verifiziert werden, wenn man die veränderten Eigenschaften der einzelnen Liganden im Feld der elektrostatischen Dipolmomente der übrigen Liganden des Systems $\langle l_i, l_j, l_k\rangle$ klassisch untersucht und auf Anteile verzichtet, die zu Paarfunktionen führen.

Das gesamte äußere Störfeld $\vec{E}'(\vec{a}_i)$ für den Liganden l_i, das Feld der permanenten elektrischen Dipole aller übrigen Liganden an der Stelle $\vec{a}_i$, ist

$$\vec{E}'(\vec{a}_i) = -\sum_{k}^{k \neq i} T_{ik} \cdot \langle \vec{m}(\bar{l}_k)\rangle .$$

Bei Verzicht auf Paarfunktionen bleibt also im System $\langle l_i, l_j, l_k\rangle$ jeweils nur das Feld desjenigen Liganden zu berücksichtigen, der in der jeweiligen Paarfunktion nicht auftritt. Daher ist z. B. für das erste Glied in $[\mathrm{Sp}\,{}^{(J)}\gamma(l_i, l_j, l_k)]^{(\tilde{1})}$ maßgebend

$$\left.\begin{aligned} \vec{E}^{(k)}(\vec{a}_i) &= -T_{ik} \cdot \langle \vec{m}(\bar{l}_k)\rangle \\ \vec{E}^{(k)}(\vec{a}_j) &= -T_{jk} \cdot \langle \vec{m}(\bar{l}_k)\rangle \end{aligned}\right\} \quad \text{für} \quad k \neq i, j .$$

Die Einflüsse dieser Felder auf die Liganden lassen sich durch Korrekturen ihrer Tensoren beschreiben, die wir einer Entwicklung nach äußeren Feldern gemäß (7) und (7a) entnehmen können. Wir ersetzen in den Definitionsgleichungen (13) für $[\mathrm{Sp}\,{}^{(J)}\gamma(l_i, l_j)]^{(\tilde{1})}$, $[\mathrm{Sp}\,{}^{(J)}\gamma(l_j, l_k)]^{(\tilde{1})}$ und $[\mathrm{Sp}\,{}^{(J)}\gamma(l_k, l_i)]^{(\tilde{1})}$ jedes Produkt von ligandenspezifischen Tensoren durch eine Summe von Produkten, in denen jeweils ein Tensor durch seine Korrektur vertreten wird, und zwar entsprechend der Vorschrift:

$$\langle m_\varrho(l_i)\rangle \to \kappa_i \sum_{\sigma} {}^{(R)}\alpha^0{}_{\varrho\sigma}(l_i)\, E'_\sigma(\vec{a}_i),$$

$$\alpha_{\varrho\sigma}(l_i) \to \kappa_i \sum_{\tau} A_{\varrho\sigma\tau}(l_i)\, E'_\tau(\vec{a}_i),$$

$$\gamma_{\varrho\sigma}(l_i) \to \kappa_i \sum_{\tau} \Gamma_{\varrho\sigma\tau}(l_i)\, E'_\tau(\vec{a}_i),$$

$$\Gamma_{\varrho\sigma\tau}(l_i) \to \frac{\kappa_i}{2} \sum_{\upsilon} \Delta_{\varrho\sigma\tau\upsilon}(l_i)\, E'_\upsilon(\vec{a}_i).$$

Der Faktor $\frac{1}{2}$ kommt dadurch zustande, daß in unserem Falle der gemischte Differentialquotient von γ nach zwei verschiedenen Feldern jeweils durch den zweiten Differentialquotienten nach dem Gesamtfeld ersetzt werden muß, um zur Definition für Δ zu kommen.

Auf diese Weise erhalten wir $[\mathrm{Sp}\,{}^{(J)}\gamma_0(l_i, l_j, l_k)]^{(\tilde{2})}$ gemäß Definitionsgleichung (15) ohne das Glied in der letzten Zeile. Das letzte Glied beschreibt einen rein quantenmechanischen Effekt, der zwar mit klassischen Größen formulierbar, aber nicht mit einer entsprechenden Überlegung abzuleiten ist und daher nur aus der quantenmechanischen Störungsrechnung entnommen werden kann.

III. Diskussion des Resultats

1. Allgemeiner Gültigkeitsanspruch und spezielle Form für Methanderivate

Aus der Theorie der Chiralitätsfunktionen kennen wir die Bedingungen für eine qualitativ vollständige Beschreibung des optischen Drehwinkels in einer Molekülklasse mit achiralem Gerüst und Liganden von der Symmetrie der Lagegruppe. Die Symmetrie des Gerüstes und die Anordnung der Ligandenplätze bestimmen darstellungstheoretische Eigenschaften der Komponenten einer qualitativ vollständigen Chiralitätsfunktion. Nach dem zweiten Näherungsverfahren werden die Komponenten jeweils durch eine Linearkombination von Funktionen beschrieben, die von einer Minimalzahl von Liganden abhängen. Diese Minimalzahlen sind für achirale Gerüste mit vier Ligandenplätzen 1, 2 und 3. Da im Modell $\bar{\mathcal{H}}$ bzw. $\tilde{\mathcal{H}}$ ohne Beeinflussung des formalen Resultats die Abschirmfelder der jeweiligen Gerüstsymmetrie anzupassen sind, kann die vorgelegte Theorie in ihrer allgemeinen Form bei allen diesen Klassen Anwendung finden. Wir haben gesehen, daß die quantenmechanische Störungsrechnung bis zur zweiten Ordnung für Gerüste dieser Art 1-, 2- und 3-Liganden-Funktionen liefert. Es ist daher anzunehmen, daß mit der zweiten Ordnung für alle diese Fälle eine qualitativ vollständige quantenmechanische Theorie des optischen Drehwinkels vorliegt. Diese Vermutung läßt sich durch explizite Diskussion der verschiedenen Molekülklassen bestätigen.

Die Diskussion der Methanderivate bezieht sich offensichtlich auf solche Molekülklassen, in denen die T_d-Bedingung zumindest bezüglich der Gerüstsymmetrie näherungsweise erfüllt ist. Aus diesem Grund interessiert uns der Satz:

> Die qualitativ vollständige Chiralitätsfunktion für alle Molekülklassen, deren Gerüste einer geometrischen Figur mit vier ausgezeichneten Punkten entsprechen, die sich stetig und *ohne Symmetrieerniedrigung* in das reguläre Tetraeder mit den vier ausgezeichneten Eckpunkten überführen läßt, enthält eine T_d-Komponente. Die T_d-Komponente transformiert sich bei Ligandenpermutationen nach der alternierenden Darstellung von $\mathfrak{S}_4$; sie kann durch eine Linearkombination aus Funktionen von drei Liganden und als einzige nicht mit Funktionen von weniger als drei Liganden approximiert werden. Für Moleküle mit der T_d-Bedingung ist die T_d-Komponente die einzige.

Solange wir also im Bereich kleiner Abweichungen von der T_d-Symmetrie des Gerüstes bleiben, kann die Komponente $\sum_{i<j<k} [\mathrm{Sp}\,^{(J)}\gamma_0(l_i, l_j, l_k)]^{(2)}$ für den Hauptbeitrag zum optischen Drehwinkel verantwortlich gemacht und Korrekturen, die Abweichungen betreffen, jeweils in störungstheoretisch niedrigerer Ordnung berücksichtigt werden. Wir haben gesehen, daß auch Abweichungen von der geforderten Symmetrie und Fixierung der Liganden in nullter oder erster Ordnung beschreibbar sind. Mit großen Abweichungen von der T_d-Bedingung verliert die zweite störungstheoretische Korrektur ihre dominierende Rolle, die vorgelegte Theorie bleibt aber kompetent.

Mit diesen Bemerkungen ist es konsequent, für eine Berechnung des optischen Drehwinkels von Methanderivaten einen Ansatz zu verwenden, in dem die zweite störungstheoretische Korrektur berücksichtigt ist, insoweit sie zu 3-Liganden-

Funktionen führt, insoweit sie zu Paarfunktionen führt, aber vernachlässigt wird. Der entsprechende Ansatz lautet

$$[\omega]^{(0+1+2)} \approx [\omega] \equiv K\left(\sum_{i}^{1,4} \mathrm{Sp}\,^{(J)}\gamma(l_i) + \sum_{i<j}^{1,4} [\mathrm{Sp}\,^{(J)}\gamma(l_i, l_j)]^{(1)} \right. \\ \left. + \sum_{i<j<k}^{1,4} [\mathrm{Sp}\,^{(J)}\gamma_0(l_i, l_j, l_k)]^{(2)} \right), \tag{16}$$

und er ist im Modell $\tilde{\mathcal{H}}$ mit den Gleichungen (13) und (15) explizit auf Eigenschaften der Liganden und auf Abstände zwischen ihnen zurückgeführt. Ebenso wie $[\omega]$ sollen in Zukunft auch Tensoren von Teilsystemen ohne Bezeichnung der störungstheoretischen Näherungsstufe im Sinne der Näherung von Ansatz (16) verstanden werden, also:

$$\begin{aligned}
&[\mathrm{Sp}\,^{(J)}\gamma(l_i, l_j)]^{(0+1+2)} \approx [\mathrm{Sp}\,^{(J)}\gamma(l_i, l_j)]^{(0+1)} \\
&\qquad \equiv \mathrm{Sp}\,^{(J)}\gamma(l_i, l_j) = \mathrm{Sp}\,^{(J)}\gamma(l_i) + \mathrm{Sp}\,^{(J)}\gamma(l_j) + [\mathrm{Sp}\,^{(J)}\gamma(l_i, l_j)]^{(1)}, \\
&[\mathrm{Sp}\,^{(J)}\gamma(l_i, l_j, l_k)]^{(0+1+2)} \\
&\approx \mathrm{Sp}\,^{(J)}\gamma(l_i, l_j, l_k) = \left\{ \begin{aligned} &\mathrm{Sp}\,^{(J)}\gamma(l_i) + \mathrm{Sp}\,^{(J)}\gamma(l_j) + \mathrm{Sp}\,^{(J)}\gamma(l_k) + [\mathrm{Sp}\,^{(J)}\gamma_0(l_i, l_j, l_k)]^{(2)} \\ &+ \mathrm{Sp}\,^{(J)}\gamma(l_i, l_j)]^{(1)} + [\mathrm{Sp}\,^{(J)}\gamma(l_j, l_k)]^{(1)} + [\mathrm{Sp}\,^{(J)}\gamma(l_k, l_i)]^{(1)} \end{aligned} \right\}.
\end{aligned} \tag{17}$$

Aus dem Text oder aus den Formeln wird jeweils zu entnehmen sein, ob es sich dabei um das Modell $\bar{\mathcal{H}}$ oder $\tilde{\mathcal{H}}$ handelt.

Die beiden Terme $[\mathrm{Sp}\,^{(J)}\gamma(l_i, l_j)]^{(0+1+2)}$ und $[\mathrm{Sp}\,^{(J)}\gamma(l_i, l_j, l_k)]^{(0+1+2)}$ bzw. ihre Vertreter in der Näherung (17), $\mathrm{Sp}\,^{(J)}\gamma(l_i, l_j)$ und $\mathrm{Sp}\,^{(J)}\gamma(l_i, l_j, l_k)$, sind jeweils allein für die optische Aktivität von Derivaten besonderer Art verantwortlich. Um dies einzusehen, erinnern wir uns an gewisse Eigenschaften unseres Modells. Ein spezieller Ligand ist definitionsgemäß ein nicht an einer Bindung beteiligtes ungepaartes Elektron des zentralen Kohlenstoffs, den wir mit dem speziellen Symbol e bezeichnen wollen. Der Ligand e ist achiral, und daher gilt $\mathrm{Sp}\,^{(J)}\gamma(e) = 0$. Außerdem ist das dazugehörige $\kappa = (n-1)/n$ gleich Null. Damit ergibt sich im Modell $\tilde{\mathcal{H}}$ mit den Gl. (13) und (15) eine stark vereinfachte Darstellung des optischen Drehwinkels $[\omega]$ für Derivate, in denen zwei bzw. einer der Liganden nur in einem radikalischen Elektron besteht, und zwar

$$\begin{aligned} &[\omega] = K\,\mathrm{Sp}\,^{(J)}\gamma(l_i, l_j) \\ \text{bzw.} \qquad &[\omega] = K\,\mathrm{Sp}\,^{(J)}\gamma(l_i, l_j, l_k)\,. \end{aligned} \tag{18}$$

$K\,\mathrm{Sp}\,^{(J)}\gamma(l_i, l_j, l_k)$ und $K\,\mathrm{Sp}\,^{(J)}\gamma(l_i, l_j)$ beschreiben die optischen Drehwinkel von Radikalen bzw. Biradikalen mit ungepaarten Elektronen an den Gerüststellen, deren Indizes in der Formel nicht auftreten.

Man kann sich leicht davon überzeugen, daß auch für höhere Multipolmomente bei der Entwicklung des Störoperators im Modell $\bar{\mathcal{H}}$ dieselben κ-Faktoren auftreten. Die Gl. (18) gelten also auch im Modell $\bar{\mathcal{H}}$. Außerdem ergeben sich entsprechende Gleichungen, wenn neben dem Rosenfeldterm auch die Korrekturterme aus (10) berücksichtigt werden.

2. T_d-*Derivate*

a) Der formale Strukturaspekt des Resultats im Modell $\bar{\mathscr{H}}$ und seine praktische Bedeutung

Für T_d-Derivate vereinfacht sich (16) zu (16a):

$$[\omega] = \sum_{i<j<k}^{1,4} [\omega(l_i, l_j, l_k)] \quad \text{mit} \quad [\omega(l_i, l_j, l_k)] = K[\mathrm{Sp}\,^{(J)}\gamma_0(l_i, l_j, l_k)]^{(2)}. \tag{16a}$$

Die Ausdrücke für $[\omega(l_i, l_j, l_k)]$, die Komponenten $K[\mathrm{Sp}\,^{(J)}\gamma_0(l_i, l_j, l_k)]^{(2)}$, bezeichnen, wie wir aus dem vorangehenden Kapitel wissen, die optischen Drehwinkel für T_d-Derivate mit den Liganden l_i, l_j, l_k an den Gerüststellen i, j, k und dem Liganden e an der nicht aufgeführten Stelle. Wenn wir in einem T_d-Derivat eine Permutation der Liganden mit symmetrieäquivalenter Fixierung vornehmen, erhalten wir nicht unterscheidbare oder gespiegelte Derivate, je nachdem, ob die Permutation gerade oder ungerade ist. Dementsprechend bleibt der Funktionswert von $K[\mathrm{Sp}\,^{(J)}\gamma_0(l_i, l_j, l_k)]^{(2)}$ ungeändert oder wechselt sein Vorzeichen.

Wir erklären eine Funktion $\varphi(l_i, l_j, l_k)$ von Eigenschaften der Liganden l_i, l_j, l_k an den Stellen zwei, drei und vier, die mit der Definitionsgleichung

$$\varphi(l_2, l_3, l_4) \equiv [\mathrm{Sp}\,^{(J)}\gamma_0(l_2, l_3, l_4)]^{(2)}$$

festgelegt ist, sich aber im Gegensatz zu $[\mathrm{Sp}\,^{(J)}\gamma_0(l_i, l_j, l_k)]^{(2)}$ immer in der Reihenfolge ihrer Argumente auf die Gerüststellen zwei, drei und vier bezieht. Aus den erwähnten Transformationseigenschaften bei Permutationen der Liganden ergibt sich damit

$$\begin{aligned}
[\mathrm{Sp}\,^{(J)}\gamma_0(l_1, l_2, l_3)]^{(2)} &= -\varphi(l_1, l_2, l_3),\\
[\mathrm{Sp}\,^{(J)}\gamma_0(l_1, l_2, l_4)]^{(2)} &= \varphi(l_1, l_2, l_4),\\
[\mathrm{Sp}\,^{(J)}\gamma_0(l_1, l_3, l_4)]^{(2)} &= -\varphi(l_1, l_3, l_4),\\
[\mathrm{Sp}\,^{(J)}\gamma_0(l_2, l_3, l_4)]^{(2)} &= \varphi(l_2, l_3, l_4).
\end{aligned}$$

Es ist zu beachten, daß die $\varphi(l_i, l_j, l_k)$ bei ungeraden Permutationen ihrer Argumente das Vorzeichen ändern; dagegen rufen entsprechende Permutationsoperatoren in den Ausdrücken $[\mathrm{Sp}\,^{(J)}\gamma_0(l_i, l_j, l_k)]^{(2)}$ eine Permutation der Indizes auch an den Basisvektoren $\vec{e}_{\varrho}^{(i)}$ hervor, und das ist ohne Einfluß auf ihren Funktionswert. Wir erhalten also Gl. (16a) in der Form

$$[\omega] = \tilde{\chi}(l_1, l_2, l_3, l_4) = K(\varphi(l_2, l_3, l_4) - \varphi(l_3, l_4, l_1) + \varphi(l_4, l_1, l_2) - \varphi(l_1, l_2, l_3)) \tag{19}$$

und haben damit das quantenmechanische Resultat für T_d-Derivate im Modell $\bar{\mathscr{H}}$ mit dem Ansatz nach dem zweiten Näherungsverfahren (2) identifiziert.

Mit einem Liganden l, der zunächst ein radikalisches Elektron e bezeichnen soll, also unter der Voraussetzung $l = e$, können wir wegen (18) dafür auch schreiben:

$$[\omega] = \tilde{\chi}(l_1, l_2, l_3, l_4) = \tilde{\chi}(l, l_2, l_3, l_4) + \tilde{\chi}(l_1, l, l_3, l_4) + \tilde{\chi}(l_1, l_2, l, l_4) + \tilde{\chi}(l_1, l_2, l_3, l). \tag{20}$$

Wenn wir nur die rechte Seite von (20) betrachten, uns von der speziellen Annahme $l = e$ lösen und jede der Chiralitätsfunktionen nach Dreiligandenfunktionen gemäß (19) zerlegen, finden wir, daß sich wegen der Transformationseigenschaften der $\varphi(l_i, l_j, l_k)$ mehrere Glieder paarweise kompensieren und schließlich die rechte Seite von (19) entsteht. Daher gilt (20) auch für $l \neq e$. Die Beziehung (20) ist also eine Funktionalgleichung für die mit unserer Theorie beschriebenen optischen Drehwinkel von T_d-Derivaten zu einem Sortiment von fünf beliebigen Liganden $l(1)$, $l(2)$, $l(3)$, $l(4)$, $l(5)$. Damit dokumentiert sich der Modellcharakter unserer Theorie in folgendem Theorem:

> Der optische Drehwinkel eines T_d-Derivates ist die Summe der optischen Drehwinkel von vier T_d-Derivaten, in denen jeweils einer der vier ursprünglichen Liganden durch einen fünften Liganden l ersetzt ist.

Funktionalgleichungen vom Typ (20) sind allgemein eine Konsequenz von Ansätzen nach dem zweiten Näherungsverfahren, die sich zum Test für die Kompetenz des Verfahrens bei der Beschreibung einer pseudoskalaren Eigenschaft an den Molekülen einer Klasse eignet. Unsere quantenmechanische Theorie zeigt, daß der Approximationsaspekt des zweiten Verfahrens für das spezielle Phänomen „optische Aktivität von T_d-Derivaten" im Rahmen eines physikalischen Modells bis zur zweiten störungstheoretischen Ordnung strenge Gültigkeit beansprucht. Eine semiempirische Bestimmung der optischen Drehwinkel von T_d-Derivaten gemäß (19) ist daher ein erstes Resultat unserer Theorie, das unabhängig von der Problematik der Multipolentwicklung in $\tilde{\mathscr{H}}$ und unabhängig von den Details in der Struktur der $[\mathrm{Sp}^{(J)}\gamma_0(l_i, l_j, l_k)]^{(2)}$ quantitativ mit dem Experiment vergleichbare Aussagen liefert.

Falls die T_d-Bedingung erfüllt ist, kann der optische Drehwinkel aller Derivate mit Liganden eines Sortiments $l(1), l(2), \ldots, l(N)$ berechnet werden, wenn die Winkel für Derivate mit einem beliebig ausgewählten Liganden $l(i)$ experimentell bekannt sind. Da mit wachsender Zahl N von verfügbaren Liganden die Zahl der verschiedenen Enantiomerenpaare $\binom{N}{4}$ stärker wächst als die zur Berechnung der optischen Drehwinkel nach (20) notwendige Zahl von experimentellen Daten $\binom{N-1}{3}$, ist das zweite Verfahren von praktischem Nutzen. Für $N = 5$ liefert Gl. (20) bereits eine nichttriviale Feststellung. Diese Methode der Berechnung ist also konsequent im Rahmen einer Theorie, die auf der Basis eines physikalisch wohlbegründeten Modells $\tilde{\mathscr{H}}$ bis zur zweiten störungstheoretischen Ordnung keine Vernachlässigung enthält. Wir haben daher deutliche Diskrepanzen mit experimentellen Daten nicht auf den unzureichenden Näherungscharakter des Verfahrens zurückzuführen, sondern dann die Gültigkeit der T_d-Bedingung in Frage zu stellen. Mit anderen Worten, wir haben in solchen Abweichungen den Hinweis dafür zu sehen, daß die Symmetrie der Liganden oder ihre Fixierung oder die Bindungswinkel nicht der T_d-Bedingung genügen, und können erwarten, daß die Komponenten erster und nullter störungstheoretischer Ordnung in unserer Theorie den dabei entstehenden zusätzlichen Beitrag zum optischen Drehwinkel beschreiben werden. Es ist ergänzend zu bemerken, daß frei drehbare Liganden mit einer Spiegelebene in der Bindungsrichtung den Verhältnissen bei starr fixierten Liganden mit T_d-Bedingung entsprechen.

Die Frage, inwieweit die T_d-Bedingung erfüllt bzw. inwieweit sie näherungsweise akzeptabel ist, kann am besten beurteilt werden, wenn wir aus Gleichung (20) eine Nullidentität machen, indem wir die Chiralitätsfunktion auf der linken

Seite als Chiralitätsfunktion für das Enantiomere auf die rechte Seite bringen. Damit haben wir auf der rechten Seite nach Multiplikation mit dem Faktor $\frac{1}{5}$ die Chiralitätsfunktion für ein äquimolares Gemisch von Derivaten, das, wie man sich leicht anhand von Fig. 1 überzeugt, nicht razemisch ist.

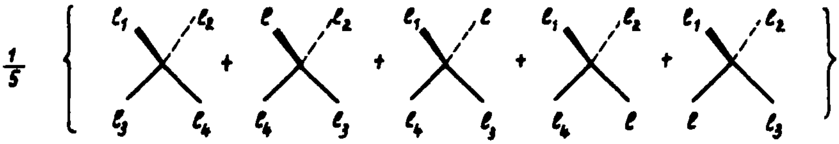

Fig. 1

Die Aussage, daß der optische Drehwinkel dieses nicht razemischen Gemisches Null sei, ist streng nicht richtig, aber exakt im Rahmen unserer Theorie und daher nach den vorausgegangenen Überlegungen als gute Näherung für T_d-Derivate anzusehen. Wir können daher den Schluß ziehen:

Die T_d-Bedingung ist erfüllt oder Abweichungen davon sind klein, wenn der molare Drehwinkel des Gemisches Fig. 1 dem Beitrag nach klein ist, verglichen mit den Drehwinkeln, die im Mittel an den reinen Substanzen gemessen werden.

b) Der optische Drehwinkel von T_d-Derivaten im Modell $\tilde{\mathscr{K}}$

Aus Anhang *B* entnehmen wir, daß für Liganden mit T_d-Bedingung der Imaginärteil von α verschwindet und die Symmetrierelationen der Tensorkomponenten von Δ und Γ zum Verschwinden jener Beiträge führen, die aus der ersten und zweiten Zeile der geschweiften Klammer in (15) stammen. (15) und alle Teilausdrücke von (15), die durch Anwendung von $\mathscr{P}_+(ijk)$ auf Glieder in der Klammer entstehen, sind gegenüber den Permutationen der Indizes i, j und k invariant. Wir können also, ohne die Gl. (15) zu zerstören, den Operator $\mathscr{O}((ij))$ auf die vierte Zeile, $\mathscr{O}((ikj))$ auf das erste Glied und $\frac{1}{2}\{\mathscr{O}((kj))+\mathscr{O}((ikj))\}$ auf das zweite Glied der fünften Zeile anwenden und erreichen damit, daß alle noch interessierenden Glieder innerhalb der Klammer den gemeinsamen Faktor κ_j enthalten. Damit erlauben die T_d-Bedingung und die Relationen ${}^{(R)}\alpha_{\varrho\sigma} = {}^{(R)}\alpha_{\sigma\varrho}$, ${}^{(R)}A_{\varrho\sigma\tau} = {}^{(R)}A_{\sigma\varrho\tau}$, ${}^{(J)}A_{\varrho\sigma\tau} = -{}^{(J)}A_{\sigma\varrho\tau}$, (15) in der Form (15a) zu schreiben:

$$[\mathrm{Sp}\,{}^{(J)}\gamma_0(l_i, l_j, l_k)]^{(\tilde{2})} = \mathscr{P}_+(ijk)\,\xi(l_i, l_j, l_k)$$

mit

$$\begin{aligned}
\xi(l_i, l_j, l_k) = 6\,\kappa_i\kappa_j^2\kappa_k \sum_{\substack{\varrho,\sigma\\ \varrho',\sigma',\tau'\\ \varrho'',\sigma''}} & (\vec{e}_\varrho^{(i)}\cdot T_{ij}\cdot\vec{e}_{\varrho'}^{(j)})\\
\cdot\Big\{ & {}^{(R)}\alpha_{\varrho\sigma}(l_i)\,{}^{(J)}\Gamma_{\varrho'\sigma'\tau'}(l_j)\;(\vec{e}_\sigma^{(i)}\cdot\vec{e}_{\sigma'}^{(j)})\;(\vec{e}_{\tau'}^{(j)}\cdot T_{jk}\cdot\{\langle\vec{m}(l_k)\rangle+\vec{c}_k\})\\
& +{}^{(J)}\gamma_{\varrho\sigma}(l_i)\,{}^{(R)}A_{\varrho'\sigma'\tau'}(l_j)\;(\vec{e}_\sigma^{(i)}\cdot\vec{e}_{\sigma'}^{(j)})\;(\vec{e}_{\tau'}^{(j)}\cdot T_{jk}\cdot\{\langle\vec{m}(l_k)\rangle+\vec{c}_k\})\\
& -{}^{(R)}\gamma_{\varrho\sigma}(l_i)\,{}^{(J)}A_{\varrho'\sigma'\tau'}(l_j)\;(\vec{e}_\sigma^{(i)}\cdot\vec{e}_{\sigma'}^{(j)})\;(\vec{e}_{\tau'}^{(j)}\cdot T_{jk}\cdot\{\langle\vec{m}(l_k)\rangle+\vec{c}_k\})\\
& +{}^{(J)}\gamma_{\varrho\sigma}(l_i)\,{}^{(R)}\alpha_{\varrho'\sigma'}(l_j)\,{}^{(R)}\alpha_{\varrho''\sigma''}(l_k)\;(\vec{e}_\sigma^{(i)}\cdot\vec{e}_{\sigma''}^{(k)})\;(\vec{e}_{\sigma'}^{(j)}\cdot T_{jk}\cdot\vec{e}_{\varrho''}^{(k)})\\
& -\frac{\pi}{c}\,{}^{(R)}\alpha_{\varrho\sigma}(l_i)\,{}^{(R)}A_{\varrho'\sigma'\tau'}(l_j)\,[\vec{a}_{ij}\cdot(\vec{e}_\sigma^{(i)}\times\vec{e}_{\sigma'}^{(j)})]\,(\vec{e}_{\tau'}^{(j)}\cdot T_{jk}\cdot\{\langle\vec{m}(l_k)\rangle+\vec{c}_k\})\\
& -\frac{\pi}{2c}\,{}^{(R)}\alpha_{\varrho\sigma}(l_i)\,{}^{(R)}\alpha_{\varrho'\sigma'}(l_j)\,{}^{(R)}\alpha_{\varrho''\sigma''}(l_k)\,[\vec{a}_{ik}(\vec{e}_\sigma^{(i)}\times\vec{e}_{\sigma''}^{(k)})]\,(\vec{e}_{\sigma'}^{(j)}\cdot T_{jk}\cdot\vec{e}_{\varrho''}^{(k)})\Big\}.
\end{aligned} \tag{15a}$$

Zur weiteren Auswertung wählen wir eine feste Bezifferung des Gerüstes nach Fig. 2 und rechtwinklige Koordinatensysteme mit den Basisvektoren $\vec{e}_r^{(i)}$, $\vec{e}_t^{(i)}$, $\vec{e}_{t'}^{(i)}$ jeweils am Durchstoßpunkt der Bindungsrichtung i mit der Oberfläche einer konzentrischen Kugel um das zentrale Kohlenstoffatom. Der Vektor $\vec{e}_r^{(i)}$ bezeichne die radiale Richtung vom Kohlenstoffatom aus, $\vec{e}_t^{(i)}$ eine Tangentialrichtung, die in der Projektion nach der Bindungsrichtung i mit einem radialen Vektor $\vec{e}_r^{(k)}$ zu $k \neq i$ übereinstimmt (vgl. Fig. 3). Eine genauere Festlegung der Koordinatensysteme ist nur für die explizite Rechnung zweckmäßig (vgl. Anhang C), für die Komponentenbezeichnung dagegen unnötig, da die jeweils drei möglichen Orientierungen des Dreibeins bezüglich der Komponenten eines nach der T_d-Bedingung fixierten Liganden symmetrieäquivalent sind.

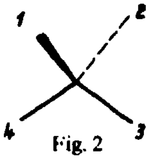

Fig. 2

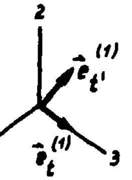

Fig. 3

Für Liganden der Symmetrie C_{3nv} mit $n \geq 1$ müssen grundsätzlich zwei mögliche Fixierungen am Gerüst unterschieden werden. Eine davon, die wir die Standardfixierung nennen, sei dadurch ausgezeichnet, daß die t-Richtung einer ligandenspezifischen Bezeichnung der Tensorkomponenten mit der Richtung von $\vec{e}_t^{(i)}$ zusammenfällt, die andere Möglichkeit ist die „staggered"-Fixierung. Sie verhält sich zur Standardfixierung wie Fig. 4a zu 4b und ist dadurch gekennzeichnet, daß die t-Komponente ligandenspezifischer Eigenschaften mit der Richtung von $\vec{e}_t^{(i)}$ einen Winkel von $\pi/3n$ einschließt. Für Liganden der Symmetrie $C_{\infty v}$ entfällt diese Unterscheidung natürlich.

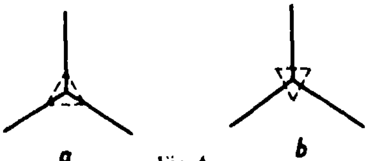

Fig. 4

Im Anhang B sind alle interessierenden Symmetrieeigenschaften von Tensorkomponenten für Liganden mit der T_d-Bedingung aufgeführt. Davon ist neben den schon benutzten Eigenschaften von Δ und Γ und dem Verschwinden des Imaginärteils von α folgendes für das Verständnis der endgültigen Formeln notwendig.

Alle Tensoren erster und zweiter Stufe, $\langle\vec{m}\rangle$, α und γ, haben für Liganden der Symmetrie C_{3nv} und $C_{\infty v}$ zylindersymmetrisches Transformationsverhalten. Das Gleiche gilt für die Komponenten von A und Γ, insoweit mindestens einer ihrer Indizes r ist. Von den übrigen Komponenten bleiben wegen der T_d-Bedingung nur zwei Typen, nämlich ${}^{(R)}A_{ttt}$ und ${}^{(J)}\Gamma_{t't'}$ zu besprechen. Sie verschwinden für Liganden der Symmetrie C_{3nv} mit $n > 1$ und $C_{\infty v}$, sie sind von Null verschieden für C_{3v}-Symmetrie und wechseln ihr Vorzeichen, wenn wir die Liganden aus der Standard- in die „staggered"-Fixierung überführen und an einer gerüstbezogenen Bezeichnung festhalten. Wir vereinfachen ihre Bezeichnung und notieren ihre Symmetrierelationen

$$
\begin{aligned}
{}^{(R)}A_t &\equiv {}^{(R)}A_{ttt} = -{}^{(R)}A_{tt't'} = -{}^{(R)}A_{t'tt'} = -{}^{(R)}A_{t't't}\,,\\
{}^{(J)}\Gamma_{t'} &\equiv {}^{(J)}\Gamma_{t't't'} = -{}^{(J)}\Gamma_{t'tt} = -{}^{(J)}\Gamma_{tt't} = -{}^{(J)}\Gamma_{ttt'}\,.
\end{aligned}
$$

Der Ausdruck (15a) und die daraus durch Anwendung der Permutationsoperatoren entstehenden unterscheiden sich durch die jeweilige Permutation entsprechender Indizes, wo immer sie in der Funktion auftreten. Wegen der symmetrieäquivalenten Fixierung der Liganden können wir bei Verwendung unserer symmetrieäquivalenten Koordinatensysteme die Anwendung der Permutationsoperatoren uminterpretieren. Wir wählen feste Basisvektoren an festen Gerüstplätzen, verstehen unter den ligandenspezifischen Tensoren Tensoren für die jeweiligen Liganden an diesen Plätzen und definieren die Anwendung eines Permutationsoperators als Vorschrift für eine Permutation von Liganden mit symmetrieäquivalenter Fixierung bezüglich dieser Plätze.

Mit den Indizes 2, 3 und 4 für Basisvektoren und einer Entscheidung über Numerierung entsprechend der Fig. 2 verwerten wir die spezielle Geometrie unseres Gerüstes für die Skalarprodukte und erhalten auf diese Weise aus den Funktionen ξ von Formel (15a) Funktionen η, in denen Basisvektoren und also auch ihre Indizes nicht mehr explizit auftreten. Da beim Übergang von den Funktionen ξ zu den Funktionen η die Geometrie der Anordnung entweder dieselbe bleibt oder gespiegelt wird, je nachdem, ob die Permutation gerade oder ungerade ist, muß im letzten Fall ein Vorzeichenwechsel auftreten. Demzufolge werden aus den Projektionsoperatoren $\mathscr{P}_+(ijk)$ Projektionsoperatoren $\mathscr{P}(ijk)$. Unter Verwendung aller im Anhang B aufgeführten Symmetriebeziehungen zwischen Tensorkomponenten finden wir über einen erheblichen Rechenaufwand schließlich das Ergebnis (21).

$$[\omega] = K(\varphi(l_2, l_3, l_4) - \varphi(l_3, l_4, l_1) + \varphi(l_4, l_1, l_2) - \varphi(l_1, l_2, l_3))$$

mit

$$\varphi(l_i, l_j, l_k) = \mathscr{P}(ijk)\, \eta(l_i, l_j, l_k) \tag{21}$$

und

$$\eta(l_i, l_j, l_k) = \frac{6}{\sqrt{3^5}}\, \frac{\kappa_i \kappa_j}{a_{ij}^3}\, \frac{\kappa_j \kappa_k}{a_{jk}^3} \sum_s^{1,9} \eta_s(l_i, l_j, l_k)\,.$$

$$\begin{aligned}
\eta_1(l_i, l_j, l_k) = {}^{(R)}\alpha_t(l_i)\Big[&4\sqrt{2}\Big(1 - \frac{a_i a_j}{a_{ij}^2}\Big)\,{}^{(J)}\Gamma_{t'}(l_j) + 2\Big(1 + 8\,\frac{a_i a_j}{a_{ij}^2}\Big)\,{}^{(J)}\Gamma_{t,r}(l_j)\\
&- \Big(1 + 3\,\frac{a_j^2 - a_i^2}{a_{ij}^2}\Big)\,{}^{(J)}\Gamma_{r,t}(l_j)\Big]\,(\langle m(l_k)\rangle + c_k)_r\Big(1 + 3\,\frac{a_k^2 - a_j^2}{a_{jk}^2}\Big),
\end{aligned}$$

$$\begin{aligned}
\eta_2(l_i, l_j, l_k) = {}^{(R)}\alpha_r(l_i)\Big[&2\sqrt{2}\Big(1 + 3\,\frac{a_i^2 - a_j^2}{a_{ij}^2}\Big)\,{}^{(J)}\Gamma_{t'}(l_j) + \Big(1 + 3\,\frac{a_i^2 - a_j^2}{a_{ij}^2}\Big)\,{}^{(J)}\Gamma_{t,r}(l_j)\\
&+ 4\Big(1 + 4\,\frac{a_i a_j}{a_{ij}^2}\Big)\,{}^{(J)}\Gamma_{r,t}(l_j)\Big]\,(\langle m(l_k)\rangle + c_k)_r\Big(1 + 3\,\frac{a_k^2 - a_j^2}{a_{jk}^2}\Big),
\end{aligned}$$

$$\begin{aligned}
\eta_3(l_i, l_j, l_k) = {}^{(J)}\gamma_t(l_i)&\Big[12\sqrt{2}\,\frac{a_i a_j}{a_{ij}^2}\,{}^{(R)}A_t(l_j) + 9\Big(1 + \frac{a_j^2 - a_i^2}{a_{ij}^2}\Big)\,{}^{(R)}A_{r,t}(l_j)\Big]\\
&\cdot(\langle m(l_k)\rangle + c_k)_r\Big(1 + 3\,\frac{a_k^2 - a_j^2}{a_{jk}^2}\Big),
\end{aligned}$$

$$\eta_4(l_i, l_j, l_k) = {}^{(R)}\gamma_t(l_i)\,{}^{(J)}A_{r,t}(l_j)\quad 3\Big(1 + 3\,\frac{a_i^2 - a_j^2}{a_{ij}^2}\Big)(\langle m(l_k)\rangle + c_k)_r\Big(1 + 3\,\frac{a_k^2 - a_j^2}{a_{jk}^2}\Big),$$

$$\eta_5(l_i, l_j, l_k) = \frac{\pi}{c}\left({}^{(R)}\alpha_t(l_i) - {}^{(R)}\alpha_r(l_i)\right)\left[2\sqrt{2}\left(1 + 3\,\frac{a_i^2 - a_j^2}{a_{ij}^2}\right) a_j\,{}^{(R)}A_t(l_j)\right.$$
$$\left. + 4\left(1 + 4\,\frac{a_i a_j}{a_{ij}^2}\right) a_j\,{}^{(R)}A_{r,t}(l_j)\right] \left(\langle m(l_k)\rangle + c_k\right)_r \left(1 + 3\,\frac{a_k^2 - a_j^2}{a_{jk}^2}\right),$$

$$\eta_6(l_i, l_j, l_k) = -\left({}^{(J)}\gamma_t(l_i) + \frac{\pi}{c} a_i\,{}^{(R)}\alpha_t(l_i)\right){}^{(R)}\alpha_r(l_j)\,{}^{(R)}\alpha_r(l_k)\; 4\left(1 + 3\,\frac{a_j^2 - a_i^2}{a_{ij}^2}\right)\left(1 + 4\,\frac{a_j a_k}{a_{jk}^2}\right),$$

$$\eta_7(l_i, l_j, l_k) = -\left({}^{(J)}\gamma_t(l_i) + \frac{\pi}{c} a_i\,{}^{(R)}\alpha_t(l_i)\right){}^{(R)}\alpha_t(l_j)\,{}^{(R)}\alpha_r(l_k)\; 2\left(1 - 4\,\frac{a_i a_j}{a_{ij}^2}\right)\left(1 + 3\,\frac{a_k^2 - a_j^2}{a_{jk}^2}\right),$$

$$\eta_8(l_i, l_j, l_k) = \left({}^{(J)}\gamma_t(l_i) + \frac{\pi}{c} a_i\,{}^{(R)}\alpha_t(l_i)\right){}^{(R)}\alpha_r(l_j)\,{}^{(R)}\alpha_t(l_k)\left(1 + 3\,\frac{a_j^2 - a_i^2}{a_{ij}^2}\right)\left(1 + 3\,\frac{a_j^2 - a_k^2}{a_{jk}^2}\right),$$

$$\eta_9(l_i, l_j, l_k) = -\left({}^{(J)}\gamma_t(l_i) + \frac{\pi}{c} a_i\,{}^{(R)}\alpha_t(l_i)\right){}^{(R)}\alpha_t(l_j)\,{}^{(R)}\alpha_t(l_k)$$
$$\cdot 4\left(1 - 4\,\frac{a_i a_j}{a_{ij}^2} + 8\,\frac{a_j a_k}{a_{jk}^2} + 4\,\frac{a_i a_j}{a_{ij}^2}\,\frac{a_j a_k}{a_{jk}^2}\right).$$

c) Vereinfachende Annahmen für die $\mathrm{T_d}$*-Komponente im Modell* $\tilde{\mathcal{K}}$

Die Gl. (21) beinhaltet grundsätzlich die Möglichkeit, die konstituierenden 3-Liganden-Funktionen für den optischen Drehwinkel auf der Basis empirischer Daten über elektromagnetische Tensoren der Liganden oder auf der Basis ihrer quantenmechanischen Bestimmung zu berechnen. Es ist klar, daß der Umfang der Definitionsgleichungen (21) drastische Vereinfachungen erstrebenswert macht. Andererseits ist es kaum möglich, physikalisch begründbare Gesichtspunkte anzugeben, mit denen wir solche Vereinfachungen erreichen, ohne dabei die Beschreibung ganzer Klassen von speziellen Derivaten auszuschließen. Es ist daher sinnvoll, in diesem Kapitel neben der Schilderung einiger allgemeiner Gesichtspunkte Vereinfachungen per definitionem vorzunehmen und an den Konsequenzen zu zeigen, daß dabei tatsächlich praktisch traktable Ausdrücke entstehen. Schließlich besteht der Wert einer allgemeinen Formel wie (21) nicht zuletzt darin, bekannte empirische oder theoretische Ansätze quantenmechanischer oder klassischer Art in den Rahmen einer allgemeinen Theorie stellen zu können und dabei ihren Kompetenzanspruch kennenzulernen und Diskrepanzen mit den Beobachtungen zu verstehen.

Ohne auf den Spezialfall einzugehen, gibt es im wesentlichen drei Approximationsaspekte, und zwar:

1. Wir vernachlässigen Spineffekte. In diesem Fall gilt ${}^{(J)}A = 0$ und damit verschwindet η_4.

2. Wir ignorieren Glieder, in denen Hyperpolarisierbarkeiten vorkommen. Diese Glieder sind, als Korrekturen der permanenten Ligandendipole interpretiert, solche, die quadratisch von induzierenden Feldern abhängen. Ihre Vernachlässigung beinhaltet also die Beschränkung auf lineare Korrekturen der Ligandendipole.

Mit dieser Annahme verschwinden in unserem Ansatz alle Glieder bis auf η_6, η_7, η_8 und η_9. Damit verschwindet aber auch die Unterscheidung der optischen Aktivität von Methanderivaten mit C_{3v}-symmetrischen Liganden in der

Standard- und der „staggered"-Fixierung, eine Differenzierung, die in den meisten Fällen keine relevanten Konsequenzen für den optischen Drehwinkel haben dürfte. Die Differenz $[\Delta\omega]$ des optischen Drehwinkels zweier Derivate, die sich durch einen Liganden in Standard- und „staggered"-Fixierung unterscheiden, kommt nur im Vorzeichen von ${}^{(R)}A_t$ und ${}^{(J)}\Gamma_{t'}$ zum Ausdruck und kann also ohne Mühe aus (21) entnommen werden.

3. Wenn wir in (21) die reziproken Abstände a_{ij}^{-1} zwischen den Entwicklungspunkten nach Abweichungen von der Kantenlänge eines regulären Tetraeders mit einem mittleren Eckenabstand a vom zentralen Kohlenstoff entwickeln, erhalten wir für $[\omega]$ eine Summe von Produkten ligandenspezifischer Eigenschaften, die formal mit (2b) identisch ist. Wir schreiben das erste Glied dieser Entwicklung auf, also die spezielle Form von (21) für gleiche Abstände $a_1 = a_2 = a_3 = a_4 = a$:

$$
\begin{aligned}
[\omega] = \frac{\sqrt{3}}{8}\,\frac{K}{(2a)^6}\Bigg[& \begin{vmatrix} 1 \\ \kappa_i(\langle m(l_i)\rangle + c_i)_r \\ \kappa_i\,{}^{(R)}\alpha_t(l_i) \\ \kappa_i^2\left(\frac{5}{\sqrt{2}}\,{}^{(J)}\Gamma_{t'}(l_i) + 8\,{}^{(J)}\Gamma_{t,r}(l_i) - {}^{(J)}\Gamma_{r,t}(l_i)\right) \end{vmatrix} \\
& + \begin{vmatrix} 1 \\ \kappa_i(\langle m(l_i)\rangle + c_i)_r \\ \kappa_i\,{}^{(R)}\alpha_r(l_i) \\ \kappa_i^2(2\sqrt{2}\,{}^{(J)}\Gamma_{t'}(l_i) + {}^{(J)}\Gamma_{t,r}(l_i) + 10\,{}^{(J)}\Gamma_{r,t}(l_i)) \end{vmatrix} \\
& + \frac{9}{\sqrt{2}} \begin{vmatrix} 1 \\ \kappa_i(\langle m(l_i)\rangle + c_i)_r \\ \kappa_i\,{}^{(J)}\gamma_t(l_i) \\ \kappa_i^2({}^{(R)}A_t(l_i) + \sqrt{2}\,{}^{(R)}A_{r,t}(l_i)) \end{vmatrix} + 3 \begin{vmatrix} 1 \\ \kappa_i(\langle m(l_i)\rangle + c_i)_r \\ \kappa_i^{(R)}\gamma_t(l_i) \\ \kappa_i^{2\,(J)}A_{r,t}(l_i) \end{vmatrix} \qquad (21\text{a}) \\
& + \frac{\pi}{c}\,a \begin{vmatrix} 1 \\ \kappa_i(\langle m(l_i)\rangle + c_i)_r \\ \kappa_i({}^{(R)}\alpha_t(l_i) - {}^{(R)}\alpha_r(l_i)) \\ \kappa_i^2(2\sqrt{2}\,{}^{(R)}A_t(l_i) + 10\,{}^{(R)}A_{r,t}(l_i)) \end{vmatrix} + \begin{vmatrix} 1 \\ \kappa_i\,{}^{(R)}\alpha_r(l_i) \\ \kappa_i({}^{(J)}\gamma_t(l_i) + \frac{\pi}{c}a\,{}^{(R)}\alpha_t(l_i)) \\ \kappa_i^2(-10\,{}^{(R)}\alpha_r(l_i) + {}^{(R)}\alpha_t(l_i)) \end{vmatrix} \\
& + \begin{vmatrix} 1 \\ \kappa_i\,{}^{(R)}\alpha_t(l_i) \\ \kappa_i\,{}^{(J)}\gamma_t(l_i) \\ \kappa_i^2({}^{(R)}\alpha_r(l_i) - \frac{49}{4}\,{}^{(R)}\alpha_t(l_i)) \end{vmatrix} \Bigg].
\end{aligned}
$$

Dabei benutzen wir die Abkürzung

$$
\begin{vmatrix} 1 \\ f(l_i) \\ g(l_i) \\ h(l_i) \end{vmatrix} = \begin{vmatrix} 1 & 1 & 1 & 1 \\ f(l_1) & f(l_2) & f(l_3) & f(l_4) \\ g(l_1) & g(l_2) & g(l_3) & g(l_4) \\ h(l_1) & h(_2) & h(l_3) & h(l_4) \end{vmatrix}.
$$

Formel (21a) ist auch eine vernünftige Näherung für ein Derivat mit sehr ähnlichen Ligandenabständen, wenn wir $a = \frac{1}{4}\sum_i^{1,4} a_i$ setzen, oder für eine Molekülklasse von Derivaten mit Liganden sehr ähnlicher Abstände aus einem Sortiment $l(1)\ldots l(N)$, wenn wir den klassenspezifischen Mittelwert $a = \frac{1}{N}\sum_{i=1}^{N} a_i$ benutzen. Wir erinnern daran (vgl. Kap. II.5), daß die a_i bzw. a sich nicht notwendig auf Ligandenschwerpunkte, sondern primär auf Stellen für optimale Konvergenz in der Multipolentwicklung beziehen, daß aber die Identifizierung beider Aspekte in vielen Fällen eine plausible Annahme ist.

Mit der zusätzlichen Annahme 2), der Vernachlässigung aller Hyperpolarisierbarkeiten, verschwinden alle Determinanten mit Ausnahme der letzten beiden.

4. (21a) verschwindet, wenn Hyperpolarisierbarkeiten vernachlässigt und $\kappa_i = 1$ gesetzt werden. Damit haben wir einen Hinweis für weitere Annahmen mit vereinfachenden Konsequenzen. Wir beziehen uns auf große Liganden und vernachlässigen Hyperpolarisierbarkeiten. Wegen $n_i \gg 1$ gilt also $\kappa_i^2 \approx \kappa_i \approx 1$, und damit rechtfertigt sich eine Formel mit der Hypothese $A = 0$, $\Gamma = 0$, $\kappa_i = 1$ für alle i. Die Abstände seien ähnlich, so daß die linearen Glieder in den Abstandsunterschieden eine ausreichende Beschreibung liefern. Wir entwickeln nach $(a(l_i) - a)/a$ an einer geeigneten Stelle a, wobei wir $a(l_i)$ statt a_i schreiben, um in den folgenden Formeln alle ligandenspezifischen Größen in der gleichen Weise zu bezeichnen, und brechen die Entwicklung mit linearen Gliedern ab. Da (21a) mit den obigen Bedingungen verschwindet, also das konstante Glied null wird, findet man die relativ einfache Formel:

$$[\omega] = \frac{3\sqrt{3}}{16}\,\frac{K}{(2a)^7}\left[\begin{vmatrix} 1 \\ -10\,{}^{(R)}\alpha_r(l_i) + {}^{(R)}\alpha_t(l_i) \\ {}^{(J)}\gamma_t(l_i) \\ a(l_i)\,{}^{(R)}\alpha_r(l_i) \end{vmatrix} + \begin{vmatrix} 1 \\ -2\,{}^{(R)}\alpha_r(l_i) + \tfrac{49}{2}\,{}^{(R)}\alpha_t(l_i) \\ {}^{(J)}\gamma_t(l_i) \\ a(l_i)\,{}^{(R)}\alpha_t(l_i) \end{vmatrix} \right.$$

$$\left. + 3\begin{vmatrix} 1 \\ {}^{(R)}\alpha_r(l_i) \\ a(l_i)\,{}^{(J)}\gamma_t(l_i) \\ {}^{(R)}\alpha_t(l_i) \end{vmatrix} - 5\,\frac{\pi a}{c}\begin{vmatrix} 1 \\ {}^{(R)}\alpha_r(l_i) \\ {}^{(R)}\alpha_t(l_i) \\ a(l_i)\,(2\,{}^{(R)}\alpha_r(l_i) + {}^{(R)}\alpha_t(l_i)) \end{vmatrix}\right]. \qquad (21\text{b})$$

Mit der zusätzlichen Annahme, daß die elektrischen Polarisierbarkeiten für alle Liganden eines Derivats etwa denselben Anisotropiefaktor haben, können wir setzen ${}^{(R)}\alpha_t(l_i) = \varepsilon\,{}^{(R)}\alpha_r(l_i)$ und erhalten aus (21b) die einfache Form

$$[\omega] = \frac{3\sqrt{3}}{16}\,\frac{K}{(2a)^7}\left(10 + \varepsilon - \frac{49}{2}\varepsilon^2\right) \begin{vmatrix} 1 & 1 & 1 & 1 \\ {}^{(R)}\alpha_r(l_1) & {}^{(R)}\alpha_r(l_2) & {}^{(R)}\alpha_r(l_3) & {}^{(R)}\alpha_r(l_4) \\ a(l_1)\,{}^{(R)}\alpha_r(l_1) & a(l_2)\,{}^{(R)}\alpha_r(l_2) & a(l_3)\,{}^{(R)}\alpha_r(l_3) & a(l_4)\,{}^{(R)}\alpha_r(l_4) \\ {}^{(J)}\gamma_t(l_1) & {}^{(J)}\gamma_t(l_2) & {}^{(J)}\gamma_t(l_3) & {}^{(J)}\gamma_t(l_4) \end{vmatrix}. \qquad (21\text{c})$$

Die speziellen Formeln (21a), (21b), (21c) sind alle von der Struktur (2b), bestehen also aus Determinanten mit der Zahl 1 in allen Spalten der ersten Zeile. Dies führt zu einer wesentlichen Erleichterung in der experimentellen Bestimmung der zu einer semiempirischen Berechnung des optischen Drehwinkels benötigten elektromagnetischen Größen. Die Ligandenqualitäten müssen nämlich wegen der genannten Eigenschaften der Determinanten nur bis auf eine gemeinsame Konstante bekannt sein. Um also z. B. ${}^{(R)}\alpha_r(l_i)$ oder ${}^{(J)}\gamma_t(l_i)$ in (21c) zu bestimmen, ist es zulässig, diese Qualität an einem achiralen Derivat zu messen, das außer dem entsprechenden Liganden l_i drei gleichartige Liganden l, beispielsweise Wasserstoff, enthält. Dieses Derivat hat die Symmetrie C_{3v}, und wir dürfen in akzeptabler Näherung annehmen, daß sich die in Rede stehenden Eigenschaften des Derivats additiv aus denen der Liganden zusammensetzen. Die Qualitäten für verschiedene Liganden unterscheiden sich von den experimentell bestimmten Qualitäten der entsprechenden Derivate also nur um einen konstanten Betrag, der ohne Einfluß auf den Wert der Determinante ist. Wir können daher für die Berechnung von (21c) die experimentellen Daten der entsprechenden Derivate benutzen.

5. Bei Derivaten, die nicht den diskutierten Voraussetzungen genügen, müssen individuelle Approximationsaspekte herangezogen werden, die wir nicht alle im einzelnen besprechen können. Es ist z. B. möglich, daß eine der obigen Voraussetzungen für drei der Liganden zutreffen, aber nicht für den vierten. Dann kann in entsprechender Weise vorgegangen werden, indem man die Näherungsannahme für diese drei Liganden macht und den vierten nach abweichenden Eigenschaften von den übrigen drei Liganden entwickelt. Auf diese oder andere Weise erhalten wir vereinfachte Formeln, die dem individuellen Charakter der einzelnen Fälle Rechnung tragen.

6. Wir nehmen einen Standpunkt ein, der gewissermaßen den empirischen Aspekt extrem betont. Wir setzen nämlich entsprechende elektrische und elektromagnetische Tensorkomponenten an den Entwicklungsstellen verschiedener Liganden einander gleich. Dies ist sicher ein Gewaltakt, der die Realität im allgemeinen völlig entstellt und dazu führt, daß formal nur die Verschiedenheit der Abstände $a(l_i)$ Anlaß zur optischen Aktivität gibt. Es ist aber möglich, dieses Vorgehen damit einigermaßen zu korrigieren, daß wir auf eine physikalische Interpretation verzichten und die Unterschiede der elektromagnetischen Eigenschaften verschiedener Liganden durch eine geeignete Wahl „repräsentativer Abstände“ gewissermaßen in Vertretung charakterisieren. Es ist also gar nicht beabsichtigt, nach einer physikalisch detaillierten Vorstellung über die Abhängigkeit der repräsentativen Längen von den elektrischen Eigenschaften der Liganden zu suchen, sondern wir machen einfach von der Tatsache Gebrauch, daß die Form (21) mit verschiedenen Abständen und im übrigen identischen Eigenschaften der Liganden eine von Null verschiedene Chiralitätsfunktion liefert, und hoffen, durch geeignete Wahl der Abstände die elektrischen und elektromagnetischen Eigenschaften summarisch erfassen und das Gesamtphänomen in akzeptabler Approximation beschreiben zu können. Die repräsentativen Abstände spielen dabei die Rolle von empirisch zu bestimmtenden Parametern $\lambda(l_i)$.

In Anbetracht dieser äußerst großzügigen Approximation begnügen wir uns mit der Feststellung, daß der Ausdruck (21) in der Umgebung eines mittleren

Abstandes a eine Funktion der $\lambda(l_i)$ ist, die als Produkt von zwei Faktoren geschrieben werden kann. Einer davon ist die Vandermondesche Determinante (2a), der andere eine in den Permutationen der Liganden totalsymmetrische Funktion der $\lambda(l_i)$. Bei gleichgesetzten elektromagnetischen Eigenschaften der Liganden führt eine Taylorreihenentwicklung von (21) nach einem mittleren Abstand a und Abbrechen mit dem Polynom niedrigsten Grades in den Abstandsdifferenzen auf die Form

$$[\omega] = \frac{C}{a^{12}} (\lambda(l_1) - \lambda(l_2))(\lambda(l_1) - \lambda(l_3))(\lambda(l_1) - \lambda(l_4)) \qquad (21\text{d})$$

$$\cdot (\lambda(l_2) - \lambda(l_3))(\lambda(l_2) - \lambda(l_4))(\lambda(l_3) - \lambda(l_4)).$$

Dabei ist neben den Parametern $\lambda(l_i)$ die Konstante C aus experimentellen Daten über den Drehwinkel zu entnehmen. Wenn wir das arithmetische Mittel $a = \frac{1}{N} \sum_{i}^{1,N} \lambda(l_i)$ der Abstände eines Ligandensortiments verwenden, ist C/a^{12} ein klassenspezifischer Parameter und die Form (21d) ist mit dem Ansatz nach dem ersten Verfahren identisch. Die zweite Möglichkeit, für jedes Derivat jeweils $a = \frac{1}{4} \sum_{i}^{1,4} \lambda(l_i)$ zu setzen, führt zu einem etwas komplizierteren Verfahren. Mit dieser Interpretation hat die Formel eine große Ähnlichkeit mit einem Ansatz von Boys [1].

IV. Schlußbemerkungen

Wir haben in dieser Arbeit auf die Diskussion von Formeln für die optische Aktivität von speziellen Methanderivaten verzichtet. Wir glauben aber, wesentliche Grenzfälle allgemeiner Art besprochen und spezielle Vereinfachungen soweit vorbereitet zu haben, daß man, von diesen Grenzsituationen ausgehend, vorgegebene Einzelfälle mit einem erträglichen Aufwand behandeln kann. Unabhängig von der Möglichkeit zur Spezialisierung haben wir ein Urteil gewonnen über die physikalische Relevanz verschiedener mathematischer Approximationen und Formeln gefunden, die eine semiempirische oder theoretische Analyse des optischen Phänomens an der ganzen Klasse chiraler Methanderivate gestatten. Wir fassen die unserer Meinung nach wesentlichsten Resultate im folgenden kurz zusammen:

1. Bei Methanderivaten gibt es einen Beitrag zur optischen Aktivität, dessen Relevanz vom Ausmaß abhängt, bis zu dem die T_d-Bedingung, eine geometrische Bedingung über Bindungswinkel, Ligandensymmetrie und Art der Fixierung von Liganden, erfüllt ist. Die T_d-Komponente des optischen Drehwinkels ist bei allen Methanderivaten von Null verschieden und ist bei T_d-Derivaten die einzige. Sie wird in unserer Theorie in zweiter störungstheoretischer Korrektur beschrieben, während alle Komponenten, die auf Abweichungen in der Geometrie zurückgehen, in erster oder nullter Ordnung erscheinen. Im Modell $\bar{\mathscr{H}}$ liefert die Störungsrechnung bis zur zweiten Ordnung die T_d-Komponente in Form des Ansatzes nach dem zweiten Näherungsverfahren. Da dieses Modell im wesent-

lichen nur fixierte Kernorte als Näherungsannahme enthält, sind der Ansatz des zweiten Verfahrens und seine Konsequenzen als quantitativ gültige Aussagen zu betrachten. Eine experimentelle Untersuchung sollte dementsprechend in einem ersten Schritt der Analyse der T_d-Komponente entsprechend der Beziehung (20) und in einem zweiten Schritt der Erklärung von Zusatzbeiträgen gewidmet werden.

2. Im Modell $\tilde{\mathscr{H}}$ wird der optische Drehwinkel explizit auf elektrische und elektromagnetische Eigenschaften der einzelnen Liganden zurückgeführt. Es besteht die Möglichkeit, durch Messungen an einfach substituierten achiralen Methanderivaten die Bestimmungsstücke für den optischen Drehwinkel chiraler Derivate empirisch festzustellen. Mit wachsender experimenteller Information darf erwartet werden, daß auch Derivate mit größerer Abweichung von der T_d-Bedingung analysiert werden können.

3. Es besteht grundsätzlich die Möglichkeit, die ligandenspezifischen Eigenschaften quantenmechanisch zu behandeln und insofern eine *ab ovo*-Rechnung durchzuführen. Auch eine solche Rechnung profitiert von unserer Theorie, da die Zahl der Derivate stärker wächst als die Zahl der konstituierenden Liganden.

4. Der Ansatz nach dem ersten Näherungsverfahren, die Vandermondesche Determinante, läßt sich nicht ohne drastische Näherungsannahmen reproduzieren. Die Parameter $\lambda(l_i)$ erhalten dabei die Bedeutung repräsentativer Abstände.

5. Insoweit experimentelle Daten mit der Möglichkeit eines Tests der aufgeführten Behauptungen vorliegen, wird die Theorie bestätigt (vgl. [12]).

V. Anhang

A. Störungsrechnung

Man findet den Rosenfeldausdruck (1) und seine Korrekturterme (10) folgendermaßen: Der Operator für die Wechselwirkung zwischen Strahlung und Materie wird als Störoperator zum Hamiltonoperator des unbeeinflußten Moleküls betrachtet, in zeitabhängiger Störungsrechnung werden die induzierten elektrischen und magnetischen Multipolmomente berechnet und die Ausdrücke über alle Orientierungen des Moleküls gemittelt. Dabei werden wegen der bei Lichtstrahlung vernachlässigbar kleinen Größe $\frac{e^2}{c^2}\,|\vec{A}|^2$ nur Beiträge berücksichtigt, die linear von den Feldern der Lichtwelle abhängen. Bei dieser Entwicklung nach Feldern der Lichtwelle, genauer nach den effektiven Feldern am Ort eines einzelnen Moleküls, treten pseudoskalare Proportionalitätsfaktoren auf, die sich mit Hilfe der Maxwellschen Gleichungen mit dem optischen Drehwinkel korrelieren lassen. Das Ergebnis ist (1) bzw. (10).

Die Störungsrechnung für (1) bzw. (10) mit $\Sigma\,\bar{\mathscr{H}}_{ij}$ bzw. $\Sigma\,\bar{\mathscr{H}}_{ij}^{[2]}$ als Störoperatoren wird nach der Rayleigh-Schrödinger-Störungstheorie durchgeführt. Da sich das Problem in einem endlichen Kasten praktisch nicht von der Situation ohne äußere Begrenzung unterscheidet, können wir darauf verzichten, das kontinuierliche Spektrum zu berücksichtigen.

Die Korrekturen erster und zweiter Ordnung von nichtentarteten Eigenwerten und Eigenvektoren $E_s^{(0)}$ und $|s\rangle^{(0)}$ des ungestörten Operators $\mathscr{H}_0$ bei Störung durch den Operator $\mathscr{V} = \Sigma\, \bar{\mathscr{H}}_{ij}$ lauten:

$$E_s^{(1)} = {}^{(0)}\langle s|\mathscr{V}|s\rangle^{(0)}, \qquad E_s^{(2)} = \sum_{t(\neq s)} \frac{{}^{(0)}\langle s|\mathscr{V}|t\rangle^{(0)}\,{}^{(0)}\langle t|\mathscr{V}|s\rangle^{(0)}}{E_s^{(0)} - E_t^{(0)}},$$

$$|s\rangle^{(1)} = \sum_{t(\neq s)} \frac{|t\rangle^{(0)}\,{}^{(0)}\langle t|\mathscr{V}|s\rangle^{(0)}}{E_s^{(0)} - E_t^{(0)}},$$

$$|s\rangle^{(2)} = \sum_{t(\neq s)} \frac{|t\rangle^{(0)}}{E_s^{(0)} - E_t^{(0)}} \left\{ \sum_{r(\neq s)} \frac{{}^{(0)}\langle t|\mathscr{V}|r\rangle^{(0)}\,{}^{(0)}\langle r|\mathscr{V}|s\rangle^{(0)}}{E_s^{(0)} - E_r^{(0)}} - \frac{{}^{(0)}\langle t|\mathscr{V}|s\rangle^{(0)}\,{}^{(0)}\langle s|\mathscr{V}|s\rangle^{(0)}}{E_s^{(0)} - E_t^{(0)}} \right\} - \frac{1}{2}\,|s\rangle^{(0)} \sum_{t(\neq s)} \frac{{}^{(0)}\langle s|\mathscr{V}|t\rangle^{(0)}\,{}^{(0)}\langle t|\mathscr{V}|s\rangle^{(0)}}{(E_s^{(0)} - E_t^{(0)})^2}.$$

Bei chiralen Methanderivaten gibt es im Modell $\bar{\mathscr{H}}$ und $\tilde{\mathscr{H}}$ außer Kramersentartung keine symmetriebedingte Entartung. Im ungestörten Modell $\mathscr{H}_0$ folgt bereits aus der C_{3v}-Symmetrie der Liganden Entartung von Moleküleigenfunktionen. Die Störungsrechnung im Entartungsfall führt zu einer unitären Transformation der entarteten Eigenfunktionen auf eine störungsadaptierte Basis und zu Zusatztermen für die auf entartete Eigenfunktionen bezogenen Matrixelemente aus Kap. II.6 und II.7. Dies hat zur Folge, daß Teilsummen über Produkte von Matrixelementen, die über orthogonale Eigenfunktionen zu einem entarteten Teilraum laufen und sich nach der nichtentarteten Störungsrechnung in der Form

$$\sum_{\lambda} {}^{(0)}\langle o|\ldots|s_\lambda\rangle^{(0)}\,{}^{(0)}\langle s_\lambda|\ldots|s_\lambda\rangle^{(0)}\,{}^{(0)}\langle s_\lambda|\ldots|s_\lambda\rangle^{(0)}\,{}^{(0)}\langle s_\lambda|\ldots|o\rangle^{(0)}$$

präsentieren, zu ersetzen sind durch

$$\sum_{\lambda,\mu,\nu\,\ldots} {}^{(0)}\langle o|\ldots|s_\lambda\rangle^{(0)}\,{}^{(0)}\langle s_\lambda|\ldots|s_\mu\rangle^{(0)}\,{}^{(0)}\langle s_\mu|\ldots|s_\nu\rangle^{(0)}\,{}^{(0)}\langle s_\nu|\ldots|o\rangle^{(0)}.$$

Entsprechendes gilt für Entartung des Grundzustandes.

Man überzeugt sich im Text ohne Mühe, daß sich aus dieser Abänderung weder an der Zerlegung des Rosenfeldausdruckes zum ganzen Molekül nach Teilsystemen noch an der Interpretation dieser Teilausdrücke etwas ändert. Da sich die quantenmechanische Definition der elektromagnetischen Tensoren bei Entartung entsprechend ändert, bleibt auch die Formulierung des Resultates in der Terminologie von Polarisierbarkeiten und Hyperpolarisierbarkeiten unverändert.

Der Rosenfeldausdruck, seine Korrekturterme und alle elektromagnetischen Tensoren sind in jeder störungstheoretischen Ordnung invariant gegenüber unitären Transformationen der Eigenfunktionen zu einem entarteten Teilraum. Aus diesem Grunde ist zu ihrer Berechnung die Kenntnis störungsadaptierter Eigenfunktionen nicht erforderlich.

B. Elektromagnetische Tensoren

Die quantenmechanische Definition für die Polarisierbarkeiten ${}^{(R)}\alpha$, ${}^{(J)}\alpha$, ${}^{(R)}\gamma$, ${}^{(J)}\gamma$ und Hyperpolarisierbarkeiten ${}^{(R)}A$, ${}^{(J)}A$, ${}^{(J)}\Gamma$ eines Systems im Grundzustand $|o\rangle$ ist folgende:

$$^{(R)}\alpha_{\varrho\sigma} = \frac{2}{h}\,\mathrm{Re}\sum_{s}\frac{\nu_{so}}{\nu_{so}^2-\nu^2}\langle o|m_\varrho|s\rangle\langle s|m_\sigma|o\rangle = {}^{(R)}\alpha_{\sigma\varrho}\,.$$

$$^{(J)}\alpha_{\varrho\sigma} = \frac{2}{h}\,\mathrm{Im}\sum_{s}\frac{1}{\nu_{so}^2-\nu^2}\langle o|m_\varrho|s\rangle\langle s|m_\sigma|o\rangle = -{}^{(J)}\alpha_{\sigma\varrho}\,.$$

$$^{(R)}\gamma_{\varrho\sigma} = \frac{2}{h}\,\mathrm{Re}\sum_{s}\frac{\nu_{so}}{\nu_{so}^2-\nu^2}\langle o|m_\varrho|s\rangle\langle s|\mu_\sigma|o\rangle\,,$$

$$^{(J)}\gamma_{\varrho\sigma} = \frac{2}{h}\,\mathrm{Im}\sum_{s}\frac{1}{\nu_{so}^2-\nu^2}\langle o|m_\varrho|s\rangle\langle s|\mu_\sigma|o\rangle\,.$$

$$\begin{aligned}
^{(R)}A_{\varrho\sigma\tau} = {} & \frac{2}{h^2}\,\mathrm{Re}\sum_{s}\frac{\nu_{so}^2+\nu^2}{(\nu_{so}^2-\nu^2)^2}\langle o|m_\varrho|s\rangle\langle s|m_\sigma|o\rangle\{\langle s|m_\tau|s\rangle-\langle o|m_\tau|o\rangle\}\\
& + \frac{2}{h^2}\,\mathrm{Re}\sum_{s,t(\neq o)}\frac{\nu_{so}}{\nu_{to}(\nu_{so}^2-\nu^2)}(\langle o|m_\varrho|s\rangle\langle s|m_\sigma|t\rangle\langle t|m_\tau|o\rangle\\
& \qquad + \langle t|m_\varrho|s\rangle\langle s|m_\sigma|o\rangle\langle o|m_\tau|t\rangle)\\
& + \frac{2}{h^2}\,\mathrm{Re}\sum_{s,t(\neq s)}\frac{\nu_{so}}{\nu_{ts}(\nu_{so}^2-\nu^2)}(\langle o|m_\varrho|s\rangle\langle t|m_\sigma|o\rangle\langle s|m_\tau|t\rangle\\
& \qquad + \langle o|m_\varrho|t\rangle\langle s|m_\sigma|o\rangle\langle t|m_\tau|s\rangle) = {}^{(R)}A_{\sigma\varrho\tau}\,.
\end{aligned}$$

$$\begin{aligned}
^{(J)}A_{\varrho\sigma\tau} = {} & \frac{2}{h^2}\,\mathrm{Im}\sum_{s}\frac{2\nu_{so}}{(\nu_{so}^2-\nu^2)^2}\langle o|m_\varrho|s\rangle\langle s|m_\sigma|o\rangle\{\langle s|m_\tau|s\rangle-\langle o|m_\tau|o\rangle\}\\
& + \frac{2}{h^2}\,\mathrm{Im}\sum_{s,t(\neq o)}\frac{1}{\nu_{to}(\nu_{so}^2-\nu^2)}(\langle o|m_\varrho|s\rangle\langle s|m_\sigma|t\rangle\langle t|m_\tau|o\rangle\\
& \qquad + \langle t|m_\varrho|s\rangle\langle s|m_\sigma|o\rangle\langle o|m_\tau|t\rangle)\\
& + \frac{2}{h^2}\,\mathrm{Im}\sum_{s,t(\neq s)}\frac{1}{\nu_{ts}(\nu_{so}^2-\nu^2)}(\langle o|m_\varrho|s\rangle\langle t|m_\sigma|o\rangle\langle s|m_\tau|t\rangle\\
& \qquad + \langle o|m_\varrho|t\rangle\langle s|m_\sigma|o\rangle\langle t|m_\tau|s\rangle) = -{}^{(J)}A_{\sigma\varrho\tau}\,.
\end{aligned}$$

$$\begin{aligned}
^{(R)}\Gamma_{\varrho\sigma\tau} = {} & \frac{2}{h^2}\,\mathrm{Re}\sum_{s}\frac{\nu_{so}^2+\nu^2}{(\nu_{so}^2-\nu^2)^2}\langle o|m_\varrho|s\rangle\langle s|\mu_\sigma|o\rangle\{\langle s|m_\tau|s\rangle-\langle o|m_\tau|o\rangle\}\\
& + \frac{2}{h^2}\,\mathrm{Re}\sum_{s,t(\neq o)}\frac{\nu_{so}}{\nu_{to}(\nu_{so}^2-\nu^2)}(\langle o|m_\varrho|s\rangle\langle s|\mu_\sigma|t\rangle\langle t|m_\tau|o\rangle\\
& \qquad + \langle t|m_\varrho|s\rangle\langle s|\mu_\sigma|o\rangle\langle o|m_\tau|t\rangle)\\
& + \frac{2}{h^2}\,\mathrm{Re}\sum_{s,t(\neq s)}\frac{\nu_{so}}{\nu_{ts}(\nu_{so}^2-\nu^2)}(\langle o|m_\varrho|s\rangle\langle t|\mu_\sigma|o\rangle\langle s|m_\tau|t\rangle\\
& \qquad + \langle o|m_\varrho|t\rangle\langle s|\mu_\sigma|o\rangle\langle t|m_\tau|s\rangle)\,,
\end{aligned}$$

$$\begin{aligned}
^{(J)}\Gamma_{\varrho\sigma\tau} = {} & \frac{2}{h^2}\,\mathrm{Im}\sum_{s}\frac{2\nu_{so}}{(\nu_{so}^2-\nu^2)^2}\langle o|m_\varrho|s\rangle\langle s|\mu_\sigma|o\rangle\{\langle s|m_\tau|s\rangle-\langle o|m_\tau|o\rangle\}\\
& + \frac{2}{h^2}\,\mathrm{Im}\sum_{s,t(\neq o)}\frac{1}{\nu_{to}(\nu_{so}^2-\nu^2)}(\langle o|m_\varrho|s\rangle\langle s|\mu_\sigma|t\rangle\langle t|m_\tau|o\rangle\\
& \qquad + \langle t|m_\varrho|s\rangle\langle s|\mu_\sigma|o\rangle\langle o|m_\tau|t\rangle)\\
& + \frac{2}{h^2}\,\mathrm{Im}\sum_{s,t(\neq s)}\frac{1}{\nu_{ts}(\nu_{so}^2-\nu^2)}(\langle o|m_\varrho|s\rangle\langle t|\mu_\sigma|o\rangle\langle s|m_\tau|t\rangle\\
& \qquad + \langle o|m_\varrho|t\rangle\langle s|\mu_\sigma|o\rangle\langle t|m_\tau|s\rangle)\,.
\end{aligned}$$

Die Tensoren A und Γ können mittels Störungsrechnung mit der Wechselwirkungsenergie zwischen elektrischem Dipolmoment und äußerem Feld als Störoperator aus den Tensoren α bzw. γ und Δ aus Γ berechnet werden (vgl. [7]). Die Formeln für die Polarisierbarkeiten gelten auch für den Entartungsfall; in den Definitionsgleichungen für die Hyperpolarisierbarkeiten A und Γ müssen entweder störungsadaptierte Eigenfunktionen vorausgesetzt werden, oder man hat Summen über Eigenfunktionen s_λ aus entarteten Teilräumen der Form

$$\sum_\lambda \langle o|\ldots|s_\lambda\rangle \langle s_\lambda|\ldots|s_\lambda\rangle \langle s_\lambda|\ldots|o\rangle$$

zu ersetzen durch

$$\sum_{\lambda,\mu} \langle o|\ldots|s_\lambda\rangle \langle s_\lambda|\ldots|s_\mu\rangle \langle s_\mu|\ldots|o\rangle\,.$$

Im Falle entarteter Grundzustände hat man in den Definitionsgleichungen das arithmetische Mittel über eine Basis für den Eigenwert E_o zu benutzen.

Bei elektrisch neutralen Systemen sind die Tensoren ${}^{(R)}\alpha$, ${}^{(J)}\alpha$, ${}^{(R)}A$, ${}^{(J)}A$ ortsunabhängig, nicht dagegen die übrigen Tensoren, da sich beim Übergang vom Ort $\vec{r}$ zum Ort $\vec{r}'$ das magnetische Moment $\langle s|\vec{\mu}|t\rangle$ gemäß Formel (5a) ändert. Damit ergeben sich die Transformationsgleichungen

$$\sum_\sigma^{1,3} {}^{(R)}\gamma_{\varrho\sigma}\,\vec{e}_\sigma = \sum_\sigma^{1,3} {}^{(R)}\gamma'_{\varrho\sigma}\,\vec{e}_\sigma - \frac{\pi}{c}\,\nu^2 \sum_\sigma^{1,3} {}^{(J)}\alpha_{\varrho\sigma}(\vec{r}'-\vec{r})\times\vec{e}_\sigma\,,$$

$$\sum_\sigma^{1,3} {}^{(J)}\gamma_{\varrho\sigma}\,\vec{e}_\sigma = \sum_\sigma^{1,3} {}^{(J)}\gamma'_{\varrho\sigma}\,\vec{e}_\sigma + \frac{\pi}{c} \sum_\sigma^{1,3} {}^{(R)}\alpha_{\varrho\sigma}(\vec{r}'-\vec{r})\times\vec{e}_\sigma\,,$$

$$\sum_\sigma^{1,3} {}^{(R)}\Gamma_{\varrho\sigma\tau}\,\vec{e}_\sigma = \sum_\sigma^{1,3} {}^{(R)}\Gamma'_{\varrho\sigma\tau}\,\vec{e}_\sigma - \frac{\pi}{c}\,\nu^2 \sum_\sigma^{1,3} {}^{(J)}A_{\varrho\sigma\tau}(\vec{r}'-\vec{r})\times\vec{e}_\sigma\,,$$

$$\sum_\sigma^{1,3} {}^{(J)}\Gamma_{\varrho\sigma\tau}\,\vec{e}_\sigma = \sum_\sigma^{1,3} {}^{(J)}\Gamma'_{\varrho\sigma\tau}\,\vec{e}_\sigma + \frac{\pi}{c} \sum_\sigma^{1,3} {}^{(R)}A_{\varrho\sigma\tau}(\vec{r}'-\vec{r})\times\vec{e}_\sigma$$

oder mit der Zusammenfassung zu komplexen Größen $t = {}^{(R)}t - i\nu\,{}^{(J)}t$

$$\sum_\sigma^{1,3} \gamma_{\varrho\sigma}\,\vec{e}_\sigma = \sum_\sigma^{1,3} \gamma'_{\varrho\sigma}\,\vec{e}_\sigma - \frac{i\pi}{c}\,\nu \sum_\sigma^{1,3} \alpha_{\varrho\sigma}(\vec{r}'-\vec{r})\times\vec{e}_\sigma\,,$$

$$\sum_\sigma^{1,3} \Gamma_{\varrho\sigma\tau}\,\vec{e}_\sigma = \sum_\sigma^{1,3} \Gamma'_{\varrho\sigma\tau}\,\vec{e}_\sigma - \frac{i\nu}{c}\,\nu \sum_\sigma^{1,3} A_{\varrho\sigma\tau}(\vec{r}'-\vec{r})\times\vec{e}_\sigma\,.$$

Damit werden die Formeln (13) und (15) verständlich.

Bei geeigneter Multiplikation von Momenten, Polarisierbarkeiten und Hyperpolarisierbarkeiten mit der Ladung e bzw. der Geschwindigkeit c erhalten wir Größen von der Dimension der Potenz einer Länge, und zwar:

$$\begin{aligned}
\left[\frac{\langle m_\varrho\rangle}{e}\right] &= \left[\frac{\langle \mu_\varrho\rangle}{e}\right] &&= cm\,,\\
[{}^{(R)}\alpha_{\varrho\sigma}] &= [{}^{(R)}\gamma_{\varrho\sigma}] &&= cm^3\,,\\
[c\,{}^{(J)}\alpha_{\varrho\sigma}] &= [c\,{}^{(J)}\gamma_{\varrho\sigma}] &&= cm^4\,,\\
[e\,{}^{(R)}A_{\varrho\sigma\tau}] &= [e\,{}^{(R)}\Gamma_{\varrho\sigma\tau}] &&= cm^5\,,\\
[ec\,{}^{(J)}A_{\varrho\sigma\tau}] &= [ec\,{}^{(J)}\Gamma_{\varrho\sigma\tau}] &&= cm^6\,.
\end{aligned}$$

Für die Tensoren ${}^{(R)}\alpha$, ${}^{(R)}\gamma$, ${}^{(J)}\gamma$, ${}^{(R)}A$, ${}^{(J)}A$, ${}^{(J)}\Gamma$ von Liganden mit der Symmetrie C_{3nv} mit $n \geqq 1$ oder $C_{\infty v}$ gelten die in Tab. 1 aufgeführten Symmetrierelationen, alle nicht aufgeführten Komponenten verschwinden. Ein permanenter elektrischer Dipol kann nur eine Komponente in Richtung $\vec{e}_r$ haben, ein permanenter magnetischer Dipol existiert nicht, auch die Komponenten von ${}^{(J)}\alpha$ sind sämtlich gleich Null.

Tabelle 1

$$\begin{aligned}
&{}^{(R)}\alpha_r \equiv {}^{(R)}\alpha_{rr}\\
&{}^{(R)}\alpha_t \equiv {}^{(R)}\alpha_{tt} = {}^{(R)}\alpha_{t't'}\\
&{}^{(R)}\gamma_t \equiv {}^{(R)}\gamma_{tt} = - {}^{(R)}\gamma_{t't'}\\
&{}^{(J)}\gamma_t \equiv {}^{(J)}\gamma_{tt'} = - {}^{(J)}\gamma_{t't}\\
&{}^{(R)}A_t \equiv {}^{(R)}A_{ttt} = - {}^{(R)}A_{tt't'} = - {}^{(R)}A_{t'tt'} = - {}^{(R)}A_{t't't}\\
&{}^{(R)}A_{r,t} \equiv {}^{(R)}A_{trt} = {}^{(R)}A_{rtt} = {}^{(R)}A_{t'rt'} = {}^{(R)}A_{rt't'}\\
&{}^{(R)}A_{t,r} \equiv {}^{(R)}A_{ttr} = {}^{(R)}A_{t't'r}\\
&{}^{(R)}A_r \equiv {}^{(R)}A_{rrr}\\
&{}^{(J)}A_{r,t} \equiv {}^{(J)}A_{trt'} = - {}^{(J)}A_{rtt'} = {}^{(J)}A_{t'rt} = - {}^{(J)}A_{rt't}\\
&{}^{(J)}\Gamma_{t'} \equiv {}^{(J)}\Gamma_{t't't'} = {}^{(J)}\Gamma_{t'tt} = - {}^{(J)}\Gamma_{tt't} = - {}^{(J)}\Gamma_{ttt'}\\
&{}^{(J)}\Gamma_{t,r} \equiv {}^{(J)}\Gamma_{tt'r} = - {}^{(J)}\Gamma_{t'tr}\\
&{}^{(J)}\Gamma_{t,r} \equiv {}^{(J)}\Gamma_{trt'} = - {}^{(J)}\Gamma_{t'rt}\\
&{}^{(J)}\Gamma_{r,t} \equiv {}^{(J)}\Gamma_{rtt'} = - {}^{(J)}\Gamma_{rt't}
\end{aligned}$$

Im Falle der Symmetrie C_{3nv} mit $n > 1$ oder $C_{\infty v}$ gilt außerdem

$$\begin{aligned}
{}^{(R)}A_t &= 0\,,\\
{}^{(J)}\Gamma_{t'} &= 0\,.
\end{aligned}$$

Da außer ${}^{(R)}A_t$ und ${}^{(J)}\Gamma_{t'}$ alle Tensorkomponenten in Tab. 1 rotationssymmetrisch bezüglich der Symmetrieachse sind, äußert sich in unseren Formeln der Unterschied zwischen Standard- und „staggered“-Fixierung nur bei Liganden mit der Symmetrie C_{3v} entsprechend den Beziehungen

$$\begin{aligned}
{}^{(R)}A_t(\text{Standard}) &= - {}^{(R)}A_{tt't'} = {}^{(R)}A_{-t,-t',-t'} = - {}^{(R)}A_t(\text{staggered})\,,\\
{}^{(J)}\Gamma_{t'}(\text{Standard}) &= - {}^{(J)}\Gamma_{t'tt} = {}^{(J)}\Gamma_{-t',-t,-t} = - {}^{(J)}\Gamma_{t'}(\text{staggered})\,.
\end{aligned}$$

Bezüglich des Tensors Δ mit der Eigenschaft $\Delta_{\varrho\sigma\tau\upsilon} = \Delta_{\varrho\sigma\upsilon\tau}$ benötigen wir für die Schlüsse im Text die Relationen

$$\begin{aligned}
\Delta_{tttt'} &= - \Delta_{t't'tt'}\,,\\
\Delta_{ttt'r} &= - \Delta_{t't't'r}\,.
\end{aligned}$$

Die folgenden Gleichungen zeigen die Transformationseigenschaften von Tensorkomponenten für C_{3nv} oder $C_{\infty v}$-symmetrische Liganden entlang der Symmetrieachse:

$$
\begin{aligned}
{}^{(J)}\gamma_t &= {}^{(J)}\gamma'_t + \frac{\pi}{c}(r'-r)\,{}^{(R)}\alpha_t\,,\\
{}^{(J)}\Gamma_{t'} &= {}^{(J)}\Gamma'_{t'} - \frac{\pi}{c}(r'-r)\,{}^{(R)}A_t\,,\\
{}^{(J)}\Gamma_{t,r} &= {}^{(J)}\Gamma'_{t,r}\,,\\
{}^{(J)}\Gamma_{r,t} &= {}^{(J)}\Gamma''_{r,t} - \frac{\pi}{c}(r'-r)\,{}^{(R)}A_{r,t}\,.
\end{aligned}
$$

Wir notieren abschließend die Definition für den Tensor des Quadrupolmomentes in Kap. II.5:

$$\Theta = \tfrac{1}{2}(3Q - \mathrm{Sp}\,Q\,1) \quad \text{mit} \quad Q = \sum_t e_t \vec r_t \vec r_t\,.$$

C. Koordinatensysteme

Zur expliziten Berechnung der Skalarprodukte $(\vec e_\varrho^{(i)}\cdot\vec e_\sigma^{(j)})$ und der Ausdrücke $(\vec e_\varrho^{(i)}\cdot T_{ij}\cdot\vec e_\sigma^{(j)})$ in Formel (15a) für T_d-symmetrische Bindungswinkel beziehen wir uns auf die Gerüstbezifferung gemäß Fig. 2 und die Koordinatensysteme gemäß Fig. 3 und denken uns ihre Orientierung weiter festgelegt, z. B. in folgender Weise: $\vec e_{t'}^{(2)}$ und $\vec e_{t'}^{(3)}$ liegen in der von $\vec a_1$ und $\vec a_4$ aufgespannten Ebene mit $(\vec e_{t'}^{(3)}\cdot\vec a_1) > 0$ und $\vec e_{t'}^{(2)} = -\vec e_{t'}^{(3)}$; $\vec e_{t'}^{(4)}$ liegt in der Ebene von $\vec a_2$ und $\vec a_3$, und es gilt $(\vec e_{t'}^{(4)}\cdot\vec a_2) > 0$ (vgl. Fig. 5).

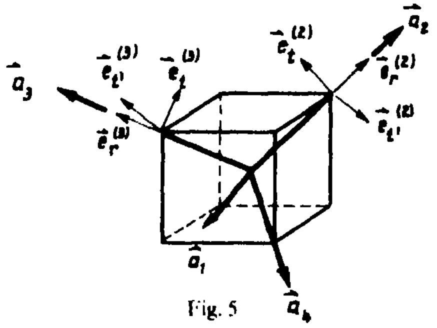

Fig. 5

Für das T_d-Gerüst gilt mit $(\vec e_r^{(i)}\cdot\vec e_r^{(j)}) = \cos\vartheta$, $\vec a_i = a_i\vec e_r^{(i)}$ und $a_{ij} = |\vec a_j - \vec a_i|$

$$\cos\vartheta = -\tfrac{1}{3},\ \sin\vartheta = \tfrac{2}{3}\sqrt{2},\ \cos\tfrac{\vartheta}{2} = \sqrt{\tfrac{1}{3}},\ \sin\tfrac{\vartheta}{2} = \sqrt{\tfrac{2}{3}}$$

und

$$a_{ij}^2 = a_i^2 + a_j^2 + \tfrac{2}{3}a_i a_j\,.$$

Die Skalarprodukte $(\vec e_\varrho^{(i)}\cdot\vec e_\sigma^{(j)})$ für die Basisvektoren an den Gerüststellen 2, 3 und 4 sind in den Tab. 2 und 3 aufgeführt, die Ausdrücke $(\vec e_\varrho^{(i)}\cdot T_{ij}\cdot\vec e_\sigma^{(j)})$ in den Tab. 4 und 5. Dabei gilt in den Tab. 3 und 5 das obere Vorzeichen für $i = 3$, das untere für $i = 2$. Es gilt ferner $(\vec e_\varrho^{(i)}\cdot\vec e_\sigma^{(j)}) = (\vec e_\sigma^{(i)}\cdot\vec e_\varrho^{(j)})$.

Wir notieren noch zwei Beziehungen zwischen den Basissystemen an den Plätzen i und j, die nicht auf ein T_d-Gerüst beschränkt sind:

$$\sum_\sigma^{1,3} (\vec e_\varrho^{(i)}\cdot T_{ij}\cdot\vec e_\sigma^{(j)})\,\vec a_{ji}\cdot(\vec e_\varrho^{(i)}\times\vec e_\sigma^{(j)}) = 0\,,$$

$$\sum_\varrho^{1,3} \vec e_\varrho^{(i)}\cdot T_{ij}\cdot\{\vec e_{\varrho'}^{(j)}\ \vec e_{\sigma'}^{(j)} - \vec e_{\sigma'}^{(j)}\ \vec e_{\varrho'}^{(j)}\}\cdot\vec e_\varrho^{(i)} = 0\,.$$

Für das T_d-Gerüst interessiert insbesondere die Beziehung

$$\vec e_r^{(i)}\cdot T_{ij}\cdot\{\vec e_t^{(j)}\,\vec e_{t'}^{(j)} - \vec e_{t'}^{(j)}\,\vec e_t^{(j)}\}\cdot\vec e_r^{(i)} = 0\,.$$

Tabelle 2

$(\vec{e}_\varrho^{(3)} \cdot \vec{e}_\sigma^{(2)})$	$\vec{e}_t^{(2)}$	$\vec{e}_{t'}^{(2)}$	$\vec{e}_r^{(2)}$
$\vec{e}_t^{(3)}$	$\frac{1}{3}$	0	$\frac{2}{3}\sqrt{2}$
$\vec{e}_{t'}^{(3)}$		-1	0
$\vec{e}_r^{(3)}$			$-\frac{1}{3}$

Tabelle 3

$(\vec{e}_\varrho^{(1)} \cdot \vec{e}_\sigma^{(4)})$	$\vec{e}_t^{(4)}$	$\vec{e}_{t'}^{(4)}$	$\vec{e}_r^{(4)}$
$\vec{e}_t^{(1)}$	$-\frac{2}{3}$	$\pm\sqrt{\frac{1}{3}}$	$-\frac{\sqrt{2}}{3}$
$\vec{e}_{t'}^{(1)}$		0	$\mp\sqrt{\frac{2}{3}}$
$\vec{e}_r^{(1)}$			$-\frac{1}{3}$

Tabelle 4

$a_{23}^3(\vec{e}_\varrho^{(3)} \cdot T_{32} \cdot \vec{e}_\sigma^{(2)})$	$\vec{e}_t^{(2)}$	$\vec{e}_{t'}^{(2)}$	$\vec{e}_r^{(2)}$
$\vec{e}_t^{(3)}$	$\frac{1}{3}\left(1+8\frac{a_2 a_3}{a_{23}^2}\right)$	0	$-\frac{\sqrt{2}}{3}\left(1+3\frac{a_2^2-a_3^2}{a_{23}^2}\right)$
$\vec{e}_{t'}^{(3)}$	0	-1	0
$\vec{e}_r^{(3)}$	$-\frac{\sqrt{2}}{3}\left(1+3\frac{a_3^2-a_2^2}{a_{23}^2}\right)$	0	$\frac{2}{3}\left(1+4\frac{a_2 a_3}{a_{23}^2}\right)$

Tabelle 5

$a_{i4}^3(\vec{e}_\varrho^{(i)} \cdot T_{i4} \cdot \vec{e}_\sigma^{(4)})$	$\vec{e}_t^{(4)}$	$\vec{e}_{t'}^{(4)}$	$\vec{e}_r^{(4)}$
$\vec{e}_t^{(i)}$	$-\frac{2}{3}\left(1-\frac{a_i a_4}{a_{i4}^2}\right)$	$\pm\sqrt{\frac{1}{3}}\left(1+2\frac{a_i a_4}{a_{i4}^2}\right)$	$\frac{\sqrt{2}}{6}\left(1+3\frac{a_4^2-a_i^2}{a_{i4}^2}\right)$
$\vec{e}_{t'}^{(i)}$	$\pm\sqrt{\frac{1}{3}}\left(1+2\frac{a_i a_4}{a_{i4}^2}\right)$	$2\frac{a_i a_4}{a_{i4}^2}$	$\pm\sqrt{\frac{1}{6}}\left(1+3\frac{a_4^2-a_i^2}{a_{i4}^2}\right)$
$\vec{e}_r^{(i)}$	$\frac{\sqrt{2}}{6}\left(1+3\frac{a_i^2-a_4^2}{a_{i4}^2}\right)$	$\pm\sqrt{\frac{1}{6}}\left(1+3\frac{a_i^2-a_4^2}{a_{i4}^2}\right)$	$\frac{2}{3}\left(1+4\frac{a_i a_4}{a_{i4}^2}\right)$

D. Die 2-Liganden-Funktionen

Das Verschwinden von 2-Liganden-Funktionen bei T_d-Derivaten kann explizit nachgewiesen werden; es wurde im Text aus der Eigenschaft geschlossen, daß die Teilsysteme $\langle l_i, l_j \rangle$ unter dieser Bedingung achiral sind. Der Beweis kann natürlich auch formal geführt werden, und wir wollen das hier für die 2-Liganden-Funktionen in erster Ordnung vorführen. In (13) stehen folgende Ausdrücke zur Debatte:

$$\sum_{\varrho,\sigma} {}^{(J)}\Gamma_{\varrho\varrho\sigma}(l_i)\,(\vec{e}_\sigma^{(i)} \cdot T_{ij} \cdot \{\langle \vec{m}(l_j) \rangle + \vec{c}_j\}),$$

$$\sum_{\substack{\varrho,\sigma\\ \varrho',\sigma'}} {}^{(R)}\alpha_{\varrho\sigma}(l_i)\, {}^{(J)}\gamma_{\varrho'\sigma'}(l_j)\,(\vec{e}_\varrho^{(i)} \cdot \vec{e}_{\sigma'}^{(j)})\,(\vec{e}_\sigma^{(i)} \cdot T_{ij} \cdot \vec{e}_{\varrho'}^{(j)}),$$

$$\sum_{\substack{\varrho,\sigma\\ \varrho',\sigma'}} {}^{(R)}\alpha_{\varrho\sigma}(l_i)\, {}^{(R)}\alpha_{\varrho'\sigma'}(l_j)\,[\vec{a}_{ij} \cdot (\vec{e}_\varrho^{(i)} \times \vec{e}_{\sigma'}^{(j)})]\,(\vec{e}_\sigma^{(i)} \cdot T_{ij} \cdot \vec{e}_{\varrho'}^{(j)}).$$

Wegen ${}^{(J)}\Gamma_{rr\sigma} = 0$ können nur die Komponenten ${}^{(J)}\Gamma_{tt\sigma}$ und ${}^{(J)}\Gamma_{t't'\sigma}$ zum ersten Ausdruck beitragen. Für $\sigma = t, r$ verschwinden aber auch diese Komponenten, für die verbleibenden gilt ${}^{(J)}\Gamma_{tt'} + {}^{(J)}\Gamma_{t't't'} = 0$, woraus das Verschwinden der ersten Zeile folgt.

Der zweite Ausdruck kann mittels

$$\alpha = \alpha_t 1 + (\alpha_r - \alpha_t)\,\vec{e}_r \circ \vec{e}_r, \qquad \gamma = \gamma_t(\vec{e}_t \circ \vec{e}_{t'} - \vec{e}_{t'} \circ \vec{e}_t)$$

und der vorletzten Beziehung aus Anhang C umgeformt werden zu

$$({}^{(R)}\alpha_r(l_i) - {}^{(R)}\alpha_t(l_i))\,{}^{(J)}\gamma_t(l_j)\,\{\vec{e}_r^{(i)} \cdot T_{ij} \cdot (\vec{e}_t^{(j)} \circ \vec{e}_{t'}^{(j)} - \vec{e}_{t'}^{(j)} \circ \vec{e}_t^{(j)}) \cdot \vec{e}_r^{(i)}\}\,.$$

Bei einem tetraedrischen Gerüst verschwindet die geschweifte Klammer.

Im dritten Ausdruck bleibt wegen der drittletzten Gleichung aus Anhang C nur das Glied mit dem Faktor $[\vec{a}_{ij} \cdot (\vec{e}_r^{(i)} \times \vec{e}_r^{(j)})]$, der seinerseits verschwindet.

Für die 2-Liganden-Funktionen der zweiten störungstheoretischen Ordnung von $\mathrm{Sp}\,{}^{(J)}\gamma$ lassen sich bis auf Ausnahmen keine geschlossenen Ausdrücke angeben, wenn man nicht von zusätzlichen Näherungsaspekten Gebrauch macht. Der explizite Nachweis für das Verschwinden dieser Funktionen bei T_d-Derivaten ist daher sehr umständlich. Er wurde aber durchgeführt und liefert das erwartete Resultat.

Literatur

1 Boys, S. F.: Proc. Royal Soc. (London) A **144**, 655, 675 (1934).
2. Buckingham, A. D.: Advances chem. Physics **12**, 107 (1967).
3 Buckingham, A. D., Longuet-Higgins, H. C.: Molecular Physics **14**, 63 (1968).
4 Chiu, Y.-N.: J. chem. Physics **50**, 5336 (1969).
5 Condon, E. U.: Rev. mod. Physics **9**, 432 (1937).
6 Condon, E. U., Altar, W., Eyring, H.: J. chem. Physics **5**, 753 (1937).
7 Haase, D., Ruch, E.: Theoret. chim. Acta (Berl.) **29**, 235 (1973).
8 Hückel, E.: Z. Elektrochem. **50**, 13 (1944).
9 Kirkwood, J. G.: J. chem. Physics **5**, 479 (1937).
10 London, F.: Trans. Faraday Soc. **33**, 8 (1937)
11 Maaskant, W. J. A., Oosterhoff, L. J.: Molecular Physics **8**, 319 (1964).
12. Richter, W. J., Richter, B., Ruch, E.: Angew. Chem. **85**, 21 (1973)
13 Rosenfeld, L.: Z. Physik **52**, 161 (1928)
14 Ruch, E.: Theoret. chim. Acta (Berl.) **11**, 183, 462 (1968).
15 Ruch, E.: Accounts Chem. Research **5**, 49 (1972).
16 Ruch, E., Schönhofer, A.: Theoret. chim. Acta (Berl.) **10**, 91 (1968).
17 Ruch, E., Schönhofer, A.: Theoret. chim. Acta (Berl.) **19**, 225 (1970).
18 Unsold, A.: Z. Physik **43**, 563 (1927).
19 Voigt, W.: Lehrbuch der Kristalloptik. Leipzig-Berlin: Teubner 1910.

Professor Dr. E. Ruch
Institut für Quantenchemie
Freie Universität Berlin
D-1000 Berlin 45, Holbeinstraße 48
Deutschland

Theoret. chim. Acta (Berl.) 29, 235—246 (1973)
© by Springer-Verlag 1973

Bemerkung zur Rayleigh-Schrödinger-Störungstheorie

Dietrich Haase und Ernst Ruch
Institut für Quantenchemie der Freien Universität Berlin

Eingegangen am 31. Juli 1972

Remarks on the Rayleigh-Schrödinger Perturbation Theory

The time-independent Hamiltonians $\mathscr{H}_0$ and $\mathscr{H} = \mathscr{H}_0 + \mathscr{V}$ have a discrete spectrum, eigenvalues, and eigenvectors $E_s^{(0)}, |s\rangle^{(0)}$ resp. $E_s, |s\rangle$. If the RS perturbation theory can be applied here then an operator $\mathfrak{p}$ with the property

$$|s\rangle^{(n+1)} = \frac{1}{n+1}\,\mathfrak{p}|s\rangle^{(n)}, \quad E_s^{(n+1)} = \frac{1}{n+1}\,\mathfrak{p}\,E_s^{(n)}$$

exists where $|s\rangle^{(n)}$ and $E_s^{(n)}$ denote the n-th order corrections of perturbation theory if $E_s^{(0)}$ is nondegenerate. In the case of degeneracy the operation $\mathfrak{p}$ remains defined and can always be used to determine perturbation corrections of quantum mechanical expressions which are invariant in zeroth order under transformations of the basis in degenerate subspaces of $\mathscr{H}_0$. The equations

$$|s\rangle = \sum_{n}^{0,\infty} |s\rangle^{(n)} = e^{\mathfrak{p}}|s\rangle^{(0)}, \quad E_s = \sum_{n}^{0,\infty} E_s^{(n)} = e^{\mathfrak{p}}\,E_s^{(0)}$$

correspond to a basis transformation where nondegenerate eigenvectors $|s\rangle^{(0)}$ and eigenvalues $E_s^{(0)}$ of $\mathscr{H}_0$ transform into eigenvectors $|s\rangle$ and eigenvalues E_s of $\mathscr{H}$. Examples show the usefulness of this formulation.

Für zeitunabhängige Hamiltonoperatoren $\mathscr{H}_0$ und $\mathscr{H} = \mathscr{H}_0 + \mathscr{V}$ mit einem diskreten Spektrum, den Eigenwerten und Eigenvektoren $E_s^{(0)}, |s\rangle^{(0)}$ bzw. $E_s, |s\rangle$ von $\mathscr{H}_0$ und $\mathscr{H}$ sei die Behandlung nach der RS-Störungstheorie gewährleistet. Dann existiert ein Operator $\mathfrak{p}$ mit der Eigenschaft

$$|s\rangle^{(n+1)} = \frac{1}{n+1}\cdot\mathfrak{p}|s\rangle^{(n)}, \quad E_s^{(n+1)} = \frac{1}{n+1}\,\mathfrak{p}\,E_s^{(n)},$$

wobei $|s\rangle^{(n)}$ und $E_s^{(n)}$ die störungstheoretischen Korrekturen n-ter Ordnung beschreiben, falls $E_s^{(0)}$ nicht entartet ist. Im Entartungsfall bleibt die Operation $\mathfrak{p}$ definiert und kann zur Bestimmung störungstheoretischer Korrekturen der quantenmechanischen Ausdrücke verwendet werden, die in nullter Näherung invariant sind gegenüber Basistransformationen in den entarteten Teilräumen von $\mathscr{H}_0$. Die Gleichungen

$$|s\rangle = \sum_{n}^{0,\infty} |s\rangle^{(n)} = e^{\mathfrak{p}}|s\rangle^{(0)}, \quad E_s = \sum_{n}^{0,\infty} E_s^{(n)} = e^{\mathfrak{p}}|s\rangle^{(0)}$$

entsprechen einer Basistransformation, bei der nichtentartete Eigenvektoren $|s\rangle^{(0)}$ und Eigenwerte $E_s^{(0)}$ von $\mathscr{H}_0$ in Eigenvektoren $|s\rangle$ und Eigenwerte E_s von $\mathscr{H}$ übergehen. Beispiele zeigen den Nutzen dieser Formulierung.

Die RS-Störungstheorie

In der RS-Störungstheorie wird die Annahme gemacht, daß die Eigenwerte E_s und Eigenvektoren $|s\rangle$ des Hamiltonoperators $\mathscr{H} = \mathscr{H}_0 + \mathscr{V}$ mit

$$\mathscr{H}|s\rangle = E_s|s\rangle \tag{1}$$

nach Potenzen des Hermiteschen Störoperators $\mathscr{V}$ entwickelt werden können. *Wir setzen voraus, daß das Spektrum von $\mathscr{H}_0$ und von $\mathscr{H}$ diskret sei, und schreiben*

$$E_s = \sum_n^{0,\infty} E_s^{(n)}, \qquad |s\rangle = \sum_n^{0,\infty} |s\rangle^{(n)}. \tag{2}$$

Die Eigenwerte $E_s^{(0)}$ und Eigenvektoren $|s\rangle^{(0)}$ des „ungestörten" Hermiteschen Operators $\mathscr{H}_0$ werden als bekannt vorausgesetzt, die $|s\rangle^{(0)}$ sollen ein vollständiges orthonormiertes Basissystem im Hilbertraum des Systems $\mathscr{H}$ bilden. Wir setzen weiter voraus, daß die Basis störungsadaptiert sei, d.h. im Entartungsfall für den ungestörten Operator die geeigneten Ausgangsfunktionen vorliegen. $E_s^{(n)}$ und $|s\rangle^{(n)}$ mit $n \geqq 1$ bezeichnen die störungstheoretischen Korrekturen n-ter Ordnung. Durch Einsetzen von (2) in (1) findet man das Gleichungssystem

$$(\mathscr{H}_0 - E_s^{(0)})|s\rangle^{(0)} = 0, \tag{3.0}$$

$$(\mathscr{H}_0 - E_s^{(0)})|s\rangle^{(1)} = -\mathscr{V}|s\rangle^{(0)} + E_s^{(1)}|s\rangle^{(0)}, \tag{3.1}$$

$$(\mathscr{H}_0 - E_s^{(0)})|s\rangle^{(2)} = -\mathscr{V}|s\rangle^{(1)} + E_s^{(1)}|s\rangle^{(1)} + E_s^{(2)}|s\rangle^{(0)}, \tag{3.2}$$

$$\vdots$$

$$(\mathscr{H}_0 - E_s^{(0)})|s\rangle^{(n)} = -\mathscr{V}|s\rangle^{(n-1)} + \sum_k^{1,n} E_s^{(k)}|s\rangle^{(n-k)}. \tag{3.n}$$

Mit orthonormierten Eigenvektoren von $\mathscr{H}_0$ führt die Forderung nach der Orthonormierung in jeder Ordnung zu den Gleichungen

$$\begin{aligned} {}^{(0)}\langle s|t\rangle^{(0)} &= \delta_{st}, \\ \sum_{\mu,\nu}^{\mu+\nu\;n} {}^{(\mu)}\langle s|t\rangle^{(\nu)} &= 0 \quad \text{für} \quad n \geqq 1. \end{aligned} \tag{4}$$

Die Gleichungssysteme (3) und (4) erlauben, $E_s^{(n)}$ und $|s\rangle^{(n)}$ rekursiv zu bestimmen. Die Lösungen für die $|s\rangle^{(n)}$ sind nicht eindeutig; ihre Verschiedenheit führt aber, wie man weiß, nur zu unterschiedlichen Phasenfaktoren in $|s\rangle$.

Durch skalare Multiplikation der Gleichungen (3) mit ${}^{(0)}\langle s|$ finden wir unter Benutzung der Hermiteizität von $\mathscr{H}_0$ die Korrekturen zur Energie $E_s^{(0)}$ in der Form (5):

$$\begin{aligned} E_s^{(1)} &= {}^{(0)}\langle s|\mathscr{V}|s\rangle^{(0)}, \\ E_s^{(2)} &= {}^{(0)}\langle s|\mathscr{V}|s\rangle^{(1)} - E_s^{(1)}\,{}^{(0)}\langle s|s\rangle^{(1)}, \\ E_s^{(3)} &= {}^{(0)}\langle s|\mathscr{V}|s\rangle^{(2)} - E_s^{(1)}\,{}^{(0)}\langle s|s\rangle^{(2)} - E_s^{(2)}\,{}^{(0)}\langle s|s\rangle^{(1)}, \\ &\;\vdots \\ E_s^{(n)} &= {}^{(0)}\langle s|\mathscr{V}|s\rangle^{(n-1)} - \sum_k^{1,n-1} E_s^{(k)}\,{}^{(0)}\langle s|s\rangle^{(n-k)}. \end{aligned} \tag{5}$$

Man findet geeignete Gleichungen für die Korrekturen der Eigenvektoren bei Verwendung der beiden Operatoren

$$\mathscr{Q}_s^{(0)} = \sum_{t \notin \mathfrak{M}_s^0} \frac{|t\rangle^{(0)}\,{}^{(0)}\langle t|}{E_s^{(0)} - E_t^{(0)}} \quad \text{und} \quad \mathscr{P}_{\mathfrak{M}_s^0}^{(0)} = \sum_{t \in \mathfrak{M}_s^0} |t\rangle^{(0)}\,{}^{(0)}\langle t|.$$

Dabei läuft die Summe $\sum\limits_{t\in\mathfrak{M}_s^0}$ über die Eigenvektoren des Teilraumes $\mathfrak{M}_s^0$ zur entarteten Energie $E_s^{(0)}$ und die Summe $\sum\limits_{t\notin\mathfrak{M}_s^0}$ über den dazu komplementären Raum, sie enthält also nur Summanden mit nichtverschwindendem Nenner $E_s^{(0)}-E_t^{(0)}$.

Wenn wir in (3) auf die Zeile (3.n) den Operator $-\mathcal{Q}_s^{(0)}$ anwenden und $\mathcal{P}^{(0)}_{\mathfrak{M}_s^0}|s\rangle^{(n)}$ auf beiden Seiten addieren, wird wegen der Identität $\sum\limits_t |t\rangle^{(0)}\,{}^{(0)}\langle t|s\rangle^{(n)}=|s\rangle^{(n)}$ aus (3) das Gleichungssystem

$$\begin{aligned}
|s\rangle^{(0)} &= \mathcal{P}^{(0)}_{\mathfrak{M}_s^0}|s\rangle^{(0)},\\
|s\rangle^{(1)} &= \mathcal{Q}_s^{(0)}\mathcal{V}|s\rangle^{(0)}+\mathcal{P}^{(0)}_{\mathfrak{M}_s^0}|s\rangle^{(1)},\\
|s\rangle^{(2)} &= \mathcal{Q}_s^{(0)}\mathcal{V}|s\rangle^{(1)}-\mathcal{Q}_s^{(0)}E_s^{(1)}|s\rangle^{(1)}+\mathcal{P}^{(0)}_{\mathfrak{M}_s^0}|s\rangle^{(2)},\\
|s\rangle^{(3)} &= \mathcal{Q}_s^{(0)}\mathcal{V}|s\rangle^{(2)}-\mathcal{Q}_s^{(0)}E_s^{(1)}|s\rangle^{(2)}-\mathcal{Q}_s^{(0)}E_s^{(2)}|s\rangle^{(1)}+\mathcal{P}^{(0)}_{\mathfrak{M}_s^0}|s\rangle^{(3)},\\
&\vdots\\
|s\rangle^{(n)} &= \mathcal{Q}_s^{(0)}\left[\mathcal{V}|s\rangle^{(n-1)}-\sum_k^{1,n-1}E_s^{(k)}|s\rangle^{(n-k)}\right]+\mathcal{P}^{(0)}_{\mathfrak{M}_s^0}|s\rangle^{(n)}.
\end{aligned}\tag{6}$$

Falls $E_s^{(0)}$ nicht entartet ist, vereinfacht sich (6) zu

$$\begin{aligned}
|s\rangle^{(0)} &= |s\rangle^{(0)}\,{}^{(0)}\langle s|s\rangle^{(0)},\\
|s\rangle^{(1)} &= \mathcal{Q}_s^{(0)}\mathcal{V}|s\rangle^{(0)}+|s\rangle^{(0)}\,{}^{(0)}\langle s|s\rangle^{(1)},\\
|s\rangle^{(2)} &= \mathcal{Q}_s^{(0)}\mathcal{V}|s\rangle^{(1)}-\mathcal{Q}_s^{(0)}E_s^{(1)}|s\rangle^{(1)}+|s\rangle^{(0)}\,{}^{(0)}\langle s|s\rangle^{(2)},\\
|s\rangle^{(3)} &= \mathcal{Q}_s^{(0)}\mathcal{V}|s\rangle^{(2)}-\mathcal{Q}_s^{(0)}E_s^{(1)}|s\rangle^{(2)}-\mathcal{Q}_s^{(0)}E_s^{(2)}|s\rangle^{(1)}+|s\rangle^{(0)}\,{}^{(0)}\langle s|s\rangle^{(3)},\\
&\vdots\\
|s\rangle^{(n)} &= \mathcal{Q}_s^{(0)}\left[\mathcal{V}|s\rangle^{(n-1)}-\sum_k^{1,n-1}E_s^{(k)}|s\rangle^{(n-k)}\right]+|s\rangle^{(0)}\,{}^{(0)}\langle s|s\rangle^{(n)}.
\end{aligned}\tag{6a}$$

Mit einer zusätzlichen Vorschrift über den Imaginärteil von ${}^{(0)}\langle s|s\rangle^{(n)}$ wird die Phase der Eigenvektoren von $\mathcal{H}$ festgelegt. Die spezielle Bedingung $Im\,{}^{(0)}\langle s|s\rangle^{(1)}=0$ führt wegen der Normierungsbedingung (4) zu ${}^{(0)}\langle s|s\rangle^{(1)}=0$; damit wird also aus der zweiten Zeile in (6a)

$$|s\rangle^{(1)}=\mathcal{Q}_s^{(0)}\mathcal{V}|s\rangle^{(0)}. \tag{7}$$

Formale Lösung für die Korrekturen $E_s^{(n)}$, $|s\rangle^{(n)}$ und der Operator $\mathfrak{p}$

Wir definieren eine Operation $\{\ \}^{(1)}$, die an störungsadaptierten Eigenkets und Eigenbras von $\mathcal{H}_0$ den Übergang zur ersten störungstheoretischen Korrektur hervorruft, auch bezüglich der Operatoren $\mathcal{H}_0$ und $\mathcal{V}$, des Einheitsoperators 1 und an Summen und Produkten von solchen Größen in folgender Weise:

$$\begin{aligned}
&\text{a)}\quad \{|s\rangle^{(0)}\}^{(1)}=|s\rangle^{(1)},\qquad \{{}^{(0)}\langle s|\}^{(1)}={}^{(1)}\langle s|\,;\\
&\text{b)}\quad \{\mathcal{H}_0\}^{(1)}=\mathcal{V},\qquad \{\mathcal{V}\}^{(1)}=0,\qquad \{1\}^{(1)}=0\,;\\
&\text{c)}\quad \{f^{(0)}+g^{(0)}\}^{(1)}=\{f^{(0)}\}^{(1)}+\{g^{(0)}\}^{(1)}\,;\\
&\text{d)}\quad \{f^{(0)}\circ g^{(0)}\}^{(1)}=\{f^{(0)}\}^{(1)}\circ g^{(0)}+f^{(0)}\circ\{g^{(0)}\}^{(1)}.
\end{aligned}\tag{8}$$

Das Produkt $f^{(0)} \circ g^{(0)}$ kann dabei irgendein Produkt zwischen den genannten Größen sein, wie z.B. ein Operatorenprodukt, ein unbestimmtes oder skalares Produkt. In der Festsetzung $\{1\}^{(1)} = 0$ drückt sich die Orthonormierungsbedingung (4) in erster Ordnung aus, denn wegen a) und d) gilt:

$$\begin{aligned} 0 &= {}^{(0)}\langle s|\{1\}^{(1)}|t\rangle^{(0)} = \sum_r \left({}^{(0)}\langle s|r\rangle^{(0)}\,{}^{(1)}\langle r|t\rangle^{(0)} + {}^{(0)}\langle s|r\rangle^{(1)}\,{}^{(0)}\langle r|t\rangle^{(0)}\right) \\ &= {}^{(0)}\langle s|s\rangle^{(0)}\,{}^{(1)}\langle s|t\rangle^{(0)} + {}^{(0)}\langle s|t\rangle^{(1)}\,{}^{(0)}\langle t|t\rangle^{(0)} = {}^{(1)}\langle s|t\rangle^{(0)} + {}^{(0)}\langle s|t\rangle^{(1)}. \end{aligned}$$

Außerdem ist damit die Operation $\{\ \}^{(1)}$ an den Eigenwerten von $\mathscr{H}_0$ für störungsadaptierte Eigenvektoren erklärt:

$$\begin{aligned} \{E_s^{(0)}\}^{(1)} &= \{{}^{(0)}\langle s|\mathscr{H}_0|s\rangle^{(0)}\}^{(1)} = {}^{(1)}\langle s|\mathscr{H}_0|s\rangle^{(0)} + {}^{(0)}\langle s|\mathscr{V}|s\rangle^{(0)} + {}^{(0)}\langle s|\mathscr{H}_0|s\rangle^{(1)} \\ &= E_s^{(0)}\left({}^{(1)}\langle s|s\rangle^{(0)} + {}^{(0)}\langle s|s\rangle^{(1)}\right) + {}^{(0)}\langle s|\mathscr{V}|s\rangle^{(0)} = {}^{(0)}\langle s|\mathscr{V}|s\rangle^{(0)} = E_s^{(1)}. \end{aligned}$$

Wir wenden die Operation $\{\ \}^{(1)}$ auf die Zeile (3.1) an und erklären sie an $|s\rangle^{(1)}$ *und $E_s^{(1)}$ durch ihre Wirkung auf die entsprechenden Ausdrücke in nullter Ordnung* gemäß (5) und (6):

$$(\mathscr{H}_0 - E_s^{(0)})\,\{|s\rangle^{(1)}\}^{(1)} = -2\mathscr{V}|s\rangle^{(1)} + 2E_s^{(1)}|s\rangle^{(1)} + \{E_s^{(1)}\}^{(1)}|s\rangle^{(0)}.$$

Der Vergleich mit der Zeile (3.2) liefert

$$\begin{aligned} \{E_s^{(1)}\}^{(1)} &= 2E_s^{(2)}, \\ \{|s\rangle^{(1)}\}^{(1)} &= 2|s\rangle^{(2)}. \end{aligned}$$

Die Orthonormierungsbedingung bleibt auch in zweiter Ordnung bestehen, denn wir erhalten

$$0 = \{{}^{(0)}\langle s|t\rangle^{(1)} + {}^{(1)}\langle s|t\rangle^{(0)}\}^{(1)} = 2\left({}^{(0)}\langle s|t\rangle^{(2)} + {}^{(1)}\langle s|t\rangle^{(1)} + {}^{(2)}\langle s|t\rangle^{(0)}\right).$$

Eine naheliegende Verallgemeinerung dieses Befundes schreiben wir als Vermutung in der Form

$$\begin{aligned} \{E_s^{(n)}\}^{(1)} &= (n+1)\,E_s^{(n+1)}, \\ \{|s\rangle^{(n)}\}^{(1)} &= (n+1)\,|s\rangle^{(n+1)}. \end{aligned} \tag{9}$$

Wir stellen fest, daß (9) für $n = 0$ und $n = 1$ gilt, nehmen also an, daß die Behauptung bis n richtig sei, und überzeugen uns von der Gültigkeit für $n+1$. Dazu wenden wir auf die Zeile für $|s\rangle^{(n)}$ im Gleichungssystem (3) die Operation $\{\ \}^{(1)}$ an und benutzen die Definition (9) für alle $\nu \leqq n$:

$$\begin{aligned} &(\mathscr{H}_0 - E_s^{(0)})\,\{|s\rangle^{(n)}\}^{(1)} \\ &= -(n+1)\,\mathscr{V}|s\rangle^{(n)} + (n+1)\,E_s^{(1)}|s\rangle^{(n)} + 2E_s^{(2)}|s\rangle^{(n-1)} + \sum_k^{2,n} (n-k+1)\,E_s^{(k)}|s\rangle^{(n-k+1)} \\ &\quad + \sum_k^{2,n-1} (k+1)\,E_s^{(k+1)}|s\rangle^{(n-k)} + \{E_s^{(n)}\}^{(1)}|s\rangle^{(0)} \\ &= -(n+1)\left[\mathscr{V}|s\rangle^{(n)} - \sum_k^{1,n} E_s^{(k)}|s\rangle^{(n-k+1)}\right] + \{E_s^{(n)}\}^{(1)}|s\rangle^{(0)}. \end{aligned}$$

Der Vergleich mit der nächsten Zeile in (3) bestätigt die Beziehungen (9).

Die Orthonormierungsbedingung in $(n+1)$-ter Ordnung bestätigt sich ebenfalls wegen

$$\begin{aligned}0 &= \left\{\sum_{\mu,\nu}^{\mu+\nu=n} {}^{(\mu)}\langle s|t\rangle^{(\nu)}\right\}^{(1)}\\ &= \sum_{\mu,\nu}^{\mu+\nu=n} \left((\mu+1)\ {}^{(\mu+1)}\langle s|t\rangle^{(\nu)} + (\nu+1)\ {}^{(\mu)}\langle s|t\rangle^{(\nu+1)}\right)\\ &= (n+1) \sum_{\mu,\nu}^{\mu+\nu=n+1} {}^{(\mu)}\langle s|t\rangle^{(\nu)}\,.\end{aligned}$$

Wir können das Problem

$$f(\mathscr{H})|s\rangle = f(E_s)|s\rangle$$

entsprechend behandeln, wenn $f(\mathscr{H})$ gemäß einer Operatorentwicklung nach Potenzen von $\mathscr{V}$ in der Form $f(\mathscr{H}) = \sum_n^{0,\infty} f^{(n)}(\mathscr{H}_0, \mathscr{V})$ gegeben ist, wobei $f^{(0)}(\mathscr{H}_0,\mathscr{V}) = f(\mathscr{H}_0)$ und $f^{(n)}(\mathscr{H}_0,\mathscr{V})$ alle Glieder enthält, in denen die Potenz $\mathscr{V}^n$ auftritt. Der Eigenwert von $f(\mathscr{H})$ zu $|s\rangle$ ist $f(E_s)$ und setzt sich aus dem Eigenwert $f(E_s^{(0)})$ zu $f(\mathscr{H}_0)$ und Korrekturen $g^{(n)}(E_s^{(0)}, E_s^{(1)}, \dots E_s^{(n)})$ zusammen, die entsprechend einer Reihenentwicklung der Funktion $f(E_s) = f(E_s^{(0)} + E_s^{(1)} + \cdots)$ an der Stelle $E_s^{(0)}$ nach Potenzen der $E_s^{(i)}\,(i = 1, 2, \dots)$ durch diejenigen Glieder gegeben sind, in denen die Summe der Ordnungen n beträgt. Wir schreiben also

$$f(E_s) = f(E_s^{(0)}) + \sum_n^{1,\infty} g^{(n)}(E_s^{(0)}, E_s^{(1)}, \dots, E_s^{(n)})\,,$$

wobei

$$g^{(1)}(E_s^{(0)}, E_s^{(1)}) = \frac{\partial f(E_s^{(0)})}{\partial E_s^{(0)}} E_s^{(1)}\,,$$

$$g^{(2)}(E_s^{(0)}, E_s^{(1)}, E_s^{(2)}) = \frac{\partial f(E_s^{(0)})}{\partial E_s^{(0)}} E_s^{(2)} + \frac{1}{2!}\,\frac{\partial^2 f(E_s^{(0)})}{\partial (E_s^{(0)})^2} (E_s^{(1)})^2 \quad \text{usw.}$$

Die konsequente Verallgemeinerung von $\{\mathscr{H}_0\}^{(1)} = \mathscr{V}$ führt zur Festsetzung

$$\{f^{(n)}(\mathscr{H}_0, \mathscr{V})\}^{(1)} = (n+1)\, f^{(n+1)}(\mathscr{H}_0, \mathscr{V})\,. \tag{8e}$$

Damit erhalten wir aus dem zu (3) analogen Rekursionsformalismus für $f(\mathscr{H})|s\rangle = f(E_s)|s\rangle$ die Beziehungen

$$\{f(E_s^{(0)})\}^{(1)} = g^{(1)}(E_s^{(0)}, E_s^{(1)})\,,$$

$$\{g^{(n)}(E_s^{(0)}, E_s^{(1)}, \dots, E_s^{(n)})\}^{(1)} = (n+1)\, g^{(n+1)}(E_s^{(0)}, E_s^{(1)}, \dots, E_s^{(n+1)})\,.$$

In Verallgemeinerung von $\{E_s^{(0)}\}^{(1)} = E_s^{(1)}$ haben wir also

$$\{f(E_s^{(0)})\}^{(1)} = \frac{\partial f(E_s^{(0)})}{\partial E_s^{(0)}} E_s^{(1)}\,. \tag{10}$$

Damit ist es möglich, die Operation $\{\ \}^{(1)}$ auch auf Größen wie $\mathscr{Q}_s^{(0)}$ anzuwenden und z.B. die Relation $\{|s\rangle^{(1)}\}^{(1)} = 2|s\rangle^{(2)}$ explizit nachzuweisen (vgl. Anhang).

Die bisherige Analyse zeigt, daß die störungstheoretische Korrektur erster Ordnung zur Korrektur n-ter Ordnung für einen Eigenvektor von $\mathscr{H}$ oder für entsprechende Matrixelemente eines Operators bis auf den Faktor $n+1$ auf die $(n+1)$-Korrektur führt. Mit der Festsetzung $\mathrm{Im}\,{}^{(0)}\langle s|s\rangle^{(1)}=0$ ist dieser Prozeß an nichtentarteten Eigenvektoren von $\mathscr{H}_0$ durch Gleichung (7) eindeutig erklärt, an entarteten Eigenvektoren dagegen erfordert die Operation $\{\ \}^{(1)}$ Informationen, die erst der Zeile (3.2) im Rekursionsformalismus (3) zu entnehmen sind.

Aus diesem Grunde untersuchen wir eine modifizierte Definition einer entsprechenden Operation $\{\ \}^{(\bar{1})}$, die eine von der Entartungsfrage unabhängige Vorschrift beinhaltet. Es gelte für jeden Eigenvektor von $\mathscr{H}_0$:

$$\{|s\rangle^{(0)}\}^{(\bar{1})}=\mathscr{Q}_s^{(0)}\mathscr{V}'|s\rangle^{(0)}=|s\rangle^{(\bar{1})},\qquad \{{}^{(0)}\langle s|\}^{(\bar{1})}={}^{(0)}\langle s|\mathscr{V}'\mathscr{Q}_s^{(0)}={}^{(\bar{1})}\langle s|\,. \tag{11}$$

Für nichtentartete Eigenvektoren von $\mathscr{H}_0$ bedeutet das:

$$|s\rangle^{(\bar{1})}=|s\rangle^{(1)},\ {}^{(\bar{1})}\langle s|={}^{(1)}\langle s|\quad\text{und}\quad E_s^{(\bar{1})}=E_s^{(1)}\,.$$

Die Gleichung $E_s^{(\bar{1})}=E_s^{(1)}$ gilt auch für störungsadaptierte Eigenvektoren aus entarteten Teilräumen, für einen beliebigen Eigenvektor $|s\rangle^{(0)}$ dagegen bezeichnet $E_s^{(\bar{1})}$ im Entartungsfall einen Erwartungswert von $\mathscr{V}'$.

Die Korrektur erster Ordnung $\mathscr{P}^{(1)}_{\mathfrak{M}_s^0}$ vom Projektionsoperator $\mathscr{P}^{(0)}_{\mathfrak{M}_s^0}$ zu einem entarteten Teilraum $\mathfrak{M}_s^0$ von $\mathscr{H}_0$ ergibt sich in der Form

$$\begin{aligned}\mathscr{P}^{(1)}_{\mathfrak{M}_s^0}&=\sum_{s\in\mathfrak{M}_s^0}\left(|s\rangle^{(1)\,(0)}\langle s|+|s\rangle^{(0)\,(1)}\langle s|\right)\\&=\sum_{s\in\mathfrak{M}_s^0}\left(\mathscr{Q}_s^{(0)}\mathscr{V}'|s\rangle^{(0)(0)}\langle s|+|s\rangle^{(0)(0)}\langle s|\mathscr{V}'\mathscr{Q}_s^{(0)}+\mathscr{P}^{(0)}_{\mathfrak{M}_s^0}|s\rangle^{(1)(0)}\langle s|+|s\rangle^{(0)(1)}\langle s|\mathscr{P}^{(0)}_{\mathfrak{M}_s^0}\right).\end{aligned}$$

Wegen (4) gilt aber

$$\begin{aligned}&\sum_{s\in\mathfrak{M}_s^0}\left(\mathscr{P}^{(0)}_{\mathfrak{M}_s^0}|s\rangle^{(1)\,(0)}\langle s|+|s\rangle^{(0)\,(1)}\langle s|\mathscr{P}^{(0)}_{\mathfrak{M}_s^0}\right)\\&\quad=\sum_{s,t\in\mathfrak{M}_s^0}\left(|t\rangle^{(0)\,(0)}\langle t|s\rangle^{(1)\,(0)}\langle s|+|s\rangle^{(0)\,(1)}\langle s|t\rangle^{(0)\,(0)}\langle t|\right)\\&\quad=\sum_{s,t\in\mathfrak{M}_s^0}|s\rangle^{(0)\,(0)}\langle t|\left({}^{(1)}\langle s|t\rangle^{(0)}+{}^{(0)}\langle s|t\rangle^{(1)}\right)=0\end{aligned}$$

und daher

$$\begin{aligned}\{\mathscr{P}^{(0)}_{\mathfrak{M}_s^0}\}^{(1)}&=\mathscr{P}^{(1)}_{\mathfrak{M}_s^0}\\&=\sum_{s\in\mathfrak{M}_s^0}\left(|s\rangle^{(0)\,(1)}\langle s|+|s\rangle^{(1)\,(0)}\langle s|\right)=\sum_{s\in\mathfrak{M}_s^0}\left(|s\rangle^{(0)\,(\bar{1})}\langle s|+|s\rangle^{(\bar{1})\,(0)}\langle s|\right)=\{\mathscr{P}^{(0)}_{\mathfrak{M}_s^0}\}^{(\bar{1})}\,.\end{aligned}$$

Damit haben wir $\{1\}^{(1)}=\{1\}^{(\bar{1})}=0$ und die Aussage, daß die Orthonormierung für gestrichene Korrekturen gültig bleibt.

Ein entsprechendes Resultat gewinnt man für Größen $\mathfrak{A}^{(0)}_{\mathfrak{M}_s^0}$ und $\mathfrak{B}^{(0)}_{\mathfrak{M}_s^0}$ der folgenden Art:

$$\begin{aligned}\mathfrak{A}^{(0)}_{\mathfrak{M}_s^0}&=\sum_{s\in\mathfrak{M}_s^0}f(E_s^{(0)})\,|s\rangle^{(0)\,(0)}\langle s|\,,\\\mathfrak{B}^{(0)}_{\mathfrak{M}_s^0}&=\sum_{s\in\mathfrak{M}_s^0}g(E_s^{(0)})\,{}^{(0)}\langle s|\mathscr{O}^{(0)}|s\rangle^{(0)}\,.\end{aligned}$$

Dabei seien f und g differenzierbare Funktionen der Energie nullter Näherung und $\mathcal{O}^{(0)}$ ein Operator, dessen störungstheoretische Korrekturen mit $\mathcal{O}^{(1)}$, $\mathcal{O}^{(2)}$ usw. bezeichnet werden.

Für die Korrekturen erster Ordnung ergibt sich mit störungsadaptierten Eigenvektoren $|s\rangle^{(0)}$

$$\{\mathfrak{A}^{(0)}_{\mathfrak{Mg}}\}^{(1)} = f(E_s^{(0)})\,\mathscr{P}^{(1)}_{\mathfrak{Mg}} + \frac{\partial f(E_s^{(0)})}{\partial E_s^{(0)}} \sum_{s\in\mathfrak{Mg}} |s\rangle^{(0)} E_s^{(1)}\,{}^{(0)}\langle s|$$

$$= f(E_s^{(0)})\,\mathscr{P}^{(\mathrm{T})}_{\mathfrak{Mg}} + \frac{\partial f(E_s^{(0)})}{\partial E_s^{(0)}} \sum_{s\in\mathfrak{Mg}} |s\rangle^{(0)} E_s^{(\mathrm{T})}\,{}^{(0)}\langle s| = \{\mathfrak{A}^{(0)}_{\mathfrak{Mg}}\}^{(\mathrm{T})}.$$

Wegen der Beziehungen

$$\mathscr{P}^{(\mathrm{T})}_{\mathfrak{Mg}} = \sum_{s\in\mathfrak{Mg}} (\mathscr{Q}_s^{(0)}\mathscr{V}'|s\rangle^{(0)}\,{}^{(0)}\langle s| + |s\rangle^{(0)}\,{}^{(0)}\langle s|\mathscr{V}'\mathscr{Q}_s^{(0)}) = \mathscr{Q}_s^{(0)}\mathscr{V}'\mathscr{P}^{(0)}_{\mathfrak{Mg}} + \mathscr{P}^{(0)}_{\mathfrak{Mg}}\mathscr{V}'\mathscr{Q}_s^{(0)}$$

und

$$\sum_{s\in\mathfrak{Mg}} |s\rangle^{(0)} E_s^{(\mathrm{T})}\,{}^{(0)}\langle s| = \sum_{s,t\in\mathfrak{Mg}} |s\rangle^{(0)}\,{}^{(0)}\langle s|\mathscr{V}'|t\rangle^{(0)}\,{}^{(0)}\langle t| = \mathscr{P}^{(0)}_{\mathfrak{Mg}}\mathscr{V}'\mathscr{P}^{(0)}_{\mathfrak{Mg}}$$

ist $\mathfrak{A}^{(1)}_{\mathfrak{Mg}}$ auf eine Summe von Produkten aus Faktoren vom Typ $\mathfrak{A}^{(0)}_{\mathfrak{Mg}}$ zurückgeführt.

Entsprechendes läßt sich für $\{\mathfrak{B}^{(0)}_{\mathfrak{Mg}}\}^{(1)}$ zeigen. Wir stellen also fest:

Es gilt $\{\mathfrak{A}^{(0)}_{\mathfrak{Mg}}\}^{(1)} = \{\mathfrak{A}^{(0)}_{\mathfrak{Mg}}\}^{(\mathrm{T})}$, $\{\mathfrak{B}^{(0)}_{\mathfrak{Mg}}\}^{(1)} = \{\mathfrak{B}^{(0)}_{\mathfrak{Mg}}\}^{(\mathrm{T})}$, und beide Ausdrücke sind, auf Größen nullter Ordnung bezogen, Summen von Produkten aus Faktoren vom Typ $\mathfrak{A}^{(0)}_{\mathfrak{Mg}}$ bzw. $\mathfrak{B}^{(0)}_{\mathfrak{Mg}}$. Daher ist die erneute Operation $\{\ \}^{(1)}$ auch durch $\{\ \}^{(\mathrm{T})}$ ersetzbar.

Da $\mathscr{Q}_s^{(0)}$ eine Summe aus Gliedern vom Typ $\mathfrak{A}^{(0)}_{\mathfrak{Mg}}$ ist, gilt insbesondere auch $\{\mathscr{Q}_s^{(0)}\mathscr{V}'|s\rangle^{(0)}\}^{(1)} = \{\mathscr{Q}_s^{(0)}\mathscr{V}'|s\rangle^{(0)}\}^{(\mathrm{T})}$, wenn $|s\rangle^{(0)}$ nichtentarteter Eigenvektor von $\mathscr{H}_0$ ist.

Zusammenfassend können wir feststellen:

Ein quantenmechanischer Ausdruck in Eigenkets und Eigenbras von $\mathscr{H}$, dessen Näherung im ungestörten System $\mathscr{H}_0$ invariant ist gegenüber einer Basistransformation in den entarteten Teilräumen von $\mathscr{H}_0$, geht durch die Operation $\{\ \}^{(\mathrm{T})}$ in die Korrektur erster Ordnung über, und die Korrektur $(n+1)$-ter Ordnung entsteht aus der Korrektur n-ter Ordnung durch Anwendung der Operation $\{\ \}^{(\mathrm{T})}$ und Multiplikation mit dem Faktor $1/n+1$.

Wir formalisieren unser Ergebnis durch Einführung eines Operators $\mathfrak{p}$, der, wie aus dem folgenden ersichtlich, nicht mit einem linearen Operator im Hilbertraum verwechselt werden darf. Er ist auf Größen $f^{(0)}$, $g^{(0)}$ anwendbar, an denen die Operation $\{\ \}^{(\mathrm{T})}$ definiert ist. $\mathfrak{p}$ wirke als Linksoperator auf alle Faktoren, die rechts davon stehen. Wir schreiben $[\mathfrak{p}.]\cdots$, wenn sich seine Wirkung nur auf den ersten Faktor eines entsprechend zerlegten Produktes beziehen soll. Entsprechend den Eigenschaften von $\{\ \}^{(\mathrm{T})}$ gilt also

$$\begin{aligned}
&\text{a)}\ \mathfrak{p}|s\rangle^{(0)} = \mathscr{Q}_s^{(0)}\mathscr{V}'|s\rangle^{(0)}, \qquad \mathfrak{p}\,{}^{(0)}\langle s| = {}^{(0)}\langle s|\mathscr{V}'\mathscr{Q}_s^{(0)};\\
&\text{b)}\ \mathfrak{p}(f^{(0)} + g^{(0)}) = \mathfrak{p}f^{(0)} + \mathfrak{p}g^{(0)};\\
&\text{c)}\ \mathfrak{p}(f^{(0)}\cdot g^{(0)}) = [\mathfrak{p}f^{(0)}]\cdot g^{(0)} + f^{(0)}\cdot\mathfrak{p}g^{(0)};\\
&\text{d)}\ [\mathfrak{p},1] = 0,\ [\mathfrak{p},\mathscr{H}_0] = \mathscr{V}',\ [\mathfrak{p},\mathscr{V}'] = 0,\ [\mathfrak{p},f(\mathscr{H}_0)] = f^{(1)}(\mathscr{H}_0,\mathscr{V}');\\
&\text{e)}\ \mathfrak{p}^n f^{(0)} = \mathfrak{p}^{n-m}(\mathfrak{p}^m f^{(0)}).
\end{aligned} \tag{12}$$

Wenn wie in c) mit $[\mathfrak{p} f^{(0)}]$ zum Ausdruck gebracht werden soll, daß $\mathfrak{p}$ nicht auf die rechts von der Klammer stehenden Faktoren wirkt, gibt es eine konsequente Schreibweise ohne Klammer. Aus

$$\mathfrak{p} f^{(0)} \circ g^{(0)} = [\mathfrak{p} f^{(0)}] \circ g^{(0)} + f^{(0)} \circ \mathfrak{p} g^{(0)} = \mathfrak{p} f^{(0)} \circ g^{(0)} - f^{(0)} \circ \mathfrak{p} g^{(0)} + f^{(0)} \circ \mathfrak{p} g^{(0)}$$

folgt nämlich $[\mathfrak{p} f^{(0)}] = \mathfrak{p} f^{(0)} - f^{(0)} \mathfrak{p}$. In dieser Formulierung hat der Operator $\mathfrak{p}$ keinen Einfluß auf nachfolgende Faktoren. Es ist daher konsequent, die Definition für die Anwendung von $\mathfrak{p}$ auf Operatoren $\mathcal{O}$ durch den Kommutator

$$[\mathfrak{p}, \mathcal{O}] = \mathfrak{p} \mathcal{O} - \mathcal{O} \mathfrak{p}$$

festzulegen, wovon in d) bereits Gebrauch gemacht ist.

Alle Operatoren $\mathcal{O}$, die von der Energiedefinition eines quantenmechanischen Systems unabhängig sind, und alle Zahlen mit dieser Eigenschaft gehören zum Koeffizientenbereich des Operators $\mathfrak{p}$. Für solche „c-Zahlen" gilt $[\mathfrak{p} c] = 0$.

Unter Verweis auf die Ergebnisse über die Operation $\{\ \}^{(T)}$ können wir folgende Konsequenz ziehen:

Für nichtentartete Eigenvektoren $|s\rangle^{(0)}$ von $\mathcal{H}_0$ gilt

$$\mathfrak{p}\,|s\rangle^{(n)} = (n+1)\,|s\rangle^{(n+1)}, \qquad \mathfrak{p}\,{}^{(n)}\langle s| = (n+1)\,{}^{(n+1)}\langle s|$$

und (13)

$$\mathfrak{p}\,E_s^{(n)} = (n+1)\,E_s^{(n+1)}, \qquad \mathfrak{p} g^{(n)}(E_s^{(0)}, E_s^{(1)}, \ldots, E_s^{(n)}) = (n+1) g^{(n+1)}(E_s^{(0)}, \ldots, E_s^{(n+1)}) .$$

Für entartete Eigenvektoren von $\mathcal{H}_0$ ist die Anwendung von $\mathfrak{p}$ gleichfalls definiert, führt aber nicht auf die Korrektur zu einem Eigenvektor von $\mathcal{H}$.

Unabhängig von der Frage der Entartung gilt die Orthonormierungsbedingung (4) für die „$\mathfrak{p}$-Korrekturen" zu einer orthonormierten Basis aus Eigenvektoren von $\mathcal{H}_0$.

Für quantenmechanische Erwartungswerte F, die in der Näherung von $\mathcal{H}_0$ invariant sind gegenüber unitären Transformationen in allen entarteten Teilräumen von $\mathcal{H}_0$, gilt ebenfalls

$$\mathfrak{p}\,F^{(n)} = (n+1)\,F^{(n+1)} . \tag{13a}$$

Für einen Operator $\mathcal{O}$ mit dieser Invarianzeigenschaft schreiben wir

$$[\mathfrak{p}, \mathcal{O}^{(n)}] = \mathfrak{p}\,\mathcal{O}^{(n)} - \mathcal{O}^{(n)}\mathfrak{p} = (n+1)\,\mathcal{O}^{(n+1)} . \tag{13b}$$

Mit der Definition

$$[\mathfrak{p}, \mathcal{O}^{(0)}]_0 = \mathcal{O}^{(0)}, [\mathfrak{p}, \mathcal{O}^{(0)}]_1 = [\mathfrak{p}, \mathcal{O}^{(0)}], [\mathfrak{p}, \mathcal{O}^{(0)}]_n = [\mathfrak{p}, [\mathfrak{p}, \mathcal{O}^{(0)}]_{n-1}]$$

gilt dann

$$\mathcal{O}^{(n)} = \frac{1}{n}\,[\mathfrak{p}, \mathcal{O}^{(n-1)}] = \frac{1}{n!}\,[\mathfrak{p}, \mathcal{O}^{(0)}]_n .$$

Wir werden im nächsten Kapitel zeigen, daß die aufgeführten Beziehungen von praktischem Interesse sind. Die folgenden Konsequenzen sind formaler Natur.

Mit der formalen Summe $e^{\mathfrak{p}} = \sum\limits_{n}^{0,\infty} \frac{1}{n!}\,\mathfrak{p}^n$ können wir für nichtentartete Eigenwerte von $\mathcal{H}_0$ die Eigenwerte und die Eigenvektoren von $\mathcal{H}$ in der Form schreiben

$$|s\rangle = e^{\mathfrak{p}}\,|s\rangle^{(0)}, \qquad \langle s| = e^{\mathfrak{p}}\,{}^{(0)}\langle s|, \qquad E_s = e^{\mathfrak{p}}\,E_s^{(0)} .$$

Für Ausdrücke F der obigen Art gilt

$$F = e^{\mathrm{p}} F^{(0)} .$$

Für Operatoren $\mathcal{O}$ können wir wegen

$$\mathcal{O} = \sum_{n}^{0,\infty} \mathcal{O}^{(n)} = \sum_{n}^{0,\infty} \frac{1}{n!} [\mathrm{p}, \mathcal{O}^{(0)}]_n = \mathcal{O}^{(0)} + [\mathrm{p}, \mathcal{O}^{(0)}] + \frac{1}{2!} [\mathrm{p}, [\mathrm{p}, \mathcal{O}^{(0)}]] + \cdots$$

$$= \left(1 + \mathrm{p} + \frac{1}{2!} \mathrm{p}^2 + \cdots\right) \mathcal{O}^{(0)} \left(1 - \mathrm{p} + \frac{1}{2!} \mathrm{p}^2 - \cdots\right)$$

die Schreibweise verwenden:

$$\mathcal{O} = e^{\mathrm{p}} \mathcal{O}^{(0)} e^{-\mathrm{p}} .$$

Speziell gilt also:

$$\mathcal{H} = e^{\mathrm{p}} \mathcal{H}_0 e^{-\mathrm{p}} .$$

Abschließend stellen wir fest:

Der Operator e^{p} bewirkt die Transformation einer orthonormierten Basis aus Eigenvektoren $|s\rangle^{(0)}$ zu $\mathcal{H}_0$ in eine andere orthonormierte Basis, in der alle Vektoren, die aus nichtentarteten $|s\rangle^{(0)}$ hervorgehen, Eigenvektoren von $\mathcal{H}$ sind.

Im folgenden soll der Nutzen des vorgetragenen Standpunktes an zwei Beispielen illustriert werden.

Beispiele

a) Ein Teilchensystem bestehe aus N Teilsystemen mit schwacher Wechselwirkung. Entsprechend soll der Hamiltonoperator

$$\mathcal{H} = \sum_{i}^{1,N} \mathcal{H}_i + \sum_{i<j}^{1,N} \mathcal{V}_{ij}$$

mit

$$\mathcal{H}_0 = \sum_{i}^{1,N} \mathcal{H}_i \quad \text{und} \quad \mathcal{V} = \sum_{i<j}^{1,N} \mathcal{V}_{ij}$$

in einen ungestörten Teil und einen Störterm zerlegt werden:

$$\mathcal{H} = \mathcal{H}_0 + \mathcal{V} .$$

Die Eigenvektoren und Eigenwerte von den Teilsystemen $\mathcal{H}_i$ seien mit $|s_i\rangle$ und E_{s_i} bezeichnet. Demnach sind die Eigenvektoren von $\mathcal{H}_0$ Produkte von der Form

$$|s\rangle^{(0)} = |s_1\rangle |s_2\rangle \cdots |s_N\rangle = |s_1 s_2 \ldots s_N\rangle .$$

Für die Eigenwerte in nullter Ordnung gilt

$$E_s^{(0)} = \sum_{i}^{1,N} E_{s_i} .$$

Wir beweisen folgenden Satz:

Für Eigenvektoren $|s\rangle$ und $|t\rangle$, die in nullter Näherung nicht entartet sind, gilt: Das Matrixelement $\langle s|A_{(m)}|t\rangle$ eines c-Operators $A_{(m)}$, der sich auf $m < N$ Teilsysteme bezieht, hat die Eigenschaft, daß die n-te störungstheoretische Korrektur eine Summe von Ausdrücken ist, die von höchstens $n+m$ Teilsystemen abhängen.

Wir beweisen die Behauptung zunächst für $n=0$ und $n=1$. Die m Teilsysteme, von denen $A_{(m)}$ abhängt, seien $\mathscr{H}_1, \mathscr{H}_2, \ldots, \mathscr{H}_m$. Dann gilt in nullter Ordnung

$$^{(0)}\langle s|A_{(m)}|t\rangle^{(0)} = \langle s_1 s_2 \ldots s_m|A_{(m)}|t_1 t_2 \ldots t_m\rangle \prod_{\kappa}^{m+1,N} \delta_{s_\kappa t_\kappa},$$

d.h. $\langle s|A_{(m)}|t\rangle$ hängt nur von den m Indizes $1, 2, \ldots, m$ ab, für die Korrektur erster Ordnung:

$$\begin{aligned}
[\langle s|A_{(m)}|t\rangle]^{(1)} &= {}^{(1)}\langle s|A_{(m)}|t\rangle^{(0)} + {}^{(0)}\langle s|A_{(m)}|t\rangle^{(1)} \\
&= \sum_{r(\neq s)} \frac{^{(0)}\langle s|\mathscr{V}|r\rangle^{(0)}}{E_s^{(0)} - E_r^{(0)}} {}^{(0)}\langle r|A_{(m)}|t\rangle^{(0)} + \sum_{r(\neq t)} {}^{(0)}\langle s|A_{(m)}|r\rangle^{(0)} \frac{^{(0)}\langle r|\mathscr{V}|t\rangle^{(0)}}{E_t^{(0)} - E_r^{(0)}} \\
&= \sum_{r(\neq s)} \sum_{i<j}^{1,N} \frac{\langle s_i s_j|\mathscr{V}_{ij}|r_i r_j\rangle}{E_{s_i} + E_{s_j} - E_{r_i} - E_{r_j}} \langle r_1 r_2 \ldots r_m|A_{(m)}|t_1 t_2 \ldots t_m\rangle \prod_{\kappa(\neq i,j)}^{1,N} \delta_{s_\kappa r_\kappa} \prod_{\kappa}^{m+1,N} \delta_{r_\kappa t_\kappa} \\
&\quad + \sum_{r(\neq t)} \sum_{i<j}^{1,N} \langle s_1 s_2 \ldots s_m|A_{(m)}|r_1 r_2 \ldots r_m\rangle \frac{\langle r_i r_j|\mathscr{V}_{ij}|t_i t_j\rangle}{E_{t_i} + E_{t_j} - E_{r_i} - E_{r_j}} \prod_{\kappa}^{m+1,N} \delta_{s_\kappa r_\kappa} \prod_{\kappa(\neq i,j)}^{1,N} \delta_{r_\kappa t_\kappa}.
\end{aligned}$$

Für Glieder mit $i>m$ und $j>m$ werden die δ-Faktoren von der Form

$$\left(\prod_{\kappa}^{1,m} \delta_{r_\kappa s_\kappa}\right) \delta_{r_i t_i} \delta_{r_j t_j} \quad \text{bzw.} \left(\prod_{\kappa}^{1,m} \delta_{r_\kappa t_\kappa}\right) \delta_{r_i s_i} \delta_{r_j s_j}.$$

Daher unterscheiden sich die entsprechenden Teilsummen aus der ersten und zweiten Zeile nur im Vorzeichen und kompensieren sich gegenseitig. Nichtverschwindende Ausdrücke genügen also der Bedingung $i \leqq m$ oder $j \leqq m$ und sind daher eine Summe von Gliedern mit höchstens $m+1$ verschiedenen Indizes.

Für die Korrektur n-ter Ordnung:

Die $(n-1)$-te Ordnung

$$[\langle s|A_{(m)}|t\rangle]^{(n-1)} = \frac{\mathfrak{p}^{n-1}}{(n-1)!} {}^{(0)}\langle s|A_{(m)}|t\rangle^{(0)}$$

ist, wie aus dem Prozeß der sukzessiven Anwendung von $\mathfrak{p}$ hervorgeht, eine Summe von Gliedern, die sich aus Faktoren vom Typ $^{(0)}\langle k|A_{(m)}|l\rangle^{(0)}$, $^{(0)}\langle p|\mathscr{V}|q\rangle^{(0)}$ und $f(E_u^{(0)} - E_v^{(0)})$ zusammensetzen. Dabei ist $f(E_u^{(0)} - E_v^{(0)})$ eine Funktion des Nenners in $\mathscr{D}_s^{(0)}$. Wir nehmen an, daß diese Produkte von nicht mehr als $n+m-1$ Indizes abhängen. Beim Übergang zur n-ten Ordnung entstehen daraus Produkte, in denen jeweils einer der Faktoren durch $\mathfrak{p}^{(0)}\langle k|A_{(m)}|l\rangle^{(0)}$ bzw. $\mathfrak{p}^{(0)}\langle p|\mathscr{V}|q\rangle^{(0)}$ ersetzt ist. In den ersten beiden Fällen können wir aus dem Vorangehenden schließen, daß die Indexmenge in konstituierenden Teilsummen höchstens um eins anwachsen kann. Es bleibt also nur noch, das Entsprechende für ein Produkt mit $\mathfrak{p}\, f(E_u^{(0)} - E_v^{(0)})$ als Faktor nachzuweisen. Sei $\mathfrak{M}$ die Indexmenge, von der f abhänge, dann können wir f, ohne etwas zu verändern, durch das Produkt von f mit einem Faktor $\prod_{\kappa \notin \mathfrak{M}} \delta_{u_\kappa v_\kappa}$ ersetzen.

Aus der Gleichung

$$\mathfrak{p}\, f(E_u^{(0)} - E_v^{(0)}) \prod_{\kappa \notin \mathfrak{M}} \delta_{u_\kappa v_\kappa}$$
$$= \frac{\partial\, f(E_u^{(0)} - E_v^{(0)})}{\partial\,(E_u^{(0)} - E_v^{(0)})} \left(\sum_{i<j}^{1,N} \{\langle u_i u_j | \mathscr{V}_{ij} | u_i u_j \rangle - \langle v_i v_j | \mathscr{V}_{ij} | v_i v_j \rangle\} \right) \prod_{\kappa \notin \mathfrak{M}} \delta_{u_\kappa v_\kappa}$$

sehen wir, daß die rechte Seite verschwindet, wenn weder i noch j zur Indexmenge $\mathfrak{M}$ gehört, d.h. auch der Faktor $f(E_u^{(0)} - E_v^{(0)})$ erhöht seine Indexmenge bei Anwendung von $\mathfrak{p}$ höchstens um eins.

Damit ist der Beweis unserer Behauptung mittels vollständiger Induktion erbracht.

b) Ein System geladener Teilchen befinde sich unter dem Einfluß eines äußeren elektrostatischen Feldes $\vec{\mathscr{E}} = \{\mathscr{E}_1, \mathscr{E}_2, \mathscr{E}_3\}$. Wir betrachten die Dipolenergie $-\sum_{\varrho}^{1,3} \mathscr{m}_\varrho \mathscr{E}_\varrho$ als Störterm für das ungestörte Ladungssystem mit dem Energieoperator $\mathscr{H}_0$. Dabei ist $\vec{\mathscr{m}} = \{\mathscr{m}_1, \mathscr{m}_2, \mathscr{m}_3\}$ der Operator des elektrischen Dipolmomentes.

Unsere Methode erlaubt die Berechnung der Polarisierbarkeit aus dem Dipolmoment, der Hyperpolarisierbarkeit aus der Polarisierbarkeit usw. Es gilt

$$\mathfrak{p}\ {}^{(0)}\langle s | \mathscr{H}_0 | s \rangle^{(0)} = -\sum_{\varrho}^{1,3} {}^{(0)}\langle s | \mathscr{m}_\varrho | s \rangle^{(0)} \mathscr{E}_\varrho\,,$$
$$\mathfrak{p}\ {}^{(0)}\langle s | \mathscr{m}_\varrho | s \rangle^{(0)} = \sum_{\sigma}^{1,3} \alpha_{\varrho\sigma}^{(0} \mathscr{E}_\sigma\,,$$
$$\mathfrak{p}\, \alpha_{\varrho\sigma}^{(0)} = \sum_{\tau}^{1,3} \beta_{\varrho\sigma\tau}^{(0)} \mathscr{E}_\tau\,.$$

Dabei sind ${}^{(0)}\langle s | \vec{\mathscr{m}} | s \rangle^{(0)}$ das elektrische Dipolmoment, $\alpha^{(0)}$ und $\beta^{(0)}$ die Tensoren der statischen elektrischen Polarisierbarkeit und Hyperpolarisierbarkeit des Systems im nichtentarteten Zusant $|s\rangle^{(0)}$ (vgl. z.B. [1]).

Eine Reihenentwicklung von $\langle s | \mathscr{H} | s \rangle$, $\langle s | \mathscr{m}_\varrho | s \rangle$ usw. nach Potenzen des Feldes $\vec{\mathscr{E}}$ kann daher in der Form geschrieben werden

$$\langle s | \mathscr{H} | s \rangle = e^{\mathfrak{p}}\ {}^{(0)}\langle s | \mathscr{H}_0 | s \rangle^{(0)}$$
$$= {}^{(0)}\langle s | \mathscr{H}_0 | s \rangle^{(0)} - \sum_{\varrho}^{1,3} {}^{(0)}\langle s | \mathscr{m}_\varrho | s \rangle^{(0)} \mathscr{E}_\varrho - \frac{1}{2!} \sum_{\varrho,\sigma}^{1,3} \alpha_{\varrho\sigma}^{(0)} \mathscr{E}_\varrho \mathscr{E}_\sigma$$
$$- \frac{1}{3!} \sum_{\varrho,\sigma,\tau}^{1,3} \beta_{\varrho\sigma\tau}^{(0)} \mathscr{E}_\varrho \mathscr{E}_\sigma \mathscr{E}_\tau - \cdots$$

$$\langle s | \mathscr{m}_\varrho | s \rangle = e^{\mathfrak{p}}\ {}^{(0)}\langle s | \mathscr{m}_\varrho | s \rangle^{(0)}$$
$$= {}^{(0)}\langle s | \mathscr{m}_\varrho | s \rangle^{(0)} + \sum_{\sigma}^{1,3} \alpha_{\varrho\sigma}^{(0)} \mathscr{E}_\sigma + \frac{1}{2!} \sum_{\sigma,\tau}^{1,3} \beta_{\varrho\sigma\tau}^{(0)} \mathscr{E}_\sigma \mathscr{E}_\tau + \cdots$$

$$\alpha_{\varrho\sigma} = e^{\mathfrak{p}} \alpha_{\varrho\sigma}^{(0)}$$
$$= \alpha_{\varrho\sigma}^{(0)} + \sum_{\tau}^{1,3} \beta_{\varrho\sigma\tau}^{(0)} \mathscr{E}_\tau + \cdots\,.$$

Während man unter Berufung auf das Hellmann-Feynman-Theorem bei Kenntnis der Entwicklung von $\langle s|\mathscr{H}(\mathcal{E}_\varrho)|s\rangle$ nach dem Parameter $\mathcal{E}_\varrho$ nur $\langle s|\mathfrak{m}_\varrho|s\rangle$ gemäß

$$\langle s|\mathfrak{m}_\varrho|s\rangle = -\frac{\partial}{\partial \mathcal{E}_\varrho}\langle s|\mathscr{H}(\mathcal{E}_\varrho)|s\rangle$$

gewinnt, nicht aber die Entwicklung von $\alpha_{\varrho\sigma}$ usw., führt die Anwendung des Operators $\mathfrak{p}$ von einer vorgegebenen Korrektur zur nächsten.

Anhang

Explizite Berechnung der zweiten Korrektur zu einem nichtentarteten Eigenvektor $|s\rangle^{(0)}$ mit dem Operator $\mathfrak{p}$:

$$|s\rangle^{(1)} = \mathfrak{p}|s\rangle^{(0)} = \mathscr{Q}_s^{(0)}\mathscr{V}|s\rangle^{(0)},$$

$$2|s\rangle^{(2)} = \mathfrak{p}\,\mathscr{Q}_s^{(0)}\mathscr{V}|s\rangle^{(0)} = [\mathfrak{p},\mathscr{Q}_s^{(0)}]\,\mathscr{V}|s\rangle^{(0)} + \mathscr{Q}_s^{(0)}\mathscr{V}\,\mathfrak{p}|s\rangle^{(0)}.$$

Wegen

$$\begin{aligned}[\mathfrak{p},\mathscr{Q}_s^{(0)}] = {} & \sum_{t\notin\mathfrak{M}}\ \sum_{r\notin\mathfrak{M}}\left(\frac{|r\rangle^{(0)}\,{}^{(0)}\langle r|\mathscr{V}|t\rangle^{(0)}\,{}^{(0)}\langle t|}{(E_s^{(0)}-E_t^{(0)})\,(E_t^{(0)}-E_r^{(0)})} + \frac{|t\rangle^{(0)}\,{}^{(0)}\langle t|\mathscr{V}|r\rangle^{(0)}\,{}^{(0)}\langle r|}{(E_s^{(0)}-E_t^{(0)})\,(E_t^{(0)}-E_r^{(0)})}\right) \\ & - \sum_{t\notin\mathfrak{M}}\frac{|t\rangle^{(0)}\,{}^{(0)}\langle t|}{(E_s^{(0)}-E_t^{(0)})^2}\left({}^{(0)}\langle s|\mathscr{V}|s\rangle^{(0)} - {}^{(0)}\langle t|\mathscr{V}|t\rangle^{(0)}\right) \\ = {} & \mathscr{Q}_s^{(0)}\left(\mathscr{V} - {}^{(0)}\langle s|\mathscr{V}|s\rangle^{(0)}\right)\mathscr{Q}_s^{(0)} - |s\rangle^{(0)}\,{}^{(0)}\langle s|\mathscr{V}\,\mathscr{Q}_s^{(0)}\mathscr{Q}_s^{(0)} - \mathscr{Q}_s^{(0)}\mathscr{Q}_s^{(0)}\mathscr{V}|s\rangle^{(0)}\,{}^{(0)}\langle s|\end{aligned}$$

ergibt sich

$$2|s\rangle^{(2)} = 2\mathscr{Q}_s^{(0)}\left(\mathscr{V} - {}^{(0)}\langle s|\mathscr{V}|s\rangle^{(0)}\right)\mathscr{Q}_s^{(0)}\mathscr{V}|s\rangle^{(0)} - |s\rangle^{(0)}\,{}^{(0)}\langle s|\mathscr{V}\,\mathscr{Q}_s^{(0)}\mathscr{Q}_s^{(0)}\mathscr{V}|s\rangle^{(0)}.$$

Der Vergleich mit (6a) bestätigt dieses Resultat bei Berücksichtigung der Normierungsbedingung

$${}^{(0)}\langle s|s\rangle^{(2)} + {}^{(2)}\langle s|s\rangle^{(0)} = -{}^{(1)}\langle s|s\rangle^{(1)} = -{}^{(0)}\langle s|\mathscr{V}\,\mathscr{Q}_s^{(0)}\mathscr{Q}_s^{(0)}\mathscr{V}|s\rangle^{(0)}$$

und der speziellen Phasenwahl $Im\,{}^{(0)}\langle s|s\rangle^{(2)} = 0$, also

$$2\,{}^{(0)}\langle s|s\rangle^{(2)} = -{}^{(0)}\langle s|\mathscr{V}\,\mathscr{Q}_s^{(0)}\mathscr{Q}_s^{(0)}\mathscr{V}|s\rangle^{(0)}.$$

Literatur

1. Buckingham, A. D.: Permanent and induced molecular moments and long-range intermolecular forces. In: Advances chem. Physics, Vol. 12, J. O. Hirschfelder, Ed., pp. 107-142. New York-London-Sydney: Interscience 1967.
2. Wigner, E. P.: Group theory and its application to the quantum mechanics of atomic spectra. New York London: Academic Press 1959.

Professor Dr. E. Ruch
Institut für Quantenchemie
Freie Universität Berlin
D-1000 Berlin 45, Holbeinstr. 48
Deutschland

Theoret. chim. Acta (Berl.) 29, 247—258 (1973)
© by Springer-Verlag 1973

Quantenmechanische Theorie der optischen Aktivität der Allenderivate im Transparenzgebiet

Dietrich Haase und Ernst Ruch

Institut für Quantenchemie der Freien Universität Berlin

Eingegangen am 20. November 1972

Quantum Mechanical Theory of Optical Rotatory Power of Allene Derivatives in the Transparent Region

The quantum mechanical theory of the optical rotatory power of methane derivatives [2] is applicable to the class of allene derivatives if one makes appropriate changes in the model Hamiltonian. We hereby find a physical interpretation for parameters already determined empiricaly in the course of experimental studies of this molecular class [7].

Die quantenmechanische Theorie der optischen Aktivität von Methanderivaten [2] wird mit entsprechenden Veränderungen des Modelloperators für die Energie auf die Klasse der Allenderivate übertragen. Dabei findet sich eine physikalische Interpretation von Parametern, die im Rahmen einer experimentellen Untersuchung [7] empirisch berechnet worden sind.

Modell und Störungsrechnung

Nach dem Muster einer algebraischen Theorie der pseudoskalaren Eigenschaften von Molekülen einer Klasse mit achiralem Molekülgerüst [8] ist das spezielle Phänomen "optische Aktivität" für Methanderivate quantenmechanisch behandelt worden [2]. Trotz der Spezialisierung auf Methanderivate dokumentieren sich in der Wahl des Modell-Energieoperators oder in der Diskussion der Störungsrechnung Züge, die an anderen Molekülklassen in entsprechender Interpretation bestehen bleiben. Beispielsweise liefert die Störungsrechnung in der benutzten Form, wie aus [3] geschlossen werden kann, bei beliebigem Gerüst den Ansatz nach dem zweiten Verfahren (vgl. [8]). Insofern liegt eine allgemeine quantenmechanische Theorie für beliebige Molekülklassen auf der Hand. Andererseits interessiert der quantitative Aspekt der Störungsrechnung, also z. B. die Frage, inwieweit die Formeln in ihrer Abhängigkeit von ligandenspezifischen Größen wie Dipolmoment, Polarisierbarkeit u. a. die optische Aktivität der Moleküle numerisch zufriedenstellend beschreiben. Experimentelle Daten zum systematischen Test von empirischen Bestimmungsstücken der formalen Theorie der optischen Aktivität [8] liegen inzwischen für Allenderivate [7] und Methanderivate [5] vor. Die physikalische Interpretation solcher Bestimmungsstücke

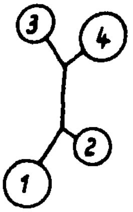

Fig. 1

liefert die quantenmechanische Analyse, wie für Methanderivate und speziell für solche mit der T_d-Bedingung in [2] gezeigt wurde. Die hier beabsichtigte Ergänzung betrifft Allenderivate und speziell solche, die wir D_{2d}-Derivate nennen wollen.

Den Derivaten des Allens oder von Kumulenen mit einer ungeraden Zahl von Kohlenstoffen ist ein Molekülgerüst der Symmetrie D_{2d} mit vier Ligandenplätzen entsprechend Fig. 1 gemein. Wir nennen sie D_{2d}-Derivate, wenn die substituierten Liganden eine Symmetrieebene besitzen und so fixiert sind, daß diese Symmetrieebene mit der jeweiligen Spiegelebene des Gerüstes zusammenfällt.

Die qualitativ vollständige Chiralitätsfunktion für D_{2d}-Derivate enthält zwei Komponenten, deren eine formal mit der von T_d-Derivaten identisch ist. Da diese T_d-Komponente in [2] ausführlich diskutiert wurde, und da aus experimentellen Befunden [7] entnommen werden darf, daß sie bei Allenderivaten offenbar keine nennenswerten numerischen Beiträge zum optischen Drehwinkel liefert, beschränken wir uns auf den verkürzten Ansatz. Er besitzt nur eine Komponente, er ist qualitativ vollständig für alle Moleküle mit mindestens zwei gleichartigen Liganden, und er erfüllt ein Additionstheorem, das in [7] und [8] ausführlich diskutiert wurde.

Der verkürzte Ansatz nach dem zweiten Näherungsverfahren lautet:

$$\tilde{\chi}(l_1, l_2, l_3, l_4) = \varphi(l_1, l_3) + \varphi(l_2, l_4) - \varphi(l_1, l_4) - \varphi(l_2, l_3) \tag{1}$$

mit

$$\varphi(l_i, l_j) = \varphi(l_j, l_i) .$$

Nach dem ersten Verfahren hat er die Form

$$\begin{aligned} \chi(l_1, l_2, l_3, l_4) &= \varepsilon[\lambda(l_1) - \lambda(l_2)]\,[\lambda(l_3) - \lambda(l_4)] \\ &= \varepsilon \begin{vmatrix} 1 & 1 \\ \lambda(l_1) & \lambda(l_2) \end{vmatrix} \begin{vmatrix} 1 & 1 \\ \lambda(l_3) & \lambda(l_4) \end{vmatrix} . \end{aligned} \tag{2}$$

die mit $\varphi(l_i, l_j) = \varepsilon \lambda(l_i)\, \lambda(l_j)$ aus (1) entsteht.

Wir diskutieren mit dem quantenmechanischen Formalismus aus [2] und unter Benutzung der dort erklärten Bezeichnungen die optische Aktivität von Allenderivaten, indem wir uns im wesentlichen darauf beschränken, Aspekte der Theorie hervorzuheben oder Resultate explizit zu formulieren, die für Methan- und Allenderivate verschieden sind. Die folgenden Betrachtungen beziehen sich ebenso auf Derivate der oben erwähnten Kumulene oder von Verbindungen mit einem anderen D_{2d}-Gerüst entsprechender Anordnung von vier Ligandenplätzen. Wir beziehen uns im Text auf Allene und vermerken, daß damit nur ein charakteristisches Beispiel für derartige Molekülklassen betrachtet wird.

Wie für Methanderivate sei das quantenmechanische Modell durch einen Energieoperator $\bar{\mathscr{H}}$ charakterisiert, in dem die Operatoren für Teilsysteme und für die Wechselwirkung zwischen diesen Systemen entsprechend wie in [2] erklärt sind.

$$\bar{\mathscr{H}} = \sum_{i}^{1,4} (\mathscr{H}_i + \mathscr{V}_i) + \mathscr{H}_G + \sum_{i<j}^{1,4} \bar{\mathscr{H}}_{ij} + \sum_{i}^{1,4} \bar{\mathscr{H}}_{iG} . \tag{3}$$

$\mathscr{H}_i + \mathscr{V}_i$ ist der Operator für einen formal gebundenen Liganden l_i einschließlich des endständigen Kohlenstoffrumpfes am Allengerüst, einer Abschirmladung $-\frac{1}{4\pi}\,\mathrm{div\,grad}\,\Phi_i$ und jener Elektronen, die die Bindung ans Gerüst besorgen. $\mathscr{V}_i$ ist die potentielle Energie der Teilchen des Liganden an der Gerüststelle i ohne den Gerüstkohlenstoff im Feld dieser Abschirmladung. Die Potentiale Φ_i und die dazugehörigen Ladungsverteilungen haben die Symmetrie C_s, Untersymmetrie der Gerüstsymmetrie D_{2d}; das Gesamtpotential $\Phi = \sum_i^{1,4} \Phi_i$ besitzt also die Symmetrie D_{2d}. $\bar{\mathscr{H}}_{ij}$, die Operatoren der Coulomb-Wechselwirkung zwischen den Liganden l_i und l_j, sind formal identisch mit denen zwischen denselben Liganden in Methanderivaten. $\bar{\mathscr{H}}_{iG}$ sind Coulombsche Wechselwirkungsoperatoren zwischen den Liganden und dem Gerüst. $\mathscr{H}_G$, der Energieoperator des Gerüstes, hat die Symmetrie D_{2d} und enthält gewünschtenfalls auch Terme, die von einem weiteren Abschirmfeld stammen.

Für Liganden, die nur aus einem Elektron bestehen, verschwinden wie beim Methan (vgl. [2]) wegen $\kappa(l_i) = 0$ die Operatoren für die Wechselwirkung mit anderen Teilsystemen. Im Modelloperator für das Allenradikal mit je einem ungepaarten Elektron an den Plätzen 1, 2, 3, 4 verschwinden daher alle Wechselwirkungsterme $\bar{\mathscr{H}}_{ij}$, die $\mathscr{H}_i + \mathscr{V}_i$ beschreiben die ungepaarten Elektronen im oben erwähnten Abschirmfeld. $\bar{\mathscr{H}}$ ist also auch noch in diesem extremen Grenzfall ein vernünftiger Modelloperator.

Zum ungestörten Hamilton-Operator

$$\mathscr{H}_0 = \sum_i^{1,4} (\mathscr{H}_i + \mathscr{V}_i) + \mathscr{H}_G$$

gehören die Eigenvektoren $|s\rangle^{(0)} = |s_1\rangle\,|s_2\rangle\,|s_3\rangle\,|s_4\rangle\,|s_G\rangle = |s_1 s_2 s_3 s_4 s_G\rangle$ und $|0\rangle^{(0)} = |0_1 0_2 0_3 0_4 0_G\rangle$ für den Grundzustand.

Wegen

$$[\mathrm{Sp}^{(J)}\gamma]^{(0)} = \sum_i^{1,4} \mathrm{Sp}^{(J)}\gamma(l_i) + \mathrm{Sp}^{(J)}\gamma(G) \tag{4a}$$

finden wir den optischen Drehwinkel in nullter störungstheoretischer Ordnung:

$$[\omega]^{(0)} = \sum_i^{1,4} [\omega(l_i)] + [\omega(G)] \tag{4b}$$

mit

$$[\omega(l_i)] = K\,\mathrm{Sp}^{(J)}\gamma(l_i) \quad \text{und} \quad [\omega(G)] = K\,\mathrm{Sp}^{(J)}\gamma(G)\,.$$

Wegen der achiralen Gerüstsymmetrie gilt $\mathrm{Sp}^{(J)}\gamma(G) = 0$, und daher verschwindet $[\omega]^{(0)}$, wenn die D_{2d}-Bedingung erfüllt ist.

Das Ergebnis der Störungsrechnung erster Ordnung mit $\sum_{i<j}^{1,4} \bar{\mathscr{H}}_{ij} + \sum_i^{1,4} \bar{\mathscr{H}}_{iG}$ als Störoperator finden wir in [2]. Der Tensor $[{}^{(J)}\gamma]^{(1)}$ ist eine Summe von Ausdrücken, die nur Eigenwerte, Eigenvektoren und Wechselwirkungsoperatoren zu jeweils einem Paar von Teilsystemen enthalten, also entweder von einem Ligandenpaar $\langle l_i, l_j\rangle$ oder von einem Liganden und dem Gerüst $\langle l_i, G\rangle$ abhängen.

Es ergibt sich also

$$[\mathrm{Sp}^{(J)}\gamma]^{(1)} = \sum_{i<j}^{1,4} [\mathrm{Sp}^{(J)}\gamma(l_i, l_j)]^{(1)} + \sum_{i}^{1,4} [\mathrm{Sp}^{(J)}\gamma(l_i, G)]^{(1)} \tag{5a}$$

und entsprechend

$$[\omega]^{(1)} = \sum_{i<j}^{1,4} [\omega(l_i, l_j)]^{(1)} + \sum_{i}^{1,4} [\omega(l_i, G)]^{(1)} \tag{5b}$$

mit

$$[\omega(l_i, l_j)]^{(1)} = K[\mathrm{Sp}^{(J)}\gamma(l_i, l_j)]^{(1)}, \qquad [\omega(l_i, G)]^{(1)} = K[\mathrm{Sp}^{(J)}\gamma(l_i, G)]^{(1)}.$$

Im Gegensatz zu T_d-Derivaten des Methans verschwinden bei D_{2d}-Derivaten des Allens nicht alle Beiträge aus der ersten störungstheoretischen Korrektur, denn nur die Teilsysteme

$$\langle l_1, l_2\rangle, \langle l_3, l_4\rangle \quad \text{und} \quad \langle l_i, G\rangle \quad \text{für alle } i$$

sind achiral.

Die Systeme

$$\langle l_1, l_3\rangle, \quad \langle l_1, l_4\rangle, \quad \langle l_2, l_3\rangle, \quad \langle l_2, l_4\rangle$$

sind dagegen chiral und liefern nichtverschwindende Beiträge in (5b). Sie sind mit dem Operator $\mathscr{P}_+(ij) = \frac{1}{2}\{\mathcal{O}(e) + \mathcal{O}((ij))\}$ im Modell $\tilde{\mathscr{K}}$ von der Form

$$\begin{aligned}[\mathrm{Sp}^{(J)}\gamma(l_i, l_j)]^{(\tilde{1})} = \frac{2\kappa_i\kappa_j}{\nu} \mathscr{P}_+(ij) \operatorname{Im} \sum_{\varrho,\sigma,\varrho',\sigma'} \Big\{ &\Gamma_{\varrho\varrho\sigma}(l_i)\,(\vec{e}_\sigma^{(i)} \cdot T_{ij} \cdot \{\langle \vec{m}(l_j)\rangle + \vec{c}_j\}) \\ &+ \alpha_{\varrho\sigma}(l_i)\,\vec{e}_\varrho^{(i)} \cdot \left(\gamma_{\varrho'\sigma'}(l_j)\,\vec{e}_{\sigma'}^{(j)} - i\,\frac{\pi}{c}\,\nu\alpha_{\varrho'\sigma'}(l_j)\,\vec{r}_j \times \vec{e}_{\sigma'}^{(j)}\right)(\vec{e}_\sigma^{(i)} \cdot T_{ij} \cdot \vec{e}_{\varrho'}^{(j)}) \Big\}.\end{aligned} \tag{6}$$

Als individuelle Bezugspunkte für die ortsabhängigen Größen $\gamma(l_i)$ und $\Gamma(l_i)$ können wieder die Ladungsschwerpunkte $\vec{r}_i$ der Kernsysteme $\mathfrak{K}_i$ gewählt werden.

Diskussion des Resultats

1. Allgemeine Form

Ähnlich wie für Methanderivate gilt für die vorliegende Molekülklasse:

> Alle geometrischen Figuren mit vier ausgezeichneten Punkten, die ohne Symmetrieerniedrigung stetig in ein D_{2d}-Gerüst (z. B. D_{2d}-symmetrisches Tetraeder mit den vier ausgezeichneten Eckpunkten) deformierbar sind, und nur solche repräsentieren mögliche Gerüste von Molekülklassen mit der Eigenschaft, daß die D_{2d}-Komponente Bestandteil der qualitativ vollständigen Chiralitätsfunktion ist.

Solange wir also im Bereich kleiner Abweichungen von der D_{2d}-Symmetrie des Gerüstes und von der D_{2d}-Bedingung bleiben und solange die Symmetrie des Gerüstes sich wesentlich von der des regulären Tetraeders unterscheidet, kann die erste störungstheoretische Ordnung von $\mathrm{Sp}^{(J)}\gamma$ für den Hauptbeitrag zum optischen Drehwinkel verantwortlich gemacht werden. Für Allenderivate solcher Art zeigen die experimentellen Befunde [7] die Zuständigkeit des verkürzten Ansatzes. Wir haben also Veranlassung, auch ohne Spezialisierung auf die D_{2d}-Bedingung, die quantenmechanische Störungsrechnung bis zur ersten

Ordnung als gute Näherung für Allenderivate zu betrachten und bekommen dementsprechend folgende Form für $[\omega]$:

$$\begin{aligned}[\omega] = [\omega]^{(0+1)} = K\Big(\sum_{i}^{1,4} \mathrm{Sp}^{(J)}\gamma(l_i) + \mathrm{Sp}^{(J)}\gamma(G) + \sum_{i<j}^{1,4} [\mathrm{Sp}^{(J)}\gamma(l_i, l_j)]^{(1)} \\ + \sum_{i}^{1,4} [\mathrm{Sp}^{(J)}\gamma(l_i, G)]^{(1)}\Big). \end{aligned} \tag{7}$$

2. D_{2d}-*Derivate im Modell* $\mathscr{H}$

Für D_{2d}-Derivate vereinfacht sich (7) zu

$$[\omega] = [\omega(l_1, l_3)] + [\omega(l_1, l_4)] + [\omega(l_2, l_3)] + [\omega(l_2, l_4)] \tag{8}$$

mit

$$[\omega(l_i, l_j)] = K[\mathrm{Sp}^{(J)}\gamma(l_i, l_j)]^{(1)}.$$

Wie in [2] definieren wir eine Funktion $\varphi(l_i, l_j)$ gemäß

$$[\varphi(l_1, l_3)] = [\mathrm{Sp}^{(J)}\gamma(l_1, l_3)]^{(1)},$$

die sich im Gegensatz zu $[\mathrm{Sp}^{(J)}\gamma(l_i, l_j)]^{(1)}$ in der Reihenfolge ihrer Argumente auf die festen Gerüststellen eins und drei bezieht. Daraus folgt für ein Derivat, in dem die Indizes der Liganden mit den Ziffern der Gerüstplätze übereinstimmen,

$$[\mathrm{Sp}^{(J)}\gamma(l_1, l_3)]^{(1)} = \varphi(l_1, l_3), \quad [\mathrm{Sp}^{(J)}\gamma(l_2, l_4)]^{(1)} = \varphi(l_2, l_4),$$

$$[\mathrm{Sp}^{(J)}\gamma(l_1, l_4)]^{(1)} = -\varphi(l_1, l_4), \quad [\mathrm{Sp}^{(J)}\gamma(l_2, l_3)]^{(1)} = -\varphi(l_2, l_3),$$

außerdem gilt

$$\varphi(l_i, l_j) = \varphi(l_j, l_i).$$

Damit ist (8) mit dem verkürzten Ansatz nach dem zweiten Näherungsverfahren identifiziert,

$$[\omega] = \tilde{\chi}(l_1, l_2, l_3, l_4) = K(\varphi(l_1, l_3) + \varphi(l_2, l_4) - \varphi(l_1, l_4) - \varphi(l_2, l_3)), \tag{9}$$

und die Komponenten $\varphi(l_i, l_j)$ sind quantenmechanisch interpretiert.

Aus (9) folgt die Beziehung

$$\begin{aligned}[\omega] = \tilde{\chi}(l_1, l_2, l_3, l_4) = \tilde{\chi}(l_5, l_2, l_6, l_4) + \tilde{\chi}(l_5, l_2, l_3, l_6) + \tilde{\chi}(l_1, l_5, l_6, l_4) \\ + \tilde{\chi}(l_1, l_5, l_3, l_6)\end{aligned} \tag{10}$$

mit beliebigen Liganden l_5, l_6. Man verifiziert diese Funktionalgleichung, indem man jede Chiralitätsfunktion der rechten Seite von Gleichung (10) nach 2-Liganden-Funktionen gemäß (9) zerlegt. In Gleichung (10) kommt folgendes Additionstheorem zum Ausdruck:

> Der optische Drehwinkel eines D_{2d}-Derivats nach dem verkürzten Ansatz des zweiten Verfahrens ist gleich der Summe der optischen Drehwinkel von vier D_{2d}-Derivaten, die man erhält, wenn man die Liganden an den Gerüststellen 1 und 3, 1 und 4, 2 und 3, 2 und 4 jeweils durch willkürlich gewählte Liganden l_5 und l_6 ersetzt.

Insofern die Störungsrechnung bis zur ersten Ordnung quantitativ zufriedenstellende Aussagen liefert, ist neben den Spezialfällen

$$\begin{aligned}\tilde\chi(l_1, l_2, l_3, l_4) + \tilde\chi(l_1, l_2, l_4, l_6) + \tilde\chi(l_1, l_2, l_6, l_3) = 0\,,\\ \tilde\chi(l_1, l_2, l_3, l_4) + \tilde\chi(l_5, l_2, l_4, l_3) + \tilde\chi(l_1, l_5, l_4, l_3) = 0\,,\end{aligned} \tag{10a}$$

die man mit $l_5 = l_1$ bzw. $l_6 = l_3$ aus (10) erhält, das Additionstheorem

$$\tilde\chi(l_1, l_2, l_3, l_4) + \tilde\chi(l_1, l_3, l_4, l_2) + \tilde\chi(l_1, l_4, l_2, l_3) = 0 \tag{11}$$

ein einfaches und experimentell nachprüfbares Kriterium für die Gültigkeit der D_{2d}-Bedingung.

3. D_{2d}-*Derivate im Modell* $\tilde{\mathscr{H}}$

Wir schreiben (6) in der Form

$$[\mathrm{Sp}\,{}^{(J)}\gamma(l_i, l_j)]^{(\mathrm{I})} = \mathscr{P}_+(ij)\,\xi(l_i, l_j) \tag{12}$$

mit der Definition:

$$\begin{aligned}\xi(l_i, l_j) = -2\kappa_i\kappa_j \sum_{\varrho,\sigma,\varrho',\sigma'} \Big\{ & {}^{(J)}\Gamma_{\varrho\varrho\sigma}(l_i)\,(\vec e^{(i)}_\sigma \cdot T_{ij} \cdot \{\langle \vec m(l_j)\rangle + \vec c_j\})\\ & + {}^{(R)}\alpha_{\varrho\sigma}(l_i)\,{}^{(J)}\gamma_{\varrho'\sigma'}(l_j)\,(\vec e^{(i)}_\varrho \cdot \vec e^{(j)}_{\sigma'})\,(\vec e^{(i)}_\sigma \cdot T_{ij} \cdot \vec e^{(j)}_{\varrho'})\\ & + {}^{(J)}\alpha_{\varrho\sigma}(l_i)\,{}^{(R)}\gamma_{\varrho'\sigma'}(l_j)\,(\vec e^{(i)}_\varrho \cdot \vec e^{(j)}_{\sigma'})\,(\vec e^{(i)}_\sigma \cdot T_{ij} \cdot \vec e^{(j)}_{\varrho'})\\ & - \frac{\pi}{2c}\,{}^{(R)}\alpha_{\varrho\sigma}(l_i)\,{}^{(R)}\alpha_{\varrho'\sigma'}(l_j)\,[\vec a_{ij} \cdot (\vec e^{(i)}_\varrho \times \vec e^{(j)}_{\sigma'})]\,(\vec e^{(i)}_\sigma \cdot T_{ij} \cdot \vec e^{(j)}_{\varrho'})\\ & + \frac{\pi}{2c}\,\nu^2\,{}^{(J)}\alpha_{\varrho\sigma}(l_i)\,{}^{(J)}\alpha_{\varrho'\sigma'}(l_j)\,[\vec a_{ij} \cdot (\vec e^{(i)}_\varrho \times \vec e^{(j)}_{\sigma'})]\,(\vec e^{(i)}_\sigma \cdot T_{ij} \cdot \vec e^{(j)}_{\varrho'})\Big\}\,.\end{aligned}$$

Die spezielle Geometrie des Allengerüstes und die D_{2d}-Bedingung erlauben, die $\xi(l_i, l_j)$ gemäß (12) weiter auszurechnen. Wir wählen dazu für jede Bindungsrichtung i ein rechtwinkliges Dreibein $\vec e^{(i)}_t, \vec e^{(i)}_{t'}, \vec e^{(i)}_r$ mit dem Vektor $\vec e^{(i)}_r$ in Bindungsrichtung und dem Vektor $\vec e^{(i)}_t$ in der Ebene der beiden benachbarten Bindungsrichtungen eines endständigen Kohlenstoffs (vgl. Fig. 2). Die Vektoren $\vec e^{(i)}_{t'}$ und $\vec e^{(k)}_{t'}$ von benachbarten Bindungsrichtungen sind also parallel und entgegengesetzt gerichtet. Alle interessierenden Symmetrieeigenschaften von Tensorkomponenten für Liganden mit der D_{2d}-Bedingung finden sich im Anhang A, ihre Indizierung entspricht derjenigen für die obigen Einheitsvektoren.

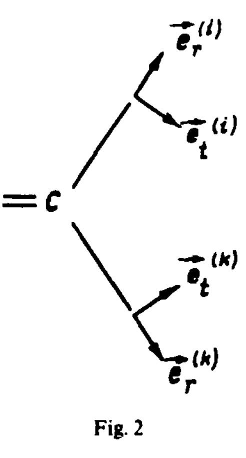

Fig. 2

Die Ausrechnung führt zu einer Formel, die sich wesentlich vereinfacht, wenn wir die Ligandensymmetrie auf C_{nv} mit $n \geqq 3$ festlegen. Da zu erwarten ist, daß diese Einschränkung bei Liganden der Symmetrie C_s oder C_{2v} in günstigen Fällen zu einer vertretbaren Vernachlässigung kleiner Korrekturen führt, wollen wir die explizite Form nur unter dieser Voraussetzung angeben.

Mit den leicht nachprüfbaren Beziehungen

$$\sum_{\varrho} [\vec{a}_{ij} \cdot (\vec{e}_{\varrho}^{(I)} \times \vec{e}_{\varrho'}^{(J)})] (\vec{e}_{\varrho}^{(I)} \cdot T_{ij} \cdot \vec{e}_{\varrho'}^{(J)}) = 0 ,$$

$$\sum_{\varrho} \vec{e}_{\varrho}^{(I)} \cdot T_{ij} \cdot (\vec{e}_{\varrho'}^{(J)} \cdot \vec{e}_{\sigma'}^{(J)} - \vec{e}_{\sigma'}^{(J)} \cdot \vec{e}_{\varrho'}^{(J)}) \cdot \vec{e}_{\varrho}^{(I)} = 0$$

und den im Anhang A aufgeführten Eigenschaften von Tensoren der Symmetrie C_{nv} mit $n \geqq 3$ finden wir:

$$\begin{aligned}\xi(l_i, l_j) = \kappa(l_i)\,\kappa(l_j) \Big\{ &-2\,[{}^{(R)}\alpha_{rr}(l_i) - {}^{(R)}\alpha_{tt}(l_i)]\; {}^{(J)}\gamma_{tt'}(l_j)\, (\vec{e}_r^{(I)} \cdot T_{ij} \cdot \{\vec{e}_t^{(J)} \cdot \vec{e}_{t'}^{(J)} - \vec{e}_{t'}^{(J)} \cdot \vec{e}_t^{(J)}\} \cdot \vec{e}_r^{(I)}) \\ &+ \frac{\pi}{c}\, [{}^{(R)}\alpha_{rr}(l_i) - {}^{(R)}\alpha_{tt}(l_i)]\, [{}^{(R)}\alpha_{rr}(l_j) - {}^{(R)}\alpha_{tt}(l_j)]\, \vec{a}_{ij} \cdot (\vec{e}_r^{(I)} \times \vec{e}_r^{(J)})\, (\vec{e}_r^{(I)} \cdot T_{ij} \cdot \vec{e}_r^{(J)}) \Big\} .\end{aligned} \tag{12a}$$

Wir beziehen diese Funktion wieder auf die Gerüstplätze eins und drei in der Reihenfolge ihrer Argumente, berechnen die Skalarprodukte gemäß Anhang B und bekommen damit nach Anwendung des Operators $\mathscr{P}_+(ij)$ die Ligandenpaarfunktion $\varphi(l_i, l_j)$ im Modell $\tilde{\mathscr{K}}$

$$\begin{aligned}\varphi(l_i, l_j) = \frac{3d}{4}\, \frac{\kappa(l_i)\,\kappa(l_j)}{a(l_i, l_j)^3} \Big[&\frac{\pi}{c} \left(\frac{1}{4} - \frac{3}{a(l_i, l_j)^2}\, b(l_i, l_j)\, b(l_j, l_i) \right) \Delta\,{}^{(R)}\alpha(l_i)\, \Delta\,{}^{(R)}\alpha(l_j) \\ &+ \frac{3}{a(l_i, l_j)^2}\, \{ b(l_i, l_j)\, \Delta\,{}^{(R)}\alpha(l_i)\, {}^{(J)}\gamma_{tt'}(l_j) + b(l_j, l_i)\, \Delta\,{}^{(R)}\alpha(l_j)\, {}^{(J)}\gamma_{tt'}(l_i) \} \Big]\end{aligned} \tag{13}$$

mit

$$a(l_i, l_j) = a(l_j, l_i) = (d^2 + d(a(l_i) + a(l_j)) + a(l_i)^2 + a(l_j)^2 + \tfrac{1}{2}\, a(l_i)\, a(l_j))^{1/2}$$

$$b(l_i, l_j) = \tfrac{1}{2} d + a(l_i) + \tfrac{1}{4} a(l_j)$$

und den Differenzen der Polarisierbarkeitskomponenten in Hauptachsenrichtung

$$\Delta\,{}^{(R)}\alpha(l_i) = {}^{(R)}\alpha_{rr}(l_i) - {}^{(R)}\alpha_{tt}(l_i) .$$

Dabei ist $a(l_i)$ der Abstand des Entwicklungspunktes für die Multipolentwicklung (Schwerpunkt des Systems $\mathfrak{R}_i$) vom benachbarten Kohlenstoffatom des Allengerüstes und d der Abstand der beiden endständigen Kohlenstoffatome im Allengerüst. Der Winkel zwischen den benachbarten Bindungsrichtungen ist mit $\frac{2\pi}{3}$ festgelegt.

Für ausdehnungsmäßig ähnliche Liganden sind die Abstände $a(l_i, l_j)$ zwischen Liganden an den Gerüststellen eins und drei nahezu dieselben, und es ist vernünftig, sich mit der Näherung eines konstanten Abstandes zu begnügen. Wir setzen also mit einem gemittelten $a(l) \approx a(l_i)$

$$a(l_i, l_j) \approx a = (d^2 + 2d a(l) + \tfrac{5}{2} a(l)^2)^{1/2}$$

und

$$b(l_i, l_j) \approx b = \tfrac{1}{2} d + \tfrac{5}{4} a(l)$$

und erhalten damit (8) in der Form

$$
\begin{aligned}
[\omega] = K\,\frac{3d}{4a^3}\Bigg[\frac{\pi}{c}\left(\frac{1}{4}-\frac{3b^2}{a^2}\right)&\begin{vmatrix} 1 & 1 \\ \kappa(l_1)\,\Delta^{(R)}\alpha(l_1) & \kappa(l_2)\,\Delta^{(R)}\alpha(l_2)\end{vmatrix} \\
&\cdot\begin{vmatrix} 1 & 1 \\ \kappa(l_3)\,\Delta^{(R)}\alpha(l_3) & \kappa(l_4)\,\Delta^{(R)}\alpha(l_4)\end{vmatrix} \\
+\frac{3b}{a^2}\Bigg\{&\begin{vmatrix} 1 & 1 \\ \kappa(l_1)\,\Delta^{(R)}\alpha(l_1) & \kappa(l_2)\,\Delta^{(R)}\alpha(l_2)\end{vmatrix}\begin{vmatrix} 1 & 1 \\ \kappa(l_3)\,{}^{(J)}\gamma_{tt'}(l_3) & \kappa(l_4)\,{}^{(J)}\gamma_{tt'}(l_4)\end{vmatrix} \\
+&\begin{vmatrix} 1 & 1 \\ \kappa(l_1)\,{}^{(J)}\gamma_{tt'}(l_1) & \kappa(l_2)\,{}^{(J)}\gamma_{tt'}(l_2)\end{vmatrix}\begin{vmatrix} 1 & 1 \\ \kappa(l_3)\,\Delta^{(R)}\alpha(l_3) & \kappa(l_4)\,\Delta^{(R)}\alpha(l_4)\end{vmatrix}\Bigg\}\Bigg].
\end{aligned}
\tag{14a}
$$

Unter der weiteren Annahme, daß die elektromagnetischen Polarisierbarkeiten der Liganden ${}^{(J)}\gamma_{tt'}(l_i)$ gegenüber den elektrischen Polarisierbarkeiten vernachlässigt werden dürfen, kommen wir schließlich zu der Form

$$
\begin{aligned}
[\omega] = K\,\frac{\pi}{c}\,\frac{3d}{4a^3}\left(\frac{1}{4}-\frac{3b^2}{a^2}\right)&\begin{vmatrix} 1 & 1 \\ \kappa(l_1)\,\Delta^{(R)}\alpha(l_1) & \kappa(l_2)\,\Delta^{(R)}\alpha(l_2)\end{vmatrix} \\
&\cdot\begin{vmatrix} 1 & 1 \\ \kappa(l_3)\,\Delta^{(R)}\alpha(l_3) & \kappa(l_4)\,\Delta^{(R)}\alpha(l_4)\end{vmatrix}.
\end{aligned}
\tag{14b}
$$

Wegen $\frac{a^2}{4} - 3b^2 < 0$ führt nach Abspaltung des Faktors (-1) die Multiplikation der zweiten Zeile in jeder der beiden Determinanten mit $\left|K\,\frac{\pi}{c}\,\frac{3d}{4a^5}\left(3b^2-\frac{a^2}{4}\right)\right|^{1/2}$ auf den verkürzten Ansatz nach dem ersten Verfahren[1]:

$$
[\omega] = -[\lambda(l_1)-\lambda(l_2)]\,[\lambda(l_3)-\lambda(l_4)]
$$

mit

$$
\lambda(l_i) = \left|K\,\frac{\pi}{c}\,\frac{3d}{4a^5}\left(3b^2-\frac{a^2}{4}\right)\right|^{1/2}\kappa(l_i)\,\Delta^{(R)}\alpha(l_i)\,.
\tag{15}
$$

4. *Vergleich mit dem Experiment*

Da aus Messungen des optischen Drehwinkels zusammen mit Runge und Kresze [7] hervorzugehen scheint, daß ein verkürzter Ansatz nach der Polynommethode quantitativ befriedigende Resultate liefert, berechnen wir $[\omega]$ nach Formel (15) an einem speziellen Allenderivat. Wir wählen optisch aktives 1,3-Dimethylallen, dessen Liganden also der Symmetriebedingung C_{nv} mit $n \geq 3$ und der D_{2d}-Bedingung genügen und für das wegen des Auftretens von

---

[1] Die hier gewählte Gerüstbezifferung geht in diejenige des regulären Tetraeders in [2] über. In [7] dagegen sind die Gerüstziffern 1 und 2 vertauscht. Aus diesem Grund entspricht dem Faktor $\varepsilon = +1$ in [7] der Faktor $\varepsilon = -1$ bei der vorliegenden Bezifferung.

Ligandenpaaren gleicher Art die T_d-Komponente verschwindet. Der verkürzte Ansatz ist dafür also qualitativ vollständig.

In der Literatur finden wir für den molaren Drehwinkel von 1,3-Dimethylallen bei der Natrium-D-Linie folgende Werte $\left(\text{in } \frac{\text{Grad/dcm}}{\text{g/cm}^3}\, \text{g}\right)$:

$$[\omega] = -17{,}2; \quad -154; \quad -118; \quad -59{,}3\,.$$

Der erste Wert bezieht sich auf Messungen in CCl_4 als Lösungsmittel und wird ohne Angabe über den Grad der optischen Reinheit mitgeteilt [10]; der zweite Wert ergibt sich aus einem Meßwert von $-10{,}8$ in Äther und einer geschätzten optischen Reinheit von 7% [11]; der dritte Wert ist im Rahmen eines klassischen Helixmodells berechnet und auf Äthanol als Lösungsmittel bezogen [1]. Der vierte Wert ist mit λ-Werten bestimmt, die sich aus Messungen der optischen Drehung an anderen Molekülen ergeben haben [7]. Dabei wurde für Äthanol als Lösungsmittel gefunden:

$$\lambda(\mathrm{H}) = 0; \quad \lambda(\mathrm{CH_3}) = 7{,}7\,.$$

Wegen der ausgezeichneten Übereinstimmung von experimentellen und theoretischen Daten, die sich mit empirischen λ-Werten von sechs Liganden bei zwölf verschiedenen Allenderivaten erreichen läßt, halten wir den Wert $-59{,}3$ für den zuverlässigsten.

Zur Berechnung von $[\omega]$ gemäß Gleichung (15) entnimmt man der Literatur folgende Werte für $\Delta^{(R)}\alpha(l_i)$ (in 10^{-25} cm^3):

$$\Delta^{(R)}\alpha(\mathrm{H}) = 0 \quad \text{und} \quad \Delta^{(R)}\alpha(\mathrm{CH_3}) = 7{,}9; \quad 20{,}9\,.$$

$\Delta^{(R)}\alpha(\mathrm{H}) = 0$ entspricht den experimentellen Erfahrungen nach Stuart [9]. Der Wert 7,9 für $\Delta^{(R)}\alpha(\mathrm{CH_3})$ folgt aus gemessenen Polarisierbarkeiten an Äthan [4], während 20,9 Messungen an Benzol und Toluol entnommen wird [9].

Es ist zu erwarten, daß der Wert für $\Delta^{(R)}\alpha(\mathrm{CH_3})$ im Falle eines Allenderivats zwischen den beiden angegebenen liegt, denn die Bindung von CH_3 an das Allengerüst repräsentiert eine Situation zwischen den zwei Extremfällen in CH_3–CH_3 und C_6H_5–CH_3. Da wir hier nur eine erste Information über die Güte der Beschreibung beabsichtigen, legen wir uns in folgender Weise auf plausible Zahlenwerte fest:

$$\Delta^{(R)}\alpha(\mathrm{H}) = 0 \quad \text{und} \quad \Delta^{(R)}\alpha(\mathrm{CH_3}) = 15\,.$$

Die geometrischen Parameter unserer Gleichung werden wie folgt zahlenmäßig festgesetzt:

$$a(l) = 1{,}5 \cdot 10^{-8}\,\text{cm}\,; \quad d = 2{,}68 \cdot 10^{-8}\,\text{cm}\,.$$

Damit ergibt sich $a = 4{,}57 \cdot 10^{-8}$ cm und $b = 3{,}22 \cdot 10^{-8}$ cm. Mit der Wellenlänge $\lambda_D = 5893 \cdot 10^{-8}$ cm für die Natrium-D-Linie und dem Brechungsindex $n = 1{,}36$ für Äthanol als Lösungsmittel ergibt sich

$$\lambda(\mathrm{H}) = 0\,, \quad \lambda(\mathrm{CH_3}) = 7{,}1\,, \quad [\omega] = -50{,}4\,,$$

während

$$\lambda(\mathrm{H})=0\,,\quad \lambda(\mathrm{CH_3})=7{,}7\,,\quad [\omega]=-59{,}3$$

den halbempirischen Befund aus [7] wiedergibt.

Schlußbemerkung

Die vorgetragene Theorie ist ein Beispiel dafür, wie aus der quantenmechanischen Theorie der optischen Aktivität von Methanderivaten mit geeignete Modifikation der Voraussetzungen andere Molekülklassen mit vier Ligandenplätzen zu behandeln sind. Die beiden Näherungsverfahren entsprechen wiede der quantenmechanischen Interpretation im Modell $\mathscr{W}$ bzw. einer vereinfachte Fassung im Modell $\tilde{\mathscr{W}}$. Beim Vergleich mit den experimentellen Befunden bei 1,3-Dimethylallen bestätigt sich das theoretisch gefundene Vorzeichen de optischen Drehwinkels und auch der errechnete Betrag im Rahmen der bei diese Vergleich möglichen Genauigkeit. *Ab ovo*-Rechnungen der Parameter in (15 oder der Bestimmungsstücke in (14b) sind natürlich ebenfalls interessant; si sind aber nicht das primäre Ziel einer Theorie über das Phänomen der optische Aktivität von Allenderivaten. Da sich diese Theorie auf eine Klasse von Verbindungen bezieht, steht in erster Linie zur Diskussion, inwieweit es gelungen ist, di individuellen Details bei den einzelnen Verbindungen mit einem klassenspezifischen Einfluß der Liganden auf die optische Aktivität quantitativ zufriedenstellend zu beschreiben.

Anhang

A. Elektromagnetische Tensoren

Die quantenmechanische Definition für die Tensoren der Polarisierbarkeite ${}^{(R)}\alpha$, ${}^{(J)}\alpha$, ${}^{(R)}\gamma$, ${}^{(J)}\gamma$ und der Hyperpolarisierbarkeit ${}^{(J)}\Gamma$ eines Systems im Grundzustand ist in [2] angegeben. In den Tab. 1 und 2 sind für Liganden der Symmetri C_s und C_{nv} ($n \geqq 3$) die nichtverschwindenden Komponenten der Polarisierbarkeitstensoren und des elektrischen Dipolmoments $\langle\vec{m}\rangle$ aufgeführt und vo Tensor ${}^{(J)}\Gamma$ die nichtverschwindenden Komponenten des Typs ${}^{(J)}\Gamma_{\varrho\varrho\sigma}$.

Tabelle 1. C_s-Symmetrie

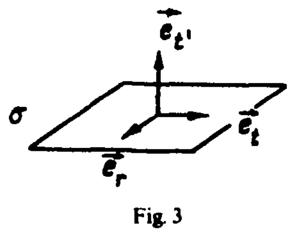

Fig. 3

$\langle\vec{m}\rangle : \langle m_r\rangle, \langle m_t\rangle$

${}^{(R)}\alpha : {}^{(R)}\alpha_{tt}, {}^{(R)}\alpha_{t't'}, {}^{(R)}\alpha_{rr}, {}^{(R)}\alpha_{tr} = {}^{(R)}\alpha_{rt}$

${}^{(J)}\alpha : {}^{(J)}\alpha_{tr} = -{}^{(J)}\alpha_{rt}$

${}^{(R)}\gamma : {}^{(R)}\gamma_{tt'}, {}^{(R)}\gamma_{t't}, {}^{(R)}\gamma_{t'r}, {}^{(R)}\gamma_{rt}$

${}^{(J)}\gamma$ wie ${}^{(R)}\gamma$

${}^{(J)}\Gamma_{\varrho\varrho\sigma} : {}^{(J)}\Gamma_{ttt'}, {}^{(J)}\Gamma_{t't't'}, {}^{(J)}\Gamma_{rrt'}$

Tabelle 2. $C_{nv}(n \geq 3)$- und $C_{\infty v}$-Symmetrie

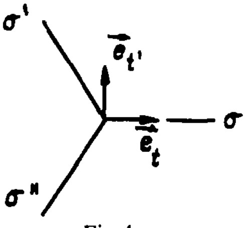

Fig. 4

$\langle \dot{m} \rangle : \langle m_r \rangle$

${}^{(R)}\alpha : {}^{(R)}\alpha_{tt} = {}^{(R)}\alpha_{t't'}, {}^{(R)}\alpha_{rr}$

${}^{(J)}\alpha = 0$

${}^{(R)}\gamma : {}^{(R)}\gamma_{tt} = -{}^{(R)}\gamma_{t't'}$

${}^{(J)}\gamma$ wie ${}^{(R)}\gamma$

$\sum_{\varrho} {}^{(J)}\Gamma_{\varrho\varrho\sigma} = 0$

B. Koordinatensysteme, Skalar- und Vektorprodukte der Basisvektoren

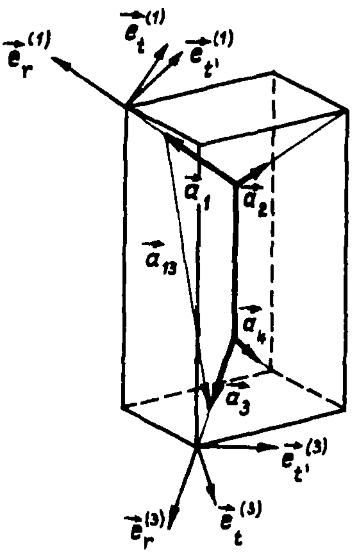

Fig. 5

Am D_{2d}-Gerüst gilt mit $(\vec{e}_r^{(1)} \cdot \vec{e}_r^{(2)}) = (\vec{e}_r^{(3)} \cdot \vec{e}_r^{(4)}) = \cos \frac{2\pi}{3} = -\frac{1}{2}$ für die Abstände a_{ij} zwischen den Orten $\vec{a}_i = a_i \vec{e}_r^{(i)}$ und $\vec{a}_j = a_j \vec{e}_r^{(j)}$:

$$a_{ij}^2 = a_i^2 + a_j^2 + a_i a_j \quad \text{für} \quad (ij) = (12), (34);$$

$$a_{ij}^2 = d^2 + d(a_i + a_j) + a_i^2 + a_j^2 + \tfrac{1}{2} a_i a_j \quad \text{für} \quad (ij) = (13), (14), (23), (24).$$

Die Skalarprodukte $(\vec{e}_\varrho^{(1)} \cdot \vec{e}_\sigma^{(3)})$, die Spatprodukte $\vec{a}_{13} \cdot (\vec{e}_\varrho^{(1)} \times \vec{e}_\sigma^{(3)})$ und die Ausdrücke $a_{13}^3(\vec{e}_\varrho^{(1)} T_{13} \vec{e}_\sigma^{(3)})$ sind in den Tab. 3, 4 und 5 aufgeführt.

Tabelle 3

$(\vec{e}_\varrho^{(1)} \cdot \vec{e}_\sigma^{(3)})$	$\vec{e}_t^{(3)}$	$\vec{e}_{t'}^{(3)}$	$\vec{e}_r^{(3)}$
$\vec{e}_t^{(1)}$	$\frac{3}{4}$	$\frac{1}{2}$	$-\frac{\sqrt{3}}{4}$
$\vec{e}_{t'}^{(1)}$	$\frac{1}{2}$	0	$-\frac{\sqrt{3}}{2}$
$\vec{e}_r^{(1)}$	$-\frac{\sqrt{3}}{4}$	$-\frac{\sqrt{3}}{2}$	$-\frac{1}{4}$

Tabelle 4

$\vec{a}_{13}(\vec{e}_\varrho^{(1)} \times \vec{e}_\sigma^{(3)})$	$\vec{e}_t^{(3)}$	$\vec{e}_{t'}^{(3)}$	$\vec{e}_r^{(3)}$
$\vec{e}_t^{(1)}$	$-\frac{1}{2}\left(\frac{1}{2}d + a_1 + a_3\right)$	$-\frac{3}{4}a_3$	$\frac{\sqrt{3}}{2}\left(\frac{1}{2}d + a_1\right)$
$\vec{e}_{t'}^{(1)}$	$-\frac{3}{4}a_1$	$d + \frac{1}{2}(a_1 + a_3)$	$-\frac{\sqrt{3}}{4}a_1$
$\vec{e}_r^{(1)}$	$\frac{\sqrt{3}}{2}\left(\frac{1}{2}d + a_3\right)$	$-\frac{\sqrt{3}}{4}a_3$	$-\frac{3}{4}d$

Tabelle 5

$$a_{13}^{3}(\vec{e}_t^{(1)}T_{13}\vec{e}_t^{(3)}) = -\frac{3}{4}\left(1-3\,\frac{(d+\frac{1}{2}a_1)(d+\frac{1}{2}a_3)}{a_{13}^2}\right)$$

$$a_{13}^{3}(\vec{e}_t^{(1)}T_{13}\vec{e}_t^{(3)}) = \frac{1}{2}\left(1+\frac{9}{2}\,\frac{a_1(d+\frac{1}{2}a_3)}{a_{13}^2}\right)$$

$$a_{13}^{3}(\vec{e}_t^{(1)}T_{13}\vec{e}_r^{(3)}) = -\frac{\sqrt{3}}{4}\left(1-3\,\frac{(d+\frac{1}{2}a_1+2a_3)(d+\frac{1}{2}a_3)}{a_{13}^2}\right)$$

$$a_{13}^{3}(\vec{e}_t^{(1)}T_{13}e_t^{(3)}) = \frac{1}{2}\left(1+\frac{9}{2}\,\frac{a_3(d+\frac{1}{2}a_1)}{a_{13}^2}\right)$$

$$a_{13}^{3}(\vec{e}_t^{(1)}T_{13}\vec{e}_t^{(3)}) = \frac{9}{4}\,\frac{a_1a_3}{a_{13}^2}$$

$$a_{13}^{3}(\vec{e}_t^{(1)}T_{13}\vec{e}_r^{(3)}) = -\frac{\sqrt{3}}{2}\left(1-\frac{3}{2}\,\frac{a_3(d+\frac{1}{2}a_1+2a_3)}{a_{13}^2}\right)$$

$$a_{13}^{3}(\vec{e}_r^{(1)}T_{13}\vec{e}_t^{(3)}) = \frac{\sqrt{3}}{4}\left(1-3\,\frac{(d+\frac{1}{2}a_1+2a_1)(d+\frac{1}{2}a_1)}{a_{13}^2}\right)$$

$$a_{13}^{3}(\vec{e}_r^{(1)}T_{13}\vec{e}_t^{(3)}) = \frac{\sqrt{3}}{2}\left(1-\frac{3}{2}\,\frac{a_1(d+\frac{1}{2}a_3+2a_1)}{a_{13}^2}\right)$$

$$a_{13}^{3}(\vec{e}_r^{(1)}T_{13}\vec{e}_r^{(3)}) = -\frac{1}{4}\left(1-3\,\frac{(d+\frac{1}{2}a_1+2a_3)(d+\frac{1}{2}a_3+2a_1)}{a_{13}^2}\right)$$

Literatur

1. Brewster, J. H.: Topics in stereochemistry, Bd. 2, S. 1 72, (Hrsg.: Eliel, F. L., Allinger, N. L.). New York: Interscience Publishers 1967.
2. Haase, D., Ruch, E.: Theoret. chim. Acta (Berl.) **29**, 189 (1973).
3. Haase, D., Ruch, E.: Theoret. chim. Acta (Berl.) **29**, 235 (1973).
4. Kirkwood, J. G.: J. chem. Physics **5**, 479 (1937).
5. Richter, W. J., Richter, B., Ruch, E.: Angew. Chem. **85**, 21 (1973).
6. Ruch, E.: Accounts Chem. Research **5**, 49 (1972)
7. Ruch, E., Runge, W., Kresze, G.: Angew. Chem. **85**, 10 (1973).
8. Ruch, E., Schönhofer, A.: Theoret chim. Acta (Berl.) **19**, 225 (1970).
9. Stuart, H. A.: Molekülstruktur, 3. Aufl., S. 422 425. Berlin-Heidelberg-New York: Springer 1967.
10. Walbrick, J. M., Wilson, J. W., Jr, Jones, W. M.: J. Amer. chem. Soc. **90**, 2895 (1968).
11. Waters, W. L., Caserio, M. C.: Tetrahedron Letters 1968, 5233.

Prof. Dr. E. Ruch
Institut für Quantenchemie
der freien Universität Berlin
D-1000 Berlin 45, Holbeinstraße 48
Deutschland

Theoret. chim. Acta (Berl.) 29, 259—268 (1973)
© by Springer-Verlag 1973

Classifications of Rearrangement Mechanisms by Means of Double Cosets and Counting Formulas for the Numbers of Classes

Werner Hässelbarth

Department of Chemistry, Princeton University

Ernst Ruch

Institut für Quantenchemie der Freien Universität Berlin

Received March 7, 1972/August 7, 1972

Rearrangements of ligands attached at given sites of a certain skeleton may be classified according to two principles: symmetry equivalence, where the same permutation of objects is related to symmetry equivalent sites and rotational equivalence, where the resulting isomers differ just by their orientation. The combination of both these principles leads to a classification wanted by experimentalists. This latter classification is shown to be correlated to double cosets, which easily allow to find the rearrangements belonging to a class in a formal way and to enumerate the distinguishable classes for any given problem.

Umordnungen von Liganden, die auf vorgegebene Plätze eines bestimmten Molekülgerüstes verteilt sind, können nach zwei Prinzipien klassifiziert werden: Symmetrieäquivalenz, gekennzeichnet durch dieselbe Permutation von Objekten bezogen auf symmetrieäquivalente Gerüstplätze, und Rotationsäquivalenz, dadurch charakterisiert, daß die entstehenden Isomere sich nur durch ihre Orientierung unterscheiden. Die Kombination dieser beiden Prinzipien führt zu einer Klassifikation, die zur Interpretation von Experimenten benötigt wird. Es wird gezeigt, daß diese Klassifikation auf Doppelnebenklassen führt, mit denen die Umordnungen einer Klasse auf formale Weise leicht zu finden sind und die Anzahl der unterscheidbaren Klassen für jedes vorgegebene Problem bestimmt werden kann.

Double Cosets and Configurations

In a previous paper [1], it has been shown that double cosets of permutation groups are the natural algebraic analogue of configurations of permutational isomers.

The representation of configurations by classes of permutations, and formulas for their enumeration, have been discussed on the basis of the concept "ordered molecule", which implies an artificial distinction between distributions of *n* numbered ligands on *n* numbered sites of a rigid molecular skeleton. The set of all ordered molecules can be classified into subsets such that each contains all those ordered molecules which cannot be distinguished if we ignore the numbers assigned to ligands and sites and disregard the orientation and conformation of a molecule. This classification is associated with a classification of ligand permutations acting on a reference ordered molecule. It has been shown [1] that these classes are the so-called double cosets of two subgroups $\mathfrak{A}$ and $\mathfrak{B}$ of the group $\mathfrak{S}_n$ of all permutations, $\mathfrak{A}$ and $\mathfrak{B}$ being chosen according to the special classification one has in mind. $\mathfrak{A}$ contains all permutations representing rotations of the whole molecule and may contain further permutations representing inner rotations or some other rearrangements which one assumes to take place independently of the attached ligands within the characteristic time of the experiment. $\mathfrak{A}$ expresses exclusively properties of the skeleton. $\mathfrak{B}$ contains all permutations of ligands of the same kind or ligands that are not distinguished by the experiment concerned and refers to the sites occupied by like ligands in the reference isomer. $\mathfrak{B}$ expresses exclusively properties of the ligands. Since the concept configuration used in chemistry should be defined by the kind of experiment considered, we may speak of $\mathfrak{A}\mathfrak{B}$-configurations.

A double coset $\mathfrak{A}x_i\mathfrak{B}$ consists of all permutations which can be written as $a x_i b$ where x_i is a given element of $\mathfrak{S}_n$, a and b are any elements respectively of $\mathfrak{A}$ and $\mathfrak{B}$.
The classification of the set $\mathfrak{S}_n$ thus obtained can be expressed as a sum of sets

$$\mathfrak{S}_n = \mathfrak{A}\mathfrak{B} \dotplus \mathfrak{A}x_2\mathfrak{B} \dotplus \cdots \dotplus \mathfrak{A}x_z\mathfrak{B} \tag{1}$$

where $\dotplus$ means the union of sets having no permutation in common.

$\mathfrak{A}\mathfrak{B}$ consists of all permutations leading from the reference isomer to ordered molecules which cannot be distinguished from the reference isomer by the experiment concerned. The permutations of $\mathfrak{A}x_i\mathfrak{B}$ with $i \neq 1$ lead to experimentally distinguishable classes of mutually non-distinguishable ordered molecules. Therefore the double cosets $\mathfrak{A}x_i\mathfrak{B}$ or representative elements of them, e.g., the x_i with $x_1 = e$ (identity permutation) may be used as symbols for configurations of permutational isomers.

The number of different configurations can be found by calculating the number z of double cosets. For this some formulas have been derived [1], which hold independently of the special type of groups we have been discussing for our purpose. We give just the one which we also want to use for the subsequent treatment of another problem.

$$z = \frac{|\mathfrak{S}_n|}{|\mathfrak{A}|\,|\mathfrak{B}|} \sum_{r=1}^{k} \frac{|\mathfrak{A} \cap \mathfrak{C}_r|\,|\mathfrak{B} \cap \mathfrak{C}_r|}{|\mathfrak{C}_r|} \tag{1a}$$

$\mathfrak{C}_r$ is a class of conjugate elements of $\mathfrak{S}_n$. $|\mathfrak{S}_n|$, $|\mathfrak{A}|$, $|\mathfrak{B}|$ and $|\mathfrak{C}_r|$ denote the number of elements of the groups $\mathfrak{S}_n$, $\mathfrak{A}$, $\mathfrak{B}$ and of the class $\mathfrak{C}_r$, and $|\mathfrak{A} \cap \mathfrak{C}_r|$, $|\mathfrak{B} \cap \mathfrak{C}_r|$ designate the number of those elements belonging to the class $\mathfrak{C}_r$ which are contained in $\mathfrak{A}$ and $\mathfrak{B}$ respectively. The sum runs over all classes $\mathfrak{C}_r$.

Double Cosets and Modes

A completely different classification problem will be shown to be soluble on a very similar basis also using double cosets. We refer again to rigid molecular skeletons with numbered sites occupied by ligands. A rearrangement of ligands on a given skeleton should be defined with reference to the numbered sites disregarding the nature of the ligands which are rearranged and disregarding the special way in which the rearrangement takes place.

If the skeleton has a certain symmetry, then there are rearrangements which effect different isomerisations but occur under precisely the same influence of the skeleton. They are related to different site numbers in a special way. Their correspondence is such that corresponding site numbers can be mapped into each other by a symmetry operation of the skeleton. Using rearrangements which correspond to symmetry operations of the skeleton we can transform a given rearrangement into a "symmetry equivalent" one. A symmetry-corresponding rearrangement followed by a given rearrangement followed again by the inverse of the first rearrangement leads to a rearrangement that is symmetry equivalent to the given one. Referring to the skeleton symmetry we will speak of the set of all rearrangements which are symmetry equivalent to a given one as of a rearrangement process. A process therefore does not imply the transition from a given molecule to a certain isomer but to a certain set of isomers.

On the other hand, if we differentiate only those rearrangements which lead from a given distribution of ligands to different isomers we have to collect as being nondistinguishable all those rearrangements which can be split into a given rearrangement followed by a rearrangement corresponding to a rotation. Such rearrangements may be called rotationally equivalent. Rotationally equivalent rearrangements lead to the same isomers.

For a demonstration of the concepts introduced above we refer to the tetragonal bipyramid (D_{4h}). The rearrangements corresponding to the permutations (12), (23), (34), (14) are mutually symmetry equivalent while the one associated with (15) is not equivalent to any of these. The rearrangements belonging to (12) and (23) e.g. are related by the reflection (13) according to (13)(23)(13) = (12).

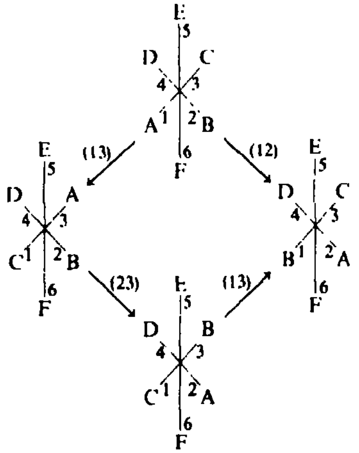

They are however not rotationally equivalent.

On the other hand the rearrangements corresponding to (12) and (134) are not symmetry equivalent, yet they are rotationally equivalent as we have (1432)(134) = (12) where (1432) represents a rotation.

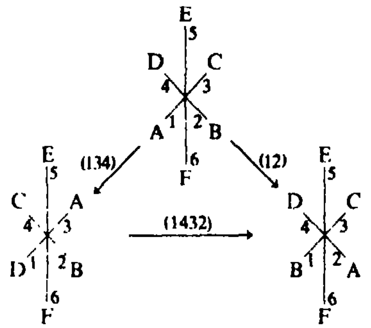

From the foregoing examples it is obvious that we have to concern ourselves with the group $\mathfrak{S}_n$ of all permutations on the n sites of a given skeleton and two subgroups $\mathfrak{G}$ and $\mathfrak{A}$ of $\mathfrak{S}_n$.

We denote by $\mathfrak{G}$ the group of permutations corresponding to the symmetry operations of the skeleton and by $\mathfrak{A}$ the subgroup of $\mathfrak{G}$ containing all permutations which correspond to proper rotations.

$\mathfrak{A}$ is a subgroup of index two in $\mathfrak{G}$ if the skeleton is achiral and all molecules with n different ligands are chiral. If σ is any permutation of $\mathfrak{G}$ not belonging to $\mathfrak{A}$, i.e. a permutation which represents an improper rotation or a reflection,

$$\mathfrak{G} = \mathfrak{A} \dotplus \sigma\mathfrak{A} = \mathfrak{A} \dotplus \mathfrak{A}\sigma$$

is the decomposition of $\mathfrak{G}$ into the subgroup $\mathfrak{A}$ and its coset.

The remaining case $\mathfrak{A} = \mathfrak{G}$ may be regarded as a special situation for which σ does not exist. It designates two types of molecular classes: either the skeleton is chiral and correspondingly all molecules are chiral (chirality order n; cf. [2]) or the skeleton is achiral but reflections are represented by permutations which are also representative for rotations. In this case all molecules are achiral provided the ligands fulfill certain symmetry conditions (chirality order 0, e.g. benzene derivatives).

The definition of symmetry and rotational equivalence reads now:

Two rearrangements x and y are symmetry equivalent if $y = g x g^{-1}$ where g is a permutation of $\mathfrak{G}$.

Two rearrangements x and y are rotationally equivalent if $y = a x$ where a is a permutation of $\mathfrak{A}$.

Rearrangements belonging to the same rearrangement process therefore are of the form $g x g^{-1}$ with a given x and any $g \in \mathfrak{G}$. Such a class of permutations is called a subclass with respect to $\mathfrak{G}$. The group $\mathfrak{S}_n$ decomposes into subclasses with respect to $\mathfrak{G}$. Each of the subclasses represents a rearrangement process.

In addition we note that a subclass with respect to $\mathfrak{G}$, $\{g x g^{-1}\}$ with any $g \in \mathfrak{G}$ can be considered to consist of two subclasses with respect to $\mathfrak{A}$, $\{a x a^{-1}\}$ and $\{a \sigma x \sigma^{-1} a^{-1}\}$ with any $a \in \mathfrak{A}$ which are either identical or disjoint.

Rotationally equivalent rearrangements are of the form $a x$ with a given x and any $a \in \mathfrak{A}$. Such a class of permutations is called a right coset of $\mathfrak{A}$. The group $\mathfrak{S}_n$ decomposes into right cosets of $\mathfrak{A}$. Each of these cosets represents a class of rotationally equivalent rearrangements effecting the same isomerisation.

It is a field of current interest to investigate the occurrence and probability of one-step rearrangement reactions as far as the influence of the skeleton is concerned, i.e. independently of the ligands varying over an appropriate assortment. Correspondingly one does not want to differentiate symmetry equivalent rearrangements. Using experiments which measure the isomerisations effected by such reactions one cannot distinguish rotationally equivalent rearrangements. For these experiments therefore distinguishable sets of rearrangements consist of symmetry equivalent rearrangements and all those rotationally equivalent to them. We call such a set a mode – a word which has been proposed by Musher [3].

Gielen and Vanlautem [4] to our knowledge were the first to give a classification according to the idea of modes for special cases (tetrahedron, square, trigonal bipyramid, octahedron) by writing down properly classified permutations. Essentially the same thing has been done by Musher [3]. But no general concept for this classification has been developed, applicable to more complicated cases. We shall give an algebraic concept of modes that allows one to work out the classification in any case whatever and to calculate the number of distinguishable classes, as we shall see below.

According to the mode concept as developed above we define:

Two rearrangements x and y are mode equivalent if y is rotationally equivalent to x or to a rearrangement which is symmetry equivalent to x, i.e. if $y = agxg^{-1}$ where a and g are permutations of $\mathfrak{A}$ and $\mathfrak{G}$ respectively.

The class $\mathfrak{M}(x)$ of rearrangements which are mode equivalent to x is the mode to which x belongs. It can be given as follows:

$$\mathfrak{M}(x) = \{agxg^{-1}\} \qquad \text{with any } a \in \mathfrak{A} \text{ and any } g \in \mathfrak{G}\,.$$

$\mathfrak{M}(x)$ is composed of two double cosets

$$\mathfrak{A}x\mathfrak{A} = \{axa'\} \qquad \text{with any} \quad a, a' \in \mathfrak{A}$$

$$\mathfrak{A}\sigma x\sigma^{-1}\mathfrak{A} = \{a\sigma x\sigma^{-1}a'\} \qquad \text{with any} \quad a, a' \in \mathfrak{A}$$

which are either disjoint or identical. Therefore $\mathfrak{M}(x)$ can be expressed as

$$\mathfrak{M}(x) = \mathfrak{A}x\mathfrak{A} \cup \mathfrak{A}\sigma x\sigma^{-1}\mathfrak{A}$$

where $\cup$ denotes the set theoretic union. If σ does not exist, $\mathfrak{M}(x)$ reduces to

$$\mathfrak{M}(x) = \mathfrak{A}x\mathfrak{A}\,.$$

Two modes $\mathfrak{M}(x)$ and $\mathfrak{M}(y)$ are either identical – if the rearrangements x and y are mode equivalent – or disjoint – if x and y are mode inequivalent. Therefore the set of all rearrangements, $\mathfrak{S}_n$, decomposes into modes $\mathfrak{M}_i = \mathfrak{M}(x_i)$:

$$\mathfrak{S}_n = \mathfrak{A} \dotplus (\mathfrak{A}x_2\mathfrak{A} \cup \mathfrak{A}\sigma x_2\sigma^{-1}\mathfrak{A}) \dotplus \cdots \dotplus (\mathfrak{A}x_z\mathfrak{A} \cup \mathfrak{A}\sigma x_z\sigma^{-1}\mathfrak{A}) \tag{2}$$

where $\mathfrak{M}_1 = \mathfrak{M}(e) = \mathfrak{A}$ is the mode of the identity rearrangement consisting of all rotations. The identity permutation e and $x_2, \ldots, x_z$ are representative permutations of the classes $\mathfrak{M}_1, \mathfrak{M}_2, \ldots, \mathfrak{M}_z$. They can be used to characterize distinct modes.

It should be explained that

1. $\mathfrak{A}x_i\mathfrak{A}$ and $\mathfrak{A}\sigma x_i\sigma^{-1}\mathfrak{A}$ may be identical or disjoint. Therefore it can happen that each class $\mathfrak{M}_i$ reduces to a double coset $\mathfrak{A}x_i\mathfrak{A}$ (trigonal bipyramid).
2. The sets $\mathfrak{A}x_i\mathfrak{A}\cup\mathfrak{A}\sigma x_i\sigma^{-1}\mathfrak{A}$ and $\mathfrak{A}x_i^{-1}\mathfrak{A}\cup\mathfrak{A}\sigma x_i^{-1}\sigma^{-1}\mathfrak{A}$ likewise are either identical or disjoint. Because they consist of mutually inverse elements, either these two classes are selfinverse or each of them contains the inverse elements of the other one. Sometimes e.g. for the trigonal bipyramid and the octahedron all classes $\mathfrak{M}_i$ are selfinverse, but generally this is not true.
3. The sets $\mathfrak{A}x_i\mathfrak{A}\cup\mathfrak{A}\sigma x_i\sigma^{-1}\mathfrak{A}$ and $\mathfrak{A}\sigma x_i\mathfrak{A}\cup\mathfrak{A}x_i\sigma^{-1}\mathfrak{A}$ are also either identical or disjoint. If they are disjoint they may be called enantiomeric modes because their rearrangements lead from a given molecule to sets of isomers which are related to each other by enantiomerism.

For experiments which do not distinguish enantiomers e.g. NMR-measurements, enantiomeric modes must be regarded as belonging to one class which we shall call a racemic mode. A classification of rearrangements given by Meakin, Muetterties *et al.* [5] for the octahedron is in agreement with the idea of racemic modes.

The set of rearrangements belonging to a racemic mode $\mathfrak{Mr}(x)$ is by definition the set theoretic union

$$\mathfrak{A}x\mathfrak{A}\cup\mathfrak{A}\sigma x\sigma^{-1}\mathfrak{A}\cup\mathfrak{A}\sigma x\mathfrak{A}\cup\mathfrak{A}x\sigma^{-1}\mathfrak{A}\,.$$

Recalling the decomposition of $\mathfrak{G}$ into the subgroup $\mathfrak{A}$ and its coset we see that the $\mathfrak{Mr}(x)$ are simply double cosets:

$$\mathfrak{Mr}(x)=\mathfrak{G}x\mathfrak{G}\,.$$

The set of all rearrangements, $\mathfrak{S}_n$, decomposes into racemic modes according to

$$\mathfrak{S}_n=\mathfrak{G}\dot{+}\mathfrak{G}x_2\mathfrak{G}\dot{+}\cdots\dot{+}\mathfrak{G}x_{z(r)}\mathfrak{G}. \tag{3}$$

The Number of Modes

Having given a well defined group theoretic class concept we turn to the problem of enumerating these classes without the need of elaborating them.

We use formula (1a) for the number of double cosets $\mathfrak{A}x\mathfrak{A}$, $\mathfrak{A}x\mathfrak{G}$, $\mathfrak{G}x\mathfrak{A}$ and $\mathfrak{G}x\mathfrak{G}$ in the corresponding decompositions

$$\mathfrak{S}_n=\mathfrak{A}\dot{+}\mathfrak{A}x_2'\mathfrak{A}\dot{+}\cdots\dot{+}\mathfrak{A}x_{z_1}'\mathfrak{A}\,, \tag{A}$$

$$\mathfrak{S}_n=\mathfrak{A}\mathfrak{G}\dot{+}\mathfrak{A}x_2''\mathfrak{G}\dot{+}\cdots\dot{+}\mathfrak{A}x_{z_2}''\mathfrak{G}\,, \tag{B}$$

$$\mathfrak{S}_n=\mathfrak{G}\mathfrak{A}\dot{+}\mathfrak{G}x_2'''\mathfrak{A}\dot{+}\cdots\dot{+}\mathfrak{G}x_{z_3}'''\mathfrak{A}\,, \tag{C}$$

$$\mathfrak{S}_n=\mathfrak{G}\dot{+}\mathfrak{G}x_2''''\mathfrak{G}\dot{+}\cdots\dot{+}\mathfrak{G}x_{z_4}''''\mathfrak{G}\,, \tag{D}$$

$$z_1=\frac{|\mathfrak{S}_n|}{|\mathfrak{A}|^2}\sum_{r=1}^{k}\frac{|\mathfrak{C}_r\cap\mathfrak{A}|^2}{|\mathfrak{C}_r|}$$

$$z_2=z_3=\frac{|\mathfrak{S}_n|}{|\mathfrak{A}|\,|\mathfrak{G}|}\sum_{r=1}^{k}\frac{|\mathfrak{C}_r\cap\mathfrak{A}|\,|\mathfrak{C}_r\cap\mathfrak{G}|}{|\mathfrak{C}_r|}$$

$$z_4=\frac{|\mathfrak{S}_n|}{|\mathfrak{G}|^2}\sum_{r=1}^{k}\frac{|\mathfrak{C}_r\cap\mathfrak{G}|^2}{|\mathfrak{C}_r|}\,.$$

Using the decomposition $\mathfrak{G} = \mathfrak{A} \dot{+} \sigma\mathfrak{A}$ and noting that $\sigma\mathfrak{A} = \mathfrak{A}\sigma = \mathfrak{A}\sigma^{-1} = \sigma^{-1}\mathfrak{A}$ we can write

$$\mathfrak{A}\mathscr{x}\mathfrak{G} = \mathfrak{A}\mathscr{x}\mathfrak{A} \cup \mathfrak{A}\mathscr{x}\sigma^{-1}\mathfrak{A}\,,$$
$$\mathfrak{G}\mathscr{x}\mathfrak{A} = \mathfrak{A}\mathscr{x}\mathfrak{A} \cup \mathfrak{A}\sigma\mathscr{x}\mathfrak{A}\,,$$
$$\mathfrak{G}\mathscr{x}\mathfrak{G} = \mathfrak{A}\mathscr{x}\mathfrak{A} \cup \mathfrak{A}\sigma\mathscr{x}\mathfrak{A} \cup \mathfrak{A}\mathscr{x}\sigma^{-1}\mathfrak{A} \cup \mathfrak{A}\sigma\mathscr{x}\sigma^{-1}\mathfrak{A}\,.$$

One can easily verify that for each quadruple $\mathfrak{A}\mathscr{x}\mathfrak{A}$, $\mathfrak{A}\sigma\mathscr{x}\mathfrak{A}$, $\mathfrak{A}\mathscr{x}\sigma^{-1}\mathfrak{A}$, $\mathfrak{A}\sigma\mathscr{x}\sigma^{-1}\mathfrak{A}$ one of the following five conditions is fullfilled

α) $\mathfrak{A}\mathscr{x}\mathfrak{A}$, $\mathfrak{A}\sigma\mathscr{x}\mathfrak{A}$, $\mathfrak{A}\mathscr{x}\sigma^{-1}\mathfrak{A}$ and $\mathfrak{A}\sigma\mathscr{x}\sigma^{-1}\mathfrak{A}$ are all identical.

β) $\mathfrak{A}\mathscr{x}\mathfrak{A}$ and $\mathfrak{A}\sigma\mathscr{x}\sigma^{-1}\mathfrak{A}$ as well as $\mathfrak{A}\sigma\mathscr{x}\mathfrak{A}$ and $\mathfrak{A}\mathscr{x}\sigma^{-1}\mathfrak{A}$ are identical.

γ) $\mathfrak{A}\mathscr{x}\mathfrak{A}$ and $\mathfrak{A}\sigma\mathscr{x}\mathfrak{A}$ as well as $\mathfrak{A}\mathscr{x}\sigma^{-1}\mathfrak{A}$ and $\mathfrak{A}\sigma\mathscr{x}\sigma^{-1}\mathfrak{A}$ are identical.

δ) $\mathfrak{A}\mathscr{x}\mathfrak{A}$ and $\mathfrak{A}\mathscr{x}\sigma^{-1}\mathfrak{A}$ as well as $\mathfrak{A}\sigma\mathscr{x}\mathfrak{A}$ and $\mathfrak{A}\sigma\mathscr{x}\sigma^{-1}\mathfrak{A}$ are identical.

ε) $\mathfrak{A}\mathscr{x}\mathfrak{A}$, $\mathfrak{A}\sigma\mathscr{x}\mathfrak{A}$, $\mathfrak{A}\mathscr{x}\sigma^{-1}\mathfrak{A}$ and $\mathfrak{A}\sigma\mathscr{x}\sigma^{-1}\mathfrak{A}$ are pairwise disjoint.

Assuming that in the decomposition (A) there occur z_α quadruples of type α, z_β of type β, z_γ of type γ, z_δ of type δ and z_ε of type ε, we can infer from the decompositions (B), (C), (D) and (2) the equations

$$\begin{aligned}
z &= z_\alpha + 2z_\beta + z_\gamma + z_\delta + 2z_\varepsilon\\
z_1 &= z_\alpha + 2z_\beta + 2z_\gamma + 2z_\delta + 4z_\varepsilon\\
z_2 &= z_\alpha + z_\beta + z_\gamma + 2z_\delta + 2z_\varepsilon\\
z_3 &= z_\alpha + z_\beta + 2z_\gamma + z_\delta + 2z_\varepsilon\\
z_4 &= z_\alpha + z_\beta + z_\gamma + z_\delta + z_\varepsilon
\end{aligned}$$

which are solved to give

$$z = z_1 + 2z_4 - z_2 - z_3\,.$$

Using formula (1a) for z_1, z_4 and $z_2 = z_3$ we get the counting formula for z

$$z = \frac{|\mathfrak{S}_n|}{|\mathfrak{A}|\,|\mathfrak{G}|} \sum_{r=1}^{k} \frac{|\mathfrak{C}_r \cap \mathfrak{A}|^2 + |\mathfrak{C}_r \cap \sigma\mathfrak{A}|^2}{|\mathfrak{C}_r|}\,. \tag{2a}$$

For the use of formula (2a) it should be mentioned that if permutations are written in the form of products of disjoint cycles it is very simple to find the numbers $|\mathfrak{C}_r \cap \mathfrak{A}|$ and $|\mathfrak{C}_r \cap \sigma\mathfrak{A}|$ by inspection, while the orders $|\mathfrak{C}_r|$ are given by

$$|\mathfrak{C}_r| = \frac{n!}{1^{r_1} r_1!\, 2^{r_2} r_2! \ldots n^{r_n} r_n!}$$

where $r_1, \ldots, r_n$ denote the numbers of cycles of length $1, 2, \ldots, n$.

Formula (1a) for $\mathfrak{A} = \mathfrak{B} = \mathfrak{G}$ gives the number $z^{(r)}$ of racemic modes

$$z^{(r)} = \frac{|\mathfrak{S}_n|}{|\mathfrak{G}|^2} \sum_{r=1}^{k} \frac{|\mathfrak{C}_r \cap \mathfrak{G}|^2}{|\mathfrak{C}_r|}\,. \tag{3a}$$

A formula for the number $z^{(p)}$ of processes which is equal to the number of subclasses with respect to the group $\mathfrak{G}$ can be given without proof

$$z^{(p)} = \frac{|\mathfrak{S}_n|}{|\mathfrak{G}|} \sum_{r=1}^{k} \frac{|\mathfrak{C}_r \cap \mathfrak{G}|}{|\mathfrak{C}_r|}\,. \tag{4a}$$

Examples

The following table gives the number z of modes for eleven examples

	Skeleton		Number of sites	Symmetry of the skeleton	Number of modes (z)
1	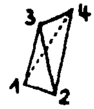	distorted tetrahedron	4	C_{2v}	6
2	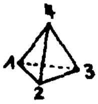	trigonal pyramid	4	C_{3v}	4
3	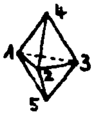	trigonal bipyramid	5	D_{3h}	6
4	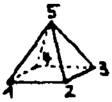	tetragonal pyramid	5	C_{4v}	7
5	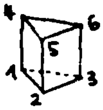	trigonal prism	6	D_{3h}	20
6	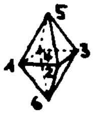	tetragonal bipyramid	6	D_{4h}	13
7	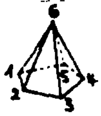	pentagonal pyramid	6	C_{5v}	24
8	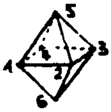	octahedron	6	O_h	5
9	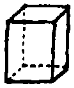	tetragonal prism	8	D_{4h}	446
10	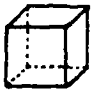	cube	8	O_h	78
11	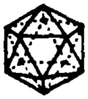	icosahedron	12	J_h	68.384

In the second table we have written down representative permutations for each mode of the first eight skeletons. The numbers in square brackets give the numbers of different isomers arising from any starting isomer through the various rearrangements belonging to any rearrangement process of the corresponding mode, provided the ligands are all different.

1: (1) [1], (12) [1], (13) [4], (123) [4], (13)(24) [1], (1324) [1]

2: (1) [1], (12) [1], (14) [3], (124) [3]

3: (1) [1], (12) [1], (14) [6], (124) [6], (14)(25) [3], (1425) [3]

4: (1) [1], (13) [1], (15) [4], (12) [4], (125) [8], (12)(35) [8], (135) [4]

5: (1) [1], (12)(45) [1], (12) [6], (123) [2], (34) [6], (12)(34) [12], (234) [12], (1432) [6], (1234) [6], (1243) [6], (142) [12], (124) [12], (14) [3], (14)(23) [6], (13)(45) [2], (1254) [6], (15)(34) [6], (1543) [6], (1345) [6], (14)(25) [3]

6: (1) [1], (13) [1], (15) [8], (135) [8], (12) [4], (125) [16], (12)(35) [16], (15)(26) [8], (1526) [8], (15)(263) [8], (15)(236) [8], (15)(36) [2], (1536) [2]

7: (1) [1], (12)(35) [1], (16) [5], (12) [5], (126) [10], (12)(36) [10], (123) [5], (1236) [5], (1263) [10], (1362) [10], (13) [5], (136) [10], (13)(26) [5], (15)(36) [5], (135) [5], (1563) [10], (1365) [10], (1325) [1], (1523) [1], (13256) [5], (16523) [5], (13)(56) [10], (1356) [5], (12)(356) [5]

8: (1) [1], (13) [1], (12) [12], (125) [8], (12)(35) [8]

Acknowledgment. The authors are most grateful to Prof. K. Mislow for his helpful encouragement of this work. One of us (E.R.) also wishes to thank Prof. Mislow for his kind hospitality during a visit of the author to Princeton, and for stimulating discussions which took place at that time.

References

1. Ruch, E., Hässelbarth, W., Richter, B.: Theoret. chim. Acta (Berl.) **19**, 288 (1970).
2. Ruch, E., Schönhofer, A.: Theoret. chim. Acta (Berl.) **19**, 225 (1970).
3. Musher, I. J.: Modes of rearrangements in phosphoranes, and Modes of rearrangements in octahedral complexes (preprints 1971).
4. Gielen, M., Vanlautem, N.: Bull. Soc. chim. Belges **79**, 679 (1970).
5. Meakin, P., Muetterties, E. L., Tebbe, F. N., Jesson, J. P.: J. Amer. chem. Soc. **93**, 4701 (1971).

Prof. Dr. E. Ruch
Institut für Quantenchemie
Freie Universität Berlin
D-1000 Berlin 45, Holbeinstraße 48
Deutschland

Theoret. chim. Acta (Berl.) 29, 269—304 (1973)
© by Springer-Verlag 1973

Theory of Chirality Functions, Generalized for Molecules with Chiral Ligands

Alden Mead, Ernst Ruch, and Alfred Schönhofer
Institut für Quantenchemie der Freien Universität Berlin

Received October 24, 1972/February 5, 1973

The theory of chirality functions described in a previous publication is generalized to allow for chiral ligands. In the earlier theory, all symmetry operations of the molecular frame could be thought of as permutations of the ligands among the sites; in the present work, improper rotations not only permute the ligands, but convert them into mirror images. The group that generates all isomers from a given ordered molecule belonging to a frame with n sites is now the "hyperoctahedral" group of order $2^n n!$ consisting of all possible combinations of permutations and site reflections. The representation theory of these groups is described, and applied to the problem of constructing qualitatively complete chirality functions, and of deciding which ligand partitions, and which isomer mixtures, are chiral. It is found useful to classify chiral representations of the covering group as "ligand specific" and "class specific". The ligand specific representations describe chiral properties which are common to all frames and arise purely from the chirality of the ligands, while the class specific representations describe the chiral properties of the frame. A number of examples are explicitly worked out.

1. Introduction and Statement of Problem

A chirality function is defined as a function which describes a pseudoscalar property of molecules belonging to a class in its dependence on the nature of the particular molecules. If the molecular class is characterized by a frame, or skeleton, with n sites for ligands, and if molecules belonging to the class are distinguished by the nature of the ligands and their distribution among the sites, then a chirality function for this class is partially determined by the frame, and depends on variables ℓ_r with indices r for the ligands.

A general theory of chirality functions [10], formulated without reference to the particular physical phenomenon being studied, enables one, under any set of special assumptions about the nature of the molecular class, to make various meaningful statements.

The frame is assumed to be achiral. If two isomers differ from one another by a rearrangement of the ligands corresponding to a symmetry operation of the frame, they must bei either identical or mirror images. This leads to a requirement on the symmetry, placement, and orientation of the ligands. Achiral ligands must be so fixed in space that all symmetry operations of the frame which leave a given site invariant are symmetry operations for the ligand found on that site. Up to now, our theory has been restricted to molecules with exclusively achiral ligands.

In this article, we drop the restriction to achiral ligands. Only symmetry operations of the first kind (pure rotations) which leave a site invariant are required to be symmetry operations for the ligand located on the site. Symmetry operations of the second kind transform chiral ligands into their mirror images[1]. The concept of isomer is to be understood as also including molecules in which chiral ligands may be replaced by their mirror images. Isomers which differ from one another only by a permutation of ligands among the sites (without inversion of any ligand) will be referred to as permutational isomers.

The basic formulation and definitions will be the same as, or analogous to, those used in [10]. $\mathfrak{G}$ is the symmetry group of the frame, $\mathfrak{D}$ the invariant subgroup of the pure rotations. The column matrix

$$L=\begin{pmatrix} l_1 \\ l_2 \\ \vdots \\ l_n \end{pmatrix} \qquad (1)$$

represents a given "ordered molecule" („geordnetes Molekül", cf. [10]). To each rotation of $\mathfrak{D}$ there corresponds a ligand permutation $\jmath$ on the fixed frame. The application of $\jmath$ to L leads to the ordered molecule

$$\jmath L=\begin{pmatrix} l_{i_1} \\ l_{i_2} \\ \vdots \\ l_{i_n} \end{pmatrix}.$$

This determines a homomorphic mapping of $\mathfrak{D}$ onto a permutation group $\mathfrak{N}$. In the case of achiral ligands, in which one need not consider their conversion to mirror images, one can also associate permutations with the rotary reflections of $\mathfrak{G}$ (elements of the coset of $\mathfrak{D}$ in $\mathfrak{G}$). In this way, all elements of $\mathfrak{G}$ may be described by pure permutations. In the case of chiral ligands, however, representation of an improper rotation must include the simultaneous transformation of all ligands into mirror images.

The operation which transforms the ligand on site k into its mirror image will be denoted by τ_k, and the mirror image of l_i by l_i^*. Thus, we have

$$\tau_k\begin{pmatrix} l_{i_1} \\ \vdots \\ l_{i_k} \\ \vdots \\ l_{i_n} \end{pmatrix}=\begin{pmatrix} l_{i_1} \\ \vdots \\ l_{i_k}^* \\ \vdots \\ l_{i_n} \end{pmatrix}.$$

τ_k is therefore a reflection, restricted to the ligand located on the site k, in a mirror plane of the frame which contains site k; or, if there is no such mirror plane, in a plane containing a symmetry axis of the first kind passing through site k; or, if there also is no such axis, in a plane chosen in such a way that the reflection leads to the natural orientation of the mirror image ligand. We shall refer to such an operation as a "site reflection".

---

[1] Note that the symmetry requirement for the ligands is automatically satisfied if the ligands are assumed to be freely rotating, or if an ensemble average over conformations is to be taken.

If $\tau_0 = \tau_1 \tau_2 \ldots \tau_n$ denotes the simultaneous site reflection of all ligands, then each improper rotation of $\mathfrak{G}$ can be represented by an operation of the form $\mathfrak{j}'\tau_0 = \tau_0 \mathfrak{j}'$, in which $\mathfrak{j}'$ denotes the corresponding rearrangement of the ligands among the sites. Thus, we find

$$\tau_0 \mathfrak{j}' L = \begin{pmatrix} l^*_{i_1} \\ l^*_{i_2} \\ \vdots \\ l^*_{i_n} \end{pmatrix}.$$

The totality of the improper rotations, i.e., the coset of $\mathfrak{D}$ in $\mathfrak{G}$ is mapped in this way onto the set of elements $\tau_0 \mathfrak{j}'$, in which $\mathfrak{j}'$ is a permutation describing only the reordering of the ligands under an improper rotation of $\mathfrak{G}$. We have the homomorphism

$$\mathfrak{G} \rightsquigarrow \bar{\mathfrak{S}}$$

of the group $\mathfrak{G}$ on $\bar{\mathfrak{S}} = \{\mathfrak{N}, \tau_0 \mathfrak{j}'\mathfrak{N}\}$.

We also have the isomorphism

$$\bar{\mathfrak{S}} \cong \mathfrak{S} = \{\mathfrak{N}, \mathfrak{j}'\mathfrak{N}\}$$

in which $\mathfrak{S}$ denotes the permutation group whose elements describe the symmetry operations of $\mathfrak{G}$ neglecting the reflection of ligands. In the case of exclusively achiral ligands, the τ_k are symmetry operations for the corresponding ligands, and it is therefore permissible, as in [10], to make use of the group $\mathfrak{S}$ instead of $\bar{\mathfrak{S}}$.

The group of all operations transforming a given ordered molecule into all its isomers, in our extended definition of the term, shall be denoted by $\bar{\mathfrak{S}}_n$. Its elements σ are pure permutations, pure site reflections and products of the two. The subgroup $\mathfrak{T}$ of site reflections on fixed sites, without simultaneous reordering, consists of all possible products $\tau_i \tau_j \ldots \tau_r$ of site reflections on sites $i, j, \ldots r$. Since the ordering does not affect the result of a sequence of site reflections on fixed sites, it follows that $\mathfrak{T}$ is a direct product of groups $\mathfrak{T}_i = \{e, \tau_i\}$, each of which consists of the unit element and the reflection on one site:

$$\mathfrak{T} = \mathfrak{T}_1 \times \mathfrak{T}_2 \times \cdots \times \mathfrak{T}_n .$$

It is clear that the result of a site reflection operation of $\mathfrak{T}$ followed by a permutation, can also be reached by the same permutation followed by site reflections on other sites. It follows that

$$\sigma = \mathfrak{j}\tau = \tau'\mathfrak{j}, \qquad \mathfrak{j}\tau\mathfrak{j}^{-1} = \tau' .$$

This, together with the commutativity of all site reflections, leads to the conclusion that $\mathfrak{T}$ is an abelian invariant subgroup of $\bar{\mathfrak{S}}_n$. The subgroup $\mathfrak{S}_n$ of the pure permutations, on the other hand, is not invariant. Since $\mathfrak{S}_n$ and $\mathfrak{T}$ have only the unit element in common, $\bar{\mathfrak{S}}_n$ is a semidirect product of $\mathfrak{T}$ and the symmetric group $\mathfrak{S}_n$:

$$\bar{\mathfrak{S}}_n = \mathfrak{T} \vee \mathfrak{S}_n , \qquad |\bar{\mathfrak{S}}_n| = n!\,2^n .$$

As in [10], with completely analogous definitions and the same reasoning, we may consider the elements of the group algebra of $\mathfrak{S}_n$ as denoting ensemble operators. Application of an element $\mathfrak{a}$ of the group algebra to a column matrix L of type (1), i.e., the application of an ensemble operator $\mathfrak{a}$ to an ordered molecule, leads to a linear combination of ordered molecules with complex coefficients,

$$\mathfrak{a}L = \Sigma a(\sigma)\sigma L\,.$$

Special ensemble operators are the projection operators

$$\mathfrak{p}_{\mathfrak{N}} = \frac{1}{|\mathfrak{N}|}\sum_{\mathfrak{j}\in\mathfrak{N}} \mathfrak{j} \quad \text{and} \quad \mathfrak{p}_{\chi} = \frac{1}{2}\{\mathfrak{p}_{\mathfrak{N}} - \mathfrak{p}_{\mathfrak{N}}\tau_0\mathfrak{j}'\}$$

which can be applied to an arbitrary $\mathfrak{a}$ to give

$$\bar{\mathfrak{a}} = \mathfrak{p}_{\mathfrak{N}}\mathfrak{a} \quad \text{and} \quad \mathfrak{p}_{\chi}\mathfrak{a} = \mathfrak{p}_{\chi}\bar{\mathfrak{a}}\,.$$

The operator $\bar{\mathfrak{a}}$ is expressible in the form

$$\bar{\mathfrak{a}} = \mathfrak{p}_{\mathfrak{N}}\sum_j \bar{a}(\sigma_j)\sigma_j \text{ with coefficients } \bar{a}(\sigma_j) = \sum_{\mathfrak{j}\in\mathfrak{N}} a(\mathfrak{j}\sigma_j)$$

and elements σ_j running through a representative system for right cosets of $\mathfrak{N}$ in $\mathfrak{S}_n$.

The coefficients $\bar{a}(\sigma_j)$ in $\mathfrak{p}_{\mathfrak{N}}\mathfrak{a}L = \Sigma\bar{a}(\sigma_j)\mathfrak{p}_{\mathfrak{N}}\sigma_j L$ refer to a collection of ordered molecules $\mathfrak{p}_{\mathfrak{N}}\sigma_j L$ differing only by their orientation in space if the numbering of sites is ignored. Therefore different $\mathfrak{p}_{\mathfrak{N}}\sigma_j L$ with $j = 1, 2\ldots$ are representative for different isomers provided the ligand assortment does not contain like ligands. Because of the equation $\mathfrak{p}_{\chi}\tau_0\mathfrak{j}' = -\mathfrak{p}_{\chi}$, for any element $\tau_0\mathfrak{j}'$ of the coset of $\mathfrak{N}$ in $\mathfrak{S}$, each coefficient in $\mathfrak{p}_{\chi}\mathfrak{a}L$ can be replaced by the negative coefficient of a corresponding enantiomer; if all coefficients of $\mathfrak{a}$ are real, $\mathfrak{p}_{\chi}\mathfrak{a}L$ can therefore be written with positive coefficients which may be interpreted as concentrations of the components of an isomeric mixture. Because the application of $\tau_0\mathfrak{j}'$ on $\mathfrak{p}_{\chi}\mathfrak{a}L$ changes the sign of all coefficients, the condition $\mathfrak{p}_{\chi}\mathfrak{a} \neq 0$ is necessary and sufficient for the existence of non-racemic mixtures $\mathfrak{a}L$ or $\bar{\mathfrak{a}}L$. $\mathfrak{p}_{\chi}\mathfrak{a}$ will be referred to as the chiral component of the ensemble operator $\mathfrak{a}$. An ensemble operator will be called chiral if $\mathfrak{p}_{\chi}\mathfrak{a} \neq 0$. Extension of the ensemble operator concept to elements of the group algebra with complex coefficients is formally permissible, making possible the formulation and solution of our problem in terms of the language and methods of representation theory.

A chirality function $\phi(|L)$ is, by definition, invariant under a reorientation of the molecule which effects a symmetry operation of the skeleton. This behaviour expressed in terms of the site numbers, corresponds to invariance under the operator $\mathfrak{p}_{\mathfrak{N}}$. Since $\phi(|L)$ changes sign under reflections of the molecule, we can define a chirality function by means of the equation

$$\mathscr{P}_{\chi}\phi(|L) = \phi(|L)\,,$$

where $\mathscr{P}_{\chi}$ is an operator corresponding to $\mathfrak{p}_{\chi}$, but operating on functions. This definition assures that $\phi(|L)$ transforms according to the chirality representation Γ_{χ} of the group $\mathfrak{S}$. For an isomer σL, the chirality function $\phi(|\sigma L)$ has the same value as another function $\phi(\sigma|L)$ of the original molecule:

$$\phi(|\sigma L) \triangleq \phi(\sigma|L)\,.$$

There are a number of qualitative requirements on a chirality function for a molecular class which must be fulfilled if the function is to give a satisfactory description of pseudoscalar observations on chiral molecules. By means of the present formalism, as derived in [10], these requirements can be collected and expressed by a *single* physically realistic property of the function for isomeric mixtures.

A linear combination of functions $\phi(\sigma|L)$, with $\sigma \in \bar{\mathfrak{S}}_n$, is related to the chirality function for a corresponding isomer mixture $\bar{a}L$ as follows:

$$\sum_{\sigma \in \mathfrak{S}_n} a(\sigma)\phi(\sigma|L) = \sum_j \bar{a}(\sigma_j)\phi(\sigma_j|L) \triangleq \sum_j \bar{a}(\sigma_j)\phi(|\sigma_j L) = \sum_{\sigma \in \mathfrak{S}_n} a(\sigma)\phi(|\sigma L).$$

Thus, seemingly completely different states of affairs for molecules and isomer mixtures lead to results which are reciprocally related. It is desirable that a chirality function not vanish for all chiral molecules in which certain numbers of identical ligands are prescribed, i.e., for molecules possessing a certain "active ligand partition". It is also desirable that a particular type of chirality function for a molecular class remain useable when the frame is continuously distorted into a frame of higher symmetry without altering the number of sites or at any intermediate point decreasing the symmetry. These and similar, seemingly trivial properties are not automatically present in the great majority of cases if functions of the usual type are used. Such properties are all encompassed in a property which we have named "qualitative completeness" („qualitative Vollständigkeit", cf. [10]), a concept which may be defined as follows in terms of isomer mixtures:

> A chirality function for molecules of a certain class is called qualitatively complete if there is no nonracemic isomer mixture for which the function is identically zero, independently of the nature of the ligands.

This definition remains meaningful for the extended concept of isomers, hence for molecules with chiral ligands; the reasons for utilizing qualitatively complete chirality functions are the same as before. The following mathematical formulation is equivalent:

> A chirality function $\phi(|L)$ is qualitatively complete if it gives rise to "regular" [9] induction from $\mathfrak{S}$ to $\bar{\mathfrak{S}}_n$.
>
> Or in other words:
>
> The functions $\phi(\sigma|L)$ for $\sigma \in \bar{\mathfrak{S}}_n$ form a basis for a representation $\bar{\Gamma}$ of $\bar{\mathfrak{S}}_n$ which, on decomposition into irreducible components $\bar{\Gamma}_r$, contains each $\bar{\Gamma}_r$ exactly as many times as the chirality representation Γ_χ is contained in $\bar{\Gamma}_r$.

If we denote this number for $\bar{\Gamma}_r$ by z_r, then we must have

$$\bar{\Gamma} = \sum_r z_r \bar{\Gamma}_r . \qquad (2)$$

As the treatment of the achiral ligand case has shown, this property expresses a structural aspect of the chirality phenomenon for a molecular class which furnishes much relevant information. A great deal of this information (such as chirality numbers, statements about active ligand partitions, and so forth) is in

As in [10], with completely analogous definitions and the same reasoning, we may consider the elements of the group algebra of $\mathfrak{S}_n$ as denoting ensemble operators. Application of an element a of the group algebra to a column matrix L of type (1), i.e., the application of an ensemble operator a to an ordered molecule, leads to a linear combination of ordered molecules with complex coefficients,

$$aL = \Sigma a(\sigma)\sigma L\,.$$

Special ensemble operators are the projection operators

$$\wp_{\mathfrak{N}} = \frac{1}{|\mathfrak{N}|}\sum_{\mathfrak{r}\in\mathfrak{N}} \mathfrak{r} \quad \text{and} \quad \wp_{\gamma} = \frac{1}{2}\{\wp_{\mathfrak{N}} - \wp_{\mathfrak{N}}\tau_0\mathfrak{r}'\}$$

which can be applied to an arbitrary a to give

$$\bar{a} = \wp_{\mathfrak{N}}a \quad \text{and} \quad \wp_{\gamma}a = \wp_{\gamma}\bar{a}\,.$$

The operator $\bar{a}$ is expressible in the form

$$\bar{a} = \wp_{\mathfrak{N}}\sum_{j}\bar{a}(\sigma_j)\sigma_j \text{ with coefficients } \bar{a}(\sigma_j) = \sum_{\mathfrak{r}\in\mathfrak{N}} a(\mathfrak{r}\sigma_j)$$

and elements σ_j running through a representative system for right cosets of $\mathfrak{N}$ in $\mathfrak{S}_n$.

The coefficients $\bar{a}(\sigma_j)$ in $\wp_{\mathfrak{N}}aL = \Sigma\bar{a}(\sigma_j)\wp_{\mathfrak{N}}\sigma_j L$ refer to a collection of ordered molecules $\wp_{\mathfrak{N}}\sigma_j L$ differing only by their orientation in space if the numbering of sites is ignored. Therefore different $\wp_{\mathfrak{N}}\sigma_j L$ with $j = 1, 2\ldots$ are representative for different isomers provided the ligand assortment does not contain like ligands. Because of the equation $\wp_{\gamma}\tau_0\mathfrak{r}' = -\wp_{\gamma}$, for any element $\tau_0\mathfrak{r}'$ of the coset of $\mathfrak{N}$ in $\mathfrak{S}$, each coefficient in $\wp_{\gamma}aL$ can be replaced by the negative coefficient of a corresponding enantiomer; if all coefficients of a are real, $\wp_{\gamma}aL$ can therefore be written with positive coefficients which may be interpreted as concentrations of the components of an isomeric mixture. Because the application of $\tau_0\mathfrak{r}'$ on $\wp_{\gamma}aL$ changes the sign of all coefficients, the condition $\wp_{\chi}a \neq 0$ is necessary and sufficient for the existence of non-racemic mixtures aL or $\bar{a}L$. $\wp_{\gamma}a$ will be referred to as the chiral component of the ensemble operator a. An ensemble operator will be called chiral if $\wp_{\gamma}a \neq 0$. Extension of the ensemble operator concept to elements of the group algebra with complex coefficients is formally permissible, making possible the formulation and solution of our problem in terms of the language and methods of representation theory.

A chirality function $\phi(|L)$ is, by definition, invariant under a reorientation of the molecule which effects a symmetry operation of the skeleton. This behaviour expressed in terms of the site numbers, corresponds to invariance under the operator $\wp_{\mathfrak{N}}$. Since $\phi(|L)$ changes sign under reflections of the molecule, we can define a chirality function by means of the equation

$$\mathscr{P}_{\chi}\phi(|L) = \phi(|L)\,,$$

where $\mathscr{P}_{\chi}$ is an operator corresponding to $\wp_{\chi}$, but operating on functions. This definition assures that $\phi(|L)$ transforms according to the chirality representation Γ_{χ} of the group $\mathfrak{S}$. For an isomer σL, the chirality function $\phi(|\sigma L)$ has the same value as another function $\phi(\sigma|L)$ of the original molecule:

$$\phi(|\sigma L) \mathrel{\hat{=}} \phi(\sigma|L)\,.$$

There are a number of qualitative requirements on a chirality function for a molecular class which must be fulfilled if the function is to give a satisfactory description of pseudoscalar observations on chiral molecules. By means of the present formalism, as derived in [10], these requirements can be collected and expressed by a *single* physically realistic property of the function for isomeric mixtures.

A linear combination of functions $\phi(\sigma|L)$, with $\sigma \in \tilde{\mathfrak{S}}_n$, is related to the chirality function for a corresponding isomer mixture $\bar{a}L$ as follows:

$$\sum_{\alpha \in \tilde{\mathfrak{S}}_n} a(\sigma)\phi(\sigma|L) = \sum_j \bar{a}(\sigma_j)\phi(\sigma_j|L) \triangleq \sum_j \bar{a}(\sigma_j)\phi(|\sigma_j L) = \sum_{\sigma \in \tilde{\mathfrak{S}}_n} a(\sigma)\phi(|\sigma L) .$$

Thus, seemingly completely different states of affairs for molecules and isomer mixtures lead to results which are reciprocally related. It is desirable that a chirality function not vanish for all chiral molecules in which certain numbers of identical ligands are prescribed, i.e., for molecules possessing a certain "active ligand partition". It is also desirable that a particular type of chirality function for a molecular class remain useable when the frame is continuously distorted into a frame of higher symmetry without altering the number of sites or at any intermediate point decreasing the symmetry. These and similar, seemingly trivial properties are not automatically present in the great majority of cases if functions of the usual type are used. Such properties are all encompassed in a property which we have named "qualitative completeness" („qualitative Vollständigkeit", cf. [10]), a concept which may be defined as follows in terms of isomer mixtures:

> A chirality function for molecules of a certain class is called qualitatively complete if there is no nonracemic isomer mixture for which the function is identically zero, independently of the nature of the ligands.

This definition remains meaningful for the extended concept of isomers, hence for molecules with chiral ligands; the reasons for utilizing qualitatively complete chirality functions are the same as before. The following mathematical formulation is equivalent:

> A chirality function $\phi(|L)$ is qualitatively complete if it gives rise to "regular" [9] induction from $\mathfrak{S}$ to $\tilde{\mathfrak{S}}_n$.

Or in other words:

> The functions $\phi(\sigma|L)$ for $\sigma \in \tilde{\mathfrak{S}}_n$ form a basis for a representation $\bar{\Gamma}$ of $\tilde{\mathfrak{S}}_n$ which, on decomposition into irreducible components $\bar{\Gamma}_r$, contains each $\bar{\Gamma}_r$ exactly as many times as the chirality representation Γ_χ is contained in $\bar{\Gamma}_r$.

If we denote this number for $\bar{\Gamma}_r$ by z_r, then we must have

$$\bar{\Gamma} = \sum_r z_r \bar{\Gamma}_r . \qquad (2)$$

As the treatment of the achiral ligand case has shown, this property expresses a structural aspect of the chirality phenomenon for a molecular class which furnishes much relevant information. A great deal of this information (such as chirality numbers, statements about active ligand partitions, and so forth) is in practice – and sometimes in principle as well – expressible only in terms of special properties of the irreducible representations of $\mathfrak{S}_n$. Among these special properties are the one-to-one correspondence between irreducible representations and so-called Young diagrams, Young operators, and a newly discovered lattice structure for Young diagrams. In the generalization to the group $\tilde{\mathfrak{S}}_n$ it is thus worthwhile to seek corresponding relations between representations and diagrams, and a corresponding lattice structure. It is equally desirable to formulate corresponding approximation procedures which lead to qualitatively complete chirality functions.

2. Properties of the Group $\tilde{\mathfrak{S}}_n$ and Its Representations

In this Section we state without proof some properties of the $\tilde{\mathfrak{S}}_n$ which we shall need. Proofs of statements in subsection 2A are to be found in the mathematical literature. Since this literature is somewhat inaccessible to the non-mathematician, we give these proofs in Appendix 1.

A. *The Group $\tilde{\mathfrak{S}}_n$, Some Subgroups, Its Young Operators and Partition Diagrams*

A class of conjugate elements in the group $\mathfrak{S}_n$ is known to be characterized by the cyclic structure of the permutations, i.e., by the type of cyclic permutation factors into which the permutations can be decomposed such that each of the numbers 1, 2,... occur in one and only one of the cycles. Like the decomposition of a certain permutation into cycles, a certain decomposition of n into a sum of integers denoting the cycle-lengths is representative for a class of conjugate elements. Such a partition of n, on the other hand, may be visualized by the lengths of rows in a partition diagram. A partition diagram of order n consists of n boxes arranged in rows and columns such that the number of boxes in a column or row does not increase if going from left to right or from top to bottom, respectively. In the case of $n = 10$, for example, one of the classes is denoted in three equivalent ways in Fig. 1.

An element of $\tilde{\mathfrak{S}}_n$ is a product of a reflection operation τ and a permutation π, which may be assumed written in cyclic form. Moreover, since each site reflection τ_j commutes with permutations not involving site (j), we may reorder the factors so that each cyclic permutation is followed immediately by reflections on sites involved in the cycle. Thus, each element of $\tilde{\mathfrak{S}}_n$ can be expressed as a product of commuting operations, each of which consists of a cyclic permutation among q sites followed by reflections on some of these sites. If the number of these reflections is even, we call the cycle even and denote it by $q^{(+)}$; if the number of reflections is odd, we call the cycle odd and denote it by $q^{(-)}$. It has been shown [11], and is also proved in Appendix 1.A, that this indexed cyclic structure determines the

(...)(...)(..)(.)(.) ⟷ (3,3,2,1,1) ⟷

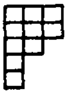

Fig. 1

$$(\ldots)^{(+)}(\ldots)^{(-)}(\ldots)^{(-)}(.)^{(+)}(.)^{(+)} \longleftrightarrow (3^{(+)},1^{(+)},1^{(+)},3^{(-)},2^{(-)}) \longleftrightarrow$$

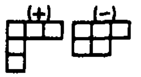

Fig. 2

classes of $\bar{\mathfrak{S}}_n$: two elements are mutually conjugate if and only if they possess the same indexed cyclic structure. Thus, a class of $\bar{\mathfrak{S}}_n$ may be represented by a partition of n into a sum of integers indexed by (+) or (−) respectively, or equivalently by a two-part diagram of order n, consisting of two ordinary diagrams, a "plus" part of order $n^{(+)}$, and a "minus" part of order $n^{(-)}$. Figure 2 shows three equivalent ways of representing one of the classes of $\bar{\mathfrak{S}}_{10}$. We will also sometimes omit the signs, separating even and odd cycles by a semicolon. In this notation, the class of Fig. 2 would be denoted by (3, 1, 1; 3, 2).

In Ref. [10], we drew much advantage from the fact that, in the case of $\mathfrak{S}_n$, there is also a one-to-one correspondence between the set of all possible diagrams of order n, $\gamma^{(r)}$, and the irreducible representations Γ_r of $\mathfrak{S}_n$:

$$\Gamma_r \leftrightarrow \gamma^{(r)}\,.$$

As we shall see presently, a precisely analogous correspondence holds between two-part diagrams $\bar{\gamma}^{(r)}$ of order n and irreducible representations $\bar{\Gamma}_r$ of $\bar{\mathfrak{S}}_n$:

$$\bar{\Gamma}_r \leftrightarrow \bar{\gamma}^{(r)}\,.$$

A two-part diagram whose n boxes are filled in any order with the symbols $1, 2, \ldots, n$ (which may be thought of as representing the numbered sites) will be called a (two-part) tableau of order n[2]. A tableau in which the numbers appear in their natural order when one reads first the plus part and then the minus part as in a book, each row from left to right and the rows from top to bottom, will be called the book tableau. For each tableau $\bar{t}^{(r)}$ belonging to the two-part diagram $\bar{\gamma}^{(r)}$, we can define some particular subgroups of $\bar{\mathfrak{S}}_n$, as follows:

Let $\mathfrak{A}^{(r)} = \mathfrak{A}^{(r+)} \times \mathfrak{A}^{(r-)}$ be the subgroup of $\mathfrak{S}_n$ containing all those permutations which effect only rearrangements within the rows of both component tableaux $t^{(r+)}$ and $t^{(r-)}$ in a tableau $\bar{t}^{(r)}$ of $\bar{\gamma}^{(r)}$ and $\mathfrak{B}^{(r)} = \mathfrak{B}^{(r+)} \times \mathfrak{B}^{(r-)}$ be the corresponding subgroup of permutations within columns.

We will sometimes denote an arbitrary member of $\mathfrak{A}^{(r+)}$ by α_+, one of $\mathfrak{A}^{(r-)}$ by α_-, with α (without a subscript) denoting an arbitrary member of $\mathfrak{A}^{(r)}$. β will play the analogous role for $\mathfrak{B}^{(r)}$.

Let $\mathfrak{T}^{(r+)}$ and $\mathfrak{T}^{(r-)}$ be subgroups of $\mathfrak{T}$ containing all site reflections in $t^{(r+)}$ and $t^{(r-)}$ respectively, and consisting of elements τ_+, τ_-.

With the semidirect products $\mathfrak{T}^{(r+)} \vee \mathfrak{A}^{(r+)}$ and $\mathfrak{T}^{(r-)} \vee \mathfrak{B}^{(r-)}$ being direct products of groups $\bar{\mathfrak{S}}_\nu$ for each row in the plus- and each column in the minus-diagram respectively we get the needed subgroups $\mathfrak{Q}^{(r)}$ and $\hat{\mathfrak{Q}}^{(r)}$ of $\bar{\mathfrak{S}}_n$ according to the following definition:

---

[2] The definition of tableau given in Ref. [10] is different from the one used here. The present definition corresponds to normal usage, and to the requirements of the present article.

$$\mathfrak{Q}^{(r)} = \mathfrak{T}^{(r+)} \vee \mathfrak{A}^{(r+)} \times \mathfrak{A}^{(r-)} \quad \text{and} \quad \hat{\mathfrak{Q}}^{(r)} = \mathfrak{B}^{(r+)} \times \mathfrak{B}^{(r-)} \vee \mathfrak{T}^{(r-)}.$$

We note that $\mathfrak{Q}^{(r)}$ and $\hat{\mathfrak{Q}}^{(r)}$ have only the unit element of $\mathfrak{S}_n$ in common,

$$\mathfrak{Q}^{(r)} \cap \hat{\mathfrak{Q}}^{(r)} = e.$$

We define the "alternating representation" of $\hat{\mathfrak{Q}}^{(r)}$ as the one having the character -1 for odd permutations and for single site reflections. Therefore an element σ of $\hat{\mathfrak{Q}}^{(r)}$ has the character $(+1)$ if both the permutation and the number of site reflections are even, or both odd, otherwise it has (-1).

The projection operators for the identity representation of $\mathfrak{Q}^{(r)}$ and for the alternating representation of $\hat{\mathfrak{Q}}^{(r)}$ which we need are

$$\mathcal{Q}^{(r)} = t^{(r+)} a^{(r+)} a^{(r-)} \quad \text{and} \quad \hat{\mathcal{Q}}^{(r)} = t^{(r-)} b^{(r-)} b^{(r+)}.$$

The factors, which are commutable, are defined as follows:

$$a^{(r+)} = \frac{1}{|\mathfrak{A}^{(r+)}|} \sum_{\alpha \in \mathfrak{A}^{(r+)}} \alpha, \quad a^{(r-)} = \frac{1}{|\mathfrak{A}^{(r-)}|} \sum_{\alpha \in \mathfrak{A}^{(r-)}} \alpha, \quad t^{(r+)} = \frac{1}{|\mathfrak{T}^{(r+)}|} \prod_{\tau_i \in \mathfrak{T}^{(r+)}} (\iota + \tau_i),$$

$$b^{(r+)} = \frac{1}{|\mathfrak{B}^{(r+)}|} \sum_{\beta \in \mathfrak{B}^{(r+)}} \varepsilon_\beta \beta, \quad b^{(r-)} = \frac{1}{|\mathfrak{B}^{(r-)}|} \sum_{\beta \in \mathfrak{B}^{(r-)}} \varepsilon_\beta \beta, \quad t^{(r-)} = \frac{1}{|\mathfrak{T}^{(r-)}|} \prod_{\tau_i \in \mathfrak{T}^{(r-)}} (\iota - \tau_i),$$

where $\varepsilon_\beta = +1$ if β is even and $\varepsilon_\beta = -1$ if β is odd.

These operators may be combined to define the Young operator

$$\mathcal{Y}^{(r)} = \mathcal{Q}^{(r)} \hat{\mathcal{Q}}^{(r)}$$

associated with the tableau in question. If the Young operator belonging to the book tableau is denoted by $\mathcal{Y}^{(r)}_b$, then any other Young operator belonging to $\bar{\mathcal{T}}^{(r)}$ may be expressed as

$$\mathcal{Y}^{(r)}_a = \sigma \mathcal{Y}^{(r)}_b \sigma^{-1}$$

with a properly chosen σ.

The Young operators possess the following properties, proved in Appendix 1.B:

Each Young operator is, apart from a constant coefficient, a primitive idempotent projecting onto a single component of an irreducible representation of $\mathfrak{S}_n$. Young operators generated by tableaux belonging to the same two-part diagram project onto equivalent irreducible representations, those from different diagrams onto inequivalent ones. Thus, the correspondence

$$\bar{\Gamma}_r \leftrightarrow \bar{\mathcal{T}}^{(r)}_i$$

is made precise by the statement that Young operators belonging to $\bar{\mathcal{T}}^{(r)}$ project onto the irreducible representation $\bar{\Gamma}_r$. All projection operators onto $\bar{\Gamma}_r$ may be expressed linearly in terms of the $\mathcal{Y}^{(r)}$ and products $\mathcal{Y}^{(r)'} \sigma \mathcal{Y}^{(r)}$. Moreover, since the number of different two-part diagrams is obviously equal to the number of classes, and hence to the number of irreducible representations, of $\mathfrak{S}_n$, we know that we obtain all irreducible representations in this way.

We will also need another subgroup of $\bar{\mathfrak{S}}_n$, called $\mathfrak{S}'_n$, which contains both $\bar{\mathfrak{S}}$ and $\mathfrak{S}_n$ as subgroups. It consists of all pure permutations, as well as $\tau_0 = \tau_1 \tau_2 \cdots \tau_n$, and products of the two, and may be defined as the direct product

$$\mathfrak{S}'_n = \mathfrak{S}_n \times \mathfrak{T}_0 \quad \text{where} \quad \mathfrak{T}_0 = \{\varepsilon, \tau_0\}\,.$$

Because the element τ_0 commutes with all permutations, classes of conjugate elements are the classes in $\mathfrak{S}_n$ and those arising by multiplication with τ_0. A characterization of classes may be given therefore by single diagrams as for $\mathfrak{S}_n$, but marked with an additional index distinguishing a class with the factor τ_0 from a class without this factor.

Because the subduction from an irreducible representation of $\mathfrak{S}'_n$ to the subgroup $\mathfrak{S}_n$ gives rise to an irreducible representation Γ_r of $\mathfrak{S}_n$ and because the subduction to the subgroup $\mathfrak{T}_0$ leads to a multiple of either the identity or alternating representation we can denote the irreducible representations of $\mathfrak{S}'_n$ by Γ_{rg} and Γ_{ru}. The corresponding notation for diagrams with an index g or u yields the one-to-one correspondence between irreducible representations of $\mathfrak{S}'_n$ and diagrams with n boxes

$$\Gamma_{rg} \leftrightarrow \gamma^{(rg)}\,, \qquad \Gamma_{ru} \leftrightarrow \gamma^{(ru)}\,.$$

Corresponding Young operators follow from those defined for the irreducible representations of $\mathfrak{S}_n$ according to

$$\mathscr{Y}^{(rg)} = \tfrac{1}{2}(\varepsilon + \tau_0)\,\mathscr{Y}^{(r)} \quad \text{and} \quad \mathscr{Y}^{(ru)} = \tfrac{1}{2}\,(\varepsilon - \tau_0)\,\mathscr{Y}^{(r)}$$

and the definition $\mathscr{Y}^{(r)} = a^{(r)} f^{(r)}$ where $a^{(r)}$ and $f^{(r)}$ refer to a single diagram $\gamma^{(r)}$ with n boxes.

B. The Regular Induction from $\mathfrak{S}_n$ and $\mathfrak{S}'_n$ to $\bar{\mathfrak{S}}_n$

As we saw in Section 1, the construction of a qualitatively complete chirality function requires the determination of the integer coefficients z_r of formula (2). z_r is the minimum number of different chirality functions transforming like linearly independent vectors of an irreducible representation space for $\bar{\Gamma}_r$ which we need, properly chosen as additional components in a qualitatively complete chirality function for each r. z_r is simultaneously the number which tells us how often the chirality representation is contained in $\bar{\Gamma}_r$. If character tables for $\bar{\mathfrak{S}}_n$ are available, z_r can be determined in a straightforward manner. If not, the characters may be calculated by means of the formula derived in appendix (1.B, Theorem 4). Even for relatively low n, however, this procedure becomes extremely tedious. The induction is much more easily carried out by means of another procedure, which we now proceed to explain. It is based on the knowledge of the readily available characters for $\mathfrak{S}'_n$ and consists of a decomposition of the induction process into the induction from $\bar{\mathfrak{S}}$ to $\mathfrak{S}'_n$ and from $\mathfrak{S}'_n$ to $\bar{\mathfrak{S}}_n$.

If the chirality representation is contained X_l times in the irreducible representation Γ'_l of $\mathfrak{S}'_n$ and if Γ'_l is contained Y_{lr} times in $\bar{\Gamma}_r$ of $\bar{\mathfrak{S}}_n$, then z_r can be determined by the formula

$$z_r = \sum_l X_l\, Y_{lr}\,.$$

As the character tables of $\mathfrak{S}'_n$ allow us to determine the X_l, our problem reduces to finding the Y_{lr}. For this purpose, we first note that a two-part diagram $\bar{\gamma}^{(r)}$ is characteristic not only for the irreducible representation $\bar{\Gamma}_r$ of $\bar{\mathfrak{S}}_n$, but also for the irreducible representation $\Gamma_{r+} \times \Gamma_{r-}$ of the direct product group $\mathfrak{S}_{n(r+)} \times \mathfrak{S}_{n(r-)}$ because $\gamma^{(r+)}$ and $\gamma^{(r-)}$ are the diagrams for the irreducible representations Γ_{r+} and Γ_{r-} of the factors $\mathfrak{S}_{n(r+)}$ and $\mathfrak{S}_{n(r-)}$.

In Appendix I.C we prove the following theorem:

The representation of $\mathfrak{S}_n$ which we get by means of the regular induction with an irreducible representation of $\mathfrak{S}_{n(r+)} \times \mathfrak{S}_{n(r-)}$ associated with the diagram pair $\bar{\gamma}^{(r)}$ is the same as that obtained by subduction of $\bar{\Gamma}_r$ to $\mathfrak{S}_n$.

Because the induction from $\mathfrak{S}_{n(r+)} \times \mathfrak{S}_{n(r-)}$ to $\mathfrak{S}_n$ is known [5a, 7], we need only reverse this process to induce from $\mathfrak{S}_n$ to $\bar{\mathfrak{S}}_n$. By a slight modification we get the step we want, the induction from $\mathfrak{S}'_n$ to $\bar{\mathfrak{S}}_n$.

The representation $[\Gamma_r]^{\bar{\mathfrak{S}}_n}$ of $\bar{\mathfrak{S}}_n$ regularly induced by Γ_r of $\mathfrak{S}_n$ is constructed as follows:

We fill a single diagram $\gamma^{(r)}$ containing n boxes with κ_1 symbols 1, κ_2 symbols 2, $\cdots \kappa_t$ symbols t subject to the conditions $\kappa_1 \geqq \kappa_2 \geqq \cdots \kappa_t$ and $\kappa_1 + \kappa_2 + \cdots + \kappa_t \leqq \frac{n}{2}$ in such a way that

1) No two symbols of the same kind may be in the same column.

2) When all the boxes containing the symbol t are removed the remaining boxes constitute a diagram; it must remain so when all boxes with t and $t-1$ are removed etc.

3) Reading from right to left along the rows, beginning with the top row and working down, one must get a "lattice permutation" of 111...22.... That is, at each point one must have read at least as many 1's as 2's, as many 2's as 3's, etc. For each way of doing this, the induced representation contains an irreducible representation whose (+) diagram is the diagram of empty boxes and whose (−) diagram has rows of lengths $\kappa_1, \kappa_2, \ldots, \kappa_t$. If the plus and minus diagram are of different order, the induced representation also contains a second irreducible representation corresponding to a two-part diagram in which the plus and minus diagrams are interchanged, otherwise not[3].

The induction from $\mathfrak{S}'_n$ to $\bar{\mathfrak{S}}_n$ is the same, except that the induced diagram pairs reduce to those with an even or odd number of boxes in the negative part according as the inducing representation is Γ_{rg} or Γ_{ru}.

In Fig. 3, we give an example of the induction from $\mathfrak{S}_7$ to $\bar{\mathfrak{S}}_7$.

With reference to the inducing process from $\mathfrak{S}'_7$ we must distinguish between the indices of the inducing representation g or u and consequently ignore induced diagram pairs with an odd or even number of boxes in the minus component. Thus, referring to Fig. 3, if the inducing representation of $\mathfrak{S}'_7$ is $(3, 2, 2)_u$, we obtain only the representations under column (u) in the figure; if it is $(3, 2, 2)_g$ we get only those in column (g).

---

[3] If the two parts are of the same order, but are not identical, there is always another allowed way of filling in the symbols which leads to the diagram pair with interchanged signs. The prescription as stated prevents this from being counted twice.

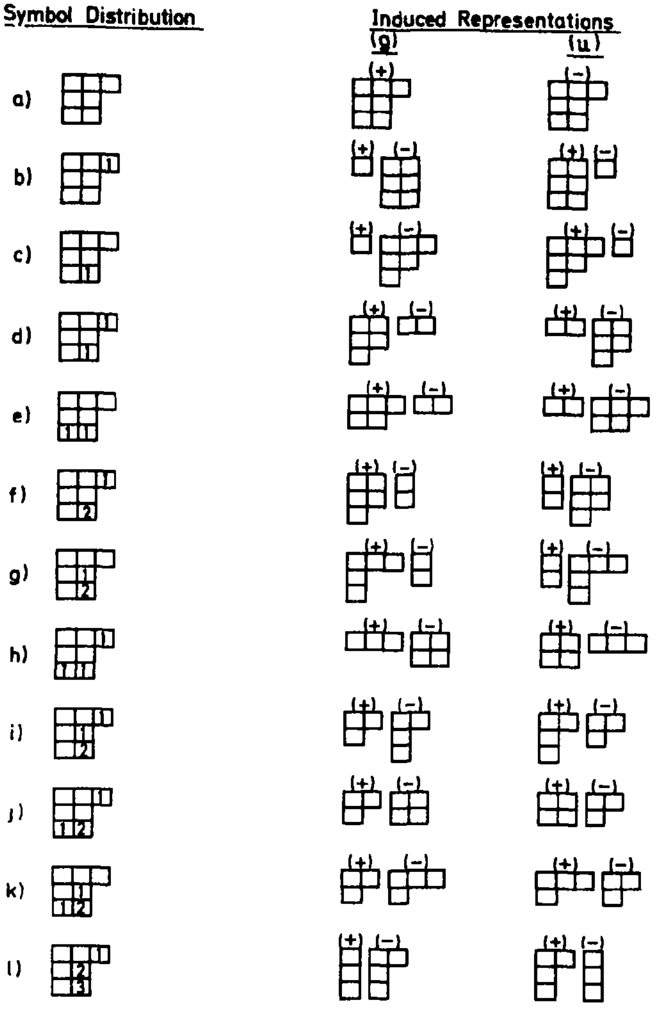

Fig. 3

C. Remainder Diagrams and the Transfer Condition

In Ref. [10], the investigation of active ligand partitions, and of other questions of physical importance, was greatly facilitated by studying the properties of the "partition lattice". In the present subsection, we lay the groundwork for an analogous treatment for the case of chiral ligands.

For single diagrams of order *n*, the partition lattice provides a very simple answer to the following question:

Consider two single diagrams of order *n*, $\gamma^{(r)}$ and $\gamma^{(l)}$, the boxes of the latter being filled with symbols 1 in the first row, 2 in the second, etc. Is it possible to transfer all the symbols into the boxes of $\gamma^{(r)}$ in such a way that no two like symbols appear in the same column? ("column condition", or "C-condition").

When this transfer is possible, we will say that the transfer condition (*T*-condition) is satisfied.

The answer to the question turned out to be: The *T*-condition is satisfied if and only if

$$\gamma^{(r)} \supset \gamma^{(l)}$$

($\gamma^{(r)}$ is greater than $\gamma^{(l)}$). The "greater" relation may be defined in three equivalent ways, viz:

i) $\gamma^{(r)} \supset \gamma^{(l)}$ if and only if $\gamma^{(l)}$ is obtained from $\gamma^{(r)}$ by moving boxes downward.

ii) Let ν_j denote the length of the j'th row of a diagram and

$$o_i = \sum_{j=1}^{i} \nu_j .$$

Then $\gamma^{(r)} \supset \gamma^{(l)}$ if and only if

$$o_i^{(r)} \geqq o_i^{(l)} \quad \text{for all } i.$$

iii) Let μ_j denote the length of the j'th column of a diagram and

$$u_i = \sum_{j=1}^{i} \mu_j .$$

Then $\gamma^{(r)} \supset \gamma^{(l)}$ if and only if

$$u_i^{(r)} \leqq u_i^{(l)} \quad \text{for all } i.$$

It is proved in Ref. [10] that these three definitions are equivalent, that the partial ordering of diagrams so defined is a lattice, and that this ordering has the stated relation to the *T*-condition.

As will become clear in the next Section, the appropriate generalization of the *T*-condition for our problem is the following:

Consider two two-part diagrams of order n, $\bar{\gamma}^{(r)}$ and $\bar{\gamma}^{(l)}$, the boxes of the latter being filled with symbols 1 in the first row, 2 in the second, etc., with the symbols in the minus part distinguished by primes. The "generalized *T*-condition" is said to be satisfied if all the symbols can be transferred into the boxes of $\bar{\gamma}^{(r)}$ in such a way that

1) No two like symbols appear in the same column of the same part of $\bar{\gamma}^{(r)}$ (primed and unprimed symbols being counted as different for this purpose); and

2) All the unprimed symbols are in the plus part of $\bar{\gamma}^{(r)}$ (though primed symbols may be in either part).

We now consider what properties the diagrams must have in order to satisfy this condition.

First, the plus part of $\bar{\gamma}^{(r)}$ must be able to accommodate all the unprimed symbols with no two like ones in the same column, though some boxes may be left unfilled. This means that the first row of $\gamma^{(r+)}$ must be long enough to accommodate all the 1's, the leftover boxes in the first row plus those in the second row enough for the 2's, etc. Continuing in this way, by reasoning exactly analogous to that used in Ref. [10] for single diagrams, one concludes that, to fulfill this part of the *T*-condition, it is necessary and sufficient that

$$o_i^{(r+)} \geqq o_i^{(l+)}, \text{ all } i.$$

Second, there must be enough different kinds of primed symbols to fill the first column of $\gamma^{(r-)}$, the unused ones plus those of which there are at least two must be enough to fill the second column, etc. Again, by reasoning analogous to that in [10], one concludes that this part of the *T*-condition is satisfied if and only if

$$u_i^{(r-)} \leqq u_i^{(l-)}, \text{ all } i.$$

The above two conditions are necessary, though not sufficient, for the *T*-condition. By means of them, we can define a "greater" relation for two-part diagrams which is analogous to the known one for ordinary diagrams, as follows:

We say that $\bar{\gamma}^{(r)} \supset \bar{\gamma}^{(l)}$ ($\bar{\gamma}^{(r)}$ greater than $\bar{\gamma}^{(l)}$) if

$$o_i^{(r+)} \geqq o_i^{(l+)}, \text{ all } i,$$

and

$$u_i^{(r-)} \leqq u_i^{(l-)}, \text{ all } i.$$

A second, equivalent, definition is: $\bar{\gamma}^{(r)}$ is greater than $\bar{\gamma}^{(l)}$ if and only if $\bar{\gamma}^{(l)}$ can be obtained from $\bar{\gamma}^{(r)}$ by moving boxes from the plus to the minus part, and/or downward within each part.

It is shown in Appendix 2.A that this partial ordering defines a lattice.

If $\bar{\gamma}^{(r)} \supset \bar{\gamma}^{(l)}$, then the above considerations show that we can transfer all the unprimed symbols into $\gamma^{(r+)}$, with no two like ones in the same column and $n_{rl} = n^{(r+)} - n^{(l+)} = n^{(l-)} - n^{(r-)}$ boxes remaining empty. Also, we can fill $\gamma^{(r-)}$ with primed symbols, no two like ones in the same column, with n_{rl} symbols not being used. In general, this partial transfer can be done in several different ways. The *T*-condition now will be satisfied if we can transfer the n_{rl} remaining unprimed symbols into the n_{rl} empty boxes with no two like symbols going into the same column. We can express this condition as a *T*-condition for ordinary diagrams as follows: First, form a diagram $\gamma^{(rl+)}$ of order n_{rl} whose column lengths are the numbers of empty boxes in the columns of $\gamma^{(r+)}$. Form another diagram $\gamma^{(rl-)}$ of order n_{rl} whose row lengths are equal to the numbers of unused primed symbols of each kind. These diagrams will be called remainder diagrams. In terms of them, the question of transferability of the unused symbols becomes: "Can all the symbols be transferred from $\gamma^{(rl-)}$ to $\gamma^{(rl+)}$ in such a way that no two symbols from the same row of $\gamma^{(rl-)}$ go into the same column of $\gamma^{(rl+)}$?" This, however, is just the ordinary *T*-condition for $\gamma^{(rl-)}$ into $\gamma^{(rl+)}$, and we know that it is satisfied if and only if $\gamma^{(rl+)} \supset \gamma^{(rl-)}$.

The remainder diagrams, however, are not uniquely determined, as the partial transfer of the symbols can in general be carried out in many ways. To satisfy the *T*-condition, we need only *one* way of doing the partial transfer which will make $\gamma^{(rl+)} \supset \gamma^{(rl-)}$. Since the two parts of the partial transfer are independent of each other, we can transfer the unprimed symbols into $\gamma^{(r+)}$ in such a way as to make $\gamma^{(rl+)}$ as large as possible, and similarly transfer the primed symbols so as to make $\gamma^{(rl-)}$ as small as possible. The possibility of doing this depends on the existence of a unique "largest remainder" for the transfer of the unprimed symbols, and a "smallest remainder" for the transfer of the primed symbols. In Appendix 2.B, it is shown that such unique largest and smallest remainders exist, and that they are constructed in the following way:

1) Largest Remainder: Given two diagrams $\gamma^{(a)}$ and $\gamma^{(b)}$, with $o_i^{(a)} \geq o_i^{(b)}$ for all i, the boxes in the first row of $\gamma^{(b)}$ being filled with 1's, the second row with 2's, etc. Transfer the symbols into the boxes of $\gamma^{(a)}$ one at a time, in any order, placing each symbol as far down as possible subject to the condition that it does not go into a column already occupied by a symbol of its own kind. If there are two or more boxes satisfying this condition and equally low down, choose the one farthest to the right. When all the symbols have been transferred, the unfilled boxes will be in diagram form without further rearrangement, and this diagram will be the largest remainder $\gamma_{\max}(\gamma^{(a)}, \gamma^{(b)})$.

The question of the smallest remainder $\gamma^{(rl-)}$ takes a completely analogous form if we reformulate it somewhat. Instead of transferring the symbols from $\gamma^{(l-)}$ into $\gamma^{(r-)}$, we imagine that the boxes of $\gamma^{(r-)}$ are transferred into $\gamma^{(l-)}$, with no two from the same column going into the same row of $\gamma^{(l-)}$. The symbols remaining uncovered by transferred boxes form the remainder. It is obvious that this is equivalent (as far as forming the remainder is concerned) to the formulation in terms of symbol transfer, and that it differs from the situation of (1) above only in the interchange of the roles of rows and columns. The construction of the smallest remainder is therefore carried out as follows:

2) Smallest Remainder: Given two diagrams, $\gamma^{(a)}$ and $\gamma^{(b)}$, with $u_i^{(a)} \geq u_i^{(b)}$ for all i, and with the first column of $\gamma^{(b)}$ filled with symbols 1, the second with 2's, etc. Transfer the symbols into the boxes of $\gamma^{(a)}$ one at a time, in any order, placing each symbol as far to the right as possible consistent with the condition that it not go into a row already occupied by a symbol of its own kind. If there are two or more allowed boxes equally far to the right, choose the one farthest down. When all the symbols have been transferred, the unfilled boxes will be in diagram form without further rearrangement, and this diagram will be the smallest remainder $\gamma_{\min}(\gamma^{(a)}, \gamma^{(b)})$.

Examples of largest and smallest remainder construction are shown in Fig. 4.

From the above discussion, we see immediately the criterion for satisfying the *T*-condition for $\bar{\gamma}^{(l)}$ into $\bar{\gamma}^{(r)}$. It is satisfied if and only if

$$1)\ \bar{\gamma}^{(r)} \supset \bar{\gamma}^{(l)} \text{ and}$$

$$2)\ \gamma_{\max}(\gamma^{(r+)}, \gamma^{(l+)}) \supset \gamma_{\min}(\gamma^{(l-)}, \gamma^{(r-)})\,.$$

We note that the *T*-condition is not transitive. For example, referring to Fig. 5, we see that the *T*-condition is satisfied for $\bar{\gamma}^{(3)}$ into $\bar{\gamma}^{(2)}$, and for $\bar{\gamma}^{(2)}$ into $\bar{\gamma}^{(1)}$, but not for $\bar{\gamma}^{(3)}$ into $\bar{\gamma}^{(1)}$.

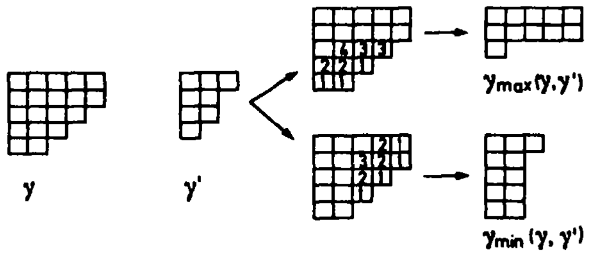

Fig. 4

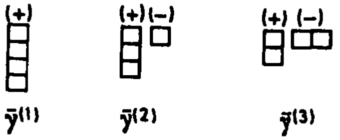

Fig. 5

In the case of $\mathfrak{S}'_n$, we have the partition lattice for $\mathfrak{S}_n$ twice, one containing all the diagrams with the index g, the other those with index u. If we allow transfer between diagrams no matter what the index, the T-condition reduces to

$\gamma^{(r)} \supset \gamma^{(l)}$ neglecting the indices g, u.

3. Active Ligand Partitions

According to the statements in the end of Section 1 and the technique developed in Section 2 we can construct qualitatively complete chirality functions for classes of molecules with chiral ligands. Approximate ansaetze for such chirality functions according to the first and second methods, of Ref. [10], shortened ansaetze for subclasses, specifications of classes according to the minimum-interaction between ligands needed for physical pseudoscalar phenomena, and other related matters, discussed in [10] for achiral ligands may be best understood on the basis of a discussion of "active ligand partitions" and their representation in the partition lattice. Analogous results in our case will be found discussing these questions with reference to chiral ligands. A ligand partition specifies the number of each type of equivalent ligands. For achiral ligands, equivalent means identical in its configuration, for chiral ligands equivalence is defined as including ligands which are identical or enantiomers. The reason for this definition will become obvious later. A ligand partition according to this definition may be characterized by a two-part diagram $\bar{\gamma}^{(l)}$ where the numbers of boxes in rows correspond to the numbers of equivalent ligands, achiral ligands being represented by $\gamma^{(l+)}$ and chiral ones by $\gamma^{(l-)}$. We denote with $L^{(l)}$ an ordered molecule with a ligand assortment belonging to the partition $\bar{\gamma}^{(l)}$.

We call a partition $\bar{\gamma}^{(l)}$ *active* if there is at least one chiral ordered molecule $L^{(l)}$. It is said to be active with respect to an ensemble operator $\mathscr{a}$ if there is an $L^{(l)}$ such that $\mathscr{a}\, L^{(l)}$ is not racemic. Recalling that negative coefficients in $\mathscr{a}$ are to be interpreted in terms of positive concentrations of enantiomers, we see that the statement that the mixture is not racemic means formally

$$\mathscr{p}_\chi \mathscr{a}\, L^{(l)} \neq 0\,,$$

i.e., the total coefficient of each particular ordered molecule in $\mathscr{p}_\chi \mathscr{a}\, L^{(l)}$ is formally not equal to zero. Conversely, the mixture is racemic if

$$\mathscr{p}_\chi \mathscr{a}\, L^{(l)} = 0\,.$$

Each ensemble operator $\mathscr{a}$ can be expressed as an achiral component plus a sum of terms of the form $\mathscr{p}_\chi \bar{\mathscr{p}}^{(r)} \mathscr{a}$, where $\bar{\mathscr{p}}^{(r)}$ is the projection operator onto an irreducible representation $\bar{\Gamma}_r$ with $z_r \neq 0$. We call $\bar{\gamma}^{(l)}$ "$\bar{\Gamma}_r$-active" if there is an $L^{(l)}$ with $\not{p}_\chi \bar{\not{p}}^{(r)} L^{(l)} \neq 0$. Obviously, $\bar{\gamma}^{(l)}$ is active with respect to a if and only if it is $\bar{\Gamma}_r$-active for some $\bar{\Gamma}_r$ with $\not{p}_\chi \bar{\not{p}}^{(r)} a \neq 0$. Equally obviously, it is active if it is $\bar{\Gamma}_r$-active for some $\bar{\Gamma}_r$. Hence, essentially all questions about active ligand partitions are answered if we can decide when a partition $\bar{\gamma}^{(l)}$ is $\bar{\Gamma}_r$-active.

We note that an ordered molecule $L^{(l)}$ is left invariant by the following operations:

(1) Permutation of any two identical ligands.

(2) Permutation of any two enantiomeric ligands followed by site reflections applied to both.

(3) Site reflections applied to achiral ligands.

Since the projection $\bar{\not{p}}^{(r)}$ can be built up out of the Young operators $\bar{\mathscr{Y}}^{(r)}$, we can study the question of $\bar{\Gamma}_r$-activity by studying the effect of the $\bar{\mathscr{Y}}^{(r)}$ (considered formally as ensemble operators) on $L^{(l)}$. Consider an arbitrary one of the $\bar{\mathscr{Y}}^{(r)}$, belonging to the tableau $\bar{t}^{(r)}$. The operator $\bar{\mathscr{Y}}^{(r)}$ antisymmetrizes with respect to the following operations:

(1) Permutation of any two ligands located on sites in the same column of $\bar{t}^{(r)}$.

(2) Site reflection on any site located in $t^{(r-)}$.

(3) Permutation of any two ligands located in the same column of $\bar{t}^{(r)}$ followed by site reflection applied to both.

Thus, if $L^{(l)}$ has any two identical or equivalent ligands on sites in the same column of $\bar{t}^{(r)}$, or any achiral ligand in a site located in $t^{(r-)}$, then $\bar{\mathscr{Y}}^{(r)}$ will antisymmetrize with respect to at least one operation which leaves $L^{(l)}$ invariant, and we have $\bar{\mathscr{Y}}^{(r)} L^{(l)} = 0$. If this is not the case, $\bar{\mathscr{Y}}^{(r)} L^{(l)} \neq 0$.

Thus, there will be an $L^{(l)}$ with $\bar{\mathscr{Y}}^{(r)} L^{(l)} \neq 0$ if and only if it is possible to distribute the symbols from $\bar{\gamma}^{(l)}$ among the sites in such a way that no symbol from $\gamma^{(l+)}$ goes into a site in $t^{(r-)}$ and no two symbols from the same row of $\bar{\gamma}^{(l)}$ go into sites in the same column of $\bar{t}^{(r)}$. This, however, is just the T-condition for $\bar{\gamma}^{(l)}$ into $\bar{\gamma}^{(r)}$. If the condition is not fulfilled, we have $\bar{\mathscr{Y}}^{(r)} L^{(l)} = 0$ for all $\bar{\mathscr{Y}}^{(r)}$ and $L^{(l)}$. If the condition is fulfilled, then for each $\bar{\mathscr{Y}}^{(r)}$ there is an $L^{(l)}$ such that $\bar{\mathscr{Y}}^{(r)} L^{(l)} \neq 0$. Since $\not{p}_\chi$ cannot be orthogonal to all the $\bar{\mathscr{Y}}^{(r)}$, it follows that, if the T-condition is satisfied, there is also an $L^{(l)}$ with $\not{p}_\chi \bar{\not{p}}^{(r)} L^{(l)} \neq 0$, and we conclude that $\bar{\gamma}^{(l)}$ is $\bar{\Gamma}_r$-active.

Summarizing, we have found that a necessary and sufficient condition for $\bar{\gamma}^{(l)}$ to be $\bar{\Gamma}_r$-active is that the T-condition be satisfied for $\bar{\gamma}^{(l)}$ into $\bar{\gamma}^{(r)}$, i.e. that

$$\bar{\gamma}^{(r)} \supset \bar{\gamma}^{(l)}$$

and

$$\gamma_{\max}(\gamma^{(r+)}, \gamma^{(l+)}) \supset \gamma_{\min}(\gamma^{(l-)}, \gamma^{(r-)}) .$$

4. $\mathscr{L}$- and $\mathscr{C}$-Partitions and the Corresponding Decomposition of Chirality Functions

In contrast to the case in which all ligands are required to be achiral, in the present case we have chirality functions which are the same for all permutational isomers, and which are present for all molecular skeletons. To study their

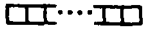

Fig. 6

properties, we note that the representation Γ_{1_u} of $\mathfrak{S}'_n$, whose diagram is shown in Fig. 6, always has $z_{1_u} = 1$, regardless of the skeleton. For the representation is one-dimensional, so z_{1_u} cannot be greater than one. On the other hand, the representation is symmetric under all $\jmath \in \mathfrak{S}_n$, in particular under those in $\mathfrak{N}$, and antisymmetric under all $\tau_0 \jmath$, in particular those in $\tau_0 \jmath' \mathfrak{N}$, so it follows that it contains Γ_χ. Moreover, Γ_{1_g} is symmetric under the elements of $\tau_0 \jmath' \mathfrak{N}$, so that always $z_{1_g} = 0$. We conclude, then, that there are always chirality functions belonging to the totally symmetric representation of $\mathfrak{S}_n$, all of these belonging to Γ_{1_u} of $\mathfrak{S}'_n$. We call these functions $\mathscr{L}$-chirality functions (ligand specific), since they arise purely from the chirality of the ligands, and are independent of the nature of the skeleton and of the distribution of the ligands among the sites.

If we define the projection operators

$$\wp_{\mathscr{L}} = \frac{1}{n!} \sum_{\jmath \in \mathfrak{S}_n} \jmath$$

and

$$\wp_{\mathscr{C}} = \iota - \wp_{\mathscr{L}},$$

then we can decompose any chirality function into independent components as follows:

$$\phi(|L) = \phi(\wp_{\mathscr{L}}|L) + \phi(\wp_{\mathscr{C}}|L).$$

The functions $\phi(\wp_{\mathscr{C}}|L)$ will be referred to as class-specific, or $\mathscr{C}$-chirality functions. Unlike the $\mathscr{L}$-chirality functions $\phi(\wp_{\mathscr{L}}|L)$, they depend on the nature of the skeleton. Because the operator $\not{p}_\chi \not{P}^{(r)}$ commutes with $\wp_{\mathscr{L}}$, this decomposition is compatible with the decomposition according to representations of $\bar{\mathfrak{S}}_n$.

The designation of a chirality function as $\mathscr{L}$ or $\mathscr{C}$, it is to be noted, refers to the representation of $\mathfrak{S}'_n$ to which it belongs, not to that of $\bar{\mathfrak{S}}_n$. The two, however, are not independent. According to the induction procedure of Section 2.B, the representations of $\bar{\mathfrak{S}}_n$ induced by Γ_{1_u} are:

$$(n-1;1), (n-3;3), \ldots.$$

There is always one $\mathscr{L}$-chirality function belonging to each of these representations, and there may be $\mathscr{C}$-chirality functions as well, depending on the skeleton. Chirality functions belonging to other representations are always $\mathscr{C}$-chirality functions.

Thus, for any $\bar{\Gamma}_r$ with $z_r \neq 0$, we may express z_r as a sum

$$z_r = z_r^{\mathscr{L}} + z_r^{\mathscr{C}}.$$

For the representations listed above, we always have $z_r^{\mathscr{L}} = 1$, $z_r^{\mathscr{C}} = z_r - 1$. For all other representations, we have $z_r^{\mathscr{L}} = 0$, $z_r^{\mathscr{C}} = z_r$.

It is easy to see that $\mathscr{L}$-chirality functions vanish identically if the ligand assortment is racemic, i.e., if the ligands are all either achiral or pairwise enantiomeric.

5. Chirality Numbers

By means of the T-condition, we may easily determine maximum numbers for identical or equivalent ligands and minimum numbers for types of nonequivalent ligands in molecules with $\bar{\Gamma}_r$-active ligand partitions $\bar{\gamma}^{(l)}$. This means, if any one of these numbers is exceeded or not reached respectively, then $\phi(\mathscr{F}^{(r)}|L^{(l)})$ vanishes even if the molecule is chiral and the isomer mixture $\mathscr{F}^{(r)}\,a\,L$ becomes racemic.

We need only the relation $\bar{\gamma}^{(r)}\supset\bar{\gamma}^{(l)}$ to derive the following relations for the lengths of first columns and rows.

$$o_1^{(r+)}\geqq o_1^{(l+)},\ u_1^{(r-)}\leqq u_1^{(l-)},\ o_1^{(r+)}+o_1^{(r-)}\geqq o_1^{(l-)},\ \max(u_1^{(r+)},u_1^{(r-)})\leqq u_1^{(l+)}+u_1^{(l-)}.$$

All these limiting numbers are attained in at least one $\bar{\Gamma}_r$-active partition; the first and the second inequalities become equalities for $\bar{\gamma}^{(r)}=\bar{\gamma}^{(l)}$ representing a $\bar{\Gamma}_r$-active partition. The third and fourth inequalities become equalities for the diagram $\bar{\gamma}^{(l)}$ whose plus part vanishes and whose minus part consists of the columns of $\gamma^{(r+)}$ and $\gamma^{(r-)}$ properly ordered. It is active as it is smaller than $\bar{\gamma}^{(r)}$ and $\max(\gamma^{(r+)},\gamma^{(l+)})=\bar{\gamma}^{(r)}\supset\min(\gamma^{(r-)},\gamma^{(l-)})$. Therefore we may conclude that for $\bar{\Gamma}_r$-active molecules

$o_1^{(r+)}$ is the maximum number of identical achiral ligands

$o_1^{(r+)}+o_1^{(r-)}$ is the maximum number of equivalent chiral ligands

$u_1^{(r-)}$ is the minimum number of inequivalent chiral ligands

$\max(u_1^{(r+)},u_1^{(r-)})$ is the minimum number of inequivalent ligands.

Each of these numbers occur in at least one $\bar{\Gamma}_r$-active ligand partition.

By forming the maxima or minima respectively of these quantities, the extrema being taken over all r with $z_r^{\mathscr{C}}\neq 0$, we get chirality numbers which are characteristic properties of the frame. It should be emphasized that the condition is $z_r^{\mathscr{C}}\neq 0$ and not $z_r\neq 0$ because the latter would only lead to trivial numbers which express the fact that a ligand partition is active for any achiral frame if it contains at least one chiral ligand. The non-trivial numbers we want should present information about the pseudoscalar properties of the particular molecular class in question. We find these "chirality numbers" from the following maxima and minima:

$$\left.\begin{array}{lll}\text{chirality order} & o^{+} & =\max\,\{o_1^{(r+)}\}\\ & o & =\max\,\{o_1^{(r+)}+o_1^{(r-)}\}\\ \text{chirality index} & u & =\min\,\{u_1^{(r-)}\}\\ & \bar{u} & =\min\,\{\max(u_1^{(r+)},u_1^{(r-)})\}\end{array}\right\}\ \begin{array}{l}\text{maxima and minima are to be}\\ \text{taken over all } r \text{ with } z_r^{\mathscr{C}}\neq 0.\end{array}$$

We call a molecule $\mathscr{C}$-chiral if its pseudoscalar property depends on the particular frame with its sites and not only on the composition of the ligand assortment, i.e., if it possesses a nonvanishing $\mathscr{C}$-chirality function. Correspondingly we call a ligand partition $\mathscr{C}$-active if there are $\mathscr{C}$-chiral molecules belonging to this ligand partition. Now we may formulate the meaning of the chirality numbers as follows:

- o^+ is the maximum number of identical achiral ligands which may be present in a $\mathscr{C}$-chiral molecule.
- o is the maximum number of equivalent ligands which may be present in a $\mathscr{C}$-chiral molecule.
- u^- is the minimum number of inequivalent chiral ligands which must be present in a $\mathscr{C}$-chiral molecule.
- $\bar{u}$ is the minimum number of inequivalent ligands which must be present in a $\mathscr{C}$-chiral molecule.

In a "chiral class" which by definition contains chiral molecules with exclusively achiral ligands, all these chiral molecules are $\mathscr{C}$-chiral. In an "achiral class" the chirality is only due to $\mathscr{L}$-chirality. Therefore, we have for any class

$$u^- = 0 .$$

For chiral classes we have proved in Ref. [10], under the restriction to achiral ligands, that the chirality order has the lower limit $n-3$ and the upper limit n which characterizes chiral skeletons. If chiral ligands are admitted we have the relation $o > o^+$ and therefore the same limits for o.

$$n-3 \leqq o \leqq n$$

6. Explicit Forms of Qualitatively Complete Chirality Functions

A. General Remarks

The general form of a qualitatively complete chirality function is

$$\phi(\,|L) = \sum_{r}^{z_r \neq 0} \phi(\bar{\mathscr{F}}^{(r)}|L)$$

where the irreducible representation $\bar{\Gamma}_r$ is induced z_r-times by the component $\phi(\bar{\mathscr{F}}^{(r)}|L)$.

According to Ref. [10], Section 2, we may achieve the required property of $\phi(\bar{\mathscr{F}}^{(r)}|L)$ starting with a set of functions $\omega_\varrho^{(r)}(\,|L)$, $\varrho = 1, 2, \ldots t_r$ for which $\bar{\mathscr{F}}^{(r)}\omega_\varrho^{(r)}(\,|L)$ does not vanish. Let the choice be such that the operator $\bar{\mathscr{Y}}^{(r)}$ does not annihilate $\omega_\varrho^{(r)}(\,|L)$ and denote the resulting projection with $\psi_\varrho^{(r)}(\,|L)$. In this section, Young operators without subscripts refer to the book tableau.

$$\bar{\mathscr{Y}}^{(r)}\omega_\varrho^{(r)}(\,|L) = \psi_\varrho^{(r)}(\,|L) \quad \text{and} \quad \omega_\varrho^{(r)}(\sigma|L) = \bar{\mathscr{Y}}_\sigma^{(r)}\omega_\varrho^{(r)}(\sigma|L) \triangleq \psi_\varrho^{(r)}(|\sigma L) .$$

Then, a component $\phi(\bar{\mathscr{F}}^{(r)}|L)$ with the desired properties is constructed by a sum of expressions

$\mathscr{P}_\chi\psi_\varrho^{(r)}(\jmath|L)$ with properly chosen ϱ and $\jmath \in \mathfrak{S}_n$[4].

These expressions, being chirality functions as well, are obviously again linear combinations of $\omega_\varrho^{(r)}(\sigma|L)$ with a given ϱ and some elements $\sigma \in \mathfrak{S}_n'$. $\psi_\varrho^{(r)}(\,|L)$ refers to the book tableau of $\bar{\gamma}^{(r)}$ and the ordered molecule (1) of Sect. 1. It transforms under site reflections as follows:

---

[4] Note that even here the group elements may be chosen to be pure permutations. This follows from the form of the projection operator $\mathscr{F}^{(r)}$ where the sum index is also confined to elements of $\mathfrak{S}_n$.

$$\mathscr{C}(\tau_i)\,\psi_\varrho^{(r)}(\,|L) \begin{array}{l} = +\psi_\varrho^{(r)}(\,|L) \text{ if } 1 \leqq i \leqq n^{(r+)} \\ = -\psi_\varrho^{(r)}(\,|L) \text{ if } n^{(r+)}+1 \leqq i \leqq n\,. \end{array}$$

Without loss of generality we may define a pseudoscalar function $\kappa(\ell_i)$ for single ligands, i.e.,

$$\mathscr{C}(\tau_i)\,\kappa(\ell_i) = \kappa(\ell_i^*) = -\kappa(\ell_i)$$

and write $\psi_\varrho^{(r)}(|L)$ in the form

$$\psi_\varrho^{(r)}(\,|L) = \kappa(\ell_{n^{(r+)}+1})\cdots\kappa(\ell_n)\,\bar{\varphi}_\varrho^{(r)}(\,|L)$$

where $\bar{\varphi}_\varrho^{(r)}(\,|L)$ satisfies the relation $e^{(r+)}a^{(r+)}e^{(r-)}a^{(r-)}\bar{\varphi}_\varrho^{(r)}(\,|L) = \bar{\varphi}_\varrho^{(r)}(\,|L)$ and is symmetric under all site reflections. From $\bar{\mathscr{Y}}^{(r)}\omega_\varrho^{(r)}(\,|L) = \psi_\varrho^{(r)}(\,|L)$ it follows that the same decomposition may be chosen for $\omega_\varrho^{(r)}(\,|L)$

$$\omega_\varrho^{(r)}(|L) = \prod_{i=n^{(r+)}+1}^{n} \kappa(\ell_i)\cdot\bar{\omega}_\varrho^{(r)}(|L)\,,$$

$\bar{\omega}_\varrho^{(r)}(|L)$ being invariant under site reflections and $e^{(r+)}a^{(r+)}e^{(r-)}a^{(r-)}\bar{\omega}_\varrho^{(r)} = \bar{\omega}_\varrho^{(r)}$. Since the above decomposition is always permissible we shall use it for the two approximate procedures of [10] which will be generalized in Section B and C. Two further remarks are worth making beforehand:

1) $\kappa(\ell_i)$ may, in principle, be chosen quite arbitrarily, though a particular choice may recommend itself in certain cases or for specific purposes. There is no need to use the same κ for different equivalent or inequivalent representations Γ_r.

2) Without loss of generality we have expressed the pseudoscalar ligand properties by *one* pseudoscalar ligand parameter κ. On the other hand, $\psi_\varrho^{(r)}(\ell_1\cdots\ell_n)$, which is a function of the scalar properties of the ligands, does not necessarily depend on values of single ligand parameters only. Rather, this is an additional postulate, which we use for an approximate type of qualitatively complete chirality function as outlined in subsection B.

B. First Procedure: Polynomials of Lowest Degree

We use the form (1) for $\omega_\varrho^{(r)}(|L)$ and choose $\bar{\omega}_\varrho^{(r)}(|L)$ to depend only upon values of a one-parameter achiral property of the single ligands $\lambda(\ell_i)$ and being a polynomial of lowest degree in $\lambda(\ell_i)$ such that the operator $e^{(r+)}a^{(r+)}e^{(r-)}a^{(r-)}$ does not annihilate $\bar{\omega}_\varrho^{(r)}(|L)$. Because this operator is the product of two commuting operators $e^{(r+)}a^{(r+)}$ and $e^{(r-)}a^{(r-)}$, for single tableaux of $\gamma^{(r+)}$ and $\gamma^{(r-)}$, we may choose $\bar{\omega}_\varrho^{(r)}(\,|L)$ as in Ref. [10] and we choose $\bar{\varphi}_\varrho^{(r)}(\,|L)$ to be a polynomial of lowest possible degree in the $\lambda(\ell_i)$. For this purpose we start with a polynomial

$$\omega(|L) = \prod_{i=n^{(r+)}+1}^{n} \kappa(\ell_i)\,\bar{\omega}(\lambda(\ell_1)\cdots\lambda(\ell_n))$$

which is of lowest degree $g^{(r)}$ in $\lambda(\ell_i)$ such that $\bar{\mathscr{Y}}^{(r)}\omega_\varrho^{(r)}(\,|L)$ does not vanish. The operator $e^{(r+)}a^{(r+)}e^{(r-)}a^{(r-)}$ in the equation $e^{(r+)}a^{(r+)}e^{(r-)}a^{(r-)}\bar{\omega}_\varrho^{(r)}(|L) = \psi_\varrho^{(r)}(|L)$ is the product of two commuting Young operators $e^{(r+)}a^{(r+)}$ and $e^{(r-)}a^{(r-)}$ for the single tableaux of $\gamma^{(r+)}$ and $\gamma^{(r-)}$. Therefore we may choose $\bar{\omega}_\varrho^{(r)}(|L)$ as in

Ref. [10] as a monomial in $\lambda(\ell_i)$ where each $\lambda(\ell_i)$ occurs in the $(i-1)$th power if i is the row number in $\gamma^{(r+)}$ or $\gamma^{(r-)}$. As we concluded from [10], this is a monomial of lowest degree which does not vanish when $\mathscr{s}^{(r+)}a^{(r+)}\mathscr{s}^{(r-)}a^{(r-)}$ is applied. Its degree is

$$g^{(r)} = \sum_{i=1}^{n} (i-1)\,(v_i^{(r+)} + v_i^{(r-)})\,.$$

The application of $\bar{\mathscr{Y}}^{(r)}$ on $\omega_\varrho^{(r)}$ leads therefore to the homogeneous polynomials

$$\bar{\mathscr{Y}}^{(r)}\omega_\varrho^{(r)}(\,|L) = \psi_\varrho^{(r)}(\,|L) = \prod_{i=n^{(r+)}+1}^{n} \kappa(\ell_i)\,\bar{\psi}_\varrho^{(r)}(\,|L)\,.$$

They are of degree $n^{(r-)}$ in κ and $g^{(r)}$ in $\lambda(\ell_i)$, and this is also true for the chirality functions $\mathscr{P}_\chi\psi_\varrho^{(r)}(\sigma\,|L)$ which can be used according to Ref. [10] to construct $\phi(\bar{\mathscr{F}}^{(r)}|\,L)$ with the required properties.

Exactly as in [10], it can be proved that a polynomial of lowest degree induces $\bar{\Gamma}_r$ only once. Therefore, we need z_r polynomials depending upon different types of parameters $\lambda^{(1)}, \lambda^{(2)}, \ldots, \lambda^{(r)}$, but the $\kappa(\ell_i)$ may be chosen to be the same. The polynomial of lowest degree depends only upon differences of the scalar parameters. This is proved by introducing new variables $\xi_1 = \Sigma\lambda(\ell_i)$, $\xi_2 = \lambda(\ell_1) - \lambda(\ell_2), \ldots, \xi_n = \lambda(\ell_{n-1}) - \lambda(\ell_n)$ and from the fact (which follows from the symmetry) that ξ_1 must occur as a factor of the polynominal if present at all. One infers as in [10] that ξ_1 does not occur if the degree is the lowest. We denote the qualitatively complete chirality function according to the first method with $\chi(\,|L)$.

C. Second Procedure: Linear Combinations of Functions Depending on as Few Ligands as Possible

In this subsection, we do not restrict the number of scalar parameters for single ligands, but we postulate that $\omega_\varrho^{(r)}(\,|L)$ depends on as few ligands as possible, again using the form:

$$\omega_\varrho^{(r)}(\,|L) = \prod_{i=n^{(r+)}+1}^{n} \kappa(l_i)\,\bar{\omega}_\varrho^{(r)}(\,|L)\,.$$

This postulate implies a minimum number of ℓ_i occurring in $\bar{\omega}_\varrho^{(r)}(\,|L)$. Assume $\bar{\omega}_\varrho^{(r)}(\,|L)$ depending on h ligands; then it is certainly totally symmetric under permutations among the remaining $n-h$ ligands. Because $\mathscr{s}^{(r+)}a^{(r+)}\mathscr{s}^{(r-)}a^{(r-)}\bar{\omega}_\varrho^{(r)}(\,|L)$ is antisymmetrical with respect to permutations within columns, ligands which do not occur in $\bar{\omega}_\varrho^{(r)}(\,|L)$ must all be in different columns. From this it follows that

$$v_1^{(r+)} + v_1^{(r-)} \geqq h\,,$$

where, if h denotes the minimum number, the equal sign is to be taken. Consequently, $\bar{\omega}_\varrho^{(r)}(\,|L)$ depends upon at least $n - v_1^{(r+)} - v_1^{(r-)}$, $\omega_\varrho^{(r)}(\,|L)$ depends therefore upon $h(r) = n - v_1^{(r+)}$ ligands and the chirality functions $\mathscr{P}_\chi\phi_\varrho^{(r)}(\sigma\,|L)$ are linear combinations of functions depending upon $h(r) = n - v_1^{(r+)}$ ligands each. They can be used to construct the components $\phi(\bar{\mathscr{F}}^{(r)}|L)$ of a qualitatively complete chirality function $\tilde{\chi}(\,|L)$ according to the second procedure outlined in Ref. [10].

Because all components of $\tilde{\chi}(|L)$ depend on a minimum number $k^{(r)}$ of ℓ_i, which cannot be decomposed into sums of functions depending on fewer variables, $k^{(r)}$ is the minimum number of ligands between which interaction has to be taken into account in order to describe the phenomenon due to $\bar{\Gamma}_r$. Recalling the chirality numbers we conclude:

> $k=n-o^+$ is the minimum interaction between ligands to be taken into account in order to describe pseudoscalar phenomena on the class in question. Of course, a qualitatively complete description also necessitates, in general, components with higher interactions.

Because of the bounds on o^+, the number k has one of the values 1, 2 or 3. This is a very useful aspect for general statements about properties of classes as pointed out in [10], or for the quantum mechanical treatment of special pseudoscalar phenomena such as the optical rotatory power shown in [3] and [4].

7. Examples

Some examples may help to make the derived results clearer. In connection with special classes (examples B, C, and D) we give the partition lattices for two, three and four sites. The chosen numbering of diagrams is arbitrary but allows one to design the representations of $\bar{\mathfrak{S}}_n$ correspondingly. With reference to given classes, all diagram pairs with $z_r^{\mathscr{C}} \neq 0$ are shaded, those for which $z_r^{\mathscr{L}} \neq 0$ have a heavy border. The induction from $\mathfrak{S}'_n$ to $\bar{\mathfrak{S}}_n$ is presented for all those diagrams of $\mathfrak{S}'_n$ which correspond to irreducible representations of $\mathfrak{S}'_n$ containing Γ_χ. In the discussed examples Γ_χ is contained only once and the induction from a given Γ' to $\bar{\mathfrak{S}}_n$ delivers each induced representation of $\bar{\mathfrak{S}}_n$ only once as well. Therefore these numbers are not mentioned. In example *D* a representation of $\bar{\mathfrak{S}}_n$ is induced from two different representations of $\mathfrak{S}'_n$. The corresponding two components for chirality functions are adapted to the originating representations of $\mathfrak{S}'_n$. The advantage of this choice becomes clear from the comparison of the T_d and D_{2d}-frame, where one of both components of D_{2d} vanishes in the T_d case.

A) $\mathscr{L}$-chirality Functions

$\mathscr{L}$-chirality functions are functions transforming according to Γ_{1u} of $\mathfrak{S}'_n$ represented by the diagram $(n)^{(u)}$. The induced representations of $\bar{\mathfrak{S}}_n$ correspond to the diagram pairs $[(n-1)^{(+)}, 1^{(-)}]$; $[(n-3)^{(+)}, 3^{(-)}]$ and so on. Because the component diagrams have not more than one row, we find with help of the derived formulas for the order $g^{(r)}$ of the polynomials and for the minimum number $h^{(r)}$ that $\bar{\omega}(|L)$ according to both methods becomes a constant. Both methods lead therefore to identical chirality functions

$$\begin{tikzcd}
 & \{(n-1)^{(+)}, (1)^{(-)}\} \leftrightarrow \sum\limits_{i=1}^{n} \kappa(\ell_i) \\
(n)^u \arrow[ur] \arrow[r] \arrow[dr] \arrow[ddr] & \{(n-3)^{(+)}, (3)^{(-)}\} \leftrightarrow \sum\limits_{i<j<k}^{i,n} \kappa(\ell_i)\kappa(\ell_j)\kappa(\ell_k) \\
 & \cdots\cdots\cdots\cdots \\
 & \cdots\cdots\cdots\cdots
\end{tikzcd}$$

B) Frame with Two Sites, Skeleton Symmetry C_s *Fig. 7, Induction Fig. 8, Partition Lattice for* $\bar{\mathfrak{S}}_2$ *Fig. 9*

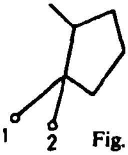

Fig. 7

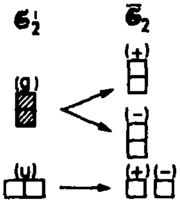

Fig. 8

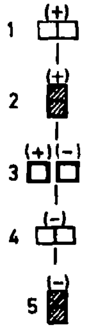

Fig. 9

$$\tilde{\chi}(\mathcal{F}^{(2)}|L) = \chi(\mathcal{F}^{(2)}|L) = \lambda(1) - \lambda(2)$$

$$\tilde{\chi}(\mathcal{F}^{(5)}|L) = \chi(\mathcal{F}^{(5)}|L) = \kappa(1)\,\kappa(2)\,[\lambda(1) - \lambda(2)]$$

$$\tilde{\chi}(\mathcal{F}^{(3)}|L) = \chi(\mathcal{F}^{(3)}|L) = \kappa(1) + \kappa(2)$$

C) Frame with Three Sites, Skeleton Symmetry C_{3v} *Fig. 10, Induction Fig. 11, Partition Lattice for* $\bar{\mathfrak{S}}_3$ *Fig. 12*

$$\chi(\mathcal{F}^{(3)}|L) = [\lambda(1) - \lambda(2)]\,[\lambda(1) - \lambda(3)]\,[\lambda(2) - \lambda(3)]$$

$$\tilde{\chi}(\mathcal{F}^{(3)}|L) = \omega(1,2) + \omega(2,3) + \omega(3,1) \quad \text{with} \quad \omega(i,k) = -\omega(k,i)$$

$$\begin{aligned}\tilde{\chi}(\mathcal{F}^{(7)}|L) &= \chi(\mathcal{F}^{(7)}|L)\\ &= \kappa(1)\,\kappa(2)\,[\lambda(1) - \lambda(2)] + \kappa(2)\,\kappa(3)\,[\lambda(2) - \lambda(3)]\\ &\quad + \kappa(3)\,\kappa(1)\,[\lambda(3) - \lambda(1)]\end{aligned}$$

$$\tilde{\chi}(\mathcal{F}^{(4)}|L) = \chi(\mathcal{F}^{(4)}|L) = \kappa(1) + \kappa(2) + \kappa(3)$$

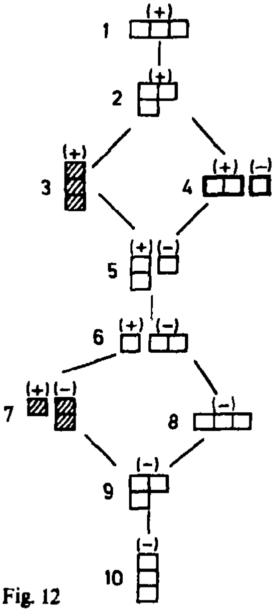

Fig. 12

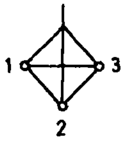

Fig. 10

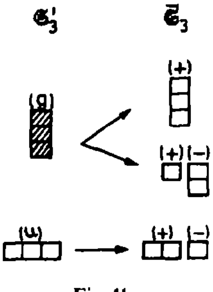

Fig. 11

D) Frame with Four Sites, Partition Lattice for $\mathfrak{S}_4$ Fig. 16

a) Skeleton symmetry D_{2d} Fig. 13, induction / / / / / shaded Fig. 15.
b) Skeleton symmetry T_d Fig. 14, induction \ \ \ \ \ shaded Fig. 15.

$$\chi(\mathcal{F}^{(3)}|L) = [\lambda(1) - \lambda(2)]\,[\lambda(3) - \lambda(4)]$$

$$\tilde{\chi}(\mathcal{F}^{(3)}|L) = \omega(1,3) - \omega(1,4) - \omega(2,3) + \omega(2,4)$$

with $\omega(i,k) = \omega(k,i)$

$$\begin{aligned}\chi_1(\mathcal{F}^{(13)}|L) = {} & 2[\kappa(1)\,\kappa(2) + \kappa(3)\,\kappa(4)]\,[\lambda(1) - \lambda(2)]\,[\lambda(3) - \lambda(4)] \\ & - [\kappa(1)\,\kappa(3) + \kappa(2)\,\kappa(4)]\,[\lambda(3) - \lambda(1)]\,[\lambda(2) - \lambda(4)] \\ & - [\kappa(1)\,\kappa(4) + \kappa(2)\,\kappa(3)]\,[\lambda(1) - \lambda(4)]\,[\lambda(2) - \lambda(3)]\end{aligned}$$

$$\begin{aligned}\tilde{\chi}_1(\mathcal{F}^{(13)}|L) = {} & 2[\kappa(1)\,\kappa(2) + \kappa(3)\,\kappa(4)]\,[\omega(1,3) - \omega(1,4) - \omega(2,3) + \omega(2,4)] \\ & - [\kappa(1)\,\kappa(3) + \kappa(2)\,\kappa(4)]\,[\omega(3,2) - \omega(3,4) - \omega(1,2) + \omega(1,4)] \\ & - [\kappa(1)\,\kappa(4) + \kappa(2)\,\kappa(3)]\,[\omega(1,2) - \omega(1,3) - \omega(4,2) + \omega(4,3)]\end{aligned}$$

with $\omega(i,k) = \omega(k,i)$

$$\tilde{\chi}(\mathcal{F}^{(9)}|L) = \chi(\mathcal{F}^{(9)}|L) = [\kappa(1) - \kappa(2)]\,[\kappa(3) - \kappa(4)]$$

$$\chi(\mathcal{F}^{(18)}|L) = \kappa(1)\,\kappa(2)\,\kappa(3)\,\kappa(4)\,[\lambda(1) - \lambda(2)]\,[\lambda(3) - \lambda(4)]$$

$$\tilde{\chi}(\mathcal{F}^{(18)}|L) = \kappa(1)\,\kappa(2)\,\kappa(3)\,\kappa(4)\,[\omega(1,3) - \omega(1,4) - \omega(2,3) + \omega(2,4)]$$

with $\omega(i,k) = \omega(k,i)$

$$\begin{aligned}\tilde{\chi}(\mathcal{F}^{(7)}|L) = \chi(\mathcal{F}^{(7)}|L) = {} & \kappa(1)\,[2\lambda(2) - \lambda(3) - \lambda(4)] + \kappa(2)\,[2\lambda(1) - \lambda(3) - \lambda(4)] \\ & + \kappa(3)\,[2\lambda(4) - \lambda(1) - \lambda(2)] + \kappa(4)\,[2\lambda(3) - \lambda(1) - \lambda(2)]\end{aligned}$$

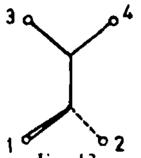

Fig. 13

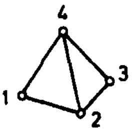

Fig. 14

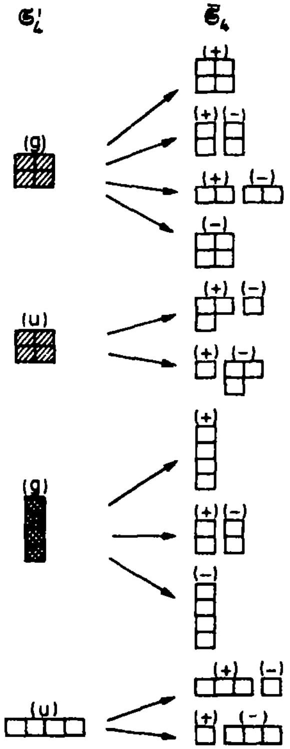

Fig. 15

$$\begin{aligned}\tilde{\chi}(\mathscr{F}^{(15)}|L) = \chi(\mathscr{F}^{(15)}|L) &= \kappa(1)\,\kappa(2)\,\kappa(3)\,[2\lambda(3)-\lambda(1)-\lambda(2)]\\ &\quad+\kappa(1)\,\kappa(2)\,\kappa(4)\,[2\lambda(4)-\lambda(1)-\lambda(2)]+\kappa(1)\,\kappa(3)\,\kappa(4)\,[2\lambda(1)\\ &\quad-\lambda(3)-\lambda(4)]+\kappa(2)\,\kappa(3)\,\kappa(4)[2\lambda(2)-\lambda(3)-\lambda(4)]\end{aligned}$$

$$\begin{aligned}\chi(\mathscr{F}^{(6)}|L) &= [\lambda(1)-\lambda(2)]\,[\lambda(1)-\lambda(3)]\,[\lambda(1)-\lambda(4)]\,[\lambda(2)-\lambda(3)]\,[\lambda(2)-\lambda(4)]\\ &\quad[\lambda(3)-\lambda(4)]\end{aligned}$$

$$\begin{aligned}\tilde{\chi}(\mathscr{F}^{(6)}|L) &= \omega(1,2,3)-\omega(1,2,4)+\omega(1,3,4)-\omega(2,3,4) \text{ with } \omega(i,k,l)\\ &\quad\text{totally antisymmetric}\end{aligned}$$

$$\begin{aligned}\chi_2(\mathscr{F}^{(13)}|L) &= [\kappa(1)\,\kappa(2)+\kappa(3)\,\kappa(4)]\,[\lambda(1)-\lambda(2)]\,[\lambda(3)-\lambda(4)]\\ &\quad+[\kappa(1)\,\kappa(3)+\kappa(2)\,\kappa(4)]\,[\lambda(3)-\lambda(1)]\,[\lambda(2)-\lambda(4)]\\ &\quad+[\kappa(1)\,\kappa(4)+\kappa(2)\,\kappa(3)]\,[\lambda(1)-\lambda(4)]\,[\lambda(2)-\lambda(3)]\end{aligned}$$

$$\begin{aligned}\tilde{\chi}_2(\mathscr{F}^{(13)}|L) &= [\kappa(1)\,\kappa(2)+\kappa(3)\,\kappa(4)]\,[\omega(1,3)-\omega(1,4)-\omega(2,3)+\omega(2,4)]\\ &\quad+[\kappa(1)\,\kappa(3)+\kappa(2)\,\kappa(4)]\,[\omega(2,3)-\omega(3,4)-\omega(1,2)+\omega(1,4)]\\ &\quad+[\kappa(1)\,\kappa(4)+\kappa(2)\,\kappa(3)]\,[\omega(1,2)-\omega(1,3)-\omega(4,2)+\omega(4,3)]\\ &\quad\text{with } \omega(i,k)=\omega(k,i)\end{aligned}$$

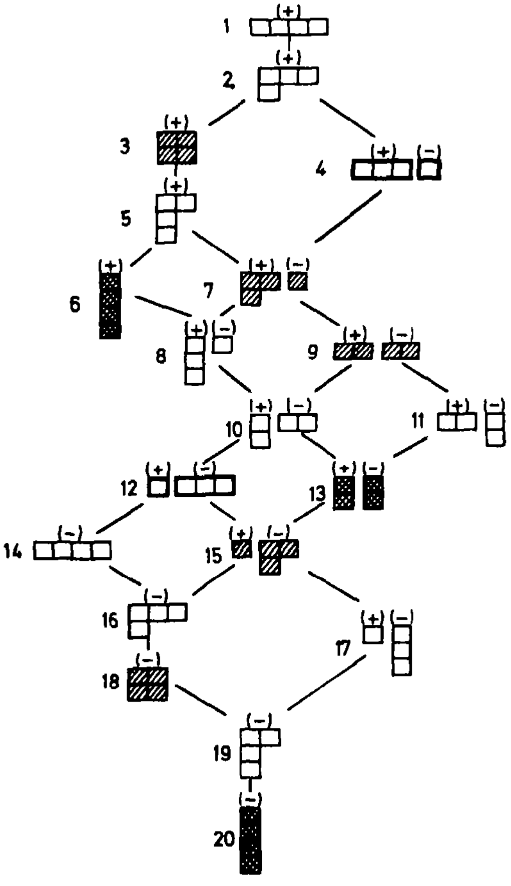

Fig. 16

$$\chi(\mathcal{T}^{(20)}|L) = \kappa(1)\,\kappa(2)\,\kappa(3)\,\kappa(4)\,[\lambda(1)-\lambda(2)]\,[\lambda(1)-\lambda(3)]\,[\lambda(1)-\lambda(4)]$$
$$\cdot[\lambda(2)-\lambda(3)]\,[\lambda(2)-\lambda(4)]\,[\lambda(3)-\lambda(4)]$$

$$\tilde{\chi}(\mathcal{T}^{(20)}|L) = \kappa(1)\,\kappa(2)\,\kappa(3)\,\kappa(4)\,[\omega(1,2,3)-\omega(1,2,4)+\omega(1,3,4)-\omega(2,3,4)]$$
with $\omega(i,k,l)$ totally antisymmetric

$$\tilde{\chi}(\mathcal{T}^{(4)}|L) = \chi(\mathcal{T}^{(4)}|L) = \kappa(1)+\kappa(2)+\kappa(3)+\kappa(4)$$

$$\tilde{\chi}(\mathcal{T}^{(12)}|L) = \chi(\mathcal{T}^{(12)}|L) = \kappa(1)\,\kappa(2)\,\kappa(3)+\kappa(1)\,\kappa(2)\,\kappa(4)+\kappa(1)\,\kappa(3)\,\kappa(4)$$
$$+\kappa(2)\,\kappa(3)\,\kappa(4)$$

a) In case of D_{2d}, $\bar{\Gamma}_{13}$ occurs twice; therefore we have to use each of the two components for Γ_{13} twice with different parameters in order to have the general ansatz according to the first method. But if we use these components only once, the ansatz is qualitatively complete and reads as follows:

$$\chi(|L) = \chi(\mathcal{T}^{(3)}|L)+\chi(\mathcal{T}^{(4)}|L)+\chi(\mathcal{T}^{(6)}|L)+\chi(\mathcal{T}^{(7)}|L)+\chi(\mathcal{T}^{(9)}|L)+(\mathcal{T}^{(12)}|L)$$
$$+\chi_1(\mathcal{T}^{(13)}|L)+\chi_2(\mathcal{T}^{(13)}|L)+\chi(\mathcal{T}^{(15)}|L)+\chi(\mathcal{T}^{(18)}|L)+\chi(\mathcal{T}^{(20)}|L)$$

(analogously for $\tilde{\chi}$).

b) In case of T_d, $\bar{\Gamma}_{13}$ occurs only once, and the ansatz is as follows:

$$\chi(|L) = \chi(\mathcal{T}^{(4)}|L)+\chi(\mathcal{T}^{(6)}|L)+\chi(\mathcal{T}^{(12)}|L)+\chi_2(\mathcal{T}^{(13)}|L)+\chi(\mathcal{T}^{(20)}|L)$$

(analogously for $\tilde{\chi}$).

8. Discussion

We have seen that, by means of the theory of the groups $\mathfrak{S}_n'$ and $\tilde{\mathfrak{S}}_n$, the theory of chirality functions can be conveniently generalized to allow for chiral ligands. Although the groups are of large order even for relatively small n, the existence of a general representation theory nevertheless makes a systematic investigation feasible.

There are two obvious directions in which the theory could be further generalized, viz:

(a) One could consider the theory, not just of pseudoscalar, but also of vector and tensor properties of molecules. This could be done with the groups already at hand, simply by considering induction, not just of the chiral representation, but of an arbitrary representation, from the molecular symmetry group to the covering group.

(b) One could allow the ligands to have arbitrary transformation properties under the symmetry operations of the frame. In this case, the covering group would no longer be $\tilde{\mathfrak{S}}_n$, but an arbitrary wreath product group [6].

Appendix 1. Representation Theory of the Groups $\tilde{\mathfrak{S}}_n$

A. General Properties: Classes

The group $\tilde{\mathfrak{S}}_n$ consists of all products $\tau\jmath$, where $\jmath$ is a member of $\mathfrak{S}_n$ (permutation of n ligands among n sites), and $\tau = \prod_j \tau(j)$, with the product running over an arbitrary subset of the n sites. The order of the group is obviously $2^n n!$ This is not a direct product group, since the τ and $\jmath$ do not necessarily commute. For example, reflection at site 1 followed by permuting 1 and 2 leaves a reflected ligand on site 2, while permutation followed by reflection on 1 leaves the reflected ligand on site 1. It is, however, a semidirect product: The subgroup $\mathfrak{T}$, consisting of all the reflection operations τ, is, as we shall see presently, an invariant subgroup, while the subgroup $\mathfrak{S}_n$ is not.

These groups were first studied by Young [11] who called them "hyperoctahedral groups". Further properties of these groups have been discussed by Frame [2]. In modern notation [6], they may be thought of as special cases of "wreath product" groups.

To elucidate the class structure, we first note that, since the operators τ do not move the ligands, we always have

$$\tau\mathfrak{p}\,\tau'\mathfrak{p}' = \tau''\mathfrak{p}\mathfrak{p}', \tag{1}$$

i.e., the permutation part ($\mathfrak{p}$) follows the multiplication table of $\mathfrak{S}_n$. The τ operators do not commute with the $\mathfrak{p}$, but they do with each other, and each τ is its own inverse.

Because of (1), we can write

$$\mathfrak{p}\tau = \tau'\mathfrak{p}, \tag{2}$$

$$\tau' = \mathfrak{p}\tau\mathfrak{p}^{-1}. \tag{3}$$

Now, if $\tau = \prod_j \tau(j)$, and $\mathfrak{p}$ takes the ligand on j to the site s_j, then $\mathfrak{p}\tau\mathfrak{p}^{-1}$ first takes the ligand on s_j to j, where it is reflected, then taken back to s_j. The net effect, therefore, is to reflect on all the sites s_j, and we have

$$\tau' = \prod_j \tau(s_j) \equiv \tau^{(s)}. \tag{4}$$

Now consider a group element $\tau\mathfrak{p}$, and conjugate it with a pure permutation $\mathfrak{r}(j \to r_j)$. Because of (3), (4), we can write

$$\mathfrak{r}\tau\mathfrak{p}\mathfrak{r}^{-1} = \tau^{(r)}\mathfrak{r}\mathfrak{p}\mathfrak{r}^{-1}.$$

It is known from the usual theory [1a, 5b] of $\mathfrak{S}_n$ that $\mathfrak{r}\mathfrak{p}\mathfrak{r}^{-1}$ has the same cyclic structure as $\mathfrak{p}$. If $\mathfrak{p}$ has the cyclic form

$$\mathfrak{p} = (j_1 j_2 \cdots j_m)(j_{m+1} j_{m+2} \cdots j_{m+m'}) \cdots,$$

then

$$\mathfrak{r}\mathfrak{p}\mathfrak{r}^{-1} = (r_{j_1} r_{j_2} \ldots r_{j_m})(r_{j_{m+1}} r_{j_{m+2}} \ldots r_{j_{m+m'}}) \ldots.$$

Also, from (4), if $\tau = \prod_j \tau(j)$, then

$$\tau^{(r)} = \prod_j \tau(r_j). \tag{5}$$

Thus, conjugation of $\tau\mathfrak{p}$ with a pure permutation gives an element whose permutation part has the same cyclic structure, and whose reflections are distributed in the same way among the sites in the permutation cycles. For example, if $\mathfrak{p}$ has l reflections on the m sites which are permuted in an m-cycle, then $\mathfrak{r}\mathfrak{p}\mathfrak{r}^{-1}$ will also have l reflections on the sites belonging to an m-cycle.

Next, we consider conjugation with a reflection, at first restricting ourselves to the case of a single reflection $\tau(j)$. We find

$$\tau(j)\,\tau\mathfrak{p}\,\tau(j)^{-1} = \tau(j)\,\tau\mathfrak{p}\,\tau(j) = \tau(j)\,\tau\,\tau(s_j)\mathfrak{p} = \tau(j)\tau(s_j)\tau\,\mathfrak{p},$$

where we have used (4), plus the fact that the τ commute with each other and are their own inverses. Conjugation with $\tau(j)$, therefore, has the same effect as multiplication with $\tau(j)\tau(s_j)$. Conjugation with a general reflection operation can be thought of as a series of successive conjugations with single reflections. By conjugating first with $\tau(j)$ and then with $\tau(s_j)$, we achieve the net result of multiplying by $\tau(j)\tau(s_j^2)$, where s_j^2 is the site to which the ligand on j is taken by two successive applications of the permutation $\mathfrak{s}$. Continuing in this way, we can multiply by any two reflections on sites belonging to the same cycle of $\mathfrak{s}$. Thus, conjugation with an arbitrary τ is equivalent to a series of operations in which one carries out two reflections on sites belonging to the same cycle of $\mathfrak{s}$. The net effect, therefore, is always to change the number of reflections in each cycle (if at all) by an even number, and all combinations are possible subject to this restriction. Conjugation with an arbitrary group element can be thought of as conjugation first with a permutation and then with a reflection. Combining the above results, we arrive at the prescription for classes given in Sec. 2.A of the text.

B. Young Operators and Irreducible Representations

Our method of proof in this subsection will closely parallel that of Boerner [1] for $\mathfrak{S}_n$. For definitions, the reader is referred to Section 2.A of the text.

Theorem 1. The number of different two-part diagrams of order n is equal to the number of classes of $\bar{\mathfrak{S}}_n$, hence also to the number of its irreducible representations.

No further proof of this theorem is needed, beyond the argument already given in Section 2.B of the text.

We now state and prove

Theorem 2. The operator $\bar{\mathscr{Y}}^{(r)}$ (defined in Section 2.B) is, up to a multiplicative constant, a primitive idempotent for the group $\bar{\mathfrak{S}}_n$ (that is, it projects onto a particular coordinate belonging to an irreducible representation). $\bar{\mathscr{Y}}$-operators from tableaux belonging to the same diagram project onto equivalent irreducible representations, while those from different diagram pairs project onto inequivalent representations. All irreducible representations are found in this way.

In the following, we omit the superscript on $\bar{\mathscr{Y}}^{(r)}$. The proof of the first part of the theorem is based on the known theorem: [1b]. If an operator $u = \Sigma u(\sigma)\sigma$, with $u(e) \neq 0$, has the property that, for all x in the group algebra,

$$uxu = gu\,, \tag{6}$$

(g a number, in general a function of x), then u is, up to a multiplicative constant, a primitive idempotent, and conversely.

We will show that $\bar{\mathscr{Y}}$ has the property (6). We first note that, for any $\alpha_+, \beta_+, \alpha_-, \beta_-$,

$$\alpha_+ a^{(r+)} = a^{(r+)};\ \alpha_- a^{(r-)} = a^{(r-)};\ b^{(r+)}\beta_+ = \varepsilon(\beta_+)\, b^{(r+)};\ b^{(r-)}\beta_- = \varepsilon(\beta_-)\, b^{(r-)}. \tag{7}$$

One also has, trivially, for arbitrary τ_+, τ_-:

$$\tau_+ b^{(r+)} = b^{(r+)}\tau_+ = b^{(r+)};\ \tau_- b^{(r-)} = b^{(r-)}\tau_- = \varepsilon(\tau_-)\, b^{(r-)}. \tag{8}$$

Because of (7) and (8), it follows that, if $c = \bar{\mathscr{Y}} x \bar{\mathscr{Y}}$ (x arbitrary), then

$$\tau_+ \alpha c \beta \tau_- = \varepsilon(\beta)\varepsilon(\tau_-) c\,. \tag{9}$$

for arbitrary α, β, τ_{+}, τ_{-}. We now show that any operator with the property (9) satisfies $c = g\bar{\mathcal{Y}}$. This will complete the proof that $\bar{\mathcal{Y}}$ has the property of u in (6), as we know that $\bar{\mathcal{Y}} x \bar{\mathcal{Y}}$ has the property (9).

We write the operator c as

$$c = \sum_{\sigma} c(\sigma)\sigma$$

where the sum goes over all group elements σ. Equation (9) means

$$\sum_{\sigma} c(\sigma)\,\tau_{+}\alpha\sigma\beta\tau_{-} = \varepsilon(\beta)\varepsilon(\tau_{-})\sum_{\sigma} c(\sigma)\sigma\,, \qquad (10)$$

for arbitrary α, β, τ_{+}, τ_{-}. First, consider terms whose permutation part is of the form $\alpha\beta$. We multiply[5] by $\tau_{+}\alpha\ldots\beta\tau_{-}$. On the left-hand side of (10), the term $\tau_{+}\alpha\beta\tau_{-}$ appears for $\sigma = e$, on the right-hand side for $\sigma = \tau_{+}\alpha\beta\tau_{-}$. We thus have, for arbitrary α, β, τ_{+}, τ_{-}

$$c(e) = \varepsilon(\beta)\,\varepsilon(\tau_{-})\,c\,(\tau_{+}\alpha\beta\tau_{-})\,.$$

This means that the coefficients $c(\sigma)$ for those terms σ which appear in $\bar{\mathcal{Y}}$ (permutation part $= \alpha\beta$) are equal to the coefficients of the same terms in $\bar{\mathcal{Y}}$, multiplied by $c(e)$. We must now show that, when the permutation part of σ is not $\alpha\beta$, $c(\sigma) = 0$. If $\sigma = \tau\jmath$, $\jmath \neq \alpha\beta$, there are two possibilities to consider:

i) $\jmath$ does not mix the (+) and (−) tableaux. In this case, σ can be written as $\tau_{+}\jmath\tau_{-}$, and it can be shown [1d] that there exist a transposition α and a transposition β such that

$$\alpha\jmath\beta = \jmath\,.$$

Choosing this $\alpha\beta$ pair, we multiply by $\tau_{+}\tau_{+}^{(\alpha)}\alpha\ldots\beta\tau_{-}^{(\beta^{-1})}\tau_{-}$. For this operation, $\varepsilon(\beta)\,\varepsilon(\tau_{-}) = -1$: β, being a transposition, is odd, and $\tau\ \tau^{(\beta^{-1})}$ is even. Applying this to our term σ, we have

$$\tau_{+}\tau_{+}^{(\alpha)}\alpha\,\tau_{+}\jmath\,\tau_{-}\beta\,\tau_{-}^{(\beta^{-1})}\tau_{-} = \tau_{+}\alpha\jmath\beta\tau_{-} = \tau_{+}\jmath\tau_{-}\,.$$

Thus, the term $\tau_{+}\jmath\tau_{-}$ appears on both sides of Eq. (10) for $\sigma = \tau_{+}\jmath\tau_{-}$, and we have

$$c(\sigma) = -c(\sigma)\,, \qquad c(\sigma) = 0\,.$$

ii) If $\jmath$ mixes the two parts, then there is at least one site j in the (−) tableau such that s_j is in the (+) tableau. We choose $\tau_{+} = \tau(s_j)$, $\tau_{-} = \tau(j)$, and multiply by $\tau_{+}\ldots\tau_{-}$. Again $\varepsilon(\beta)\,\varepsilon(\tau_{-}) = -1$. We find

$$\tau_{+}\tau\jmath\tau_{-} = \tau(s_j)\tau\tau(s_j)\jmath = \tau\jmath\,.$$

The term $\tau\jmath$, therefore, appears on both sides of (10) for $\sigma = \tau\jmath$ and we have again $c(\tau\jmath) = -c(\tau\jmath)$, $c(\tau\jmath) = 0$.

This completes the proof that $\bar{\mathcal{Y}}$ is a number times a primitive idempotent. To prove the statement about equivalence of representations, we must consider the behavior of the $\bar{\mathcal{Y}}$ operators under conjugation. We first consider conjugation with a pure reflection operator $\tau = \tau_{+}\tau_{-}$. We obtain

$$\tau\bar{\mathcal{Y}}\tau^{-1} = \tau\bar{\mathcal{Y}}\tau = \tau_{+}\tau_{-}\ell_{+}\mathcal{Y}_{+}\mathcal{Y}_{-}\ell_{-}\tau_{-}\tau_{+} = \tau_{+}\ell_{+}\mathcal{Y}_{+}\tau_{+}\tau_{-}\mathcal{Y}_{-}\ell_{-}\tau_{-}\,, \qquad (11)$$

---

[5] This notation means: multiply on the left by $\tau_{+}\alpha$, on the right by $\beta\tau_{-}$.

where $\mathcal{Y}_+ = a^{(r+)}b^{(r+)}$, $\mathcal{Y}_- = a^{(r-)}b^{(r-)}$, and we abbreviate $\ell^{(r+)}$, $\ell^{(r-)}$ with ℓ_+, ℓ_-.

Consider the portion $\ell_+\mathcal{Y}_+\tau_+$. It may be written, apart from the normalization factors, as

$$\ell_+\mathcal{Y}_+\tau_+ = \ell_+\Sigma\varepsilon(\beta_+)\alpha_+\beta_+\tau_+ = \ell_+\Sigma\,\varepsilon(\beta_+)\tau_+^{(\alpha_+\beta_+)}\alpha_+\beta_+ = \ell_+\mathcal{Y}_+$$

where we have used (4) and (8). With another application of (8), we have $\tau_+\ell_+\mathcal{Y}_+\tau_+ = \ell_+\mathcal{Y}_+$. Similarly, one proves

$$\tau_-\mathcal{Y}_-\ell_-\tau_- = \mathcal{Y}_-\ell_- .$$

Thus, we see that

$$\tau\bar{\mathcal{Y}}\tau^{-1} = \bar{\mathcal{Y}} . \tag{12}$$

We now take up the conjugation of the Young operator $\bar{\mathcal{Y}} = \bar{\mathcal{Y}}(\bar{t})$ with an arbitrary element $\sigma = \tau\pi$. Let $\bar{t}'$ be the tableau obtained from $\bar{t}$ by applying the permutation π, and denote the corresponding operators also by primes. We find

$$\begin{aligned}\sigma\bar{\mathcal{Y}}\sigma^{-1} &= \tau\pi\ell_+\mathcal{Y}_+\mathcal{Y}_-\ell_-\pi^{-1}\tau = \tau\tau'_+\pi\mathcal{Y}_+\mathcal{Y}_-\pi^{-1}\ell'_-\tau\\ &= \tau\ell'_+\mathcal{Y}'_+\mathcal{Y}'_-\ell'_-\tau = \tau\bar{\mathcal{Y}}'\tau = \bar{\mathcal{Y}}' ,\end{aligned} \tag{13}$$

where we have used (4), (12), and a trivial generalization of a theorem [1e] on the conjugation of ordinary Young operators: $\pi\mathcal{Y}\pi^{-1} = \mathcal{Y}'$.

Now, a necessary and sufficient condition [1f] for the equivalence of the representations generated by two idempotents $\bar{\mathcal{Y}}$ and $\bar{\mathcal{Y}}'$ is that there exist some x in the group algebra such that

$$\bar{\mathcal{Y}}'x\bar{\mathcal{Y}} \neq 0. \tag{14}$$

First, let $\bar{\mathcal{Y}}, \bar{\mathcal{Y}}'$ belong to the same diagram. Then, because of (13), there is a group element σ with the property $\sigma\bar{\mathcal{Y}}\sigma^{-1} = \bar{\mathcal{Y}}'$. It follows that

$$\bar{\mathcal{Y}}'\sigma\bar{\mathcal{Y}} = \bar{\mathcal{Y}}'\sigma\bar{\mathcal{Y}}\sigma^{-1}\sigma = \bar{\mathcal{Y}}'^2\sigma = k\,\bar{\mathcal{Y}}'\sigma \neq 0$$

where we have used the fact that $\bar{\mathcal{Y}}'$ is a multiple of an idempotent, $\bar{\mathcal{Y}}'^2 = k\,\bar{\mathcal{Y}}' \cdot \bar{\mathcal{Y}}'\sigma = \sigma\bar{\mathcal{Y}}$ is not zero, since if it were, $\bar{\mathcal{Y}}' = \sigma\bar{\mathcal{Y}}\sigma^{-1}$ would also be zero. Thus, the condition (14) is satisfied with $x = \sigma$, and we conclude that the representations are equivalent.

If $\bar{\mathcal{Y}}, \bar{\mathcal{Y}}'$ refer to different diagrams, then there are two possibilities:

i) $n_+ \neq n'_+$. In this case, there is at least one site j which belongs to the $(-)$ part of $\bar{t}$ and to the $(+)$ part of $\bar{t}'$ (or vice versa). Thus, $\ell'_+(\ell_+)$ contains $(e+\tau_j)$ as a factor, and $\ell_-(\ell'_-)$ contains $(e-\tau_j)$. Hence, either $\ell'_+\ell_- = 0$ or $\ell'_-\ell_+ = 0$, and we have

$$\bar{\mathcal{Y}}'\bar{\mathcal{Y}} = \ell'_+\mathcal{Y}'_+\mathcal{Y}'_-\ell'_-\ell_+\mathcal{Y}_+\mathcal{Y}_-\ell_- = \ell'_-\mathcal{Y}'_+\mathcal{Y}'_-\ell'_+\ell_-\mathcal{Y}_+\mathcal{Y}_-\ell_+ = 0 .$$

ii) $n_+ = n_-$. If the sites are divided differently between the $(+)$ and $(-)$ parts of the two tableau pairs, then again there is a site which belongs to the $(+)$ part of one pair and to the $(-)$ part of the other, and we see, just as in case (i), that $\bar{\mathcal{Y}}'\bar{\mathcal{Y}} = 0$. If they are distributed in the same way, then it follows immediately from a known theorem [1g] that either

$$\mathcal{Y}'_+\mathcal{Y}_+ = 0, \quad \text{or} \quad \mathcal{Y}'_-\mathcal{Y}_- = 0 .$$

Hence,

$$\mathcal{Y}'\mathcal{Y} = \ell'_+ \ell'_- \mathcal{Y}'_+ \mathcal{Y}'_- \mathcal{Y}_- \mathcal{Y}_+ \ell_+ \ell_- = \ell'_+ \ell'_- \mathcal{Y}'_- \mathcal{Y}'_+ \mathcal{Y}_+ \mathcal{Y}_- \ell_+ \ell_- = 0 .$$

Thus, for tableau pairs belonging to different diagram pairs,

$$\bar{\mathcal{Y}}'\bar{\mathcal{Y}} = 0 . \tag{15}$$

But also, for any group element σ,

$$\bar{\mathcal{Y}}'\sigma\bar{\mathcal{Y}} = \bar{\mathcal{Y}}'\sigma\bar{\mathcal{Y}}\sigma^{-1}\sigma = \bar{\mathcal{Y}}'\bar{\mathcal{Y}}''\sigma = 0 ,$$

where $\bar{\mathcal{Y}}''$ is the Young operator generated according to (13) from $\bar{\mathcal{Y}}$ by σ. Since $\bar{\mathcal{Y}}''$ refers to the same diagram as $\bar{\mathcal{Y}}$, the last equality follows from (15). For an arbitrary element x of the group algebra, we have

$$\bar{\mathcal{Y}}' x \bar{\mathcal{Y}} = \sum_{\sigma} x(\sigma)\, \bar{\mathcal{Y}}'\sigma\bar{\mathcal{Y}} = 0 .$$

Thus, the condition (14) cannot be satisfied, and the two representations are inequivalent.

The Young operators, therefore, generate a set of inequivalent irreducible representations equal in number to the number of different two-part diagrams. But, according to Theorem 1, this is also equal to the number of classes in the group, hence to the total number of inequivalent irreducible representations. Hence, we have found all the irreducible representations.

This completes the proof of Theorem 2, which encompasses the statements made in Section 2.A of the text.

We now proceed to define a "standard two-part tableau", analogously to the definition of the "standard tableau" in the usual theory of $\mathfrak{S}_n$.

A standard two-part tableau is a tableau in which, in each part, reading from left to right along the rows, or from top to bottom along the columns, the numbers always increase.

Theorem 3. The $\bar{\mathcal{Y}}$ operators corresponding to different standard tableaux (same diagram) are linearly independent. The number of different standard tableaux is equal to the dimension of the corresponding irreducible representation.

Proof. For each distribution (d) of the sites between the (+) and (−) parts, arrange the standard tableau pairs in "dictionary" order [1h], $\bar{t}_{d1}$, $\bar{t}_{d2}$, ... If $\bar{\mathcal{Y}}$, $\bar{\mathcal{Y}}'$ belong to different d's, then $\bar{\mathcal{Y}}\bar{\mathcal{Y}}' = 0$ because of the orthogonality of the ℓ parts, as used in the proof of Theorem 2. Within the same d, a trivial generalization of a known theorem [1i] gives

$$\bar{\mathcal{Y}}_{dk}\bar{\mathcal{Y}}_{di} = 0 \quad \text{for} \quad i < k. \tag{16}$$

Now consider a linear combination

$$\sum_{d,j} a_{dj}\bar{\mathcal{Y}}_{dj} = 0 .$$

Multiplication from the right by $\bar{\mathcal{Y}}_{d1}$ gives zero for all terms except $d1$, from which we conclude $a_{d1} = 0$. Then we multiply from the right by $\bar{\mathcal{Y}}_{d2}$, and conclude $a_{d2} = 0$. Continuing in this way, we find that all the $a_{dj} = 0$, which proves the linear independence.

Because of the linear independence, it follows [1j] that the number of standard tableaux, $F_{\bar{\Gamma}}$, belonging to a given representation $\bar{\Gamma}$ cannot be greater than the dimension of the representation. We show the equality by showing that

$$\sum_{\bar{\Gamma}} F_{\bar{\Gamma}}^2 = n!\,2^n, \text{ the order of the group}.$$

For a diagram pair with $n_+ = l$, $n_- = n-l$, there are $\frac{n!}{l!\,(n-l)}$ distributions d. For each d, the two parts must separately be standard tableaux, and the number of ways of achieving this is just the product $F_l^{(\gamma_+)} F_{n-l}^{(\gamma_-)}$ of the number of standard tableaux belonging to the $(+)$ and $(-)$ diagrams, γ_+ and γ_-. Hence

$$F_{\bar{\Gamma}} = \frac{n!}{l!\,(n-l)!} F_l^{(\gamma_+)} F_{n-l}^{(\gamma_-)}.$$

The sum of the squares is

$$\sum_{\bar{\Gamma}} F_{\bar{\Gamma}}^2 = \sum_{l=0}^{n} \frac{(n!)^2}{(l!)^2[(n-l)!]^2} \sum_{\gamma_+,\gamma_-} F_l^{(\gamma_+)2} F_{n-l}^{(\gamma_-)2}.$$

From the theory of $\mathfrak{S}_n$, we know that

$$\sum_{\gamma} F_l^{(\gamma)2} = l!.$$

Hence,

$$\sum_{\bar{\Gamma}} F_{\bar{\Gamma}}^2 = \sum_{l=1}^{n} \frac{(n!)^2}{l!\,(n-l)!} = n!\,2^n,$$

which completes the proof.

We now turn our attention to the calculation of the characters of the irreducible representations. For a two-part diagram $\bar{\gamma} = (\gamma_+, \gamma_-)$ we can use the $\mathscr{Y}$ operators for the standard tableaux, applied to some suitable function or set of functions (of suitable variables, such as properties of ligands on sites), to generate a complete set of linearly independent basis functions which will transform among themselves under $\mathfrak{S}_n$ according to the representation $\bar{\Gamma}$. Functions corresponding to different d's will already be orthogonal because of their different reflection symmetries. Within a given d, we can assume that the functions ψ_{dj} have been orthogonalized and normalized.

Now consider the effect of a group element σ with cycle structure

$$\xi = (\nu_1^{(+)}, \nu_2^{(+)}, \ldots; \nu_1^{(-)}, \nu_2^{(-)}, \ldots).$$

The character $\chi_\xi^{(\bar{\Gamma})}$ is the sum of the diagonal elements $\sigma_{dj;dj}$ in the F expressions

$$\sigma\psi_{dj} = \sum_{d',j'} \sigma_{dj;d'j'}\, \psi_{d'j'}.$$

If d is such that σ mixes the two parts, then the diagonal element is zero, since $\sigma\psi$ gives a function belonging to another d. Hence, only those d contribute to the character for which each cycle of σ has all its members (sites) in the same part of the tableau pair. In other words, the cycle structure ξ breaks up into parts ξ_+, ξ_-, of cycles belonging completely to the $(+)$ and $(-)$ parts, respectively. Within such a d, however, the permutation part of σ acts simply as a direct product of two operators: one a member of $\mathfrak{S}_{n_+}$, with cycle structure ξ_+ in a space belonging to the representation Γ_+; the other a member of $\mathfrak{S}_{n-}$, cyclic structure ξ_-, in a space belonging to the representation Γ_-. As for the reflections, those in ξ_+ simply multiply by unity, while each reflection in ξ_- multiplies by (-1). The overall effect, then, is simply to multiply by ε_d, where $\varepsilon_d = \pm 1$ according as the number of odd cycles in ξ_- is even or odd. So we find the character

Theorem 4.

$$\chi_{\xi}^{(\bar{\Gamma})} = \sum_{d}' \varepsilon_d \chi_{\xi_+}^{(\Gamma_+)} \chi_{\xi_-}^{(\Gamma_-)}$$

where the sum goes over the above-described "compatible" distributions d. In this way, the character for $\bar{\mathfrak{S}}_n$ can be calculated from the known ones for the $\mathfrak{S}_n$.

As an example, we calculate the character of $\bar{\mathfrak{S}}_6$ belonging to the representation

$\bar{\Gamma} \leftrightarrow$ 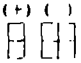

for the class with cycle structure

$$\xi = (1, 2; 1, 2).$$

The different contributions are:

d	ξ_+	ξ	ε_d	$\chi_{\xi_+}^{(\Gamma_+)}$	$\chi_{\xi_-}^{(\Gamma_-)}$	contribution to χ
1.	(2;)	(1; 1, 2)	1	−1	0	0
2.	(; 2)	(1, 2; 1)	−1	−1	0	0
3.	(1; 1)	(2; 2)	−1	1	2	−2

Total character $= -2$.

It should be noted that d's which differ in the exchange of two cycles of the same kind count as different. Thus, in the above example, the first two d's would still be different for the class (1, 2, 2; 1)

C. Induction and Subduction Between $\bar{\mathfrak{S}}_n$, $\mathfrak{S}'_n$, $\mathfrak{S}_n$

A representation $\bar{\Gamma}$ of $\bar{\mathfrak{S}}_n$, applied only to the members of the subgroup $\mathfrak{S}_n$ "subduces" a representation of $\mathfrak{S}_n$, in general reducible, which may be broken up into its irreducible parts. Symbolically

$$\bar{\Gamma} \rightarrow \sum_{\Gamma} C_{\bar{\Gamma}\Gamma} \Gamma . \tag{17}$$

Because of the Frobenius induction theorem [1b, 9], $C_{\bar{\Gamma}\Gamma}$ is also the number of times $\bar{\Gamma}$ is contained in the representation of $\bar{\mathfrak{S}}_n$ "regularly induced" by the representation Γ of $\mathfrak{S}_n$. From the general formula for coefficients in terms of characters, we have

$$C_{\bar{\Gamma}\Gamma} = \frac{1}{n!} \sum_{\omega} \chi^{(\Gamma)}(\omega) \chi^{(\bar{\Gamma})}(\omega)$$

where the sum goes over all $\jmath$, i.e., over all members of the subgroup $\mathfrak{S}_n$. Because of Theorem 4, the expression can be rewritten as

$$C_{\bar{\Gamma}\Gamma} = \frac{1}{n!} \sum_{\jmath} \chi^{(\Gamma)}(\jmath) \sum_{d}{}' \chi_{\xi_+}^{(\Gamma_+)} \chi_{\xi_-}^{(\Gamma_-)}.$$

In this case, $\jmath$ contains no odd cycles, so we have $\varepsilon_d = 1$ for all d. The sum goes over all $\jmath$, and for each $\jmath$ over all "compatible" d. However, it may equally well be thought of as a sum over d, and for each d over compatible $\jmath$, i.e., $\jmath \in (\mathfrak{S}_{n_+} \times \mathfrak{S}_{n_-})$. Thus, it may also be written as

$$C_{\bar{\Gamma}\Gamma} = \frac{1}{n!} \sum_{d} \sum_{\jmath}{}' \chi^{(\Gamma)}(\jmath) \chi_{\xi_+}^{(\Gamma_+)} \chi_{\xi_-}^{(\Gamma_-)}.$$

The sum over $\jmath$ is obviously independent of d, with the consequence that the sum over d just gives the number of different d's, $\frac{n!}{n_-!\, n_+!}$. So we find

$$C_{\bar{\Gamma}\Gamma} = \frac{1}{n_+!\, n_-!} \sum_{\jmath \in (\mathfrak{S}_{n_+} \times \mathfrak{S}_{n_-})} \chi^{(\Gamma)}(\jmath) \chi_{\xi_+}^{(\Gamma_+)} \chi_{\xi_-}^{(\Gamma_-)}.$$

This is obviously just the number of times the representation $(\Gamma_+ \times \Gamma_-)$ is contained in the representation of $(\mathfrak{S}_{n_+} \times \mathfrak{S}_{n_-})$ subduced by Γ. The answer to this subduction problem is known, however, and corresponds to the procedure used in the text [5a, 7].

As for subduction from $\bar{\mathfrak{S}}_n$ to $\mathfrak{S}'_n$, we note that the representation $\bar{\Gamma}$ is g or u with respect to the operator τ_0 according as n_- is even or odd, and that further subduction to $\mathfrak{S}_n$ must give (17). Clearly, therefore, in the subduced representation of $\mathfrak{S}'_n$ by a $\bar{\Gamma}$ with even n_-, each representation Γ_g appears $C_{\bar{\Gamma}\Gamma}$ times, the Γ_u not at all; if n_- is odd, the roles of g and u are reversed.

In induction from $\mathfrak{S}'_n$ to $\bar{\mathfrak{S}}_n$, the procedure is reversed: In the representation induced by Γ_g, each $\bar{\Gamma}$ with even n_- appears $C_{\bar{\Gamma}\Gamma}$ times, the others not all; in that induced by Γ_u, those with odd n_- appear $C_{\bar{\Gamma}\Gamma}$ times, the others not at all. This completes the justification for the induction (subduction) procedures described in Section 2.C and used in the text.

Appendix 2. Proofs of Assertions Made in Section 3

A. Lattice Structure of $\supset$ Relation

The set of diagram pairs is a partial ordering defined by

$$\bar{\gamma}^{(r)} \supset \gamma^{(l)} \leftrightarrow o_i^{(r+)} \geqq o_i^{(l+)}, \qquad u_i^{(r-)} \leqq u_i^{(l-)}.$$

Contention: It is also a lattice.

Proof. The union of $\bar{\gamma}^{(1)}$ and $\bar{\gamma}^{(2)}$ must be larger, therefore provided it is existent it must satisfy the condition

$$o_i \geqq \max(o_i^{(1)}, o_i^{(2)}),$$
$$u_i \leqq \min(u_i^{(1)}, u_i^{(2)}).$$

Let us construct "pseudo diagram" γ with the partial sums

$$o_i^{(+)} = \max(o_i^{(1)}, o_i^{(2)}),$$
$$u_i^{(-)} = \min(u_i^{(1)}, u_i^{(2)});$$

because of

$$\begin{aligned} u_i^{(-)} - u_{i+1}^{(-)} &= 2u_i^{(-)} - u_{i-1}^{(-)} - u_{i+1}^{(-)} = 2\min(u_i^{(1)}, u_i^{(2)}) - \min(u_{i-1}^{(1)}, u_{i-1}^{(2)}) \\ &\quad - \min(u_{i+1}^{(1)}, u_{i+1}^{(2)}) \geqq 2\min(u_i^{(1)}, u_i^{(2)}) \\ &\quad - \min(u_{i-1}^{(1)} + u_{i+1}^{(1)}, u_{i-1}^{(2)} + u_{i+1}^{(2)}) \\ &= \min(2u_{i-1}^{(1)} + 2\mu_i^{(1)}, 2u_{i-1}^{(2)} + 2\mu_i^{(2)}) \\ &\quad - \min(2u_{i-1}^{(1)} + \mu_i^{(1)} + \mu_{i+1}^{(1)}, 2u_{i-1}^{(2)} + \mu_i^{(2)} + \mu_{i+1}^{(2)}) \geqq 0 \end{aligned}$$

the lengths of columns do not increase with increasing indices. Therefore $\gamma^{(-)}$ is a diagram; the pseudodiagram $\gamma^{(+)}$ has rows for which increasing cannot be excluded. Let us take therefore the columns of $\gamma^{(+)}$, they do not increase with increasing indices as follows from the construction of $\gamma^{(+)}$. Now we construct the diagram $\gamma'^{(+)}$ with the same columns. For this we have $o_i'^{(+)} \geqq o_i^{(+)}$. Any single diagram which is larger has other columns, therefore it is the smallest single diagram. It follows that the diagram pair with $o_i'^{(+)}$ and $u_i'^{(-)} = u_i^{(-)}$ is the smallest of all larger ones and we may call it union of $\bar{\gamma}^{(1)}$ and $\bar{\gamma}^{(2)}$ $(\bar{\gamma}^{(1)}, \bar{\gamma}^{(2)})$.

B. "*Largest Remainder*"

In the beginning of this section, we consider the largest remainder prescription with the transfer being carried out in a particular order: First the 1's, then the 2's, etc. At the end, we will see that the order is irrelevant.

To prove the validity of the prescription, we start with some definitions and preliminary remarks.

We call two allowed arrangements of the symbols among the boxes "equivalent" if they have the same remainder. Since the remainder, as well as the C-condition, depends only on the number of symbols in each column, we can assume without loss of generality that all symbols in a given column are piled up at the bottom of the column. Now, for fixed number of symbols in each column, we define a "standard" arrangement as one in which the 1's are placed as low down as is compatible with (C) and the fixed column distribution (number of symbols in each column), the 2's as low as is compatible with (C), the column distribution, and the placement of the 1's, etc.

Now, starting with an arbitrary arrangement $\mathscr{A}$, we can rearrange it into standard form as follows:

We rearrange the symbols among the occupied boxes so that the 1's are at the bottoms of the $\nu_1^{(b)}$ longest occupied columns (i.e., in the $\nu_1^{(b)}$ lowest-lying occupied boxes with no two in the same column), the 2's are at the bottoms of the $\nu_2^{(b)}$ longest columns of the remainder which still have space available, etc. This standard arrangement $\mathscr{A}_s$ is equivalent to $\mathscr{A}$, as the same boxes are occupied as before, though not necessarily by the same symbols. Now, if we can move an entire pile of symbols from one column into a longer, previously unoccupied one, we obtain an arrangement with a larger remainder than $\mathscr{A}_s$, since we have increased the length of a shorter column of the remainder at the expense of a longer one. Let us do this with all the "1-piles" (piles with 1's at the bottoms), i.e., move the 1-piles into the ν_1 longest columns of $\gamma^{(a)}$, choosing the columns farthest to the right in case of ties. (This will not displace any other piles, as the 1-piles already are in the longest occupied columns.) The resulting arrangement has the 1's placed according to the prescription, and has a larger remainder than does $\mathscr{A}_s$. It is standard as far as the placement of the 1's is concerned; if it is not also standard for the other symbols, we rearrange them as before to form a standard arrangement, $\mathscr{A}'_s$ whose remainder is larger than that of $\mathscr{A}_s$. Similarly, we now move the 2-piles (the 2's, plus whatever else may be on top of them) into longer columns (of $\gamma^{(a)}$ minus the squares already occupied by 1's) where possible and rearrange into a standard arrangement, $\mathscr{A}''_s$, in which the 1's and 2's are arranged according to the prescription and whose remainder is larger than that of $\mathscr{A}'_s$, hence also larger than that of $\mathscr{A}_s$. Continuing this procedure for the 3's, 4's, etc., we end up with the prescribed arrangement. Its remainder is greater than that of $\mathscr{A}_s$, hence also greater than that of the equivalent arrangement $\mathscr{A}$. But $\mathscr{A}$ was arbitrary, so the prescribed arrangement has a larger remainder than any other, and the validity of the prescription is proved.

It is evident from the nature of the proof that the prescription is, as claimed in Section 3, independent of the order of placement of the symbols. To prove the prescription for another order of placement, one need only redefine "standard arrangement" in such a way that first preference (i.e., the lowest available places) is given to the symbols which are to go in first, then those which go in next, etc.

References

1 Boerner, H.: Darstellungen von Gruppen, zweite Auflage. Berlin: Springer Verlag 1967. English Translation: Representations of groups, 2'nd Edition. Amsterdam: North Holland Publishing Co., 1970. The following chapter and page numbers refer to the second German edition: (a) Kap. II.2, pp. 28–9, (b) Kap. III, Satz 3.9, p. 58, (c) Kap. IV, Satz 2.5, p. 106; (d) Kap. IV, Satz 2.8, 2.9, p. 107; (e) Kap. IV, Satz 2.1, p. 104, (f) Kap. III, Satz 3.8, p. 58, (g) Kap. IV, Satz 3.2, p. 109; (h) Kap. IV, p. 110; (i) Kap. IV, Satz 4.4, p. 111, (j) Kap. III.4, pp. 60–67; (k) Kap. III, Satz 13.1, p. 92.
2 Frame, J. S.: Nagoya Math. J. **27**, 585 (1966)
3. Haase, D., Ruch, E.: Theoret. chim. Acta (Berl.) **29**, 189 (1973).
4 Haase, D., Ruch, E.: Theoret. chim. Acta (Berl.) **29**, 247 (1973).
5 Hamermesh, M.: Group theory. Reading, Mass.: Addison-Wesley, 1962. (a) Ch. 7–12, pp. 249–54, (b) Ch. 1–5, pp. 24–6.
6 Kerber, A.: Representations of permutation groups I. Berlin. Springer Verlag 1971.
7 Littlewood, D. E.: The theory of group characters. Oxford: Oxford University Press 1950.
8 Ruch, E.: Theoret. chim. Acta Berl. **11**, 183 (1968).
9. Ruch, E., Schönhofer, A.: Theoret. chim. Acta Berl. **3**, 291 (1965).
10. Ruch, E., Schönhofer, A.: Theoret. chim. Acta Berl. **19**, 225 (1970).
11 Young, A.: Proc. London Math. Soc. (2) **31**, 273 (1930).

Alden Mead
Chemistry Department
University of Minnesota
Minneapolis, Minnesota 55455
USA

Ernst Ruch
Institut für Quantenchemie
Freie Universität Berlin
D 1000 Berlin 45, Holbeinstraße 48
Germany

Alfred Schönhofer
Technische Universität Berlin
Lehrstuhl III für Theoretische Physik
D 1000 Berlin 12, Straße des 17. Juni 135
Germany

Theoret. chim. Acta (Berl.) 29, 305—311 (1973)
© by Springer-Verlag 1973

Commentationes

Application of SCF-Perturbation Theory to Hydrogen Bonding in Water Dimers

Reiner Sustmann and Fritz Vahrenholt
Organisch Chemisches Institut der Universität, 4400 Münster, Federal Republic of Germany

Received May 5, 1972/November 28, 1972

The usefulness of Self-consistent perturbation theory and of a variation perturbation treatment both in semiempirical form (CNDO/2) is tested by application to hydrogen bonding in water dimers. The results are comparable to variational calculations. A splitting of the total energy in various components provides insight into the nature of hydrogen bonding.

Die Anwendbarkeit von SCF-Störungstheorie und eines Variationsstörverfahrens, beide in semiempirischer Form (CNDO/2), wird an der Wasserstoffbrückenbindung im dimeren Wasser geprüft. Die Ergebnisse sind vergleichbar mit Variationsrechnungen. Eine Aufspaltung der Gesamtenergie in verschiedene Komponenten vermittelt einen Einblick in die Natur der Wasserstoffbrückenbindung.

Introduction and Methods of Calculation

A self-consistent perturbation theory for interacting electron systems, based on a perturbation of the Fock-Dirac density matrix [1], has recently been developed [2]. The semiempirical MINDO version [3] of this theory was applied successfully to problems in chemical reactivity [4]. It has now been rewritten for the CNDO/2 [5] approximation [6]. The usefulness of such a theory for intermolecular forces is compared to a variation perturbation treatment which makes use of zero order SCF-wave functions but is not self consistent. This latter theory had been developed by Pople [7] and was applied by Pople and Schofield [8] to π-electron systems. It has been extended to two electron perturbations in order to treat interacting electron systems [9] and was programmed for the CNDO/2 approximation [10].

Both formalisms are based on the same zero order wave function and therefore give identical results for the first order energy [2, 4]. Incorporation of the change in nuclear repulsion gives a first order change of total energy:

$$\delta E^{(1)} = \sum_{kl} [q_k q_l \gamma_{kl} + (14.399/R_{kl} - \gamma_{kl}) C_k C_l] \tag{1}$$

$q_{k(l)}$ are the excess charges of atoms k and l of the two subsystems K and L. γ_{kl} represents the repulsion of two electrons on atom k and l at the distance R_{kl} and $14.399/R_{kl}$ is the repulsion of two point charges in eV. $C_{k(l)}$ are core charges. The first term in Eq. (1) depends on excess charges and will be called charge interaction, the second term also coulombic in nature includes most of what commonly is considered to be steric hindrance and will be called steric interaction.

The second order energy in the semiempirical SCF-perturbation theory is obtained as the sum of a covalent term (2) and an electrostatic contribution (3) [4]. This is independent of the MINDO or CNDO approximation.

$$\delta E^{(2)}_{\mathrm{COV.}} = \tfrac{1}{2} \sum_{\mu\lambda} P'^{KL}_{\mu\lambda} H'^{KL}_{\lambda\mu} + \tfrac{1}{2} \sum_{\kappa\nu} P'^{LK}_{\kappa\nu} H'^{LK}_{\nu\kappa} , \tag{2}$$

$$\delta E^{(2)}_{\mathrm{elec.}} = \tfrac{1}{2} \sum_{kl} (Q'_k q_l + Q'_l q_k) \gamma_{kl} \, . \tag{3}$$

Both (2) and (3) [11] depend on the change in the first order density matrix. The change in electron distribution in the subsystems ($Q'_{k(l)}$) should be negligible for the interaction of neutral molecules. Therefore (3) should have no significance in these cases.

The second order energy in the variation perturbation treatment differs from (2) and (3). According to Pople the perturbed wave function ψ is expanded as linear combination of the ground state ψ_0 and singly excited singlet states.

$$\psi = a \psi_0 + \sum_{s>0} b_s \psi_s \, . \tag{4}$$

The second order energy is given by Eq. (5) where H' is defined as in Ref. [2].[1]

$$\delta E^{(2)} = - \sum_{s>0} \frac{\langle \psi_0 | H' | \psi_s \rangle \langle \psi_s | H' | \psi_0 \rangle}{E_s - E_0} \, . \tag{5}$$

Carrying this through one obtains in the CNDO/2 approximation:

$$\delta E^{(2)} = -2 \sum_{u}^{\mathrm{occ}} \sum_{p}^{\mathrm{unoc}} \left| \sum_{\mu} \sum_{\lambda} c_{u\mu} c_{p\lambda} \beta_{\mu\lambda} \right|^2 E_u^{p\,-1} \tag{6a}$$

$$-2 \sum_{p}^{\mathrm{occ}} \sum_{u}^{\mathrm{unoc}} \left| \sum_{\lambda} \sum_{\mu} c_{p\lambda} c_{u\mu} \beta_{\lambda\mu} \right|^2 E_p^{u\,-1} \tag{6b}$$

$$-2 \sum_{u}^{\mathrm{occ}} \sum_{r}^{\mathrm{unoc}} \left[\sum_{\mu} \sum_{l} c_{u\mu} c_{r\mu} \gamma_{\mu l} q_l \right]^2 E_u^{r\,-1} \tag{6c}$$

$$-2 \sum_{p}^{\mathrm{occ}} \sum_{q}^{\mathrm{unoc}} \left[\sum_{\lambda} \sum_{k} c_{p\lambda} c_{q\lambda} \gamma_{\lambda k} q_k \right]^2 E_p^{q\,-1} \tag{6d}$$

The terms (6a) and (6b), being a function of resonance integrals $\beta_{\mu\lambda}$, express the covalent interaction of the systems K and L analogous to (2); (6c) and (6d) are. similar to (3), electrostatic in nature. All terms are devided by an excitation energy (7).[2] For (6a) and (6b) this is a charge transfer excitation energy, for (6c) and (6d) a local excitation energy. It is interesting to note that the significance of

---

[1] A comment on the definition of H' may be useful at this point. As was pointed out in Ref. 2 ψ_0 is not an eigenfunction of H_0. This difficulty has also been recognized by others and has been solved by using projection operator techniques [Yaris, R.: J. chem. Physics **44**, 3894 (1966); Murrell, J. N., Shaw, G.: J. chem. Physics **46**, 1768 (1967)]. Kreek and Meath [J. chem. Physics **50**, 2289 (1969)] point out, that a satisfactory intermolecular perturbation theory can be formulated by neglecting electron exchange. This assumption is also a consequence of the CNDO approximation which is used in the present treatment.

$$E^i_j = \langle \psi_{i\to j}|H_0|\psi_{i\to j}\rangle - \langle \psi_0|H_0|\psi_0\rangle\,. \tag{7}$$

(6a) and (6b) should be the greater the lower the charge transfer excitation energies. This parallels results of independent electron models where the excitation energy (7) is replaced by the differences of orbital energies.

Application to Hydrogen Bonding in Water Dimers

The hydrogen bond of water dimers is by no means a new subject as the *ab initio* [11–14, 23] and semiempirical [15–18] calculations demonstrate. The energy and geometry of possible intermolecular complexes has been studied extensively. The aim of this communication is to show the usefulness of SCF-perturbation theory for hydrogen bonding. Perturbational approaches had been deviced by Bratoz [19], by van Duijneveldt and Murrell [20], and van Duijneveldt-van de Ridt and van Duijneveldt [24]. Bratoz evaluates the linear water hydrogen bond using as a basis the occupied and unoccupied hydroxy bond orbitals and a lone pair of the oxygen atom of the hydrogen acceptor in a colinear p-orbital. The problem is then solved analogous to our variation perturbation treatment. His final formula resembles the sum of our first and second order energy. It does not contain a second order electrostatic term and treats the short range repulsion (term 2 in Eq. (1)) by an exponential with empirical parameters. The difficulty in assessing the different quantities caused this theory to remain a qualitative one. Van Duijneveldt and Murrell [20] also restrict themselves to the linear O···H—O fragment. The free electron pair occupies a sp^2 – hybrid orbital. A long range perturbation theory for small intermolecular overlap [21] is applied to this model. However, this theory does not take proper account of short range interactions. For the hydrogen bond it does not lead to an energy minimum. Van Duijneveldt-van de Ridt and van Duijneveldt [24] have extended this latter theory in order to account for this failure. Recently Santry and Bacon [22] proposed an SCF-perturbational approach to treat hydrogen bonding similar to our theory [2, 4].

In our calculations we followed earlier investigations for the linear, bifurcated and cyclic water dimers [14]. The energy components are listed in Table 1 for the SCF-perturbation treatment and the variation perturbation calculations. The linear arrangement has been compared to a direct CNDO/2 calculation. The total SCF-perturbation energies agree within 1–2% (convergence limit for the maximum change of an element in the 1. order density matrix was ≤ 0.001). The value of the second order variation perturbation energy in the linear complex is smaller than the SCF-value. This becomes more pronounced the closer the separation of the two molecules, i.e. the higher the perturbation.

The superposition of the repulsive first order energy and the attractive second order energy yields potential curves which are almost identical to full variational calculations. Yet the perturbation calculations provide more insight. The first

---

[2] We use the following index convention: u, v: MO's in K; p, q: MO's in L; μ, ν: AO's in K; κ, λ: AO's in L

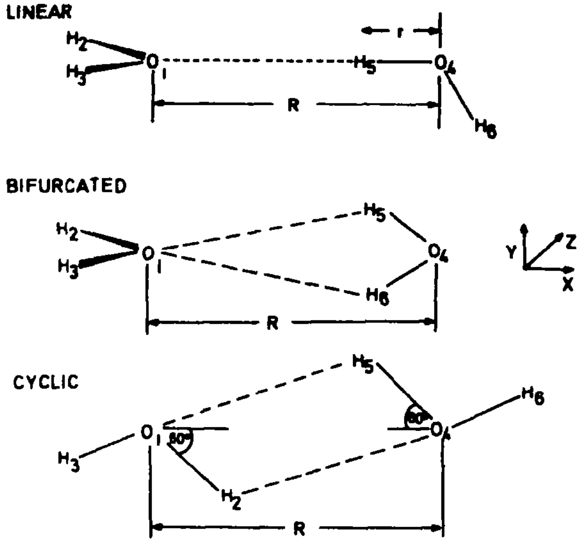

Fig. 1. Geometries of the linear, bifurcated and cyclic water dimers

order energy and the second order energy both can be split into two components. This has been done for the SCF-results in Fig. 2. The picture is dominated by the steric and the covalent contributions. The charge interactions are small (of the order of 1–2 kcal/mole) and do not show significant distance dependence. The second order electrostatic effects ((3), (6c) and (6d)) are negligible. They amount to 1–2% of the second order energy and are omitted from Fig. 2. The most stable structure is the linear. Even though the total energy for the other complexes is comparable the individual components differ appreciably.

Table 1 Perturbation energies for the linear (a), bifurcated (b) and cyclic (c) water dimers of Fig. 1 in kcal/mole. SCF = self consistent perturbation theory; VP = Variation perturbation theory; $E_{CNDO/2}$ = direct CNDO/2 calculation

	R(Å)	$\delta E^{(1)}$	$\delta E^{(2)}_{SCF}$	$\delta E^{(2)}_{VP}$	E^{total}_{SCF}	E^{total}_{VP}	$E_{CNDO/2}$
a	3.0	1.290	− 3.952	− 3.838	−2.662	−2.548	−2.811
	2.8	3.651	− 8.001	− 7.703	−4.350	−4.052	−4.468
	2.53	13.137	−19.306	−18.352	−6.168	−5.215	−6.255
	2.4	23.742	−28.425	−26.817	−4.683	−3.075	−4.844
b	3.0	0.034	− 1.041	− 1.045	−1.007	−1.011	
	2.8	0.497	− 2.059	− 2.064	−1.563	−1.568	
	2.44	3.703	− 6.303	− 6.315	−2.600	−2.612	
	2.4	4.470	− 7.063	− 7.077	−2.593	−2.608	
c	3.0	0.109	− 0.635	− 0.636	−0.525	−0.527	
	2.4	2.786	− 4.651	− 4.616	−1.866	−1.830	
	2.25	5.390	− 7.432	− 7.376	−2.042	−1.986	
	2.2	6.690	− 8.663	− 8.601	−1.973	−1.911	

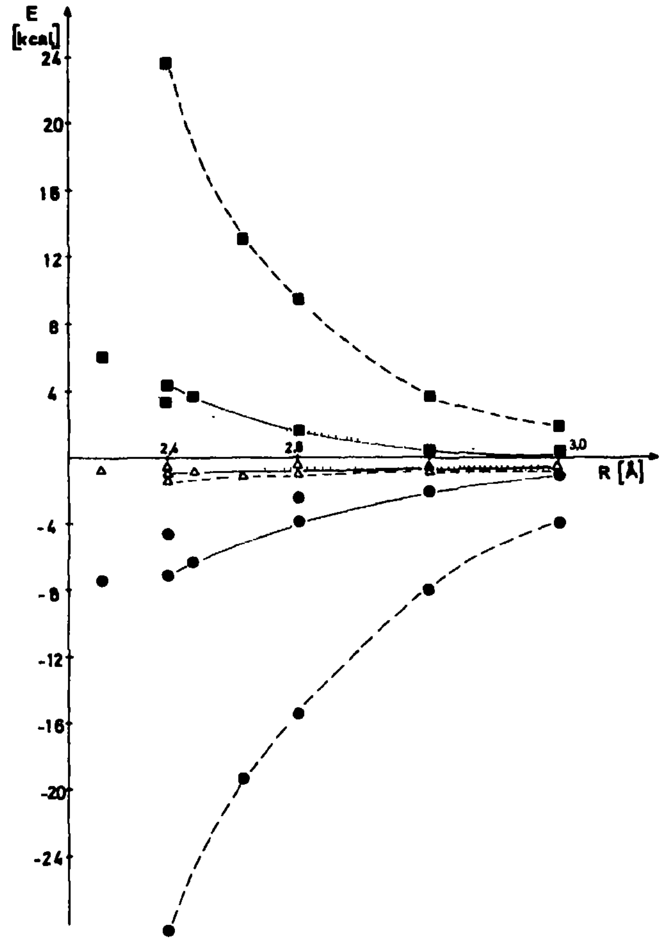

Fig. 2. Steric interactions (■), charge interactions (△) and covalent contributions (●) for the linear (- - - -), bifurcated (——) and cyclic (······) water dimers of Fig. 1

The SCF-perturbation theory allows a further splitting of the second order energy in contributions from the individual atomic orbitals of the subsystems [4]. This has been done for the $2s_1$ and $2p_{x1}$ atomic orbitals of the electron pair donor (for numbering see Fig. 1), the $1s_5$ atomic orbital of the bridged hydrogen atom and the $2p_{x4}$ atomic orbital of the second water molecule in Table 2. A comparison shows that these energy components amount to almost all of the second order energy. The variation perturbation theory elucidates that charge transfer interactions from the electron pair donor to unoccupied molecular orbitals of the hydrogen donor are responsible for more than 90% of the second order energy.

This detailed analysis justifies nicely the models of Bratoz [19] and of van Duijneveldt and Murrell [20]. Yet their approaches have limitations. Besides the restrictions mentioned earlier they are not capable to consider non linear struc-

Table 2. Second order contributions (kcal/mole) by atomic orbitals of the linear structure. For numbering and coordinate system see Fig. 1

R(Å)	$2s_1$	$2p_{x1}$	$1s_5$	$2p_{x4}$	Sum
3.0	0.705	− 1.204	− 2.139	0.126	− 3.922
2.8	− 1.440	2.426	− 4.407	0.309	− 7.964
2.53	− 3.517	− 5.779	− 11.026	1.027	− 19.295
2.4	− 5.209	− 8.429	− 16.623	1.792	28.469

tures. Therefore the influence of other atoms or groups in a molecule can not be assessed.

The cyclic and bifurcated structure are both less stable. The steric energies are more favourable because the intermolecular distances of the hydrogen and oxygen atom are greater. However, the covalent stabilization also decreases. The variation perturbation treatment traces this back to smaller charge transfer interactions from the oxygen lone pair to the unoccupied orbitals of the hydrogen donor.

Conclusions

The perturbational evaluation of water dimers not only provides comparable results to variation calculations but furthermore yields insight into the factors determining the most stable structure. The splitting of the total energy into four components reveals that coulombic forces (due to the polarity of the molecules) are not important in determining the most stable complexes. Rather the interplay of steric and covalent contributions gives rise to the observed minimum structure. The variation perturbation theory yields good results as long as the perturbation remains small. It has the advantage of shorter computation times and the possibility of interpretations similar to independent electron perturbation theory. The SCF-CNDO/2-perturbation program, the variation perturbation program will be available from QCPE. Further work on hydrogen bonding will be published in due time.

Acknowledgments. This work was supported by Deutsche Forschungsgemeinschaft. Computer time was provided by the Computation Centre of the university in Münster.

References

1. McWeeny, R.: Chem. Physics Letters **1**, 567 (1968).
2. Sustmann, R., Binsch, G.: Molecular Physics **20**, 1 (1971).
3. Baird, N. C., Dewar, M. J. S.: J. chem. Physics **50**, 1262 (1969)
4. Sustmann, R., Binsch, G.: Molecular Physics **20**, 9 (1971).
5. Pople, J. A., Santry, D. P., Segal, G. A.: J. chem. Physics **43**, S 129 (1965). Pople, J. A., Segal, G. A.: J. chem. Physics **43**, S 136 (1965); **44**, 3289 (1966).
6 Sustmann, R., Ansmann, A., Vahrenholt, F.: J. Amer. chem. Soc. **94**, 8099 (1972). Ansmann, A.: Diplomarbeit. Universität Münster 1971.
7. Pople, J. A.: Proc. Royal Soc. (London) A **233**, 233 (1955).
8. Pople, J. A., Schofield, P.: Proc. Royal Soc. (London) A **233**, 241 (1955).
9. Sustmann, R.: Habilitationsschrift, Universität Münster 1970.

10. Vahrenholt, F.: Diplomarbeit, Universität Münster 1971.
11. Diercksen, G. H. F.: Theoret. chim. Acta (Berl.) **21**, 335 (1971).
12. Morokuma, K., Pedersen, L.: J. chem. Physics **48**, 3275 (1968).
13. Del Bene, J., Pople, J. A.: Chem. Physics Letters **4**, 426 (1969).
14. Kollman, P. A., Allen, L. C.: J. chem. Physics **51**, 3286 (1969).
15. Murthy, A. S. N., Rao, C. N. R.: Chem. Physics Letters **2**, 123 (1968).
16. Hoyland, J. R., Kier, L. B.: Theoret. chim. Acta (Berl.) **15**, 1 (1969).
17. Schuster, P., Funck, T.: Chem. Physics Letters **2**, 587 (1968).
18. Kollman, P. A., Allen, L. C.: J. Amer. chem. Soc. **92**, 753 (1970).
19. Bratoz, S.: Advances in quant. Chemistry **3**, 209 (1967).
20. Van Duijneveldt, F. B., Murrell, J. N.: J. chem. Physics **46**, 1759 (1967); Murrell, J. N.: Chem. in Britain **13**, 107 (1970).
21. Murrell, J. N., Randic, M., Williams, D. R.: Proc. Royal Soc. A**284**, 566 (1965).
22. Bacon, J., Santry, D. P.: J. chem. Physics **55**, 3743 (1971).
23. Kollman, P. A., Allen, L. C.: J. Amer. chem. Soc. **93**, 4991 (1971).
24. Van Duijneveldt-van de Ridt, J., van Duijneveldt, F. B.: J. Amer. chem. Soc. **93**, 5644 (1971).

Dr. Reiner Sustmann
Organisch Chemisches Institut der Universität
D-4400 Münster, Orleansring 23
Federal Republic of Germany

Theoret. chim. Acta (Berl.) 29, 313—317 (1973)
© by Springer-Verlag 1973

Sesquiacetylenes

J. Y. Becker, A. Y. Meyer, and J. Klein
Department of Organic Chemistry, Hebrew University, Jerusalem

Received March 23, 1972

All-valence-electron SCF calculations support the linear "sesquiacetylenic" geometry in propargylic dianions. The two accompanying univalent cations are close to the central carbon, with an angle MC^2M of 90°. The migration of lithium in allylic systems is interpreted as an intramolecular sigmatropic rearrangement.

SCF-Rechnungen unter Benutzung aller Valenzelektronen stützen die lineare "sesquiacetylen"-ähnliche Geometrie in Propargyldianionen. Die beiden zugehörigen Kationen befinden sich in der Nähe des zentralen Kohlenstoffatoms und bilden einen MC^2M-Winkel von 90°. Die Wanderung des Lithiums in allylartigen Systemen wird als intramolekulare sigmatrope Umlagerung interpretiert.

Des calculs SCF pour tous les électrons de valence sont en faveur de la géométrie linéaire «sesquiacétylénique» dans les dianions propargyliques. Les deux cations univalents correspondants sont proches du carbone central avec un angle MC^2M de 90°. La migration du lithium dans les systèmes allyliques est interprétée comme un réarrangement intramoléculaire sigmatrope.

It has been shown [1–4] that two or more protons can be abstracted from a propargylic system ($RCH_2C{\equiv}CCH_2R$) and that this abstraction occurs preferentially on the same carbon [4], leading to $[RCH_2C{\equiv}CCR]^{-2}$ rather than to $[RCHC{\equiv}CCHR]^{-2}$. Also, in $PhC{\equiv}CCH_3$, the second proton is removed faster than the first, so that 1 mole of BuLi produces half a mole of dianion, no monoanion being detectable [4]. Furthermore [4], the NMR spectrum of $[RCH{=}CHCC{\equiv}CR]^{-2}$ shows that, unlike in monoanions, the charge is localized in the propargylic system. The phenomena were attributed to the stability of an eight-pi-electron system, when based on a linear, terminally substituted, three-carbon segment. The arrangement was termed [4] extended-acetylene or sesquiacetylene.

Here we report that SCF–MO calculations, of the CNDO/2-type [5], support the hypothesis of linearity and indicate that the sesquiacetylenic structure (*I*) is more stable than a twisted, allenic disposition (*II*). In these calculations, performed by a current [6] computer-program, we considered as

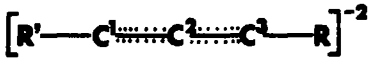

I

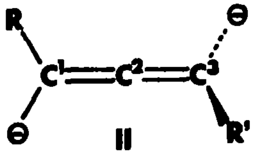

II

models several geometries of dianions derivable from propyne ($CH_3C{\equiv}CH$) and 2-butyne ($CH_3C{\equiv}CCH_3$). Geometrical details and computed energies are given in Tables 1 and 2. Despite certain limitations of the method [7], the energies are expected to reflect the order of stability of the various species.

As for input geometries, both allenic and acetylenic bond-lengths, as well as intermediate situations, were examined; in the Tables, however, only results for *lowest-energy* structures are reported. For example, in the case of $C^1H_3C^2C^3C^4H$ (fifth species in Table 1), the energy was found to augment steadily as one passes from the acetylenic arrangement [$r(C^2C^3) = r(C^3C^4) = 1.20$ Å; $E = -843.04$ eV] to the allenic [$r(C^2C^3) = r(C^3C^4) = 1.31$ Å; $E = -838.56$ eV]. Also, at each value of $r(CC)$, the stablest arrangement has $r(C^4H) = 1.08$ Å [values in the range 1.060 Å (allenic) to 1.096 Å (tetrahedral) were examined]. Accordingly, Table 1 reports only the case with $r(C^2C^3) = r(C^3C^4) = 1.20$ Å, $r(C^4H) = 1.08$ Å.

For the derivative of propyne ($[CHCCH]^{-2}$), a sesquiacetylenic linear structure, with equal CC-bond lengths, is found (Table 1) to be more stable, and to correspond to higher bond-populations, than any allenic arrangement; it is also endowed of a more pronounced charge-alternation. As for the Li atoms, it is seen (Table 2) that the optimal arrangement has them close to the central carbon (C^2), with an angle LiC^2Li of 90° (*III*); an angle of 180°, although characterized by a lower Li–Li repulsion, still corresponds to a higher total energy.

The two, almost degenerate, highest-occupied molecular orbitals have the following (overlap-renormalized) forms:

$$\begin{aligned}\varphi(\mathrm{HOMO}) = {} & 0.4\,[x(C^1) - x(C^3) - z(C^1) + z(C^3)] \\ & + 0.3\,[y(Li^1) + y(Li^2)] + \cdots\end{aligned}$$

$$\begin{aligned}\varphi(\mathrm{HOMO}-1) = {} & 0.46\,[x(C^1) - x(C^3) + z(C^1) - z(C^3)] \\ & + 0.2\,[y(Li^1) - y(Li^2)] + \cdots\end{aligned}$$

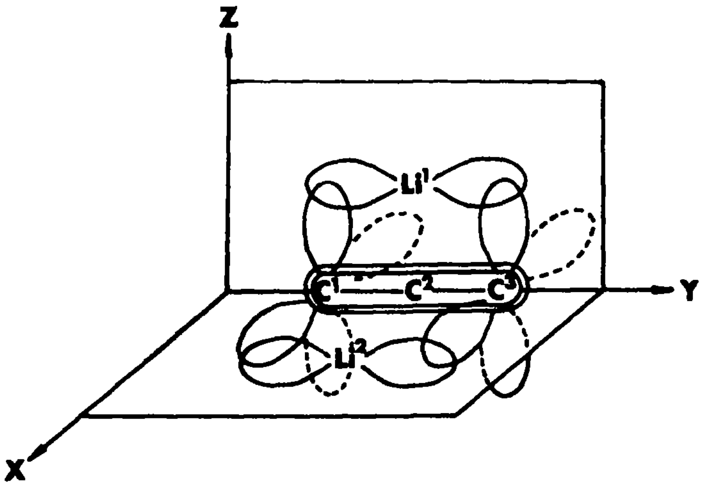

III

Table 1. CNDO/2 results for dianions

Dianion structure	Energy (eV)	Atomic population		Overlap population	
		Carbon	Hydrogen	CC	CH
I,[a] $R'=R=H$	−600.46	C^1, −0.905 C^2, +0.185	−0.188	1.506	0.788
I,[b] $R'=R=H$	−599.18	C^1, −0.852 C^2, +0.042	−0.169	1.419	0.790
II,[b] $R'=R=H$	−600.12	C^1, −0.776 C^2, −0.040	−0.204	1.209	0.547
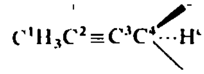 $C^1H_3C^2{\equiv}C^3C^4\cdots H^c$	−842.71	C^1, +0.146 C^2, −0.643 C^3, +0.115 C^4, −0.780	H^1, −0.220 H^4, −0.178	C^1C^2, 1.115 C^2C^3, 1.423 C^3C^4, 1.169	C^1H, 0.611 C^4H, 0.522
$C^1H_3C^2{=}C^3{-}C^4{-}H^d$	−843.04	C^1, +0.176 C^2, −0.693 C^3, +0.182 C^4, −0.768	H^1, −0.244 H^4, −0.167	C^1C^2, 1.157 C^2C^3, 1.431 C^3C^4, 1.576	C^1H, 0.591 C^4H, 0.789
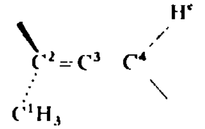 $C^2{=}C^3\ C^4\ H^e$, C^1H_3	−840.31	C^1, +0.163 C^2, −0.668 C^3, +0.032 C^4, −0.816	H^1, −0.211 H^4, −0.080	C^1C^2, 0.872 C^2C^3, 1.182 C^3C^4, 1.184	C^1H, 0.635 C^4H, 0.491
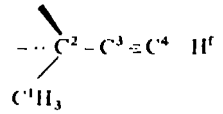 $C^2{-}C^3{\equiv}C^4\ H^f$, C^1H_3	−838.92	C^1, +0.150 C^2, −0.909 C^3, −0.026 C^4, −0.455	H^1, −0.207 H^4, −0.138	C^1C^2, 0.784 C^2C^1, 0.904 C^3C^4, 1.583	C^1H, 0.643 C^4H, 0.797
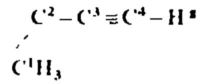 $C^2{-}C^3{\equiv}C^4{-}H^g$, C^1H_3	−840.91	C^1, +0.204 C^2, −0.745 C^3, +0.049 C^4, −0.592	H^1, −0.261 H^4, −0.133	C^1C^2, 0.921 C^2C^3, 0.869 C^3C^4, 1.633	C^1H, 0.583 C^4H, 0.796

[a] Distance $r(C^1C^2) = r(C^2C^3) = 1.202$ Å, as in acetylenes [12, 13], $r(C^1H) = r(C^2H) = 1.060$ Å, as in acetylene [14].

[b] $r(C^1C^2) = r(C^2C^3) = 1.310$, $r(C^1H) = r(C^3H) = 1.070$ Å, as in allene [13].

[c] $r(C^1C^2) = 1.460$ Å as in propyne [12, 13], $r(C^2C^3) = r(C^3C^4) = 1.203$ Å, $r(C^1H) = r(C^4H) = 1.096$ Å [12]; C^1 and C^4 tetrahedral, with lone pairs occupying ligand positions.

[d] $r(C^1C^2) = 1.460$ [12, 13], $r(C^2C^3) = r(C^3C^4) = 1.200$, $r(C^1H) = 1.096$, $r(C^4H) = 1.080$ Å [12]; C^1 tetrahedral, C^4 linear.

[e] $r(C^1C^2) = 1.460$ [12, 13], $r(C^2C^3) = r(C^3C^4) = 1.310$ as in allene [12], $r(C^1H) = 1.096$, $r(C^4H) = 1.080$Å [12]; C^2 and C^4 trigonal, with lone pairs occupying ligand positions

[f] $r(C^1C^2) = 1.540$ [14], $r(C^2C^3) = 1.460$ [12, 13], $r(C^3C^4) = 1.212$ [12], $r(C^1H) = 1.096$ [12], $r(C^4H) = 1.057$ Å as in acetylene [14]; C^2 tetrahedral, with lone pairs occupying ligand positions.

[g] As in *f*, but C^2 trigonal.

Table 2. CNDO/2 results for dilithio derivatives of propyne

Dilithio derivative[a]	Energy (eV)	Atomic population Carbon	Lithium	Hydrogen	Overlap population CC	CLi	CH
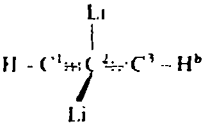	-647.11	C^1, −0.481 C^2, +0.217	+0.260	+0.112	1.342	0.154	0.798
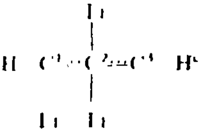	644.99	C^1, −0.586 C^2, +0.202	+0.389	+0.097	1.335	0.183	0.778
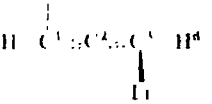	644.32	C^1, −0.492 C^2, +0.237	+0.256	+0.118	1.381	0.339	0.768
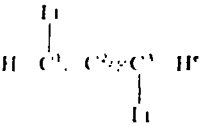	642.49	C^1, 0.601 C^2, +0.023	+0.390	+0.096	1.384	0.387	0.763
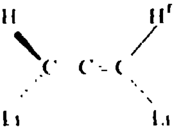	-641.59	C^1, −0.439 C^2, +0.103	+0.349	+0.039	1.240	0.682	0.682

[a] The following were taken for all structures, except the last: $r(C^1C^2) = r(C^2C^3) = 1.202$ Å, as in acetylenes [12, 13], $r(CLi) = 2.2$ Å, as the shortest CLi-bond in solid CH_3Li [15] and CH_3CH_2Li [16], $r(CH) = 1.060$ Å [14], angle HCC of 180°. For the last (allenic): $r(C^1C^2) = r(C^2C^3) = 1.310$, $r(CH) = 1.070$ Å, as in allene [12], $r(CLi) = 2.2$ Å [15, 16], angle HCC of 120°.

[b] $LiC^2Li = 90$

[c] $LiC^2Li = 180$

[d] LiC^1C^3Li torsion angle 90

[e] LiC^1C^3Li torsion angle 180.

[f] $HCLi = 120$

We note that the contribution of C^2 is here insignificant, and that electrons are distributed mainly in $2p_y$ orbitals of Li and in the perpendicular $2p_x$ and $2p_z$ of the terminal carbons. φ(HOMO) also corresponds to a pi-bond between the two Li-atoms. The lithium p_y bridges thus C^1 and C^3, while C^2 is in the MO node (*III*). Hence, incidentally, an explanation for the easy migration of Li in allylic systems [8–10], which we interpret as *intramolecular*, rather than intermolecular, and accompanied by inversion. It is thus an allowed [11] sigmatropic rearrangement.

The bond between the lithiums and C^2 evolves from deeper MO's and has some pi-character. This is illustrated by the following (last MO but one):

$$\varphi = 0.14\,[H^1 - H^2] + 0.46\,[s(C^1) - s(C^3)] \\ - 0.28\,y(C^2) - 0.07\,[y(Li^1) + y(Li^2)]\,.$$

References

1. Eberly, K. C., Adams, H. E.: J. organomet. Chem. **3**, 165 (1967).
2. West, R., Correy, P. A., Mines, I. C.: J. Amer. chem. Soc. **87**, 3788 (1965).
   West, R., Jones, P. C.: J. Amer. chem. Soc. **91**, 6156 (1969).
3. Mulvaney, J. E., Folk, I. C., Newtor, D. J.: J. org. Chem. **32**, 1674 (1967).
4. Klein, J., Brenner, S.: J. Amer. chem. Soc. **91**, 3094 (1969). - J. organomet. Chem. **18**, 291 (1969). - Tetrahedron **26**, 2345, 5807 (1970).
   Klein, J., Gurfinkel, E.: J. org. Chem. **34**, 3952 (1969).
5. Pople, J. A., Segal, G. A.: J. chem. Physics **44**, S 3289 (1966).
6. Clark, P. A., Ragle, J. L.: CNDOTWO-SCF-LCAO-MO, QCPE Catalogue, Vol. VII (1971), program 100, Indiana University.
7. Daudel, R., Pullman, A. (Eds.). Aspects de la chimie quantique contemporaine, pp. 34–48. Paris: Editions du CNRS 1971.
8. Johnson, C. S., Wiener, M. A., Waugh, J. S., Seyferth, D.: J. Amer. chem. Soc. **83**, 1306 (1961).
9. Seyferth, D., Jula, T. F.: J. organomet. Chem. **8**, 13 (1967).
10. Freedman, H. H., Sandel, V. R., Thill, B. P.: J. Amer. chem. Soc. **89**, 1762 (1967).
    West, R., Purmort, J. I., McKinley, S. V.: J. Amer. chem. Soc. **90**, 797 (1968).
    Waack, R., Doran, M.: J. Amer. chem. Soc. **85**, 1651 (1963).
    Kuwata, K.: Bull. chem. Soc. Japan **33**, 1091 (1960).
11. Woodward, R. B., Hoffmann, R.: Angew. Chem. international Ed. **8**, 781 (1969).
12. Sutton, L. E. (Scient. Editor): Tables of interatomic distances and configuration in molecules and ions. London: The Chemical Society 1958 and 1965.
13. Cartmell, E., Fowler, G. W. A.: Valence and molecular structure, 3rd Ed., p. 126 and 151. London: Butterworths 1966.
14. Cottrell, T. L.: The strength of chemical bonds, p. 272. London: Butterworths 1954.
15. Weiss, E., Lucken, E. A. C.: J. organomet. Chem. **2**, 200 (1964).
16. Dietrich, H.: Acta crystallogr. **16**, 681 (1963).

Dr. A. Y. Meyer
Department of Organic Chemistry
Hebrew University
Jerusalem, Israel

Theoret. chim. Acta (Berl.) 29, 319 - 334 (1973)
© by Springer-Verlag 1973

Le spectre d'absorption électronique du trichloroamminoplatinate de potassium cristallisé

Edmond Francke et Claude Moncuit

Département de Recherches Physiques, Laboratoire associé au CNRS n° 71 Université Paris VI et Département de Physique, Université d'Orléans

Reçu le 1 août 1972/8 novembre 1972

Electronic Absorption Spectra of Crystallized $K[PtCl_3(NH_3)] \cdot H_2O$

Absorption spectra of single crystals with light polarized parallel to the principal axes at room temperature and at 10 °K, have been recorded. The spectra, including spin-orbit coupling, has been calculated by means of the values of the parameters characterising the schemes *A* and *B*, suggested for K_2PtCl_4 by Martin *et al.* The "Angular-Overlap model" is applied in order to evaluate the result of the substitution of one Cl by one NH_3.

On a mesuré les spectres d'absorption de monocristaux en lumière polarisée selon chacun des axes principaux, à la température ambiante et à 10 °K. On a d'autre part calculé les spectres, compte tenu de l'interaction spin-orbite, avec les valeurs des paramètres caractérisant les schémas *A* et *B* proposés par Don S. Martin *et al.* pour K_2PtCl_4, en utilisant le «Modèle de recouvrement angulaire» pour évaluer l'effet de la substitution d'un Cl par un NH_3.

Einkristall-Absorptionsspektren wurden mit polarisiertem Licht, parallel zu den Hauptachsen, bei gewöhnlicher Temperatur und bei 10 °K gemessen. Unter Berücksichtigung der Spin-Bahn-Kopplung wurden die Spektren mit Hilfe der jeweiligen Parametersätze, die Martin *et al.* für $PtCl_4$ vorgeschlagen hatten und die im folgenden mit *A* und *B* bezeichnet werden, berechnet. Schließlich wurde der Substitutionseffekt NH_3 gegen Cl nach dem „Angular-Overlap" Modell abgeschätzt.

Introduction

L'ion complexe $[PtCl_4]^{2-}$ a déjà été l'objet d'un certain nombre de travaux théoriques et expérimentaux, [1] à [10]. Martin et ses collaborateurs, qui ont étudié de manière approfondie les propriétés optiques et magnétiques de K_2PtCl_4 cristallisé [4 – 6], proposent le classement des orbitales à caractère 5*d* prépondérant, dans l'ordre des énergies croissantes, selon:

A) $a_{1g}(d_{z^2}) < e_g(d_{yz}, d_{zx}) < b_{2g}(d_{xy}) \ll b_{1g}(d_{x^2-y^2})$ ou

B) $e_g(d_{yz}, d_{zx}) \lesssim a_{1g}(d_{z^2}) < b_{2g}(d_{xy}) \ll b_{1g}(d_{x^2-y^2})$.

Selon ces auteurs le classement B apparaît le plus convenable pour rendre compte des faits expérimentaux, sans que le classement A puisse cependant être absolument rejeté. C'est, d'ailleurs, à ce schéma A qu'aboutissent les calculs des énergies des orbitales moléculaires de ce complexe [7, 8]. Pourtant, la transition $a_{1g}(d_{z^2}) \rightarrow b_{1g}(d_{x^2-y^2})$ n'a pas été identifiée de manière tout à fait sûre dans le spectre d'absorption de K_2PtCl_4 [9]. Nous nous sommes proposé de contribuer à cette recherche en mesurant le spectre d'absorption en lumière polarisée, à basse température, de $K[PtCl_3(NH_3)] \cdot H_2O$ cristallisé qui offre l'avantage d'une

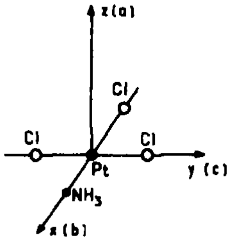

Fig. 1. Schéma de l'ion $[\mathrm{Pt\,Cl_3(NH_3)}]^-$

symétrie orthorhombique et permet ainsi une investigation aussi complète q possible de la polarisation des transitions.

La structure cristalline de ce composé est connue [11]. L'ion comple $[\mathrm{Pt\,Cl_3(NH_3)}]$, plan, possède quatre liaisons platine-«ligand» à peu près orth gonales entre elles et a sensiblement la symétrie du groupe ponctuel C_{2v}. L axes moléculaires x, y et z que nous choisissons comme il est indiqué sur la Fig. sont respectivement parallèles aux axes cristallographiques b, c et a.

Nous donnons dans le Tableau 1, les polarisations des transitions de dipô électrique permises comme transitions électroniques pures dans la symétrie C et les polarisations des transitions vibroniques permises par perturbation vibr tionelle par les modes β_1 et β_2. Le dénombrement des modes de vibrations intern de l'ion complexe, en considérant NH_3 comme une entité, s'effectue en eff selon: $4\alpha_1, 3\beta_1, 2\beta_2$.

Avec ce choix des axes moléculaires (Fig. 1) et en conservant les axes x et dirigés vers les «ligands» dans le cas de l'ion $[\mathrm{Pt\,Cl_4}]^{2-}$ de symétrie D_{4h}, il e possible d'établir la corrélation entre les représentations des groupes D_{4h} et C telle qu'elle est mentionnée dans le Tableau 2.

Tableau 1. Polarisations des transitions électroniques pures et vibroniques vers les différents ét excités de l'ion $[\mathrm{Pt\,Cl_3(NH_3)}]$

Symétrie de l'état excité	Transition électronique pure	Transition vibronique Mode β_1	Mode β_2
A_1	x	y	z
A_2	–	z	y
B_1	y	x	–
B_2	z	–	x

Tableau 2. Corrélation entre les représentations des groupes D_{4h} et C_{2v}

D_{4h}	C_{2v}	D_{4h}	C_{2v}
A_{1g}	A_1	A_{1u}	A_2
A_{2g}	B_1	A_{2u}	B_2
B_{1g}	A_1	B_{1u}	A_2
B_{2g}	B_1	B_{2u}	B_2
E_g	$A_2 + B_2$	E_u	$A_1 + B_1$

On prévoit ainsi que les transitions vers les états excités $A_{2g}(d_{xy}\to d_{x^2-y^2})$ $B_{1g}(d_{z^2}\to d_{x^2-y^2})$ et $E_g(d_{yz}, d_{zx}\to d_{x^2-y^2})$ de la symétrie D_{4h} doivent être permises dans la symétrie C_{2v}, polarisées selon y, z et x respectivement. La détermination de la polarisation devrait donc contribuer efficacement à l'identification de ces transitions.

Résultats expérimentaux

Nous avons préparé le composé $K[Pt\,Cl_3(NH_3)]$ à partir de $[Pt\,Cl_2(NH_3)_2]$ *cis*, selon la méthode indiquée par Lebedinsky et Golovnja [12]. Par évaporation lente, isotherme de solutions aqueuses saturées, nous avons obtenu le monohydrate $K[Pt\,Cl_3(NH_3)]\cdot H_2O$ sous forme de cristaux prismatiques assez volumineux ($10 \times 5 \times 3$ mm^3) pour permettre la taille et l'orientation de lames cristallines de dimensions suffisantes pour une étude optique. Nous avons ainsi examiné des lames parallèles aux trois plans principaux: $zx(ab)$, $xy(bc)$ et $yz(ca)$.

Nous avons mesuré l'absorption de 2000 à 8000 Å au moyen d'un spectrophotomètre Cary 14 et utilisé pour les mesures à la température de l'hélium liquide un cryostat dans lequel le cristal se trouve en contact direct avec le gaz froid.

Nous représentons sur la Fig. 2 le spectre d'absorption des solutions aqueuses légèrement acidifiées par H Cl, fraîchement préparées. Ce spectre comporte, dans la région examinée, un épaulement vers 24500 cm^{-1} et trois maxima situés à 29200, 33500 et 48500 cm^{-1}. Nous avons également représenté sur cette figure

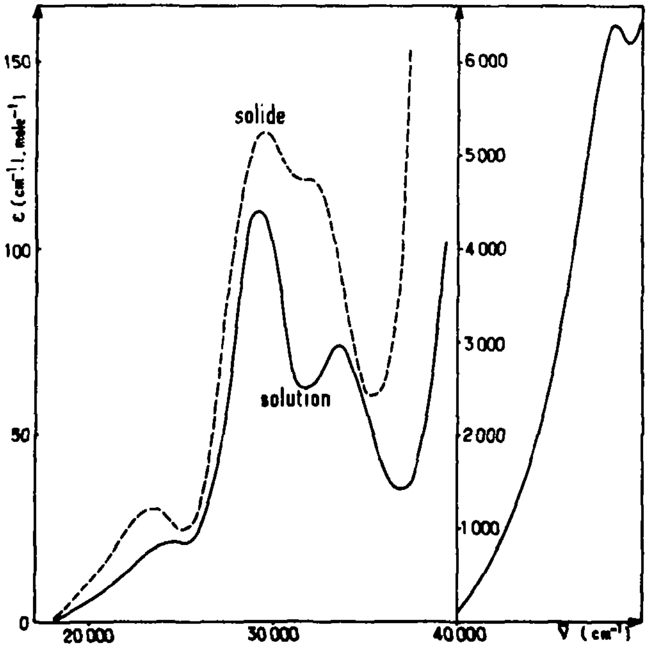

Fig. 2. Spectre d'absorption de $K[Pt\,Cl_3(NH_3)]\cdot H_2O$

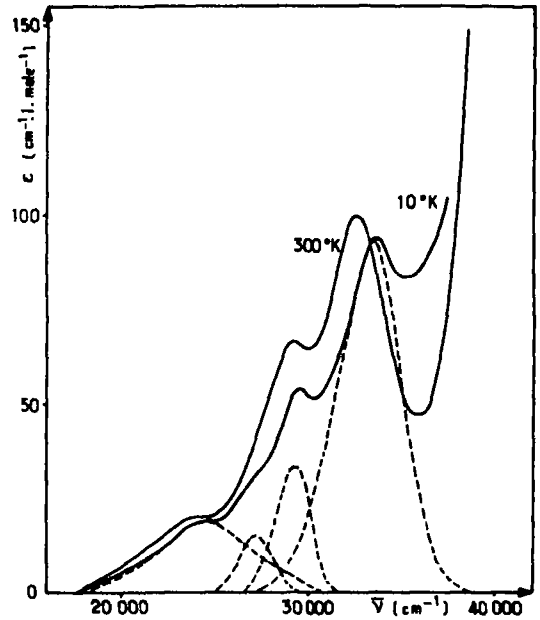

Fig. 3. Spectre d'absorption polarisé selon x de $K[PtCl_3(NH_3)]\cdot H_2O$

le spectre d'absorption non polarisé du composé à l'etat solide, obtenu en faisant la moyenne pondérée, $\varepsilon = \frac{1}{3}(\varepsilon_x + \varepsilon_y + \varepsilon_z)$ des coefficients d'absorption suivant chacun des axes x, y et z. Bien que les maxima soient un peu déplacés, ce spectre est assez semblable à celui des solutions. Les spectres d'absorption obtenus à la température ordinaire et à une température voisine de 10 °K, polarisée en x, y et z, sont représentés sur les Figs. 3, 4 et 5 respectivement. A la température ordinaire, le spectre polarisé en x présente un épaulement vers 24000 cm^{-1} et deux maxima à 29400 et 32800 cm^{-1}. Les spectres polarisés en y et z ne comportent que deux maxima situés à 23000 et 29400 cm^{-1} pour la polarisation y, à 23500 et 33000 cm^{-1} pour la polarisation z.

L'examen des spectres obtenus à 10 °K montre que ces spectres résultent de la présence d'un plus grand nombre de bandes. Il apparait notamment un épaulement supplémentaire, vers 28000 cm^{-1}, dans les spectres polarisés en x et en z, et la bande à 23000 cm^{-1} du spectre polarisé en y présente un début de résolution en deux composantes. Les minima présentés par ces spectres forment des vallées moins profondes. Cette altération du spectre peut être due à une modification de l'échantillon cristallin à basse température. Cette modification est cependant réversible car nous avons pu vérifier que le spectre du cristal ramené à la température ambiante était identique à celui qui avait été obtenu avant refroidissement. Nous avons analysé les spectres en courbes de Gauss afin de déterminer les positions des bandes, $\bar{\nu}$, et leurs forces d'oscillateur, f, mentionnées dans le Tableau 3. Dans les régions du spectre où la séparation n'est pas suffisante pour permettre une résolution en courbes gaussiennes dépourvue d'ambiguïté, la détermination des forces d'oscillateur est peu précise et,

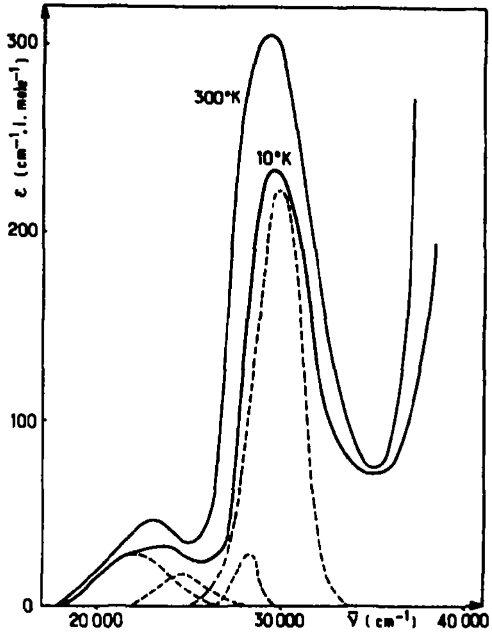

Fig. 4. Spectre d'absorption polarisé selon y de $K[Pt\,Cl_3(NH_3)] \cdot H_2O$

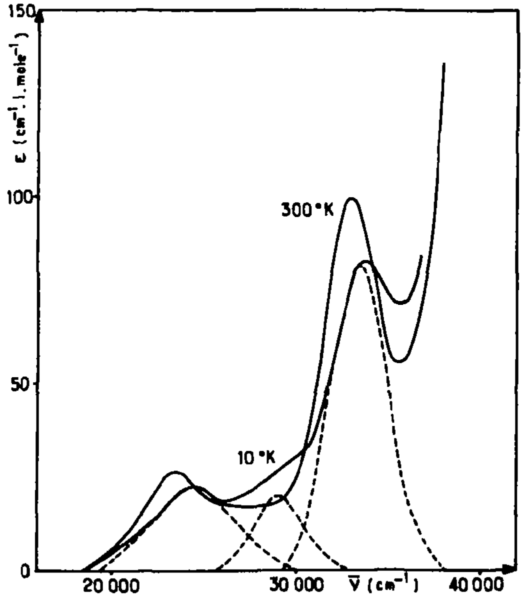

Fig. 5. Spectre d'absorption polarisé selon z de $K[Pt\,Cl_3(NH_3)] \cdot H_2O$

dans ce cas, les valeurs calculées sont indiquées entre parenthèses. La résolution en courbes de Gauss des spectres obtenus à basse température est reportée sur les Figs. 3, 4 et 5.

Tableau 3. Spectre d'absorption de $K[PtCl_3(NH_3)].H_2O$ cristallisé

	T = 300 K			T = 10 K		
	$\bar{\nu}$(cm^{-1})	ε	$f \times 10^3$	$\bar{\nu}$(cm^{-1})	ε	$f \times 10^3$
Polaris x	24000	20	0,63	24400	18	0,45
				(27200)	(15)	0.14
	29200	57	0,94	29600	33	0,30
	32800	94	1,73	33600	92	1,52
Polaris y				(22000)	(29)	(0,57)
	23000	46	1,10	(24500)	(18)	(0,24)
	(28000)	(46)	(0,25)	(28300)	(29)	(0,19)
	29200	290	4,60	29600	224	3,19
Polaris z	23600	27	0,57	24400	22	0,42
	(28400)	(18)	(0,25)	(29200)	(20)	(0,27)
	33000	100	1,66	33600	82	1,36

Discussion et interprétation des résultats

Le spectre d'absorption des solutions aqueuses fraîches de $K[PtCl_3(NH_3)] \cdot H_2O$ représenté sur la Fig. 2 est analogue à celui des solutions de K_2PtCl_4, bien que déplacé vers le violet de 3000 à 4000 cm^{-1} environ. Ces résultats sont en accord avec ceux de Chatt *et al.* [1]. On observe en outre une bande intense à 48500 cm^{-1}. Cette bande est manifestement l'analogue de la bande de transfert de charge observée vers 46000 cm^{-1} dans le spectre de $[PtCl_4]^{2-}$ et peut être attribuée à une transition «$\pi(Cl) \rightarrow 5d_{x^2-y^2}$». La similitude du spectre pondéré des cristaux et du spectre des solutions (Fig. 2) conduit à penser que les actions intermoléculaires existant dans le réseau cristallin sont négligeables. Il apparait donc que le spectre d'absorption du cristal $K[PtCl_3(NH_3)] \cdot H_2O$ est celui de l'ion $[PtCl_3(NH_3)]$ et qu'il est possible de prévoir ce spectre à partir de celui de l'ion $[PtCl_4]^{2-}$ si on sait évaluer les conséquences de la substitution d'un «ligand» Cl par un «ligand» NH_3. A cet effet la méthode exposée sous le nom de «Modéle de recouvrement angulaire» par Jørgensen et ses collaborateurs [13 - 15] semble très appropriée.

Energie des orbitales «à caractère d» dans le modèle de recouvrement angulaire

Dans le cas d'un chromophore MX_4 de symétrie D_{4h}, les énergies des orbitales moléculaires σ antiliantes (a_{1g}, b_{1g}) et π antiliantes (b_{2g}, e_g), mesurées à partir de l'énergie d'une orbitale d non liante, s'obtiennent en fonction des paramètres e_σ et e_π du modèle de recouvrement angulaire comme:

$$\varepsilon(a_{1g}) = e_\sigma, \quad \varepsilon(b_{1g}) = 3e_\sigma, \quad \varepsilon(b_{2g}) = 4e_\pi, \quad \varepsilon(e_g) = 2e_\pi. \quad [13].$$

Lorsque le «ligand» X est un halogène, on a $e_\pi/e_\sigma \simeq 0{,}25$ à $0{,}30$ [14]. Il en résulte l'ordre des énergies: $e_g < b_{2g} \lesssim a_{1g} \ll b_{1g}$. Si ce classement vaut pour des complexes faiblement covalents, il ne peut être conservé pour $[PtCl_4]^{2-}$ puisque les résultats expérimentaux conduisent dans ce cas à attribuer à l'orbitale a_{1g} l'énergie la plus basse, sinon sensiblement égale à celle de l'orbitale e_g [5]. Cette stabilisation de l'orbitale a_{1g} s'explique par la participation de l'orbitale 6 *s*, ce qui diminue beaucoup la densité électronique de l'orbitale a_{1g} dans le plan de l'ion complexe et rend cette orbitale moins antiliante [7, 8].

Nous pouvons tenir compte de l'interaction avec l'orbitale 6 *s*, assez simplement, de la manière suivante. Soit une orbitale moléculaire ψ, formée d'une orbitale du métal φ_M, et d'une combinaison de symétrie appropriée, φ_X, des orbitales des «ligands». On suppose, selon le principe du modèle de recouvrement angulaire, que l'effet antiliant est proportionnel au carré de l'intégrale de recouvrement de groupe S_{MX}, des orbitales φ_M et φ_X, puisque l'énergie de l'orbitale ψ, ainsi qu'il ressort d'un calcul de perturbation au 2ème ordre peut s'écrire [14]:

$$E \simeq H_M + S^2_{MX}\frac{H^2_X}{H_M - H_X}.$$

H_M et H_X désignent respectivement les énergies des orbitales φ_M et φ_X.

Soit, dans le cas présent, $\varphi_M = (1+\lambda^2)^{-\frac{1}{2}}(5d_{z^2} + \lambda 6s)$, il vient:

$$S^2_{MX} = \frac{(1+\lambda\varrho)^2}{1+\lambda^2} S^2_{5d_{z^2},X}, \quad \text{en posant} \quad \varrho = \frac{S_{6s,X}}{S_{5d_{z^2},X}}$$

d'où:

$$\varepsilon(a_{1g}) = H_M - H_{5d} + \frac{(1+\lambda\varrho)^2}{1+\lambda^2} S^2_{5d_{z^2},X}\frac{H^2_X}{H_M - H_X}$$

qui tend, pour $\lambda = 0$, vers $S^2_{5d_{z^2},X}\dfrac{H^2_X}{H_{5d} - H_X} = e_\sigma$. Par suite:

$$\varepsilon(a_{1g}) = a + be_\sigma$$

en posant:

$$a = H_M - H_{5d} \simeq \frac{\lambda^2}{1+\lambda^2}(H_{6s} - H_{5d})$$

et $b = \dfrac{(1+\lambda\varrho)^2}{1+\lambda^2}\dfrac{H_{5d} - H_X}{H_M - H_X} \simeq \dfrac{(1+\lambda\varrho)^2}{1+\lambda^2}$ puisque H_{6s} et $H_{5d} \gg H_X$.

L'orbitale φ_X est une combinaison d'orbitales 3*s* et 3*p* des «ligands». D'après [7] on a: $\dfrac{S_{6s,3p}}{S_{5d_{z^2},3p}} = -\dfrac{0{,}5298}{0{,}1440} = -3{,}679$ et $\dfrac{S_{6s,3s}}{S_{5d_{z^2},3s}} = -\dfrac{0{,}3676}{0{,}1101} = -3{,}339$. Comme, de plus, les orbitales 3*p* interviennent de manière prèpondérante, nous prendrons $\varrho = \dfrac{S_{6s,X}}{S_{5d_{z^2},X}} = -3{,}679$. Il en résulte que *b* s'annule, c'est-à-dire que l'orbitale a_{1g} est non liante pour $\lambda = 0{,}272$. Son énergie est alors égale à $a_0 = a(\lambda = 0{,}272)$. Les énergies des orbitales 6*s* et 5*d*, qui sont mêlées dans φ_M, ne sont pas très différentes. Avec $H_{6s} - H_{5d} = 6350\,\mathrm{cm}^{-1}$ [8], on trouve $a_0 \simeq 450\,\mathrm{cm}^{-1}$. Notons que selon Basch et Gray [7], l'orbitale 6*s* intervient dans la formation de l'orbitale a_{1g} avec un coefficient égal à 0,302, ce qui correspond dans le modèle utilisé ici à une valeur $\lambda \simeq 0{,}32$, donc sensiblement au cas extrême où cette orbitale est non liante et a l'energie la plus basse.

D'après le calcul précédent, l'énergie antiliante de l'orbitale moléculaire a_{1g} s'exprime par: $\varepsilon(a_{1g}) = a + be_\sigma$. Ce résultat est formellement identique à celui qu'on obtiendrait si l'orbitale atomique φ_M était représentée uniquement par l'orbitale d_{z^2}, mais en remplaçant le paramètre d'énergie e_σ par le paramètre effectif $(a + be_\sigma)$, qui dépend par l'intermédiaire des quantités a et b du coefficient λ avec lequel intervient l'orbitale 6s dans cette orbitale φ_M. Les paramètres e_σ, e_π et λ peuvent être obtenus d'après:

$$\varepsilon(b_{1g}) - \varepsilon(b_{2g}) = 3e_\sigma - 4e_\pi\,,$$
$$\varepsilon(b_{2g}) - \varepsilon(e_g) = 2e_\pi\,,$$
$$\varepsilon(e_g) - \varepsilon(a_{1g}) = 2e_\pi - (a + be_\sigma)\,.$$

Selon le schéma A [5], on a pour $PtCl_4^{2-}$:

$$\varepsilon(b_{1g}) - \varepsilon(b_{2g}) = 26\,100\,\mathrm{cm}^{-1}\,,$$
$$\varepsilon(b_{2g}) - \varepsilon(e_g) = 4100\,\mathrm{cm}^{-1}\,,$$
$$\varepsilon(e_g) - \varepsilon(a_{1g}) = 8100\,\mathrm{cm}^{-1}\,.$$

Ces valeurs donneraient $e_\sigma = 11\,433\,\mathrm{cm}^{-1}$, $e_\pi = 2050\,\mathrm{cm}^{-1}$, $a + be_\sigma = -4000\,\mathrm{cm}^{-1}$. Avec ces valeurs de e_σ et de e_π, on obtient $\varepsilon(a_{1g}) = -4000\,\mathrm{cm}^{-1}$, c'est à dire que l'orbitale a_{1g} serait σ liante. Ceci n'est cependant pas compatible avec le modèle utilisé ici dans lequel on prévoit cette orbitale σ antiliante ou à la limite, non liante. Il semble préférable, afin de surmonter cette difficulté à interpréter le schéma A, d'admettre que ce schéma correspond au cas limite où l'orbitale a_{1g} est non liante et que le paramètre e_π peut ne pas avoir exactement la même valeur s'il s'agit d'une liaison π dans le plan de l'ion complexe $(e_{\pi\parallel})$ ou dans le plan perpendiculaire $(e_{\pi\perp})$.

On aurait alors:

$$\varepsilon(b_{1g}) - \varepsilon(b_{2g}) = 3e_\sigma - 4e_{\pi\parallel}\,,$$
$$\varepsilon(b_{2g}) - \varepsilon(e_g) = 4e_{\pi\parallel} - 2e_{\pi\perp}\,,$$
$$\varepsilon(e_g) - \varepsilon(a_{1g}) = 2e_{\pi\perp} - a_0\,.$$

D'où, avec $a_0 = 450\,\mathrm{cm}^{-1}$, $e_\sigma = 12\,917\,\mathrm{cm}^{-1}$, $e_{\pi\parallel} = 3162\,\mathrm{cm}^{-1}$, $e_{\pi\perp} = 4275\,\mathrm{cm}^{-1}$. D'autre part, selon le schéma B [5], avec: $\varepsilon(b_{1g}) - \varepsilon(b_{2g}) = 25\,700\,\mathrm{cm}^{-1}$, $\varepsilon(b_{2g}) - \varepsilon(e_g) = 4800\,\mathrm{cm}^{-1}$, $\varepsilon(e_g) - \varepsilon(a_{1g}) = -300\,\mathrm{cm}^{-1}$, on trouverait: $e_\sigma = 11\,767\,\mathrm{cm}^{-1}$, $e_{\pi\parallel} = e_{\pi\perp} = e_\pi = 2400\,cm^{-1}$ *et* $a + be_\sigma = 5100\,\mathrm{cm}^{-1}$, ce qui donne $\lambda = 0{,}093$.

Nous envisagerons maintenant la substitution d'un «ligand» Cl par un «ligand» NH_3 qui conduit à l'ion $[PtCl_3(NH_3)]^-$ représenté schématiquement sur la Fig. 1. Dans cette symétrie C_{2v}, nous avons les orbitales de symétrie $1a_1(5d_{z^2}, 6s)$, $2a_1(5d_{x^2-y^2})$, $a_2(5d_{yz})$, $b_1(5d_{xy})$ et $b_2(5d_{zx})$. Puisque le «ligand» NH_3 est essentiellement σ donneur, on peut admettre que le paramètre e'_π, c'est-à-dire $e_\pi(NH_3)$, est sensiblement nul. Les énergies des orbitales π antiliantes s'obtiennent ainsi selon:

$$\varepsilon(a_2) = 2e_\pi\,; \quad \varepsilon(b_1) = 3e_\pi\,; \quad \varepsilon(b_2) = e_\pi\,.$$

Le calcul des énergies des orbitales de type a_1 peut être effectué commodément dans le formalisme du potentiel de contact où l'action des «ligands» est représenté par un potentiel singulier V_S, qui n'agit que dans leur voisinage immédiat [14, 15]. Dans le cas présent:

$$V_S = \frac{4\pi}{5} \sum_k e_\sigma(k)\, \delta(\Omega - \Omega_k), \qquad k = \mathrm{NH_3, Cl}$$

qui est nul partout sauf dans la direction $\Omega_k(\theta_k, \varphi_k)$. Les éléments de matrice de V_S dans la base $(|1a_1\rangle = (1+\lambda^2)^{-\frac{1}{2}}(5d_{z^2} + \lambda 6s)$; $|2a_1\rangle = 5d_{x^2-y^2})$ s'obtiennent comme:

$$\langle 1a_1 | V_S | 1a_1 \rangle = \frac{1}{4}\left[3(a + be_\sigma) + (a' + b'e'_\sigma)\right],$$

$$\langle 1a_1 | V_S | 2a_1 \rangle = \frac{\sqrt{3}}{4}\left[\sqrt{(a + be_\sigma)\, e_\sigma} - \sqrt{(a' + b'e'_\sigma)\, e'_\sigma}\right],$$

$$\langle 2a_1 | V_S | 2a_1 \rangle = \frac{3}{4}\left[3e_\sigma + e'_\sigma\right].$$

Les paramètres accentués e'_σ, a' et b', correspondent au «ligand» NH_3 et leurs valeurs peuvent être déduites du spectre d'absorption de l'ion $[Pt(NH_3)_4]^{2+}$. Le spectre des solutions de $[Pt(NH_3)_4](ClO_4)_2$ comporte deux bandes peu résolues: l'une à 43100 cm^{-1}, attribuée aux transitions $^1A_{1g} \to {}^1A_{2g}, {}^1E_g$, l'autre à 46080 cm^{-1}, attribuée à la transition $^1A_{1g} \to {}^1B_{1g}$ [9]. Un calcul approché indique alors que les valeurs $b' = 0$ (donc $a' = a_0$) et $e'_\sigma \simeq 14500$ cm^{-1} semblent convenables.

Energie des états de l'ion $[PtCl_3(NH_3)]^-$

L'état de plus basse énergie de l'ion $[PtCl_3(NH_3)]^-$ est un état essentiellement constitué par l'état singulet $^1A_1$ I$[\ldots(1a_1)^2(a_2)^2(b_1)^2(b_2)^2]$. Les configurations excitées dans lesquelles un électron est assigné à l'orbitale $2a_1$ donnent naissance aux états $^{1,3}A_1$ II$[\ldots 1a_1\, 2a_1]$, $^{1,3}A_2[\ldots 2a_1\, a_2]$, $^{1,3}B_1[\ldots 2a_1\, b_1]$, $^{1,3}B_2[\ldots 2a_1\, b_2]$. Ces états sont scindés par l'interaction spin-orbite en plusieurs composantes dont le nombre et le type de symétrie s'obtiennent par réduction de la représentation produit direct, Γ (fonction orbitale) $\times\, \Gamma$ (fonction de spin). Nous indiquons dans le Tableau 4 les fonctions spin-orbitales appartenant à la configuration fondamentale et aux configurations excitées envisagées ici, classées selon leurs propriétés de transformation dans l'espace produit direct, espace des fonctions orbitales × espace des fonctions de spin.

Nous avons calculé les éléments de la matrice qui représente dans cette base l'hamiltonien $H' = V_S + V_{ES} + V_{SO}$, où V_S désigne le potentiel singulier du modèle de recouvrement angulaire qui rend compte de l'action des «ligands» sur les électrons de l'atome métallique, V_{ES} et V_{SO} les potentiels d'interaction de répulsion électronique et d'interaction spin-orbite, selon les méthodes habituelles. Nous donnons dans le Tableau 5 l'expression de ces éléments de matrice, en fonction des paramètres du modèle de recouvrement angulaire, des paramètres de Racah d'interaction électrostatique, A, B *et* C, et du paramètre d'interaction spin-orbite ζ.

Tableau 4. Fonctions de base

$\|A_1(^1A_1\ \mathrm{I})\rangle = \|(1a_1)^2(a_2)^2(b_1)^2(b_2)^2\|$	
$\|A_1(^1A_1\ \mathrm{II})\rangle = \frac{1}{\sqrt{2}}(\|1a_1^+\ 2a_1\| - \|1a_1\ 2a_1^+\|)$	$\|B_1(^1B_1)\rangle = \frac{1}{\sqrt{2}}(\|2a_1^+\ b_1^-\| - \|2a_1^-\ b_1^+\|)$
$\|A_1(^3A_2)\rangle = \frac{1}{\sqrt{2}}(\|2a_1^+\ a_2^+\| - \|2a_1\ a_2\|)$	$\|B_1(^3A_1)\rangle = \frac{1}{\sqrt{2}}(\|1a_1^+\ 2a_1^-\| + \|1a_1^-\ 2a_1^+\|)$
$\|A_1(^3B_1)\rangle = \frac{1}{\sqrt{2}}(\|2a_1^+\ b_1\| + \|2a_1\ b_1^+\|)$	$\|B_1(^3A_2)\rangle = \frac{1}{\sqrt{2}}(\|2a_1^+\ a_2^-\| + \|2a_1^-\ a_2\|)$
$\|A_1(^3B_2)\rangle\ \frac{1}{\sqrt{2}}(\|2a_1^+\ b_2^+\| + \|2a_1\ b_2\|)$	$\|B_1(^3B_2)\rangle = \frac{1}{\sqrt{2}}(\|2a_1^+\ b_2^+\| - \|2a_1^-\ b_2^-\|)$
$\|A_2(^1A_2)\rangle\ \frac{1}{\sqrt{2}}(\|2a_1^+\ a_2\|\quad \|2a_1\ a_2^+\|)$	$\|B_2(^1B_2)\rangle = \frac{1}{\sqrt{2}}(\|2a_1^+\ b_2^-\| - \|2a_1\ b_2^+\|)$
$\|A_2(^3A_1)\rangle\ \frac{1}{\sqrt{2}}(\|1a_1^+\ 2a_1^+\|\quad \|1a_1\ 2a_1\|)$	$\|B_2(^3A_1)\rangle\ \frac{1}{\sqrt{2}}(\|1a_1^+\ 2a_1^+\| + \|1a_1^-\ 2a_1\|)$
$\|A_2(^3B_1)\rangle\ \frac{1}{\sqrt{2}}(\|2a_1^+\ b_1^+\| + \|2a_1\ b_1\|)$	$\|B_2(^3A_2)\rangle = \frac{1}{\sqrt{2}}(\|2a_1^+\ a_2\| + \|2a_1^-\ a_2^+\|)$
$\|A_2(^3B_2)\rangle\ \frac{1}{\sqrt{2}}(\|2a_1^+\ b_2\| + \|2a_1\ b_2^+\|)$	$\|B_2(^3B_1)\rangle = \frac{1}{\sqrt{2}}(\|2a_1^+\ b_1^+\|\quad \|2a_1^-\ b_1\|)$

(les sous-couches «d» complétes sont omises, excepté pour $|A_1(^1A_1\ \mathrm{I})\rangle$)

Dans l'approximation où l'interaction avec les états excités des configurations dans lesquelles deux électrons sont assignés à l'orbitale $2a_1$ est négligée (nous avons vérifié, en comparant avec les résultats de Martin *et al.* [5], que dans le cas de $[\mathrm{Pt\,Cl_4}]^2$ négliger l'interaction de configuration ne modifiait pas les résultats de façon significative, au plus 500 cm^{-1}), nous obtenons à une constante additive près les énergies des états considérés ici de l'ion $[\mathrm{Pt\,Cl_3(NH_3)}]^-$ comme les valeurs propres de cette matrice. Nous avons effectué ce calcul selon le schéma A et selon le schéma B, en conservant les valeurs des paramètres d'interaction électrostatique F_2 et F_4 $(B = F_2 - 5F_4, C = 35F_4)$ et d'interaction spin-orbite $\alpha(=\zeta/2)$, choisies par Martin *et al.* pour $[\mathrm{Pt\,Cl_4}]^{2-}$ dans les cas A et B [5]. Il ne semble pas, en effet, que la substitution d'un «ligand» Cl par un «ligand» $\mathrm{NH_3}$ puisse entraîner des modifications importantes des valeurs de ces paramètres. Les résultats de ce calcul sont indiqués dans le Tableau 6 et confrontés avec les positions des bandes des spectres mesurés à basse température sur la Fig. 6.

Intensités relatives des transitions dipolaires électriques permises

Les nombreuses transitions vers les états excités à caractère triplet prépondérant issus du couplage spin-orbite, permises comme transitions électroniques pures dans la symétrie C_{2v} ou permises par perturbation vibronique, ont une énergie très voisine. Les spectres sont trop mal résolus pour qu'il soit possible de tenter une identification de ces transitions. Il est cependant nécessaire de tenir

Tableau 5. Eléments de matrice

Représentation A_1	
$\langle {}^1A_1\,\mathrm{I}\vert\,\vert{}^1A_1\,\mathrm{I}\rangle = \Delta - \frac{3}{4}(3e_\sigma + e'_\sigma) + 4B + 3C$	$\langle {}^3B_1\vert\,\vert{}^3A_2\rangle = \alpha$
$\langle {}^1A_1\,\mathrm{II}\vert\,\vert{}^1A_1\,\mathrm{I}\rangle = \dfrac{\sqrt{3}}{2\sqrt{2}}\left(\sqrt{(a+be_\sigma)e_\sigma} - \sqrt{a_0 e'_\sigma}\right)$	$\langle {}^3B_1\vert\,\vert{}^3B_1\rangle = \Delta - \frac{3}{4}(3e_\sigma + e'_\sigma) - 3e_{\pi\parallel} + 4B$
$\langle {}^1A_1\,\mathrm{II}\vert\,\vert{}^1A_1\,\mathrm{II}\rangle = \Delta - \frac{3}{4}(3e_\sigma + e'_\sigma) - \frac{1}{4}a_0 - \frac{3}{4}(3e_\sigma + e'_\sigma) + 2C$	$\langle {}^3B_2\vert\,\vert{}^1A_1\,\mathrm{I}\rangle = \sqrt{2}\alpha$
$\langle {}^3A_2\vert\,\vert{}^1A_1\,\mathrm{I}\rangle = i\sqrt{2}\alpha$	$\langle {}^3B_2\vert\,\vert{}^1A_1\,\mathrm{II}\rangle = -\sqrt{3}\alpha$
$\langle {}^3A_2\vert\,\vert{}^1A_1\,\mathrm{II}\rangle = i\sqrt{3}\alpha$	$\langle {}^3B_2\vert\,\vert{}^3A_2\rangle = i\alpha$
$\langle {}^3A_2\vert\,\vert{}^3A_2\rangle = \Delta - \frac{3}{4}(3e_\sigma + e'_\sigma) - 2e_{\pi\perp} - 5B$	$\langle {}^3B_2\vert\,\vert{}^3B_1\rangle = -i\alpha$
$\langle {}^3B_1\vert\,\vert{}^1A_1\,\mathrm{I}\rangle = i2\sqrt{2}\alpha$	$\langle {}^3B_2\vert\,\vert{}^3B_2\rangle = \Delta - \frac{3}{4}(3e_\sigma + e'_\sigma) - e_{\pi\perp} - 5B$
$\langle {}^3B_1\vert\,\vert{}^1A_1\,\mathrm{II}\rangle = 0$	
Représentation A_2	
$\langle {}^1A_2\vert\,\vert{}^1A_2\rangle = \Delta - \frac{3}{4}(3e_\sigma + e'_\sigma) - 2e_{\pi\perp} + B + 2C$	$\langle {}^3B_1\vert\,\vert{}^3B_1\rangle = \Delta - \frac{3}{4}(3e_\sigma + e'_\sigma) - 3e_{\pi\parallel} + 4B$
$\langle {}^3A_1\vert\,\vert{}^1A_2\rangle = i\sqrt{3}\alpha$	$\langle {}^3B_2\vert\,\vert{}^1A_2\rangle = -i\alpha$
$\langle {}^3A_1\vert\,\vert{}^3A_1\rangle = \Delta - \frac{3}{4}(a + be_\sigma) - \frac{1}{4}a_0 - \frac{3}{4}(3e_\sigma + e'_\sigma) - 8B$	$\langle {}^3B_2\vert\,\vert{}^3A_1\rangle = -\sqrt{3}\alpha$
$\langle {}^3B_1\vert\,\vert{}^1A_2\rangle = -\alpha$	$\langle {}^3B_2\vert\,\vert{}^3B_1\rangle = -i\alpha$
$\langle {}^3B_1\vert\,\vert{}^3A_1\rangle = 0$	$\langle {}^3B_2\vert\,\vert{}^3B_2\rangle = \Delta - \frac{3}{4}(3e_\sigma + e'_\sigma) - e_{\pi\perp} - 5B$
Représentation B_1	
$\langle {}^1B_1\vert\,\vert{}^1B_1\rangle = \Delta - \frac{3}{4}(3e_\sigma + e'_\sigma) - 3e_{\pi\parallel} + 4B + 2C$	$\langle {}^3A_2\vert\,\vert{}^3A_2\rangle = \Delta - \frac{3}{4}(3e_\sigma + e'_\sigma) - 2e_{\pi\perp} - 5B$
$\langle {}^3A_1\vert\,\vert{}^1B_1\rangle = 0$	$\langle {}^3B_2\vert\,\vert{}^1B_1\rangle = -i\alpha$
$\langle {}^3A_1\vert\,\vert{}^3A_1\rangle = \Delta - \frac{3}{4}(a + be_\sigma) - \frac{1}{4}a_0 - \frac{3}{4}(3e_\sigma + e'_\sigma) - 8B$	$\langle {}^3B_2\vert\,\vert{}^3A_1\rangle = \sqrt{3}\alpha$
$\langle {}^3A_2\vert\,\vert{}^1B_1\rangle = \alpha$	$\langle {}^3B_2\vert\,\vert{}^3A_2\rangle = i\alpha$
$\langle {}^3A_2\vert\,\vert{}^3A_1\rangle = -i\sqrt{3}\alpha$	$\langle {}^3B_2\vert\,\vert{}^3B_2\rangle = \Delta - \frac{3}{4}(3e_\sigma + e'_\sigma) - e_{\pi\perp} - 5B$
Représentation B_2	
$\langle {}^1B_2\vert\,\vert{}^1B_2\rangle = \Delta - \frac{3}{4}(3e_\sigma + e'_\sigma) - e_{\pi\perp} + B + 2C$	$\langle {}^3A_2\vert\,\vert{}^3A_2\rangle = \Delta - \frac{3}{4}(3e_\sigma + e'_\sigma) - 2e_{\pi\perp} - 5B$
$\langle {}^3A_1\vert\,\vert{}^1B_2\rangle = -\sqrt{3}\alpha$	$\langle {}^3B_1\vert\,\vert{}^1B_2\rangle = i\alpha$
$\langle {}^3A_1\vert\,\vert{}^3A_1\rangle = \Delta - \frac{3}{4}(a + be_\sigma) - \frac{1}{4}a_0 - \frac{3}{4}(3e_\sigma + e'_\sigma) - 8B$	$\langle {}^3B_1\vert\,\vert{}^3A_1\rangle = 0$
$\langle {}^3A_2\vert\,\vert{}^1B_2\rangle = i\alpha$	$\langle {}^3B_1\vert\,\vert{}^3A_2\rangle = -\alpha$
$\langle {}^3A_2\vert\,\vert{}^3A_1\rangle = -i\sqrt{3}\alpha$	$\langle {}^3B_1\vert\,\vert{}^3B_1\rangle = \Delta - \frac{3}{4}(3e_\sigma + e'_\sigma) - 3e_{\pi\parallel} + 4B$

$(\Delta = [\frac{3}{2}(a + be_\sigma) + \frac{1}{2}a_0 + \frac{3}{2}(3e_\sigma + e'_\sigma) + 6e_{\pi\parallel} + 6e_{\pi\perp}] + [28A - 42B + 21C]; \alpha = \frac{1}{2}\zeta)$

compte de l'interaction spin-orbite pour expliquer l'intensité relativement élevée de certaines de ces transitions, en particulier de celles qui sont responsables des bandes observées vers 24000 cm^{-1} pour chacune des polarisations.

Les transitions permises dans la symétrie C_{2v} sont au nombre de quatre pour chaque polarisation: celle dont le nombre d'ondes est le plus élevé, vers un état à caractère singulet, doit être la plus intense, les trois autres vers des états excités à caractère triplet doivent avoir une intensité plus faible. Le calcul des intensités relatives de ces transitions peut être effectué de la manière suivante.

Soit un état excité $n\Gamma_i$, de vecteur propre

$$|n\Gamma_i\rangle = c_{ni}\,|\Gamma_i({}^1\Gamma_i)\rangle + \sum_j c_{ni,j}\,|\Gamma_i({}^3\Gamma_j)\rangle\,.$$

Pour l'état fondamental on a:

$$|1A_1\rangle = c_1\,|A_1({}^1A_1\,\mathrm{I})\rangle + c'_1\,|A_1({}^1A_1\,\mathrm{II})\rangle + \sum_j c_{1j}\,|A_1({}^3\Gamma_j)\rangle \simeq |A_1({}^1A_1\,\mathrm{I})\rangle\,.$$

Tableau 6. Energies des états de $[\mathrm{Pt\,Cl_3(NH_3)}]^-$

Schéma A		Schéma B	
Etat	Energie (cm^{-1})	Etat	Energie (cm^{-1})
$1A_1$		$1A_1$	-
$1B_2$	18312	$1B_1$	19720
$1B_1$	18375	$1B_2$	19773
$2A_1$	18526	$1A_2$	20492
$1A_2$	21532	$2A_1$	21227
$2B_1$	21862	$2B_1$	22165
$3A_1$	23073	$2B_2$	23384
$2A_2$	23485	$2A_2$	23657
$2B_2$	24204	$3A_1$	24080
$3B_2$	26221	$3B_2$	27256
$3A_2$	26661	$3A_2$	28056
$4A_1$	26781	$4A_1$	28674
$3B_1$	28486	$3B_1$	29068
$4B_1$	29875	$4B_1$	30550
$4A_2$	30971	$4A_2$	32598
$4B_2$	33912	$5A_1$	33532
$5A_1$	36695	$4B_2$	34389

Calculées dans le schéma A, avec: $e_\sigma = 12917$ cm^{-1}, $e'_\sigma = 14600$ cm^{-1}, $e_{\pi\parallel} = 3162$ cm^{-1}, $e_{\pi\perp} = 4275$ cm^{-1}, $a = a_0 = 450$ cm^{-1}, $b = 0$; $B = 675$ cm^{-1}, $C = 2275$ cm^{-1}; $\alpha = 1500$ cm^{-1} et, dans le schéma B, avec: $e_\sigma = 11767$ cm^{-1}, $e'_\sigma = 14300$ cm^{-1}, $e_{\pi\parallel} = e_{\pi\perp} = 2400$ cm^{-1}, $a + be_\sigma = 5100$ cm^{-1}, $a_0 = 450$ cm^{-1}, $B = 550$ cm^{-1}, $C = 1890$ cm^{-1}; $\alpha = 1700$ cm^{-1}.

La force d'oscillateur de la transition permise $1A_1 \rightarrow n\Gamma_i$, s'obtient donc en fonction du moment de dipôle de transition selon:

$$f(1A_1 \rightarrow n\Gamma_i) \simeq 1{,}085 \times 10^5 \times \varepsilon(n\Gamma_i) \times |c_{ni}\langle\Gamma_i(^1\Gamma_i)|\,P\,|A_1(^1A_1\ 1)\rangle|^2$$

et d'une manière analogue $f(1A_1 \rightarrow n'\Gamma_i)$, d'où:

$$f(1A_1 \rightarrow n'\Gamma_i) \simeq \frac{\varepsilon(n'\Gamma_i)}{\varepsilon(n\Gamma_i)}\left|\frac{c_{n'i}}{c_{ni}}\right|^2 f(1A_1 \rightarrow n\Gamma_i).$$

Cette expression permet, connaissant les énergies ε des transitions vers les états excités $n\Gamma_i$ et $n'\Gamma_i$ d'une part, et les coefficients c_{ni} et $c_{n'i}$ d'autre part, de calculer les forces d'oscillateur des transitions permises vers les états de symétrie Γ_i, en fonction de la force d'oscillateur de l'une d'elles, par exemple celle de plus forte intensité. Nous avons ainsi évalué les forces d'oscillateur des transitions vers les états «triplets» relativement à la force d'oscillateur de la transition vers l'état «singulet». Les résultats de ce calcul que nous avons effectué pour les schémas A et B sont donnés dans le Tableau 7. Nous les avons également schématisés sur la Fig. 6 afin de permettre la comparaison avec les résultats expérimentaux.

Ces transitions peuvent apparaître polarisées différemment par suite de couplage vibronique, ainsi qu'il est vu au Tableau 1. En admettant que les intensités relatives des composantes vibroniques ne sont pas très différentes de celles des transitions permises, la calcul précédent donne aussi un ordre de grandeur des composantes vibroniques des transitions vers les états de type A_1, B_1 et B_2.

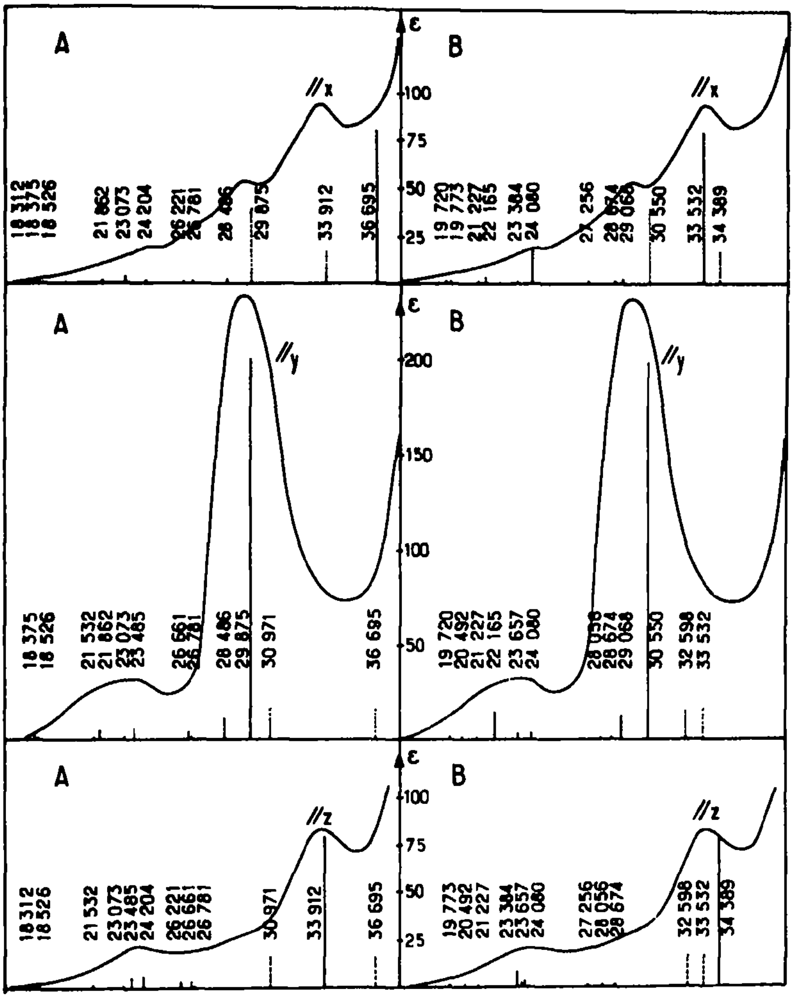

Fig. 6. Spectres d'absorption à 10 K de K[Pt $Cl_3(NH_3)$] · H_2O, polarisés en x, y et z. Les transitions prévues pour chaque polarisation, selon les schémas A et B, sont figurés par des traits (pleins s'il s'agit de transitions permises, discontinus s'il s'agit de transitions vibroniques) de longueur proportionnelle à leur force d'oscillateur. La valeur de la force d'oscillateur de la transition vers l'état «singulet» est fixée arbitrairement, mais relativement à celle-ci les forces d'oscillateur des transitions vers les états «triplets» sont dans le rapport indiqué dans le Tableau 6

Il n'est pas possible d'évaluer aussi simplement les forces d'oscillateur relatives des transitions vers les états de type A_2. Ces transitions, permises par perturbation vibronique, possèdent une certaine intensité grace au mélange de la composante singulet et des composantes triplets avec des états de symétrie convenable. Or ce mélange s'effectue dans une proportion qui peut être différente selon les cas et par suite les résultats du calcul selon la méthode exposée apparaissent peu sûrs. Indiquons pour mémoire qu'on obtient: 0,013, 0,353, 0,211 et 1,000 pour les

Tableau 7. Forces d'oscillateur relatives des transitions

Schéma A			Schéma B		
Etat excité	Energie (cm^{-1})	F. d'osc relative	Etat excité	Energie (cm^{-1})	F. d'osc. relative
$2A_1$(0,095)	18 526	0,005	$2A_1$(0,141)	21 227	0,017
$3A_1$(0,243)	23 073	0,040	$3A_1$(0,477)	24 080	0,220
$4A_1$(0,077)	26 781	0,005	$4A_1$(0,040)	28 674	0,002
$5A_1$(0,962)	36 695	1,000	$5A_1$(0,861)	33 532	1,000
$1B_1$(0,151)	18 375	0,016	$1B_1$(0,061)	19 720	0,003
$2B_1$(0,162)	21 862	0,021	$2B_1$(0,290)	22 165	0,071
$3B_1$(0,231)	28 486	0,057	$3B_1$(0,239)	29 068	0,063
$4B_1$(0,947)	29 875	1,000	$4B_1$(0,925)	30 550	1,000
$1B_2$(0,067)	18 312	0,003	$1B_2$(0,061)	19 773	0,002
$2B_2$(0,312)	24 204	0,082	$2B_2$(0,359)	23 384	0,102
$3B_2$(0,222)	26 221	0,045	$3B_2$(0,076)	27 256	0,005
$4B_2$(0,921)	33 912	1,000	$4B_2$(0,928)	34 389	1,000

La valeur indiquée entre parenthèses pour chaque état excité est le module du coefficient avec lequel intervient la composante singulet dans le vecteur propre.

états $1A_2$(0,105), $2A_2$(0,519), $3A_2$(0,376) et $4A_2$(0,760) respectivement, dans le cas du schéma A, et 0,022, 0,171, 0,060 et 1,000 pour les états $1A_2$(0,162), $2A_2$(0,419), $3A_2$(0,229) et $4A_2$(0,863) respectivement, dans le cas du schéma B.

Confrontation avec les résultats expérimentaux

La comparaison des spectres obtenus à la température ambiante et à la température de 10 K (Figs. 3, 4, 5 et Tableau 3) fait apparaître à basse température une diminution de la force d'oscillateur des bandes. Cette diminution affecte plus ou moins tout le spectre et montre que les bandes présentent un caractère vibronique, au moins en partie.

Selon le schéma A comme selon le schéma B, il apparait que la bande à 29600 cm^{-1} polarisée en y est due essentiellement à la transition vers l'état «singulet» $4B_1$. Cette bande peut, en outre, contenir la bande due à la transition vers l'état «triplet» $3B_1$, du côté des petits nombres d'onde, et la bande due à la transition vibronique vers le «singulet» $4A_2$, du côté des grands nombres d'onde (Fig. 6). L'attribution à la transition $1A_1 \rightarrow 4B_1$ est confirmée par la présence de la petite bande à 29600 cm^{-1} polarisée en x, qui doit être due, comme il est attendu avec cette polarisation, à la composante vibronique de cette transition.

De même, dans le schéma A et dans le schéma B, la bande à 33600 cm^{-1}, polarisée en z, s'explique par la transition vers l'état «singulet» $4B_2$, avec la participation de la transition vibronique, $\rightarrow 4A_2$, dans le pied de cette bande, vers les basses fréquences.

L'interprétation de la bande à 33600 cm^{-1}, polarisée en x, diverge suivant le modèle choisi. Selon le schéma B, cette bande résulte en partie de la transition vers le singulet $5A_1$, en partie de la composante vibronique polarisée en x de la transition vers le «singulet» $4B_2$. Les composantes vibroniques polarisées en y et en z de la transition vers $5A_1$ (33532 cm^{-1}) n'apparaissent pas distinctement, mais on peut supposer qu'elles contribuent au même titre que la transition vibronique vers l'état $4A_2$ (32598 cm^{-1}), du côté des grands nombres d'ondes à l'intensité de la bande à 29600 cm^{-1} polarisée en y, et à la bande à 33600 cm^{-1} polarisée en z. Selon le schéma A, cette bands à 33600 cm^{-1} polarisée en x résulte essentiellement de la composante vibronique de la transition vers le «singulet» $4B_2$. Cette transition, permise dans la symétrie C_{2v} avec la polarisation z, rend compte en grande partie, comme on l'a vu, de la bande observée également à 33600 cm^{-1} dans le spectre polarisé en z. La transition vers le «singulet» $5A_1$ doit se trouver, selon le schéma A, à un nombre d'ondes plus élevé, mais n'a pu être observée.

Les bandes dues aux transitions vers les états à caractère triplet sont en général très mal résolues et il n'est guère possible d'en donner une interprétation. Compte tenu des positions et des intensités relatives calculées, aussi bien selon le schéma A que selon le schéma B, il apparaît cependant que la bande à 24400 cm^{-1}, polarisée en x, peut résulter de la transition vers le «triplet» $3A_1$ et de la composante vibronique de la transition vers le «triplet» $2B_2$, prévues vers 23000 – 24000 cm^{-1}. De même, la bande à 24400 cm^{-1} polarisée en z, doit être due principalement à la transition vers le «triplet» $2B_2$, et peut être aussi en partie à la transition vibronique vers le «triplet» $2A_2$, prévue vers 23500 cm^{-1}. Enfin, la bande polarisée en y, dont le maximum se situe vers 23300 cm^{-1}, peut résulter notamment de la transition vers le «triplet» $2B_1$, du côté des petits nombres d'onde, et de la transition vibronique vers le triplet $2A_2$, du côté des grands nombres d'onde.

Les bandes à 29600 cm^{-1}, polarisée en y, et à 33600 cm^{-1}, polarisée en z, que nous pensons être dues essentiellement aux transitions vers les «singulets» $4B_1$ et $4B_2$ respectivement, se placent mieux dans le schéma A qui prévoit ces transitions à 29875 et 33912 cm^{-1}, que dans le schéma B (Fig. 6). Mais la divergence entre ces deux schémas apparaît surtout dans l'interprétation de la bande à 33600 cm^{-1}, polarisée en x, puisque dans un cas cette bande s'explique principalement par la transition vers le «singulet» $5A_1$ (schéma B) et que dans l'autre cette bande résulte de la composante vibronique selon x de la transition vers le «singulet» $4B_2$ (schéma A). Malheureusement l'expérience ne fournit pas d'argument décisif qui permette de conclure. Le caractère vibronique au moins partiel de cette bande dont l'intensité décroit à basse température va à l'encontre de l'attribution, $1A_1 \rightarrow 5A_1$, transition permise dans la symétrie C_{2v}. On peut donc penser qu'il s'agit plutôt ici de la composante vibronique selon x de la transition, $1A_1 \rightarrow 4B_2$, permise selon z et qui explique bien la bande observée au même nombre d'ondes dans le spectre polarisée en z. Mais les bandes observées à 33600 cm^{-1} en x et en z ont à peu près la même intensité et la distinction entre transition permise par la symétrie C_{2v} et transition permise par perturbation vibrationelle n'apparait alors pas possible, contrairement à ce qui avait lieu pour la transition $1A_1 \rightarrow 4B_1$. D'autre part, on devrait selon le schéma A observer la transition vers le «singulet» $5A_1$, à environ 37000 cm^{-1}, ou peut être au delà vers 39000 – 40000 cm^{-1} si on admet que cette transition (principalement $d_{z^2} \rightarrow d_{x^2-y^2}$) est responsable de la bande qui apparait sous forme d'épaulement vers 37000 cm^{-1} dans le spectre de K_2PtCl_4 [9]. Nous n'avons pu l'observer dans le cas de $K[PtCl_3(NH_3)] \cdot H_2O$.

Références

1. Chatt, J., Gamlen, G. A., Orgel, L. E.: J. chem. Soc. (London) 486 (1958).
2. Fenske, R F., Martin Jr., Don S., Ruedenberg, K.: Inorg. Chemistry **1**, 441 (1962).
3. Gray, H. B., Ballhausen, C. J.: J. Amer. chem. Soc. **85**, 260 (1963).
4. Martin, Jr., Don S., Lenhardt, C. A.: Inorg. Chemistry **3**, 1368 (1964).
5. Martin, Jr., Don S., Tucker, M. A., Kassman, A. J.: Inorg. Chemistry **4**, 1862 (1965); **5**, 1298 (1966).
6. Martin, Jr, Don S., Foss, J G., McCarville, M., Tucker, M. A., Kassman, A. J.: Inorg. Chemistry **5**, 491 (1966).
7. Basch, H., Gray, H. B : Inorg. Chemistry **6**, 365 (1966).
8. Cotton, F. A., Harris, C. B : Inorg. Chemistry **6**, 369 (1966).
9. Mason III, W R., Gray, H. B.: J. Amer. chem Soc. **90**, 5721 (1968).
10. McCaffery, A J., Schatz, P. N., Stephens. P. J.: J. Amer. chem. Soc. **90**, 5730 (1968).
11. Jeannin, Y. P., Russel, D R.: Bull. Soc. franç. minéralog. cristallogr. **91**, 540 (1968).
12. Lebedinský, V V, Golovnja, V V.: Gmelins Handbuch der Anorg. Chemie **68**, 421 (1957).
13. Jørgensen, C. K., Pappalardo, R., Schmidtke, H H.: J. chem. Physics **39**, 1422 (1963).
14. Jørgensen, C K., J. physique radium **26**, 825 (1965).
15. Schäffer, C. E., Jørgensen, C. K : Molecular Physics **9**, 401 (1965).

Dr. C. Moncuit
Département de Physique
Université d'Orléans
F 45-Orléans-La Source, France

Theoret. chim. Acta (Berl.) 29, 335—343 (1973)
© by Springer-Verlag 1973

Transition Energies and Oscillator Strengths for Electronic Spectra of Non Planar Conjugated Molecules. I. Polyphenyls

A. Gamba, G. F. Tantardini, and M. Simonetta

C.N.R. Centre for the Studium of Relationship between Structure and Chemical Reactivity
and Institute of Physical Chemistry University of Milano

Received August 22, 1972

Ultraviolet spectra of terphenyls and quaterphenyls are theoretically investigated by "Molecules in Molecules" (MIM) method and compared with experiment. Oscillator strengths are evaluated using the gradient operator and the mixed dipole-gradient operator. The results are compared with those obtained by the dipole-length operator. The calculation of oscillator strengths *via* the gradient operator is shown to be in general the most successful. All the components of the "primitive integral", necessary for non planar π-electron systems, are reported.

Die Ultraviolettspektren von Terphenylen und Quaterphenylen wurden mit Hilfe der "Molekül im Molekül" (MIM) Methode theoretisch untersucht und mit den experimentellen Resultaten verglichen. Mit einem Gradient-Operator und einem gemischten Dipol-Gradient-Operator wurden die Oszillatorenstärken berechnet und mit Rechnungen mit Dipollängen-Operatoren verglichen. Es wird gezeigt, daß die Berechnung von Oszillatorenstärken mit dem Gradient-Operator im allgemeinen am erfolgreichsten ist. Es werden alle Komponenten des "primitiven Integrals", die für nicht planare π-Elektronensysteme nötig, angegeben.

Les spectres dans l'ultraviolet des triphényles et des quadriphényles sont étudiés théoriquement par la méthode «Molécules dans les molécules» (MIM) et comparés à l'expérience. Les forces oscillatrices sont évaluées en utilisant l'opérateur gradient et l'opérateur mixte gradient dipolaire. Les résultats sont comparés avec ceux obtenus avec l'opérateur longueur dipolaire. Le calculades, forces oscillatrices à l'aide de l'opérateur gradient s'avère plus convenable. On reproduit toutes les composantes de «l'intégrale primitive», nécessaires pour les systemes d'électrons π non plans.

1. Introduction

It has been shown that the use of "Molecules in Molecules" (MIM) method of calculation allows a quantitative interpretation of electronic spectra of hydrocarbons [1] and azines [2]. Calculated singlet-singlet, singlet-triplet and triplet-triplet transition energies and oscillator strengths are in excellent agreement with experimental data for all molecules and ions for which MIM calculation has been performed [1–3].

The MIM method has also been successful in the study of UV spectra of phenyl- and naphthyl-naphthalenes [4], spiroconjugated [5] and homoconjugated molecules [6] where the π-electron system is far from planarity.

The series of diphenyl, *ortho*, *meta*, *para* terphenyls and symmetric *ortho*, *meta*, *para* quaterphenyls seemed to us a particularly interesting case for a further test of this theory. To this aim the UV absorption spectra of these molecules in

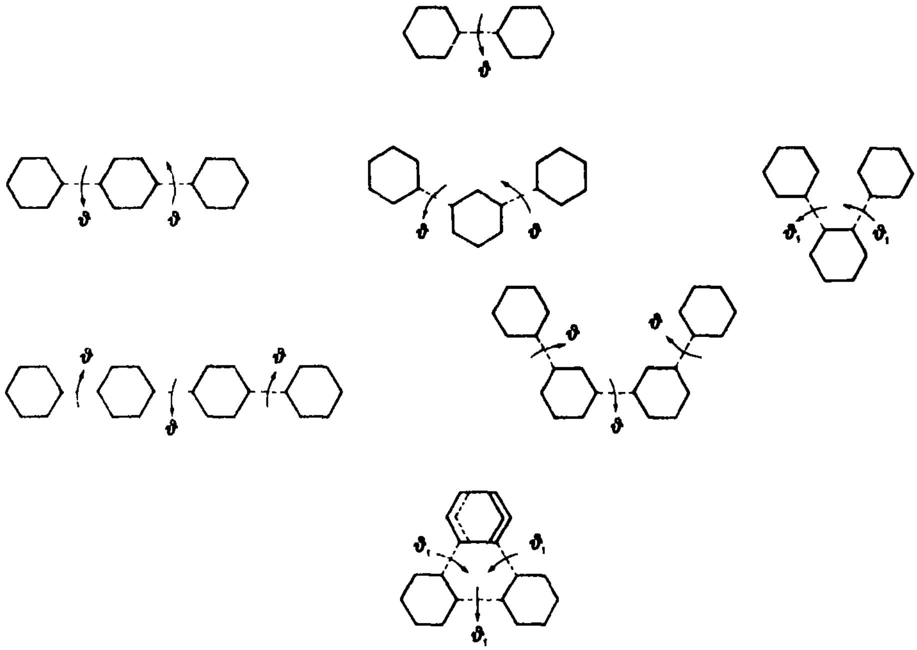

Fig. 1 Molecular geometry and fragmentation scheme for considered molecules $\vartheta = 40$, $\vartheta_1 = 53$

different solvents have been measured.[1] A complementary problem was the choice of the best operator to be used in calculating oscillator strengths when the MIM wavefunctions are the basis functions. As usual [4, 7] preliminary to excitation energy calculations a conformational analysis has been carried out to determine the ground-state geometry.

Fig. 1 shows the geometries of all molecules considered in the present paper as well the fragmentation scheme.

2. Experimental

2.1. Materials

Terphenyls and quaterphenyls were pure KEK products. For ultraviolet absorption measurements, spectrograde solvents were used.

2.2. Ultraviolet Spectra

Ultraviolet absorption spectra in the wavelength region 1750–3500 Å were measured at room temperature by a recording ultraviolet spectrophotometer Beckman DK–2A. In the far ultraviolet region short-path cells with suprasil silica windows were employed: their optical path was fixed at 0.02 cm. Recording was carried out in a purified nitrogen stream (oxygen content ≦0.2 ppm). In the near ultraviolet region standard cell with optical path of 1 cm were used.

---

[1] Except for *o*-quaterphenyl, for which a sample of sufficient high purity was not available.

Table 1. Excitation energies, oscillator strengths calculated through dipole moment operator (f_1), gradient operator (f_2) and their mean ($\sqrt{f_1 \times f_2}$), and corresponding experimental values for diphenyl[a]

ΔE_{calc}(eV)		ΔE_{exp}(eV)			f_1	f_2	$\sqrt{f_1 \times f_2}$	f_{exp}	
		sol.	vap.	solid				sol.	vap.
$^1A_1$	5.959								
	6.310								
	6.530								
	7.350								
$^1B_1$	4.900	5.02	5.22	5.08	0.871	0.419	0.604	0.33	0.31
	6.115	6.19	6.43		1.121	0.517	0.761	0.90	
	6.577				0	0	0		
	7.200				0.160	0.157	0.158		
$^1B_2$	4.531				0	0	0		
	6.047	6.05			0.448	0.227	0.319	shoulder	
	6.556				0	0	0		
	7.362		7.40		1.487	0.554	0.945		0.70
$^1B_3$	4.533		4.16	4.27	0	0.0002	0	0.0004[b]	
	5.842				0.100	0.055	0.074		
	6.578				0	0	0		
	6.996				0.152	0.055	0.092		

[a] Energy values and experimental oscillator strengths are taken from Table 6 in Ref. [7].

[b] $\varepsilon_{max} = 20$ [7]; f evaluated from the relationship: $f = 2 \cdot 10^{-5}\, \varepsilon_{max}$.

Table 2. Excitation energies, oscillator strengths calculated through dipole moment operator (f_1), gradient operator (f_2), and their mean ($\sqrt{f_1 \times f_2}$), and corresponding experimental values for terphenyls

	ΔE_{calc}(eV)	ΔE_{exp}(eV)[a]	f_1		f_2		$\sqrt{f_1 \times f_2}$		f_{exp}[a]
o-terphenyl	4.995	4.998	0.383		0.198		0.275		0.29
	5.243	5.332	1.204		0.552		0.815		0.56
	5.962	6.003	0.288	1.314	0.149	0.649	0.207	0.923	0.91
	6.028		0.589		0.284		0.409		
	6.154		0.437		0.216		0.307		
	6.230	6.357	0.478	0.706	0.222	0.294	0.326	0.453	0.62
	6.236		0.090		0.039		0.060		
	6.366		0.138		0.033		0.067		
m-terphenyl	4.777	5.019	0.337	1.839	0.169	0.950	0.239	1.322	0.96
	4.912		1.502		0.781		1.083		
	5.888	6.076	0.195	1.203	0.108	0.635	0.145	0.874	1.01
	5.948		0.316		0.166		0.229		
	5.973		0.692		0.361		0.500		
	6.342	6.390	0.185	0.783	0.055	0.275	0.102	0.464	0.62
	6.528		0.598		0.220		0.363		
p-terphenyl	4.480	4.491	1.430		0.790		1.063		0.80
	5.855	6.032	0.125	2.013	0.118	1.055	0.159	1.457	1.21
	5.926		0.435		0.228		0.315		
	5.995		1.363		0.709		0.983		
	6.963	6.457	0.226	1.015	0.088	0.518	0.141	0.699	0.37
	7.010		0.120		0.185		0.149		
	7.071		0.660		0.245		0.405		

[a] Solvent: n-hexane.

Table 3. Excitation energies, oscillator strengths calculated through dipole moment operator (f_1), gradient operator (f_2), and their mean ($\sqrt{f_1 \times f_2}$), and corresponding experimental values for quaterphenyls

	ΔE_{calc}(eV)	ΔE_{exp}(eV)	f_1		f_2		$\sqrt{f_1 \times f_2}$		f_{exp}
o-quaterphenyl	5.076		0.987		0.494		0.698		
	5.249		1.330		0.598		0.882		
	5.892		0.471		0.228		0.328		
m-quaterphenyl	4.664		0.324		0.196		0.252		
	4.819	5.008	1.156	2.759	0.652	1.528	0.868	2.053	1.30
	4.886		1.279		0.680		0.933		
	5.732		0.159		0.102		0.127		
	5.939	6.046	0.509	1.005	0.275	0.544	0.374	0.739	
	6.098		0.337		0.167		0.238		
p-quaterphenyl	4.242	4.216	2.258		1.282		1.606		0.93
	5.902	5.988	1.392		0.799		1.054		

---

[a] In cyclohexane

[b] In CH_2Cl_2. In cyclohexane the compounds exhibit low solubility.

Spectra were recorded in several solvents: spectra for the same molecule in different solvents were so close to each other that only the data relative to measurements in *n*-hexane for terphenyls and cyclohexane for quaterphenyls have been reported (see Tables 1–3): apparently the influence of the solvent is not relevant. Transition intensities were calculated according to the relationship

$$f = 4.32 \times 10^{-9} \cdot \int \varepsilon(\nu)\, d\nu .$$

Owing to the low solubility of quaterphenyls in *n*-hexane and cyclohexane, *f* values for these molecules have been obtained from spectra measured in CH_2Cl_2.

3. Calculations

3.1. Conformational Analysis

The geometry of the ground state of diphenyl has been the subject of several investigations [7, 8]. We used in the present paper the following geometry [7]: all C–C–C angles equal to 120°; intra-ring C–C distance 1.40 Å; C–C inter-ring distance equal to 1.48 Å; inter-ring twist angles 40°. For terphenyls the same values for geometrical parameters were assumed except for the twist angle. The total energy has been calculated as the sum of π-electron energy (obtained by MIM calculations) and non-bonded interactions, and has been minimized with respect to the two inter-ring twist angles. However the minimum in all cases was obtained for a geometry showing C_2 symmetry.

Computations were carried on following exactly the same line as in previous work [4, 7]. The results are shown in Fig. 2. To save a large amount of computing time the geometry of quaterphenyls was assumed, namely C_2 symmetry with inter-ring distances and twist angles equal to values of the corresponding terphenyls. This assumption is supported by the results obtained for *para* and *meta* terphenyl as compared with diphenyl.

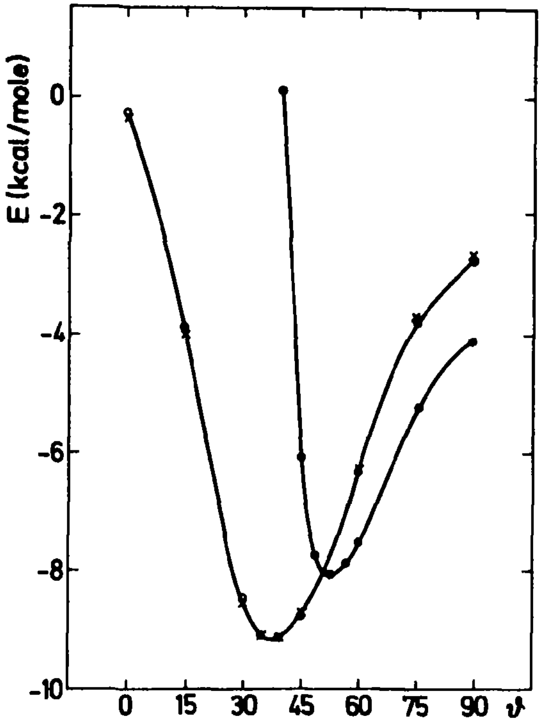

Fig. 2. Total energy *vs* twist angle ○ *p*-terphenyl, × *m*-terphenyl, ● *o*-terphenyl (π-electron energy calculated by MIM method). Curves for *p*- and *m*-terphenyls are practically coincident

3.2. MIM *Calculations*

These calculations were performed following the fragmentation scheme reported in Fig. 1. Details of the method have been described before [1] and are not reported here.

Only ground state and singly excited configurations have been included. Excitation energies are reported in Tables 1–3.

MIM wavefunctions have been used in the calculation of oscillator strengths. There is some discussion on the choice of the operators to be used in such calculations. Namely the use of transition moment, transition gradient and the geometric mean of the two alternative values have been recommended [9–11]. The relative merits of the different operators as well as of different values for the $2p_z$ carbon orbital exponent have been discussed [12, 13], but no definitive criterium to justify a choice on practical or theoretical grounds has been offered. For this reason we report in Table 1, 2, 3 oscillator strengths obtained by the three different methods using a Slater orbital exponent $\xi = 1.625$.

3.3. Primitive Integrals

In the calculation of transition gradient, primitive integral such as $I_{pq} = \langle \chi_p | \text{grad} | \chi_q \rangle$ on the atomic orbitals χ centered on p and q atoms are necessary. Owing to non-planarity of π-electron systems considered in this paper, all the components of the primitive integrals are necessary. They have been calculated according to the following formulae:

$$\begin{array}{cccc}
 & k=x & k=y & k=z \\
\left\langle p_x^P \middle| \frac{\partial}{\partial k} \middle| p_x^Q \right\rangle & 0 & 0 & -\xi F(\varrho) \\
\left\langle p_x^P \middle| \frac{\partial}{\partial k} \middle| p_y^Q \right\rangle & 0 & 0 & 0 \\
\left\langle p_x^P \middle| \frac{\partial}{\partial k} \middle| p_z^Q \right\rangle & -\xi F(\varrho) & 0 & 0 \\
\left\langle p_y^P \middle| \frac{\partial}{\partial k} \middle| p_y^Q \right\rangle & 0 & 0 & -\xi F(\varrho) \\
\left\langle p_y^P \middle| \frac{\partial}{\partial k} \middle| p_z^Q \right\rangle & 0 & -\xi F(\varrho) & 0 \\
\left\langle p_z^P \middle| \frac{\partial}{\partial k} \middle| p_z^Q \right\rangle & 0 & 0 & -\xi G(\varrho)
\end{array}$$

where:

$$p_k^Q = \pi^{-1/2} \cdot \xi^{5/2} \cdot k_Q \cdot e^{-\xi r_Q} \qquad (k = x, y, z)$$

$$F(\varrho) = \varrho e^{-\varrho}(\varrho^2 + 3\varrho + 3)/15\,,$$

$$G(\varrho) = \varrho e^{-\varrho}(\varrho^3 - 2\varrho^2 - 9\varrho - 9)/15\,,$$

$$\varrho = \xi R\,.$$

The not reported matrix elements can be obtained by using the antihermitian property of the gradient operator. The relationship between local and external coordinates systems is shown in Fig. 3.

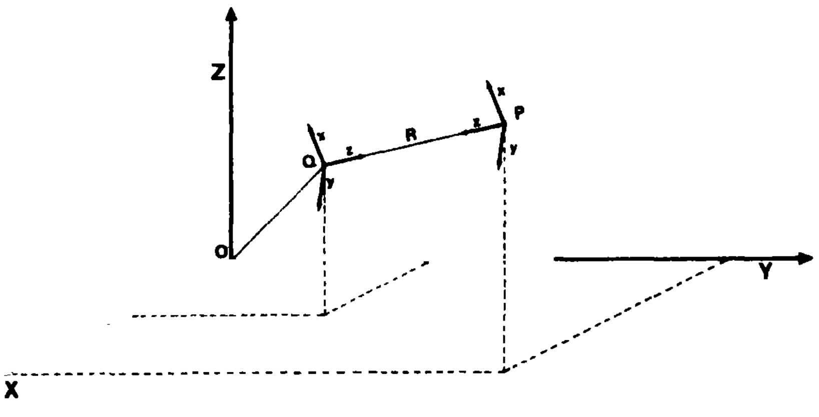

Fig. 3. Local and external coordinate systems for the calculation of transition gradients

Table 4. Calculated $T_1 \leftarrow S_0$ and most intense $T_j \leftarrow T_1$ transitions for quaterphenyls

		ΔE(eV)	f_1	f_2*	$\sqrt{f_1 \times f_2}$*
o-quaterphenyl	$T_1 \leftarrow S_0$	3.377			
	$T_j \leftarrow T_1$	1.854	0.001	0.	0.
		2.496	0.044	0.001	0.001
		2.586	0.099	0	0.003
		2.737	0.239	0.002	0.021
		2.936	0.030	0.001	0.004
m-quaterphenyl	$T_1 \leftarrow S_0$	3.206			
	$T_j \leftarrow T_1$	1.885	0.010	0	0.001
		1.899	0.002	0	0.001
		2.742	0.395	0.003	0.003
		2.844	0.240	0.002	0.002
		2.897	0.030	0	0
p-quaterphenyl	$T_1 \leftarrow S_0$	3.111			
	$T_j \leftarrow T_1$	2.544	0.884	0.006	0.075
		2.838	0.004	0	0
		2.993	0.029	0	0.002

* 0 means $< 10^{-3}$.

3.4. Excitation Involving Triplet States

MIM calculations for excitations involving triplet states in diphenyl and the three terphenyls have been reported before [3, 7].

In Table 4 we collected the calculated values for excitation energies and oscillator strengths of $T_1 \leftarrow S_0$ and $T_j \leftarrow T_1$ transitions in quaterphenyls. Unfortunately no experimental data are available for comparison.

4. Discussion

A recent X-ray determination of the molecular structure of *para*-terphenyl has shown this molecule to be nearly planar [14]. However this finding is not in contrast with our results. The nearly planar configuration given by X-ray results may correspond to a mean configuration and not to equilibrium configuration. Besides it has been shown in the case of diphenyl [8] that the planar configuration in the crystal is due to the action of packing forces. In the case of p, p'-bitolyl the packing of molecules in the crystal is such that twist angle for the molecule in the crystal is 36° and 40° for the two molecules in the asymmetric unit [15]. A similar angle of twist ($\vartheta = 33°$) is found in 4,4'-dinitrobiphenyl [16] and 4-nitrobiphenyl [17]. As usual in the MIM method the agreement of calculated and experimental singlet-singlet transition energy is excellent for all molecules. This is evident from Fig. 4, where a regression line is shown to correlate the experimental transition energies of all known bands with the corresponding calculated values for the whole series of molecules. Oscillator strengths have been calculated by means of the dipole-length, dipole-velocity expressions and their geometrical mean. Our systems differ from the ones that have been previously used for a

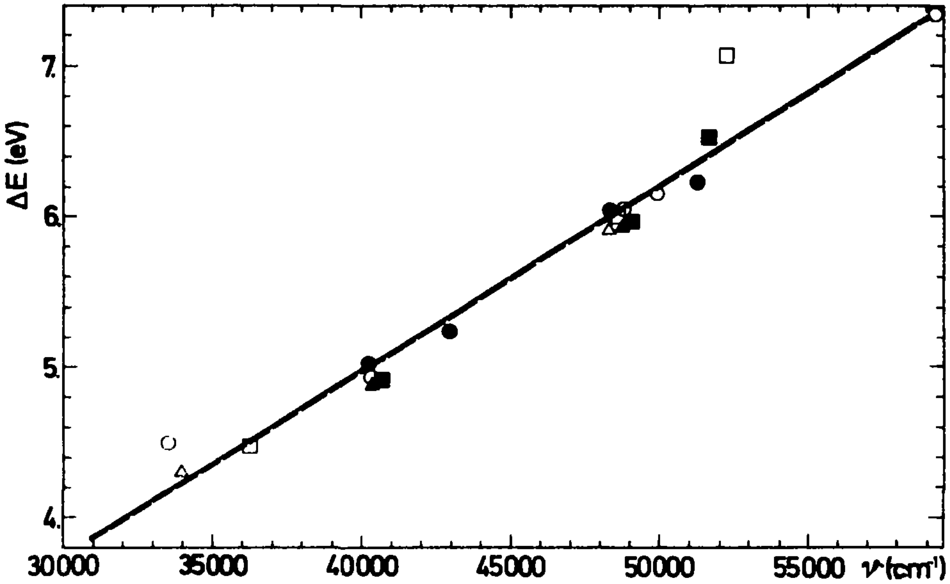

Fig. 4. Regression line for theoretical excitation energy of the first bands versus observed frequencies in polyphenyls (solid line). The dotted line corresponds to exact agreement between theory and experiment. Correlation coefficient $r = 0.997$, $n = 18$. ○ diphenyl, ● *o*-terphenyl, □ *p*-terphenyl, ■ *m*-terphenyl, △ *p*-quaterphenyl, ▲ *m*-quaterphenyl

test of this kind in two aspects: we are using MIM wave-functions and we consider non planar conjugated molecules, where σ-π interactions may be particularly significant.

It may be pointed out that in general a better agreement is obtained when the gradient operator is used. This rule is not without exception as for example in the fourth band of *ortho*-terphenyl. However it is worthwhile to point out that the agreement between experimental and calculated oscillator strengths when using gradient operator is always good even in cases when dipole operator does a better job, while the f_1 values may sometimes be far off the experimental values. On the basis of the small series of molecules which has been used in the present test it seems that the use of gradient operator together with MIM wavefunctions may be recommended.

References

1. Favini, G., Gamba, A., Simonetta, M.: Theoret. chim. Acta (Berl.) **13**, 175 (1969).
2. Simonetta, M., Gamba, A., Rusconi, E.: The Israel acad. sciences and humanities (Jerusalem) **1970**, 213.
3. Gamba, A., Tantardini, G. F., Simonetta, M.: Theoret. chim. Acta (Berl.) **23**, 336 (1972).
4. Gamba, A., Rusconi, E., Simonetta, M.: Tetrahedron **26**, 871 (1970).
5. Gamba, A., Tantardini, G. F., Simonetta, M.: Theoret. chim. Acta (Berl.) **20**, 12 (1971).
6. Bellobono, I. R., Gamba, A., Simonetta, M.: Rendiconti Acc. Naz. Lincei **49**, 102 (1970).
7. Gamba, A., Tantardini, G. F., Simonetta, M.: Spectrochim. Acta, **28** A, 1877 (1972).
8. Casalone, G., Mariani, C., Mugnoli, A., Simonetta, M.: Molecular physics **15**, 339 (1968).

9. Hansen, A. E.: Molecular Physics **13**, 425 (1967).
10. Chong, D. P.: Molecular Physics **14**, 275 (1968).
11. Yue, C. P., Chong, D. P.: Molecular Physics **14**, 487 (1968).
12. de Bruijn, S.: Chem. Physics Letters **5**, 428 (1970).
13. Hush, N. S., Williams, M. L.: Chem. Physics Letters **8**, 179 (1971).
14. Bandour, P. J. L.: Acta crystallogr. B **28**, 1649 (1972).
15. Casalone, G., Mariani, C., Mugnoli, A., Simonetta, M.: Acta crystallogr. B**25**, 1741 (1969).
16. Booustra, E. G.: Acta Crystallogr. **16**, 816 (1963).
17. Casalone, G., Simonetta, M.: private communication.

Prof. Dr. M. Simonetta
Institute of Physical Chemistry
University of Milano
Via Saldini 50
I-20133 Milano, Italy

Theoret. chim. Acta (Berl.) 29, 345—357 (1973)
© by Springer-Verlag 1973

Simplified Non-Empirical Excited States Calculations

Part II. Interpretation of the Electronic Transitions in the Vacuum-UV Spectrum of Ethylene

I. Fischer-Hjalmars and J. Kowalewski

Institute of Theoretical Physics and Institute of Inorganic and Physical Chemistry
University of Stockholm, S-11346 Stockholm, Sweden

Received December 14, 1972

The simple non-empirical method for calculating excited electronic states that we have presented recently has been applied on Rydberg states of ethylene. All kinds of *ns*, *np* and *nd* series have been studied using a Gaussian basis set including *s*, *p* and *d* functions. Calculated values of energy, oscillator strengths and other properties have been compared with the experimental spectrum. Assignments of all the observed series have been proposed.

Die vor kurzem von den Verfassern entwickelte Methode zur Berechnung von angeregten elektronischen Zuständen wird auf Rydberg-Zustände angewendet. Alle *ns*-, *np*- und *nd*-Serien werden unter Benutzung eines Gaußschen Basissatzes mit *s*-, *p*- und *d*-Funktionen untersucht. Die errechneten Energiewerte, Oszillatorstärken und sonstigen Eigenschaften werden mit dem experimentellen Spektrum verglichen und den beobachteten Serien zugeordnet.

1. Introduction

The far UV spectrum of ethylene has been carefully investigated experimentally [1]. The vibrational structure of the bands corresponding to the different electronic transitions is generally well understood and the geometry of the resulting excited states has been established in some detail. However, the correlation of the experimentally found Rydberg series with group-theoretical symbols or semi-united atom orbital symbols is rather incomplete and somewhat ambiguous. Most theoretical calculations on excited states of ethylene, for example Refs. [2–7], have been concerned with the $\pi \rightarrow \pi^*$ excited $T\,{}^3B_{1u}$ and $V\,{}^1B_{1u}$ states. Assignments of some Rydberg transitions were recently proposed by Buenker *et al.* [8], using a very elaborate combined SCF and CI method, and by Betts and McKoy [9], using a semiempirical model potential method. However, neither of these calculations is quite complete, as no basis functions of *d*-type were employed, though some of the Rydberg series obviously have this symmetry, and as no transition probabilities were computed.

We have recently suggested a new simplified non-empirical method for excited state calculations [10] and applied it on the *ns* and *npσ* Rydberg series of ethylene. We have now found it warranted to perform similar calculations on the remaining *p* and *d* Rydberg series of this molecule to further contribute to the interpretation of the spectrum.

The method is based on describing excited states by mixing singly excited configurations. By using the frozen core approximation combined with the natural orbital transformation [11, 12], the excited state wavefunctions can actually be referred to single configurations with one electron transferred from a ground state orbital - in this study of ethylene, a π-orbital -- to an excited state natural orbital. Besides transition energies, also oscillator strengths and some properties of the excited states may easily be computed.

In Section 2 we present the details of the basis sets used and the ground state calculations. Section 3 describes the results of the excited state calculations on the *ndσ*, *ndδ*, *npπ* and *ndπ* Rydberg series. In Section 4 our results are compared with the experimental spectrum and with earlier assignments.

2. Computational Details

As discussed in Ref. [10] it is possible to divide the Gaussian function basis set in a natural way into two parts, the normal state basis functions, NGTF's, and the Rydberg state basis functions, RGTF's. These two sets seem to be rather independent [10].

The basis sets adopted in the present study were similar to the basis used previously [10]. As before, the NGTF's were chosen as the ethylene-optimized set of 56 Gaussians, determined by Schulman *et al.* [13]. The RGTF's however were chosen somewhat differently. Among the diffuse Gaussians centered at the molecular midpoint, the *s*-type functions were replaced by *d*-type functions. The orbital exponents of these functions were chosen three times as large as those of the corresponding *s*-type functions of Ref. [10] in order to keep the maximas of the radial distributions at the same distance from the midpoint. For all seven Rydberg series investigated here, a total of 46 RGTF's is needed if the accuracy is to be comparable with that of Ref. [10]. Inclusion of all these functions would lead to an inadmissible computational time for the ground state SCF-MO part of the calculation. This part was carried out with the IBMOL program version 4 [14]. As pointed out in Ref. [10], much higher efficiency may be reached if separate calculations are performed for particular classes of excited states. Accordingly, three separate SCF-MO calculations with different RGTF subsets were accomplished, cf. Table 1.

Table 1. Diffuse basis functions (RGTF's) added to the normal state basis functions in the different calculations on Rydberg states of ethylene

Rydberg orbitals	Types and numbers of RGTF's per center															Total number
	C				H	Molecular midpoint										
	s	p_x	p_y	p_z	s	s	p_x	p_y	p_z	$d\sigma$[a]	$d\delta'$[a]	d_{xy}	d_{xz}	d_{yz}	3s	of RGTF's
$s, p\sigma$[b]	2			1	1	4		-	4			-		-	-	18
$d\sigma, d\delta'(a_g)$	2			1	1					4	4		–	-	4	22
$p\pi_y, d\pi_y$			1		1			4		-		–		4	--	14
$p\pi_x, d\pi_x, d\delta''(b_{1g})$		1					4			–		4	4		–	14

[a] $d\sigma = d_{2z^2-x^2-y^2}$, $d\delta' = d_{x^2-y^2}$. [b] Calculations carried out in Ref. [10].

Table 2. Ground state energies and π-orbital energies (in a.u.) of the different calculations

Rydberg orbitals	Total number of RGTF's	Ground state energy	π-orbital energy
	0	-77.90830^{a}	-0.3914^{a}
$s, p\sigma$	18	-77.91451^{b}	-0.38728^{b}
$d\sigma, d\delta'(a_g)$	22	-77.91501	-0.38665
$p\pi_y, d\pi_y$	14	-77.91035	-0.39610
$p\pi_x, d\pi_x, d\delta''(b_{1g})$	14	-77.90985	-0.39449

[a] Values from Ref. [13]. [b] Values from Ref. [10].

All calculations were carried out with the experimental ground state equilibrium geometry as given by Allen and Plyler [15]. With this geometry the ethylene molecule belongs to the point group D_{2h}. The coordinate system was chosen according to the recommendation by Mulliken [16], the molecule lying in the yz plane with CC bond and z-axis collinear.

Total energies and π-orbital energies obtained in the three different calculations are listed in Table 2, which also includes the corresponding results obtained previously [10, 13]. As mentioned in Ref. [10], the effect of different RGTF sets on the ground state properties is of minor significance. This is also borne out by the present results, cf. Table 2.

3. Results

3.1. B_{3u} and B_{2u} States – $nd\sigma$ and $nd\delta$ Rydberg Series

Excitations from the occupied π-orbital ($1b_{3u}$) and belonging to the B_{3u} species are of the type $1b_{3u} \to ma_g$, $m \geqq 4$. There are three kinds of semi-united atom orbitals (UAO) belonging to a_g in the D_{2h} group notation, *i.e.* *ns*, *ndσ* and *ndδ'* ($nd_{x^2-y^2}$). Thus, the assignment of excited states as belonging to Rydberg series of specified symmetry may be somewhat intricate when mixing of configurations is allowed. This fact was observed and discussed already in [10], where the *ns* series was considered. In the present study, a mixing of thirteen $1b_{3u} \to ma_g$, $m = 4, \ldots, 16$, configurations resulted in eight singlets and eight triplets below the ionization limit, 10.521 eV, calculated according to Koopmans' theorem. By inspecting the natural orbitals corresponding to the singlets it was possible to classify the lowest of these states as originating from the $\pi \to 3s$ excitation. The excitation energy was found to be 7.52 eV, the same as obtained in Ref. [10]. The fact that this state is comparatively well described here although no *s*-type Gaussian centered at the molecular midpoint has been explicitely included, is probably due to the presence of three equivalent *dσ*-functions. Their sum, $d_{x^2} + d_{y^2} + d_{z^2} = r^2 e^{-\alpha r^2}$, is a radial function, more similar to a 3*s* orbital than the usual *s*-type Gaussians, $e^{-\alpha r^2}$. For this reason it has been included in Table 1 under the heading 3*s*. The classification of the higher states was less straight-forward. It was of some guidance to study the contours of the natural

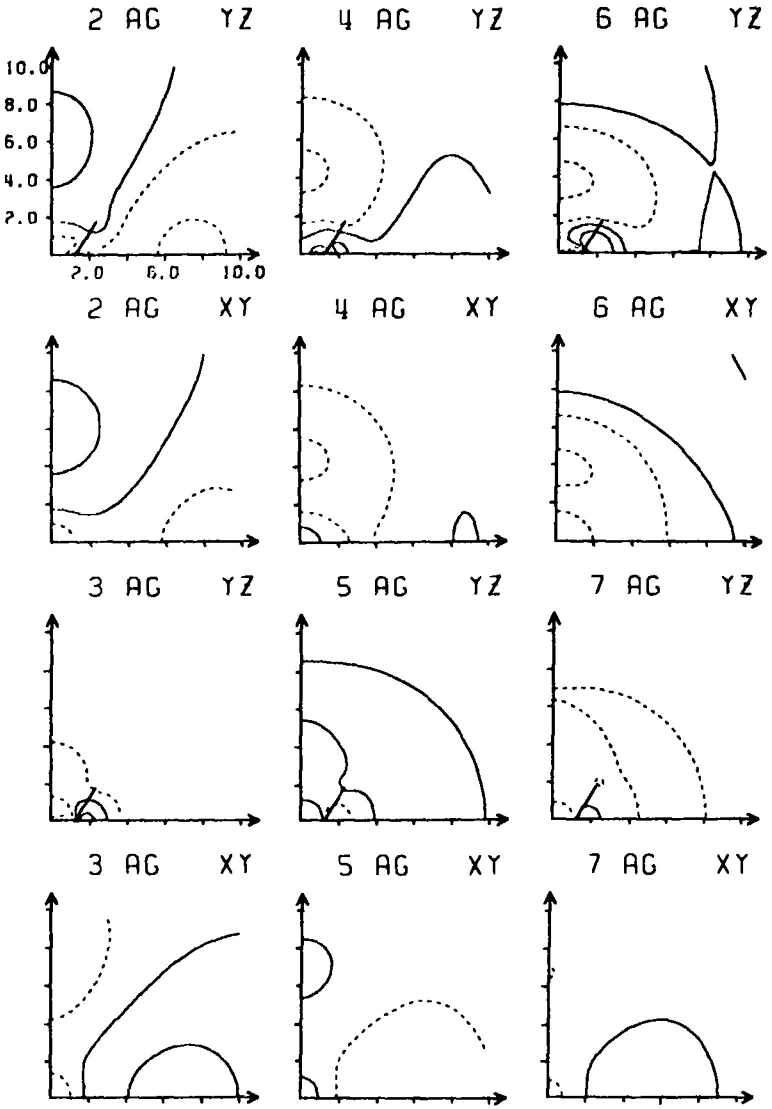

Fig. 1. Contours of a_g natural orbitals of $d\sigma$ and $d\delta'$ types in the molecular yz-plane and in the perpendicular xy-plane. The vertical axis is the y-axis in all cases. Solid lines indicate positive loops and broken lines negative loops. In the yz-plane the CH-bonds are indicated. Orbitals numbered 2, 4, 6 were assigned as $4d\sigma$, $5d\sigma$, $6d\sigma$. Orbitals numbered 3, 5, 7 were assigned as $3d\delta'$, $4d\delta'$, $5d\delta'$. (Length scale in a.u.)

Rydberg orbitals corresponding to the various states. In Fig. 1 contours of the natural orbitals corresponding to the six next higher singlets are presented both in the molecular yz-plane and in the perpendicular xy-plane. The natural Rydberg orbitals numbered 2, 4 and 6 in the figure were assigned as $4d\sigma$, $5d\sigma$ and $6d\sigma$ respectively, while the orbitals denoted 3, 5 and 7 were assigned as $3d\delta'$, $4d\delta'$ and $5d\delta'$. No assignment was made for the eighth B_{3u} state obtained in this calculation.

Table 3. Some lower B_{3u} (13 conf.) and B_{2u} (4 conf.) states of ethylene. (Energies in eV)

Rydberg orbital	Singlet vertical transition energy	Singlet-triplet splitting	$(n-\delta)^2$	δ	r_{max} of the outermost loop (a.u.)	Oscillator strength	IP-adjusted singlet energy
B_{3u} $4d\sigma(a_g)$	8.992	0.009	8.90	1.02	7	10^{-4}	8.98[a]
$5d\sigma$	9.633	0.024	15.32	1.08	18	0.002	9.62[a]
$6d\sigma$	9.904	0.057	22.05	1.3	30	0.013	9.89[a]
B_{3u} $3d\delta'(a_g)$	9.036	0.048	9.16	−0.03	7	0.016	9.03[a]
$4d\delta'$	9.684	0.027	16.29	−0.04	20	0.010	9.67[a]
$5d\delta'$	9.985	0.015	25.38	−0.04	35	0.006	9.98[a]
B_{2u} $3d\delta''(b_{1g})$	9.271	0.019	9.29	−0.05	7	0.019	9.04[b]
$4d\delta''$	9.907	0.009	16.43	−0.05	20	0.009	9.68[b]
$5d\delta''$	10.204	0.005	25.62	−0.06	35	0.005	9.98[b]

[a] $E(\mathrm{IP}) = 10.521$. [b] $E(\mathrm{IP}) = 10.734$.

Excitations from the occupied π-orbital and belonging to the B_{2u} species are of the type $1b_{3u} \rightarrow mb_{1g}$, $m \geq 1$. No orbital of the b_{1g} symmetry is obtained from the valence basis set. The virtual molecular orbitals belonging to this species are linear combinations of the four d_{xy} RGTF's centered at the molecular midpoint. No assignment problems were thus encountered. The principal quantum number of the lowest orbital in the $nd\delta''$ series must be $n = 3$ since no core ancestor is present. This principal quantum number value is also confirmed by a study of the orbital radial density along the $x = y$, $z = 0$ line, as no node except those at origo and infinity is present.

Some properties calculated for the Rydberg $nd\sigma$ and $nd\delta$ states are collected in Table 3. The singlet-triplet splittings are very small as anticipated for Rydberg states.

The $(n-\delta)^2$ values were found from the relation [17]:

$$E_n = E(\mathrm{IP}) - \frac{R}{(n-\delta)^2}\,. \tag{1}$$

They lead to quantum defects, δ, which are reasonably constant within the $nd\sigma$ series and almost exactly constant within the two $nd\delta$ series. The values of $E(\mathrm{IP})$, the ionization potentials used in Eq. (1), were obtained from Koopmans' theorem, which is consistent with our method of calculating the transition energies, cf. Ref. [10]. It should be pointed out that we assume the first member of the $nd\sigma$ series to have the principal quantum number $n = 4$, since in agreement with Merer and Mulliken [1] we interpret the $3a_g$ MO of the ground state as the $3d\sigma$ UAO, cf. [10]. This interpretation is at variance with the assignment of Buenker *et al.* [8], who correlate the $3a_g$ MO with the $3s$ UAO and consequently assume the Rydberg $nd\sigma$ series to start with $n = 3$. Such an assignment would of course lead to δ-values very different from those of Table 3. Our δ-values seem however to be consistent with experiments, see Table 6 below. The high values may be understood as a result of the strong penetration of the $nd\sigma$ orbitals into the molecular core. The penetration is obviously much lower for the $nd\delta$ orbitals.

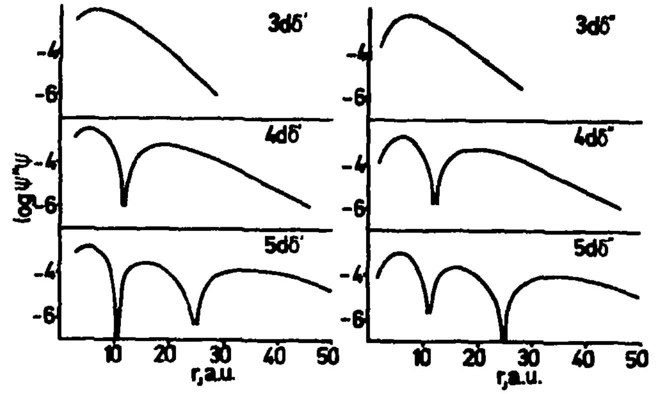

Fig. 2. Logarithm of charge density vs distance from the molecular midpoint along the z-axis (CC-axis) for $nd\delta'$ and $nd\delta''$ natural orbitals

According to Mulliken [17] the $(n-\delta)^2$ values should be equal to the distance between origo and the position of maximum radial density of the outermost loop, r_{max} in Table 3. The r_{max} values were estimated from density plots similar to those of Fig. 2. The agreement with Mulliken's formula is moderately good. The $^1A_g \rightarrow {}^1B_{3u}$ and $^1A_g \rightarrow {}^1B_{2u}$ transitions are symmetry allowed and the oscillator strengths were computed using dipole transition moments.

It should be stressed that the $nd\sigma$ and $nd\delta'$ series on the one hand and the $nd\delta''$ series on the other have been computed using different ground state calculations, cf. Section 2. Therefore a comparison between the energy values of these series cannot be made until all values have been related to a common reference point. Since Rydberg states are closely connected with ionized states and since our method of calculation parallels Koopmans' theorem, we have chosen to refer the calculated excitation energies to a common value of the ionization potential. Thus, from the primarily computed excitation energies, listed in the second column of Table 3, we have subtracted the difference between the E(IP)-value from Koopmans' theorem and the experimental value, 10.51 eV [18]. These IP-adjusted energies are given in the last column of Table 3. After the adjustment, the near degeneracy of the $d\delta$ levels becomes clear. This result can be theoretically justified as follows. The levels are degenerate in the isoelectronic oxygen molecule. Since the high density regions of these particular Rydberg orbitals do not interfere with the molecular skeleton, the exchange of an oxygen atom for a CH_2 group should only have a minor influence. The radial density plots for both types of $nd\delta$ orbitals are shown in Fig. 2. It should be noted that not only the positions of maximal density for all the loops fall at the same distance from the molecular midpoint, but even the form of the curves is extremely alike.

3.2. A_g and B_{1g} States – $np\pi$ Rydberg Series

The semi-united atom $p\pi$ orbitals belong in ethylene to the symmetry species b_{3u} and b_{2u} for π_x and π_y respectively. No other s, p or d UAO belongs to any of these irreducible representations of the D_{2h} group and thus no assignment

Table 4. Some lower A_g (6 conf.) and B_{1g} (7 conf.) states of ethylene. (Energies in eV)

Rydberg orbital	Singlet vertical transition energy	Singlet-triplet splitting	$(n-\delta)^2$	δ	r_{max} of the outermost loop (a.u.)	IP-adjusted singlet energy
A_g $3p\pi_x(b_{3u})$	8.645	0.324	6.51	0.45	6	8.42[a]
$4p\pi_x$	9.669	0.104	12.76	0.43	16	9.44[a]
$5p\pi_x$	10.092	0.050	21.19	0.40	29	9.86[a]
$6p\pi_x$	10.328	0.048	33.5	0.2	43	10.10[a]
B_{1g} $3p\pi_y(b_{2u})$	8.298	0.048	5.49	0.66	5	8.03[b]
$4p\pi_y$	9.581	0.016	11.37	0.63	14	9.31[b]
$5p\pi_y$	10.071	0.008	19.24	0.61	25	9.80[b]
$6p\pi_y$	10.313	0.005	29.3	0.6	42	10.04[b]

[a] $E(\mathrm{IP}) = 10.734$. [b] $E(\mathrm{IP}) = 10.778$.

problems caused by the mixing occur for these orbitals. The $1b_{3u} \to mb_{3u}$, $m \geq 2$, transitions generate states of A_g symmetry. Mixing six configurations of this type, with $m = 2, \ldots 7$, gave four singlets and triplets below the ionisation limit, 10.734 eV. The $1b_{3u} \to mb_{2u}$, $m \geq 2$ transitions generate states of B_{1g} symmetry. Four singlets and triplets below the ionization limit, 10.778 eV, were obtained by mixing seven configurations with $m = 2, \ldots, 8$.

Transitions to these states from the ground state are only quadrupole allowed and the dipole oscillator strengths are thus zero. Some properties calculated for the B_{1g} and A_g excited states are summarised in Table 4. A comparison of uncorrected energy values indicates the $B_{1g}(np\pi_y)$ states to be throughout lower than the corresponding $A_g(np\pi_x)$ states. Further, previously studied $B_{2g}(np\sigma)$ states [10] seem to lie below both kinds of $np\pi$ states. After an IP-adjustment, the order of increasing energy becomes instead $\pi_y < \sigma < \pi_x$ for every value of n. Singlet-triplet splittings are very small for the π_y series but rather large for the π_x series. This might have been expected since the considerable overlap between the ground state occupied π-orbital and the Rydberg π_x orbitals leads to substantial values of the exchange integrals between these orbitals. The quantum defects are rather constant within the series. The lowest δ-values are found in the $np\pi_x$ series, which obviously has the smallest penetration into the core. Mulliken's relation between $(n-\delta)^2$ and r_{max} is fulfilled moderately well also here; r_{max} is always found to be larger for the $np\pi_x$ than for the $np\pi_y$ orbitals in agreement with this relation. The general appearance of the orbital radial densities is rather similar and resembles also the curves for the $np\sigma$ orbitals [10].

3.3. A_u and B_{1u} States *ndπ Rydberg Series*

The semi-united atom $d\pi$ orbitals belong in ethylene to the symmetry species b_{2g} and b_{3g} for $d\pi_x$ and $d\pi_y$ respectively. The $1b_{3u} \to mb_{3g}$, $m \geq 2$ transitions generate states of A_u symmetry. Seven configurations of this type were mixed resulting in three pairs of states (singlets and triplets) below the ionization limit.

The states were assigned as corresponding to the Rydberg orbitals $4d\pi_y$, $5d\pi_y$ and $6d\pi_y$. The first member of the series has the principal quantum number $n = 4$, because the core orbital $1b_{3g}$ correlates with the $3d\pi_y$ UAO. The $^1A_g \rightarrow {}^1A_u$ transitions are strictly forbidden and the transition probabilities are thus zero.

The $1b_{3u} \rightarrow mb_{2g}$, $m \geqq 1$, transitions generate states of B_{1u} symmetry. Mixing seven configurations of this type with $m = 1, \ldots, 7$ led to four pairs of states below the ionization limit. However, the lowest pair of these states, with configuration $(1b_{3u})^1\ (1b_{2g})^1$, is not of Rydberg type but represents the spectroscopic V and $T(\pi \rightarrow \pi^*)$ states. The unadjusted energies of these states are 8.85 eV and 3.68 eV respectively. The T state is presumably described rather satisfactorily, the too low energy compared with experiment being caused by the difference in correlation energy. The description of the V state on the other hand is probably rather deficient, as its computed energy is about 1 eV too high. The basis set used in this study is supposedly not flexible enough and besides, the reorganisation energy, approximately counterweighting the correlation change for Rydberg states, may be rather large for the V state. The oscillator strength computed for the $N\,^1A_g \rightarrow V\,^1B_{1u}$ transitions is 0.47. An interesting feature shown by the natural orbital of π^* type, corresponding to the V state, is a lack of a maximum in the radial density curve outside the molecular frame, which clearly distinguishes this orbital from the higher excited natural orbitals of b_{2g} symmetry.

Calculated properties of the $B_{1u}(nd\pi_x)$ and $A_u(nd\pi_y)$ states are summarized in Table 5. The energies of the $nd\pi_y$ states are distinctly lower than the $nd\pi_x$ energies, and consequently the difference in quantum defects is quite large. However, it is not unlikely that the present description of the whole $nd\pi_x$ series is inferior to that of the other Rydberg series. The reason for this is the unsatisfactory description of the first, non-Rydberg member of the series, the V state. As already mentioned, its energy was computed 1 eV too high. Since the higher members of the series must be orthogonal to this first member, the whole series may be pushed to too high energy levels, implying somewhat too small δ-values. The penetration of the $nd\pi_y$ orbitals is obviously large since their loops point in almost the same direction as the C–H bonds. Low singlet-triplet splitting for

Table 5. Some lower B_{1u} (7 conf.) and A_u (7 conf.) states of ethylene. (Energies in eV)

	Rydberg orbital	Singlet vertical transition energy	Singlet-triplet splitting	$(n-\delta)^2$	δ	r_{max} of the outermost loop (a.u.)	Oscillator strength	IP-adjusted singlet energy
B_{1u}	$4d\pi_x(b_{2g})$	9.657	0.320	12.62	0.45	13	0.158	9.43[a]
	$5d\pi_x$	10.071	0.128	20.49	0.47	26	0.061	9.84[a]
	$6d\pi_x$	10.332	0.106	33.75	0.2	38	0.071	10.10[a]
A_u	$4d\pi_y(b_{3g})$	9.310	0.010	9.27	0.94	7		9.04[b]
	$5d\pi_y$	9.955	0.005	16.53	0.93	20	–	9.67[b]
	$6d\pi_y$	10.251	0.003	25.9	0.9	35	—	9.98[b]

[a] $E(\mathrm{IP}) = 10.734$. [b] $E(\mathrm{IP}) = 10.778$.

these states is quite obvious too; with their special form, the exchange integrals between them and the occupied π-orbital must be extremely low. On the other hand, the $nd\pi_x$ orbitals have high density in the same part of space as the core π-orbital, resulting in a larger singlet-triplet splitting than for other Rydberg states. In accordance with Mulliken's relation, the larger $(n-\delta)^2$ values in the $nd\pi_x$ series are accompanied by larger $r_{\max}$ values, *i.e.* larger diffuseness of the orbitals. ${}^1A_g \rightarrow {}^1B_{1u}$ transitions are fully allowed and their oscillator strengths were computed. The $\pi \rightarrow 4d\pi_x$ transition is predicted to be very strong, even stronger than $\pi \rightarrow 3s$, the first Rydberg transition. It should be remembered, however, that no estimate of the Franck-Condon integral has been made within the present computational scheme. This integral may change the relative oscillator strengths by a considerable factor. In particular, the integral is likely to be much larger for a bonding Rydberg orbital, e.g. $3s$, than for an antibonding, e.g. $4d\pi_x$. Hence, the above comparison between the strength of different transitions must not be considered as conclusive.

4. Discussion of the Spectrum

The higher Rydberg states in ethylene have been studied experimentally by Price and Tutte [19], who discovered several transitions belonging to one Rydberg series and two transitions belonging to other series. Wilkinson [20] identified several other transitions belonging to four Rydberg series in all. He even suggested assignments of most of the vibrational bands. Wilkinson also found some bands that he did not assign, conjecturing that they might belong to a fifth Rydberg series.

In previous theoretical investigations [8, 9] attempts have been made to assign group-theoretical symbols and semi-united atom Rydberg orbital symbols to the series, by Wilkinson named nR, nR', nR'', nR'''.

In the present investigation we are also concerned with this problem. For which reason, the results of the present calculations and of our previous ones [10] are listed together in Table 6 in order of increasing energy. The IP-adjusted values have been given since they are most suitable for a direct comparison between different calculations, cf. the above discussion. Oscillator strengths f and quantum defects δ are also listed. The experimental material included in Table 6 has been taken from Wilkinson [20], Merer and Schoonveld [21] and Ross and Lassettre [22]. The latter authors have found a forbidden transition at 7.45 eV. The values of ν_{vertical}, r_0 and δ, reported as experimental, have been estimated by us from the information given in Refs. [20–22]. The r_0-values are not the same as in Ref. [20] since we have used another ground-state value, *i.e.* $r_0 = 1.339$ Å.

The assignment we propose here are obvious from our tabular setup. They coincide with previous assignments in several cases. There is no doubt that the nR series originates from $\pi \rightarrow ns$ transitions, the $2R$ band at 7.11 eV from the transition to the $3s$ Rydberg orbital, the $3R$ band at 8.90 eV to the $4s$ orbital and the $4R$ band at 9.62 eV to the $5s$ orbital. These assignments agree with those of previous authors [1, 8, 9, 20], the only diversity being a difference in principal quantum number, advocated by Buenker *et al.* [8]. This point was discussed in

Table 6. Calculated properties of the lower singlet Rydberg states of ethylene compared with experiments. Energy values in eV

State	Calculations				Experiments [20–22]				
	Rydberg orbital MO(UAO)	Energy (IP-adj.)	f	δ	Label	ν_{00}	$\nu_{\mathrm{vert}}^{a}-\nu_{00}$	r_0^{a}	δ^{a}
$^1B_{3u}$ [b]	$4a_g(3s)$	7.49	0.05	0.9	$2R$	7.11	0.2	1.41	1.0
$^1B_{1g}$	$2b_{2u}(3p\pi_y)$	8.03	0	0.7	-	7.45		—	0.9
$^1B_{2g}$ [b]	$3b_{1u}(3p\sigma)$	8.19	0	0.6	$3R'$	8.26	0	1.44	0.5
^1A_g	$2b_{3u}(3p\pi_x)$	8.42	0	0.5					
$^1B_{3u}$	$5a_g(4d\sigma)$	8.98	10^{-4}	1.0	$4R'''$	9.05	0.1	1.39	0.9
$^1B_{3u}$	$6a_g(3d\delta')$	9.03	0.02	−0	$3R''$	8.62	0.3	1.41	0.3
$^1B_{2u}$	$1b_{1g}(3d\delta'')$	9.04	0.02	−0					
^1A_u	$2b_{3g}(4d\pi_y)$	9.04	0	0.9					
$^1B_{3u}$ [b]	$7a_g(4s)$	9.06	0.02	0.9	$3R$	8.90	0.1	1.39	1.1
$^1B_{1g}$	$3b_{2u}(4p\pi_y)$	9.31	0	0.6					
$^1B_{2g}$ [b]	$4b_{1u}(4p\sigma)$	9.38	0	0.5	$4R'$	9.36	0.1	1.47	
$^1B_{1u}$	$2b_{2g}(4d\pi_x)$	9.43	0.16	0.5		9.11	-	--	0.9
^1A_g	$3b_{3u}(4p\pi_x)$	9.44	0	0.4					
$^1B_{3u}$	$8a_g(5d\sigma)$	9.62	0.002	1.1					
^1A_u	$3b_{3g}(5d\pi_y)$	9.67	0	0.9					
$^1B_{3u}$	$9a_g(4d\delta')$	9.67	0.01	−0	$4R''$	9.51		1.49	0.3
$^1B_{2u}$	$2b_{1g}(4d\delta'')$	9.68	0.01	−0					
$^1B_{3u}$ [b]	$10a_g(5s)$	9.74	0.003	0.8	$4R$	9.62	0		1.1

[a] Values estimated by the present authors. [b] Values from Ref. [10].

our precedent paper [10]. In the nR series our calculated values are seen to lie 0.1-0.2 eV above our appraisal of vertical transition energies. Our assignment of the forbidden transition at 7.45 eV is also in harmony with previous suggestions [1, 8].

The nR' series is observed to be weaker than the nR series [20], the strength of the first member, $3R'$, being lower than that of $3R$, yet slightly larger than that of $4R$. For the nR' series, different assignments have been suggested previously. Betts and McKoy assigned it as a $nd\sigma$ series, $n=4, 5, \ldots$. Buenker *et al.* [8] discussed the possibility of $3R'$ being either $3d\delta$ or $3d\sigma$. Our assignment is $3p\sigma$. This might seem questionable since the transition to the $^1B_{2g}$ state is not dipole allowed. However, it is well known that both the ion and the Rydberg states do not have planar equilibrium conformations but are somewhat twisted [1, 7, 20, 21]. By arbitrarily twisting the molecule the point group D_{2h} is transferred into the group D_2 where transitions to all B-states are allowed. To evaluate the effect of twisting on the oscillator strengths we have carried out calculations on the Rydberg ns and $np\sigma$ series with a twisted conformation (cf. Merer and Schoonveld [21]):

$$r(\mathrm{C{-}C}) = 1.41\,\text{Å}\,, \quad r(\mathrm{C{-}H}) = 1.11\,\text{Å}\,, \quad \angle\,\mathrm{CCH} = 120^\circ\,,$$

and the dihedral angle = 25°. The same basis set as in Ref. [10] was used. Some results from calculations within the frozen core approximation are displayed in

Table 7. Some lower singlet $B_{3(u)}$ and $B_{2(g)}$ states of ethylene with twisted conformation, see text for details. Results from frozen core approximation. Energy values in eV

Rydberg orbital	Vertical transition energy in D_2 geometry	Transition energy to D_2 state from D_{2h} ground state[a]	Vertical transition energy in D_{2h} geometry[b]	Oscillator strengths for vertical transitions	
				D_2	D_{2h}[b]
3*s*	6.72	7.33	7.52	0.029	0.045
4*s*	8.28	8.89	9.09	0.016	0.022
5*s*	8.97	9.58	9.77	0.002	0.003
3*pσ*	7.41	8.02	8.22	0.005	0
4*pσ*	8.60	9.21	9.41	0.001	0
5*pσ*	9.06	9.67	9.86	10^{-4}	0

[a] $E_0(D_{2h}) = -77.91451$ a.u., $E_0(D_2) = -77.89211$ a.u.

[b] Values from Ref. [10].

Table 7. Nine configurations were used for the B_3 states and ten for the B_2 states. Calculations mixing all singly excited configurations were also performed (extended CI of Ref. [10]) including thirtyeight B_3 and forty B_2 configurations. The deviation between these two rather different CI-treatments in no case exceeded 0.01 eV, although the $\sigma-\pi$ separability is lost by twisting. In agreement with previous, more elaborate studies we found that all Rydberg states were stabilized by twisting, cf. columns three and four of Table 7. Oscillator strengths obtained with twisted (D_2) and planar (D_{2h}) conformations are compared in the last two columns. It is noticeable that the strength obtained for the $B_2(3p\sigma)$ state is even larger than for the $4R(5s)$ state, thus supporting our assignment. The experimental energy values of the nR' series, 8.26 eV and 9.36 eV, are rather close to the energies calculated for the transitions to the $B_2(3p\sigma)$ and $B_2(4p\sigma)$ states, *i.e.* 8.19 eV and 9.38 eV respectively (cf. Table 6). Furthermore, the comparatively large values of r_0 indicate that the nR' Rydberg orbitals are likely to be antibonding. Experimental and theoretical δ-values are also in good accord and of a magnitude typical for Rydberg *np* states. On the other hand, the previous assignments of the Rydberg orbital of $3R'$ as $3d\delta$ [8] or $4d\sigma$ [9] are not supported by our results. We obtained energy values for both these states close to 9 eV, *i.e.* 0.7 eV above the experimental value. In view of our good results for the nR series, it is rather unlikely that the nR' series should be so badly described by our model. It should also be noted that the previous treatments [8, 9] did not include *d*-functions in their basis sets.

The $3R''$ system consists of several strong, diffuse bands with maximum intensity at $3R''_{20}$ (8.96 eV), 0.34 eV above the 00-band. Its unusual appearance led us to consider that it might be composed of two superimposed transitions of almost equal energy. Since our calculations of IP-adjusted energies indicate that the $B_{3u}(3d\delta')$ and $B_{2u}(3d\delta'')$ states are almost degenerate, we propose that both these states contribute to the $3R''$ system. A justification for this proposal is given by the fact that during twisting the B_3 and B_2 states will approach each other and finally become exactly degenerate in the D_{2d} (perpendicular) geometry. The calculated energies are found about 0.1 eV above the vertical transitions. The intensities as well as the small r_0-value of $3R''$ are in harmony with our assignment. Our conclusion is in partial agreement with that of Betts and McKoy [9], who assigned $3R''$ as $3d\delta'(a_g)$ and an unassigned band at 8.92 eV as $3d\delta''(b_{1u})$. A different interpretation of $3R''$ was given by Buenker *et al.* [8]. As already mentioned these authors suggested that $3R''$ and $3R'$ may correspond to $3d\sigma$ and $3d\delta$, with some preference for $3R''$ being $3d\sigma$. As mentioned, none of these two investigations included *d*-functions in the basis sets. Both interpretations must therefore be considered as somewhat speculative.

Among the observed bands, not yet discussed here, the $4R'''$ system is by far the most important. This system is composed of several rather intense bands. Following a suggestion by Wilkinson, Betts and McKoy [9], as well as Buenker *et al.* [8], assigned the Rydberg orbital involved as $d\pi_x$, and presumably $4d\pi_x$. This assignment is supported by our result that the oscillator strength calculated for this transition is as large as 0.16. However, it is difficult to understand how the r_0-value of the $4R'''$ state (1.39 Å) could be compatible with an antibonding $(d\pi_x)$ Rydberg orbital. This r_0-value should be compared to the CC-distance of the ion $C_2H_4^+$ which is found to be 1.41 ± 0.01 Å [21]. For this reason we tentatively assign $4R'''$ as $B_{3u}(4d\sigma)$ (accordant with r_0 and δ values, but not quite in harmony with the calculated oscillator strength) and the rather intense 9.11 eV transition as $B_{1u}(4d\pi_x)$, cf. Table 6. An interchange of these two assignments might be considered. A more definite conclusion would however require much more elaborate calculations. The most intense band of the $4R'''$ system is found very close to the 9.11 eV band [20]. In contrast, our energy values of the two states under discussion indicate a separation of 0.4 eV. However, as already mentioned, we expect all members of the $nd\pi_x$ series to be less adequately represented in our model than the other Rydberg series. Therefore, this deficiency is not a very serious argument against our assignments.

It should be pointed out that the order of the lowest states as computed with our method agrees completely with the results of Buenker *et al.* [8]. However, their very elaborate method does not easily allow either a description of the higher states or calculation of oscillator strengths. Both these things can easily be achieved by our method. In view of the simplicity of the method and its characteristic of being completely ab initio the results collected in Table 6 must be considered as very satisfactory and promising for continued application.

Acknowledgements. Part of this work has been supported by grants from the Swedish Natural Science Research Council.

We are indebted to Mrs. Janina Kowalewska for drawing the figures. One of us (J.K.) gratefully acknowledges support from Professor Ragnar Vestin.

References

1. Merer, A. J., Mulliken, R. S.: Chem. Reviews **69**, 639 (1969).
2. Robin, M. B., Basch, H., Kuebler, N. A., Kaplan, B. E., Meinwald, J.: J. chem. Physics **48**, 5037 (1968). - Basch, H., McKoy, W.: J. chem. Physics **53**, 1628 (1970).
   Shibuya, T., McKoy, V.: J. chem. Physics **54**, 1738 (1971).
3. Dunning, T. H., Jr., Hunt, W. J., Goddard III, W. A.: Chem. Physics Letters **4**, 147 (1969).
4. Levy, B., Ridard, J.: Chem. Physics Letters **15**, 49 (1972).
5. Ryan, J. A., Whitten, J. L.: Chem. Physics Letters **15**, 119 (1972).

6. Bender, C. F., Dunning, T. H., Jr., Schaefer III, H. F., Goddard III, W. A., Hunt, W. J.: Chem. Physics Letters **15**, 171 (1972).
7. Buenker, R. J., Peyerimhoff, S. D., Hsu, H. L.: Chem. Physics Letters **11**, 65 (1971).
8. Buenker, R. J., Peyerimhoff, S. D., Kammer, W. E.: J. chem Physics **55**, 814 (1971).
9. Betts, T., McKoy, V.: J. chem. Physics **54**, 113 (1971).
10. Fischer-Hjalmars, I., Kowalewski, J.: Theoret. chim. Acta (Berl.) **27**, 197 (1972).
11. Löwdin, P.-O.: Physic. Rev. **97**, 1474 (1955).
12. Fischer-Hjalmars, I.: Trans. International Symp. Mol. Structure and Spectroscopy, B **205** (1962).
13. Schulman, J. M., Hornback, C. J., Moskowitz, J. W.: Chem. Physics Letters **8**, 361 (1971).
14. Veillard, A.: IBMOL Version 4, Special IBM Technical Report, San Jose (1968).
15. Allen, H. C., Plyler, E. K.: J. Amer. chem. Soc. **80**, 2673 (1958).
16. Mulliken, R. S.: J. chem. Physics **23**, 1997 (1955).
17. Mulliken, R. S.: J. Amer. chem. Soc. **86**, 3183 (1964).
18. Eland, J. H. D.: Int. J. Mass Spectrom. Ion Physics **2**, 471 (1969).
19. Price, W. C., Tutte, W. T.: Proc. Royal Soc. (London) A **174**, 207 (1940).
20. Wilkinson, P. G.: Canad. J. Physics **34**, 643 (1956).
21. Merer, A. J., Schoonveld, L.: Canad. J. Physics **47**, 1731 (1969).
22. Ross, K. J., Lassettre, E. N.: J. chem. Physics **44**, 4633 (1966)

Prof. I. Fischer-Hjalmars
Institute of Theoretical Physics
University of Stockholm
Vanadisvägen 9
S-11346 Stockholm, Sweden

Theoret. chim. Acta (Berl.) 29, 359–374 (1973)
© by Springer-Verlag 1973

Couplage vibronique et anisotropie paramagnétique dans un complexe cubique $^2T_2$ soumis à un champ trigonal

O. Kahn

Ecole Nationale Supérieure de Chimie de Paris, 11, rue Pierre et Marie Curie, 75.005 Paris, France

S. F. A. Kettle

School of Chemical Sciences, University of East Anglia, Norwich, England

Reçu le 30 octobre 1972

Vibronic Coupling and Paramagnetic Anisotropy of a Cubic Complex $^2T_2$ Subjected to a Trigonal Field

The influence of vibronic coupling on the average paramagnetism and the paramagnetic anisotropy of a cubic complex, the electronic ground state $^2T_2$ of which is perturbed by a trigonal field, is investigated. It is necessary to introduce the following parameters: the spin-orbit coupling coefficient λ, the vibronic coupling coefficient x, the frequency $h\omega_\varepsilon$ of the E modes of vibration, the splitting Δ of the $^2T_2$ level in the trigonal field and the covalence parameter k.

For given x and $\varrho\left(=\frac{3\lambda}{2h\omega_\varepsilon}\right)$, the influence of the vibronic coupling is more important if in the trigonal field the electronic ground state of the complex is ^2E than if it is ^2A. For given x and $v\left(=\frac{\Delta}{\lambda}\right)$, the smaller $|\varrho|$, the greater the influence of vibronic coupling. The respective effects of vibronic coupling and covalence are compared. Finally, the case of the first row transition-metal complexes is briefly discussed.

Introduction

Nous avons dans un article précédent [1] auquel nous nous référons fréquemment étudié l'influence du couplage vibronique sur le paramagnétisme d'un complexe cubique dont l'état électronique est $^2T_2$[1]. En d'autres termes, nous avons tenu compte de ce que toute molécule possède des modes de vibration non totalement symétriques de sorte que la configuration d'équilibre de cette molécule n'est qu'une configuration moyenne. Lorsque l'état électronique fondamental de la molécule est dégénéré, celui-ci peut se coupler avec certains modes de vibration; l'approximation de Born-Oppenheimer dans laquelle on étudie le mouvement électronique en supposant les noyaux fixes dans leur position d'équilibre n'est alors plus valable.

Pour étudier théoriquement le paramagnétisme de complexes de métaux de transition en tenant compte du couplage vibronique, la théorie de Van Vleck [2] reste parfaitement applicable; mais alors les sommations qui interviennent dans la formule classique donnant la susceptibilité molaire en fonction de la température:

---

[1] Par complexe cubique nous entendons aussi bien complexe tétraédrique dont la symétrie est T_d que complexe octaédrique dont la symétrie est O_h. Dans ce dernier cas, l'état électronique considéré est $^2T_{2g}$. Pour simplifier, nous garderons la notation $^2T_2$.

$$\chi = -\frac{N\sum_n [(E_n^{(1)})^2/kT - 2E_n^{(2)}] \exp(-E_n^{(0)}/kT)}{\sum_n \exp(-E_n^{(0)}/kT)} \tag{1}$$

doivent être faites sur les différents niveaux vibroniques pour lesquels il intervient un couplage entre état électronique et modes de vibration et non sur les seuls niveaux électroniques.

Dans un complexe cubique dont l'état électronique est un triplet orbital, les modes de vibration qui se couplent avec l'état électronique sont ceux qui se transforment comme les représentations irréductibles E et T_2 du groupe cubique (E_g et T_{2g} si le complexe est octaédrique). Nous avons supposé avec Sturge [3] que le couplage vibronique engendré par les modes de vibration T_2 peut être négligé et avons introduit le paramètre x [4] qui définit l'importance du couplage vibronique engendré par les modes de vibration E. $x = 0$ correspond à l'approximation de Born-Oppenheimer dans laquelle le couplage vibronique est négligé; $x = 1$ correspond à un fort couplage vibronique. Lorsque x devient très grand ($x > 2$), on tend vers une distorsion tétragonale statique de la molécule. Nous avons montré que la variation du paramagnétisme en fonction de la température est d'autant plus modifiée par l'introduction du couplage vibronique que le paramètre $\varrho = \frac{3\lambda}{2\hbar\omega_E}$ où λ est le coefficient de couplage spin-orbite et $\hbar\omega_E$ la fréquence des modes de vibration E, est en valeur absolue plus faible. De plus il a été trouvé que l'influence du couplage vibronique est proche de celle de la covalence qui tend à réduire le moment orbital d'un facteur constant k mais non rigoureusement identique.

Nous nous proposons maintenant de poursuivre l'étude de l'influence du couplage vibronique sur les propriétés magnétiques des complexes cubiques ${}^2T_2$ en supposant qu'au champ de ligands cubique se superpose un champ axial engendrant une distorsion statique trigonale du complexe donc une anisotropie magnétique. L'existence d'une telle distorsion trigonale dans un complexe cubique ${}^2T_2$ a fréquemment été soit prouvée expérimentalement par radiocristallographie [5], soit supposée dans le but d'interpréter les propriétés magnétiques [6–8]. L'influence d'un champ axial sur le paramagnétisme d'un complexe cubique ${}^2T_2$ a été étudiée théoriquement par Figgis [9] puis par Gerloch [10]. Ces deux auteurs cependant ne tiennent pas compte de ce qu'outre une distorsion statique, le complexe subit des distorsions dynamiques correspondant aux modes de vibration non totalement symétriques et que certains de ces modes peuvent se coupler avec l'état électronique. Il nous a alors paru intéressant d'étendre les études de Figgis et Gerloch en tenant compte du couplage vibronique.

Figgis ne distingue pas dans son article un champ axial trigonal d'un champ axial tétragonal et de fait, si on considère que l'état fondamental ${}^2T_2$ est très séparé en énergie des états excités et que l'on néglige le couplage vibronique, l'effet du champ axial, qu'il soit trigonal ou tétragonal, est de diviser le niveau ${}^2T_2$ en un niveau orbitalement non dégénéré (${}^2A_1$ ou ${}^2B_2$) et un niveau orbitalement doublement dégénéré (${}^2E$) séparé du précédent de Δ. Ce paramètre Δ définit alors de façon univoque l'influence du champ axial sur la susceptibilité magnétique moyenne et l'anisotropie magnétique. Gerloch étudie le cas où l'état fondamental $^2T_2$ est perturbé par un champ tétragonal et envisage deux modèles: le modèle $^2T_2$ où l'état fondamental est très séparé des états excités et le modèle ^2D applicable aux ions d^9 en champ tétraédrique où il tient compte de la séparation $10\,Dq$ des niveaux $^2T_2$ et ^2E dans le complexe cubique. Les résultats qu'il obtient dans le premier modèle peuvent parfaitement être étendus au cas d'une distorsion trigonale alors que ceux obtenus dans le modèle ^2D seraient modifiés si la distorsion était trigonale. Même en supposant qu'il n'y a pas d'états excités proches en énergie de l'état fondamental (modèle $^2T_2$), il est nécessaire de distinguer la nature de la distorsion axiale, trigonale ou tétragonale, dès lors qu'on inclut le couplage vibronique dans la théorie. En effet une distorsion trigonale fait passer la symétrie du complexe de O_h à D_{3d} ou de T_d à C_{3v}; les coordonnées normales Q_2 et Q_3 correspondant aux modes de vibration E dans le complexe cubique restent dégénérées. Par contre, une distorsion tétragonale fait passer la symétrie de O_h à D_{4h} ou de T_d à C_{4v}; Q_2 et Q_3 ne sont plus dégénérés et se transforment respectivement comme A_1 et B_1. On peut dire que les niveaux vibrationnels correspondant aux modes de vibration E dans le complexe cubique ne sont pas perturbés par une distorsion trigonale alors qu'ils le sont par une distorsion tétragonale. Le problème de l'influence du couplage vibronique sur un ion $^2T_2$ perturbé par un champ tétragonal a été abordé par Kamimura et Mizuhashi [11, 12].

Par rapport à l'étude précédente [1], le seul paramètre supplémentaire que nous avons introduit est Δ compté positivement lorsque le niveau fondamental est le niveau orbitalement non dégénéré $^2A_1$. Les autres paramètres sont λ le coefficient de couplage spin-orbite, k le paramètre de covalence, la fréquence $\hbar\omega_\varepsilon$ des modes de vibration E et le paramètre de couplage vibronique x. Pour exprimer les résultats, nous définirons deux paramètres supplémentaires $v = \dfrac{\Delta}{\lambda}$ et $\varrho = \dfrac{3\lambda}{2\hbar\omega_\varepsilon}$.

Enfin, dans l'exposé des résultats, nous nous attacherons d'une part à montrer en quoi l'introduction du couplage vibronique modifie les résultats présentés par Figgis et Gerloch, d'autre part à comparer les influences sur l'anisotropie magnétique du couplage vibronique et de la covalence dont on sait qu'elle tend à réduire le moment orbital du facteur k.

Méthode de Calcul

La méthode de calcul utilisée est tout à fait similaire à celle qui a été décrite en détail dans le précédent article [1], n'était ce que dans l'hamiltonien vibronique $\mathscr{H}$ du complexe, un terme H_D de perturbation due au champ trigonal est rajouté. $\mathscr{H}$ s'écrit alors:

$$\mathscr{H} = H_E + H_N + H_D + H_{SO} \tag{2}$$

où H_E, H_N et H_{SO} sont respectivement les hamiltoniens électronique, nucléaire et de couplage spin-orbite.

Rappelons ici l'action de la distorsion trigonale et du couplage spin-orbite sur l'état électronique ${}^2T_2$ en absence de couplage vibronique. La distorsion trigonale sépare le niveau ${}^2T_2$ en un niveau ${}^2A_1$ situé à $-\frac{2\Delta}{3}$ et un niveau ${}^2E$ situé à $+\frac{\Delta}{3}$. Le couplage spin-orbite sépare lui-même le niveau ${}^2E$ en deux composantes Γ_4 et Γ_5 qui se réfèrent aux représentations du double groupe D_3' ($\Gamma_4 = E_{1,2}$ et $\Gamma_5 = E_{3,2}$). Au premier ordre Γ_4 et Γ_5 sont situés respectivement à $\frac{\Delta}{3} \pm \frac{\lambda}{2}$. Le niveau ${}^2A_1$ n'est pas perturbé au premier ordre par le couplage spin-orbite et donne un niveau Γ_4. Au second ordre, on sait que les deux niveaux Γ_4 issus respectivement de ${}^2E$ et ${}^2A_1$ interagissent. Ces résultats sont schématisés dans la Fig. 1 où nous avons pris $\lambda = 100\,\mathrm{cm}^{-1}$ et $\Delta = -500\,\mathrm{cm}^{-1}$, d'où $v = -5$.

En développant (2) en série taylorienne en fonction des n coordonnées normales de vibration Q_k et en ne tenant compte que du couplage vibronique engendré par les modes de vibration E du groupe cubique, $\mathscr{H}$ s'écrit:

$$\mathscr{H} = H_E^0 + H_N + H_D + H_{SO} + \left(\frac{\partial H_E}{\partial Q_2}\right)_0 Q_2 + \left(\frac{\partial H_E}{\partial Q_3}\right)_0 Q_3 \tag{3}$$

équation dans laquelle H_E^0, H_N et H_{SO} ont été explicités précédemment [1] et où Q_2 et Q_3 sont les coordonnées normales de vibration se transformant comme la représentation irréductible E du groupe cubique.

Les fonctions de base sont les fonctions de l'approximation de Born-Oppenheimer $\psi_i^0 s_u \varphi^{m,n}$ qui diagonalisent $H_E^0 + H_N$. ψ_i^0 sont les fonctions propres de H_E^0 pour l'état électronique fondamental, s_u les fonctions du doublet de spin ($s_1 = \alpha$; $s_2 = \beta$) et $\varphi^{m,n}$ les fonctions propres de H_N dans l'approximation harmonique où m et n réfèrent aux nombres quantiques de vibration correspondant à Q_2 et Q_3. Les termes H_D, H_{SO} et $\left(\frac{\partial H_E}{\partial Q_2}\right)_0 Q_2 + \left(\frac{\partial H_E}{\partial Q_3}\right)_0 Q_3$ sont considérés comme des perturbations dont les ordres de grandeur sont suffisamment proches pour qu'elles puissent être diagonalisées en même temps.

La distorsion H_D ne perturbe pas les niveaux vibrationnels $\hbar\omega_\varepsilon(m+n+1)$; H_D peut alors être considéré comme un opérateur purement électronique et nous avons:

$$\langle \psi_i^0 s_u \varphi^{m,n} | H_D | \psi_j^0 s_{u'} \varphi^{m',n'} \rangle = H_{Dij}\,\delta_{uu'}\,\delta_{mm'}\,\delta_{nn'} \tag{4}$$

H_{Dij} est un élément de la matrice carrée d'ordre 3:

$$H_D = \begin{array}{ccc} \psi_1^0 & \psi_2^0 & \psi_3^0 \\ \hline 0 & -\frac{\Delta}{3} & -\frac{\Delta}{3} \\ & 0 & -\frac{\Delta}{3} \\ & & 0 \end{array} \tag{5}$$

où ψ_1^0, ψ_2^0 et ψ_3^0 se transforment respectivement comme les orbitales atomiques d_{xy}, d_{yz} et d_{zx}.

Remarquons qu'une distorsion tétragonale perturberait les niveaux vibrationnels $\hbar\omega_\varepsilon(m+n+1)$ et qu'il aurait été alors nécessaire d'introduire dans le calcul un nouveau paramètre δ égal à $\hbar(\omega_2-\omega_3)$.

Du fait de la distorsion, le paramètre de covalence qui apparaît dans les éléments matriciels de la perturbation H_{SO} est anisotrope et en toute rigueur nous devrions introduire les paramètres $k_\parallel$ et $k_\perp$ correspondant à la réduction du moment orbital suivant l'axe principal et perpendiculairement à cet axe. En fait, pour simplifier un problème dont le nombre de paramètres est déjà fort élevé, nous gardons un seul paramètre k que l'on peut considérer comme un paramètre de covalence moyen.

Une fois obtenue par diagonalisation de $\mathcal{H}$ les énergies et fonctions vibroniques, on applique la perturbation Zeeman. Les éléments matriciels sur la base des fonctions électroniques $\psi_i^0 s_u$ des opérateurs $\hat{\mu}_\parallel$ et $\hat{\mu}_\perp$, moments magnétiques suivant l'axe de la distorsion et perpendiculairement à cet axe, sont respectivement en unités atomiques:

$$\hat{\mu}_\parallel=\begin{array}{cccccc}
\psi_1^0 s_1 & \psi_1^0 s_2 & \psi_2^0 s_1 & \psi_2^0 s_2 & \psi_3^0 s_1 & \psi_3^0 s_2 \\
\hline
\frac{\sqrt{3}}{3} & \frac{\sqrt{3}}{3}(1-i) & \frac{i\sqrt{3}}{3}k & 0 & -\frac{i\sqrt{3}}{3}k & 0 \\
 & -\frac{\sqrt{3}}{3} & 0 & \frac{i\sqrt{3}}{3}k & 0 & -\frac{i\sqrt{3}}{3}k \\
 & & \frac{\sqrt{3}}{3} & \frac{\sqrt{3}}{3}(1-i) & \frac{i\sqrt{3}}{3}k & 0 \\
 & & & -\frac{\sqrt{3}}{3} & 0 & \frac{i\sqrt{3}}{3}k \\
 & & & & \frac{\sqrt{3}}{3} & \frac{\sqrt{3}}{3}(1-i) \\
 & & & & & -\frac{\sqrt{3}}{3}
\end{array} \tag{6}$$

$$\hat{\mu}_\perp=\begin{array}{cccccc}
\psi_1^0 s_1 & \psi_1^0 s_2 & \psi_2^0 s_1 & \psi_2^0 s_2 & \psi_3^0 s_1 & \psi_3^0 s_2 \\
\hline
\frac{\sqrt{2}}{2} & -\frac{\sqrt{2}}{2} & 0 & 0 & \frac{i\sqrt{2}}{2}k & 0 \\
 & -\frac{\sqrt{2}}{2} & 0 & 0 & 0 & \frac{i\sqrt{2}}{2}k \\
 & & \frac{\sqrt{2}}{2} & -\frac{\sqrt{2}}{2} & \frac{i\sqrt{2}}{2}k & 0 \\
 & & & -\frac{\sqrt{2}}{2} & 0 & \frac{i\sqrt{2}}{2}k \\
 & & & & \frac{\sqrt{2}}{2} & -\frac{\sqrt{2}}{2} \\
 & & & & & -\frac{\sqrt{2}}{2}
\end{array}. \tag{7}$$

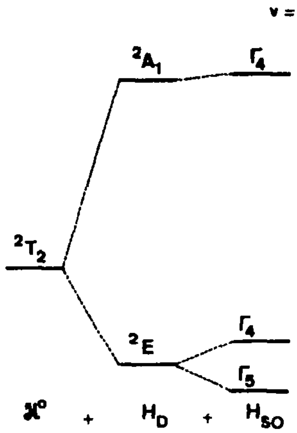

Fig. 1

Les perturbations Zeeman parallèle et perpendiculaire à l'axe de la distorsion sont diagonalisées sur la nouvelle base des fonctions vibroniques. On calcule alors les coefficients Zeeman du premier et du second ordre et obtient les susceptibilités magnétiques molaires $\chi_{\parallel}$ et $\chi_{\perp}$ par application de la formule (1). La susceptibilité magnétique moyenne $\bar{\chi}$ est données par:

$$\bar{\chi} = \tfrac{1}{3}(\chi_{\parallel} + 2\chi_{\perp}) \tag{8}$$

Les moments magnétiques effectifs $\mu_{\parallel}$, $\mu_{\perp}$ et $\bar{\mu}$ exprimés en Magnétons de Bohr se déduisent des susceptibilités magnétiques molaires selon:

$$\mu_{\parallel} = \left(\frac{3kT\chi_{\parallel}}{N\beta^2}\right)^{1/2} \tag{9}$$

et deux relations équivalentes pour $\mu_{\perp}$ et $\bar{\mu}$.

Nous avons limité la base des fonctions de Born-Oppenheimer à $m+n=2$. De la sorte le calcul requiert des diagonalisations de matrices hermitiques d'ordre 36, ce qui, au point de vue du temps de calcul, revient à diagonaliser des matrices réelles symétriques d'ordre 72. Du fait de la distorsion trigonale, aucune transformation unitaire ne perment de réduire l'ordre des matrices à diagonaliser. On notera que la base de départ est moins large que celle que nous avions utilisée dans l'article précédent [1]. Cette réduction de la base nous a été imposée afin de limiter le temps de calcul à 15 heures sur IBM 360/75. Les valeurs de $\bar{\mu}$ obtenues pour $v=0$, c'est-à-dire en absence de distorsion trigonale, sont légèrement différentes de celles obtenues précédemment lorsque $x \neq 0$. Cette différence reste faible pour $x=1$. La forme générale des courbes de variation du paramagnétisme en fonction de la température pour différentes valeurs de x n'est pas appréciablement modifiée par la réduction de la base.

Résultats et discussions

Les résultats seront discutés à partir de tableaux et schémas qui couvriront les principales conséquences de l'introduction du couplage vibronique dans la théorie du paramagnétisme d'un complexe cubique subissant une distorsion trigonale.

Intéressons-nous d'abord au moment magnétique effectif moyen. Dans le Tableau 1, nous avons donné les valeurs de $\bar{\mu}$ en fonction de $\frac{kT}{\lambda}$ pour $\varrho = 0,3$ et différentes valeurs de $v(-8 \leqq v \leqq 8)$ et de $x(x = 0; 0,5; 1)$ en négligeant la covalence ($k = 1$). Ce tableau concerne donc le cas où le coefficient de couplage spin-orbite est positif (ion d^1 hexacoordiné en environnement D_{3d} et ion d^5 tétracoordiné en

Tableau 1. Moment magnétique effectif d'un ion ${}^2T_2$ soumis à un champ trigonal en fonction de $\frac{kT}{\lambda}$, v et x et pour $\varrho = 0,3$ et $k = 1$

$\varrho = 0,3$ $k = 1$ $x = 0$

$\frac{kT}{\lambda}$:	0,1	0,2	0,3	0,4	0,5	0,6	0,8	1,0	1,2	1,4	1,6	1,8	2,0
$v = 8$	1,60	1,61	1,63	1,64	1,66	1,67	1,70	1,73	1,76	1,79	1,82	1,84	1,87
5	1,51	1,54	1,56	1,59	1,61	1,64	1,68	1,73	1,77	1,82	1,85	1,89	1,92
2	1,23	1,31	1,38	1,44	1,50	1,56	1,66	1,75	1,82	1,87	1,92	1,95	1,98
1	0,96	1,10	1,22	1,33	1,43	1,51	1,65	1,76	1,83	1,89	1,93	1,97	1,99
0	0,63	0,89	1,09	1,26	1,39	1,49	1,65	1,76	1,84	1,89	1,94	1,97	2,00
−1	0,64	0,92	1,13	1,28	1,41	1,50	1,65	1,76	1,83	1,89	1,93	1,96	1,99
−2	0,63	0,92	1,14	1,30	1,42	1,51	1,65	1,75	1,82	1,88	1,92	1,96	1,99
−5	0,63	0,91	1,13	1,30	1,43	1,52	1,65	1,74	1,80	1,85	1,89	1,93	1,96
−8	0,63	0,91	1,13	1,30	1,42	1,52	1,65	1,73	1,79	1,84	1,87	1,90	1,93

$\varrho = 0,3$ $k = 1$ $x = 0,5$

$\frac{kT}{\lambda}$:	0,1	0,2	0,3	0,4	0,5	0,6	0,8	1,0	1,2	1,4	1,6	1,8	2,0
$v = 8$	1,57	1,59	1,60	1,62	1,63	1,65	1,68	1,70	1,73	1,76	1,79	1,81	1,83
5	1,52	1,54	1,57	1,59	1,62	1,64	1,68	1,73	1,76	1,80	1,83	1,86	1,88
2	1,29	1,35	1,42	1,48	1,53	1,58	1,67	1,73	1,78	1,82	1,86	1,89	1,92
1	1,08	1,20	1,32	1,42	1,50	1,57	1,67	1,74	1,79	1,83	1,87	1,90	1,92
0	0,81	1,07	1,26	1,39	1,49	1,56	1,67	1,74	1,79	1,84	1,87	1,90	1,93
−1	0,84	1,11	1,22	1,40	1,50	1,57	1,67	1,74	1,79	1,83	1,86	1,89	1,91
−2	0,82	1,12	1,30	1,42	1,50	1,57	1,67	1,74	1,79	1,83	1,86	1,89	1,92
−5	0,78	1,09	1,29	1,42	1,50	1,56	1,65	1,71	1,76	1,80	1,84	1,86	1,89
−8	0,77	1,08	1,28	1,42	1,50	1,56	1,66	1,72	1,76	1,80	1,83	1,86	1,88

$\varrho = 0,3$ $k = 1$ $x = 1$

$\frac{kT}{\lambda}$:	0,1	0,2	0,3	0,4	0,5	0,6	0,8	1,0	1,2	1,4	1,6	1,8	2,0
$v = 8$	1,60	1,61	1,62	1,64	1,65	1,66	1,69	1,71	1,74	1,76	1,78	1,80	1,83
5	1,54	1,56	1,58	1,60	1,62	1,64	1,68	1,72	1,75	1,78	1,80	1,83	1,85
2	1,33	1,39	1,45	1,51	1,56	1,59	1,66	1,70	1,74	1,77	1,80	1,83	1,85
1	1,12	1,25	1,37	1,45	1,52	1,57	1,63	1,68	1,72	1,76	1,79	1,82	1,84
0	0,98	1,23	1,39	1,49	1,56	1,60	1,68	1,73	1,77	1,80	1,83	1,86	1,88
−1	1,01	1,24	1,38	1,47	1,54	1,59	1,66	1,71	1,75	1,79	1,82	1,84	1,87
−2	0,98	1,26	1,40	1,49	1,55	1,60	1,67	1,72	1,76	1,79	1,82	1,85	1,87
−5	0,96	1,26	1,42	1,51	1,57	1,61	1,67	1,72	1,76	1,79	1,82	1,84	1,87
−8	0,93	1,25	1,41	1,51	1,57	1,61	1,67	1,72	1,76	1,79	1,81	1,84	1,86

environnement C_{3v} dans la limite d'un champ fort). Lorsque v est positif, l'état fondamental est $^2A_1$. Au premier ordre cet état ne se couple pas avec les modes de vibration E puisque les intégrales du type $\left\langle {}^2A_1 \left| \frac{\partial H_E}{\partial Q_k} \right| {}^2A_1 \right\rangle$ avec $k = 1$ et 2 sont nulles. Le niveau $^2A_1$ n'est perturbé par le couplage vibronique qu'au second

Tableau 2. Moment magnétique effectif d'un ion $^2T_2$ soumis à un champ trigonal en fonction de $\frac{kT}{|\lambda|}$, v et x et pour $\varrho = -0,3$ et $k = 1$

$\varrho = -0,3$ $k = 1$ $x = 0$

$\frac{kT}{\lvert\lambda\rvert}$	0,1	0,2	0,3	0,4	0,5	0,6	0,8	1,0	1,2	1,4	1,6	1,8	2,0
$v = 8$	2,10	2,20	2,26	2,29	2,31	2,31	2,30	2,29	2,28	2,28	2,27	2,27	2,27
5	2,09	2,20	2,27	2,31	2,33	2,34	2,34	2,34	2,34	2,34	2,33	2,33	2,33
2	2,05	2,18	2,29	2,36	2,40	2,43	2,45	2,45	2,45	2,43	2,42	2,41	2,40
1	2,00	2,16	2,30	2,39	2,45	2,49	2,51	2,50	2,48	2,47	2,45	2,43	2,42
0	1,95	2,14	2,30	2,42	2,49	2,52	2,53	2,52	2,50	2,48	2,46	2,44	2,43
− 1	2,03	2,16	2,27	2,36	2,43	2,46	2,49	2,49	2,48	2,46	2,45	2,43	2,42
2	2,06	2,12	2,18	2,24	2,29	2,33	2,38	2,40	2,41	2,41	2,41	2,40	2,39
5	1,94	1,97	1,99	2,01	2,03	2,05	2,09	2,13	2,16	2,19	2,21	2,23	2,25
8	1,88	1,89	1,90	1,92	1,93	1,94	1,97	1,99	2,02	2,04	2,07	2,09	2,11

$\varrho = -0,3$ $k = 1$ $x = 0,5$

$\frac{kT}{\lvert\lambda\rvert}$	0,1	0,2	0,3	0,4	0,5	0,6	0,8	1,0	1,2	1,4	1,6	1,8	2,0
$v = 8$	1,92	2,05	2,11	2,13	2,14	2,14	2,14	2,14	2,14	2,15	2,15	2,16	2,17
5	1,90	2,04	2,11	2,14	2,15	2,16	2,17	2,17	2,17	2,18	2,19	2,19	2,20
2	1,83	2,01	2,11	2,17	2,20	2,21	2,22	2,22	2,23	2,23	2,23	2,23	2,24
1	1,80	2,01	2,14	2,21	2,24	2,25	2,25	2,25	2,25	2,25	2,25	2,25	2,25
0	1,75	2,00	2,15	2,22	2,25	2,26	2,27	2,26	2,26	2,26	2,26	2,26	2,26
− 1	1,85	2,01	2,13	2,20	2,23	2,24	2,25	2,25	2,25	2,25	2,25	2,25	2,26
− 2	1,93	2,01	2,07	2,12	2,15	2,18	2,20	2,21	2,22	2,22	2,23	2,23	2,24
− 5	1,87	1,90	1,92	1,94	1,96	1,98	2,01	2,04	2,07	2,09	2,11	2,12	2,13
− 8	1,86	1,87	1,89	1,90	1,91	1,93	1,95	1,97	2,00	2,02	2,04	2,06	2,07

$\varrho = -0,3$ $k = 1$ $x = 1$

$\frac{kT}{\lvert\lambda\rvert}$	0,1	0,2	0,3	0,4	0,5	0,6	0,8	1,0	1,2	1,4	1,6	1,8	2,0
$v = 8$	1,83	1,96	2,01	2,03	2,04	2,04	2,04	2,05	2,06	2,07	2,08	2,09	2,10
5	1,79	1,94	2,00	2,03	2,04	2,04	2,05	2,06	2,07	2,08	2,09	2,10	2,11
2	1,74	1,93	2,02	2,05	2,07	2,07	2,08	2,09	2,10	2,11	2,12	2,13	2,14
1	1,66	1,90	2,01	2,05	2,06	2,07	2,08	2,08	2,09	2,10	2,11	2,12	2,13
0	1,66	1,93	2,05	2,09	2,10	2,11	2,11	2,11	2,12	2,13	2,14	2,15	2,16
− 1	1,74	1,93	2,03	2,07	2,09	2,09	2,10	2,11	2,11	2,12	2,13	2,14	2,15
− 2	1,86	1,94	2,00	2,04	2,06	2,07	2,08	2,09	2,10	2,11	2,12	2,13	2,13
− 5	1,88	1,90	1,92	1,94	1,95	1,97	1,99	2,02	2,03	2,05	2,06	2,07	2,08
− 8	1,85	1,86	1,88	1,89	1,90	1,91	1,93	1,95	1,97	1,99	2,01	2,02	2,04

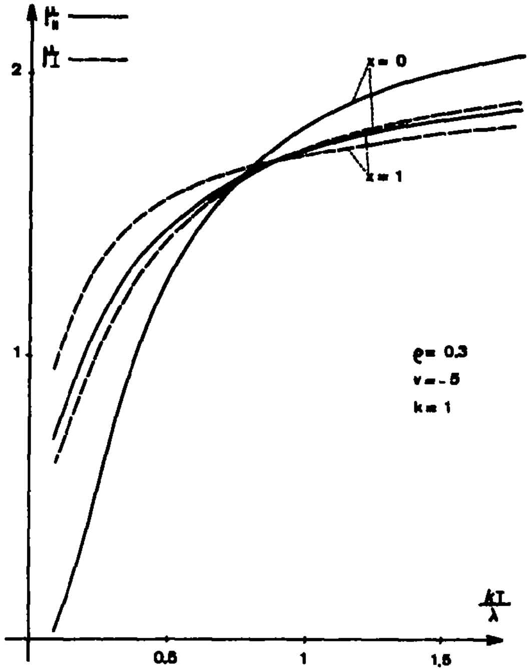

Fig 2

ordre, les intégrales du type $\left\langle {}^2A_1 \left| \frac{\partial H_E}{\partial Q_k} \right| {}^2E \right\rangle$ étant différentes de zéro. On constate en effet que l'influence du couplage vibronique sur le paramagnétisme pour $v > 0$ est faible et ce d'autant plus que v est plus grand, donc que les composantes Γ_4 et Γ_5 de ${}^2E$ sont plus séparées en énergie de ${}^2A_1$. Par contre, pour $v < 0$, le niveau fondamental est ${}^2E$ qui se couple au premier ordre avec les modes de vibration E puisque $\left\langle {}^2E \left| \frac{\partial H_E}{\partial Q_k} \right| {}^2E \right\rangle$ est différent de zéro et le couplage vibronique modifie de façon sensible la variation de $\bar{\mu}$ en fonction de $\frac{kT}{\lambda}$.

Le Tableau 2 ne diffère du précédent qu'en ce que $\varrho = -0{,}3$. Il concerne donc le cas où λ est négatif (ion d^5 hexacoordiné en environnement D_{3d} dans la limite du champ fort et ion d^9 tétracoordiné en environnement C_{3v}). Lorsque v est positif, le niveau fondamental est ${}^2E$ et le couplage vibronique modifie sensiblement la variation du paramagnétisme en fonction de la température alors que, pour $v < 0$, le niveau fondamental est ${}^2A_1$ et l'influence du couplage vibronique est faible. Les deux Tableaux 1 et 2 doivent être comparés à ceux de l'article de Figgis [9] où les valeurs de $\bar{\mu}$ sont données en fonction de $\frac{kT}{\lambda}$, v et k en négligeant le couplage vibronique ($x = 0$).

Dans la Fig. 2, est représentée la variation de $\mu_\parallel$ et $\mu_\perp$ en fonction de $\frac{kT}{\lambda}$ lorsque $\varrho = 0{,}3$, $v = -5$ et cela dans le cas d'un couplage vibronique nul ($x = 0$)

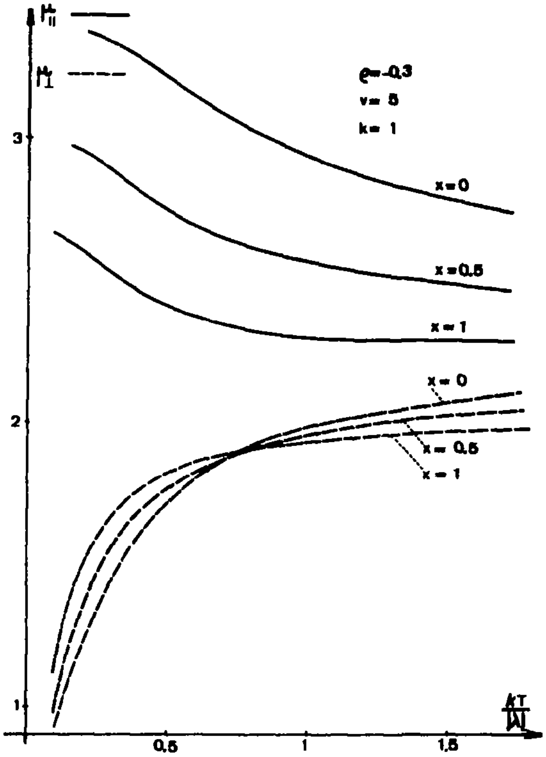

Fig. 3

et d'un couplage vibronique important ($x = 1$). On constate que, comme attendu, le couplage vibronique qui diminue la contribution orbitale du paramagnétisme entraîne une diminution de l'anisotropie magnétique définie par $\mu_{\parallel} - \mu_{\perp}$. En fait, pour $\lambda > 0$, l'anisotropie magnétique, même en absence de couplage vibronique, reste faible et nous nous intéresserons uniquement par la suite au cas des complexes avec $\lambda < 0$ pour lesquels l'anisotropie magnétique est nettement plus importante. Ainsi la Fig. 3 donne la variation de $\mu_{\parallel}$ et $\mu_{\perp}$ en fonction de $\frac{kT}{|\lambda|}$ et cela pour $\varrho = -0{,}3$, $v = 5$ et $x = 0$, 0,5 et 1. On vérifie que l'anisotropie magnétique, importante pour $x = 0$, tend à diminuer lorsque x croît. On remarque que le couplage vibronique modifie beaucoup plus fortement $\mu_{\parallel}$ que $\mu_{\perp}$.

La Fig. 4 se déduit aisément de la Fig. 3 et donne les variations de l'anisotropie magnétique $\mu_{\parallel} - \mu_{\perp}$ en fonction de $\frac{kT}{|\lambda|}$ pour les mêmes valeurs des paramètres ϱ, v et x.

Sur la Fig. 5, nous avons représenté la variation de $\mu_{\parallel} - \mu_{\perp}$ en fonction de v pour $\varrho = -0{,}3$, $\frac{kT}{\lambda} = -1$ et $x = 0$, 0,5 et 1. Lorsque v est positif, c'est-à-dire lorsque l'état fondamental est ^2E, l'anisotropie croît avec v mais cette croissance est d'autant plus lente que x est plus grand. Pour $v = 0$, bien évidemment $\mu_{\parallel} - \mu_{\perp} = 0$

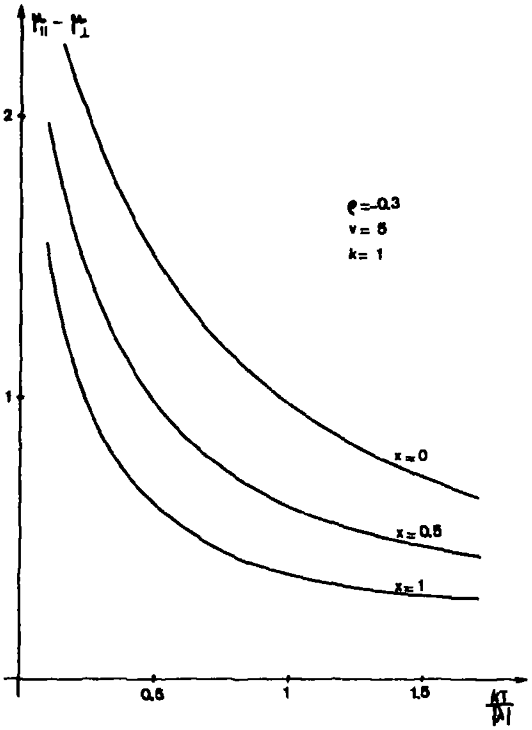

$\mu_\parallel - \mu_\perp$
2
1
$\varrho = -0.3$
$v = 5$
$k = 1$
$x = 0$
$x = 0.5$
$x = 1$
0.5
1
1.5
$\frac{kT}{|\lambda|}$

Fig. 4

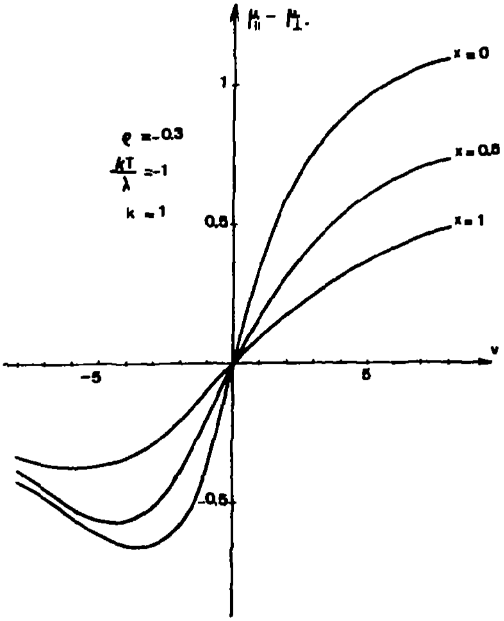

$\mu_\parallel - \mu_\perp$
$x = 0$
1
$x = 0.5$
$\varrho = -0.3$
$\frac{kT}{\lambda} = -1$
$k = 1$
0.5
$x = 1$
v
-5
5
-0.5

Fig. 5

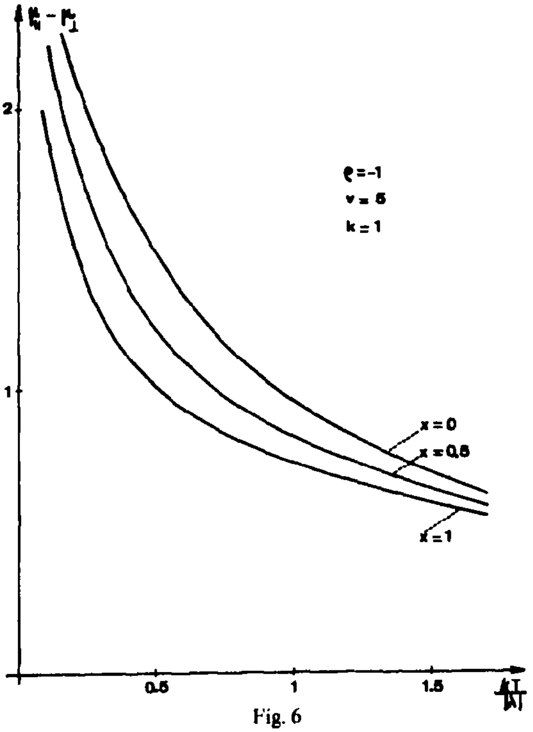

Fig. 6

et pour $v < 0$, comme déjà observé par Gerloch [10], l'anisotropie passe par un maximum en valeur absolue et tend vers zéro lorsque le niveau fondamental ^2A est très séparé du niveau ^2E. Le moment orbital est alors détruit par la distorsion et $\mu_\parallel$ et $\mu_\perp$ sont égaux à $\sqrt{3}$.

Nous avons vu précédemment que l'influence du couplage vibronique sur le paramagnétisme était d'autant plus faible que le paramètre ϱ en valeur absolue était plus grand. Ce résultat peut à nouveau être vérifié dans cette étude. Pour cela nous avons tracé sur la Fig. 6 la variation de $\mu_\parallel - \mu_\perp$ en fonction de $\frac{kT}{|\lambda|}$ pour $\varrho = -1$, $v = 5$ et $x = 0$, 0,5 et 1. Cette courbe doit être comparée à celle de la Fig. 4 et cette comparison confirme que la diminution de l'anisotropie magnétique engendrée par le couplage vibronique est nettement plus faible lorsque $\varrho = -1$ que lorsque $\varrho = -0{,}3$.

Enfin jusqu'à présent dans les Tableaux 1 et 2 et les Figs. 2 à 6, nous avons négligé la covalence en posant $k = 1$. Nous voulons maintenant comparer l'influence de la covalence à celle du couplage vibronique. Pour cela, sur la Fig. 7, nous avons à nouveau représenté $\mu_\parallel - \mu_\perp$ en fonction de $\frac{kT}{|\lambda|}$ lorsque λ est négatif et v égal à 5, en posant $x = 0$ et en donnant à k les valeurs 1, 0,8 et 0,6. On peut constater que les effets de la covalence et du couplage vibronique sont très similaires;

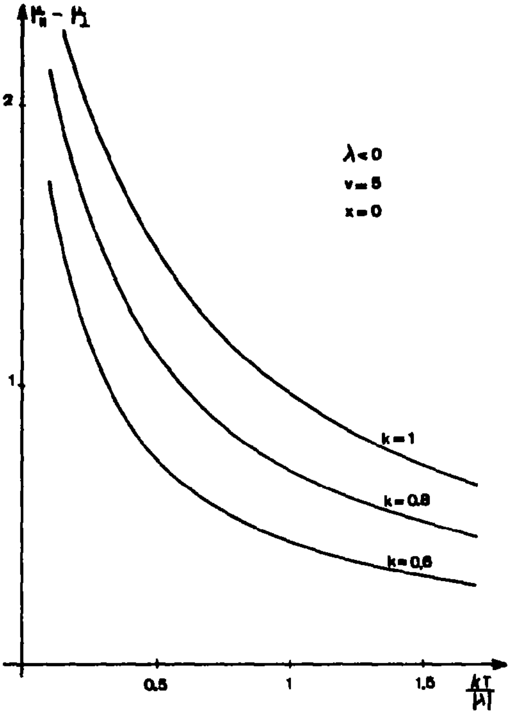
$\mu_\parallel - \mu_\perp$
2
1
$\lambda < 0$
$v = 5$
$x = 0$
k = 1
k = 0.8
k = 0.6
0.5
1
1.5
$\frac{kT}{|\lambda|}$

Fig. 7

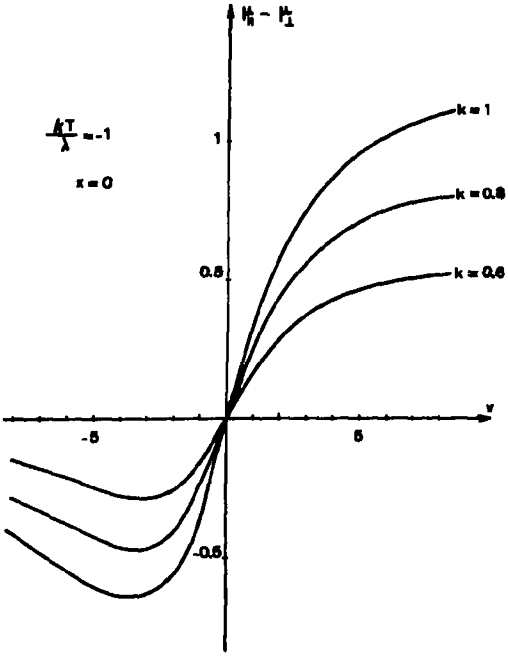
$\mu_\parallel - \mu_\perp$
$\frac{kT}{\lambda} = -1$
$x = 0$
1
0.5
-0.5
k = 1
k = 0.8
k = 0.6
-5
5
v

Fig. 8

tous deux entrainent une diminution de l'anisotropie magnétique, mais ils ne sont pas rigoureusement équivalents. Par exemple pour $\frac{kT}{|\lambda|} = 1{,}7$, la courbe $x = 1$ de la Fig. 4 passe par le même point que la courbe $k = 0{,}6$ de la Fig. 7. Ces deux courbes cependant ne sont pas superposables; elles ne possèdent que ce point commun. La même constatation peut être faite si dans la Fig. 8, on trace la variation de $\mu_{\parallel} - \mu_{\perp}$ en fonction de v pour λ négatif, $\frac{kT}{\lambda} = -1$, $k = 1$, 0,8 et 0,6 et compare les courbes tracées à celles de la Fig. 5. Par exemple les courbes $x = 1$ de la Fig. 5 et $k = 0{,}6$ de la Fig. 8 ont trois points communs ($v \sim 8$, $v = 0$ et $v \sim -3$) mais ne sont pas du tout superposables. Rappelons ici que k a la signification d'un paramètre de covalence moyen et qu'en toute rigueur il faudrait introduire deux paramètres de covalence $k_{\parallel}$ et $k_{\perp}$ pour tenir compte de l'anisotropie créée par la distorsion.

Conclusion

Nous avons introduit le couplage vibronique dans la théorie du paramagnétisme d'un complexe cubique $^2T_2$ subissant une distorsion trigonale. Nous avons pour cela considéré que l'état électronique peut se coupler avec les modes de vibration E du complexe cubique de sorte que l'approximation de Born-Oppenheimer ne peut plus être utilisée. L'écart à l'approximation de Born-Oppenheimer est déterminé par le paramètre de couplage vibronique x. Nous avons en fait simplifié le problème vibronique en négligeant le couplage entre l'état électronique et les modes de vibrations T_2 du complexe cubique. De la sorte nous devons considérer que la distorsion statique trigonale résulte non pas d'un effet Jahn-Teller mais de l'environnement cristallin; c'est par exemple le cas de Ti^{3+} dans le rubis, le corundum, de l'alun de césium et de titane, de l'acétylacétonate de titane, etc [5].

Les résultats de cette étude confirment et étendent ceux qui avaient été obtenus précédemment: L'influence du couplage vibronique sur les propriétés magnétiques est similaire de celle de la covalence mais non rigoureusement identique. Le couplage vibronique réduit la contribution orbitale au paramagnétisme mais d'un facteur qui n'est pas indépendant de la température alors que k, le paramètre de covalence, est supposé indépendant de la température. Cette réduction de la contribution orbitale au paramagnétisme entraîne une diminution de l'anisotropie magnétique créée par la distorsion trigonale. Cet effet du couplage vibronique dépend outre de x, de $v = \frac{\Delta}{\lambda}$ et $\varrho = \frac{3\lambda}{2\hbar\omega_c}$. Lorsque v et λ ont le même signe, Δ est positif et l'état fondamental $^2A_1$, au premier ordre, n'est pas perturbé par le couplage vibronique. Au contraire, si v et λ sont de signes contraires, Δ est négatif et l'état fondamental ^2E est au premier ordre perturbé par le couplage vibronique dont l'influence sur le paramagnétisme du complexe peut être importante. Sasaki et Obata [13] ont étudié un problème voisin; en admettant qu'en absence de couplage vibronique, la susceptibilité magnétique suit une loi de Curie-Weiss, ils ont montré que l'introduction du couplage vibronique conduit à une réduction de la susceptibilité magnétique d'un facteur dépendant de la température. Ils n'ont cependant pas précisé l'influence du couplage spin-orbite sur cet effet.

En ce qui concerne le paramètre ϱ, plus celui-ci est grand en valeur absolue, moins le couplage vibronique influence les propriétés magnétiques. Ainsi, lorsque $|\varrho|$ dépasse 2, le couplage vibronique ne joue à peu près plus aucun rôle dans l'interprétation du paramagnétisme. Il est alors possible d'examiner pour quels complexes ${}^2T_2$, le couplage vibronique est susceptible d'influer sur le paramagnétisme. Si nous supposons que les ions des métaux de transition sont ceux de la premère série (Ti à Cu) et qu'ils sont situés dans un champ de ligands dont les atomes coordinateurs appartiennent à la première ligne de la classification périodique, on peut admettre que la fréquence $h\omega_\varepsilon$ est de l'ordre de $400\,\mathrm{cm}^{-1}$. En retenant comme valeurs des coefficients de couplage spin-orbite, celles données par Dunn [11], on arrive aux conclusions suivantes: en ce qui concerne les ions d^1 en champ octaédrique, le couplage vibronique peut jouer un rôle important pour Ti^{3+} ($\lambda = 155\,\mathrm{cm}^{-1}$) et n'être pas négligeable pour V^{4+} ($\lambda = 250\,\mathrm{cm}^{-1}$). Ce rôle devient très faible pour Cr^{5+} ($\lambda = 380\,\mathrm{cm}^{-1}$). En ce qui concerne les ions d^5 en champ fort, le couplage vibronique est susceptible de jouer un rôle très important dans les propriétés magnétiques de V^0 ($\lambda = \pm 95\,\mathrm{cm}^{-1}$). Un fort effet Jahn-Teller dynamique a déjà été postulé pour $\mathrm{V(CO)_6}$ [12]. Si l'influence du couplage vibronique ne peut a priori être négligé pour Cr^{+} ($\lambda = \pm 190\,\mathrm{cm}^{-1}$) ou même Mn^{2+} ($\lambda = \pm 300\,\mathrm{cm}^{-1}$), elle est sans doute très faible pour Fe^{3+} ($\lambda = \pm 460\,\mathrm{cm}^{-1}$). Enfin pour les ions d^9 en champ tétraédrique tels que Cu^{2+} qui possèdent un fort coefficient de couplage spin-orbite ($\lambda = -830\,\mathrm{cm}^{-1}$ pour Cu^{2+}), le couplage vibronique éventuel est sans effet sur les propriétés magnétiques. Ce qui précède ne préjuge pas de la valeur du paramètre de couplage vibronique x dont le calcul théorique, à partir des fonctions électroniques ψ_i^0, est extrêmement difficile, x et les autres paramètres introduits dans cette étude peuvent être déterminés par recherche du meilleur accord entre variations expérimentale et théorique du paramagnétisme en fonction de la température. Cela a été fait dans le cas de $\mathrm{TiF_6Na_3}$. Si nous définissons à partir des moments effectifs moyens calculés et expérimentaux $\bar{\mu}_{\mathrm{cal}}$ et $\bar{\mu}_{\mathrm{exp}}$ le facteur d'accord $R = \dfrac{\sum|\bar{\mu}_{\mathrm{cal}} - \bar{\mu}_{\mathrm{exp}}|}{\sum \bar{\mu}_{\mathrm{exp}}}$, nous obtenons pour 15 mesures entre 77 et 300 °K un accord presque parfait correspondant à $R = 0{,}002$ pour $x = 0{,}50$, $k = 0{,}80$, $h\omega_\varepsilon = 450\,\mathrm{cm}^{-1}$, $\lambda = 155\,\mathrm{cm}^{-1}$ et $\Delta = 200\,\mathrm{cm}^{-1}$. Sans introduction du couplage vibronique, le meilleur accord obtenu par Hatfield *et coll.* [16] correspond à $R = 0{,}009$. Sans doute ne faut-il pas surestimer la signification d'un tel accord; ainsi que nous l'avions noté précédemment [1], le nombre de paramètres introduits permet une trop grande flexibilité dans l'obtention des courbes théoriques. Le test serait nettement plus sévère si, dans le cas d'un cristal axial, nous cherchions à retrouver théoriquement les variations de $\mu_\parallel$ et $\mu_\perp$. Il nous apparait cependant clairement que pour les composés des métaux de transition dont l'état fondamental est un triplet orbital, l'écart à l'approximation de Born-Oppenheimer engendré par le couplage vibronique peut être un facteur important dans l'interprétation des propriétés magnétiques dès lors que le couplage spin-orbite n'est pas trop important.

References

1. Kahn, O., Kettle, S. F. A.: Theoret. chim. Acta (Berl.) **27**, 187 (1972).
2. Van Vleck, J. H.: The theory of electronic and magnetic susceptibilities. Oxford University Press (1932).
3. Sturge, M. D.: Solid State Physics **91** (1967).
4. Kahn, O., Kettle, S. F. A.: Molecular Physics à paraître.
5. Gladney, H. M., Swalen, J. D.: J. chem. Physics **42**, 1999 (1965).
6. Dutta-Roy, K. S., Chakravarty, A. S., Buse, A.: Indian J. Physics Proc. Indian Assoc. Cultivat. Sci. **38**, 483 (1959).
7. Bleaney, B., Bogle, G. S., Cooke, A. H., Duffus, R. J., O'Brien, M. C. M., Stevens, K. W. H.: Proc. Physics Soc. **268**, 57 (1955).
8. Van Vleck, J. H.: J. chem. Physics **7**, 61 (1939).
9. Figgis, B. N.: Trans. Faraday Soc. **57**, 198 et 204 (1961).
10. Gerloch, M.: J. chem. Soc. **1968**, 2023.
11. Kamimura, H., Mizuhashi, S.: J. appl. Physics **39**, 684 (1968).
12. Mizuhashi, S.: J. physic. Soc. Japan **26**, 468 (1969).
13. Sasaki, K., Obata, Y.: J. physic. Soc. Japan **28**, 1157 (1970).
14. Dunn, T. M.: Trans. Faraday Soc. **57**, 1441 (1961).
15. Hass, H., Sheline, R. K.: J. Amer. chem. Soc. **88**, 3219 (1966).
16. Nassif, P. J., Couch, T. W., Hatfield, W. E., Villa, J. F.: Inorg. Chemistry **10**, 368 (1971).

Dr. O. Kahn
Ecole Nationale Supérieure
de Chimie de Paris
11, rue Pierre et Marie Curie
F-75005 Paris, France

Theoret. chim. Acta (Berl.) 29, 375—382 (1973)
© by Springer-Verlag 1973

Relatio

Molecular Dipole Polarizabilities Based on MINDO/1 and MINDO/2 Wavefunctions*

H. Meyer and A. Schweig

Fachbereich Physikalische Chemie, D-3550 Marburg (Lahn), Biegenstr. 12

Received September 27, 1972

Molecular dipole polarizability values are derived from a MINDO/1 - and MINDO/2 "finite perturbation treatment". The results are, especially in the MINDO/1 case, surprisingly good.

Introduction

The "finite perturbation theory" independently developed by Cohen and Roothaan [1] and by us [2–5], and subsequently given this name by Pople *et al.* [6], provided an exceptional stimulus to the calculation of second and higher order properties (dipole [1–5, 7–19] and quadrupole [10, 13] polarizabilities, susceptibilities [20], shielding [20] and coupling [21–25] constants, hyperpolarizabilities [5, 8, 10, 11, 26], and transition polarizabilities [27]). Since this theory, when applied at the CNDO/2 level [28], gives values for molecular dipole polarizabilities which are too low, we tested two other valence electron methods, MINDO/1 and MINDO/2 [29], for the same purpose. Is is the aim of this note to point out the unexpected result that these methods give much better results than the CNDO/2 method.

Method

Restricting ourselves for the present objective to the diagonal components α_{ii} of the molecular polarizability, we may describe the field dependence of the molecular dipole moment by [30]

$$\mu_i = \mu_i^{(0)} + \alpha_{ii} F_i + \cdots, i = x, y, z \qquad (1)$$

where μ_i and $\mu_i^{(0)}$ are the i-components of the total and permanent dipole moment, respectively, and F_i the strength of the uniform electric field applied in the i-direction. In order to incorporate F_i into the Hamiltonian operator, we have to add to the core matrix H^c the field dependent matrix F, whose elements are the same for all of the three above mentioned valence electron procedures and which have been listed previously [17] [1]. For several values of F_i, values of μ_i are computed, and α_{ii} is obtained using the method of least squares to express μ_i according to (1) as a power series in F_i.

---

* Part 15 of Properties of molecules in electric fields. Part 14: Schweig, A.: Angew. Chem., (in press).

[1] Some of the formulae in [17] are presented incorrectly and should be applied with caution.

Results and Discussion

Tables 1–3 list the calculated MINDO/1, MINDO/2 and CNDO/2[2] polarizabilities (Table 1 the α_{zz}, Table 2 the α_{xx} and α_{yy} components and Table 3 the mean polarizabilities $\alpha=(\alpha_{xx}+\alpha_{yy}+\alpha_{zz})/3)$ together with previously calculated or experimental values. The orientation of molecules relative to the Cartesian coordinate system indicated in the Tables is chosen so that the coordinate axes and the principal polarizability axes coincide.

The Tables reveal two interesting results:

1) The quality of the calculated values clearly increases in the series: CNDO/2→MINDO/2→MINDO/1. This result is surprising, since previous experience [54] has shown MINDO dipole moments to be inferior to those calculated by CNDO/2.

2) Whereas MINDO polarizabilities of linear molecules along the molecular axis (α_{zz}) generally agree well with the experimental values, the polarizabilities perpendicular to the axis (α_{xx}) are much too low. A similar situation prevails in planar molecules (H_2O, C_2H_4) where the MINDO polarizabilities in the molecular plane (α_{zz} and α_{xx}) are much better (especially in the MINDO/1 case) than the polarizability perpendicular to the plane, (α_{yy}) being again much too low.

These results show that the semiempirical MINDO- "finite perturbation method" represents a practical combination of methods for predicting satisfactory numerical values of molecular polarizabilities along the axis for linear molecules and in the plane for planar systems. However, if equally good polarizabilities perpendicular to the molecular axis (linear molecules) or molecular plane are needed, the inclusion of some sort of polarization functions in the semiemperical method seems to be unavoidable.

Table 1. Polarizability component α_{zz} (in 10^{-24} cm^3)

Molecule[a]	MINDO/1	MINDO/2	CNDO/2	Calculated	Experimental[b]
H – H	1.02	0.47	0.455 [17]	0.971 [13]	1.028 [49]
				0.945 [32]	0.934 [50]
				0.21 [33]	
				1.293 [34]	
				1.92 [35]	
				1.664 [36]	
N ≡ N	2.79	2.78	1.153 [17]	1.10 [33]	2.23_1 [49]
				4.67 [34]	2.38 [50]
				3.84 [35]	
				5.746 [36]	
				1.56 [38]	
F – F	2.25		0.936 [17]	1.904 [36]	
				2.248 [37]	
				1.08 [38]	
				2.15 [39]	

---

[2] All CNDO/2 polarizability values have been recalculated by us. In case of large discrepancies between our values and those of Hush and Williams, both values are listed in the Tables.

Table 1 (Continued)

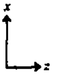 Molecule[a]	MINDO/1	MINDO/2	CNDO/2	Calculated	Experimental[b]
C≡O	2.85	2.26	1.070 [17]	2.11 [13] 1.67 [13] 1.76 [13] 4.32 [34] 4.803 [36] 3.222 [37] 3.264 [40]	2.33_2 [49] 2.60 [50]
O=C=O	4.44	3.93	1.994 [17]		4.03 [49] 4.93 [51]
N=N=O	5.58	5.73	2.58	3.65 [13] 4.07 [13]	4.97 [49] 4.86 [50]
F–H	0.60		0.327 [31]	0.830 [16] 0.32 [33] 0.63 [33] 1.002 [37] 0.859 [39] 0.779 [41] 0.732 [42] 0.808 [42] 0.616 [43] 0.791 [45]	
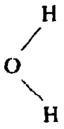	0.67	0.33	0.22 [31]	1.452 [40] 0.749 [40] 1.073 [41] 1.067 [41] 0.88 [43] 1.162 [44] 1.00 [45] 1.150 [46] 0.489 [46]	
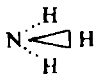	0.53	0.53	0.21 0.651 [31]	1.624 [41]	2.41 [49] 2.42 [50]
CH_4	1.64	1.05	0.65 [31]	2.30 [18] 2.58 [35] 3.176 [40] 1.889 [41]	2.60 [50] 2.62 [52]
H–C≡N	4.71	3.36	1.52 1.862 [31]	1.845 [40] 1.831 [47]	3.92 [50]
H–C≡C–H	5.09	3.86	2.121 [17]		4.73 [49] 5.12 [50]
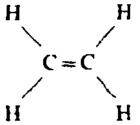	5.45	4.29	2.46	4.20 [16] 2.40 [33] 4.08 [33] 5.61 [48]	

---

[a] Experimental bond lengths and angles are used.

[b] Optical polarizabilities unless otherwise specified.

Table 2. Polarizability components α_{xx} and α_{yy} (10^{-24} cm^3)

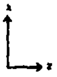 Molecule[a]	MINDO/1		MINDO/2		CNDO/2		Calculated		Experimental[b]
H – H	0.00		0.00		0.000 [17]		0.678 [32] 0.00 [33] 0.801 [34] 0.24 [35] 0.572 [36]		0.714 [49] 0.718 [50]
N ≡ N	0.60		0.60		0.394 [17]		0.40 [33] 1.27 [34] 0.72 [35] 1.098 [36] 1.954 [37] 0.94 [38]		1.53_5 [49] 1.45 [50]
F - F	0.03				0.04 0.017 [17]		0.390 [36] 0.949 [37] 0.30 [38] 0.77 [39]		
C ≡ O	0.95		0.90		0.709 [17]		1.55 [34] 1.283 [36] 2.088 [37] 2.013 [40]		1.80_0 [49] 1.625 [50]
O = C = O	0.73		0.50		0.322 [17]				1.93 [49] 2.14 [51]
N = N = O	0.71		0.70		0.42				2.01 [49] 2.07 [50]
F - H	0.04		-		0.03 0.000 [31]		0.03 [33] 0.22 [33] 0.364 [34] 0.377 [36] 0.791 [37] 0.623 [39] 0.525 [41]		
	α_{xx}	α_{yy}	α_{xx}	α_{yy}	α_{xx}	α_{yy}	α_{xx}	α_{yy}	
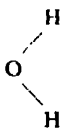	1.42	0.15	0.37	0.14	0.63	0.09 [31]	1.651 1.071 1.191 1.202 1.44 1.279 1.83 1.247 0.840	1.226 [40] 0.589 [40] 0.918 [41] 0.920 [41] 0.63 [43] 1.069 [44] 0.53 [45] 1.011 [46] 0.165 [46]	
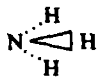	1.88		0.83		0.65 1.045 [31]		1.742 [41]		2.12 [49] 2.18 [50]

Table 2 (Continued)

 Molecule	MINDO/1	MINDO/2	CNDO/2	Calculated	Experimental[b]
CH_4	1.64	1.05	0.65 [31]	2.30 [18] 2.58 [35] 3.176 [40] 1.889 [41]	2.60 [50] 2.62 [52]
H – C ≡ N	0.97	0.77	0.46 0.025 [31]	1.845 [40] 1.831 [47]	1.92 [50]
H – C ≡ C – H	0.73	0.54	0.33 0.000 [17]		2.87 [49] 2.43 [50]
	α_{xx} α_{yy}	α_{xx} α_{yy}	α_{xx} α_{yy}	α_{xx} α_{yy}	
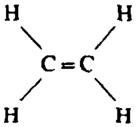	3.72 1.02	2.00 0.79	1.09 0.49	2.28 16 1.10 0.50 [33] 2.86 1.77 [33] 3.96 3.38 [48]	

[a] Experimental bond lengths and angles are used.

[b] Optical polarizabilities unless otherwise specified.

Table 3. Mean polarizability $\alpha(10^{-24}\ cm^3)$

 Molecule[a]	MINDO/1	MINDO/2	CNDO/2	Calculated	Experimental[b]
H – H	0.34	0.16	0.152 [17]	0.767 [32] 0.07 [33] 0.965 [34] 0.80 [35] 0.936 [36]	0.819 [49] 0.79 [50]
N ≡ N	1.33	1.33	0.647 [17]	0.63 [33] 2.40 [34] 1.76 [35] 2.648 [36] 2.651 [37] 1.15 [38]	1.76_7 [49] 1.76 [50]
F – F	0.77	–	0.339 0.323 [17]	0.895 [36] 1.382 [37] 0.56 [38] 1.23 [39]	
C ≡ O	1.58	1.35	0.829 [17]	2.44 [34] 2.283 [36] 2.466 [37]	1.97_7 [49] 1.95 [50] 1.94 1.98^c

Table 3 (Continued)

 Molecule[a]	MINDO/1	MINDO/2	CNDO/2	Calculated	Experimental[b]
O=C=O	1.97	1.64	0.879 [17]	2.430 [40]	2.63 [49] 2.92 [51] 2.62 2.89[c] 2.59 2.92[c]
N N O	2.33	2.38	1.14		3.00 [49] 3.00 [50] 2.92 3.08[c] 2.92 3.10[c]
F H	0.23		0.129 0.109 [31]	0.13 [33] 0.36 [33] 0.506 [34] 0.528 [36] 0.861 [37] 0.702 [39] 0.610 [41]	2.46 [44]
H O H	0.75	0.28	0.32 [31]	1.443 [40] 0.803 [40] 1.061 [41] 1.063 [41] 0.98 [43] 1.170 [44] 1.12 [45] 1.136 [46] 0.489 [46]	1.49 [53] 1.46 1.49[c]
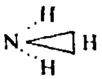	1.43	0.73	0.50 0.914 [31]	1.703 [41]	2.22 [49] 2.26 [50] 2.16 2.46[c] 2.18 2.34[c]
CH_4	1.64	1.05	0.65 [31]	2.30 [18] 2.58 [35] 3.176 [40] 1.889 [41]	2.60 [50] 2.62 [52] 2.57 2.59[c] 2.54 2.62[c]
H–C≡N	2.22	1.63	0.81 0.637 [31]	1.845 [40] 1.831 [47]	2.59 [50] 2.50 2.50[c] 2.54 4.99[c]
H–C≡C–H	2.18	1.65	0.927 0.707 [17]		3.49 [49] 3.33 [50] 3.40 3.91[c] 3.45 3.96[c]
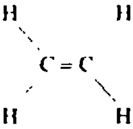	3.40	2.36	1.35	1.33 [33] 2.90 [33] 4.32 [48]	4.22 [49] 4.26 [50] 4.08 4.24[c]

---

[a] Experimental bond lengths and angles are used.

[b] Optical polarizabilities unless otherwise specified.

[c] Calculated from polarization values given in [50], the first value from the electronic polarization, the second from the total polarization (electronic + atomic polarization).

Acknowledgement. This work was supported by the Deutsche Forschungsgemeinschaft and the Fonds der Chemischen Industrie. We thank Dr. M. T. Reetz for reading the manuscript.

References

1. Cohen, H. D., Roothaan, C. C. J.: J. chem. Physics **43**, S 34 (1965).
2. Schweig, A.: Dissertation, Marburg 1964.
3. Schweig, A., Dimroth, K., Kuhn, H.: In Optische Anregung organischer Systeme, 1966. Weinheim: Verlag Chemie S. 765.
4. Schweig, A.: Chem. Physics Letters **1**, 163 (1967).
5. Schweig, A.: Chem. Physics Letters **1**, 195 (1967).
6. Pople, J. A., McIver, J. W., Ostlund, N. S.: J. chem. Physics **49**, 2960 (1968).
7. Cohen, H. D.: J. chem. Physics **43**, 3558 (1965).
8. Cohen, H. D.: J. chem. Physics **45**, 10 (1966).
9. Schweig, A.: Z. Naturforsch. **22a**, 724 (1967).
10. Schweig, A.: Molecular Physics **14**, 533 (1968).
11. Schweig, A.: Molecular Physics **15**, 1 (1968).
12. Schweig, A.: Chem. Physics Letters **3**, 542 (1969).
13. McLean, A. D., Yoshimine, M.: J. chem. Physics **46**, 3682 (1967).
14. Pople, J. A.: J. chem. Physics **49**, 2960 (1968).
15. Seibold, K., Navangul, H., Labhart, H.: Chem. Physics Letters **3**, 275 (1969).
16. Navangul, H., Labhart, H.: Theoret. chim. Acta (Berl.) **17**, 239 (1970).
17. Hush, N. S., Williams, M. L.: Chem. Physics Letters **5**, 507 (1970).
18. Teixeira-Dias, J. J. C., Murrel, J. N.: Molecular Physics **19**, 329 (1970).
19. Varma, C. A. G. O., Oosterhoff, L. J.: Chem. Physics Letters **8**, 1 (1971).
20. Pople, J. A.: J. chem. Physics **53**, 613 (1970).
21. Pople, J. A.: Chem. Physics Letters **1**, 461 (1967).
22. Pople, J. A., McIver, J. W., Jr., Ostlund, N. S.: J. chem. Physics **49**, 2965 (1968).
23. Ostlund, N. S., Newton, M. D., McIver, J. W., Jr., Pople, J. A.: J. Magnet. Resonance **1**, 298 (1969).
24. Maciel, G. E.: J. Amer. chem. Soc. **92**, 5829 (1970).
25. Nakatsuji, H., Hirao, K., Kato, H., Yohazawa, T.: Chem. Physics Letters **6**, 541 (1970).
26. Hush, N. S., Williams, M. L.: Theoret. chim. Acta (Berl.) **25**, 346 (1972).
27. Schweig, A.: Chem. Physics Letters **4**, 266 (1969).
28. Pople, J. A., Beveridge, D. L.: Approximate molecular orbital theory. New York: McGraw-Hill 1970.
29. Dewar, M. J. S.: Molecular orbital theory of organic chemistry. New York: McGraw-Hill Book Company 1969.
30. Buckingham, A. D.: Quart. Rev. chem. Soc. **13**, 183 (1959).
31. Hush, N. S., Williams, M. L.: Chem. Physics Letters **6**, 163 (1970). CNDO/2 values obtained from Eq. (1).
32. Kolos, W., Wolniewicz, L.: J. chem. Physics **46**, 1426 (1967).
33. Davies, D. W.: Molecular Physics **17**, 473 (1969).
34. Kolker, H. J., Karplus, M.: J. chem. Physics **39**, 2011 (1963).
35. Applequist, J., Carl, J. R., Fung, K. K.: J. Amer. chem. Soc. **94**, 2952 (1972).
36. Sadlej, A. J.: Theoret. chim. Acta (Berl.) **21**, 159 (1971).
37. O'Hare, J. M., Hurst, R. P.: J. chem. Physics **46**, 2356 (1967).
38. Davies, D. W.: Molecular Physics **20**, 605 (1971).
39. Stevens, R. M., Lipscomb, W. N.: J. chem. Physics **40**, 2238 (1964); **41**, 184 (1964); **41**, 3710 (1964).
40. Liebmann, S. P., Moskowitz, J. W.: J. chem. Physics **54**, 3622 (1971).
41. Moccia, R.: Theoret. chim. Acta (Berl.) **8**, 192 (1967).
42. McLean, A. D., Yoshimine, M.: J. chem. Physics **47**, 3256 (1967).
43. Drossbach, P., Schmittinger, P.: Z. Naturforsch. A **25**, 823 (1970); **25**, 834 (1970) (given: $\alpha_{zz} = -0.88 \cdot 10^{-24}\,\mathrm{cm}^3$).
44. Arrighini, G. P., Guidotti, C., Salvetti, O.: J. chem. Physics **52**, 1037 (1970).
45. Benedict, W. S., Gailer, N., Plyler, E. K.: J. chem. Physics **24**, 1139 S (1956).
46. Arrighini, G. P., Maestro, M., Moccia, R.: Chem. Physics Letters **1**, 242 (1967).
47. Arrighini, G. P., Guidotti, C., Maestro, M., Moccia, R., Salvetti, O.: J. chem. Physics **49**, 2224 (1968).
48. Denbigh, K. G.: Trans. Faraday Soc. **36**, 936 (1940).

49. Bridge, N. J., Buckingham, A. D.: Proc. Royal Soc. **295** A, 334 (1966).
50. Landolt-Börnstein: Zahlenwerte und Funktionen, Vol. 1, Part 3. Berlin: Springer 1951.
51. Le Fèvre, C. G., Le Fèvre, R. J. W.: Revs. Pure Appl. Chem. **5**, 261 (1955).
52. Watson, H. E., Ramaswamy, K. L.: Proc. Royal Soc., Ser. A. 156, 144, Rg. (1936).
53. Hölemann, P., Goldschmidt, H.: Z. physik. Chem. Abt. B **24**, 199, Rg. (1934).
54. Klopman, G., O'Leary, B.: Fortschr. chem. Forsch. **15**, Heft 4 (1970).

Prof. Dr. A. Schweig
Fachbereich Physikalische Chemie
Philipps-Universität Marburg
D-3550 Marburg (Lahn)
Biegenstr. 12
Federal Republic of Germany

Instructions to Authors

1. *Manuscripts* should be submitted in duplicate, typed in double-line spacing on one side of he paper only. Form and contents should be carefully checked to exclude the need for corrections n proof. To speed up publication, authors will receive only one set of proofs: provisionally numbered age proofs. Authors are requested to correct typographical errors only; they will be charged for orrections involving changes, additions, or deletions to the original manuscript.

Formulae should be typewritten whenever possible, special attention being given to the placing of in-ices and exponents so that they are recognizable as such even though there is no difference in size. Formulae should preferably be written in a "linear" form, e.g. exp$(-\varepsilon/kT)$ instead of $e^{-\frac{\varepsilon}{kT}}$). Special typefaces Greek, Script) should be shown by underlining in color. To avoid confusing the printer, please se red for Greek and green for Script, and underline in brown for bold face. Characters which are asily confused, e.g. 0 (zero) and capital O (letter) or 1 (figure one) and small *l* (letter), should have ome special distinguishing mark. When formulae are inserted by hand, small letters should be nderlined once and capital letters twice.

2. *Illustration copies* (graphs and structural formulae) should be drawn in Indian ink in clean niform lines and sent in on separate sheets. Please mark in the margin of the manuscript where iagrams and tables should be inserted. Captions, which should be brief, should be typed separately nd attached to the manuscript.

3. Original papers should be preceded by a *summary* (not more than 100 words) in English, German and French. (The editorial staff is willing to translate English summaries if asked.) Short notes need only an English summary. Papers not written in English should have an *English title* for use by such journals as Current Contents.

4. *Literature references* should be numbered and listed at the end of the paper. They should e cited as follows: *journal papers* — names and initials of all authors, journal in the accepted abbreviation, volume and page number, year; *books* — names of authors, full title, edition, place, publisher nd year. References should be cited in the text by number.

5. 75 *offprints* of each paper will be supplied free of charge; additional copies may be ordered at cost price.

6. *Editorial enquiries* should be addressed to:
Prof. Dr. Hermann Hartmann, Theoretica chimica Acta, D-6500 Mainz, Geschwister Scholl-Straße 2, Akademie der Wissenschaften und der Literatur zu Mainz

Manuscripts should be sent to the Editor or to one of the Co-editors:

Prof. Dr. Carl J. Ballhausen, Chemical Laboratory IV, H. C. Ørstedinstitutet, Universitetsparken 5, København Ø, Danmark,
Prof. Dr. Ronald D. Brown, Monash University, Department of Chemistry, P. O. Box 92, Clayton, Victoria, Australia 3168,
Prof. Dr. Edgar Heilbronner, Physikalisch-Chemisches Institut der Universität Basel, CH-4000 Basel, Klingelbergstraße 80, Switzerland,
Prof. Dr. J. Jortner, Department of Chemistry, Tel-Aviv University, Tel-Aviv, Israel,
Prof. Dr. Masao Kotani, 36-4 Sanno 3 chome, Ota-ku, Tokyo 143, Japan,
Prof. Dr. Jaroslav Koutecký, Československá Akademie Věd. Ústav Fyzikální Chemie, Praha 2-Vinohrady, Máchova 7, ČSSR,
Prof. Dr. Jack W. Linnett, Department of Physical Chemistry, Lensfield Road, Cambridge, England,
Prof. Dr. E. E. Nikitin, Institute of Chemical Physics, Academy of Sciences, Vorobyevskoye Chaussée 2b, Moskwa V-334, USSR,
Prof. Dr. Ralph G. Pearson, Department of Chemistry, Northwestern University, Evanston, Illinois 60201, USA,
Prof. Dr. Bernard Pullman, Université de Paris, Institut de Biologie physico-chimique, 13, rue Pierre Curie, Paris V, France,
Prof. Dr. Klaus Ruedenberg, Department of Chemistry, Iowa State University of Science and Technology, Ames, Iowa 50010, USA,
Prof. Dr. Camille Sandorfy, Université de Montréal, Case Postale 6128, Montréal, Canada,
Prof. Dr. Massimo Simonetta, Istituto di Chimica Fisica dell'Università di Milano, Via Saldini, 50, Milano, Italia,
Prof. Dr. Oktay Sinanoğlu, Department of Chemistry, Yale University, 225 Prospect Street, New Haven, Conn. 06520, USA.

Hinweise für die Autoren

1. *Manuskripte* werden mit einer Kopie, auf einseitig beschriebenen Blättern mit doppeltem Zeilenabstand erbeten. Die Manuskripte müssen formal wie inhaltlich so durchgearbeitet sein, daß Änderungen in den Korrekturfahnen unnötig sind. Zur Abkürzung der Publikationszeit erhalten die Autoren nur *eine* Seitenkorrektur mit provisorischen (*kursiven*) Seitenzahlen. Es sollen darin nur Satzfehler berichtigt werden. Nachträgliche (vom Manuskript abweichende) Korrekturen müssen den Autoren berechnet werden.

Alle Formeln sind möglichst mit der Maschine zu schreiben. Dabei ist darauf zu achten, daß Indices und Exponenten trotz des fehlenden Größenunterschiedes genau als solche zu erkennen sind. Besondere Lettern (griechische, Script) sind durch farbige Unterstreichungen zu kennzeichnen. Zur Vereinfachung für den Setzer wird gebeten, griechische Buchstaben rot, Scripttypen grün und halbfette braun zu unterstreichen. Auch einander ähnliche Zeichen, z. B. 0 (Null) und O (Buchstabe) oder 1 (Eins) und *l* (Buchstabe) sind besonders zu kennzeichnen. Bei handgeschriebenen Formeln ist bei allen vorkommenden Alphabeten zwischen Groß- und Kleinbuchstaben (durch doppeltes bzw. einfaches Unterstreichen) zu unterscheiden.

2. *Abbildungsvorlagen* werden als Tuschezeichnungen mit tiefschwarzem einheitlichen Strich auf besonderen Blättern erbeten. Am Manuskriptrand ist deutlich ihre Plazierung und die von Tabellen zu vermerken. Kurze Abbildungsunterschriften sollen am Schluß des Manuskripts beigefügt werden.

3. Bei Originalarbeiten wird um je eine *Zusammenfassung* (nicht über 100 Wörter) in Englisch, Deutsch und Französisch, bei Kurzmitteilungen um eine in Englisch gebeten. (Übersetzung ins Französische kann in der Redaktion vorgenommen werden.) Nichtenglischen Arbeiten soll außerdem eine englische Titelübersetzung beigefügt werden.

4. *Literaturangaben* sind am Schluß der Arbeit zusammenzustellen und zu numerieren. Sie enthalten Namen und nachgestellte Initialen aller Autoren, den nach den internationalen Regeln gekürzten Zeitschriftentitel, Band-, Seiten- und Jahreszahl; bei *Büchern* Autorennamen, vollen Titel, Auflage, Ort, Verlag und Jahr. Zitierung im Text erfolgt mit Nummer.

5. Von jeder Arbeit werden 75 *Sonderdrucke* kostenlos zur Verfügung gestellt. Weitere Separata können von den Autoren zum Selbstkostenpreis bezogen werden.

6. *Redaktionelle Anfragen* sind zu richten an:
Theoretica Chimica Acta, Prof. Dr. Hermann Hartmann.
Manuskripte können an alle Mitherausgeber eingesandt werden. Adressen umstehend.

Indications pour les auteurs

1. Les *manuscripts* seront envoyés en deux exemplaires dactylographiés au recto seulement. Tant la forme extérieure que le contenu doivent avoir leur aspect définitif, afin que des corrections sur les épreuves ne soient plus nécessaires. Afin d'accélérer la publication, les auteurs ne recevront qu'une seule épreuve dont les pages seront numérotées provisoirement. Seul les fautes de typographie devront être corrigées; toute autre correction entraînant des modifications, additions ou suppressions au texte original sera facturée aux auteurs. Dans la mesure du possible les formules doivent être tapées à la machine. On veillera à ce que les indices et les exposants soint facilement reconnaissables lorsqu'ils ne sont pas différenciés par leur taille. Sinon, ils devront être inscrits à la main. Les lettres spéciales (grecques, script) doivent être soulignées en couleur. Pour simplifier le travail du typographe, on recommande de souligner en rouge les lettres grecques et en vert les script. Les lettres grasses seront soulignées en brun. Dans la mesure où des caractères manuscrits sont utilisés on distinguera (même pour les caractères latins) les majuscules, qu'on soulignera deux fois, des minuscules, soulignées une fois. Des difficultés spéciales naissent du fait que les machines à écrire ne font pas, en général, de différence entre 0 (zéro) et O (lettre) ainsi qu'entre 1 (un) et *l* (lettre). Dans ce cas, des signes distinctifs sont absolument indispensables.

2. Des *graphiques* et des formules développées doivent être tracés en lignes noires à l'encre de Chine. Veuillez indiquer dans la marge du manuscrit où les graphiques et les tableaux doivent être disposés.

3. Les travaux originaux doivent comporter de brefs *résumés* (100 mots maximum), rédigés dans les 3 langues: anglais, français et allemand. Le résumé des communications brèves doit être rédigé en anglais. (Sur demande, le résumé original peut être traduit par la rédaction, en allemand). Pour faciliter la documentation un titre anglais doit être ajouté à chaque article n'étant pas écrit en anglais.

4. Les *références* bibliographiques seront numérotées et rassemblées à la fin du texte. Les citations se présenteront comme suit: noms et initiales de tous les auteurs, titre du journal abrégé selon les règles internationales, tome, numéros des pages et année. Les *livres* seront cités précédés du nom de l'auteur, titre complet, édition, lieu de publication, éditeur et date de parution. Les références dans le texte doivent être indiquées par des numéros.

5. 75 *tirés à part* de chaque article seront remis gratuitement aux auteurs. Pour les exemplaires supplémentaires le prix de revient sera facturé aux auteurs.

6. *Les demandes au rédacteur* doivent être adressées à
Theoretica Chimica Acta, Prof. Dr. Hermann Hartmann.
Les *manuscrits* peuvent être envoyés à tous les co-éditeurs (adresses susmentionnées).